

**Investigation of radiation-induced  
vascular abnormalities in  
glioblastoma tumour recurrences  
and the role of DOCK4 on  
pathological vessel development**

Anastasia Anindya Widyadari

Submitted in accordance with the requirements for the degree of  
Doctor of Philosophy (PhD)

The University of Leeds  
Leeds Institute of Medical Research

March 2022

The candidate confirms that the work submitted is her own and that appropriate credit has been given where reference has been made to the work of others.

This copy has been supplied on the understanding that it is copyright material and that no quotation from the thesis may be published without proper acknowledgment.

The right of Anastasia Anindya Widyadari to be identified as Author of this work has been asserted by Anastasia Anindya Widyadari in accordance with the Copyright, Designs and Patents Act 1988.

*I dedicate this piece to my grandfather, Gembor.  
Not a day has passed that I do not think of you.*

## **Acknowledgements**

First and foremost, I would like to express my deepest gratitude to both of my parents, Ririn and Anton, and my brother Abirama. Without your generosity and belief in me, my enthusiasm for science would have not been realised, and this thesis would have never seen the light of day. My partner, Adam Urwick, I am indebted to your kindness, your patience and grace. You encouraged me, pushed me to the limits I would have never realised myself. You never fail to make me laugh and smile even on the toughest days. I love you; it is an honour to have you by my side and no words can fully express my gratitude.

Sincere gratitude is given to both of my supervisors, Dr Georgia Mavria and Dr Mihaela Lorger. Georgia, you have been a remarkable supervisor, friend, and mentor. Your enthusiasm for science is unparalleled. I will miss our long-winded discussions about science and life, thank you for believing in me more than I did myself. Mihaela, I thank you for your sincerity and reinforcement throughout the past four years. You helped and encouraged me through the toughest times of my PhD. Day and night for the past four years the both of you have encouraged me to strive for better, as a person and as a researcher.

To Laura Heskin, your support is second to none, you believed in me, cared, listened, and picked me up when I reached rock bottom. I am grateful you are in my life, and I love you with all my might. When I look back to this time, I will think of Gary Shaw. Your encouragement, patience, and understanding are unrivalled. I appreciate you from the bottom of my heart. Helen Carrasco Hope, who have been there for me from day 1 of this journey, I have so much love for you, and I am eternally thankful we crossed paths. Safoura Mohajerani, your care, kindness and strength has made even the hardest lab days, delightful. Teklu Egnuni, this work would have never existed without you. I am grateful to have worked under you and your support has been invaluable. Chiara Galloni, thank you for being the best mentor, post-doc, and friend I could ask for. Filomena Esteves, although short but sweet, I will never forget our beautiful friendship. Jan Bilton, Debra Evans, I cannot thank you enough for your patience, and assistance with the animal work.

Dr Safarina Malik, thank you for your continued support and encouragement to pursue my dream as a researcher, I dream to become like you. To Triana Hadiprawoto, my soul sister, thank you for all the weight you have carried with me. Iva, my mentor, who has reminded me to never forget the bigger picture and encouraged me through and through, thank you. To Anna Tsunematsu, thank you for existing and loving, for I would not be here without you. Last but not least, to Professor Harry Mellor and Dr Sandra Bell, thank you for making my PhD *viva* examination a memorable and delightful experience.

To everyone I have crossed paths with, has mentored me, danced with me, and worked with me over the past four years, I sincerely thank you, your contribution does not go unnoticed. Lastly, I would like to acknowledge and give honour to all the animals involved in this study and throughout the history of scientific discovery. I am grateful for the scientific advances they have made possible for humankind, and for all the lives they have unknowingly saved.

## **Abstract**

Glioblastoma (GBM) is the most lethal form of brain tumour with an overall median survival of 12-15 months with current standard therapy of maximal safe surgery, radiotherapy and temozolomide chemotherapy. Abnormalities in the vascular niche are associated with defective vessel function and development of hypoxia, promoting disease progression and resistance to various anti-cancer therapies. Current anti-angiogenic therapies for GBM have not been promising in the clinic, contributing to no improvement in overall patient survival.

Analysis of patient GBM tumours in our laboratory had shown augmentation of vascular abnormalities, including increase in vascularisation, larger lumen size and increase in mature blood vessels in recurrences compared to primary tumours. However, the precise nature of those vascular abnormalities and how they are affected by radiotherapy was not understood. This study explores the effects of radiotherapy on the vascularisation of regrown tumours with the use of an experimental CT2A murine glioma model. Similar to the vascular changes identified in the GBM patient recurrences, abnormal vascularisation was augmented in regrown tumours post radiotherapy in the experimental model. Larger lumen size, increase in vessel length and overall surface area covered by blood vessels were abnormalities identified in CT2A tumours regrown post radiotherapy.

Hypoxia has been shown previously to result in the formation of vessels with large lumens *via* the action of VEGF. Blood vessel enlargement in experimental recurrence tumours was associated with decreased vascular permeability and elevated hypoxia in the recurrent tumours post irradiation. While smaller and larger calibre blood vessels exhibited comparable levels of extravasation in unirradiated primary tumours, enlarged blood vessels showed increased extravasation and normoxia in their vicinity, suggesting that vessel enlargement is an adaptation response to vascular dysfunction and hypoxia in the regrown tumours post radiotherapy. DOCK4 (dedicator of cytokinesis 4) is a member of the DOCK180 family of guanine nucleotide exchange factors (GEFs) and GEF for the small GTPase Rac1, shown to operate downstream of VEGF signalling in

organotypic co-cultures *in vitro* and to regulate blood vessel lumen size in *in vivo*. In CT2A tumours grown in global *Dock4* heterozygous knockout mice to overcome homozygous *Dock4* deletion embryonic lethality, blood vessel enlargement was reversed in tumours regrown post radiotherapy treatment, while DOCK4 played no role in the vascularisation of primary tumours. Additionally, regrown tumours post radiotherapy also exhibited higher number of blood vessels associated with  $\alpha$ -SMA positive pericytes. This increase in blood vessel maturation that was unaffected by *Dock4* deletion and had no impact on blood vessel permeability.

Further *in vivo* experiments using CT2A tumours grown in the *Dock4* endothelial conditional homozygous knockout mice showed that in primary tumours *Dock4* may act as a blood vessel growth suppressor, however more experiments are necessary in the future to exclude the action of compensatory mechanisms in response to knocking out both of the *Dock4* alleles in endothelial cells. The experiments were underpowered to confirm an endothelial cell autonomous role of *Dock4* deletion in the reversal of blood vessel enlargement in regrown irradiated CT2A tumours.

In summary, the study shows that in GBM tumours regrown post radiotherapy there is VEGF-driven augmentation of blood vessel calibre and growth to counteract radiation driven vasculopathy and elevated hypoxia in the regrown tumours. The resulting vasculature is also more mature with elevated pericyte coverage. Co-option of blood vessels situated in the peri-tumoural area treated with radiotherapy following surgical resection, and subsequent tumour-induced modification would provide an explanation for the abnormal function of the vasculature in the regrown tumours, and resistance to current anti-angiogenic therapies. The CT2A experimental model of tumour regrowth established here can be used to further elucidate the contribution of therapies on vascular abnormality. Elucidating the mechanisms of radiation-induced aberrant vascularisation may lead to the development of new blood vessel-targeting therapies and/ or provide rationale and alternative avenues for modifying existing therapies.

## Table of Contents

<b>Acknowledgements</b> .....	<b>iv</b>
<b>Abstract</b> .....	<b>vi</b>
<b>Table of Contents</b> .....	<b>viii</b>
<b>List of Figures</b> .....	<b>xiii</b>
<b>List of Tables</b> .....	<b>xviii</b>
<b>List of Abbreviations</b> .....	<b>xix</b>
<b>Chapter 1 Introduction</b> .....	<b>1</b>
1.1 Glioblastoma (GBM) .....	2
1.2 GBM Molecular Classification .....	2
1.3 Prevalence and Pathological features of GBM .....	6
1.4 Current treatment of GBM.....	8
1.4.1 Standard care of therapy for GBM .....	8
1.4.2 The use of Bevacizumab.....	10
1.4.3 GBM Recurrence.....	11
1.4.4 Histological and molecular features of GBM recurrence .....	14
1.5 Brain tumour microenvironment.....	15
1.5.1 Perivascular Niche .....	17
1.5.2 Hypoxic Niche .....	19
1.5.3 Invasive Tumour Niche.....	20
1.6 Endothelial cells .....	21
1.6.1 Vascular Pericytes.....	22
1.6.2 Astrocytes.....	26
1.6.3 Tumour associated macrophages (TAMs) .....	26
1.7 Interaction of GSCs with the GBM tumour microenvironment .....	28
1.8 Vascular development of GBM .....	29

1.8.1	Developmental Angiogenesis.....	29
1.8.2	Blood vessel development in GBM .....	30
1.9	Mouse models of GBM .....	40
1.9.1	Xenograft models.....	40
1.9.2	Syngeneic models .....	41
1.9.3	Genetically engineered mouse models.....	41
1.9.4	Emerging alternative models .....	42
1.10	Effect of radiotherapy on GBM.....	42
1.10.1	Effect of radiotherapy on GBM tumour growth .....	42
1.10.2	Effect of radiotherapy on GBM tumour vasculature .....	46
1.11	Dedicator of Cytokinesis 4 (DOCK4) .....	51
1.11.1	Rho GTPases .....	51
1.11.2	Guanine Nucleotide Exchange Factors (GEFs).....	52
1.11.3	The role of DOCK4 in cancer.....	54
1.11.4	The role of DOCK4 in vascular development and angiogenesis.....	58
1.12	Previous work leading to this thesis .....	59
1.13	Aims.....	64
<b>Chapter 2 Materials and Methods .....</b>		<b>65</b>
2.1	Cell Culture techniques.....	66
2.1.1	Cell lines .....	66
2.1.2	Culturing mammalian cell lines .....	66
2.1.3	Freezing stocks .....	66
2.1.4	Standard solutions .....	67
2.1.5	Irradiation of cells.....	67
2.2	Biochemistry.....	68
2.2.1	Cell supernatant collection.....	68

2.2.2 ELISA.....	68
2.3 Immunostaining.....	68
2.3.1 Immunohistochemistry (IHC) .....	68
2.3.2 Immunofluorescence (IF) .....	71
2.3.3 Mouse-on-Mouse (M.O.M) immunofluorescence staining ..	75
2.4 Image processing and quantifications.....	75
2.4.1 Randomisation of samples and images .....	75
2.1.1 CD31 .....	75
2.1.2 F4/80.....	76
2.1.3 $\alpha$ -SMA.....	76
2.1.4 GLUT-1 .....	77
2.1.5 BSA-AlexaFluor555 .....	77
2.5 Microscopes .....	78
2.5.1 Zeiss AxioImager Z1 upright .....	78
2.5.2 Nikon A1R confocal .....	78
2.5.3 Nikon Eclipse E1000.....	79
2.6 <i>In vivo</i> experiments .....	79
2.6.1 Mouse strain and breeding .....	79
2.6.2 Intracranial implantation of cancer cells.....	80
2.6.3 Irradiation .....	81
2.6.4 IVIS Imaging .....	81
2.6.5 Terminal Perfusion.....	82
2.6.6 <i>In vivo</i> sample processing.....	82
2.7 Statistical analysis.....	84
<b>Chapter 3 Effects of radiotherapy on pathological vessel development of tumour recurrences.....</b>	<b>85</b>
3.1 Introduction .....	86

3.2 Characterisation of blood vessel morphology in the CT2A murine GBM model .....	88
3.3 Irradiation of CT2A tumours .....	101
3.4 Increased angiogenesis and lumenisation in radiotherapy treated regrown tumours .....	104
3.5 Increased F4/80 positive areas in radiotherapy treated regrown CT2A tumours .....	113
3.6 Summary .....	118
<b>Chapter 4 Effects of radiotherapy on blood vessel maturation, permeability, and hypoxia .....</b>	<b>120</b>
4.1 Introduction .....	121
4.2 Characterisation of $\alpha$ -SMA+ cells/pericytes in the intracranial CT2A glioblastoma tumour implantation model .....	123
4.2.1 Optimisation of $\alpha$ -SMA staining .....	124
4.3 Effects of radiotherapy on blood vessel association with $\alpha$ -SMA positive pericytes. ....	128
4.4 Effect of radiotherapy on blood brain barrier (BBB) integrity and blood vessel permeability .....	139
4.5 Pilot experiment for the analysis of blood vessel permeability in response to radiotherapy .....	142
4.6 Establishing a method to analyse BSA-AlexaFluor555 extravasation .....	148
4.7 Analysis of tracer extravasation in the control and radiotherapy treated regrown tumours in the pilot experiment .....	152
4.8 Analysis of tracer extravasation in regrown tumours post radiotherapy in a larger tumour cohort .....	156
4.9 Blood vessel association with $\alpha$ -SMA positive cells does not alter tracer extravasation in control tumours or tumours regrown after radiotherapy .....	174

4.10 Decreased tracer extravasation from blood vessels with lumen size $\leq 10\mu\text{m}$ in irradiated regrown tumours.....	177
4.11 Decreased tracer extravasation from blood vessels with shorter length in irradiated regrown tumours .....	181
4.12 Increased hypoxia marked by GLUT1 expression in radiotherapy treated regrown tumours.....	184
4.13 Summary.....	189
<b>Chapter 5 Effects of <i>Dock4</i> deletion on radiotherapy-induced blood vessel vascular changes .....</b>	<b>191</b>
5.1 Introduction .....	192
5.2 Characterisation of blood vessels in CT2A tumours implanted intracranially in <i>Dock4</i> heterozygous knockout mice in response to irradiation .....	194
5.3 <i>Dock4</i> heterozygous deletion reverses radiotherapy-induced effects on blood vessel development.....	198
5.4 <i>Dock4</i> heterozygous deletion does not reverse the radiation-induced effects of blood vessel– $\alpha$ -SMA+ pericyte association..	208
5.5 Intracranial implantation of CT2A glioma cell line in endothelial <i>Dock4</i> conditional knockout mice.....	213
5.6 Characterisation of CT2A tumours injected intracranially in endothelial <i>Dock4</i> conditional knockout mice .....	226
5.7 Intracranial implantation of CT2A glioma cell line in endothelial <i>Dock4</i> conditional knockout mice in the repeat experiment.....	234
5.8 Characterisation of early excised CT2A tumours injected intracranially in endothelial <i>Dock4</i> conditional knockout mice. ..	244
5.9 Blood vessel tracer extravasation in early excised intracranial CT2A tumours in endothelial <i>Dock4</i> conditional knockout mice	252
5.10 <i>Dock4</i> endothelial deletion stimulates blood vessel formation in blood vessels of CT2A tumours injected intracranially .....	259
5.11 Summary.....	263

<b>Chapter 6 Discussion .....</b>	<b>265</b>
6.1 Introduction .....	266
6.2 The use of the CT2A tumour model .....	267
6.3 The vascularisation of GBM recurrences .....	269
6.4 Blood vessel enlargement in regrown tumours post-irradiation ..	271
6.5 Elevated hypoxia in regrown tumours post-irradiation .....	272
6.6 Radiotherapy promotes blood vessel association with $\alpha$ -SMA positive cells.....	274
6.7 Blood vessel enlargement but not the increase in $\alpha$ -SMA association is reversed by <i>Dock4</i> genetic deletion .....	276
6.8 Effects of radiotherapy on blood vessel permeability.....	279
6.9 Other changes observed in regrown post radiotherapy CT2A tumours .....	283
6.10 Effects of endothelial <i>Dock4</i> deletion on tumour vessel development .....	285
6.11 Concluding remarks .....	287
<b>Appendices .....</b>	<b>290</b>
<b>Appendix 1 - Summary of <i>in vivo</i> experiments conducted and/or analysed within this study.....</b>	<b>291</b>
<b>Appendix 2 - Scanned images of CT2A tumours in WT and <i>Dock4</i>het mice, control and regrown post radiotherapy used for quantification.....</b>	<b>294</b>
<b>Appendix 3 - Python source code and output used in image randomisation for analysis of immunohistochemistry sections.....</b>	<b>297</b>
<b>Appendix 4 - Observed peritumoral invasion in control and regrown intracranially implanted CT2A tumours. ....</b>	<b>298</b>
<b>Appendix 5 - Visualisation of blood vessel co-option in CT2A tumours intracranially implanted in WT and <i>Dock4</i>Het mice. ....</b>	<b>300</b>

<b>Appendix 6 - Pattern of tracer extravasation from tumour mass to non-tumour bearing brain parenchyma in CT2A control non-irradiated tumour.....</b>	<b>302</b>
<b>Appendix 7 - Vascularisation and tracer extravasation of normal mouse brain treated with radiotherapy. ....</b>	<b>304</b>
<b>Appendix 8 - Graphical representation of the process of blood vessel tracer quantification and macros generated for automation. ....</b>	<b>306</b>
<b>Appendix 9 - Conditional <i>Dock4</i> knockout model generated by Ozgene.....</b>	<b>309</b>
<b>Appendix 10 - Increased VEGF secretion in conditioned medium of CT2A cells treated with radiotherapy.....</b>	<b>311</b>
<b>Appendix 11 - The application of statistical methods: Student's t-test and ANOVA.....</b>	<b>314</b>
<b>References.....</b>	<b>316</b>

## List of Figures

Figure 1.1 Regions of human brain where GBM commonly develops...	7
Figure 1.2 Standard of care therapy for GBM.....	10
Figure 1.3 Glioblastoma tumour niches.....	16
Figure 1.4 Modes of neovascularisation in GBM. ....	35
Figure 1.5 Early effects of irradiation on GBM vasculature. ....	47
Figure 1.6 Four groups of the DOCK family proteins. ....	53
Figure 1.7 Domain structure of DOCK4. ....	54
Figure 1.8 The role of DOCK4 as a Rac1 activator.....	55
Figure 1.9 Schedule of CT2A-Luc tumour growth, irradiation, and excision following intracranial implantation in WT and <i>Dock4</i> heterozygous knockout ( <i>Dock4</i> het) mice.....	63
Figure 3.1 CT2A tumours present aberrant and convoluted vascular morphology compared to normal brain.....	90
Figure 3.2 Selection of areas within a CT2A tumour section for vascular characterisation.....	95
Figure 3.3 Blood vessel morphology in different CT2A tumour sections. ....	98
Figure 3.4 Variability of lumen number and diameter between tumour sections and samples.....	100
Figure 3.5 Representative images of CT2A blood vessel morphology in control and radiotherapy treated regrown tumours.....	106
Figure 3.6 Increase in blood vessel lumenisation and lumen size in radiotherapy treated regrown tumours.....	108
Figure 3.7 Radiotherapy increased blood vessel length and surface area in regrown tumours.....	110
Figure 3.8 Radiotherapy affects neither the thickness nor the branching of blood vessels. ....	112

<b>Figure 3.9 Higher F4/80 positive areas in radiotherapy treated regrown tumours.....</b>	<b>117</b>
<b>Figure 4.1 <math>\alpha</math>-SMA+ cells could not be detected by immunohistochemistry in CT2A tumours. ....</b>	<b>124</b>
<b>Figure 4.2 Blood vessel staining in CT2A tumours with different markers by immunofluorescence.....</b>	<b>126</b>
<b>Figure 4.3 <math>\alpha</math>-SMA+ blood vessels are readily detectable by immunofluorescence staining of CT2A tumours.....</b>	<b>127</b>
<b>Figure 4.4 Visualisation of <math>\alpha</math>-SMA positive blood vessels in regrown tumours following radiotherapy treatment.....</b>	<b>131</b>
<b>Figure 4.5 Increased abundance <math>\alpha</math>-SMA positive blood vessels observed in histological sections of regrown tumours following radiotherapy treatment.....</b>	<b>133</b>
<b>Figure 4.6 Scoring of blood vessel pericyte association. ....</b>	<b>135</b>
<b>Figure 4.7 Quantification of <math>\alpha</math>-SMA+ blood vessels show increase in <math>\alpha</math>-SMA tight association after radiotherapy. ....</b>	<b>137</b>
<b>Figure 4.8 Schedule of CT2A tumour implantation, irradiation, and tracer injection in a pilot experiment. ....</b>	<b>141</b>
<b>Figure 4.9 Monitoring of CT2A tumour growth following irradiation in the tracer extravasation pilot experiment.....</b>	<b>147</b>
<b>Figure 4.10 Schematic of processing of CT2A bearing brains for visualisation of BSA-AlexaFluor555 tracer extravasation in histological sections. ....</b>	<b>150</b>
<b>Figure 4.11 Visualisation of <math>\alpha</math>-SMA, CD34/Endomucin and BSA-AlexaFluor555 tracer for quantification. ....</b>	<b>151</b>
<b>Figure 4.12 Irradiated regrown tumour in pilot experiment demonstrates higher tracer extravasation. ....</b>	<b>154</b>
<b>Figure 4.13 Monitoring of CT2A tumour growth following irradiation in the tracer extravasation repeat experiment. ....</b>	<b>161</b>

<b>Figure 4.14 CT2A Tumours regrown after irradiation display reduced tracer extravasation compared to untreated tumours. ....</b>	<b>168</b>
<b>Figure 4.15 Quantification of tracer-positive pixels of extravasation around blood vessels shows decreased extravasation in irradiated regrown tumours compared to control. ....</b>	<b>170</b>
<b>Figure 4.16 Liver control samples of tracer injected mice display a comparable amount of tracer between control and irradiated group.....</b>	<b>173</b>
<b>Figure 4.17 <math>\alpha</math>-SMA+ cell association with tumour blood vessels does not contribute to the differences in tracer extravasation between control and irradiated tumours.....</b>	<b>176</b>
<b>Figure 4.18 Blood vessels with smaller lumens show the largest reduction in tracer extravasation in CT2A regrown tumours following radiotherapy. ....</b>	<b>180</b>
<b>Figure 4.19 Blood vessels with shorter lengths have the lowest tracer extravasation in irradiated regrown tumours.....</b>	<b>183</b>
<b>Figure 4.20 Increased hypoxia in regrown tumours after irradiation marked by GLUT-1 expression. ....</b>	<b>188</b>
<b>Figure 5.1 Morphology of blood vessels of CT2A tumours grown intracranially in WT and <i>Dock4</i>het mice in control conditions and following irradiation and tumour re-growth. ....</b>	<b>197</b>
<b>Figure 5.2 Reduction of overall vessel area of irradiated CT2A tumours grown intracranially in <i>Dock4</i>het compared to WT mice. ....</b>	<b>202</b>
<b>Figure 5.3 Reduction of blood vessel lumen size of irradiated CT2A tumours grown intracranially in <i>Dock4</i>het compared to WT mice.</b>	<b>205</b>
<b>Figure 5.4 Reduction of blood vessel length of irradiated CT2A tumours grown intracranially in <i>Dock4</i>het compared to WT mice.</b>	<b>207</b>
<b>Figure 5.5 Association of blood vessels with <math>\alpha</math>-SMA positive cells in response to <i>Dock4</i> heterozygous genetic deletion. ....</b>	<b>212</b>

<b>Figure 5.6 Schedule of CT2A-Luc tumour growth, irradiation, and excision in Cdh5(PAC)-CreERT2; Dock4 fl/fl mice (endothelial Dock4 conditional knockout mice) following tamoxifen induction.</b>	<b>217</b>
<b>Figure 5.7 Monitoring of CT2A tumour growth in control and irradiated WT or endothelial Dock4 conditional knockout mice by bioluminescence imaging.</b>	<b>222</b>
<b>Figure 5.8 Endothelial Dock4 deletion detected by IHC in CT2A tumours grown intracranially in endothelial Dock4 conditional knockout mice.</b>	<b>225</b>
<b>Figure 5.9 Morphology of blood vessels of CT2A tumours grown intracranially in endothelial Dock4 conditional knockout mice.</b>	<b>230</b>
<b>Figure 5.10 Quantification of blood vessel growth, abundance, and size of blood vessel lumens in control and irradiated CT2A tumours growing intracranially in Dock4 conditional knockout mice.</b>	<b>233</b>
<b>Figure 5.11 Altered schedule of excision of CT2A tumours in repeat experiment in Dock4 conditional knockout mice due to early presentation of neurological symptoms.</b>	<b>237</b>
<b>Figure 5.12 Monitoring of CT2A tumour growth in control and irradiated Dock4 conditional knockout mice by bioluminescence imaging (repeat experiment).</b>	<b>241</b>
<b>Figure 5.13 Morphology of blood vessels of CT2A tumours grown intracranially in Dock4 conditional knockout mice.</b>	<b>248</b>
<b>Figure 5.14 Quantification of blood vessel growth, abundance, and size of blood vessel lumens in early excised CT2A tumours growing intracranially in Dock4 conditional knockout mice.</b>	<b>251</b>
<b>Figure 5.15 Quantification of tracer extravasation from blood vessels in control and irradiated CT2A tumours growing intracranially in Dock4 conditional knockout mice.</b>	<b>255</b>
<b>Figure 5.16 Quantification of tracer abundance in livers of mice injected with BSA-AlexaFluor555.</b>	<b>258</b>

<b>Figure 5.17 Stimulation of blood vessel growth, abundance, and size of blood vessel lumens in tumours growing intracranially in <i>Dock4</i> conditional knockout mice compared to WT controls. ...</b>	<b>262</b>
<b>Figure 6.1 Observed changes in tumour blood vessels of primary and recurrent GBM tumours. ....</b>	<b>292</b>

## List of Tables

Table 1.1 Reported vascular aberrations observed in GBM patient samples and <i>in vivo</i> models of GBM .....	32
Table 2.1 List of commonly used standard solutions in the study. ....	67
Table 2.2 List of primary and secondary antibodies used in immunohistochemistry. ....	70
Table 2.3 List of primary and secondary antibodies used in immunofluorescence.....	73
Table 3.1 Blood vessel readouts used in the study for vascular characterisation. ....	92
Table 3.2 List of CT2A tumour control and irradiated tumour samples for the investigation of the effects of radiotherapy on vascularisation.....	103
Table 4.1 List of CT2A tumour control and irradiated tumour samples analysed in the tracer extravasation experiment.....	162
Table 5.1 CT2A tumour samples grown intracranially in endothelial <i>Dock4</i> conditional knockout mice.....	223
Table 5.2 CT2A tumour samples grown intracranially in <i>Dock4</i> conditional knockout mice (repeat experiment). ....	242
Table 4.1 List of CT2A tumour control and irradiated tumour samples analysed in the tracer extravasation experiment.....	162
Table 5.1 CT2A tumour samples grown intracranially in endothelial <i>Dock4</i> conditional knockout mice. ....	223
Table 5.2 CT2A tumour samples grown intracranially in <i>Dock4</i> conditional knockout mice (repeat experiment). ....	242

## List of Abbreviations

2ME2	2-methoxyestradiol
$\alpha$ -KG	Alpha ketoglutarate
$\alpha$ -SMA	Alpha smooth muscle actin
ADAM10	ADAM Metallopeptidase Domain 10
ADAMTS1	ADAM Metallopeptidase with Thrombospondin Type 1 Motif 1
ADS	Antibody diluent solution
AKT	Protein kinase B
AML	Acute myeloid leukemia
ANG-1	Angiopoeitin-1
ANG-2	Angiopoeitin-2
ARB	Angiotensin-1 receptor blocker
ASD	Autism spectrum disorder
BBB	Blood brain barrier
BMDC	Bone marrow derived cells
BMDM	Bone marrow derived macrophages
BSA	Bovine serum albumin
BTB	Blood tumour barrier
BV	Blood vessel(s)
CAIX	Carbonic anhydrase 9
CBCT	Cone beam computer tomography
CCL2	C-C Motif Chemokine Ligand 2
CCL5	C-C Motif Chemokine Ligand 5
CCR5	Chemokine receptor type 5
CD105	Cluster of differentiation 105
CD13	Cluster of differentiation 13
CD133	Cluster of differentiation 133
CD144	Cluster of differentiation 144
CD31	Cluster of differentiation 31 (PECAM-1)
CD34	Cluster of differentiation 34
CD45	Cluster of differentiation 45
CDKN2A	Cyclin Dependent Kinase Inhibitor 2A
CHEO	Children Hospital of Eastern Ontario

CHI3L1	Chitinase 3 Like 1
CLX	Cell line xenografts
CNS	Central nervous system
CSF	Cerebrospinal fluid
CT	Computerised tomography
CVH	Chronic vascular hyperplasia
CXCL12	C-X-C Motif Chemokine Ligand 1
CXCR	C-X-C motif chemokine receptors
CXCR4	C-X-C motif chemokine receptor 4
DAB	3,3'-Diaminobenzidine
DAPI	4',6-diamidino-2-phenylindole
DH	Dbl Homology
DHR	Dock Homology Region
DHR1	Dock Homology Region 1
DHR2	Dock Homology Region 2
DIC	Differential interference contrast
DLL4	Delta Like Canonical Notch Ligand 4
DMEM	Dulbecco's Modified Eagle Medium (DMEM)
DMSO	Dimethyl sulfoxide
DNA	Deoxyribonucleic acid
DOCK	Dedicator of Cytokines
DOCK1	Dedicator of Cytokines 1
DOCK2	Dedicator of Cytokines 2
DOCK3	Dedicator of Cytokines 3
DOCK4	Dedicator of Cytokines 4
Dock4het	Dock4 heterozygous knockout mice
DOCK5	Dedicator of Cytokines 5
DOCK6	Dedicator of Cytokines 6
DOCK7	Dedicator of Cytokines 7
DOCK8	Dedicator of Cytokines 8
DOCK9	Dedicator of Cytokines 9
DOCK10	Dedicator of Cytokines 10
DOCK11	Dedicator of Cytokines 11
DPX	Dibutylphthalate Polystyrene Xylene
DSB	Double strand break

EC	Endothelial cell
ECM	Extracellular matrix
EGF	Endothelial growth factor
EGFR	Epidermal growth factor receptor
ELISA	Enzyme-linked immunoassay
ELMO	Engulfment and cell motility
EMT	Epithelial to mesenchymal transition
EPC	Endothelial progenitor cell
ERK1	Extracellular signal-regulated protein kinase 1
ETV2	ETS Variant Transcription Factor 2
FCS	Foetal Calf Serum
FGF	Fibroblast growth factor
FITC	Fluorescein isothiocyanate
GAP	GTPase activating proteins
GBM	Glioblastoma
GDI	Guanine dissociation inhibitors
GDP	Guanine diphosphate
GEF	Guanine nucleotide exchange factors
GEMM	Genetically engineered mouse models
GFAP	Green fluorescent activated protein
GLI2	GLI Family Zinc Finger 2
GLUT-1	Glucose transporter 1
GMP	Glomeruloid microvascular proliferation
Grp124	Probable G-protein coupled receptor 124
GSC	Glioma stem cells
GTP	Guanine triphosphate
HCAEC	Human coronary artery endothelial cells
HGF	Hepatocyte growth factor
HH	Hedgehog pathway
HIF	Hypoxia Inducible Factor
HRP	Horseradish peroxidase
HUVEC	Human umbilical vein endothelial cells
ICAM	Intercellular adhesion molecule
IDH	Isocitrate dehydrogenase

IDH1	Isocitrate dehydrogenase 1
IDH2	Isocitrate dehydrogenase 2
IF	Immunofluorescence
IFN- $\gamma$	Interferon gamma
IHC	Immunohistochemistry
IL-10	Interleukin 10
IL-1 $\beta$	Interleukin 1 beta
IL-2	Interleukin 2
IL-6	Interleukin 6
IL-8	Interleukin 8
IMRT	Intensity-modulated radiotherapy
IP	Intraperitoneal
IV	Intravascular
JAG1	Jagged Canonical Notch Ligand 1
KO	Knockout
L1CAM	L1 cell adhesion molecule
LFNG	LFNG O-fucosylpeptide 3-beta-N-acetylglucosaminyltransferase
LIMR	Leeds Institute of Medical Research
LTBP4	Latent-transforming growth factor beta-binding protein 4
MAP	Mitogen-activated protein kinase
MDS	Myelodysplastic syndrome
Met	Tyrosine-protein kinase Met
MGMT	O <sup>6</sup> -methylguanine-DNA-methyltransferase
MHC 1	Major histocompatibility complex 1
MHC 2	Major histocompatibility complex 2
MLH1	MutL homolog 1
MMP1	Matrix metalloproteinase 1
MMP16	Matrix metalloproteinase-16
MMP2	Matrix metalloproteinase 2
MMP9	Matrix metalloproteinase 9
MMR	Mismatch repair
MRI	Magnetic resonance imaging
MSH2	MutS Homolog 2
MSH6	MutS Homolog 6

NCAM	Neural cell adhesion molecule
NCRI	National Cancer Research Institute
NEFL	Neurofilament Light Chain
NES	Nestin
NF- $\kappa$ B	Nuclear factor kappa B
NF1	Neurofibromatosis type 1
NG2	Neuron-glia antigen 2
NICE	National institute of care and excellence
NOD	Non-obese/diabetic
NOS	Not otherwise specified
NOTCH	Notch homolog
NOTCH3	Notch homolog 3
NSG	NOD scid gamma mouse
NVU	Neurovascular unit
OLIG2	Oligodendrocyte Transcription Factor 2
PAS	Periodic acid schiff staining
PBS	Phosphate buffered saline
PCNA	Proliferating cell nuclear antigen
PCV	Procarbazine, lomustine and vincristine
PDGF	Platelet-derived growth factor
PDGFB	Platelet-derived growth factor beta
PDGFR	Platelet-derived growth factor receptor
PDGFRA	Platelet-derived growth factor receptor A
PDX	Patient-derived xenografts
PECAM	Platelet endothelial cell adhesion molecule 1
PEDF	Pigment epithelium-derived factor
PFA	Paraformaldehyde
PGF	Placental growth factor
PGK1	Phosphoglycerate kinase 1
PH	Pleckstrin Homology
PI3K	Phosphatidylinositol (3,4,5)-trisphosphate
PIP3	Phosphoinositide 3-kinase
PKCs	Protein kinase, catalytic subunit
PLVAP	Plasmalemma vesicle associated protein

PTCH	Patched
PTEN	Phosphatase and tensin homolog
PVN	Perivascular niche
RAS	Rat sarcoma virus
RB	Retinoblastoma
RCAS	Replication-Competent Avian with Splice acceptor
RFP	Red fluorescent protein
RNA	Ribonucleic acid
RO2	Organic peroxy radicals
ROBO4	Roundabout guidance receptor
ROI	Region of interest
ROS	Reactive oxygen species
RT	Radiotherapy
RTK	Receptor tyrosine kinase
SARRP	Small animal radiation research platform
SCID	Severe combined immunodeficiency trait
SDF-1	Stromal cell-derived factor 1
SH3	Src-Binding
SH3YL1	SH3 domain-containing YSC84-like protein 1
SLC12A5	Solute Carrier Family 12 Member 5
SLIT2	Slit Guidance Ligand 2
SMC	Smooth muscle cell
SMO	Smoothened
SOX2	SRY (Sex determining region Y)-box 2
SRS	Stereotactic radiosurgery
SSB	Single strand breaks
TAM	Tumour associated macrophages
TBS	Tris buffered saline
TBST	Tris buffered saline + Tween
TEM	Tie2-expressing Monocytes
TERT	Telomerase Reverse Transcriptase
TGCA	The Cancer Genome Atlas
TGF- $\beta$	Transforming growth factor beta
TMZ	Temozolomide

TNF- $\alpha$	Tumour necrosis factor alpha
TOP2A	DNA Topoisomerase II Alpha
TP53	Tumour protein 53
USV	Ultrasonic vocalisation
VE-Cadherin	Vascular endothelial cadherin
VEGF	Vascular endothelial growth factor
VEGFR2	Vascular endothelial growth factor receptor 2
VM	Vasculogenic mimicry
VPF	Vascular permeability factor
VSMC	Vascular smooth muscle cells
VWF	Von Willebrand factor
WHO	World health organisation
WNT	Wingless-related integration site
WT	Wild type
ZO-1	Zonula occludens 1

# **Chapter 1**

## **Introduction**

## **1.1 Glioblastoma (GBM)**

Brain tumours, together with other central nervous system tumours, are among the most feared of all cancers. Brain tumours account for 3% of all cancer cases, with over 12,000 people diagnosed between 2015 and 2017 in the UK alone (Cancer Research UK, 2020). Glioblastoma (GBM) is the most aggressive brain tumour and most frequent tumour subtype diagnosed (Wanis et al., 2021). Proving challenging to treat, more than two thirds of adults diagnosed with GBM die within 2 years of diagnosis (Gilbert et al., 2014). Dr Rudolf Virchow was the first to identify GBM in 1863 as a tumour with glial cell origins (Agnihotri et al., 2013). Originally thought to arise solely from glial cells, recent evidence suggests that high grade gliomas, including GBM, may arise from multiple cell types with neural stem cell-like properties (Couturier et al., 2020).

GBMs are classified as either primary or secondary. Primary GBMs are defined as tumours that arise without a known precursor, whereas secondary GBMs are tumours with clinical, radiologic, or histopathological evidence that the tumour developed from a lower-grade malignancy (Parsons et al., 2008). Although histologically indistinguishable, primary, and secondary GBMs are distinct in the genetic alterations that occur during their evolution, a finding that was first reported in 1996 by H. Ohgaki and colleagues. Genetic alterations of the epidermal growth factor receptor (EGFR) gene such as overexpression, phosphatase and tensin homolog (PTEN) gene mutation or entire loss of chromosome 10 were the seen most frequently in primary GBM (Ohgaki and Kleihues, 2013). Genetic alterations involving tumour protein 53 (TP53) and IDH1 gene mutations were more frequently seen in secondary GBM (Nobusawa et al., 2009).

## **1.2 GBM Molecular Classification**

The World Health Organisation (WHO) tumour grading is used for diagnosis and to predict therapeutic outcome. The 2007 WHO classification categorises glioblastoma multiforme as a grade IV neoplasm which is assigned to neoplasms that are mitotically active and cytologically malignant with a fast disease evolution and typically fatal outcome (Louis et al., 2007). Utilising microarray technology,

Phillips and co-workers classified GBM into three subtypes: Proneural, Proliferative and Mesenchymal (Phillips et al., 2006). Patients with GBM of Proneural subtype have a better prognosis and are more commonly seen in younger patients. Expression of proteins associated with neurons such as neural cell adhesion molecule (NCAM) and gamma-aminobutyric acid type B receptor subunit 1 (GABBR1) are frequently expressed in GBM tumours with Proneural subtype (Phillips et al., 2006). The Proliferative subtype was defined as one with up-regulated proliferation markers such as DNA topoisomerase II alpha (TOP2A) and proliferating nuclear cell antigen (PCNA) (Phillips et al., 2006). Distinctively, the Mesenchymal subtype displays elevated angiogenesis markers including platelet endothelial cell adhesion molecule gene (PECAM) and vascular endothelial growth factor (VEGF) (Phillips et al., 2006). These three subtypes provide the foundation of further molecular GBM classification.

As a result of genomic and transcriptomic profiling of 206 GBM patient samples carried out by The Cancer Genome Atlas Research Network (TCGA) 601 genes with genetic alterations were identified in GBM providing evidence on the true complexity of the mutational signature of GBM (The Cancer Genome Atlas Research, 2008). A set of three core signalling pathways commonly altered were reported in the study, namely the retinoblastoma (Rb) pathway, the tumour protein p53 (p53) pathway and receptor tyrosine kinase (RTK)/Ras/phosphoinositide 3-kinase (PI3K) signalling pathway. Prognostic factors for treatment response were also identified in different studies namely the methylation status of the promoter of the MGMT (O<sup>6</sup>-methylguanine-DNA methyltransferase) gene which is involved in DNA repair (Hegi et al., 2005). GBM patients with MGMT gene promoter methylation and hence lower transcription of the MGMT gene show increased survival compared to patients without MGMT gene promoter methylation (Hegi et al., 2005).

Following the development of large-scale next generation sequencing methods, GBM was subsequently categorised into four subtypes based on differences in genetic expression profiles: Classical, Mesenchymal, Proneural and Neural (Verhaak et al., 2010). EGFR amplification, characterised by chromosome 7 amplification paired with chromosome 10 loss was observed in 100% of the

Classical subtype along with lack of TP53 gene mutations, and cyclin-dependent kinase inhibitor 2A (CDKN2A) gene deletion which affects the RB pathway and its components (Verhaak et al., 2010). Nestin encoded by the NES gene, a neural stem cell marker, along with components of the Notch (NOTCH3, JAG1, LFNG) and Sonic hedgehog pathways (SMO, GAS1, GLI2) are all highly expressed in the Classical subtype. Patients presenting with Classical subtype have significant improvement in mortality when treated with aggressive treatments of radiotherapy and chemotherapy (Verhaak et al., 2010). Mesenchymal subgroup tumours have extensive necrosis and inflammation and contain the highest number of mutations in the NF1 (Neurofibromatosis type 1) tumour suppressor gene. It is also characterised by displayed expression of mesenchymal markers i.e., Chitinase3-like 1 (CHI3L1) and MET receptor tyrosine kinase. Genes that participate in the tumour necrosis superfamily pathway and nuclear factor kappa-light-chain-enhancer of activated B cells (NF- $\kappa$ B) pathway are highly expressed in the Mesenchymal subtype. Although Mesenchymal subtypes respond well to therapy, they have increased potential for invasion (Verhaak et al., 2010) and also the worst overall prognosis among all subtypes (Colman et al., 2010). Recent work shows that vascular endothelial growth factors (VEGF) A and B, and angiopoietins (ANG) 1 and 2 are responsible for angiogenesis and they are highly upregulated in the Mesenchymal subtype compared to other subtypes (Sharma et al., 2017). Colman et al., have demonstrated that there is an association between the mesenchymal-angiogenic phenotype in GBM and a stem-like phenotype (Colman et al., 2010), which is correlated with worse outcome in GBM patients receiving standard therapy (Murat et al., 2008).

Platelet-derived growth factor receptor alpha (PDGFRA) and point mutations in the IDH1 gene are two major genetic alterations seen in the Proneural subtype (Verhaak et al., 2010). TP53 gene mutations and loss of heterozygosity were common in this subtype and elevated levels of expression of oligodendrocytic development genes such as oligodendrocyte transcription factor (OLIG2) was seen in this subtype. Tumour suppressor and inhibitor of stem cell proliferation p21, is suppressed by high expression of OLIG2 which leads to increased proliferation (Dennis et al., 2012). Lastly, Neural subtype has similar genetic expression when compared to normal brain tissue and respond better to

radiotherapy and chemotherapy (Zhang et al., 2020). Neural subtype is characterised by expression of neural markers e.g., Solute carrier family 12 members 5 (SLC12A5) and neurofilament light peptide (NEFL). Although showing no significant improvement in response to aggressive treatments, patients presenting with tumours of Proneural subtype may have better survival rates. In 2017, Wang et al. found that the median survival of Classical, Mesenchymal and Proneural GBM are 14.7, 11.5 and 17.0 months, respectively (Wang et al., 2017). In the study, they also observed that a macrophage/microglia-rich phenotype can shape a GBM Mesenchymal phenotype, suggesting that tumour-associated glial cells and microglia may contribute to an overall worse prognosis (Wang et al., 2017).

In 2016, the WHO presented a major restructuring of classification which includes applying not only histological but also molecular features as a defining feature in classification of tumour entities. The term 'multiforme' was omitted from the original name, glioblastoma multiforme. However, the abbreviation GBM was kept for disambiguation (Louis et al., 2016). Glioblastoma under the 2016 classification was categorised into two types of isocitrate dehydrogenase (IDH) mutation: IDH-mutant glioblastoma and IDH-wildtype glioblastoma, or a third NOS (not otherwise specified) designation for a tumour lacking a diagnostic mutation. Epithelioid glioblastoma, mainly observed in younger adults was also added as a new variant of GBM under IDH-wild type GBM (Louis et al., 2016).

Parsons and colleagues were the first to describe IDH1 gene mutations in glioblastoma (Parsons et al., 2008). The IDH1 gene encodes for isocitrate dehydrogenase 1 which plays an enzymatic role in the citric acid (Krebs) cycle (Ohgaki and Kleihues, 2013). They reported that mutations in the IDH1 gene are correlated with increased overall survival; mutations are seen in secondary tumours; and are commonly found in young patients (Parsons et al., 2008). IDH1/2 gene mutation results in the reduced conversion of isocitrate to  $\alpha$ -ketoglutarate ( $\alpha$ -KG) and increased levels of the transcription factor hypoxia-inducible factor 1 $\alpha$  (HIF-1 $\alpha$ ) and its targets (e.g. glucose transporter 1 [GLUT-1], vascular endothelial growth factor (VEGF) and phosphoglycerate kinase 1

[PGK1]) (Zhao et al., 2009). The oxidative decarboxylation of isocitrate to  $\alpha$ -KG also has a protective role of cells from reactive oxygen species (ROS) which can cause DNA damage (Al-Khallaf, 2017). In glioma, IDH gene mutations are frequently heterozygous missense mutations, occurring most commonly in codon R132 of IDH1 or codon R172 of the IDH2 gene (Singh et al., 2017). A study by Songtao et al., showed that IDH gene mutation was positively correlated with the presence of MGMT promoter methylation and patients presenting with IDH-mutant compared to IDH-wild type GBM have a higher overall survival and are shown to respond better to temozolomide (Songtao et al., 2012). Overall, IDH-mutant gliomas have distinct characteristics to IDH-wild type. Hence, significant changes were made in the most recent 5<sup>th</sup> edition of WHO classification of the CNS tumours (2021). Substantial evidence over the years has shown that the presence of one or more of three genetic parameters: TERT (Telomerase Reverse Transcriptase) gene promoter mutation; EGFR gene amplification; combined gain of entire chromosome 7 and loss of entire chromosome 10 are sufficient to assign the maximum (IV) WHO grade to gliomas (Louis et al., 2021). Thus, as a result, Glioblastomas are now classified as IDH-wild type tumours along with any of those three genetic parameters; an entirely separate diagnosis from astrocytoma IDH-mutant grade 2 to 4 (Louis et al., 2021).

### **1.3 Prevalence and Pathological features of GBM**

With a possibility of developing at any age, the peak incidence age of GBM is between 50 to 70 years and is more common in men than women (Cancer Research UK, 2020). Rare hereditary syndromes such as Li-Fraumeni, neurofibromatosis type 1 and 2, Cowden and Turcot are associated with increased risk of developing gliomas (Baldi and Loiseau, 2012); however, for the majority of gliomas, the underlying cause has not been identified. The most common location with 95% prevalence where GBM develops is the supratentorial region (upper part of the brain) of the cerebral hemispheres (Nakada et al., 2011). GBMs that develop deeply into the thalamus and basal ganglia and the eloquent cortices of the brain i.e. regions that directly control language and motor sensory functions are inaccessible to surgical resection, and therefore result in particularly poor prognosis (Nakada et al., 2011) (Figure 1.1).

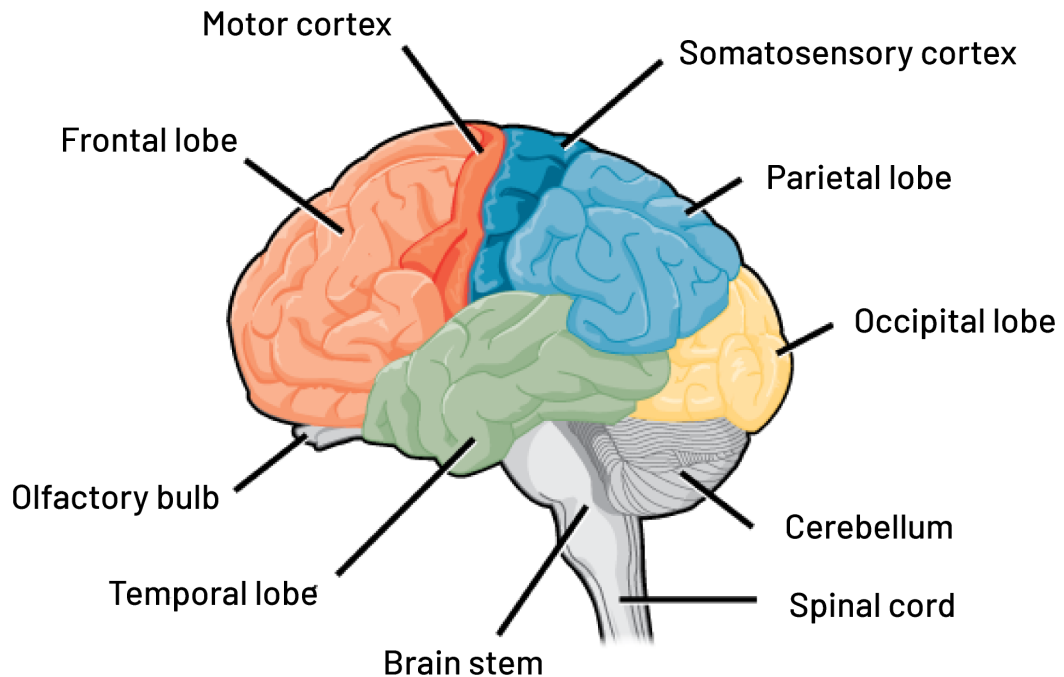


**Figure 1.1 Regions of human brain where GBM commonly develops.**

Primary GBM tumours commonly develop in the supratentorial area which is the upper part of the brain. This includes the cerebrum (four lobes including the temporal, frontal, parietal, and occipital). Other areas of the brain where GBMs may develop include the choroid plexus, pineal gland, hypothalamus, pituitary gland, and optic nerve. *The human cerebral cortex includes the frontal, parietal, temporal, and occipital lobes.* 2020. Lumen Learning. [Online]. [Accessed 14 October 2021]. Available from: <https://courses.lumenlearning.com/wm-biology2/chapter/brain/>

Clinically, patients with GBM may present with frequent and progressive headache, cognitive difficulties and personality changes, gait imbalance, papilloedema (swelling of the optic nerve due to increased intracranial pressure), sensory loss and seizures (Omuro and DeAngelis, 2013). When a brain tumour is suspected, patients are recommended to undergo brain magnetic resonance imaging (MRI) with and without contrast, and computerised tomography (CT) scans for patients unable to undergo MRI. GBM is typically characterised by a large, single, irregular shaped lesion arising normally in the white matter

(D'Alessio et al., 2019). Resembling histological features of anaplastic astrocytoma, both tumours are characterised by increased cellularity, nuclear atypia and mitotic activity (Agnihotri et al., 2013). In addition, GBMs are also characterised by necrotic areas and proliferation of vascular endothelial cells with glomeruloid structure (Rojiani and Dorovini-Zis, 1996) denoting vascular tortuosity.

Metastasis into the extracranial tissues is uncommon; however, GBM's extensive infiltration to the surrounding brain parenchyma is also one of the clinical hallmarks of all GBM subtypes (Claes et al., 2007). The extensive invasion of gliomas was first described by Hans Joachim Scherer in 1938. Scherer's study concluded that glioma cells migrate along existing brain structures (now called Scherer's secondary structures). This includes perineural growth (around neurons), perivascular growth (around blood vessels), intrafascicular growth (tumour cells migrating along white matter tracts), and surface or subpial growth (under the pia mater) (Scherer, 1938; Cuddapah et al., 2014). Additionally, glioma cells also secrete proteases, including membrane type matrix metalloproteinase 1 (MMP1), MMP2 and MMP9, which can degrade the extracellular matrix (ECM), forming paths for migration (Cuddapah et al., 2014).

## **1.4 Current treatment of GBM**

### **1.4.1 Standard care of therapy for GBM**

Despite improvement in the understanding of the cellular and molecular characteristics, GBM remains an incurable disease. There are several standard approaches in GBM management which include maximum surgical resection, radiotherapy, and chemotherapy. Considering the infiltrative nature of GBM to its surrounding normal tissues, the entirety of the tumour would not be able to be removed during surgical resection. However, surgery is crucial to reduce the bulk of the tumour and alleviate symptoms prior to radiotherapy and chemotherapy and providing tumour tissue available for histologic and molecular tumour characterisation (Omuro and DeAngelis, 2013). Corticosteroid treatment has proven to be effective in reducing intracranial pressure and severity of symptoms in the early development of tumours (Nakada et al., 2011).

The heterogeneous nature of glioblastoma contributes to the difficulty in glioblastoma treatment and management. Personalised therapy is the current best therapeutic approach, by integrating individual patient's tumour histopathologic presentations and molecular subtypes. Therefore, treatment options would largely depend on whether it is a primary or secondary GBM, age of the patient and time of diagnosis. After maximum surgical resection, adjuvant radiotherapy combined with chemotherapy, is the most common mode of treatment (Figure 1.2). The typical dose of ionizing radiation is 60 Gy divided into 30 fractions (Omuro and DeAngelis, 2013). Concomitantly with radiotherapy, the DNA alkylating agent temozolomide is administered orally. TMZ works by cell cycle arrest at the G2/M checkpoint, which leads to cancer cell apoptosis (Alonso et al., 2007). The use of oral TMZ was supported by the randomised phase 3 study which found that combination treatment of TMZ and radiotherapy increased the median survival to 15 months (Stupp et al., 2005). GBM patients with methylated *MGMT* promoter tumours were more likely to respond better, and benefit from the supplementation of TMZ compared to treatment with radiotherapy alone (Hegi et al., 2005).

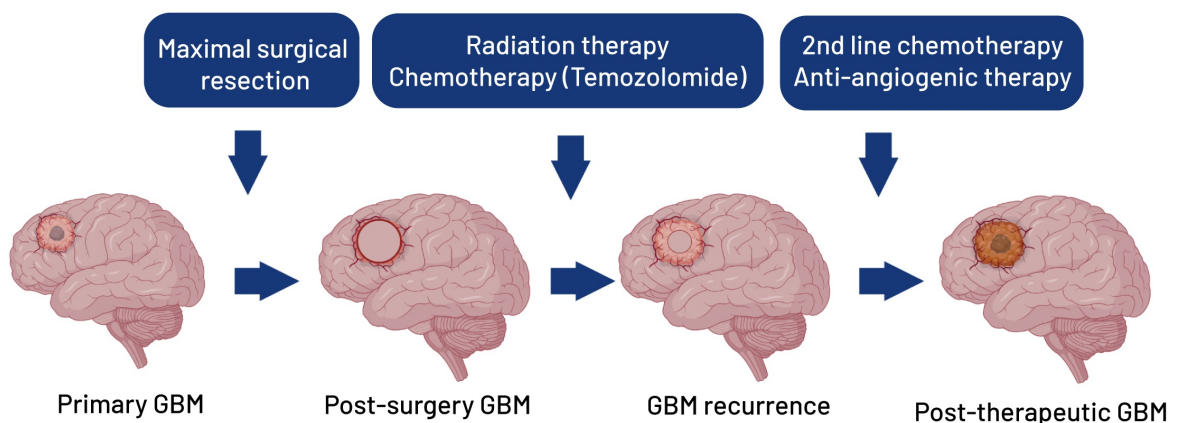


## **Figure 1.2 Standard of care therapy for GBM.**

Illustration shows the progression of GBM development in standard care and second line therapy. Primary GBM patients are treated firstly with surgery followed by radiation and temozolomide chemotherapy. However, eventually GBM tumours recur, due to persistent glioblastoma stem cells (GSC) and remaining resistant cancer cells. Second line treatment agents include chemotherapeutic agents such as temozolomide and Bevacizumab. Adapted from Rosińska, S., 2021. Created with BioRender.com.

### **1.4.2 The use of Bevacizumab**

In 2004, bevacizumab (Avastin®) was approved for clinical use, in the US. Bevacizumab is a monoclonal antibody which works by selectively binding to free VEGF-A in the circulation preventing the attachment to VEGF receptors and subsequent activation of downstream pro-angiogenic pathways (Nakada et al., 2011). GBM is a highly vascularised solid tumour and VEGF is one of the primary growth factors which promotes angiogenesis. The formation of new blood vessels subsequently results in the tumour having the ability to access nutrients and oxygen for growth and progression. VEGF stimulates vascular permeability, and thus bevacizumab treatment has been associated with reduction in vasogenic brain oedema. However, the phase 3 AVAglio study (BO21990), a randomised, double-blind, placebo-controlled trial on the evaluation of the effect of combining bevacizumab to radiotherapy-TMZ for treatment of newly diagnosed GBM, has not shown promise. The addition of bevacizumab results in an increase in median progression-free survival of 10.6 months versus 6.2 months for placebo group; however, overall survival did not improve significantly (Chinot et al., 2014). Unfortunately, a higher number of patients given bevacizumab instead of a placebo drug experienced grade 3 or higher adverse events (Chinot et al., 2014).

In a clinically relevant *in vivo* study using rats, the use of bevacizumab as a treatment resulted in a 68% increase in tumour cell invasion into the surrounding brain parenchyma (Keunen et al., 2011). Recent work by Sandmann et al. has evaluated the use of bevacizumab in the context of GBM molecular subtypes.

The work showed evidence of significant overall survival advantage of 17.1 months versus 12.8 months (placebo group) in patients with *IDH1*-wild type GBM, but only in the proneural subgroup (Sandmann et al., 2015). Another challenge in the development of anti-angiogenic drugs is that not all vessel formation in GBM is induced by VEGF. GBM tumours have alternative modes of neovascularisation which supports tumour growth. Therefore, greater research effort is needed to target various aspects of blood vessel formation in GBM.

### **1.4.3 GBM Recurrence**

Despite advances in molecular characterisation and development of personalised approaches to treatment, almost every GBM tumours recur (Stupp et al., 2009) and due to treatment resistance, recurrence is still a major challenge in the clinic. The development of treatment for recurrent GBM has had to rely on primary GBM samples although there are growing evidence of the significant pathological and molecular differences between primary and recurrent GBM (Campos et al., 2016). In the UK, current treatment for patients with recurrent GBM include second surgical resection, reirradiation, temozolomide chemotherapy and the chemotherapy combination drug PCV (procarbazine, lomustine and vincristine) (Niyazi et al., 2011; NICE, 2018). Depending on the infiltrative nature of the tumour, around up to a quarter of people with recurrent GBM can undergo a second surgical resection of the tumour (Mandl et al., 2008; Niyazi et al., 2011).

Currently, there are over 50 clinical studies in the literature on reirradiation of gliomas (Reviewed in Nieder et al., 2016). Although the risk of severe radiation-induced complications after reirradiation including symptomatic radiation necrosis – an inflammatory reaction at the site of irradiation resulting in necrotic degeneration of brain tissue, causing mild to severe neurological symptoms (Sayan et al., 2020) – remains, reirradiation has recently emerged as an effective and safe treatment option for some patients with recurrent GBM (Reviewed in Minniti et al., 2021). For patients with recurrent GBM, stereotactic radiosurgery (SRS) may be given alone or in combination with systemic therapy. With a median SRS dose of 15-18 Gy, the overall survival for patients given SRS reirradiation ranges from 7.5 to 13 months. The progression-free survival time

ranges between 4.4 to 6 months (Reviewed in Minniti et al., 2021). Combs *et al.* analysed a database of 172 patients with recurrent glioma treated with fractionated stereotactic radiotherapy, including 59 patients diagnosed with GBM, which led to median survival after reirradiation of 8 months for GBM patients (Combs et al., 2005). Another study by Kong et al., analysed 65 GBM patients with a median time of initial diagnosis to recurrence of 4.3 months. The study demonstrated that the median progression-free survival after reirradiation was 4.6 months (Kong et al., 2008). Thus, the available literature suggests that reirradiation is safe in a number of selected patients (Nieder et al., 2016), with median survival ranging between 6 to 12 months (Minniti et al., 2021). However, more studies are needed to support this conclusion so that reirradiation can be offered to patients with recurrent GBM as standard treatment (Nieder et al., 2016).

Marucci et al. reported that recurrent GBM tissues consist of large areas of necrosis with low content of vital tumour cells compared to the primary tumour (Marucci et al., 2015). Recurrences mainly develop locally, with roughly two-thirds of tumours recur within 2 cm of the tumour margin (De Bonis et al., 2013). The rest recur in a different lobe from the initial tumour bulk, on the contralateral hemisphere or the infratentorial region (region of the brain containing the cerebellum) (Nifterik et al., 2006; De Bonis et al., 2013). In 2015, Kim *et al.* demonstrated using whole-exome sequencing on 15 pairs of local and 7 pairs of distant GBM recurrences that occur far from the initial bulk is a result from tumour cells that had invaded the brain at an early stage of the disease. They found that primary and distant recurrent tumours only shared an average 25% of the mutations compared to an average of 70% for primary and local recurrences (Kim et al., 2015).

Glioma cancer cells with stem-cell like features, also known as glioblastoma stem cells (GSCs), have been suggested recently to contribute and influence tumour growth and recurrence (Campos et al., 2016). These stem-like cells are characterised by slow-cycling tumour cells with resistance to radiotherapy and chemotherapy, higher self-renewal potential, and increased ability to form into tumours (Singh et al., 2004). GSCs are successful in their development into

recurrence tumours due to overexpression of DNA damage repair enzymes (Bao, Wu, McLendon, et al., 2006), ability to grow under hypoxic conditions (Z. Li et al., 2009), and marked overexpression of CD133 (marker of stem cell) which is associated with drug resistance to drugs such as temozolomide, paclitaxel and carboplatin (Liu et al., 2006; Q. Liu et al., 2009). Although there is limited evidence of the role of GSCs in recurrent GBM, CD133 – a GSC marker – is correlated with therapy resistance *in vitro* and increased tumour formation *in vivo* (Campos et al., 2016). CD133 is overexpressed in recurrent GBM (Tamura et al., 2013) and overexpression negatively correlates with patient survival (Zeppernick et al., 2008). Understanding of GBM recurrence is limited due to low availability of paired primary and recurrent patient samples which is crucial for understanding the genetics and patterns of growth of recurrent GBM.

The optimum protocol for the treatment for recurrent GBM has yet to be defined. Although second surgery has been shown to increase overall survival by 5-11 months with preserved neurological status (Ringel et al., 2016; Antoine et al., 2020) less than 50% of patients are eligible (Helseth et al., 2010; Woodroffe et al., 2020). Intensity-modulated radiotherapy (IMRT) – a type of radiotherapy that enables precise conformation of radiation dose to the shape of the tumour, sparing healthy tissues (Taylor and Powell, 2004) – is being used at an increasing rate to treat recurrence GBM with a median survival of 10.1 months from treatment (Voynov et al., 2002). With the risk of radiation necrosis, reirradiation in combination with bevacizumab is common in the clinic (Gutin et al., 2009). Study by Cuneo et al., employed 49 patients with recurrent GBM treated with SRS alone or in combination with bevacizumab. The authors showed that there was an increase of 28% in 1-year overall survival time when patients were treated with SRS in combination with bevacizumab compared to SRS alone (Cuneo et al., 2012). Other therapeutic options include temozolomide rechallenging (Perry et al., 2008), tumour-treating fields (non-invasive therapy using electric fields which disrupts mitosis of cancer cells) (Stupp et al., 2012) and lomustine or bevacizumab or in combination (Wick et al., 2017).

#### 1.4.4 Histological and molecular features of GBM recurrence

GBM is subject to high degree of plasticity especially upon recurrence. For a long time GBM has been hypothesised to switch from Proneural to Mesenchymal subtypes (Phillips et al., 2006). Gene expression profiles from 96 paired primary and recurrence tumours conducted by Q. Wang et al., revealed that the Mesenchymal subtype was the most stable subtype; Proneural and Mesenchymal subtypes increased in frequency in recurrences which are associated with poor outcome; while the Classical subtype was the least abundant in recurrences (Wang et al., 2017). Another study by J. Wang, et al. also supported this finding with two primary tumours switching to Mesenchymal, two to Proneural and one to Neural subtype in recurrences, while also the Mesenchymal subtype at recurrence was associated with worse overall survival (Wang et al., 2016). In the same study, they reported a mutation in the latent-transforming growth factor beta-binding protein 4 (*LTBP4*) gene in 11% of recurrence tumours associated with poorer patient survival (Wang et al., 2016). *LTBP4* is a key regulator in the transforming growth factor beta (TGF- $\beta$ ) pathway which is crucial in many biological processes including proliferation, and epithelial-to-mesenchymal transition (EMT) (Massagué, 2008).

Management of primary tumours through therapies has been shown to contribute to molecular changes and patterns of recurrence. Andor et al. analysed 10 paired patient samples treated with radiotherapy and TMZ and reported a higher number of mutations in the recurrent tumours (Andor et al., 2014). Studies by Stark et al. and Felsberg et al. revealed the expression status of DNA mismatch repair (MMR) genes known to be important in dictating tumour response to TMZ: genes MutL homolog 1 (*MLH1*), MutS homolog 2 (*MSH2*), MutS homolog 6 (*MSH6*) (Stark et al., 2010; Felsberg et al., 2011). Reduced expression of MMR genes is frequently seen in GBM recurrences (Felsberg et al., 2011) and loss of *MSH6* have been implicated with the development of recurrence GBM during TMZ treatment (Cahill et al., 2007). Stark et al., reported a downregulation of the *MLH1* gene in the recurrent tumours from 42 paired samples from patients treated with combined radiotherapy and TMZ chemotherapy (Stark et al., 2010). Study by Felsberg et al., reported a reduced expression of *MSH6* in recurrent tumours when compared to primary tumours (n=43 paired patients) (Felsberg et al., 2011).

Hence reduced expression of MMR genes appears to play a significant role in GBM resistance to therapies and recurrence.

## **1.5 Brain tumour microenvironment**

The tumour microenvironment consists of many different cell types that support cancer cells including endothelial cells, pericytes, fibroblasts and immune cells (Quail and Joyce, 2013). In GBM, the microenvironment is composed of a wide variety of non-neoplastic stromal cells i.e., the vasculature, immune cells and glial cells, and its high heterogeneity has resulted in the compartmentalisation of distinct regions known as tumour niches (Hambardzumyan and Bergers, 2015). These niches harbour GSCs and also orchestrate the communication between tumour and host cell populations to promote growth and protection of GSCs (Schiffer et al., 2015; Hambardzumyan and Bergers, 2015). In GBM, at least three tumour niches can exist in one single tumour with the vasculature as the main conductor: the perivascular tumour niche (PVN), the hypoxic tumour niche and the invasive tumour niche (Figure 1.3).

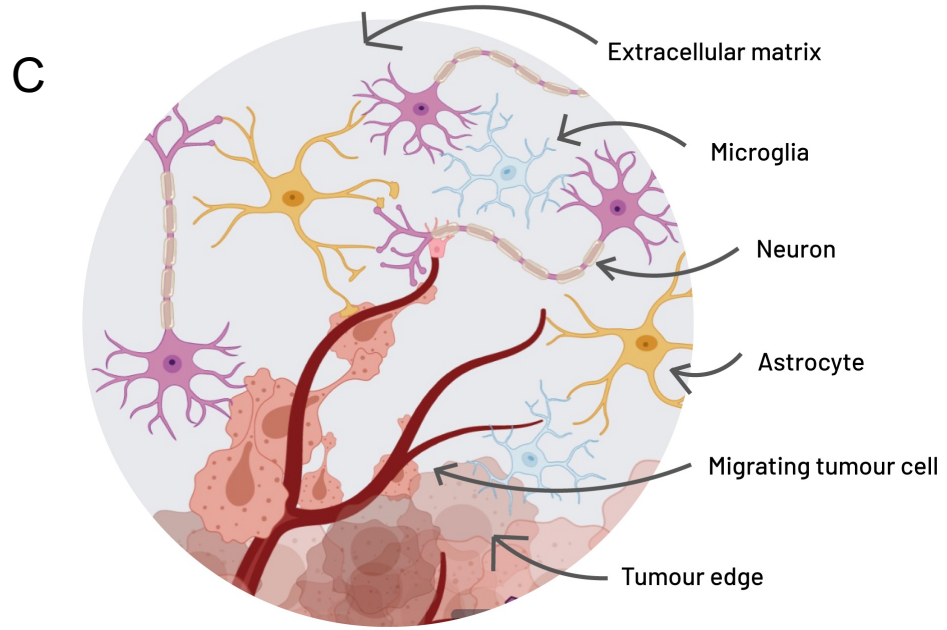
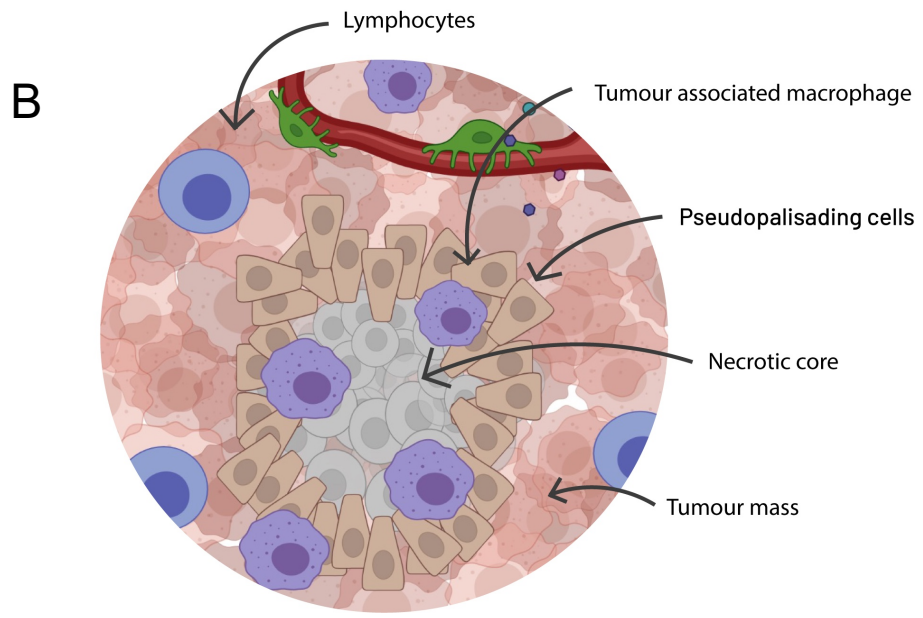
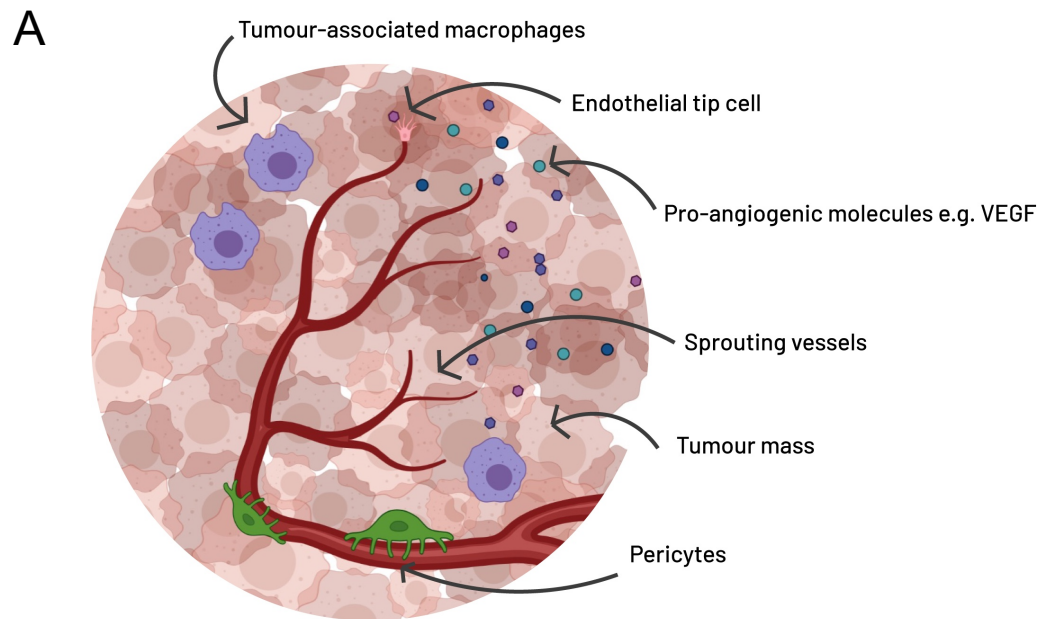


### **Figure 1.3 Glioblastoma tumour niches.**

Illustration shows the different tumour niches present in GBM. **(A)** the perivascular GBM niche provides a supportive environment for growth of glioma like stem cells. It consists of structures involved in vascular development including endothelial cells, pericytes and macrophages. **(B)** The hypoxic GBM niche is characterised by pseudopalisading cells with a necrotic core. Hypoxia in this niche occurs through induction of hypoxia inducible factor  $1\alpha$  (HIF-1  $\alpha$ ). **(C)** The invasive GBM niche provides expansion of the tumour with glioma cells migrating along the blood vessels. Adapted from De Vleeschouwer, S. and Bergers, G., 2017. (Vleeschouwer and Bergers, 2017). Created with BioRender.com.

#### **1.5.1 Perivascular Niche**

The perivascular niche is one of the most significant microenvironments in brain tumours, and a central hub for therapeutic resistance (Seano, 2018). A highly aberrant, leaky, and tortuous vasculature is one highly distinct characteristic of GBM, predominantly promoted by the elevated levels of VEGF. Angiogenic growth factors such as VEGF, fibroblast growth factor (FGF) and platelet-derived growth factor (PDGF) are all produced by the tumour cells. Closely associated with various components in the niche including – but not limited – to endothelial cells and pericytes, glioma stem cells (GSCs) often reside in the perivascular niche (Seano, 2018). GSCs are a sub-population of tumour cells which share phenotypic similarities with neural stem cells (Bulstrode et al., 2017) including expression of markers such as CD133, SOX2 ((Sex-determining region Y)-box2) and Nestin (Lee et al., 2006). GSCs marked by CD133 and Nestin expression are strongly associated with the blood vessels surrounding them also have been shown to produce high amounts of VEGF (Bao, Wu, McLendon, et al., 2006; Calabrese et al., 2007). In the perivascular tumour niche, GSCs lie in close proximity with the highly angiogenic abnormal vasculature of GBM. VEGF is the main modulator of angiogenesis, it results in pericyte detachment and vascular basement membrane degradation resulting in enlarged vessels (or otherwise known as “mother vessels”) which are highly susceptible to chronic vascular hyperplasia (CVH) and are highly leaky (Dvorak, 2015). Blood vessels in GBM

are phenotypically aberrant, a common phenotype observed being glomeruloid microvascular proliferation (GMP), which received its name from its close resemblance of kidney glomeruli.

The PVN not only hosts GSCs but also saves them from depletion (Scadden, 2006). Previous studies have demonstrated the role of ephrin-B2 as critical driver of both perivascular invasion (Krusche et al., 2016) and GSC self-renewal (Binda et al., 2014). Ephrin-B2 belongs to the Eph/ephrin family of receptor tyrosine kinases and their membrane-bound ligands, with widespread roles in both normal and cancer development (Pasquale, 2010). EphA2 knockdown is associated with reduced self-renewal abilities, reduced stem marker expression, and decreased tumorigenicity (Miao et al., 2015). Interestingly, protein ligands that are responsible for angiogenesis, are also responsible for stem cell self-renewal. For example, PEDF (pigment epithelium-derived factor), which maintains neural stem cell self-renewal is a potent angiogenesis regulator (Pumiglia and Temple, 2006; Ramírez-Castillejo et al., 2006). Additionally, in an important study by Bao et al. whereby isolated GSCs from human GBM biopsy specimens were implanted into the brains of immunocompromised mice, the authors demonstrated that GSCs secreted elevated levels of VEGF, which were further induced by hypoxia (Bao, Wu, Sathornsumetee, et al., 2006). In the same study, they demonstrated using an *in vitro* model of angiogenesis that GSC-conditioned medium increased EC migration and vascular tube formation (Bao, Wu, Sathornsumetee, et al., 2006).

The relationship between ECs and GSCs have shown to be mutually beneficial and mediated *via* multiple mechanisms. The canonical sonic hedgehog pathway – highly active in GBM (O'Brien et al., 2010) – is activated by the binding of three hedgehog ligands: Shh, Ihh and Dhh to the trans-membrane protein Patched (PTCH) and the G-protein coupled receptor Smoothened (Smo) (Skoda et al., 2018). Study by Yan et al., showed that the stemness of GSCs is regulated by endothelial cells through activation of the Sonic Hedgehog pathway (SHH). The authors show that ECs upregulate the expression of GSC-associated genes in both U251 and GL261 glioma cells (Yan et al., 2014), and importantly that Sonic hedgehog ligand (Shh) secreted from endothelial cells mediates the activation of SHH pathway and promote GSC-like phenotype in glioma cells (Yan et al., 2014).

In addition to SHH signalling, other studies have shown that tumour ECs release nitric oxide and NOTCH ligand which promote stem-like characteristics in GBM (Hovingaa et al., 2010; Zhu et al., 2011). In the PVN, tumour associated macrophages (TAMs) and microglia orchestrate many tumour sustaining roles such as stimulation of cancer cell proliferation, and regulation of inflammation (Zhai et al., 2011; Li and Graeber, 2012; Szulzewsky et al., 2015).

### **1.5.2 Hypoxic Niche**

Hypoxia is one of the defining features of malignant glioma (Evans et al., 2004) and is primarily regulated by hypoxia-inducible factors (HIFs). With the poor and aberrant formation of GBM vasculature, a dysfunctional blood vessel system exists and causes both slow blood flow and inconsistent oxygen delivery to the tumour. Under hypoxic conditions, HIF-1 subsequently activates genes whose protein products result in the increase in oxygen availability or mediate the metabolic adaptation of cells to oxygen deprivation (Zagzag et al., 2006). VEGF is one of the genes upregulated during hypoxia, through HIF-1  $\alpha$ , resulting in a proangiogenic response.

Necrotic areas are normally surrounded by pseudopalisading GBM cancer cells. These cells are severely hypoxic, overexpress HIF-1 which is activated in low oxygen conditions, and secrete proangiogenic factors such as VEGF and interleukin-8 (IL-8) (Rong et al., 2006). GBM cells grown in hypoxic conditions in culture compared to normoxic conditions are more migratory (20-60% increase) (Brat et al., 2004). Although the cause of hypoxia-induced migration is unclear, studies suggest that the formation of pseudopalisades are due to tumour cells migrating towards peripheral vessels suggesting that pseudopalisading cells represent an actively migrating population (Zagzag et al., 2000; Brat et al., 2004). In necrotic areas, more than 50% of vessels are thrombosed (Hambardzumyan and Bergers, 2015), which results in tumour cells actively migrating away from hypoxic areas creating the peripheral formation of pseudopalisading tumour cells (F.J. II et al., 2006; Rong et al., 2006). Studies have also shown that GSCs are supported by hypoxic tumour niches (Seidel et al., 2010). In contrast to PVN, the hypoxic tumour niche develops around necrotic areas where hypoxia inducible

factors (HIF-1/2) in hypoxic regions hosts, maintains, and protects GSCs from chemotherapy and radiotherapy (Christensen et al., 2008; Seidel et al., 2010). Hypoxia promotes the expansion of GSCs through the PI3K/ Akt (protein kinase B), and extracellular signal-regulated kinase 1/2 (ERK1/2) cascade (Bar et al., 2010).

Counterintuitively, impaired oxygen delivery and necrosis does not slow down tumour growth, rather it results in poor prognosis of diffuse gliomas (a term for tumours of the central nervous systems ranging from WHO II to grade IV tumours including glioblastomas) (Hambardzumyan and Bergers, 2015). Consequently, HIF-1 $\alpha$  and its signalling pathway have been a vital target in cancer chemotherapy (Reviewed in Shirai et al., 2021; Ikeda and Kakeya, 2021). For example, the drug EZN-2968, a third-generation antisense oligonucleotide (synthetic, chemically modified chains of nucleotides that can modulate gene expression *via* different mechanisms (Roberts et al., 2020)), has been developed to target HIF-1 $\alpha$  mRNA. *In vitro* studies employing U373 GBM cells show that EZN-2968 can potently inhibit HIF-1 mRNA expression thus inhibiting tumour growth (Greenberger et al., 2008). 2-Methoxyestradiol (2ME2), or otherwise known as Panzem®, is a derivative of estradiol which works by dysregulating HIF-1 (Ikeda and Kakeya, 2021). Phase II clinical trials in patients with recurrent GBM treated with Panzem® in combination with temozolomide chemotherapy (NCT00481455) showed a 6-month progression-free survival, increased median overall survival in patients receiving at least one dose of the treatment (National Institute of Health, 2007).

### **1.5.3 Invasive Tumour Niche**

GBM cells are highly invasive, often employing co-option as the mode of deriving blood supply (which will be discussed further in this chapter), to colonise blood vessels in the normal brain parenchyma (Westphal and Lamszus, 2011). The invasive tumour niche is associated with functional brain vasculature situated at the border of the tumour with the normal brain parenchyma (Hambardzumyan and Bergers, 2015). In addition, GBMs are able to “switch on” the invasive mode in response to antiangiogenic therapy through activation of the receptor tyrosine

kinase MET in the presence or absence of hypoxia (Rubenstein et al., 2000; Pàez-Ribes et al., 2009). VEGF ablation results in increased tumour invasion through enhanced MET phosphorylation through disruption of the VEGFR2:MET complex which keeps MET inactive (Eckerich et al., 2007; Iwamoto et al., 2009; Rose and Aghi, 2010). Invading glioma cells are also highly influenced by microglial cells which promote migration. GBM cells secrete colony stimulating factor 1 (CSF1) which is a microglia attractant, and in response, microglia produce epidermal growth factor (EGF) which has been shown to promote migration of the GBM cell line GL261 (Coniglio et al., 2012).

## **1.6 Endothelial cells**

The BBB in normal brain is formed by endothelial cells lining the blood vessels supported by cells of the neurovascular unit (NVU) including pericytes and astrocytes (Abbott, 2013). It has been hypothesised that glioma-associated endothelial cells (EC) in GBM are intrinsically different compared to ECs in the normal brain (Charalambous et al., 2006) which may have contributed to the ineffectiveness of antiangiogenic therapies that solely target molecules expressed by normal ECs (Neri and Bicknell, 2005). Tumour ECs may be recruited by more than one way and may be derived from multiple origins. The first mechanism being normal ECs recruited into the tumour site by the release of angiogenic growth factors by cells that express markers of activated ECs (Bussolati et al., 2003). Another hypothesised mechanism is tumour ECs being derived from endothelial progenitor cells (EPCs) migrated to the tumour site and differentiated into blood vessels, hence expressing EPC markers such as CD34 (Traweek et al., 1991). Furthermore, tumour-derived ECs having similar chromosomal aberrations as the tumour cells they are associated with, has served as evidence of tumour cells transdifferentiating into ECs (Streubel et al., 2004). Additionally, using an *in vitro* model, Soda et al., demonstrated that a hypoxic microenvironment may promotes transdifferentiation of GSCs into endothelial-like cells and incorporate themselves into blood vessels (Soda et al., 2011).

There are multiple markers that readily detect GBM ECs including vWF, CD31, VE-Cadherin (or CD144) and CD105 (Alessandri et al., 1999; Charalambous, Hofman, et al., 2005; Miebach et al., 2006). Morphological characterisation by Charalambous et al. showed that GBM-derived ECs have altered expressions of CD31 and CD144 (Charalambous et al., 2006). VE-Cadherin is a tight junction protein that is crucial in maintaining BBB integrity and its downregulation results in elevated blood vessel leakiness (Davies, 2002). It also plays instrumental roles in angiogenesis and tubule formation and growth (Griffioen, 1997; Wright et al., 2002). With GBM known to have leaky and aberrant blood vessels architecture, it is not unexpected that gliomas lose VE-Cadherin expression (Miebach et al., 2006) and other tight junction proteins such as claudin-1, claudin-5 and occludins (Liebner et al., 2000; Papadopoulos et al., 2001). In a study utilising primary cultures of GBM-derived ECs taken from the tumour core, it was observed that these glioma-associated endothelial cells have a significantly slower rate of proliferation compared to normal brain ECs (Charalambous et al., 2006). GBM-derived ECs have also been reported to be more migratory than normal brain ECS and

have increased expression of growth factors such as VEGF and IL-8 (Charalambous, Pen, et al., 2005; Charalambous, Hofman, et al., 2005).

### **1.6.1 Vascular Pericytes**

Pericytes were first described almost a century ago as cells that wrap around blood capillaries (*peri*: around, *cyte*: cell) and are embedded within the basement membrane of microvessels (Bergers and Song, 2005). Pericytes in the normal brain serve as the supportive cells of blood vessels, but also perform complex communication functions such as exchange of molecules and ions with endothelial cells through physical contact mediated *via* gap junctions (a type of cell junction in which adjacent cells are connected via protein channels) between endothelial cells and pericytes (Bergers and Song, 2005). Pericytes also exhibit a smooth-muscle actin cell phenotype through expression of alpha-smooth muscle actin ( $\alpha$ -SMA). However, it has been unclear whether pericytes are actually smooth-muscle cells (SMCs), or cells with SMC characteristics with the ability to transform into SMCs (Bergers and Song, 2005).

Lineage-tracing studies have shown that pericytes have different developmental origins, and in the CNS, they are mainly derived from the neural crest (Bergwerff et al., 1998). In respect to their recruitment to the peri-endothelial location in the brain, this is mediated *via* ECs releasing PDGF-B which attracts pericytes, and subsequently binds to PDGFR $\beta$  – a receptor expressed on the surface of mesenchymal pericyte progenitor cells (Armulik et al., 2011). The relationship between ECs and pericytes is highly dynamic and mutually symbiotic. ECs survival relies on pericytes' production of VEGF, and the supportive role of pericytes protects ECs from VEGF withdrawal suggesting that pericytes are able to confer resistance to anti-VEGF therapies (Carmeliet and Jain, 2011).

Another important molecular modulator of pericyte recruitment and blood vessel stabilisation is the angiopoetins and TIE receptor system. ECs express the receptor tyrosine kinase TIE2 (Sundberg et al., 2002) which is stimulated by Angiopoietin-1 (ANG-1) and angiopoietin-2 (ANG-2). ANG-1 is involved in vessel maturation *via* stimulation of TIE2, contributing to maintenance of vascular stability and quiescence (Augustin et al., 2009); while Ang-2 destabilises blood vessels for vessel growth and sprouting (Bergers and Song, 2005). Another signalling pathway involved in vessel stabilisation is activation of TGF- $\beta$ 1 through EC-pericyte contact which results in reduction in endothelial cell proliferation and migration, (Orlidge and D'Amore, 1987; Sato and Rifkin, 1989) and promotes differentiation of perivascular cells into pericytes contributing further to blood vessel stability (Ramsauer and D'Amore, 2002).

Several widely accepted pericyte markers include platelet-derived growth factor receptor beta (PDGFR $\beta$ ), chondroitin sulfate proteoglycan 2 (NG2), alanyl membrane aminopeptidase (CD13),  $\alpha$ -SMA, and Desmin (Armulik et al., 2005; Krueger and Bechmann, 2010). However, due to the diverse characteristics, functions and origins of pericytes, it is important to note that currently there is no single general pan-pericyte molecular marker (Armulik et al., 2011). In 2005, using the Rip1Tag2 transgenic mouse model of pancreatic neuroendocrine tumours, Song et al., showed that PDGFR $\beta$ <sup>+</sup> perivascular cells are distinct from

mature pericytes; which are ones that express  $\alpha$ -SMA or desmin markers (S. Song et al., 2009). This study has provided some understanding of how different markers relate to different pericyte cell states.

In the normal developing brain, pericytes play a critical role in the formation and regulation of a functional and stable BBB and the lack of pericytes result in oedema and extravasation of plasma proteins in the brain (Armulik et al., 2010). Pericytes in tumours are different from normal pericytes. In general, tumour pericytes in glioblastoma, pancreatic islet carcinoma and mammary carcinomas are more loosely attached to blood vessels (Bergers and Song, 2005). However, tumour pericytes might still use the same signalling mechanisms of PDGF $\beta$  and their associations to blood vessels (Abramsson et al., 2003; Bergers and Song, 2005). This was demonstrated by the reduction in pericyte abundance in the tumour vasculature in a tumour model grown in *pdgfb*-deficient mice (Abramsson et al., 2003; Bergers and Song, 2005). However, PDGFR- $\beta$ + pericytes have a dual role, in that blockade of PDGFB has been implicated with excessive leakage and they may also promote malignancy (Abramsson et al., 2003). A more recent study has suggested that the SDF-1/CXCR4 axis may also be important in recruiting tumour pericytes (S. Song et al., 2009). Pericytes in tumours are more loosely associated to the vasculature and seem to be dramatically reduced in abundance in comparison to normal tissue, especially in GBM (Carmeliet and Jain, 2011). Interestingly, Morikawa et al. observed a higher abundance of  $\alpha$ -SMA expressing pericytes in GBM compared to the normal brain (Morikawa et al., 2002). Charalambous et al., argued that around 50% of glioma-associated ECs express  $\alpha$ -SMA+ cells (Charalambous et al., 2006). In their analysis of normal and GBM-derived ECs isolated from normal human brain or human GBM tissue, the expression of  $\alpha$ -SMA positive mural cells was absent from control ECs (non-tumour) (Charalambous, Hofman, et al., 2005). Due to  $\alpha$ -SMA being implicated in the initiation of cell contraction and cell migration, in the same study they suggested that the enhanced migratory ability of tumour ECs may directly related to expression of  $\alpha$ -SMA by tumour ECs (Charalambous et al., 2006). In addition, although previously reported otherwise, recent study by Alarcon-Martinez et al., demonstrated that in addition to venules and arterioles, capillary

pericytes in mice also express  $\alpha$ -SMA (Alarcon-Martinez et al., 2018), potentially serving  $\alpha$ -SMA as a common pericyte marker.

Furthermore, pericytes exhibit immunomodulatory properties. Their expression of functional pattern recognition receptors means that they can sense and respond to pro-inflammatory stimuli by secreting chemokines and cytokines such as tumour necrosis factor alpha (TNF- $\alpha$ ), interleukin-1 $\beta$  (IL-1 $\beta$ ) and interferon gamma (IFN- $\gamma$ ) (Charalambous et al., 2006). Pericytes also express the intercellular adhesion molecule-1 (ICAM-1) and major histocompatibility complex molecules 1 and 2 (MHC I and II) enhancing the ability to present antigen to T-cells (Balabanov et al., 1999). Lastly, in the context of immune modulation, pericytes also have been shown to create an immunosuppressive microenvironment through Treg modulation (Navarro et al., 2016).

Recent findings support the notion that targeting the pericytes in the tumour vasculature might improve the clinical outcome of GBM. Elegant *in vivo* work by Cheng et al. has shown that GSCs in GBM are able to transdifferentiate into pericytes and remodel the perivascular niche to support both blood vessel function and tumour growth (Cheng et al., 2013). Not only that, but using *in vivo* cell lineage tracing, the authors demonstrated that GSCs are able to generate the majority of vascular pericytes. The recruitment of these GSC-derived pericytes to the ECs is modulated by the SDF-1/CXCR4 (C-X-C motif chemokine receptor 4) signalling (Cheng et al., 2013). Importantly, selectively targeting GSC-derived pericytes resulted in halting of neovasculature formation and inhibition of tumour growth (Cheng et al., 2013). This study was later supported by findings by Zhou et al., which showed that targeting pericytes that are derived from GSCs may enhance drug delivery by specifically targeting the BBB (Zhou et al., 2017). A recent paper by Zhang et al., elucidated the role of pericyte in enhancing DNA damage repair in GBM cells in the perivascular niche, resulting in tumour chemoresistance to temozolomide (Zhang et al., 2021). The authors demonstrated that pericytes secrete C-C motif chemokine ligand 5 (CCL5) which activates the C-C motif chemokine receptor 5 (CCR5) in GBM cells, resulting in the activation of the Akt-dependent DNA-protein kinase catalytic subunit pathway

(AKT-DNA-PKcs), thus augmenting DNA double strand break (DNA-DSB) repair and rescinding TMZ-induced GBM cell death (Zhang et al., 2021). Their study highlighted the importance on CCL5-CCR5 signalling as a potential target in improving chemotherapy efficacy for GBM.

### **1.6.2 Astrocytes**

Another component of the BBB in addition to ECs and pericytes are astrocytes. Astrocytes are the most abundant of all glial cells and is responsible for many functions of the CNS. Generally, astrocytes provide support for neurons and maintain BBB integrity. They participate in the regulation of blood flow, synaptic activity and transmitter homeostasis (Reviewed in (Zhou et al., 2017) and are also able to respond to infection, injury, ischemia and neurodegeneration (Reviewed in Pekny and Nilsson, 2005). Glial fibrillary acidic protein (GFAP) is a cytoskeletal protein commonly used to identify astrocytes (O'Brien et al., 2013). Studies have also shown that glioma associated astrocytes, are distinctively different to their normal counterparts (O'Brien et al., 2013).

Astrocytes have been shown to display MHC II which suggests a relationship with helper T cells (Katz et al., 2012). In a study by Kostianovsky et al., astrocytes have also been observed to interact with microglia and infiltrating monocytes, and to modulate an immunosuppressive microenvironment. The study demonstrated that GBM-derived malignant astrocytes not only result in suppression of TNF secretion by microglia and monocytes, but also disable the recruitment of T cells (Kostianovsky et al., 2008). An important function of astrocytes is their contribution to the BBB structure and its induction of tight junction formation between ECs (Goldstein, 1988). In the BBB, a layer of what is called the glia limitans is where astrocytic endfeet processes provide structural support to the barrier. These astrocytic endfeet express the water channel aquaporin-4 (O'Brien et al., 2013). Astrocytes have been implicated in the enhancement of tumour cell growth (Reviewed in O'Brien et al., 2013). A recent study by Mega et al. has shown that astrocytes are able to enhance GBM cell growth and proliferation in *in vitro* studies of both GBM cell lines and patient-derived cultures (Mader and Brimberg, 2019).

### **1.6.3 Tumour associated macrophages (TAMs)**

The majority of immune cells that reside in brain tumours are tumour associated macrophages (TAMs) (Graeber et al., 2002) and have been observed to comprise up to 50% of the tumour bulk (Morantz et al., 1979). Until now, it is still a challenge to distinguish macrophage populations from microglia accurately without the use of lineage tracing. For research using *in vivo* mouse models, researchers utilise CD45 expression levels to distinguish microglia characterised by low CD45 expression, to bone marrow-derived myeloid cells (BMDMs) which in contrast express high CD45 levels (Landry et al., 2020).

In the brain tumour microenvironment, two ontogenically distinct TAM populations exist, including tissue-resident microglia and BMDMs (Hambardzumyan et al., 2015). It has been described that, microglia reside more on the invasive edge of the tumour while BMDMs are more abundant in the tumour core and are attracted to the hypoxic niche (Darmanis et al., 2017). Landry et al., have also shown that BMDMs residing in the core evolve into a more pro-inflammatory phenotype over time (Landry et al., 2020). Although still widely described by their activation state of M1 macrophages having anti-tumour effects and M2 macrophages having pro-tumoral effects (Li et al., 2019) this linear M1-M2 phenotypic balance has been disputed (Quail and Joyce, 2013).

It has been previously described that TAMs in the brain promote tumour growth and that high TAMs abundance is associated with higher tumour grade and poorer patient prognosis (Komohara et al., 2008; Hambardzumyan et al., 2015). TAMs promote tumour growth in several ways. TAMs have been observed to be reside in close proximity to ECs (Wang et al., 2018) and this gives them their ability to facilitate intravasation of tumour cells through the vasculature into the bloodstream (Quail and Joyce, 2013). This is mediated through a paracrine loop whereby tumour cells respond to EGF secreted by macrophages, and macrophages respond to the tumour cell-secreted colony stimulating factor 1 (CSF-1) (Brown et al., 2017). Inhibition of CSF-1 receptor (CSF-1R) has shown to deplete (Coniglio et al., 2012) or depolarise TAMs (Pyonteck et al., 2013) which

in turn suppresses glioma tumour growth. TAMs are able to inhibit both adaptive and innate antitumour immunity. M2-polarised TAMs secrete immunosuppressive molecules including TGF- $\beta$ , interleukin 10 (IL-10) and arginase-1 (Arg-1) which inhibits T-cell immune response (Munder et al., 1998; Terabe et al., 2003; Sheng et al., 2015). A population of VEGF-A expressing Tie2-expressing macrophages (TEM), which are closely in contact with blood vessels exhibit pro-angiogenic effects which promote tumour growth (De Palma et al., 2005).

Vascular damage due to radiation and anti-VEGF therapy have been shown to promote the accumulation of BMDMs that differentiate into TAMs (Roh-Johnson et al., 2014). In GBM, the abrogation of blood vessels leads to increased hypoxia and upregulation of HIF-1 $\alpha$  which promotes elevated levels of the ligand CXCL12 (SDF-1) recruiting monocytes expressing CXCR4 (C-X-C motif chemokine receptor 4) (Brown et al., 2017). However, in a phase II study, inhibiting colony stimulating factor 1 receptor (CSF-1R) using Pexidartinib (PLX-3397) in recurrent GBM showed no efficacy (Butowski et al., 2016) while other clinical trials targeting TAMs have yet to show promise.

## **1.7 Interaction of GSCs with the GBM tumour microenvironment**

GSCs in GBM were first described in 2002 and contribute extensively to tumour progression (Ignatova et al., 2002). Although one universal marker for GSC does not exist, there are a number of available markers widely used to identify GSCs including SOX2, CD133, Nestin, OLIG2, NanoG, Musashi and Oct4 (Reviewed in (Cheng et al., 2013). Nestin is a crucial marker in GBM. Increased levels of Nestin have been shown to be correlated with lower survival rates (Zhang et al., 2008).

GSCs have also been implicated in chemoresistance and have been linked to GBM recurrence (Huang et al., 2010; Ahmed et al., 2013) as explained previously in Section 1.4.3 discussing GBM Recurrence. GSCs are also highly invasive.

Studies have shown their ability to lead cancer cells residing at the tumour edge to drive tumour recurrence following surgical resection (Cheng et al., 2011). In addition, their ability to switch between aerobic glycolysis and oxidative phosphorylation makes them metabolically more flexible and resistant to complex microenvironments (Vlashi et al., 2011). In the context of angiogenesis, GSCs play a significant role in this process by the overexpression of angiogenic factors such as VEGF and SDF-1 $\alpha$  and in *in vivo* tumour models, knockdown of which factors has been shown to affect blood vessel formation and tumour formation (Folkens et al., 2009).

## **1.8 Vascular development of GBM**

### **1.8.1 Developmental Angiogenesis**

The vascular network is formed through intricate and complex processes essential for vertebrate development. A number of different signalling pathways cooperate in CNS angiogenesis in organizing precise timing and spatial organisation of the CNS vascular network, including, but not limited to VEGF, Dll4/Notch, Slit2/Robo4 (slit guidance ligand 2/roundabout guidance receptor 4) and Wnt (wingless-related integration site) signalling (Mancuso et al., 2008). The CNS vasculature is highly complex and protected by the blood brain barrier (BBB) – an extensive coverage and precisely modulated communication system between endothelial cells, pericytes, and astrocytes (Mancuso et al., 2008). Although vasculogenesis – a process occurring during embryogenesis whereby mesoderm-derived angioblasts differentiate into ECs and form a *de novo* primary vascular plexus (Harrigan et al., 2003), most of the CNS vasculature is formed through the process of angiogenesis (Mancuso et al., 2008). After the primary vascular plexus is formed, angiogenesis can take place (Wacker and Gerhardt, 2011). Angiogenesis is a process whereby blood vessels grow from pre-existing blood vessels (Risau, 1997). The vasculature in the brain, like other vascular networks in the body have to go through the process of growth, stabilisation, branching, pruning and specialisation.

ECs migrate from the pial surface towards the subventricular zones, take one of two phenotypes as a tip or stalk cell, and angiogenesis commences (Lee et al., 2009). In the brain, VEGF signalling, canonical Wnt signalling, Integrin  $\alpha_v\beta_8$ , TGF $\beta$  signalling and *Grp124* (Probable G-protein coupled receptor 124) have all been identified as essential CNS developmental regulators for angiogenesis and BBB formation (Mancuso et al., 2008). VEGF/Nrp-1 (Neuropilin 1) signalling is thought to be key player in CNS angiogenesis (Raab et al., 2004). VEGFR2 activation in ECs results in the activation of the MAP (mitogen activated protein) kinase and PI3 kinase/Akt pathways which mediates survival and proliferation of ECs (Olsson et al., 2006). Wnt signalling on the other hand has been shown to be specifically activated in CNS endothelium and is also essential in the expression of GLUT-1 and Claudin-3 (Stenman et al., 2008) both which are components of the BBB. Research using transgenic zebrafish by Umans et al. has demonstrated that in the CNS, angiogenesis and barrierogenesis (differentiation of EC acquiring BBB properties) occur simultaneously (Umans et al., 2018). For optimal functioning, newly formed blood vessels are stabilised by the recruitment of mural cells and formation of the extracellular matrix (Umans et al., 2018). This process is modulated by signalling pathways including the PdgfB/Pdgfr- $\beta$ , TGF $\beta$ /Endoglin and Angiopoetin/Tie2 pathways (Lee et al., 2009).

### **1.8.2 Blood vessel development in GBM**

In 1971, Judah Folkman proposed that in order for tumours to grow over 1-2 mm, it must regulate a system of blood vessels for nutrient delivery and removal (Wu et al., 2015). When it subsequently reaches over 2 mm in diameter, a hypoxic microenvironment often in combination with oncogenic pathways promote angiogenesis in order to compensate for the high demand in oxygen and nutrients. Angiogenesis is one of the hallmarks of GBM (Winkler et al., 2018) and the blood vessels are widely known to be tortuous, highly permeable, highly covered by  $\alpha$ -SMA pericytes, large in size and diameter and structurally and functionally disorganised (Yuan et al., 1994; Monsky et al., 1999; Bullitt et al., 2005). Although some of the BBB characteristics present in the normal brain are retained in tumours, the blood vessels are highly permeable.

In GBM, growth factors such as VEGF, hepatocyte growth factor (HGF), fibroblast growth factor (FGF) and platelet derived growth factor (PGF) are all elevated (Brat et al., 2005; Reiss et al., 2005; Shih and Holland, 2006). Generally, VEGF is the main proangiogenic factor driving the aberrant formation of blood vessels in tumours and can be modulated by a variety of oncogenes and tumour suppressor genes such as RAS (Rat sarcoma virus) (Winkler et al., 2018) and MYC (Rak et al., 1995). VEGF is also known as vascular permeability factor (VPF) because of its role in increasing microvascular permeability (Baudino et al., 2002). The increase in vascular permeability is crucial in brain tumours as increase in tumour size is directly correlated with excessive increase in oedema and increased interstitial fluid pressure (Boucher et al., 1997). Peritumoral oedema in GBM results in increased intracranial pressure and is also associated with poorer prognosis (Vallon et al., 2014). In addition, high interstitial fluid pressure results in poorer drug delivery (Jain, 1994).

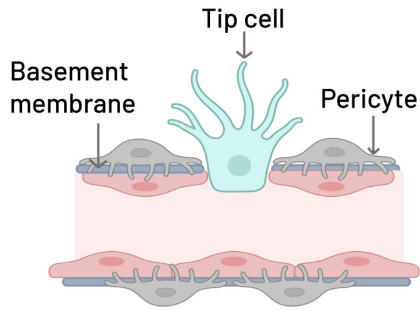
**Table 1.1 Reported vascular aberrations observed in GBM patient samples and *in vivo* models of GBM**

<b>No.</b>	<b>Sample type used in the study</b>	<b>Reported aberrations</b>	<b>Reference</b>
1.	U87 intracranially implanted in brain of immunodeficient mice	Dilated and tortuous vessels. Disorganised new capillaries	(Jain et al., 2007)
2.	U87 and U251 intracranially and subcutaneously implanted in brain of male nude mice	Highly permeable. Wide junctions in endothelial lining, extensive fenestration, disorganised basement membrane	(Hobbs et al., 1998; Roberts et al., 1998)
3.	GBM patient samples (n = 18)	Abnormal pericyte coverage	(Wesseling et al., 1995)
4.	Patient-derived glioma xenografts GBM22, GBM39 and GBM14	Displaced astrocytic endfeet from vessel basement membrane	(Watkins et al., 2014)
5.	GBM patient samples (n = 3)	Loss of pericyte coverage in peritumoral region	(Bertossi et al., 1997)
6.	GBM patient samples (n = 24)	Presence of glomeruloid vascular structures	(Rojiani and Dorovini-Zis, 1996)

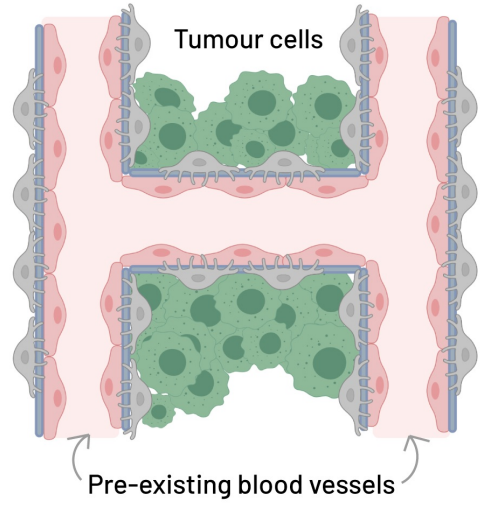
Table shows a selective list of published reported aberrations observed both in *in vivo* GBM models and also in patients with GBM.

There are several mechanisms which both normal tissues and tumour cells use to derive blood supply that have been described in the literature – all of which have been shown to be relevant to some extent in GBM. This includes vessel co-option, sprouting angiogenesis, vasculogenesis, vascular mimicry and endothelial transdifferentiation (Reviewed in Hardee and Zagzag, 2012) (Figure 1.4).

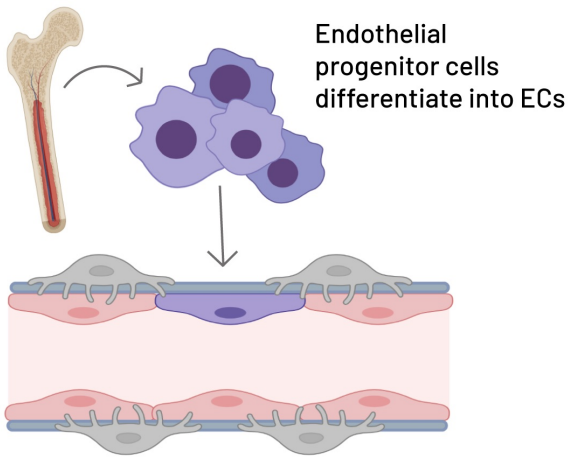
A. Sprouting angiogenesis



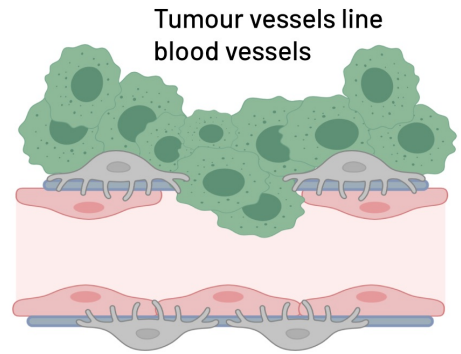
B. Vessel co-option



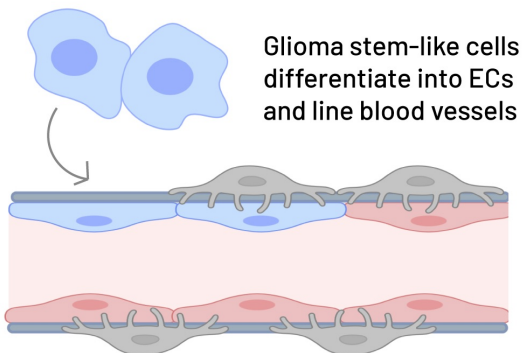
C. Vasculogenesis



D. Vascular mimicry



E. Tumour cell -> EC differentiation



Key

-  Endothelial cells
-  Pericytes
-  Tumour cells
-  Basement membrane
-  Tip cell
-  Endothelial progenitor cells
-  Glioma stem-like cells

**Figure 1.4 Modes of neovascularisation in GBM.**

Diagram depicts the different observed modes of GBM cells deriving its own blood supply. **(A)** Sprouting angiogenesis is the formation of new blood vessels from pre-existing vascular network driven by proangiogenic factors to increase oxygen and nutrient supply to tumour mass. **(B)** Vascular co-option of tumour cells hijacking pre-existing blood vessels. **(C)** Vasculogenesis is the formation of new blood vessels from endothelial progenitor cells (EPC) residing in the bone marrow. **(D)** Vascular mimicry occurs when tumour cells form functional blood vessel tubular-like structures by lining the tumour vessel. **(E)** Tumour cell to endothelial cell differentiation occurs when glioma stem-like cells (GSCs) differentiate into ECs and form tumour blood vessels. Adapted from Carmeliet, P. and Jain, RK., 2011 (Carmeliet and Jain, 2011). Created with BioRender.com.

### 1.8.2.1 Vessel Co-option

In GBM, vascular co-option is one of the initial mechanisms in which gliomas initiate and form their vasculature (Hardee and Zagzag, 2012). Blood vessel co-option is defined as a non-angiogenic process which involves the utilisation of pre-existing vasculature of normal blood vessels by tumour cells by cuff formation (Hardee and Zagzag, 2012). Cancer cells move along the abluminal surface of normal vessels and attach in close proximity to the vessels, resulting in cancer cells obtaining its metabolic demands and subsequent tumour growth around normal, functioning blood vessels (Hardee and Zagzag, 2012; Kuczynski et al., 2019). Using a C6 rat glioma model, Holash et al. were the first to demonstrate vessel co-option through histological analysis (Holash et al., 1999). ANG-2 is expressed in co-opted vessels, and co-option may aid as means for cancer cells to spread throughout the brain without intravasation (Holash et al., 1999). Co-option may take place in glioma without the detachment of pericyte from the EC, and by rather utilising and hijacking pericyte function (Nagano et al., 1993). The alternative also occurs, with tumour cells displacing astrocytes and pericytes, both methods promoting tumour growth by altering BBB function (Caspani et al., 2014).

Co-option modelled in orthotopic models of GL261 mouse cell line and rat glioma model CNS-1, have been observed to persist through to late-stage disease (Baker et al., 2014). Using orthotopic models of glioma and brain metastases, treatment with anti-angiogenic therapies have resulted in a more infiltrative tumour growth, resulting in increased migration of cancer cell towards pre-existing blood vessels (Rubenstein et al., 2000; De Groot et al., 2010; Keunen et al., 2011; Baker et al., 2014). With the abrogation of angiogenic vessels and cancer cells integrating into pre-existing blood vessels, there appears to be a delayed switch from angiogenesis to vessel co-option (Rubenstein et al., 2000; Kunkel et al., 2001; Navis et al., 2013). This delayed switch of mechanism post antiangiogenic treatments is yet to be elucidated; however, a study suggests that WNT signalling in glioma cells may play a key role. Griveaeu et al., demonstrated that Olig2<sup>+</sup> oligodendrocyte precursor-like glioma cells invade the brain parenchyma by co-option and preserve the blood brain barrier (Griveau et al.,

2018). Importantly, the authors found that both *Wnt7a/7b* deletion or pharmacologic Wnt inhibition halts vessel co-option and improves TMZ efficacy (Griveau et al., 2018).

### **1.8.2.2 Sprouting angiogenesis**

After tumour cells co-opt a healthy functioning normal vessel, they continue their growth by adopting a sprouting angiogenesis method. Sprouting angiogenesis is the best studied mode of angiogenesis in both developmental and pathological vasculature growth and is also the most common mechanism for most tumours. Glioma-associated sprouting angiogenesis is controlled by the balance between pro-angiogenic signals and factors that promote vessel quiescence. It begins by ANG-2 and TIE-2 mediated breakdown of existing stable vessels characterised by detachment of mural cells from the vessel wall, degradation of the basement membrane and vessel dilation (Holash et al., 1999; Reiss et al., 2005). ECs then acquire tip or stalk phenotype mediated by the delta-like 4 (DLL4)/Notch pathway (Holash et al., 1999; Reiss et al., 2005). Tip cells follow guidance signals such as ephrins and semaphorins and stalk cells proliferate and elongate forming a lumen and fuse with another vessel branch to establish a perfused neovessel (Hellström et al., 2007).

For a blood vessel to become functional, it must become mature and stable. Stalk cells attract pericytes through signals such as PDGF-B, ANG-1 and basement membrane is deposited to stabilise the vessels (Jain et al., 2007). However, GBM blood vessels form into an abnormal vascular network with abnormal perfusion (Jain et al., 2007). Upregulation of VEGF due to hypoxia is mediated through upregulation of HIF-1 $\alpha$  in which together with HIF-1 $\beta$  form the HIF transcription factor responsible for VEGF gene transcription (Hardee and Zagzag, 2012). Another pathway that is upregulated by hypoxia is the SDF-1 $\alpha$ /CXCR4 axis which has also been shown to be important in GBM neovascularisation (Hardee and Zagzag, 2012). *In vivo*, SDF-1 $\alpha$  has been shown to induce sprouting and branching (Zagzag et al., 2006).

### **1.8.2.3 Vasculogenesis**

Vasculogenesis is the process of tumour neovascularisation that involves the differentiation of circulating bone marrow-derived cells (BMDCs) known as endothelial progenitor cells (EPCs) to mature endothelial cells covering blood vessels (Salmaggi et al., 2004). However, recent research has elucidated that in addition to bone-marrow derived EPCs, TAMs are also able to differentiate into ECs and macrophages (Hardee and Zagzag, 2012). The key pathways involved in vasculogenesis mediating EPC recruitment, include the CXCR4/SDF-1 $\alpha$  pathway and ANG-2/TIE-2 pathway, both of which can be upregulated by HIF-1 (Lewis et al., 2007). A notable study by Kioi et al. demonstrated that inhibition of vasculogenesis through CXCR4/SDF-1 $\alpha$  pathway using the CXCR4 inhibitor AMD3100 in addition to radiotherapy results in the inhibition of recurrence tumour growth in an orthotopic mouse model of U251 GBM cells (Kioi et al., 2010).

### **1.8.2.4 Vasculogenic Mimicry**

Vasculogenic mimicry (VM) is another mechanism of glioma vascularisation where tumour cells mimic ECs and line the tumour vessels to form functional vessel-like network (Kioi et al., 2010). Although it was not observed until 2005 in glioma, it is commonly observed in melanoma. Briefly, vasculogenic mimicry can be identified and quantified according to the standard described by Folberg et al. using periodic acid-Schiff (PAS) staining (Folberg et al., 2000). Folberg et al., characterised VMs as highly patterned distinct vascular channels with a PAS-positive basement membrane and is absent of ECs (Folberg et al., 2000). Yue and Chen et al. described this phenomenon in 2 out of 45 human astrocytoma samples of grade IV based on Folberg's standard for VM characterisation (Yue and Chen, 2005). However, recent studies have suggested that PAS by itself may not be sufficient as a biomarker for VM (Racordon et al., 2017; Valdivia et al., 2019). Further research using organotypic co-culture model of glioma cells and ECs demonstrated that glioma cells incorporate themselves into EC vessel network and under angiogenic conditions, glioma cells are able to assemble themselves into vascular networks with the absence of EC markers (suggesting

that they did not transdifferentiate, rather mimic the EC) (Yue and Chen, 2005). This suggests that vascular radioresistance (a process by which vascular structures develop resistance to ionising radiation and adapt to the radiotherapy-induced changes (Tang et al., 2018)) may be aided by the presence of glioma stem cells lining the blood vessels. Although limited, there is sufficient evidence to support that vasculogenic mimicry exists in human GBM (Shaifer et al., 2010). However, its mechanism and degree of contribution to GBM pathological vascularisation is still unclear.

#### **1.8.2.5 Endothelial Transdifferentiation**

The process of vasculogenic mimicry have been implicated to be linked with subsequent transdifferentiation of tumour cells to other cell types, such as endothelial cells (Hendrix et al., 2003). Endothelial transdifferentiation is the process in which tumour cells transdifferentiate into an endothelial phenotype (Zhao et al., 2018). In 2011, Soda et al. demonstrated using an *in vitro* differentiation assay that hypoxia induces the differentiation of glioma cells into ECs and this process does not require VEGF (Soda et al., 2011). They described that these tumours derived endothelial cells are functional, they are resistant to anti-VEGF therapy and that they also exist in human GBMs (Soda et al., 2011). Ricci-Vitiani et al., demonstrated that a variable number of ECs in primary glioblastoma (between 20% and 90%) showed aneuploidy with a significant number exhibiting genomic alterations found in glioma cells (Ricci-Vitiani et al., 2010). In more recent work using chromatin immunoprecipitation sequencing (ChIP-Seq) and RNA sequencing (RNA-seq), Zhao elucidated that the expression of ETS variant transcription factor 2 (ETV2) drives transdifferentiation of CD133-positive, nestin-positive cells into an endothelial phenotype in the zebrafish brain (Zhao et al., 2018). They also found that ETV2 not only is highly expressed in GBM, but GBM tumour cells with ETV positivity co-express endothelial genes (Zhao et al., 2018). Additionally, a study by Deshors et al., comparing trans-differentiation of GSCs to ECs in culture in the absence or presence of irradiation, showed that trans-differentiated GSCs form tubule-like structures both *in vitro*, and blood vessels in Matrigel plugs *in vivo*, more effectively post irradiation, suggesting a role for irradiation in the process of trans-differentiation (Deshors et al., 2019). The Tie2 signalling pathway was

upregulated in the irradiated GSCs and drove the increase in vascularisation (Deshors et al., 2019).

## **1.9 Mouse models of GBM**

In order to understand GBM further and to improve of treatments for patients, the use of mouse models is crucial; however, the recapitulation of the diffuse and infiltrative nature of GBM in mouse models has proven to be a challenge. There are four distinct types of preclinical rodent models that are most commonly used: cell-line xenografts (CLX) of human origin, patient derived xenografts (PDX) of human origin, syngeneic models of mouse origin and genetically engineered mouse models (GEMM) (Deshors et al., 2019). In glioma research, xenograft and syngeneic mouse models are the most commonly utilised. The location of cancer cell implantation is as important as choosing the most suitable tumour cell line in order to accurately recapitulate the tumour characteristics seen in patients (Hicks et al., 2021).

### **1.9.1 Xenograft models**

In CLX models, cells that are commonly implanted into the mouse include U87, 8251, T98G and A172. (Irtenkauf et al., 2017). CLX tumours tend to grow with very distinct boundaries which do not recapitulate the infiltrative nature of GBM patient samples (Brighi et al., 2020; Akter et al., 2021). However, owing to its rapid and reproducible nature, the CLX model is use widely for glioma research. PDX models on the other hand, involve the direct xenotransplantation of human biopsy tissue preserving the features in the tumour of origin (Brighi et al., 2020). Xenotransplantation was first demonstrated using a rat glioma cell line in both neonatal and adult mice in 1986 (Brighi et al., 2020). It has been shown that compared to CLX models, PDX tumours recapitulate the patient tumours more accurately, in particular the vascular characteristic and the blood brain barrier (Brighi et al., 2020), and thus would be useful in research involving the invasiveness of GBM and interactions with the stroma. However, the use of immune-deficient mice is required in PDX models to reduce the risk of rejection which poses limitations for studies investigating immune responses and interaction of different components of the microenvironment.

Examples of glioma CLX models commonly used in studies include TG1 human GBM cell line or T98 and U87 glioma cell lines grown in non-obese/diabetic (NOD) / severe combined immunodeficient (SCID) mice which lack mature T and B lymphocytes or grown in nude mice (Reviewed in Hicks et al., 2021). Examples of glioma PDX models of GBM used in *in vivo* studies in published literature include patient derived GBM cells grown in either NSG (Kerstetter-Fogle et al., 2020), nude (Sarkaria et al., 2006) or in NOD/SCID/IL2rg<sup>-/-</sup> (interleukin 2 receptor subunit gamma) (Joo et al., 2013).

### **1.9.2 Syngeneic models**

Syngeneic models that are commonly used in glioma research include GL261 and CT2A cell lines. These models were generated by injection of the carcinogen 3-methylcholantrene which induced tumour development that recapitulated GBM tumours (Shultz et al., 2005). In these models, immunocompetent mice are used for tumour growth which gives an advantage for research involving the tumour interactions with the microenvironment. However, limitations of this model include lack of stepwise genetic progression often seen in human tumours including GBM (Hicks et al., 2021). The use of syngeneic mouse models also exclusively involves mouse tissues and genetic background, which have proven challenging to translate to human tumours for the development of treatments. Similar to PDX models, syngeneic models have been described previously to have distinct tumour boundaries (Akter et al., 2021).

### **1.9.3 Genetically engineered mouse models**

GEMMS or genetically engineered mouse models are generated by manipulating the mouse genetic background to induce tumour development (Akter et al., 2021) in immunocompetent mice. To induce specific genetic alterations in mice, the commonest method for site-specific recombination is the use of the cre/LoxP system to activate oncogenes and signalling pathways involved in gliomagenesis. This is a process by which cyclisation recombinase (cre) mediates recombination between two LoxP sites (Reviewed in Noorani, 2019). Another system of GEMM production that is less commonly employed in models of glioma and other cancers is the replication competent ASLV long terminal repeat with a splice

acceptor vector system (RCAS) system. (Richmond and Su, 2008). There are numerous advantages of using this model including the ability to activate relevant genes and pathways at specific time points. Summarised extensively in a review by Imran Noorani (Noorani, 2019), examples of key published GEMM models of GBM includes a model by Holland et al., in which a *Kras*<sup>G12D</sup> mutation and a constitutively active Akt mutant were generated using RCAS vectors (Holland et al., 2000). Histologically, lesions resembling that of human GBMs were observed when both of the mutations were expressed. Zhu et al. generated a transgenic mice model overexpressing EGFRvIII (Epidermal Growth Factor Receptor Variant III) in combination with homozygous deletions leading to loss of PTEN (phosphatase and tensin homolog) and INK4A (encoded by the CDKN2A gene) (Zhu et al., 2009). This model requires administration of adenovirus transducing Cre recombinase injections into the brain for activation of gene deletion.

#### **1.9.4 Emerging alternative models**

Further from mouse models, there is development of alternative tumour models in *Drosophila melanogaster* (fruit flies) which shares 75% of functional orthologs with human genes (Reiter et al., 2001); *Danio rerio* (zebrafish) currently used for research on early tumorigenesis; as well as canine brain tumour models (Reiter et al., 2001).

### **1.10 Effect of radiotherapy on GBM**

#### **1.10.1 Effect of radiotherapy on GBM tumour growth**

Rapidly proliferating cancer cells are more susceptible to ionising radiation, hence, radiation therapy has been largely successful in treating different cancers (Bernier et al., 2004). The effects of ionising radiation damage can be classified into two categories: direct effects and indirect effects. Direct effect is when the damage results from the ionising radiation itself, mainly by damage to the DNA, subsequently resulting in cell death and reduction of cell populations. Radiation cause damage to the DNA by single strand breaks (SSB) or double strand breaks (DSB) in the cell. DSBs, if unrepaired, is the most lethal type of DNA damage which normally results in cell death (Baskar et al., 2014). However, damaged

cells that survive may later induce carcinogenesis or result in a different type of pathogenesis. Indirect radiation damage is when ionising radiation hits the water molecules and other organic molecules in the cells, producing free radicals such as hydroxyl ( $\text{HO}\cdot$ ) and peroxy radicals ( $\text{RO}_2\cdot$ ) (Desouky et al., 2015). Free radicals are unstable atoms possessing an unpaired electron in the structure which is very reactive. This reactive electron reacts with DNA molecules and give rise to molecular structural damage. The number of the free radicals produced by ionising radiation is dependent on the total dose given (Desouky et al., 2015). It has been elucidated that the majority of damage from radiation is from indirect action, due to the high content of water in cells (Saha, 2013). Cells undergo a stress response within less than a microsecond after the ionising radiation hits (Azzam et al., 2012). Compared to normal cells, cancer cells repair radiation-induced damage more slowly, and produce more DNA breaks than the normal cells (Shahidi et al., 2007; Mohseni-Meybodi et al., 2009).

The use of radiotherapy in the clinic for treatment of brain tumours has been implemented from as early as the 1940s. By the 1970s, the use of whole brain irradiation had come to a halt, due to the advancement of imaging techniques which could be used to focus irradiation to the tumour area sparing the normal brain. The dose-dependent effects of radiotherapy on GBM were first demonstrated by Walker et al., where they showed that doses of 50-60 Gy were associated with improvement in survival compared to doses less than 45 Gy which were less efficacious (Walker et al., 1979). By the 1980s, the use of magnetic resonance imaging (MRI) in combination with radiotherapy began to be incorporated. The use of MRI with T1-weighted and T2 weighted image datasets improved definition of the tumour target volume (Gzell et al., 2017). In the present times, intensity-modulated radiotherapy (IMRT) is used, and it allows the delivery of restrictive targeted radiation, sparing surrounding areas. IMRT is achieved by delivering multiple beamlets of radiation from various angles towards a target. IMRT has proven to be beneficial in efficient coverage of target especially meeting the organ dose constraints of critical structures in the brain, and dose conformity for tumours of irregular shapes (Suzuki et al., 2003; Burnet et al., 2014).

There has been growing interest and evidence in the benefits of hypofractionation regimen of radiotherapy for newly diagnosed GBM. Study by Ammirati et al. assessing the efficacy of treating primary GBM, with 52.5 Gy radiotherapy in 15 fractions in combination with TMZ, demonstrated that patients had a median survival of 12.7 months (Ammirati et al., 2014). Similarly, ultra-hypofractionated regimes of 60 Gy radiotherapy in 10 fractions in combination with TMZ has been performed in the clinic. Reddy et al., showed that using this ultra-hypofractionated regime in patients, the median overall survival was 16.6 months (Reddy et al., 2012). Unfortunately, no studies have shown improved survival benefits in patients when compared to standard fractionation (Gzell et al., 2017).

A phase 3 trial conducted by the European Organisation for Research and Treatment of Cancer in 2004 (NCT00006353), employed 573 patients and demonstrated an improved progression-free and overall survival in GBM patients following maximal safe resection treated with concomitant and adjuvant temozolomide, an oral alkylating agent, and radiation therapy (Stupp et al., 2009). In the trial, combined treatment of TMZ and radiotherapy for GBM resulted in 1.9% overall survival for radiotherapy alone and 9.8% overall survival for combined at 5 years; however, patients that has successfully undergone combination treatment eventually died due to recurrence (Stupp et al., 2009). In the same study, they demonstrated that *MGMT* promoter methylation status was the strongest predictor for patients benefitting from TMZ chemotherapy. The authors suggested that the development of alternative strategies is crucial for patients with unmethylated *MGMT* (Stupp et al., 2009).

Radiotherapy is one of the most important treatment regimens; however, radioresistance and recurrence post-irradiation are a challenging predicament. As a standard, radiation oncologists add a further 2 cm margin to the apparent tumour bulk (which is termed the clinical target volume), with the aim of including infiltrating cells surrounding the tumour mass while sparing healthy tissues (Price and Gillard, 2011). Studies have shown that, 93% of recurrence occur in the field of irradiation (within 2 cm of the original tumour margin), 5% are marginal and only 2% were distant (McDonald et al., 2011). One of the biggest limitations of radiotherapy of solid tumours is that it enhances the formations of hypoxic niches,

which harbour GSCs (Rycaj and Tang, 2014). Sustained hypoxia triggers mechanisms that is important for GSC maintenance including HIF signalling, epithelial-mesenchymal transition, and autophagy. In GBM, *in vitro* studies have shown that HIF-1 $\alpha$  along with Notch signalling drive the maintenance of GSC (Qiang et al., 2012). Recent *in vitro* studies of GBM cell lines have demonstrated that ionising radiation results in enhanced GSCs stemness by activation of autophagy (self-eating) through the Wnt/ $\beta$ -catenin pathway, resulting in enhanced GSC radioresistance (Tsai et al., 2021).

Glioma stem like tumour cells (GSCs), are crucial drivers of radioresistance and recurrence in GBM (Prager et al., 2020). Although the molecular mechanisms driving resistance in GBM has yet to be elucidated in full, GSCs have been shown to be highly resistant to ionising radiation. This is achieved by GSCs ability to repair themselves in response to radiation-induced damage and their pro survival mechanisms (Bao, Wu, McLendon, et al., 2006; Kang et al., 2008). In a 2016 study, De Bacco et al., elucidated the role of MET in the ability of GSCs to resist radiation in GBM. The authors described a novel mechanism in which MET promotes GSC radioresistance by modulation of DNA damage response and repair via AKT signalling (De Bacco et al., 2016).

GSCs' ability to thrive in harsh and complex microenvironment and highly invasive potential makes them successful in driving tumour recurrence. As explained in previous sections, GSCs have metabolic plasticity, meaning they are able to oscillate between aerobic glycolysis and oxidative phosphorylation depending on oxygen availability (Shibao et al., 2018). This adaptation renders them metabolically more flexible and resistant to complex microenvironments (Vlashi et al., 2011). Using an intracranial implantation model of GSCs versus non-stem tumour cells isolated from a GBM xenograft (D456), Cheng et al. demonstrated that GSCs display greater invasive capacity into the surrounding normal tissue, compared to non-stem tumour cells (Cheng et al., 2011). Additionally, the authors also observed an increase in invasion-associated proteins including MMP16 (matrix metalloproteinase 16), L1CAM (cell adhesion molecule) and ADAMTS1 (a disintegrin and a metalloprotease with thrombospondin motifs 1) in GSCs compared to non-stem tumour cells (Cheng

et al., 2011). DNA damage caused by radiation triggers GSC-specific, NF- $\kappa$ B driven switch towards the more aggressive mesenchymal subtype (Bhat et al., 2013). It is possible that radiotherapy may result in the survival of highly proliferative GSCs adapted to rapid repair from DNA damage (Prager et al., 2020). Targeting resistant populations of GSCs in GBM remain crucial for the future enhanced success of radiotherapy treatments.

### **1.10.2 Effect of radiotherapy on GBM tumour vasculature**

Vascular remodelling is a hallmark of radiation damage. This is characterised by increased permeability, detachment from the basement membrane, and endothelial cell death (Langley et al., 1997; Heckmann et al., 1998) (Kouam et al., 2019) (Figure 1.5). Depending on whether the blood vessels are derived through sprouting angiogenesis, co-option or vasculogenesis, tumour vessels may lack basement membrane and pericyte coverage. This renders the blood vessels more permeable and more radiosensitive than mature vessels in the normal brain parenchyma (Jain, 2003; Barker et al., 2015). The microvasculature is highly susceptible to radiotherapy (Baker and Krochak, 1989). Morphological changes in the vasculature induced by radiation includes thickening of the intimal layer of the blood vessel, and development of thrombosis and fibrosis (Reviewed in Barker et al., 2015). As a result of ionising radiation, endothelial activation occurs, resulting in a switch from a quiescent phenotype to a pro-inflammatory phenotype characterised by increased endothelial cell production of interleukin-6 (IL-6), interleukin-8 (IL-8), C-C motif chemokine ligand 2 (CCL2) post-irradiation (Baselet et al., 2017; Jaillet et al., 2017). Prolonged or repeated ionising radiation results endothelial dysfunction (Deanfield et al., 2007).

In addition, partially due to hypoxia, levels of VEGF and angiotensin is elevated in GBM in response to irradiation, promoting cancer progression by VEGF-induced angiogenesis (Kil et al., 2012; Januel et al., 2015). This was evidenced in a study by Kil et al., using two GBM cell lines (U251 and LN18) which demonstrated that extracellular VEGF concentration increased after the cells were irradiated with a range of doses between 0.5 to 10 Gy (Kil et al., 2012). Importantly, the authors showed using cell motility assay that there was an

increase in glioma cell motility when grown in irradiated conditioned medium. In the case of angiotensin, Januel et al. analysed 81 GBM patients, some which were already being treated with angiotensin-II receptor 1 blockers (ARBs) used for the treatment of high blood pressure. The authors found that patients who were treated with ARBs after radiotherapy treatment were functionally independent for longer compared to patients not treated with ARBs (Januel et al., 2015). The authors elaborated that Ang2 inhibitors works by inhibiting angiogenesis, marked by reduced VEGF secretion and VEGF receptor transactivation by Ang2 demonstrated in a subcutaneous C6 rat glioma model (Arrieta et al., 2005). Additionally, Ang2 inhibitors can improve oxygen delivery at tumour site, improving radiosensitivity (Chauhan et al., 2013).

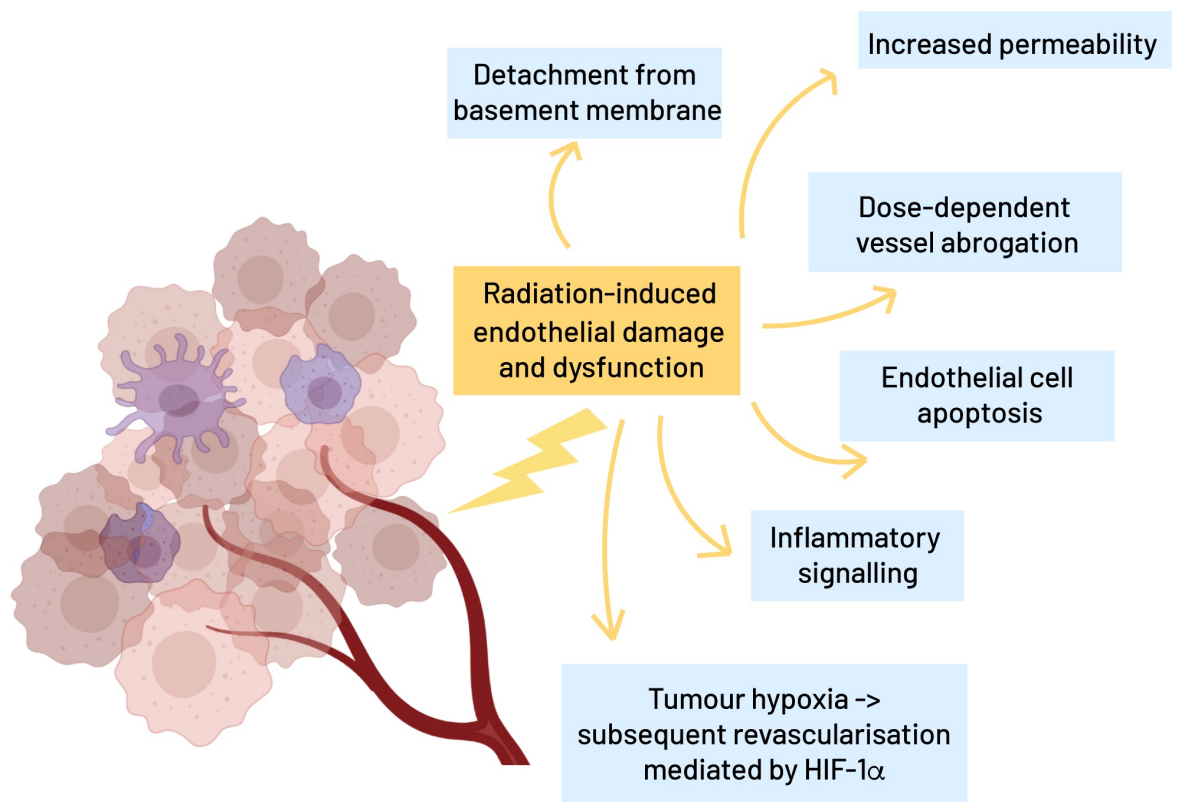


**Figure 1.5 Early effects of irradiation on GBM vasculature.**

Damage from ionising radiation leads to the dysfunction of endothelial cells. Depending on the dose, radiation has been shown to result in increased permeability, detachment of ECs from the basement membrane and apoptosis, and activation of inflammatory cascades. When the tumour mass is irradiation, vessel abrogation due to radiation results in induction of hypoxia and results in tumour revascularisation either via vasculogenesis or angiogenesis. Created with BioRender.com.

It has been long known that ionising radiation induces changes to the blood brain barrier function due damage to the endothelium in non-tumour conditions (Trnovec et al., 1990; D'Avella et al., 1992; Rubin et al., 1994). To elaborate briefly, in the study by Rubin et al., rats were given irradiation at 60 Gy and disruption of BBB was detected. The authors described the disruption as discrete vasculature leakage, severe loss of capillary network and necrosis (Rubin et al., 1994). In a review paper by Park et al., the authors showed that there was an increase in vascular permeability post-irradiation (at different doses), in *in vivo* tumours models of non-small-cell lung cancer, rectal cancer, colon tumour and Walker breast carcinoma, to name a few (Reviewed in Park et al., 2012). In all of these studies, vessel permeability was measured early after irradiation (24 to 72 hours). A study using Walker 256 tumours, a rat mammary carcinoma used as an animal model of bone-metastatic cancer, irradiated with 20 Gy shows that 2 days after irradiation, vascular permeability decreased markedly (C. Song et al., 2009). This supports *in vivo* studies using a squamous cell carcinoma line (SCCVII), which demonstrate that the increase in vessel permeability post-irradiation is transient (Kobayashi et al., 2004). Although there is limited evidence in the case of vessel permeability in glioblastoma tumours, in a retrospective study by Qin et al., analysing the response of 14 GBM patients, the authors demonstrated that shortly after radiation therapy with doses of 30-40 Gy, there was increased BBB permeability measured by <sup>99m</sup>Tc-glucoheptonate imaging (Qin et al., 1990). Based on this observation, the authors suggest that improved permeability may improve the delivery of chemotherapy (Qin et al., 1990). In a more recent study employing a F98 glioma model implanted in rats, Bouchet et al., observed that radiation resulted in increase tumour vascular permeability (monitored by MRI) which peaked at day 7 but subsequently decreased to normal control levels at day 14 (Bouchet et al., 2017). However, to our knowledge, until now still very little is known about the effects of radiation on vessel permeability of recurrent tumours, especially in GBM.

Although the mechanism of increased vascular permeability post-irradiation is still not fully elucidated, one long-proposed mechanism is the radiation-mediated damage to endothelial cells (Potchen et al., 1972). Damage to endothelial cells results in clefts or gross disruption of cells, resulting in transvascular trafficking of

macromolecules (Potchen et al., 1972). The transient abrogation of endothelial cells lining the blood vessels may result in openings which facilitates entry of macromolecules. A more recent study of irradiated primary human coronary artery endothelial cells (HCAEC), elucidated that ionising radiation increases the permeability of endothelium through a disintegrin and metalloproteinase domain-containing protein 10 (ADAM10)-mediated cleavage of vascular endothelial cadherin (VE-cadherin) (Kabacik and Raj, 2017). Kabacik et al., showed that there was a radiation dependent increase in VE-cadherin cleavage by ADAM10 (Kabacik and Raj, 2017). The same observation was demonstrated in HUVEC cells (Kouam et al., 2019). Kobayashi et al., suggest that the restoration of damaged endothelial cells by circulating stem cells could explain the transient nature of vessel permeability (Kobayashi et al., 2004).

In the context of vessel architecture, a study by Donnelly et al., using subcutaneous GL261 model of GBM, demonstrated 10Gy irradiation resulted in reduced tumour vasculature to 37% 3 days post-irradiation and that the majority of functioning vasculature post irradiation was situated in the periphery of tumours (Donnelly et al., 2001). A study by Kioi et al., showed that in the intracranially implanted U251 GBM model, irradiation with 15Gy results in reduction of CD31 positive cells to 25% of control, increase in hypoxic area marked by pimonidazole staining, and decrease in blood perfusion to 10% of control in tumours 2 weeks post-irradiation (Kioi et al., 2010).

The increase in tumour hypoxia alongside with increased vascular permeability triggers infiltration of immune cells into the brain parenchyma; including increased recruitment of macrophages following radiotherapy (Tabatabai et al., 2006; Wang et al., 2013). This is driven by radiation-induced chronic inflammation which results in high intracellular nitric oxide in glioma cells (Kim et al., 2013) resulting in stabilisation of HIF-1 (Kaur et al., 2005). SDF-1 expression induced by HIF-1 upregulation promotes the radiation-induced recruitment of macrophages to the tumours. The increase in macrophage infiltration, as described previously, is associated with poor prognosis (Sørensen et al., 2018). Recent study by Wei et al., expanded on this knowledge using a GL261 syngeneic mouse model and demonstrated that glioma associated macrophage cells induce the activation of

endothelial cells via secretion of TNF- $\alpha$ . This resulted in aberrant GBM angiogenesis and resistance to the antiangiogenic drug B20.4.1.1 (mouse analogue of Bevacizumab) (Wei et al., 2021).

The molecular mechanisms of revascularisation of GBM tumour recurrences remain unknown. However, different signalling mechanisms have been proposed including the vasculogenesis pathway. Studies from the lab of J. Martin Brown have given evidence that blocking the pathway involved in vasculogenesis can prevent tumour recurrence. In 2010, they showed that *in vivo*, irradiation induces the recruitment of bone marrow-derived cells (BMDCs), cells which are known to contribute to vasculogenesis. BMDC recruitment was mediated via the SDF-1/CXCR4 axis and inhibition using AMD3100, a clinically approved small molecule inhibitor of SDF-1/CXCR results in abrogation of recurrence when combined with irradiation (Kioi et al., 2010). Subsequently, their study in 2014 demonstrated that blocking the chemokine SDF-1 following irradiation using NOX-A12 (an RNA oligonucleotide), inhibits tumour recurrences in rats (Liu et al., 2014). However, in response to the studies on vasculogenesis, Jain et al., published a commentary which states that vasculogenesis is not the major contributor to revascularisation in GBM recurrences. Rather, the surviving ECs in irradiated tumours are the major drivers of revascularisation via the angiogenic pathway (Kozin et al., 2011; Kozin et al., 2012). However, the authors expanded that there is limited proof in the literature to support this argument. To summarise, the data in the literature on mechanisms of revascularisation in recurrence tumour are incomplete and inconsistent (Kozin et al., 2012). To quote from the commentary: “most studies in the published literature have focused on early vascular effects, and late post-radiation stages have been less explored (Kozin et al., 2012). Thus, understanding the radiation-induced effect on the tumour vasculature is important for maximising the efficacy of radiotherapy and greater advancement is needed in this field.

## 1.11 Deducator of Cytokinesis 4 (DOCK4)

### 1.11.1 Rho GTPases

Rho GTPases are a family of highly conserved guanine nucleotide binding proteins (G proteins) with low molecular weight (~21 kDA) encoded by 20 genes (Clayton and Ridley, 2020) and belong to the Ras superfamily. Rho GTPases act as a molecular switch in intracellular signal transduction pathways (Clayton and Ridley, 2020) and are known for their key roles as regulators of the actin cytoskeleton amongst other functions including neuronal development (Clayton and Ridley, 2020).

Rho GTPases are further divided into seven subfamilies, namely Rho, Rac, Cdc42, Rnd, RhoD, RhoBTB and RhoH with RhoA, Rac1 and Cdc42 being the most extensively studied (Etienne-Manneville and Hall, 2002; Gadea and Blangy, 2014; Kobayashi et al., 2014). Each modulating different pathways, RhoA regulates actomyosin contractility and formation of actin stress fibres and focal adhesions necessary for cell motility (Coleman and Olson, 2002; Takai et al., 2021); it has been long known that Rac is responsible for the production of lamellipodia and membrane ruffles (Ridley et al., 1992); and Cdc42 has been shown to instigate the formation of actin-rich filopodia, and is required for directional migration (Kozma et al., 1995; Nobes and Hall, 1995). Using an endothelial specific deletion of Cdc42 in ECs by a Tie2-Cre driver line (or Cdc42<sup>Tie2KO</sup>), Barry et al., showed that endothelial Cdc42 is crucial for developmental blood vessel formation, and that loss of endothelial *Cdc42* results in embryonic lethality due to defects in tubulogenesis and blood circulation (Barry et al., 2015). Using a conditional endothelial specific *Rac1* knockout in a Cre/Flox approach, Tan et al., showed that loss of endothelial *Rac1 in vivo* resulted in embryonic lethality midgestation, and that endothelial *Rac1* deficient embryos developed defective blood vessels and lacked small-branching blood vessels (Tan et al., 2008). Due to their role in the control of the actin cytoskeleton and cell migration, in cancer, Rho GTPases were proposed to be pro-tumorigenic. However, activating mutations of Rho proteins are rare in human cancers (Stankiewicz and Linseman, 2014), although overexpression is common, and is correlated with tumour progression (Stankiewicz and Linseman, 2014; Clayton

and Ridley, 2020). Rho GTPases have also been implicated in angiogenesis through their modulation of blood vessel proliferation and migration (Bryan and D'Amore, 2007), branching and lumen morphogenesis (Abraham, Scarcia, Bagshaw, McMahon, et al., 2015). In pathological angiogenesis, Rho GTPases also have been shown to modulate HIF activation (Turcotte et al., 2003), and the production of pro-angiogenic factors in cancer cells (Van Golen et al., 2000).

### **1.11.2 Guanine Nucleotide Exchange Factors (GEFs)**

The majority of Rho GTPases cycle between two forms: GDP-bound inactive form or GTP-bound active form (Jaffe and Hall, 2005) and this cycling is controlled by three classes of regulatory molecules. Guanine nucleotide exchange factors (GEFs) mediate the exchange of GDP to GTP; GTPase activating proteins (GAPs) inactivate Rho GTPases by stimulating the intrinsic ability of Rho GTPases to hydrolyse GTP to GDP; and guanine dissociation inhibitors (GDIs) sequester GTPases in the cytosol in a GDP-bound state (Svensmark and Brakebusch, 2019). Rho GEFs are divided further into two families, the Deducator of Cytokinesis related proteins (DOCK) 180 family GEFs and the Dbl-like family. The presence of a Dbl homology (DH) domain followed by a pleckstrin homology (PH) domain is characteristic of the Dbl-like RhoGEFs (Rossman et al., 2005).

The DOCK180 family GEFs were discovered much later and have 11 members to the family (Côté and Vuori, 2002). The presence of two evolutionary conserved domains: the lipid-binding Dock homology region-1 (DHR-1) and the GEF DHR-2 modules is characteristic of the DOCK family (Côté and Vuori, 2002). DOCK GEFs are also referred to as atypical GEFs due to the lack of a Dbl domain (Rossman et al., 2005; Clayton and Ridley, 2020). The DOCK family is further subdivided into four categories: DOCK-A which are Rac GEFs consists of DOCK1, DOCK2 and DOCK5; DOCK-B, also Rac GEFs consists of DOCK3 and DOCK4; DOCK-C which are Rac or Cdc42 GEFs consists of DOCK6, DOCK7 and DOCK8; and DOCK-D which are Cdc42 GEFs consists of DOCK9, DOCK10 and DOCK11 (Reviewed in Rossman et al., 2005; Clayton and Ridley, 2020) (Figure 1.6).

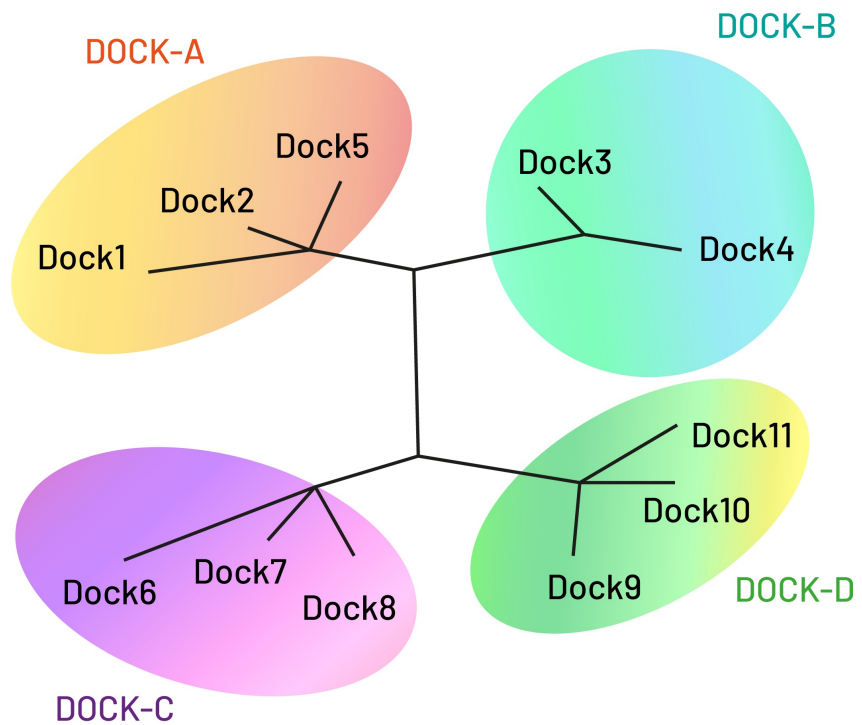


**Figure 1.6 Four groups of the DOCK family proteins.**

11 members of the DOCK protein family divided into four groups on the basis of primary-sequence conservation. DOCK-A includes DOCK-1, -2, and -5. DOCK-B includes DOCK-3 and -4. DOCK-C includes DOCK-6, -7 and -8. DOCK-D includes Dock-9, -10 and -11. Adapted from Rossman et al., 2005, (Rossman et al., 2005).

### 1.11.3 The role of DOCK4 in cancer

DOCK4 is a member of the DOCK180 family of Rho GEFs and a GEF for Rac1. The structure and arrangement of the domains of DOCK4 highly resembles that of other DOCK180 family proteins and is characterised by the presence of DHR1 and DHR2 (DOCK homology regions 1 and 2) domains (Brugnera et al., 2002; Côté and Vuori, 2002). The DHR1 domain binds to phosphatidylinositol 3,4,5-triphosphate (PIP3) which mediates cell elongation and motility (Côté and Vuori, 2002). DHR2 on the other hand, activates Rac by functioning as a guanine nucleotide exchange factor (Côté and Vuori, 2002; Meller et al., 2002; Watabe-Uchida et al., 2006). In addition, at its proline rich C-terminus, DOCK4 also contains a unique set of motifs including a Src-binding (SH3) site, and a proline rich C-terminus (Kobayashi et al., 2014) (Figure 1.7).



**Figure 1.7 Domain structure of DOCK4.**

DOCK4 is comprised of the DHR1 and DHR2 domains, both which are conserved in all mammalian DOCK family proteins. On the N-terminus, DOCK4 has an SH3 domain, and on the C-terminus, a proline rich (PxxP) domain.

Several studies show that DOCK4 is a key activator of Rac1 signalling (Figure 1.8). In 2006, Hiramoto et al., demonstrated using HEK293T cells that when the DHR-2 domain of DOCK4 is mutated, the activation of Rac1 by DOCK4 is suspended, suggesting that Rac activation occurs in the DHR-2 domain (Hiramoto et al., 2006). In the same study, they also demonstrated that RhoG small GTPase and its effector ELMO (Engulfment and cell motility) regulates DOCK4 and promotes cell migration through Rac1 activation (Hiramoto et al., 2006). In 2008, Upadhyay et al. contributed to the new understanding of DOCK4's role in Wnt/ $\beta$ -catenin signalling pathway via Rac1 activation important in cell proliferation and migration, and also tumorigenesis using HEK293T and

NIH3T3 cells, both which have an intact Wnt pathway (Upadhyay et al., 2008). In the study they elucidated the molecular link between the  $\beta$ -catenin degradation complex and DOCK4-Rac1 resulting in  $\beta$ -catenin activation and stabilisation using *in vitro* assays including TopFlash reporter assay, and a transgenic zebrafish Wnt/ $\beta$ -catenin reporter line (Upadhyay et al., 2008).

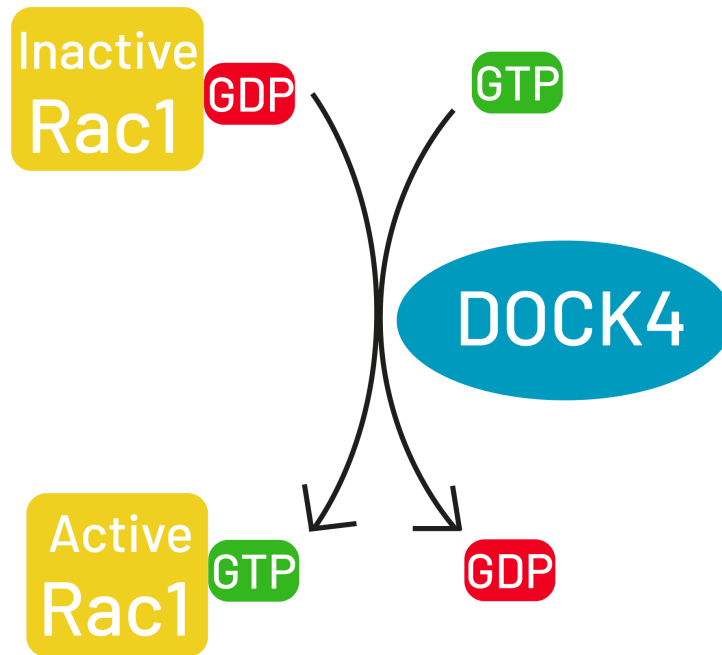


**Figure 1.8 The role of DOCK4 as a Rac1 activator.**

Resting state inactive Rac1 bound to GDP is activated by DOCK4 by the dissociation of GDP and binding of GTP. DOCK4 promotes this nucleotide exchange and results in an active GTP-bound Rac1.

DOCK4 is also expressed in the brain and plays crucial roles in the CNS development. Ueda et al. showed that DOCK4 plays a vital role in dendritic growth and branching and that DOCK4 localises to the dendritic spines and is important in the formation of the spine through Rac and cortactin activation (Ueda et al., 2008; Ueda et al., 2013). *Dock4* has been identified as a risk gene for neuropsychiatric disorders. So far, *Dock4* genetic polymorphisms (mainly single nucleotide polymorphisms) has been found to be associated with several neuropsychiatric and neurodevelopmental disorders including dyslexia

(Pagnamenta et al., 2010), autism (Maestrini et al., 2010) and schizophrenia (Pagnamenta et al., 2010; Alkelai et al., 2012). A study by Yang et al. analysed ultrasonic vocalisation (USV) of mice pups to study development of early life language deficits in autism spectrum disorder (ASD) (Yang et al., 2021). Using a recently generated *Dock4* KO line the authors demonstrated that mice lacking *Dock4* can be utilised as a model for studies exploring ASD-like social communication in mouse models (Yang et al., 2021).

DOCK4 is considered as an ambiguous GEF due to its dual role as an inhibitor or a promoter to disease development including cancer (Gadea and Blangy, 2014). *Dock4* was initially identified as a gene disrupted during tumorigenesis, more specifically its role as a tumour suppressor (Yajnik et al., 2003). Yajnik et al., demonstrated that genetic deletion of *Dock4* resulted in defects in adherens junction formation through Rap GTPase, resulting in a more invasive phenotype *in vivo* and that reconstitution of DOCK4 restored those effects (Yajnik et al., 2003). The potential tumour suppressing ability of DOCK4 was analysed in osteosarcoma cells with *Dock4* deletion. It was found that cells engineered to express wild-type DOCK4 produced smaller nodules compared to osteosarcoma cells expressing Pro718Leu-DOCK4 (missense mutation at the C-terminal motif-1 region). Those Pro718Leu-DOCK4 expressing cells were also more invasive in nature suggesting that DOCK4 possesses tumour suppressing capabilities. The authors also screened 44 human cancer cells lines from a broad range of tumour types and sequenced their coding sequence region (Yajnik et al., 2003). The authors demonstrated that *Dock4* mutations are present in various human cancer lines, including human prostate and ovarian cancer (Yajnik et al., 2003).

The tumour suppressor role of DOCK4 was seen in other cancers including one observed by Kjeldsen and Viegaard in patients with normal karyotype acute myeloid leukemia (NK-AML). A rare submicroscopic, monoallelic deletion at 7q31.1 encompassing the major 3' region of the DOCK4 gene was seen in one out of 21 patients which presented with rapid disease progression and dismal outcome (Kjeldsen and Veigaard, 2013). Furthermore Kuo et al. identified DOCK4 as one of the most commonly seen homozygous deletion mutations in patients with ovarian serous carcinoma and suggested the tumour suppressor

role of DOCK4 (Kuo et al., 2009). Zhou et al., implicated *Dock4* as a pathogenic gene in myelodysplastic syndromes (MDS). They demonstrated that the expression of DOCK4 is reduced due to either deletion of chromosome 7q or hypermethylation (Zhou et al., 2011). Subsequent study by Sundaravel et al., showed that reduced DOCK4 expression causes the dysplastic erythroid morphology in MDS, by disruption of actin cytoskeleton in developing red blood cells (Sundaravel et al., 2015). In the context of GBM – in particular GBM stem-like cells – Debruyne et al. demonstrated that the overexpression of DOCK4 suppresses the tumorigenicity of GBM stem-like cells (Debruyne et al., 2018). In the study, the authors found that in proliferative SOX2 and OLIG2 positive GBM cells was positively correlated with a reduced expression of DOCK4 (Debruyne et al., 2018). This finding relates to the regulation of GSK3 and  $\beta$ -catenin and DOCK4 regulatory pathway in GBM where nuclear  $\beta$ -catenin translocation promotes a non-proliferative state in GBM and repression of stemness markers (Debruyne et al., 2018). Importantly, they showed that increased DOCK4 expression in GBM was associated with a better patient prognosis (Debruyne et al., 2018).

There is growing evidence of a tumour promoting, migration inducing, role of DOCK4. Demonstrated by Kobayashi et al., the authors provided evidence for the interaction between SH3YL1 (SH3 domain-containing YSC84-like protein 1), a phosphoinositide-binding protein, and the C-terminal proline-rich region of DOCK4 in MDA-MB-231 cell line (triple negative breast cancer) (Kobayashi et al., 2014). This interaction promotes DOCK4-mediated Rac activation, resulting in formation of actin-rich protrusions which drives cell movement (Kobayashi et al., 2014). Furthermore, recent research by Westbrook et al., on early breast cancer demonstrated the association of high DOCK4 expression with disease malignancy and higher risk of future bone metastasis (Westbrook et al., 2019). The authors gave evidence that DOCK4 knockdown inhibited the early-stage migration of MDA-MB-231 cells. Notably, they indicated that DOCK4 may be a valuable prognostic biomarker for patients with early breast cancer (Westbrook et al., 2019). Furthermore, Yu et al., identified DOCK4 as a key target of the TGF- $\beta$ /Smad signalling pathway which was directly correlated with increased metastasis of lung adenocarcinoma to livers (Yu et al., 2015). Altogether, studies

over the years have shown that DOCK4 can have tumour suppressing or tumour promoting roles depending on the type of cancer and tumour models used.

#### **1.11.4 The role of DOCK4 in vascular development and angiogenesis**

There is growing evidence in the critical role of DOCK proteins in the complex mechanisms of blood vessel formation in development and disease. To date, 7 out of 11 DOCK proteins have been implicated with the regulation of blood vessel formation (E. Benson and Southgate, 2021). DOCK4 is expressed widely in tissues including in human umbilical vein endothelial cells (HUVECs) (Van Buul et al., 2014). Initially, DOCK4 involvement in vascular-type cells was elucidated by Kang et al. which showed that DOCK4 was one of the DOCK proteins expressed in vascular smooth muscle cells (VSMCs) upstream of *mir-21*, a microRNA involved in cardiovascular diseases and tumorigenesis (Kang et al., 2012). In this same study they showed that DOCK4 downregulation using small interfering RNA (siRNA), also reduced vSMC motility and contraction (Kang et al., 2012).

Research by Abraham et al., using a coculture angiogenesis system gave evidence to the importance of *Dock4* in various vessel processes namely endothelial cell-cell adhesion, filopodia formation and tubule development (Abraham, Scarcia, Bagshaw, McMahon, et al., 2015). ECs were seeded onto a confluent layer of fibroblast and after 14 days lumens were 3D reconstructed. Their results showed that knockdown of DOCK4 led to a significant decrease in vessel branching, vessels developed thinner tubules and had fewer lateral cell-cell contacts and a marked decrease in lumenised tubes (Abraham, Scarcia, Bagshaw, McMahon, et al., 2015). DOCK4 acting as a Rac1 GEF working downstream of the angiogenic factor VEGF was also described in the study (Abraham, Scarcia, Bagshaw, McMahon, et al., 2015). However, *in vivo* homozygous deletion of *Dock4* led to early embryonic lethality. *Dock4* heterozygous deleted mice implanted intracranially with EO771 breast cancer cell line developed tumour vessels with smaller calibre lumens; however, pericyte coverage remained unchanged. The same trend was also seen in developmental

angiogenesis in embryos of *Dock4* heterozygous mice (Abraham, Scarcia, Bagshaw, McMahon, et al., 2015). Although more research is required, so far there is promising evidence that DOCK4 regulates vascular processes including tubule formation and remodelling, lateral cell-cell contact and lumen formation. Up to this date, published literature on the role of DOCK4 in GBM tumour vessel formation does not exist.

## **1.12 Previous work leading to this thesis**

Previous work in the laboratory had shown that blood vessels in primary GBM patient tumours show varying degrees of blood vessel abnormality when compared to the normal brain (Egnuni, T., PhD Thesis), with some blood vessels showing enlarged lumens, coverage by nestin positive cells – a stem cell marker associated with transdifferentiation of GBM cancer stem cells to endothelial cells (Soda et al., 2011) – and high degree of tortuosity (glomeruloid morphology). In the GBM patient samples, there was a significantly higher abundance of blood vessels with larger calibre around (20-50  $\mu\text{m}$  and over 50  $\mu\text{m}$ ) when compared to smaller calibre blood vessels (10-20  $\mu\text{m}$ ) (Egnuni, T., PhD Thesis). Further investigation shows that the nestin positive cells, were distinct from the blood vessels and lacking other stem cell markers such as OLIG2 (Oligodendrocyte transcription factor) and SOX2 (SRY-box 2). These nestin positive cells were positive for the pericyte markers  $\alpha\text{-SMA/PDGFR}\beta$  (Egnuni, T., PhD Thesis). When the primary and recurrence tumours were compared, the observed blood vessel abnormalities were highly augmented in all the GBM recurrence tumours that had undergone radiotherapy and temozolomide chemotherapy treatment (Egnuni, T., PhD Thesis).

In order to assess the potential contribution of radiotherapy to blood vessel abnormality of recurrences, an experimental murine glioma model of treatment and tumour regrowth was set up. The experimental set up, performed by Dr T., Egnuni, is shown in Figure 1.9. CT2A-Luc glioma cells stably expressing luciferase which allows non-invasive imaging of intracranial tumour growth by IVIS bioluminescence imaging, were treated with fractionated irradiation, at a dose that allows most tumours to regrow (2 x 5Gy), delivered to the mouse brains

(whole brain irradiation) on days 7 and 8 after implantation using SARRP (small animal radiation research platform). Following regression, the irradiated tumours were allowed to regrow. Mice were sacrificed and tumour bearing brains were excised for analysis in this thesis. Control, non-irradiated tumours were excised at days 18 or 19 after intracranial implantation on presentation of neurological symptoms, and irradiated tumours 11 days following regression (29 days after intracranial implantation). Tumour regression following radiotherapy treatment was confirmed by MRI and histological staining 18 days after irradiation.

In addition, in order to determine the early effects of radiotherapy on the vasculature of experimental CT2A tumours, some control and irradiated tumours were excised 3 days after irradiation (11 days after intracranial implantation). These tumours were analysed by Dr T., Egnuni. The analysis showed that blood size (vessel length and lumen diameter) decreased significantly post-irradiation.

The day 18 or 19 for controls and day 29 for irradiation and regrowth excised tumour bearing brains were analysed for vascularisation by myself in this study with the results shown in Chapter 3 of this thesis.

In order to assess the effects of *Dock4* genetic deletion, CT2A-Luc tumours were implanted both in WT and in heterozygous *Dock4* knockout mice (Abraham, Scarzia, Bagshaw, McMahon, et al., 2015). The use of heterozygous *Dock4* knockout mice was necessary because of the embryonic lethality of the global homozygous *Dock4* knockout model. The results of the analysis of CT2A tumours grown in the *Dock4* heterozygous knockout mice under control or irradiation conditions are presented in Chapter 5.

Prior to the start of this PhD a *Dock4* conditional knockout model was generated by Ozgene, imported, and bred in the St James's Biological Services facility (Appendix 9) which was also used in intracranial tumour growth and irradiation experiments presented in Chapter 5.

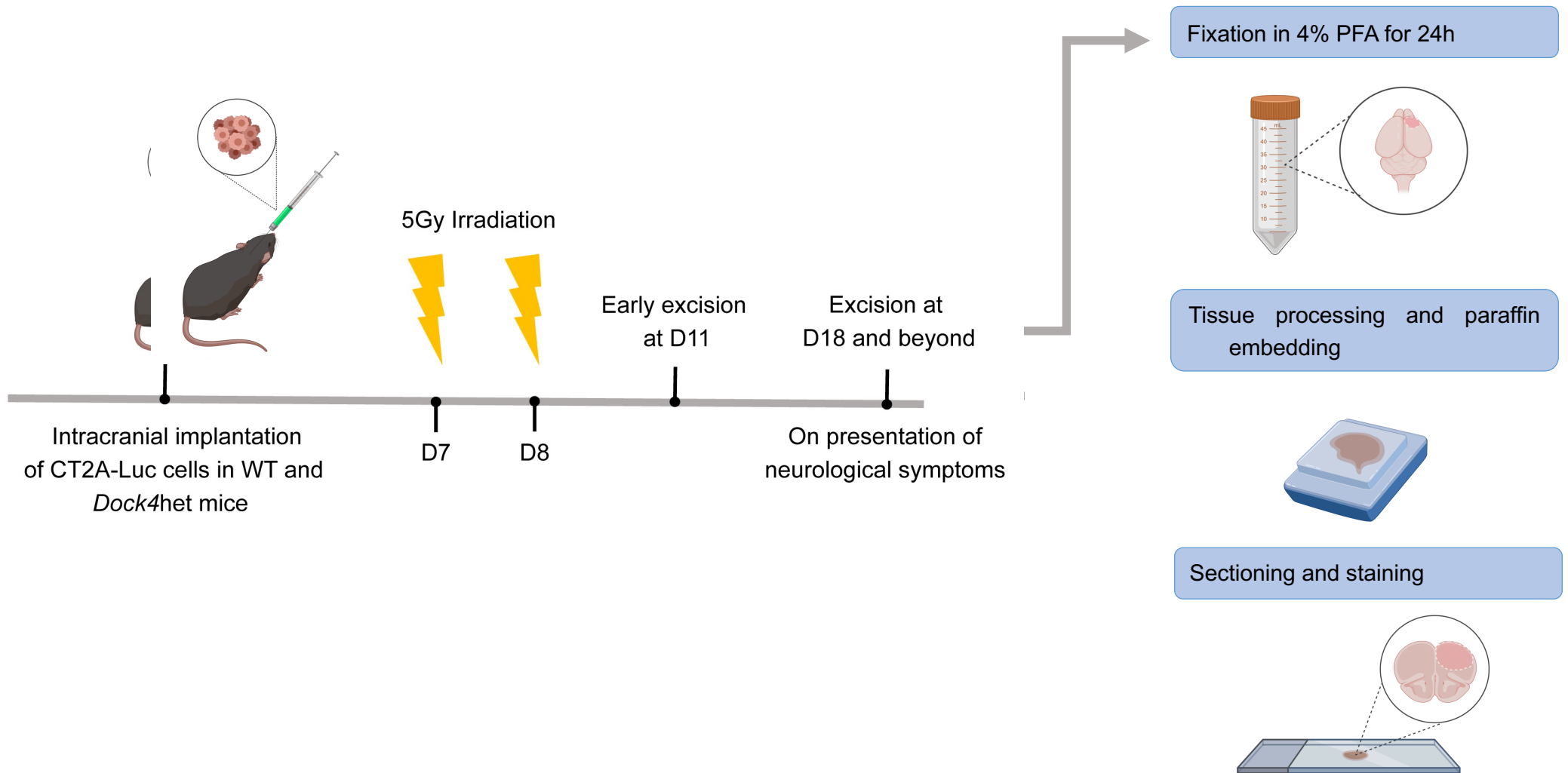


**Figure 1.9 Schedule of CT2A-Luc tumour growth, irradiation, and excision following intracranial implantation in WT and *Dock4* heterozygous knockout (*Dock4* het) mice.**

CT2A-Luc murine glioma cells ( $1 \times 10^5$ ) were injected intracranially into the striatum of C57BL/6 wild type mice (WT) and *Dock4* heterozygous knockout mice (*Dock4*het). Tumour growth was followed non-invasively by IVIS bioluminescence imaging and on day 6 mice were randomised for irradiation. Fractionated irradiation (2 x 5Gy) was delivered on days 7 and 8 following implantation using SARRP and following regression the irradiated tumours were allowed to regrow. Mice were sacrificed on day 11 (early excised irradiated group) day 18 (non-irradiated control group) and day 29 (late excised irradiated group). Mouse brains were subsequently excised, fixed and embedded in paraffin

## 1.13 Aims

The overarching aim of the project has been to investigate whether radiotherapy contributes to the blood vessel abnormality observed in GBM patient recurrence samples using an experimental system of tumour recurrence. The objectives were as follows:

### **1) Assess the effects of radiotherapy on pathological vessel development of tumour recurrences.**

This was done through analysis of phenotypic changes of blood vessels in CT2A tumours implanted intracranially, regrown after radiotherapy treatment in comparison to non-irradiated control tumours. The effects of radiotherapy were determined on overall vascularisation, blood vessel size and maturation in regrown tumours.

### **2) Determine the effects of any aberrancies on blood vessel functionality and levels of tumour hypoxia.**

Blood vessel permeability was assessed by means of intravenous injection of fluorescent-conjugated tracer (BSA-Alexa Fluor555) and hypoxia by staining for glucose transporter 1 (GLUT-1).

### **3) Investigate the effects of *Dock4* deletion on radiotherapy-induced blood vessel vascular changes**

The study of *Dock4* in pathological vessel development of CT2A tumours employed the use of both the global *Dock4* heterozygous knockout mouse model, and the *Dock4* endothelial homozygous conditional knockout mouse model described above. Immunohistochemical analysis techniques assessed the effects of heterozygous *Dock4* deletion in blood vessel abnormality in regrown tumours; and the effects of endothelial *Dock4* deletion on CT2A blood vessel formation.

# **Chapter 2**

## **Materials and Methods**

## **2.1 Cell Culture techniques**

### **2.1.1 Cell lines**

The CT2A murine glioma cell line originated from David Stojdl and Charles Lefebvre of the Children's Hospital of Eastern Ontario (CHEO) Research institute in Ottawa, Canada and was kindly donated by Dr Wurdak's group of the Leeds Institute of Medical Research (LIMR), University of Leeds.

### **2.1.2 Culturing mammalian cell lines**

CT2A lines were cultured in Dulbecco's Modified Eagle Medium (DMEM) (Sigma-Aldrich) supplemented with 10% foetal calf serum (FCS) (Gibco), 1% L-Glutamine (Gibco) and 1% Penicillin and Streptomycin (Gibco). Cells were cultured in T75 or T150 and kept in a humidified incubator at 37°C with 5% CO<sub>2</sub>. To passage cells, media was completely removed, and cells were washed once with PBS. Cells were then trypsinised with 1 ml TrypLE™ Express (1X) (ThermoFisher), split according to experimental requirements, transferred to a new flask with fresh medium, and kept in a humidified incubator at 37°C with 5% CO<sub>2</sub>.

### **2.1.3 Freezing stocks**

To generate frozen cell stocks for long term storage, 80% confluent cells were washed once in PBS and trypsinised as described above. Once completely detached, cells were re-suspended in media and transferred to a falcon tube. Cells were spun down at 700 rpm at 4°C and once a pellet was deposited on the bottom of the tube, the supernatant was aspirated, and the pelleted cells re-suspended in cold freezing down media consisting of 90% FCS and 10% dimethyl sulfoxide (DMSO). Cells were then aliquoted into cryogenic vials and stored at -80°C prior to long term storage in liquid nitrogen. Frozen cells were recovered by thawing a frozen aliquot in a 37°C water bath and transferring cells to an appropriate flask required for culturing. To remove the DMSO, cells were spun down in the falcon tube after thawing and resuspended in fresh medium before cultured in a T75 or T150 flask.

### 2.1.4 Standard solutions

List of commonly used solutions used throughout this thesis are shown in Table 2.1. Solutions were either purchased or prepared in the lab according to experimental requirements.

**Table 2.1 List of commonly used standard solutions in the study.**

No.	Solution	Recipe / Catalogue No.
1.	10X TBS	900 ml ddH <sub>2</sub> O, 24.2 g Tris-base, 80 g NaCl. pH adjusted to 7.6 with concentrated HCl
2.	TBST	900 ml ddH <sub>2</sub> O, 100 ml 1X TBS, 1ml Tween-20
3.	PBS	500ml disH <sub>2</sub> O + 2 PBS tablets (P4117, Sigma) + 1 PBS tablet (BR0014G, OXOID)
4.	Access Revelation	Antigen Retrieval (MP-607-X500, MenaPath)
5.	Antibody diluent solution	0.01M phosphate-buffered normal saline (0.87% NaCl), pH 7.2 to 7.4 PBS containing 0.1% bovine serum albumin (BSA) and 0.1% sodium azide as a preservative
6.	4% Paraformaldehyde	20 g Paraformaldehyde in 500 ml ddH <sub>2</sub> O heated at 55°C, 50 ml 10X PBS. pH adjusted to ~7.5 with 1M NaOH
7.	25% Sucrose	160 ml ddH <sub>2</sub> O, 50 g Sucrose, 9.2 ml 0.5M NaH <sub>2</sub> PO <sub>4</sub> , 30.8 ml Na <sub>2</sub> HPO <sub>4</sub>

### 2.1.5 Irradiation of cells

For the purpose of ELISA experiments, CT2A murine glioma cells were grown to 90% confluence in T75 flasks, and  $1 \times 10^5$  cells were then plated into 6-well plates one day prior to irradiation. Plates were secured with polyfilm to avoid spillage and placed on ice for transfer to the SBS facility. Plates were then irradiated using a RS 2000 Biological Research Irradiator (Rad Source Technologies) at 5 Gy, 10 Gy, 15 Gy and 20 Gy. Cells were then maintained in a humidified incubator at

37°C with 5% CO<sub>2</sub>. At 24, 48, and 72 hours, 1 ml of supernatant was collected and stored at -20°C. Cells from respective wells were then washed with PBS, trypsinised and counted using a haemocytometer.

## **2.2 Biochemistry**

### **2.2.1 Cell supernatant collection**

For ELISA experiments, 500 µl of supernatant was collected carefully into Eppendorf tubes using a pipette and was spun down at 13000 rpm for 5 minutes at 4°C. Supernatant was then recollected and stored at -20°C for long term storage. Collection was done at specific timepoints depending on the experiment.

### **2.2.2 ELISA**

The Quantikine Human VEGF Immunoassay was used to measure VEGF<sub>165</sub> in supernatants. Supernatants were thawed using a warm water bath and spun down at 13000 rpm for 5 minutes at 4°C. ELISA was performed in accordance with the manufacturer's protocol.

## **2.3 Immunostaining**

### **2.3.1 Immunohistochemistry (IHC)**

Paraffin-embedded mouse brain tumour tissue samples were orientated to have the prefrontal cortex facing down during the embedding process, sectioned at 4 µm thickness, and mounted on SuperFrost+ microscope slides (Thermo Fisher Scientific). Slides were placed on a slide heater at 70°C for 20 minutes and, immediately after, the antigen retrieval process was carried out using 10X MenaPath Access Revelation solution using a pressure cooker at a maximum temperature for 40 minutes. A separate staining pot filled with prepared TBST was also placed in the pressure cooker to heat. Once finished, slides were immediately washed in heated TBST (1 x TBS and 0.1% Tween-20) followed by cooling down by washing under a running tap water for 1 minute. Excess water was carefully removed from the slides and an ImmEdge™ Hydrophobic Barrier

Pen (Vector Laboratories) was used to circle around the brain tumour tissue sample on each slide.

All endogenous antibodies were blocked using Peroxidase Blocking Solution BloxAll (Vector Laboratories) for 20 minutes in a humidified chamber. After completion, slides were washed in TBST for 5 minutes before being incubated for another 20 minutes using 10X Casein Solution (Vector Laboratories) at 1/10 dilution in Antibody Diluent Solution (ADS) (Invitrogen) to avoid non-specific binding. Excess casein was removed from the slides and, without washing, slides were then incubated with 100 ml primary antibody diluted in ADS at the right concentration depending on the antibody (Table 2.2). Slides were incubated in a humidified chamber either overnight at 4°C or for 1 hour at room temperature.

Once primary incubation had finished, slides were washed in TBST 3 times for 3 minutes each and incubated with the appropriate secondary antibody for 30 minutes at room temperature. Subsequently, slides were again washed 3 times for 3 minutes each time and slides were then incubated for 5 minutes with ImmPACT DAB peroxidase substrate Vector (Vector Laboratories) in which oxidised DAB forms a brown precipitate that is insoluble in alcohol and most organic solvents at the location of HRP. Once completed, slides were then washed under running tap water for 1 minute.

Slides were then counterstained through the process of applying Haematoxylin, washing under running tap water, and using Scotts' tap water substitute and washing under running tap water for 1 minute each. Immediately after, slides were dehydrated in 100% ethanol for 4 x 1 minutes each, finished off with xylene at 3 x 2 minutes each, mounted with a glass coverslip using DPX mountant, and then left to dry completely overnight before imaging.

**Table 2.2 List of primary and secondary antibodies used in immunohistochemistry.**

<b>Primary antibodies</b>					
<b>No.</b>	<b>Antibody</b>	<b>Host Species</b>	<b>Species reactivity</b>	<b>Dilution</b>	<b>Company / Catalogue No.</b>
1.	Polyclonal anti-CD31	Rabbit	Human, Mouse	1:30	Abcam / ab28364
2.	Monoclonal anti-F4/80	Rabbit	Mouse, Rat, Human	1:200	Abcam / ab16911
3.	Polyclonal anti- $\alpha$ -SMA	Rabbit	Rat, Mouse, Human	1:200	Proteintech / 55135-1-AP
4.	Polyclonal anti- $\alpha$ -SMA	Rabbit	Mouse, Human	1:100	Abcam / ab5694
5.	Monoclonal anti-RFP	Mouse	Mouse, Human	1:1000	GeneTex / GTX82561
<b>Secondary antibodies</b>					
<b>No.</b>	<b>Antibody</b>	<b>Host Species</b>	<b>Species reactivity</b>	<b>Dilution</b>	<b>Company / Catalogue No.</b>
1.	HRP Goat anti-rabbit	Goat	Rabbit	Ready to use	Vector lab / MP-7451
2.	Mouse on Mouse biotinylated Anti-Mouse IgG reagent	Horse	Mouse	Ready to use	Vector lab / MKB-2225

### **2.3.2 Immunofluorescence (IF)**

Paraffin mouse brain tumour tissue samples were prepared and treated exactly the same as in immunohistochemistry process above (Section 2.3.1) until the primary antibody step. For both paraffin and frozen embedded immunofluorescence double staining samples, a calculated cocktail of antibody concentration was used. Samples were incubated with an appropriate primary antibody in a dark humidified chamber overnight at 4°C. After this step, and after 3 x 3 washing with TBST, 100 ml of the appropriate secondary antibody (Table 2.3) diluted at 1/500 in ADS was added to the slides and incubated for 30 minutes at room temperature. Immediately after secondary antibody incubation, slides were again washed in TBST 3 times for 3 minutes each. In order to reduce autofluorescence, 80-100 ml Vector® TrueVIEW® Autofluorescence Quenching Kit (Vector Laboratories) was used at a 1:1:1 ratio and incubated for 1-5 minutes depending on the antibody used. To stain the nuclei, 100 ml 1µg/ml DAPI diluted in ADS was added to the slides and incubated for 10 minutes. 50 ml Vectashield® Antifade Mounting Medium (Vector Laboratories) was used to mount the slides and the coverslip was set in place using a transparent nail varnish along the edges.

For immunofluorescence of frozen mouse brain tumour tissue samples, slides stored at -20°C were left at room temperature for half an hour prior to staining. Slides were then twice washed in PBS at 3 minutes each. Immediately after, one drop of BloxAll was added to the slides as the first blocking step, followed by Casein diluted at 1/10 concentration in ADS. The primary antibody, depending on single or double staining, prepared prior to this step is diluted at the appropriate concentration in ADS and 100 ml is added to slides immediately. Depending on the antibody, primary samples were incubated with the primary antibody either overnight at 4°C or for 1 hour at 37°C in a dark humidified chamber. Routine 3 x 3 minutes washes in TBST were done post-primary antibody incubation and samples were treated in exactly the same as paraffin mouse brain tumour tissue samples (Section 2.3.1) from this step onwards.

**Table 2.3 List of primary and secondary antibodies used in immunofluorescence.**

<b>Primary antibodies</b>					
<b>No.</b>	<b>Antibody</b>	<b>Host Species</b>	<b>Species reactivity</b>	<b>Dilution</b>	<b>Company / Catalogue No.</b>
1.	Monoclonal Anti-Endomucin (V.7C7)	Rat	Mouse, Rat	1:100	Santa Cruz Biotech / sc-65495
2.	Monoclonal anti-actin, $\alpha$ -SMA Cy3™ Conjugated	Mouse	Human, Frog, Sheep, Mouse, Rat, Canine	1:400	Sigma-Aldrich / C1698
3.	Monoclonal anti-actin, $\alpha$ -SMA FITC- Conjugated	Mouse	Human, Frog, Sheep, Mouse, Rat, Canine	1:200	Sigma-Aldrich / F3777
4.	Monoclonal anti-CD34	Rat	Mouse	1:100	BioLegend / 119301
5.	Polyclonal anti-CD31	Rabbit	Human, Mouse	1:100	Abcam / ab28364
6.	Polyclonal anti-GLUT-1	Rabbit	Human, Mouse	1:100	Sigma-Aldrich / 07-1401

<b>Secondary antibodies</b>					
<b>No.</b>	<b>Antibody</b>	<b>Host Species</b>	<b>Species reactivity</b>	<b>Dilution</b>	<b>Company / Catalogue No.</b>
1.	AlexaFluor 647	Goat	Rat	1:500	ThermoFisher/A-21247
2.	AlexaFluor 488	Goat	Rabbit	1:500	ThermoFisher/A-11070
3.	AlexaFluor 488	Goat	Rat	1:500	ThermoFisher/A-11006
4.	DAPI (4',6-diamidino-2-phenylindole) for nucleic acid staining	N/A	N/A	1ug/ml	Sigma-Aldrich/D9542

### **2.3.3 Mouse-on-Mouse (M.O.M) immunofluorescence staining**

The use of Vector® Mouse on Mouse (M.O.M™) Kits and M.O.M™ reagents decrease non-specific background staining that results from the presence of endogenous mouse antibodies. M.O.M kit was used for antibodies raised in mouse listed on Table 2.4. Single and multiple IF staining using the M.O.M kit was performed based on the manufacturer's protocol.

## **2.4 Image processing and quantifications**

### **2.4.1 Randomisation of samples and images**

The original numbering of tumour samples was randomised by another researcher by generation and allocation of a new set of numbers for each sample unknown to the primary researcher. Subsequently, images of stained tumour samples captured using a microscope were saved as numbered files. Images selected for use in the analysis were chosen by random via generation of a simple random number generator using a Python code run on Mac Terminal application. Source code and output is shown in Appendix Chapter (Appendix 3). The key for the original tumour samples was retained by the randomiser until full analysis was complete.

### **2.1.1 CD31**

Stained CD31 slides were scanned using an Apeiro AT Virtual Slide scanner carried out by the Leeds Histology service and analysed using Aperio ImageScope Software. Using the shapes tool, at low magnification, 500  $\mu\text{m}^2$  numbered square boxes were placed accordingly on the viable non-necrotic section of the tumour tissue. At least 75% of the tumour region of the specimen was covered by the boxes. The random number generator was then used to select 5 boxes from each sample. For each tumour sample, three different brain sections at a minimum of 100  $\mu\text{m}$  apart were analysed to account for intra-tumoral variation. An overall image of the section covered with boxes was taken, and images of individual boxes at 40x magnification were then acquired for

quantification. Further characterisations of the vasculature were then carried out using ImageJ software (Version 2.0.0). The number of CD31 positive blood vessels were counted using the ROI manager tool in ImageJ software.

### **2.1.2 F4/80**

Stained F4/80 slides were scanned using an Apeiro AT Virtual Slide scanner and analysed using Aperio ImageScope Software. The Positive Pixel Count Algorithm was used for quantification; this is a built-in algorithm in which quantifies the amount of specific stain present in a scanned slide image. The algorithm has built-in threshold values. For the use of this algorithm, SVS files of scanned slides (provided by Virtual Pathology at Leeds) were uploaded to ImageScope software. The F4/80 positivity was quantified using this method based on the Pixel Positive Count Algorithm Aperio User Guide.

### **2.1.3 $\alpha$ -SMA**

Slides were double stained by immunofluorescence for Endomucin/CD34 for blood vessel visualisation and  $\alpha$ -SMA as a pericyte marker. Using a Zeiss AxioImager Z1 Upright microscope, 20 random images from each sample were taken first by visualising the Endomucin/CD34 channel only to avoid bias in selecting  $\alpha$ -SMA positive areas, followed by capturing images of both Endomucin/CD34 and  $\alpha$ -SMA. For each group (control and radiotherapy), three mice from experiment 1 and one mouse from experiment 3 were used for quantification (Appendix 1). Quantification for  $\alpha$ -SMA includes percentage  $\alpha$ -SMA positive blood vessels defined as pericytes within 20  $\mu$ m radius of the vessel periphery; percentage of  $\alpha$ -SMA tight association defined as over 20% of the vessel periphery ensheathed by  $\alpha$ -SMA positive pericytes; and percentage  $\alpha$ -SMA loose association defined as over 20% of the vessel periphery with unattached  $\alpha$ -SMA positive pericytes. This quantification is described in detail in Figure 4.6.

#### **2.1.4 GLUT-1**

Slides were double stained by immunofluorescence for CD34/Endomucin for blood vessels visualisation and GLUT-1 as a hypoxia marker. Tumour sections from five mice from experiment 4 (Appendix 1) were used in the analysis. A total of ten images from two sections 100  $\mu\text{m}$  apart was captured using a Nikon A1R confocal microscope. GLUT-1 quantification was done using ImageJ software. ND2 files multichannel images were obtained from confocal microscope and imported using the Bio-Formats<sup>©</sup> Package plug-in (Open Microscopy Environment), installed as described in the user guide. Multichannel images were then converted into 8-bit from 16-bit images and channels was split to isolate GLUT-1 (green) channel. GLUT-1 positive blood vessels were removed from the quantification along with folded areas, damaged areas, and areas out of focus. Chosen measurements was set using the 'Set measurements' tool on ImageJ and area, mean gray value, integrated density and area fraction were selected. Mean fluorescent intensity (concentration of GLUT-1 positivity in the sections) of each image (integrated density divided by area) was quantified. Regions absent of GLUT-1 staining were quantified to identify the background pixel value and subtracted from all values. Thresholding was not applied to images as background fluorescence were omitted from each value and binary images were not required for this quantification. Subsequent GLUT-1 quantification was performed by MSc student Tehniat Ali.

#### **2.1.5 BSA-AlexaFluor555**

Slides were double stained by immunofluorescence for CD34/Endomucin for blood vessels visualisation and  $\alpha$ -SMA as pericyte marker and visualised alongside fluorescent conjugated BSA-AlexaFluor555. Tumour sections from five mice from experiment 4 (Appendix 1) were used in the analysis. Blood vessel permeability was analysed by determining the extravascular area positive for BSA-AlexaFluor555 tracer using ImageJ software. This was determined within a 40 $\mu\text{m}$  radius around each blood vessel to allow for extravasation to be accurately determined for individual vessels. 60x magnification images comprising a minimum of 1 to a maximum of 3 blood vessels were used in the analysis.

A macro generated in-house using the ImageJ macro language (IJM), was used to threshold images and automate quantification (Appendix 9 A). The procedure within the macro is as follows: Using manually the threshold tool, minimum and maximum threshold values were determined using several images of low and high extravasation to determine suitable threshold values subsequently used for quantification of all images. As the focus of quantification lies on tracer accumulation within the extravascular area, accumulation with the blood vessel wall was removed using the ImageJ 'clear' tool and omitted from the quantification. Next, the region of interest within the distance of 40  $\mu\text{m}$  around the blood vessels was drawn. Circles of 40  $\mu\text{m}$  diameter were placed surrounding the blood vessels (CD34/Endomucin positive staining) and an outline was drawn using the 'freehand tool' on ImageJ. Areas falling outside the 40  $\mu\text{m}$  diameter were removed using the 'clear outside' tool on ImageJ. With the region of quantification established, thresholds determined previously were applied to the image, the image was converted into binary mode, and tracer positivity was measured in pixels (integrated density value). A graphical representation of the process is shown in Appendix 9 B.

## **2.5 Microscopes**

### **2.5.1 Zeiss AxioImager Z1 upright**

Immunofluorescence-stained samples were visualised using a Zeiss AxioImager Z1 upright microscope. This is a computer-controlled, motorised microscope with brightfield, differential interference contrast (DIC) and widefield fluorescence imaging capabilities, allowing for multi-dimensional data acquisition. Zeiss AxioVision software was used to control microscope functions and x20 and x40 objectives were used to obtain images. Throughout this study this microscope was used for rapid visualisation and image acquisition of IF stained slides.

### **2.5.2 Nikon A1R confocal**

For imaging of immunofluorescence-stained samples at high resolution and quality, an advanced fully automated Nikon A1R confocal microscope was used equipped with a hybrid confocal scan head incorporating a resonant scanner for

high-speed imaging, and Galvano scanner for high-resolution image acquisition. The NIS-Elements C Advanced Software Platform (Nikon Instruments) was used to control microscope functions and a x20, x60 and x100x objectives were used to obtain images. Image tiling sequence was used to produce large images via stitching images of adjacent microscopic fields.

### **2.5.3 Nikon Eclipse E1000**

For imaging of immunohistochemically stained samples (without use of whole slide scanning), the Nikon Eclipse E1000 microscope was used in the study. This is a fixed-stage upright microscope configured to capture images in bright-field, phase contrast and epi-fluorescence modes. A 10x, 20x or 40x objective was used to obtain the images.

## **2.6 *In vivo* experiments**

All *in vivo* experimentation was conducted in accordance with the Animal (Scientific Procedures) Act 1986 and NCRI Guidelines. The protocols were approved locally by the University of Leeds Animal Welfare and Ethical Review Committee and project licenses for the work were issued by the Home Office: P67C4EBE, PEA0105B1, P85C8BDBF.

### **2.6.1 Mouse strain and breeding**

All mice were bred and kept at St James' Biological Services (SBS) animal facility Clinical Sciences Building, St James' University Hospital, where their welfare was maintained with the help of SBS staff.

Heterozygous *Dock4* knockout mice (Abraham et al, 2015) were maintained on C57BL/6 background through regular crossing and the pups were biopsied for genotyping at 3 weeks of age. Genotyping was carried out externally by Transnetyx (TN, USA).

*Dock4* endothelial conditional knockout mice were generated by OzGene, Australia, and crossed to *Cdh5*(PAC)-CreERT2; Rosa26-Tdtomato mice imported from the Beatson Institute, Glasgow. To generate the line Endothelial *Dock4* deletion was induced by activating the expression of Cre-ERT2 under the control of the endothelial specific *Cdh5* (encodes VE-cadherin) promoter. For Cre activation mice were injected intraperitoneally with 2mg tamoxifen for 5 consecutive days. Intracranial implantation of tumours was two weeks after cessation of tamoxifen treatment. *Cdh5*(PAC)-CreERT2; Rosa26-Tdtomato; *Dock4* fl/fl mice were used to confirm Cre activity in blood vessels following induction through staining with an antibody against RFP (recognises the TdTomato protein which is an RFP variant). Positive staining indicates that active Cre deletes the floxed STOP codon downstream of the TdTomato gene allowing expression detected by the anti-RFP antibody. Tumour samples growing in *Cdh5*(PAC)-CreERT2; *Dock4*fl/fl; Rosa26-Tdtomato (Cre+) or *Dock4*fl/fl; Rosa26-Tdtomato (Cre-) *Dock4* conditional mice were stained with anti-RFP to confirm Cre activity in the tumour blood vessels.

### **2.6.2 Intracranial implantation of cancer cells**

For intracranially implanted glioma tumours, the syngeneic murine cell line CT2A-Luc was used. 2-3 weeks prior to the planned *in vivo* experiment, CT2A cells were thawed and cultured for 2 weeks in order for them to reach exponential growth before injection. One day prior to the planned injection day, mice were briefly anaesthetised using isoflurane and their head regions were shaved using a hair clipper. A stereotaxic machine was used for intracranial injections as previously described (Lorger et al., 2009) and injections were done with two mice restrained at the same time.

Throughout the process, a source of isoflurane and oxygen generator was connected through one tube and a scavenger unit to draw out isoflurane waste was connected through another tube. Ear bars were applied to fix the heads firmly for injection and Lubrithal (Dechra) eye gel was applied to both eyes. Mice were injected with 5 mg/ml Metacam (Boehringer Ingelheim) subcutaneously and 2.5% Baytril (BAYER) intramuscularly prior to making a small skin incision on the head. The area of injection was cleaned with ethanol and Hibiscrub and was left to dry

to expose the skull. A hole was drilled 1 mm to the right of and anterior to the bregma using a surgical micro bone drill. A Hamilton syringe with 30 G needle was filled with cancer cells and injected 3 mm deep into the striatum with the stereotaxic machine ruler as a guide. 2  $\mu$ l of CT2A cells were injected 1  $\mu$ l at a time separated by a 1-minute interval and the needle was gradually withdrawn 1 mm at a time with a gap of 30 seconds apart. Lamp-heated bone wax (Medline Industries) was applied to seal the burr hole and the skin incision was glued back together using Vetbond Tissue Adhesive (3M).

Mice were left to recover at 37°C in the Small Animal Recovery Chamber before returning them to their respective cages. After 24 hours mice were again given 5 mg/ml Metacam and routinely monitored subsequently.

### **2.6.3 Irradiation**

Mice were randomised one day prior to irradiation according to the most recent IVIS readings. Mice in the treatment group received fractionated whole-brain irradiation of 5 Gy for 2 consecutive days at day 7 and 8 post tumour implantation using Small Animal Radiation Research Platform (SARRP) (Xstrahl Medical & Life Sciences). Prior to irradiation, mice were imaged using Cone Beam Computed Tomography (CBCT). The image acquired was loaded to the Muriplan treatment planning system software for dose planning, organ contouring and aligning the beam with the brain position. The beam was aligned such that the irradiation beam precisely covered the whole brain. A 10 mm<sup>2</sup> square field collimator was centred on the tumour as defined by the isocentre (the point in space through which the central ray of the radiation beam passes). This process was done under anaesthesia using isoflurane and once treatment had been completed mice were allowed to recover at 37°C in the Small Animal Recovery Chamber before being returned to their respective cages.

### **2.6.4 IVIS Imaging**

Observation of tumour growth of CT2A-Luc implanted mice was done using a non-invasive IVIS<sup>®</sup> Spectrum in vivo imaging system (PerkinElmer) twice a week with a maximum of 8 IVIS imaging per mouse in total. Mice were injected

subcutaneously with D-Luciferin Sodium Salt (Regis Technologies) and after 20 minutes mice were anaesthetised using isoflurane and imaged immediately. Resulting images were analysed using IVIS spectrum software.

### **2.6.5 Terminal Perfusion**

Depending on the experimental protocol, mice of the same group were taken down by terminal perfusion either simultaneously at a specified timepoint, or individually when a mouse developed neurological symptoms. Mice were injected intraperitoneally with 0.05  $\mu$ l of Pentobarbital and were monitored until they showed no response to the pedal reflex assessment through a hind limb toe pinch. A skin incision was made through the abdomen to expose the thoracic cavity. The heart was then firmly held using curved forceps and the right atria was clipped followed by dark venous blood flowing through the cavity. Using a 10 ml syringe and 30 G needles, mice were steadily perfused with 15 ml of cold PBS followed by 15 ml of 4% paraformaldehyde (PFA). Skin and the skull cap were removed to expose the brain and, using blunt tipped forceps, the brain was gently lifted forwards for collection. Brains were then further fixed in 4% PFA overnight at 4°C or for 6 hours for tracer injected samples.

### **2.6.6 *In vivo* sample processing**

#### **2.6.6.1 Paraffin embedding and microtome sectioning**

Mouse brains collected for paraffin embedding from *in vivo* experiments were kept in 4% PFA overnight at 4°C and transferred the next day into 70% ethanol for long term storage. Brain samples were individually transferred to tissue embedding cassettes. The tissues were processed using an automatic tissue processor which includes dehydration through a sequence of using graded ethanol, clearing using xylene, and finally wax infiltration using paraffin wax at 60°C. Cassettes were taken out of the tissue processor and were then transferred to the embedding centre to form tissue blocks. Tissue samples were taken out of the cassettes, a mould was filled with molten paraffin, and the samples were set in place with the frontal lobe facing down. A cassette was then placed on top of the mould, topped up with more wax, and placed on a cold plate to solidify. Paraffin embedded samples were stored at 4°C for long term storage.

Coronal sections of the brain were sectioned at 5  $\mu\text{m}$  thickness anterior to posterior. The brain was carefully sliced until it reached the tumour site which was visualised rapidly using quick H&E staining. Brain tumour sections were allowed to flatten out using a paraffin section mounting bath kept at 45°C. Sections were then mounted on labelled Superfrost Plus™ slides (Thermo Scientific). A minimum of 30 sections were collected. Tissues were left overnight in the slide drying incubator at 37°C and subsequently stored in microscope slide boxes at 4°C.

#### **2.6.6.2 O.C.T. frozen embedding and cryostat sectioning**

Mouse brains collected for O.C.T. embedding and freezing from *in vivo* experiments were kept in 4% PFA for 6 hours at 4°C and then transferred to 25% sucrose for 24 hours or until the tissue sank to the bottom of the falcon tubes. This was carried out to prevent tissue damage through ice crystal formations by substitution of water molecules with sucrose. Samples were washed three times in PBS for 5 minutes each time to remove sucrose. Working inside a fume hood, a small polystyrene box was filled with approximately one third full of liquid nitrogen and a small plastic container was also filled with iso-pentane (VWR International). Using large forceps, a plastic container with iso-pentane was transferred into the liquid nitrogen until the iso-pentane was half frozen. Labelled Peel-A-Way™ square embedding moulds (Sigma-Aldrich) were filled with O.C.T. compound (VWR International) and brain tissues were placed frontal lobe side down, avoiding air bubbles in the process. Using large forceps, O.C.T. moulds with tissue were transferred into the cold isopentane until the O.C.T. started to freeze while the tissue was held at the desired embedding position. Once the O.C.T. was completely frozen, the mould was transferred immediately into a Styrofoam box filled with dry ice. Frozen samples were wrapped in aluminium foil and stored at -80°C for long term storage.

Frozen brain tissue samples were sectioned using a cryostat (Leica Biosystems) set at -20°C. Coronal sections of the brain were sectioned at 10  $\mu\text{m}$  thickness anterior to posterior. The brain was carefully sliced until the tumour site was

reached, which was visualised rapidly using quick H&E staining. Sections were then mounted on labelled Superfrost Plus™ slides (Thermo Scientific). A minimum of 20 sections from each tumour was collected. Tissues were left at room temperature for 30 minutes following sectioning and wrapped in aluminium to protect from light. Slides were subsequently stored at -20°C for long term storage.

## **2.7 Statistical analysis**

Data were analysed using Microsoft Excel software (version 16.52). Statistical analysis and determination of P-values was carried out using Student's t-test. For student's t-test, a P-value of less than 0.05 was considered as statistically significant. Graphs were produced using GraphPad Prism 9 software.

# **Chapter 3**

## **Effects of radiotherapy on pathological vessel development of tumour recurrences**

### 3.1 Introduction

The high propensity of GBM tumours to recur, is one of the causes of the dismal prognosis of patients with GBM. The one distinguishing pathological feature of GBM from its lower-grade glial tumour counterparts is microvascular proliferation (Das and Marsden, 2017). Given the highly vascular nature of GBM, research into targeting the blood vessels has become significant in the field. However, despite the apparent dependence of these tumours on the vasculature, anti-angiogenic therapies such as bevacizumab, have not been promising in the clinic. Although short-term effects of ionising radiation on the tumour vasculature have been reported including increased vessel permeability, detachment from basement membrane and increased EC apoptosis (Heckmann et al., 1998; Bussink et al., 2000; El Kaffas et al., 2013), evidence on the impacts of radiotherapy on GBM recurrent tumours are still limited. In a seminal paper by Kioi et al. published in 2010, the authors suggested that vasculogenesis and not angiogenesis, is at the core of revascularisation in glioma recurrence (Kioi et al., 2010). Their study improved our understanding of the GBM recurrent vasculature and suggested revascularisation mechanisms as an alternative to angiogenesis.

Previous work in our laboratory had shown that the vasculature in GBM patient tumours is highly abnormal, characterised by Nestin positivity, and blood vessels with large lumen size. Morphologically, there was also an abundance of blood vessels with glomeruloid morphology, previously shown to contribute to worse patient prognosis (Birner et al., 2003). When quantified, those abnormalities increased in recurrent tumours in two separate patient cohorts from St. James's University hospital and Imperial Teaching hospitals. Additionally, the nestin positive blood vessels expressed the pericyte markers:  $\alpha$ -SMA and PDGFR $\beta$ .

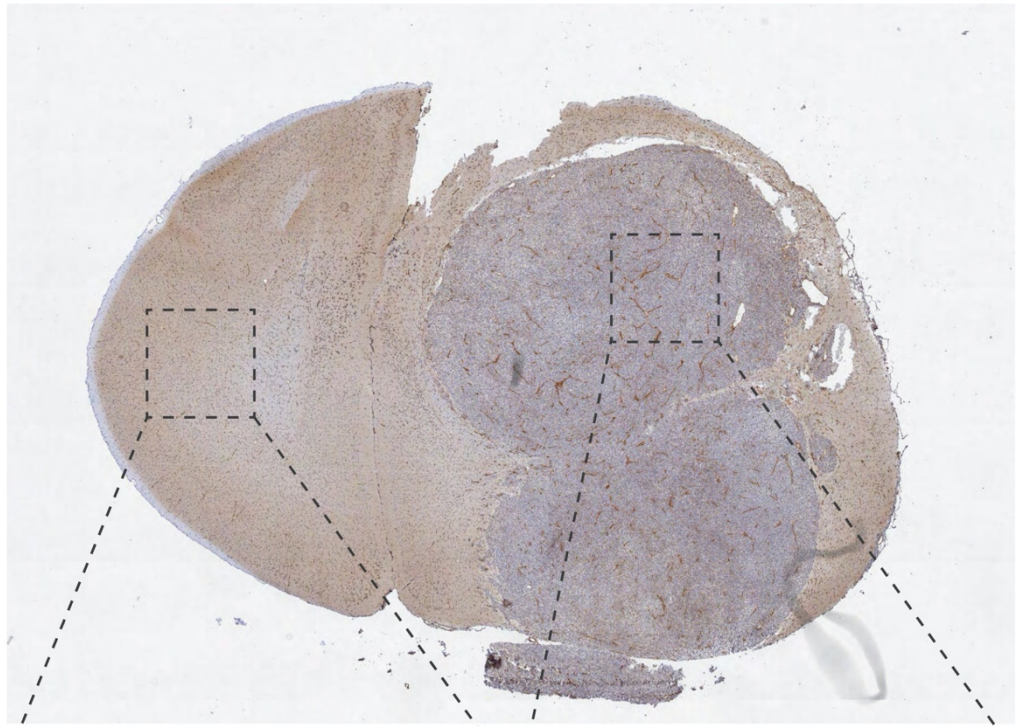
The differences seen in blood vessel pathology of the GBM patient recurrent tumours described above suggest the presence of vascular remodelling, which is a hallmark of ionising radiation injury (Gupta and Burns, 2018). Thus, it is plausible that radiotherapy may contribute to the development of blood vessel abnormalities that persist in recurrent tumours. There is growing evidence suggesting that radiotherapy-induced changes in the brain tumour

microenvironment promote tumour recurrence and aggressiveness (Gupta and Burns, 2018). Alternatively, this might be a normal progression of tumour growth. To investigate this further, an *in vivo* experiment using a clinically relevant irradiation protocol was set up and performed by Dr Tek Egnuni prior the start of this project using the CT2A syngeneic mouse glioblastoma model. During this experiment, mice were sacrificed at two timepoints, 3 days after irradiation for the purpose of understanding the early effects of radiotherapy on blood vessel morphology, and on the presentation of neurological symptoms when irradiated tumours had regrown to a tumour size similar to that of control tumours (measured by bioluminescence imaging platform IVIS). Early excised tumour samples exhibited shorter length of blood vessels, smaller blood vessel lumen size and lower percentage of vessels with detectable lumens (Egnuni et al, unpublished data). I set out to characterise the long-term effects of radiation in control (non-irradiated) tumours and tumours regrown after irradiation.

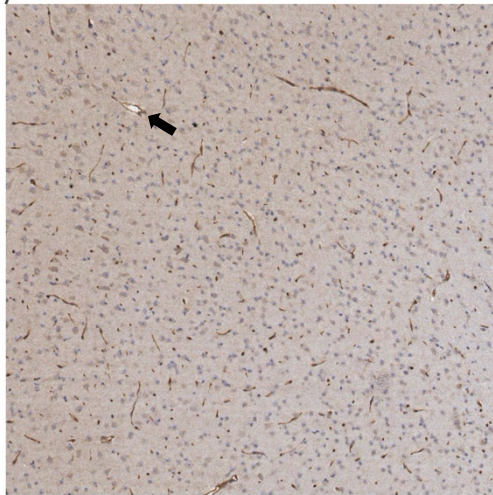
### **3.2 Characterisation of blood vessel morphology in the CT2A murine GBM model**

1 x 10<sup>5</sup> CT2A cells were injected into the striatum of 8-10 weeks old syngeneic C57BL/6 mice and tumour progression was monitored non-invasively using IVIS bioluminescence imaging. Mice were randomised into two groups based on IVIS signal intensity of D6 and one group was treated with 5Gy dose of radiotherapy for two consecutive days (7 and 8). Tumours were left to grow, and control mice were sacrificed from day 18 upon presentation of neurological symptoms. Radiotherapy treated mice were sacrificed starting from day 29 upon presentation of neurological symptoms. Tumours were excised from both groups at relatively similar sizes and IVIS signal intensity. Samples of mouse brains were subsequently processed, embedded in paraffin and serial sectioned at 5 µm thickness at the coronal plane from anterior to posterior starting from the olfactory region. Slides were stained with an anti-CD31 antibody to visualise blood vessels, counterstained with haematoxylin to visualise nuclei and scanned using Apeiro AT Virtual Slide Scanner.

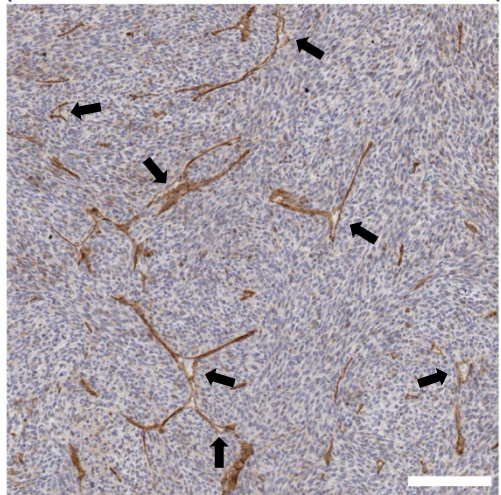
In patient GBM samples blood vessels are aberrant with distinct characteristic features: glomeruloid morphology, large lumen diameter and strong Nestin positivity (Egnuni et al, unpublished data). In the CT2A mouse tumours similar characteristics were observed. Blood vessels within the tumour showed aberrant and convoluted morphology compared to blood vessels in the normal brain as shown in Figure 3.1. Haematoxylin was used to visualise the tumour area, characterised by higher cellularity when compared to the normal brain region. The image of the normal brain area blood vessels visualised using CD31 depicts a conventional architecture of brain vasculature, with blood vessels ranging from 5-50 µm. However, a convoluted and aberrant morphology of vessels can be seen in the image of the tumour region. Sizes of the blood vessels were visually larger in the tumour region, up to around 450 µm in length, and more and larger lumens could be identified.



CD31



Normal brain



Tumour

**Figure 3.1 CT2A tumours present aberrant and convoluted vascular morphology compared to normal brain.**

1 x 10<sup>5</sup> CT2A cells were injected into the striatum of 8-10 weeks old syngeneic C57BL/6 mice and intracranial tumours were allowed to develop for a minimum of 18 days. Images show sections of tumour bearing mouse brains stained by immunohistochemistry for the endothelial cell marker CD31, and haematoxylin to mark nuclei. Images show tumour area and surrounding normal brain. Black arrows point to blood vessel lumens. Scale bar = 100  $\mu$ m.

To convert visual observations into a set of quantitative data, a list of readouts was generated shown in Table 3.1. Only the tumour region was considered for quantification over the course of the study. For measurement of lumens size the smallest lumen measured reliably under 20x magnification used for this analysis was 10  $\mu$ m. The length and thickness were considered of blood vessels over 20  $\mu$ m in length. The readouts were chosen based on the previous work on analysis of patient samples, in order to confirm that the vasculature of experimental CT2A tumours used in this project resembles that of the patient tumour vasculature. To maintain objectivity and eliminate bias, all quantifications were done blindly following image randomisation as described in the Materials and Methods Chapter (Section 2.4.1).

Selection of areas within the tumour section needed to be chosen methodically to ensure that the areas included are representative of the whole tumour area. The slides were scanned using AT Aperio Virtual Slide Scanner and visualised using ImageScope software. The numbered square tool of ImageScope was used to lay out 500 x 500  $\mu$ m (0.25 mm<sup>2</sup>) boxes covering approximately 75% of the whole tumour area as shown in Figure 3.2. Using a random number generator, five 500 x 500  $\mu$ m areas were selected and were individually captured at 20x magnification for quantification using ImageJ. Necrotic regions were excluded from the analysis. To take intra-tumoral heterogeneity into account 3 sections situated 100  $\mu$ m apart (coronal plane direction) from each brain sample were analysed.

As evident in Figure 3.3, blood vessel morphology appeared to be heterogeneous in different sections in terms of blood vessel lumen size and length. As an example, area 13 of section 2 in Figure 3.3 appeared to have blood vessels with longer length and fewer lumens with smaller diameters when compared to area 9 of section 3, which appeared to have larger lumen diameters and a higher number of blood vessels with smaller length (Figure 3.3). Figure 3.4 shows that there is quantifiable variability between the lumen sizes and number of lumens between different tumours and in different sections from each tumour. Figure 3.4 A shows that the average lumen size in sample 1 is 18  $\mu\text{m}$  with section 2 showing the highest abundance of visible lumens (14). The tumour in Figure 3.4 B shows different blood vessel morphology by no visible lumens in section 1; three lumens with a range of lumen diameters in section 2; in section 3 lumen size and abundance are more similar to sample 1 (Figure 3.4 A) with an average lumen size of 18  $\mu\text{m}$ . Lastly, sample 3 (Figure 3.4C) showed low variability of lumen size amongst different sections with average lumen size of 18  $\mu\text{m}$ . Altogether, this analysis shows a level of inter- and intra-tumoral heterogeneity in blood vessel morphologies for which reason analyses were performed using 3 mice per condition on 3 sections 100  $\mu\text{m}$  apart for each tumour.

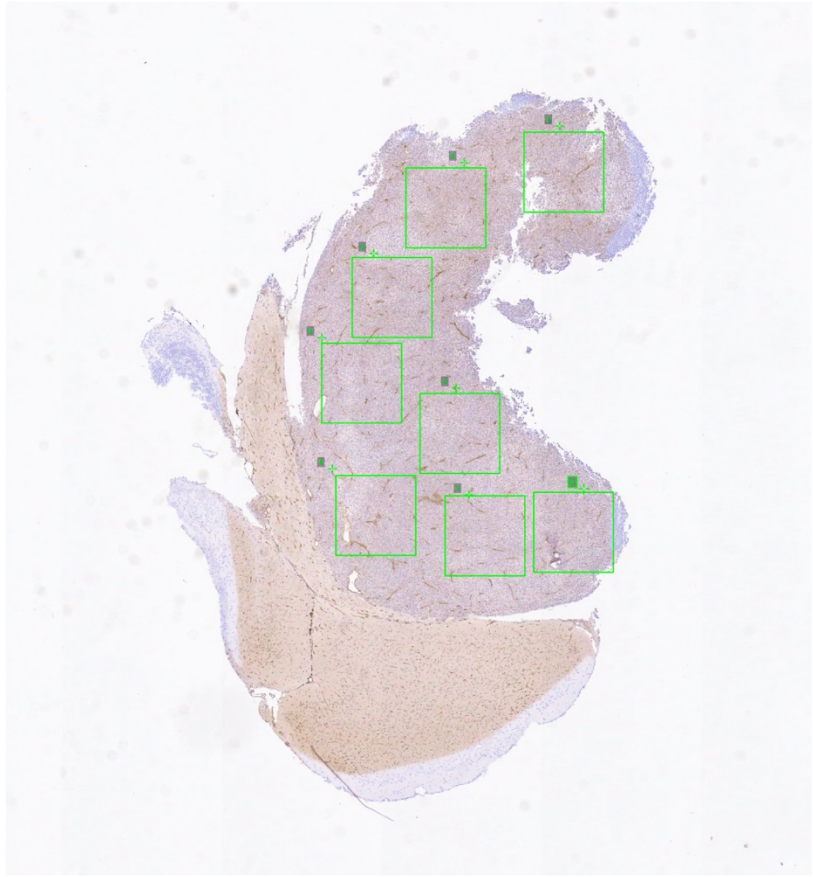
**Table 3.1 Blood vessel readouts used in the study for vascular characterisation.**

<b>No.</b>	<b>Readout</b>	<b>Definition/ Method</b>	<b>Cut-off points</b>
1.	BV area coverage	Total pixels of all vessels including visibly lumenised blood vessels per field	N/A
2.	BV lumen size	Best fit circle	Smallest size identified at 20x magnification = 10 $\mu\text{m}$ diameter
3.	% lumenisation	Visibly lumenised blood vessels as percentage of total	>10 $\mu\text{m}$ diameter
4.	BV thickness	Non lumenised blood vessels only	> 20 $\mu\text{m}$ length
5.	BV length	Individual blood vessel length	>20 $\mu\text{m}$ length
6.	Total length	Sum of all blood vessel lengths including lumenised per field	>20 $\mu\text{m}$ length
7.	Branch points	Total number of branch points per field	N/A
8.	Branch point index	Branch points divided by total length	N/A

List of readouts used for blood vessel characterisation. Blood vessels were identified on the basis of CD31 staining by immunohistochemistry and visualized at 20x magnification. Quantifications were conducted blind following image randomisation as described in Materials and Methods (Chapter 2, Section 2.4.2).

A

CD31



B

CD31

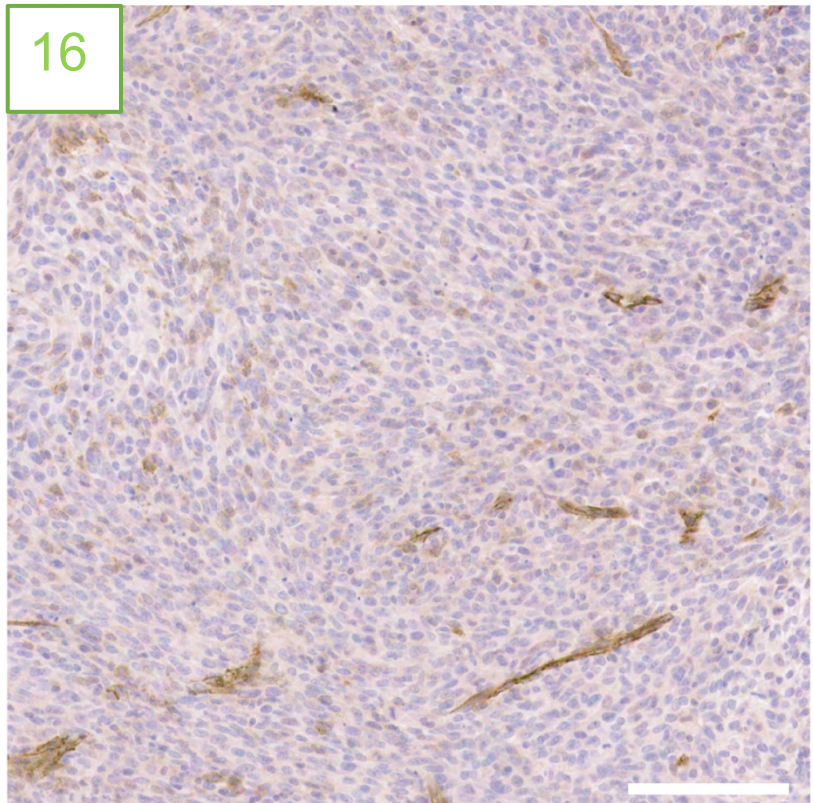


**Figure 3.2 Selection of areas within a CT2A tumour section for vascular characterisation.**

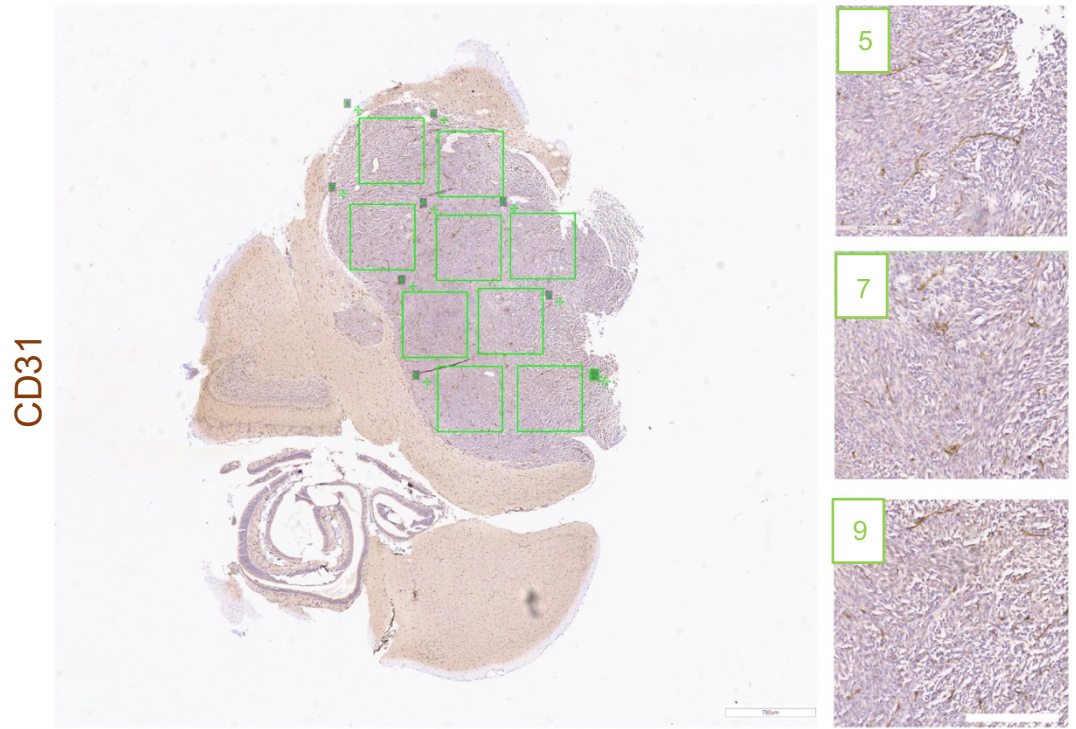
Sections of mouse brains bearing CT2A tumours were stained using the endothelial marker CD31 and haematoxylin. Slides were scanned using Aperio AT Virtual Slide Scanner and visualised using ImageScope software. The numbered square tool of ImageScope was used to define areas for quantification.

(A) Image of a scanned section with defined 500  $\mu\text{m}$  x 500  $\mu\text{m}$  areas marked cover at least 75% of the entire tumour area. Five 500  $\mu\text{m}$  x 500  $\mu\text{m}$  areas from each section were randomly selected for quantification using a random number generator.

(B) Magnified image of an example area (16) captured using ImageScope for blood vessel characterisation. Blood vessels of different lengths can be observed, and there is lack of blood vessels with visible lumens. Scale bar = 100  $\mu\text{m}$ .

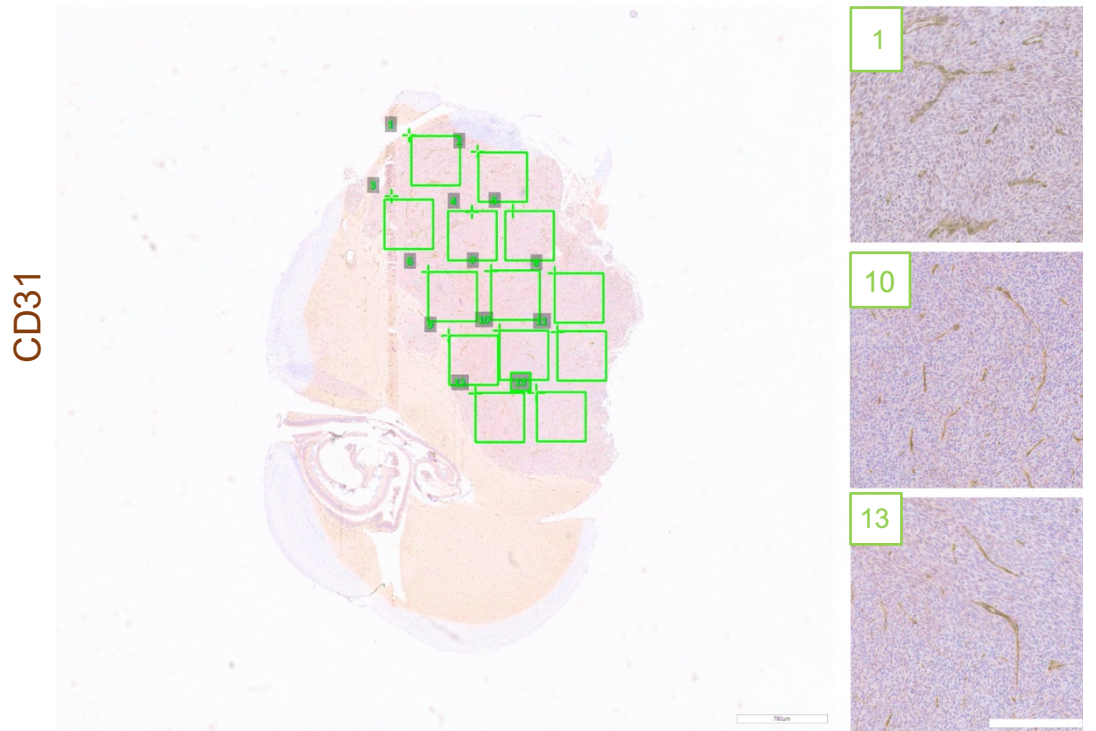
A

Section 1



B

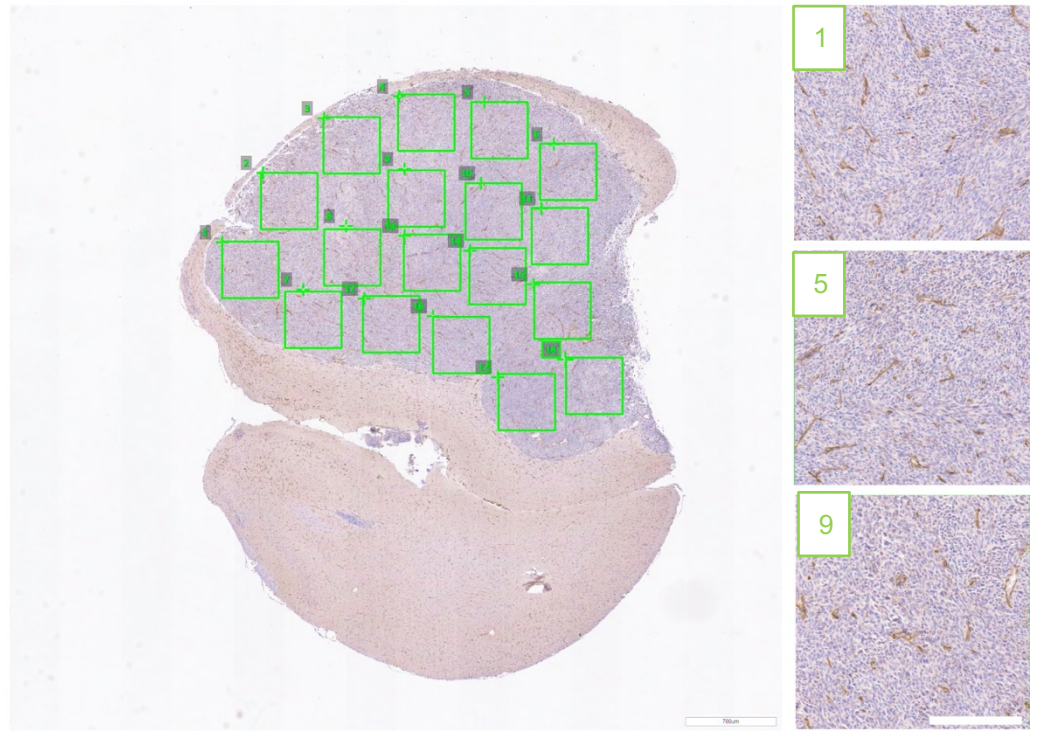
Section 2



C

Section 3

CD31



D

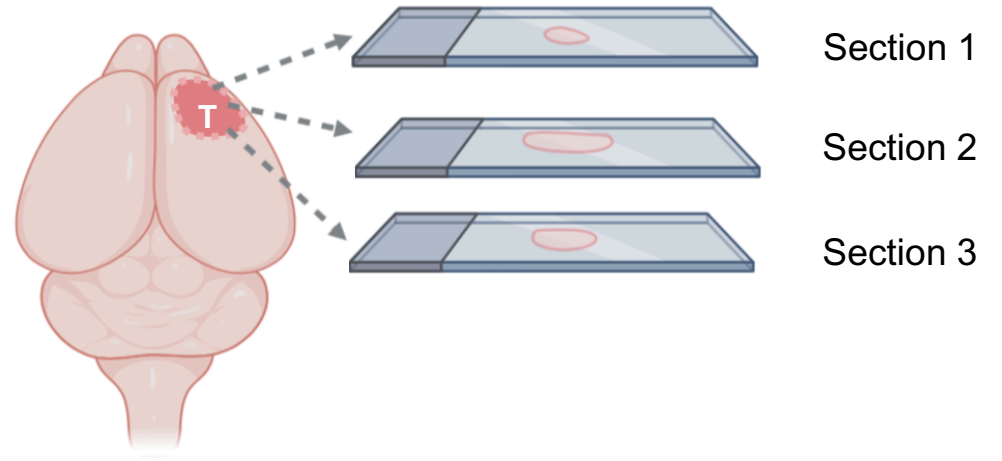


**Figure 3.3 Blood vessel morphology in different CT2A tumour sections.**

Serial sections of mouse brains bearing CT2A tumours were stained for CD31 and haematoxylin. Slides were scanned and five 500  $\mu\text{m}$  x 500  $\mu\text{m}$  areas were randomly selected for capture from each of 3 sections.

(A-C) Images show appearance of blood vessels at three different sections (A, B and C) 100  $\mu\text{m}$  apart from one mouse. Left-hand side panels show scanned slides at 1x magnification. Right-hand side panels show 500  $\mu\text{m}$  x 500  $\mu\text{m}$  areas at 20x magnification. Note the apparent variability of blood vessel length and lumenisation in different sections. Scale bar = 200  $\mu\text{m}$ .

(D) Schematic of the approximate positioning of the three sections within the tumour mass (T).



**Figure 3.4 Variability of lumen number and diameter in tumour sections and samples.**

Serial sections of mouse brains bearing CT2A tumours were stained for CD31 and haematoxylin. Slides were scanned and 500  $\mu\text{m}$  x 500  $\mu\text{m}$  areas were obtained from three different tumour sections at 100  $\mu\text{m}$  apart. The lumen diameter of all blood vessels with detectable lumen ( $>10$   $\mu\text{m}$ ) was measured.

(A-C) Dot plots of blood vessel lumen diameters in different sections of CT2A tumours growing in 3 separate control mice. The tumours had equivalent sizes as assessed by bioluminescence imaging (IVIS). Error bars represent the SEM. P-values between different sections are non-significant unless stated otherwise. n = number of blood vessels with visible lumens.

### 3.3 Irradiation of CT2A tumours

Analysis of patient samples performed previously in the lab had shown that the prevalence of abnormal blood vessel morphologies significantly increased in recurrent tumours. Recurrent tumours had larger blood vessel calibre and lumen size and there was higher abundance of blood vessels with glomeruloid morphology (Egnuni et al, unpublished data). Preliminary analysis of CT2A tumours showed both similarity and differences in the vascular morphology between patient samples and the CT2A experimental model. Despite the presence of blood vessel tortuosity in intracranial CT2A tumours (Figure 3.1) there was an absence of glomeruloid blood vessel morphology in this model that resembled patient tumour glomeruloid blood vessel architecture. Previous analyses had shown that this was similar in the GL261 intracranial model (Egnuni, unpublished data). This may be due to experimental tumours being grown to a relatively smaller size compared to human tumours, in line with the severity limits of the intracranial implantation procedure. However, potential differences between control and irradiated tumours could be analysed in terms of blood vessel abundance, lumenisation and vessel calibre.

An intracranial CT2A irradiation experiment was set up by Dr Teklu Egnuni to investigate the potential contribution of radiotherapy on increased blood vessel abnormality, which was previously observed in the patient recurrence samples (Chapter 1, Section 1.11). As shown in Previous work leading to this thesis section (Chapter 1, Figure 1.9), on day 0 CT2A cells ( $1 \times 10^5$ ) were injected into the striatum of 8-10 weeks old syngeneic C57BL/6 mice. On days 7 and day 8 the radiotherapy group mice were treated with 5Gy dose of whole-brain radiotherapy on each day using Small Animal Radiation Research Platform (SARRP) and tumours were left to regrow. Tumour growth was monitored using IVIS. Two groups were set up, early and late excision, in which early excised tumours were sacrificed 4 days post-radiation. Late excised tumours were sacrificed at the onset of neurological symptoms starting from day 18.

Analysis was then required of tumours that had been allowed to regrow post irradiation to assess the potential involvement of radiotherapy in the vascular

abnormality of patient recurrent tumours. The schematic in Figure 1.9 shows the treatment and excision timepoint of the 'late' excised tumours that were analysed in this study. Control unirradiated tumours were taken from day 18 post implantation on presentation of neurological symptoms. Radiotherapy treated tumours were then taken individually starting on day 29 also upon the presentation of neurological symptoms. Control and radiotherapy treated tumours were excised at relatively similar sizes according to IVIS bioluminescence imaging readings. I contributed to the experiment from the onset of processing of mouse brain tumour samples, paraffin embedding, and sectioning at the coronal plane starting from the olfactory bulb.

Table 3.2 shows the list of samples analysed in this study. The excision days are shown of control and irradiated mice together with IVIS signal intensity on the day of excision. Throughout this report, the use of the terms 'radiotherapy treated tumours' and 'regrown tumours' may be used interchangeably. However, both terms refer to the same group of regrown tumours post radiotherapy treatment.

**Table 3.2 List of CT2A tumour control and irradiated tumour samples for the investigation of the effects of radiotherapy on vascularisation.**

<b>Mouse ID</b>	<b>Age at intracranial implantation (weeks)</b>	<b>Sex</b>	<b>Irradiation</b>	<b>Tumour excision day post injection</b>	<b>Final IVIS signal (D18)</b>	<b>Neurological symptoms (Y/N)</b>
653	8	F		19	1.56E+08	Y
743	8	F		18	5.78E+06	Y
692	8	F		19	2.25E+08	Y
702	10	F	X	29	3.63E+06	Y
673	9	F	X	35	2.11E+06	Y
691	8	F	X	35	1.38E+06	Y

List of late excised samples used for blood vessel characterisation of control and regrown tumours in this study including sex, age at injection, treatment, excision days and date, and presence of neurological symptoms.

### **3.4 Increased angiogenesis and lumenisation in radiotherapy treated regrown tumours**

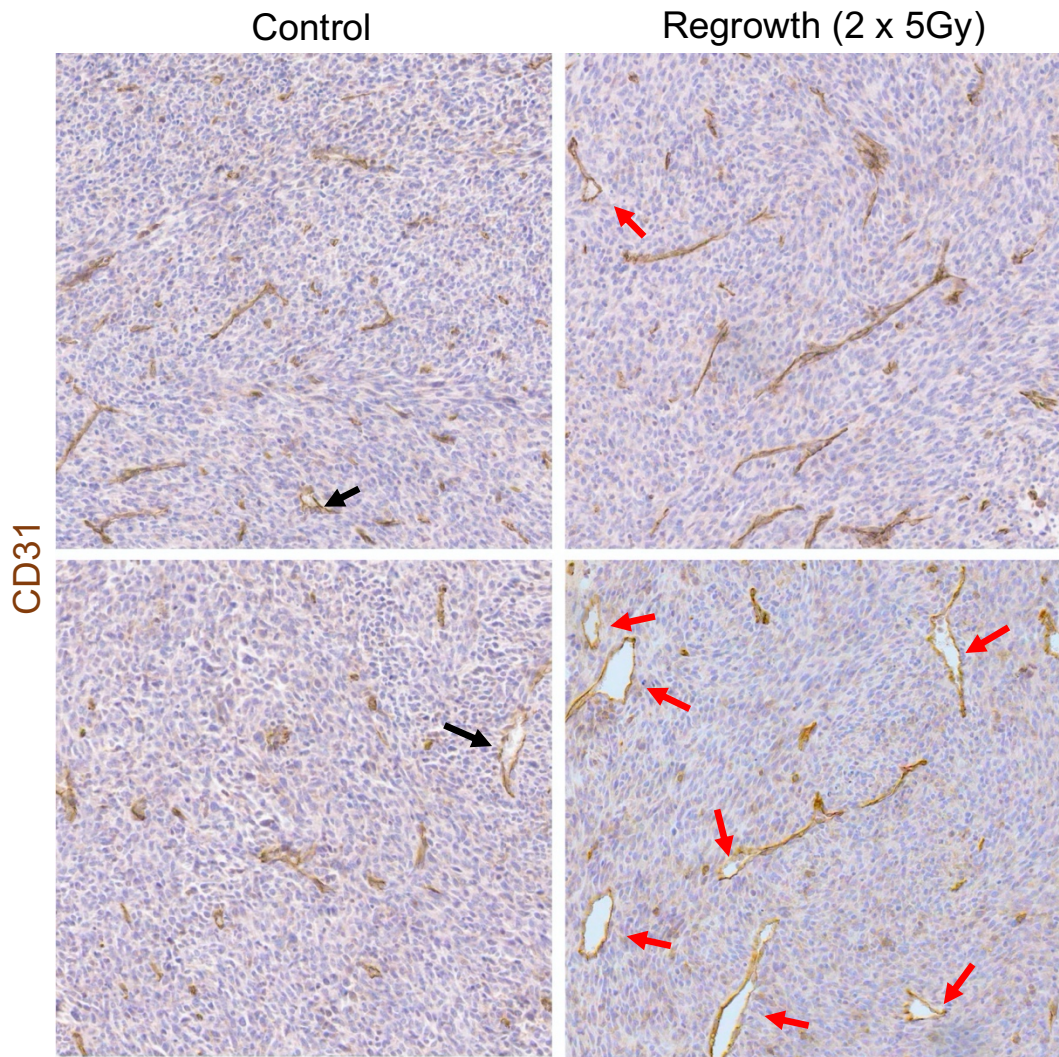
Control and radiotherapy treated tumours were sectioned and stained by immunohistochemistry with an antibody against CD31 for blood vessel visualisation. Figure 3.5 shows four 500  $\mu\text{m}$  x 500  $\mu\text{m}$  areas used in the quantification that represent the discernible differences between the blood vessels in the control and radiotherapy treated regrown tumours. Control tumours in the figure appears to have a much lesser number of visibly lumenised blood vessels, while the majority of the blood vessels are shorter in length and also have less branches. Blood vessels in radiotherapy treated tumours on the other hand appeared to have a higher number of visible lumens, larger lumen size, larger length of individual blood vessels, and they appeared more branched.

Visually, the blood vessels in the radiotherapy treated regrown CT2A tumours displayed a similar phenotype to the blood vessels in the recurrent patient tumour samples (Egnuni, T., PhD Thesis). Visual observations were taken further into quantification based on the criteria in Table 3.1. Using this approach, as shown in Figure 3.6, aligned with the initial observation, subsequent quantification shows that there was a significant increase in the percentage of blood vessels with visible lumens in the radiotherapy treated regrown tumours compared to unirradiated controls. The radiotherapy treated tumours relative to the control tumours showed over twice the degree of lumenisation of blood vessels. Furthermore, when individual lumens were analysed the blood vessels in radiotherapy-treated tumours had lumen sizes significantly larger than blood vessels in untreated controls (Figure 3.6B). The mean lumen size was 16.9  $\mu\text{m}$  for control and 24.1  $\mu\text{m}$  for radiotherapy-treated tumours. Taking these two into account, when lumen size was quantified for blood vessels with 10-20  $\mu\text{m}$  diameter and diameter larger than 20  $\mu\text{m}$ , the percentage of blood vessel possessing smaller lumen size did not differ significantly between control and regrown tumours. In contrast, the percentage of blood vessels with lumen size larger than 20  $\mu\text{m}$  was significantly higher in the radiotherapy-treated tumours (Figure 3.6). Taken together these data shown that radiotherapy not only

increased the formation of blood vessels with visible lumens, but the sizes of those lumens were also markedly larger.

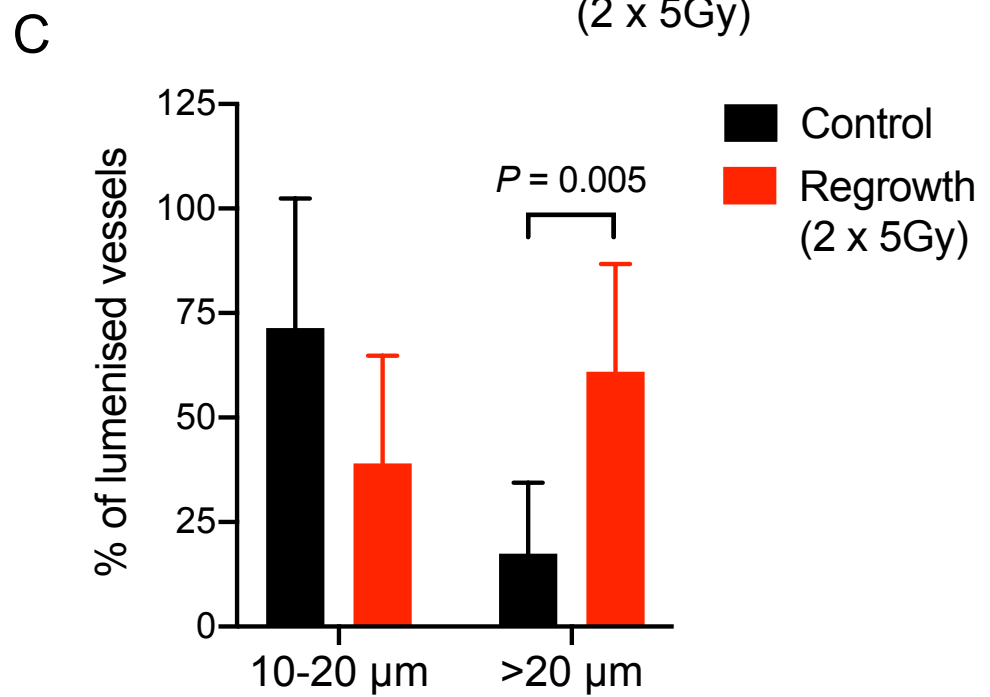
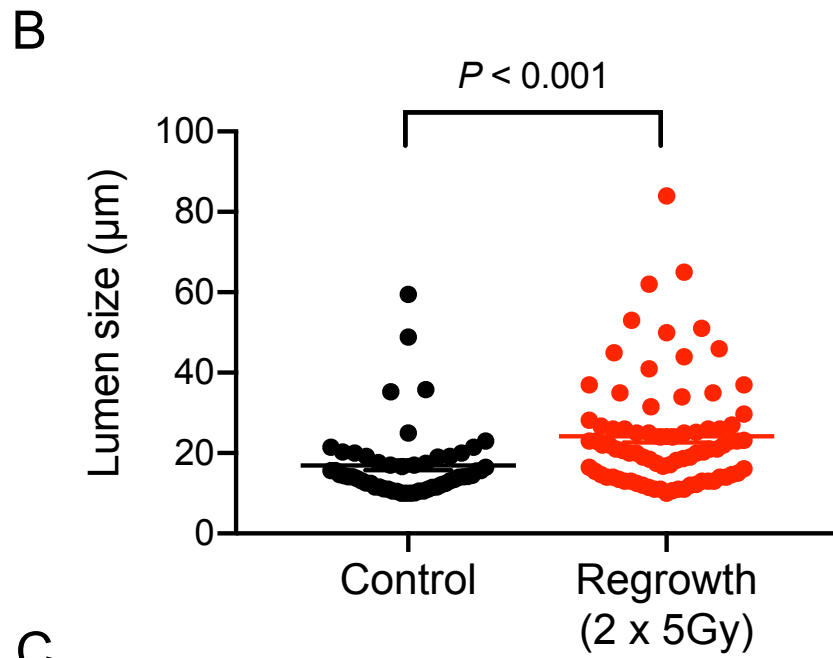
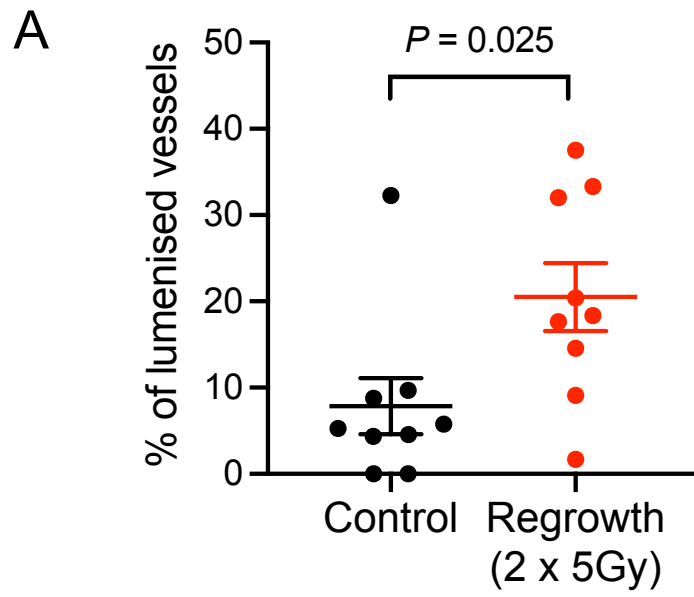
Apart from size and prevalence of blood vessels with visible lumens, another characteristic that was distinguishable in the recurrent patient samples was blood vessel length and area covered by blood vessels. Figure 3.7 A shows that there was a significantly higher overall vessel area coverage per 500  $\mu\text{m}$  x 500  $\mu\text{m}$  area in the regrown irradiated tumours compared to control. Vessel area coverage was calculated as the total tumour area covered by blood vessels including visibly lumenised blood vessels (Table 3.1). Vessel area coverage for control and for irradiated tumours were 29,669.9 and 40,207.7 ( $10^4$  pixels per 1.25  $\text{mm}^2$ ), respectively, equating to an increase of 35.5% in surface area following irradiation and regrowth. Figure 3.7B also shows that irradiation resulted in a statistically significant longer length of blood vessels with an average of 90.5  $\mu\text{m}$  for irradiated tumours and 66.7  $\mu\text{m}$  for control tumours corresponding to an increase of 35.7%. Another important characteristic of vascularisation is the thickness and branching of blood vessels (Blanco and Gerhardt, 2013). As seen in Figure 3.8 A there was no significant difference in terms of blood vessel thickness between control and irradiated tumours. The thickness of blood vessel of control tumours averages at 9.2  $\mu\text{m}$  whereas the average thickness of irradiated tumour blood vessels was 8.6  $\mu\text{m}$ . The branching point index was measured as the number of branches per total vessel length within a microscopic field (Table 3.1).

Figure 3.8 B shows that there is no significant difference between the branch point index of control versus radiotherapy treated regrown tumours. Altogether, the quantifications conducted show that there is an increase in the overall area covered by blood vessels in the radiotherapy treated regrown tumours compared to untreated controls due to the greater size and prevalence of lumenised vessels and longer blood vessel lengths. Therefore, not only the blood vessels with visible lumens in the irradiated tumours are larger, but there also appears to be an increase in vascularisation in the radiotherapy treated regrown tumours.



**Figure 3.5 Representative images of CT2A blood vessel morphology in control and radiotherapy treated regrown tumours.**

Serial sections of late excised mouse brains (day 18 onwards post-implantation) bearing CT2A tumours were stained for CD31 and haematoxylin. Representative images of 500  $\mu\text{m}$  x 500  $\mu\text{m}$  tumour areas from 2 different sections are shown to highlight the differences in blood vessel morphology between untreated control and irradiated regrown tumours. Note that blood vessels are longer and with more lumens in the irradiated tumours. Arrows indicate lumens in control tumours (black) and irradiated tumours (red). Scale bar = 100  $\mu\text{m}$ .



**Figure 3.6 Increase in blood vessel lumenisation and lumen size in radiotherapy treated regrown tumours.**

Blood vessel lumenisation and lumen size in control and radiotherapy treated regrown tumours were quantified using ImageJ from scanned slides of three different tumour sections at 100  $\mu\text{m}$  distance.

(A) Dot plot shows significant increase in percentage of blood vessels with lumens in radiotherapy treated tumours compared to untreated controls.

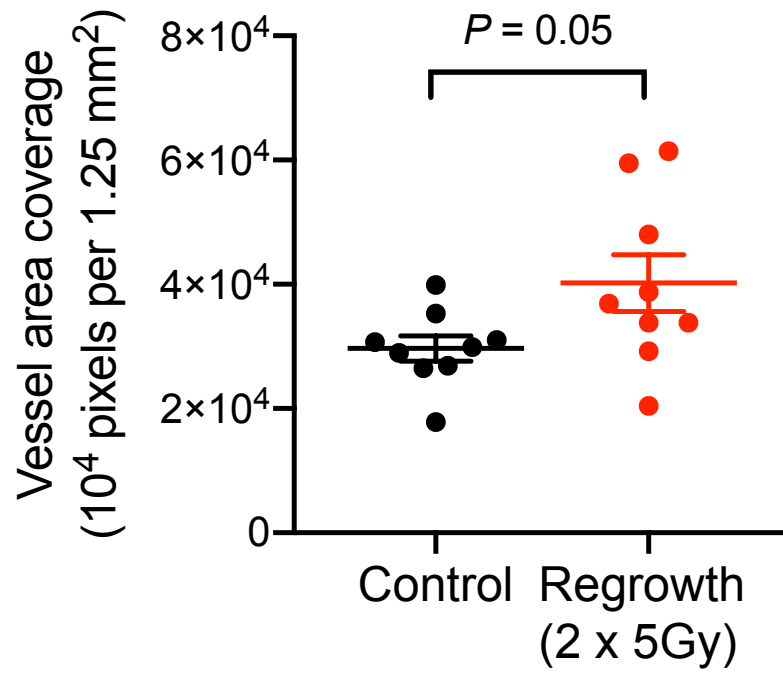
(B) Dot plot shows significant increase in lumen diameter in radiotherapy treated tumours compared to control.

(C) Bar chart shows the percentage of blood vessels with lumens with the indicated diameters. Graph shows a significant difference between the percentage of vessels with lumens of  $>20 \mu\text{m}$  in control versus radiotherapy treated tumours.

A and C: n = number of sections quantified from 3 mice per condition: control = 9, radiotherapy = 9. Each value the average of 5 randomly selected  $500 \times 500 \mu\text{m}$  areas.

B: n = total number of blood vessels with visible lumens quantified from 3 mice per condition: control = 55, radiotherapy = 81.

A



B

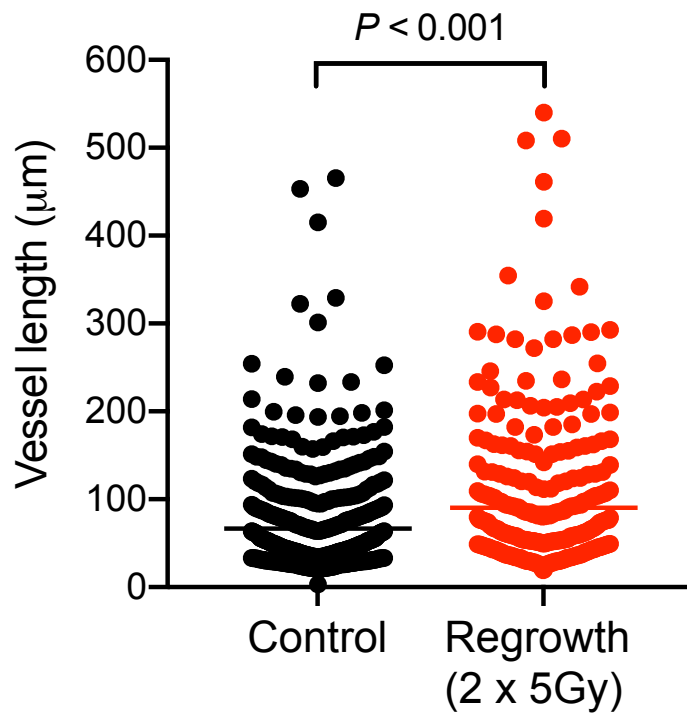


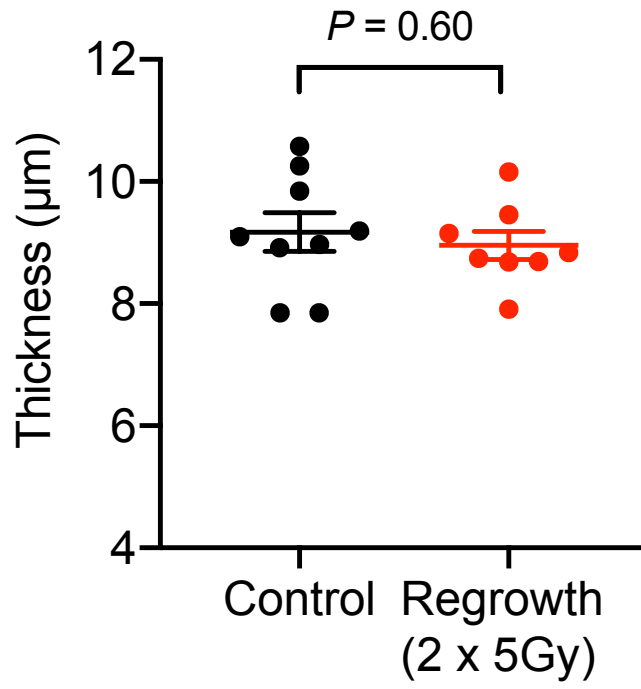
**Figure 3.7 Radiotherapy increased blood vessel length and surface area in regrown tumours.**

Blood vessel area coverage and vessel length were quantified in control and radiotherapy treated regrown tumours using ImageJ from scanned slides from three different tumour sections 100  $\mu\text{m}$  apart.

(A) Dot plot shows an increase in vessel area coverage in radiotherapy treated tumours compared to unirradiated controls. n = number of sections per group quantified from 3 mice per condition: control and radiotherapy = 9. Each value the average of 5 randomly selected 500 x 500  $\mu\text{m}$  areas.

(B) Dot plot shows significant increase in blood vessel length in radiotherapy treated tumours compared to unirradiated controls. n = number of blood vessels quantified from 3 mice per condition: control = 574, radiotherapy = 346.

A



B

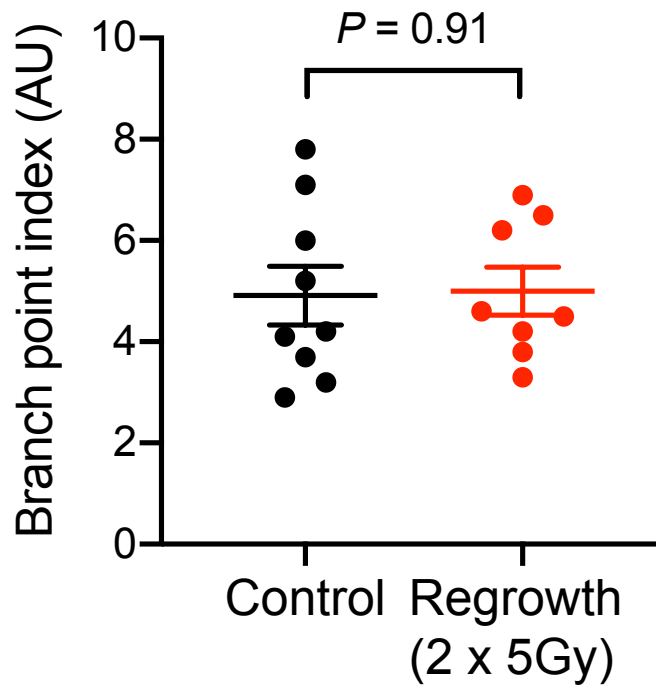


**Figure 3.8 Radiotherapy affects neither the thickness of the vessel wall nor the branching of blood vessels.**

Blood vessel thickness and branching were quantified in control and radiotherapy treated regrown tumours using ImageJ from scanned slides of from three different tumour sections 100  $\mu\text{m}$  apart.

(A) Dot plot shows no significant difference in the thickness of blood vessels in radiotherapy treated tumours compared to unirradiated controls.

(B) Dot plot shows no significant difference in the branch point index between radiotherapy treated tumours compared to unirradiated controls.

n = number of sections per group quantified from 3 mice per condition: control = 9, radiotherapy = 8. Each value the average of 5 randomly selected 500 x 500  $\mu\text{m}$  areas.

### **3.5 Increased F4/80 positive areas in radiotherapy treated regrown CT2A tumours**

Tumour associated macrophages (TAMs) not only play a significant role in immunity but may also promote tumour growth through their influence of tumour angiogenesis. TAMs are distinct from brain microglia with regards to their origin and where they reside. Whereas microglia are resident in the brain, TAMs infiltrate the tumour from the blood stream and tend to reside in the hypoxic niche mainly in the centre of the tumour mass where they are attracted through HIF-1 $\alpha$  activation (Darmanis et al., 2017). In various solid tumours including brain and breast cancers, it has been shown that TAMs accumulate in these hypoxic regions post-vessel abrogation from stress signals such as irradiation and trigger a proangiogenic cascade (Reviewed in Ribatti et al., 2007).

Therefore, given the observed increase in vascularisation in the irradiated tumours, an analysis of the abundance of macrophages in the control and irradiated regrown tumours was conducted. Sections were stained with the major macrophage and microglia marker F4/80 by immunohistochemistry. Due to time constraints, only one section from each tumour was quantified. Figure 3.9 A shows representative images of the F4/80 positive areas in unirradiated control tumours and B in irradiated regrown tumours. As shown, the control tumours have small number of cells positive for F4/80. In contrast, irradiated regrown tumours exhibit a much higher abundance of F4/80 positive cells, and the F4/80 antibody staining is stronger as compared to control tumours.

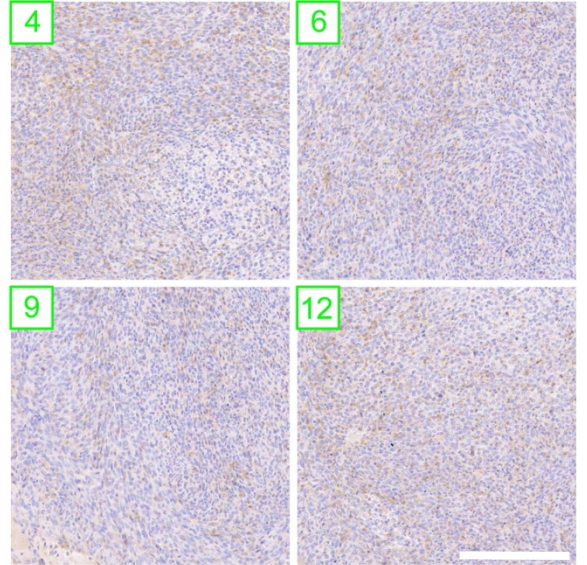
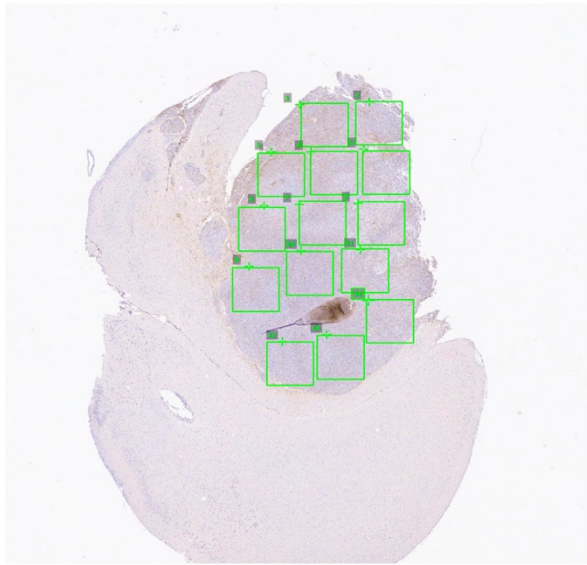
Using the Aperio Positive Pixel Count algorithm on ImageScope software, an automated quantification was possible. Positive Pixel Count algorithm automatically quantifies the amount of a specific stain present in a scanned slide image in pixels, and this was used to quantify more accurately F4/80 positive areas. The algorithm outputs four distinct categories of antibody staining: negative, low positivity, positive and high positivity. Although only one section from each tumour was quantified, as shown on Figure 3.9 C, irradiated regrown tumours showed significant increase in F4/80 positive areas in irradiated tumours compared to untreated controls ( $P = 0.05$ ). These data suggest that increased

macrophage activation in recurrent tumours post radiotherapy may play a role in the development of the aberrant vasculature of recurrent tumours.

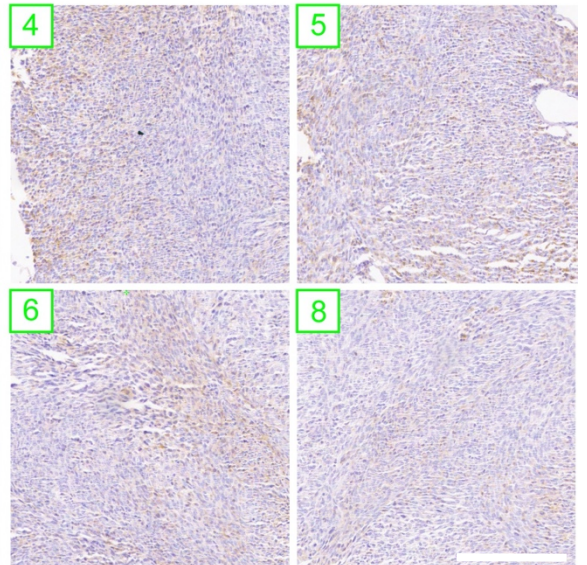
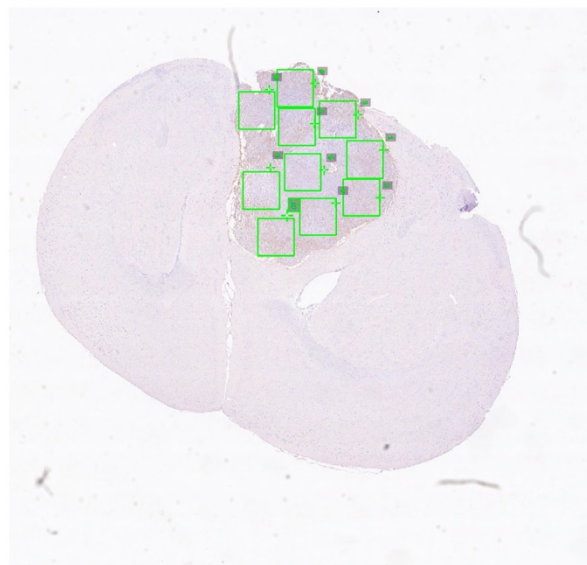
A

Control

F4/80



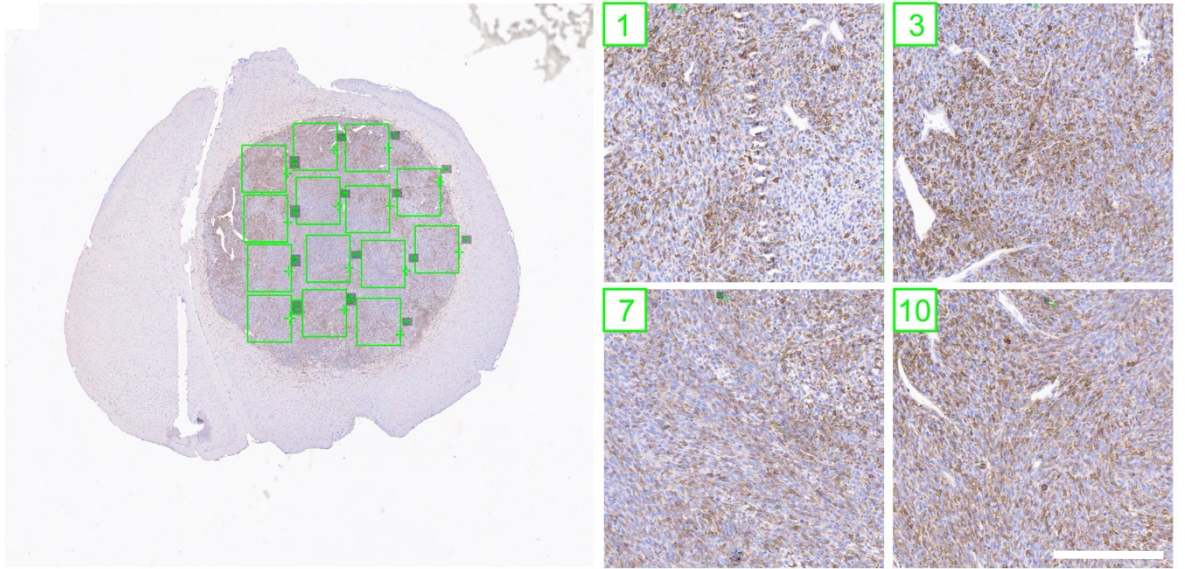
F4/80



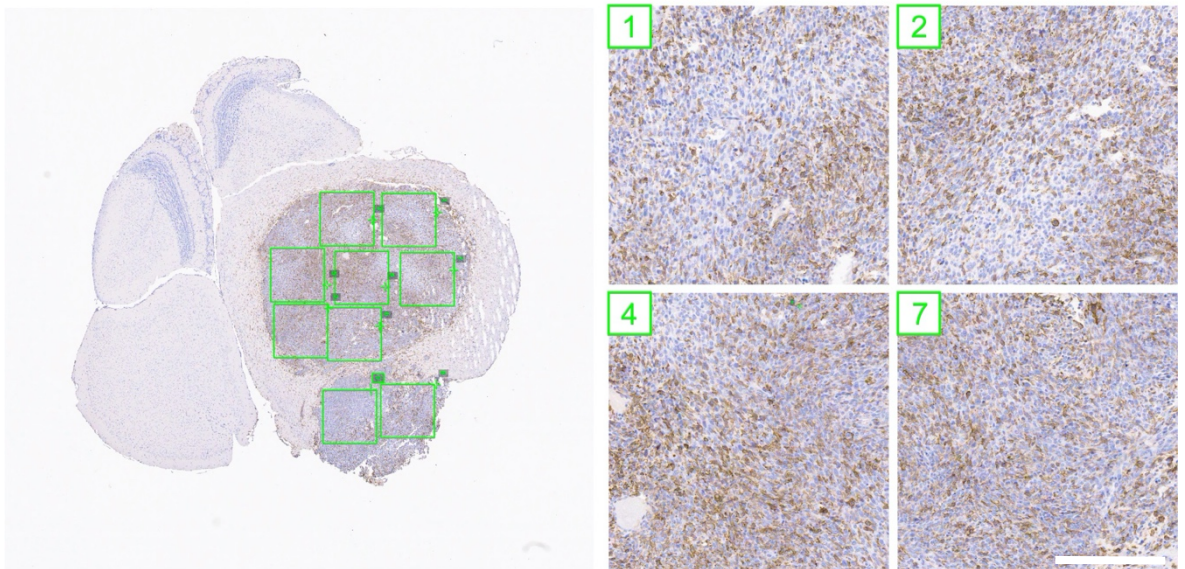
**B**

Regrowth (2 x 5Gy)

F4/80



F4/80



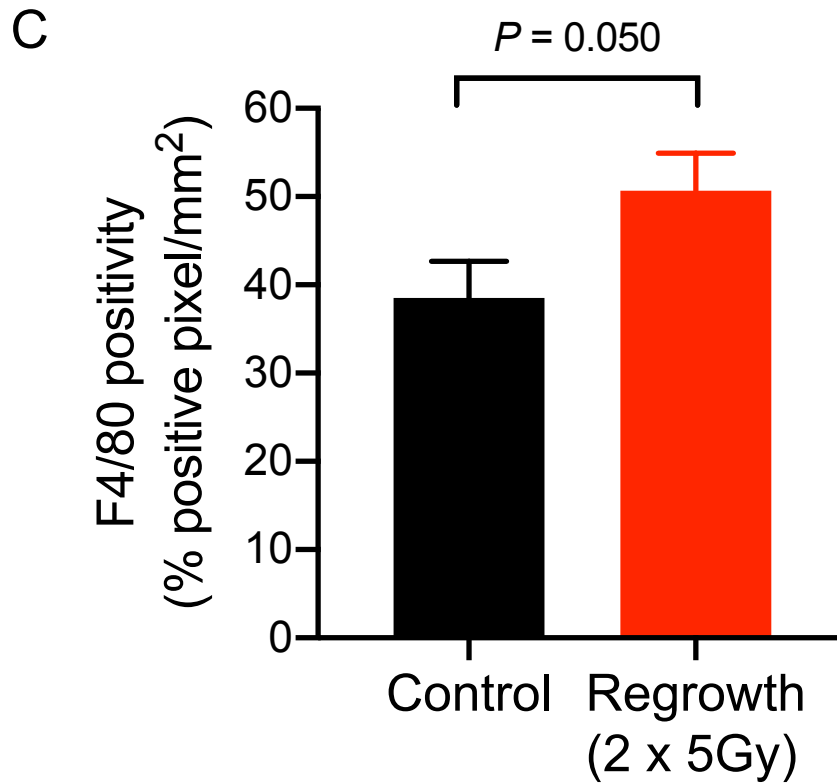


**Figure 3.9 Higher F4/80 positive areas in radiotherapy treated regrown tumours.**

Sections of late excised mouse brains bearing CT2A tumours were stained using F4/80 antibody and haematoxylin. Whole slides were scanned, and quantifications were conducted using Aperio Positive Pixel Count algorithm of ImageScope software. Algorithm output gives staining positivity based on four distinct categories: negative, low positivity, positive and high positivity.

(A, B) Representative images of CT2A tumour sections stained with F4/80 antibody taken at 1x (left panel) and 20x (right panel) magnification of control and regrown post radiotherapy CT2A tumours.

(C) Dot plot shows an increase in F4/80 positive areas in radiotherapy treated mice compared to unirradiated control. Sum of area positive with F4/80 staining are included in this graph.  $n =$  number of  $500\ \mu\text{m} \times 500\ \mu\text{m}$  areas quantified from 3 mice per condition: control = 15, radiotherapy = 14.

### 3.6 Summary

In this chapter, I used an orthotopic CT2A glioma model to investigate changes in blood vessel morphology and abundance in tumours regrown post-delivery of clinically relevant fractionated radiation. Using the endothelial cell marker CD31, I initially compared the CT2A tumour blood vessels to the normal brain blood vessels. Tumour blood vessels were larger, aberrant, and convoluted compared to the normal brain blood vessels. To consider intra- and inter-tumoral heterogeneity of each of the tumours, an analysis was then conducted to look at the differences in blood vessel morphology at different areas of the tumour and in different tumours. Three sections at 100  $\mu\text{m}$  apart, were selected and analysis showed that there is variability amongst those areas, as there was variability amongst the different tumours analysed. This was important to consider as intra-tumoral heterogeneity is a classic characteristic of GBM. Similarly, in the *in vivo* model, I observed that different regions of the tumour had distinct blood vessel morphology, with different patterns from one tumour to another. Thus, taking account of different sections provides a more accurate analysis of the blood vessel characteristic of the tumour. Next, I characterised the vessel morphology of control unirradiated and regrown irradiated tumours. Irradiation was based on a published model of glioblastoma regrowth post fractionated radiotherapy delivered at 2 x 5Gy dose (Kioi et al., 2010). A set of readouts for quantification were blood vessel area coverage, lumen size, vessel length, branching and thickness.

Quantifications conducted blind with respect to the identity of the samples revealed a significant increase in blood vessel lumenisation, lumen size, blood vessel length and overall blood vessel area coverage. In recurrent patient tumours, parallel to the experimental model, the same trend of augmentation of these blood vessel traits was also observed supporting the hypothesis that radiotherapy contributes to the development of blood vessel abnormalities in recurrent tumours. In addition, I also investigated another key player in the GBM tumour microenvironment that may influence angiogenesis, tumour associated macrophages (TAMs). The quantifications showed that there was an increase in F4/80 positive macrophage expression in the radiotherapy-treated regrown tumours.

There are some limitations in the data presented in this chapter with respect to sample size. Although the analysis differences in morphology of control and regrowth tumours are striking, ideally, a repeat experiment would have been advantageous to confirm these phenotypes. In reference to the macrophage data, analysis of additional tumour sections would have been advantageous. It is important to take into account intra-tumoral heterogeneity and including more sections to the analysis would provide a better understanding of the degree of macrophage infiltration post radiotherapy in this model. In addition, methodologically, implementing a more quantitative method such as flow cytometry would be useful in providing further information on macrophage abundance and numbers, rather than stained area.

In the following chapter further vessel abnormality in the regrown tumours is further analysed, in the context of blood vessel pericyte coverage, permeability and hypoxia status.

## **Chapter 4**

# **Effects of radiotherapy on blood vessel maturation, permeability, and hypoxia**

## 4.1 Introduction

Another characteristic observed in the recurrent GBM patient tumours was increased coverage by Nestin positive,  $\alpha$ -smooth muscle actin ( $\alpha$ -SMA) positive pericyte/ smooth muscle cells. The presence of pericyte coverage is a hallmark of vessel maturation (Armulik et al., 2005). In developmental angiogenesis, pericyte recruitment to blood vessels occurs in the later stages of the angiogenic cascade that results in blood vessel stabilisation and maturation (Herbert and Stainier, 2012). Pericytes contribute to blood vessel maturation through their physical interaction endothelial cells providing mechanical stability, and through the release of growth factors acting via paracrine signalling pathways (Bergers and Song, 2005). A study by Armulik et al. utilised the PDGF-B retention motif knockout (*Pdgfb*<sup>ret/ret</sup>) to generate a pericyte-deficient mutant mouse model. They demonstrated in the study that lack of pericytes in mice during development results in extravasation of plasma proteins from the brain vasculature, due to breakdown of the blood brain barrier (BBB) (Armulik et al., 2010).

In tumours, studies have shown that pericytes play a role in blood vessel stability and permeability (Östman and Corvigno, 2018); however, in cancer, irregular pericytes are frequently observed. It has been reported that in tumours pericytes are commonly loosely associated with the blood vessels and are lower in abundance (Benjamin et al., 1998; Morikawa et al., 2002). A study by Zhou et al. has shown that, pericyte density is correlated with poor GBM patient prognosis; and chemotherapeutic efficacy can be improved by targeting glioma stem cell-derived pericytes (Zhou et al., 2017). Furthermore, pericytes enhance GBM chemoresistance to temozolomide through CCL5-CCR5 paracrine signalling (Zhang et al., 2021). These findings highlight the capacity of pericytes in maintaining an advantageous niche for GBM tumour survival and influencing the outcome of therapies for GBM.

In the patient samples, the abundance of pericytes was augmented in the recurrent patient samples (Egnuni et al., unpublished data). Thus, I sought to investigate whether the increase in pericyte abundance was due to irradiation. Following optimisation pericytes in tumour sections were marked with an antibody against  $\alpha$ -SMA. Pericyte-positive blood vessels were then quantified in the

untreated control, and the regrown post radiation treatment tumours. To investigate whether any observed changes in pericyte association influenced permeability, I set up experiments injecting intravenously fluorophore-conjugated bovine serum albumin (BSA) as a tracer to assess blood vessel permeability. Tracer positive pixels around blood vessels were measured using Image J software, while tracer abundance the mouse livers was used as a tracer injection control. To understand the impact of any differences in permeability on blood vessel functionality, I concluded this part of the study by analysing tumour hypoxia by staining the tumours for the hypoxia marker GLUT1 (Mayer et al., 2012).

## **4.2 Characterisation of $\alpha$ -SMA+ cells/pericytes in the intracranial CT2A glioblastoma tumour implantation model**

In order to investigate a potential effect of radiotherapy on mural cell/ pericyte recruitment and blood vessel maturation it was necessary to use an established marker that would detect pericytes in the CT2A tumour model used in the experiment. Although there is a multitude of markers available to identify pericytes, a single pericyte-specific marker has not been identified as yet, potentially due to variability in different organs and different stages of blood vessel development (Armulik et al., 2005; Armulik et al., 2011). In this study  $\alpha$ -SMA was chosen as a tumour pericyte marker. Although absent in quiescent pericytes in normal tissues,  $\alpha$ -SMA is a useful marker for pathological conditions such as tumour angiogenesis and inflammation (Gerhardt and Betsholtz, 2003), and has been shown to readily mark brain tumour vascular pericytes and SMCs (Armulik et al., 2011; Zhou et al., 2017). Furthermore,  $\alpha$ -SMA has been shown to detect pericytes in the GL261 model of glioma (Reis et al., 2012).

As anti- $\alpha$ SMA staining using two different antibodies was non-specific in its application using immunohistochemical staining as shown in Figure 4.1, further optimisation was necessary using a different  $\alpha$ -SMA antibody and immunofluorescence staining (IF). After trial of commonly used endothelial cell markers CD31, CD34 and Endomucin for use in IF (Figure 4.2) a cocktail antibody of CD34 and Endomucin (denoted as CD34/Endomucin) was used in all IF experiments for blood vessel visualisation, due to its specificity, lack of background staining, and ability to stain small capillary blood vessels in the normal brain (non-tumour area). Double IF with CD34/Endomucin and  $\alpha$ -SMA (Sigma-Aldrich, C6198) showed that  $\alpha$ -SMA positive cells were readily detectable in intracranial CT2A tumours (Figure 4.3).

#### 4.2.1 Optimisation of $\alpha$ -SMA staining

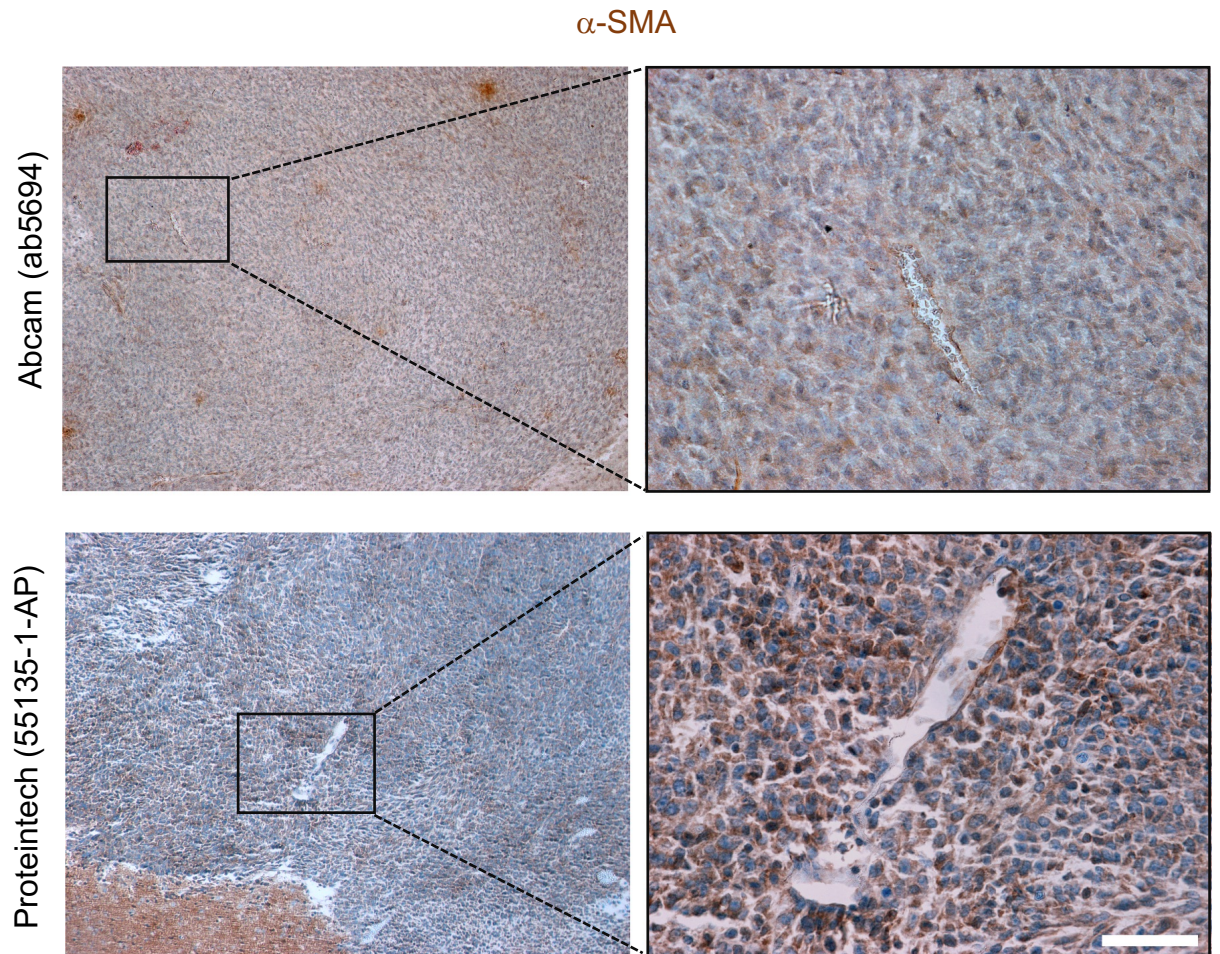


**Figure 4.1  $\alpha$ -SMA<sup>+</sup> cells could not be detected by immunohistochemistry in CT2A tumours.**

Sections of mouse brains implanted with CT2A tumours were stained for  $\alpha$ -SMA using different antibodies and counterstained with haematoxylin. Images of stained sections were captured at 10x and 40x magnification using a Nikon Eclipse 1000 microscope and ImageJ software was used for visualisation. Shown are representative images. Note that the staining detected is non-specific. Scale bar = 200  $\mu$ m.

Tumour

Normal Brain

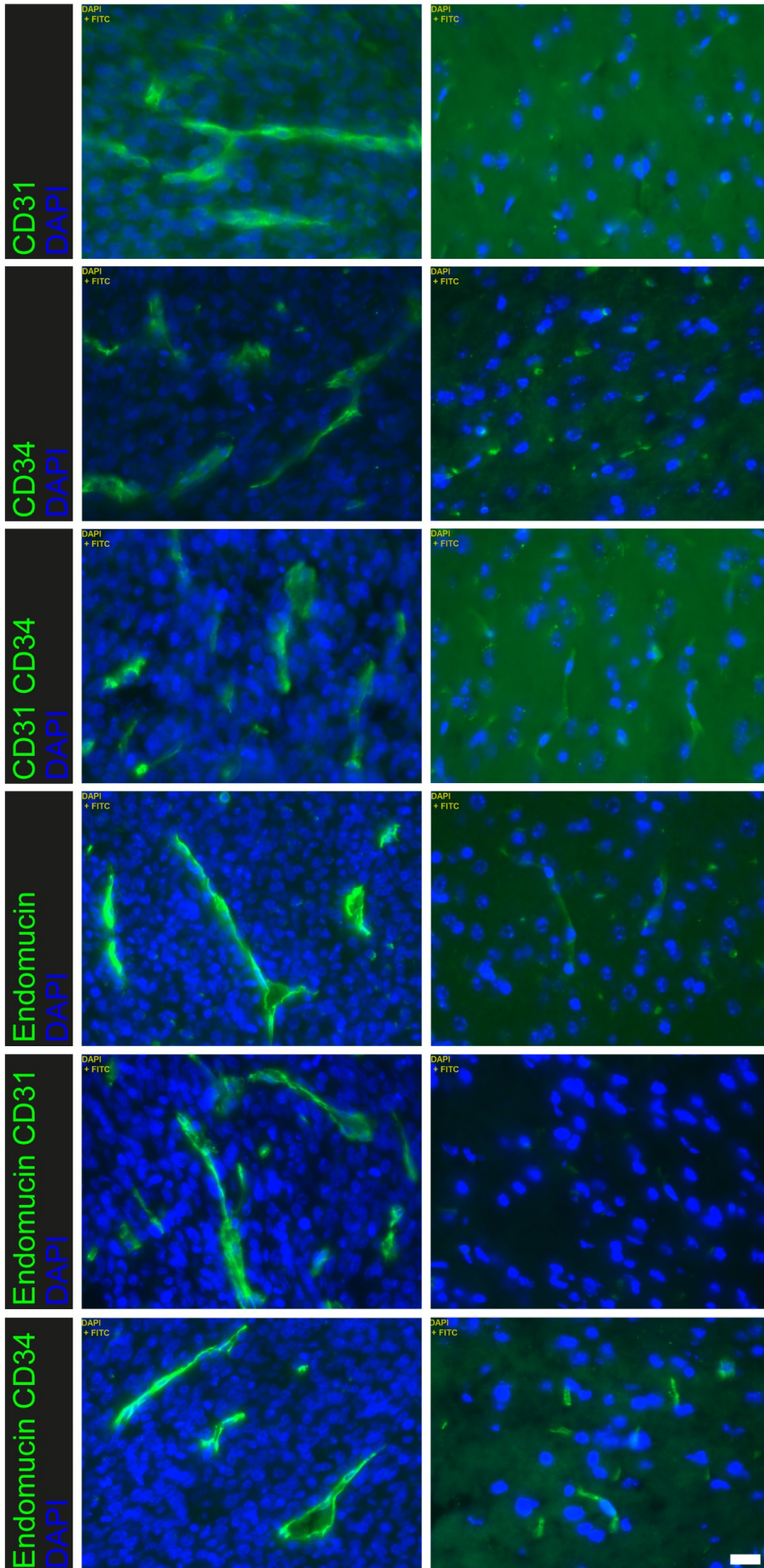


**Figure 4.2 Blood vessel staining in CT2A tumours with different markers by immunofluorescence.**

Sections of mouse brains implanted with CT2A tumours were stained for the endothelial markers CD31, CD34, Endomucin or combinations, and DAPI to mark nuclei. Images of stained tumour and peritumoral normal brain were captured at 40x magnification using a Zeiss AxioImager Z1 upright microscope. Note that the tumour area has higher cellularity compared to normal brain visualised by DAPI staining. CD34/Endomucin/ marks blood vessels in both tumour and normal brain effectively. Scale bar = 20  $\mu\text{m}$ .

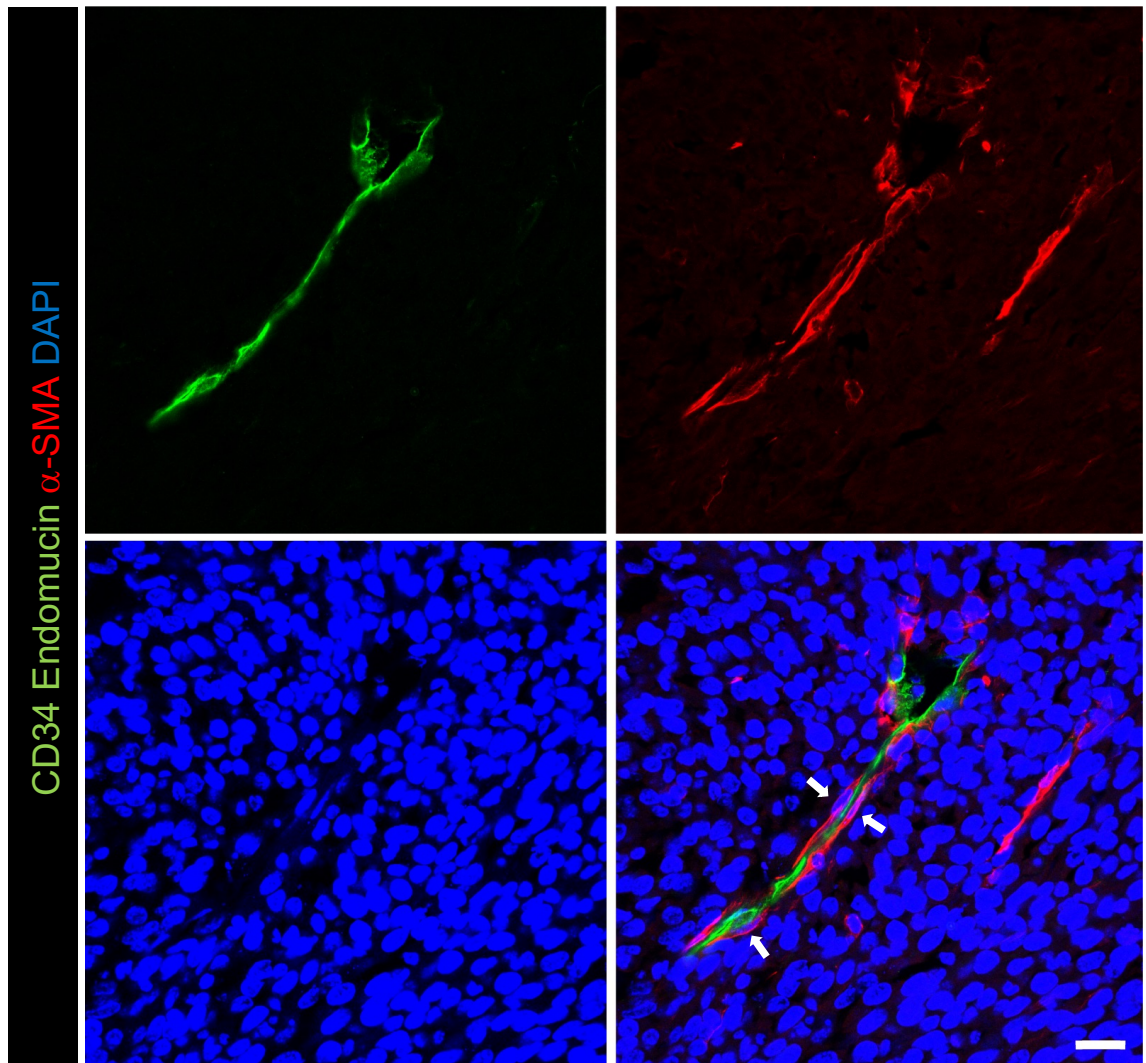


**Figure 4.3  $\alpha$ -SMA+ blood vessels are readily detectable by immunofluorescence staining of CT2A tumours.**

Sections of mouse brains implanted with CT2A tumours were stained for CD34/Endomucin,  $\alpha$ -SMA and DAPI. Images were captured at 60x magnification using a Nikon A1R Confocal microscope. The image depicts a blood vessel covered by  $\alpha$ -SMA+ cells. Arrows point to  $\alpha$ -SMA+ cells in close proximity to ECs. Scale bar = 20  $\mu$ m.

### **4.3 Effects of radiotherapy on blood vessel association with $\alpha$ -SMA positive pericytes.**

The study that led to this work (Chapter 1, Section 1.11) shown increased association of blood vessels with nestin/  $\alpha$ -SMA positive cells in recurrent tumours following radiotherapy and temozolomide chemotherapy (Egnuni et al., unpublished data). To investigate whether radiotherapy can contribute to this phenotype, I investigated whether experimental CT2A tumours that regrow after radiation therapy recapitulate the  $\alpha$ -SMA expression patterns observed in the recurrent patient tumours by staining the experimental tumours described in the irradiation experiment in Chapter 3 for CD34/Endomucin and  $\alpha$ -SMA. Fractionated irradiation (2 x 5Gy) was delivered to mouse brains bearing CT2A-Luc tumours using SARRP at days 7 and 8 post intracranial injection, and following regression and regrowth the tumours were excised, processed, and sectioned as described in Materials and Methods (Chapter 2, Section 2.4)

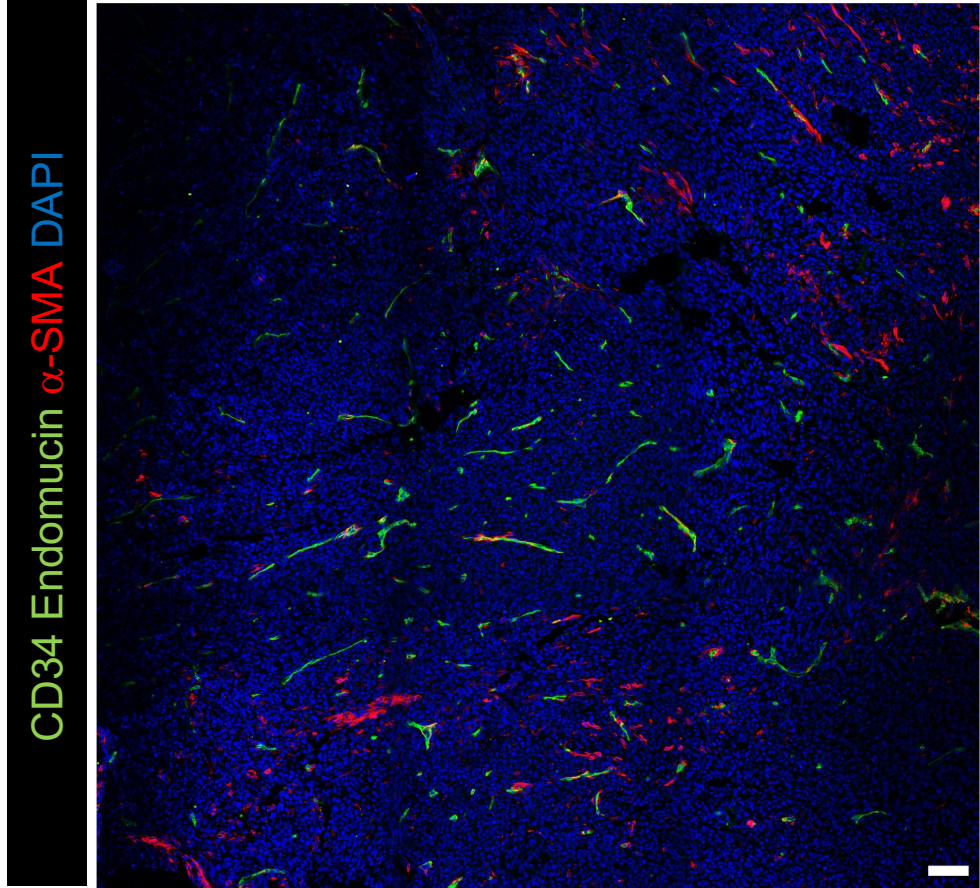
From each brain tumour three sections 100  $\mu$ m apart, were stained, and multiple microscopic fields were visualised using a Nikon A1R confocal microscope. Visually, the tumours that regrew after irradiation showed a higher overall abundance of  $\alpha$ -SMA+ expression (Figure 4.4). This was further evidenced when the stained sections were imaged at higher magnification (60x) and additionally, there appeared to be an increase in  $\alpha$ -SMA positive cells tightly associated with CD34/Endomucin positive blood vessels in the radiotherapy treated tumours (Figure 4.5). Hence, I set out to quantify the abundance of  $\alpha$ -SMA+ cells and association with blood vessels in control tumours and tumours regrown after radiotherapy. Three distinct types of blood vessels could be observed in terms of their association with pericytes based on the previously described characteristics of tumour pericytes by Morikawa and colleagues (Morikawa et al., 2002). Blood vessels with  $\alpha$ -SMA positive cells within their vicinity (defined as 20 $\mu$ m radius from the blood vessel periphery), were classified as pericyte positive (Figure 4.6 A-B). Pericyte-positive blood vessels were further classified as having tight or loose pericyte association as shown in Figure 4.6B.  $\alpha$ -SMA positive tight associated blood vessels were defined as having over 20% of the vessel periphery covered by  $\alpha$ -SMA+ cells (overlapping or adjoining expression of

CD34/Endomucin and  $\alpha$ -SMA);  $\alpha$ -SMA positive loose associated blood vessels were defined as having loosely associated but not adjoining  $\alpha$ -SMA+ cells (Figure 4.6A-B). Bias was avoided in quantification by selecting areas with CD34/Endomucin positive blood vessels without  $\alpha$ -SMA channel present. Subsequently, a multicolour CD34/Endomucin and  $\alpha$ -SMA image was captured. In addition, the identities of control and irradiated tumours were unknown (blinded quantification).

Visual observations were subsequently taken forward for quantification using the scoring criteria described in Figure 4.6 A. Aligned with the visual observation made, the graphs in Figure 4.7 show that there was a statistically significant increase in the percentage of CD34/Endomucin blood vessels associated with  $\alpha$ -SMA+ cells in tumours that regrew after radiotherapy compared to the non-irradiated control tumours; with mean values of 81.7% and 61.9% respectively. Furthermore, when classified into tight and loose pericyte association, Figure 4.7 B and C shows that there was a statistically significant increase in tight but not loose pericyte association in regrown tumours. This suggests that in the regrown tumours blood vessels recruit pericytes more efficiently than in the unirradiated, control tumours.

Therefore, consistent with the observations in the recurrent tumour patient samples, the experimental CT2A tumours treated with radiotherapy demonstrated an increase not only in vascularisation and blood vessel calibre (Chapter 3), but also in the association of  $\alpha$ -SMA+ cells with blood vessels.

Control



2 x 5Gy

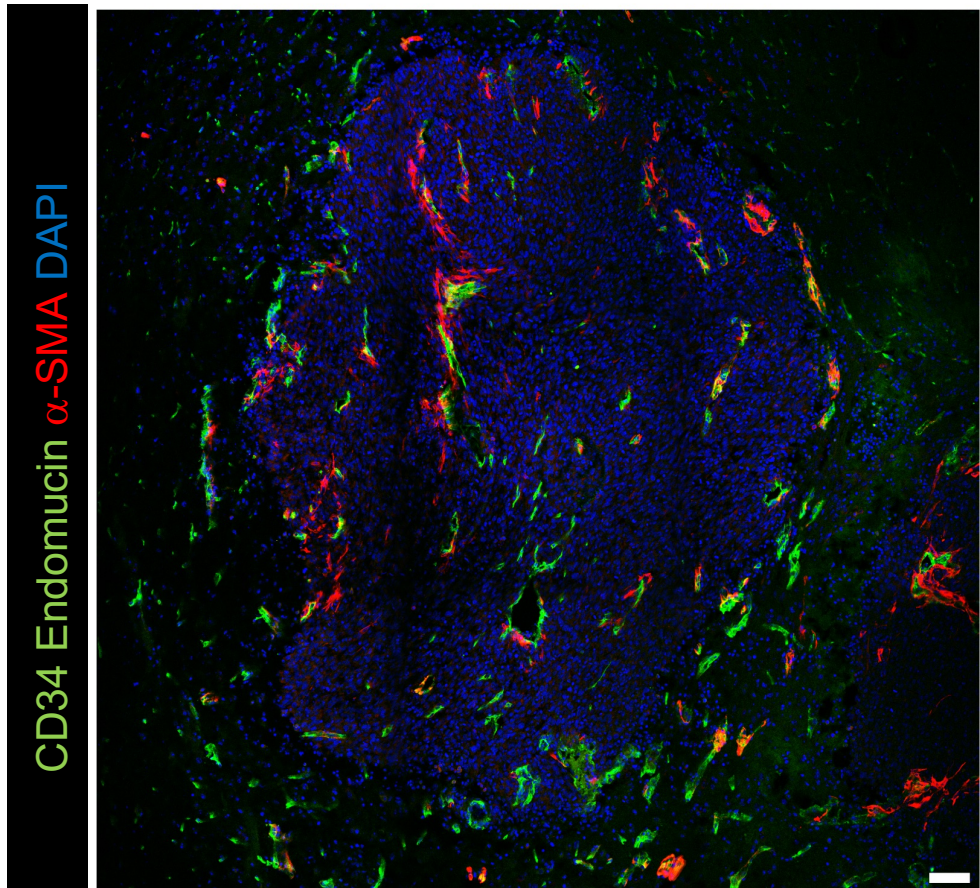
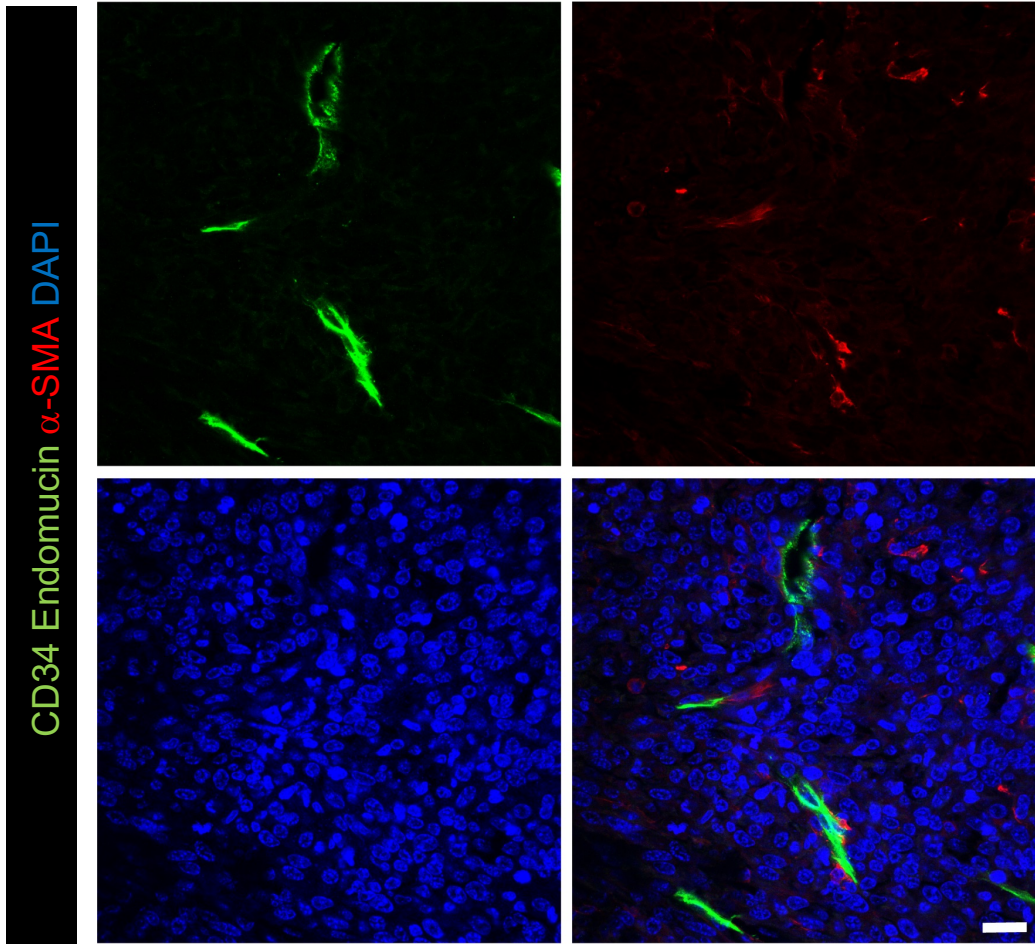


**Figure 4.4 Visualisation of  $\alpha$ -SMA positive blood vessels in regrown tumours following radiotherapy treatment.**

Sections of mouse brains bearing CT2A tumours were stained for CD34/Endomucin,  $\alpha$ -SMA and DAPI. 3 x 3 images were captured at 20x magnification and tiled at 5% overlap using the NIS-Elements C Advanced Software Platform. Images shown are representative from control and irradiated tumours. Note the abundance of  $\alpha$ -SMA+ blood vessels in the radiotherapy treated tumour. DAPI was enhanced in the bottom panel. Scale bar = 20  $\mu$ m.

Control



2 x 5Gy

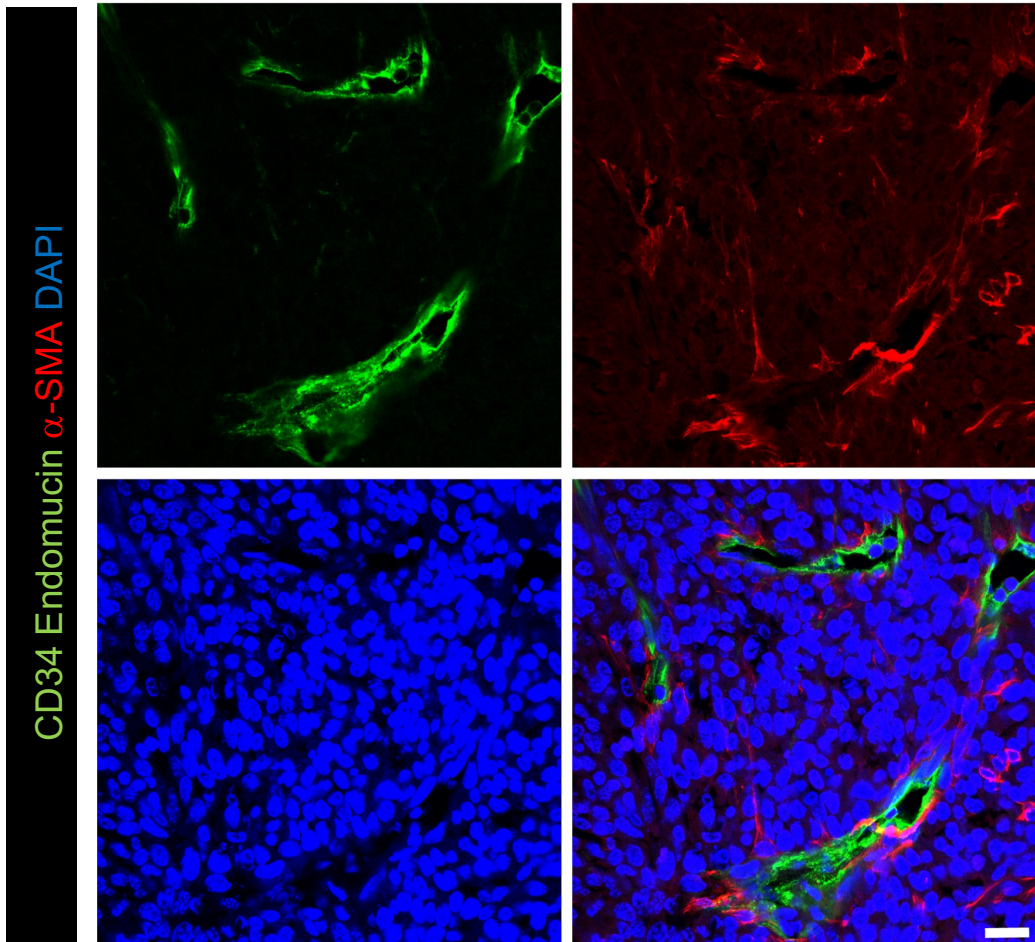


**Figure 4.5 Increased abundance  $\alpha$ -SMA positive blood vessels observed in histological sections of regrown tumours following radiotherapy treatment.**

Sections of mouse brains bearing CT2A tumours were stained for CD34/Endomucin,  $\alpha$ -SMA and DAPI. Images were captured at 60x magnification using a Nikon A1R confocal microscope. Images shown are representative from control and irradiated tumours. Scale bar = 20  $\mu$ m.

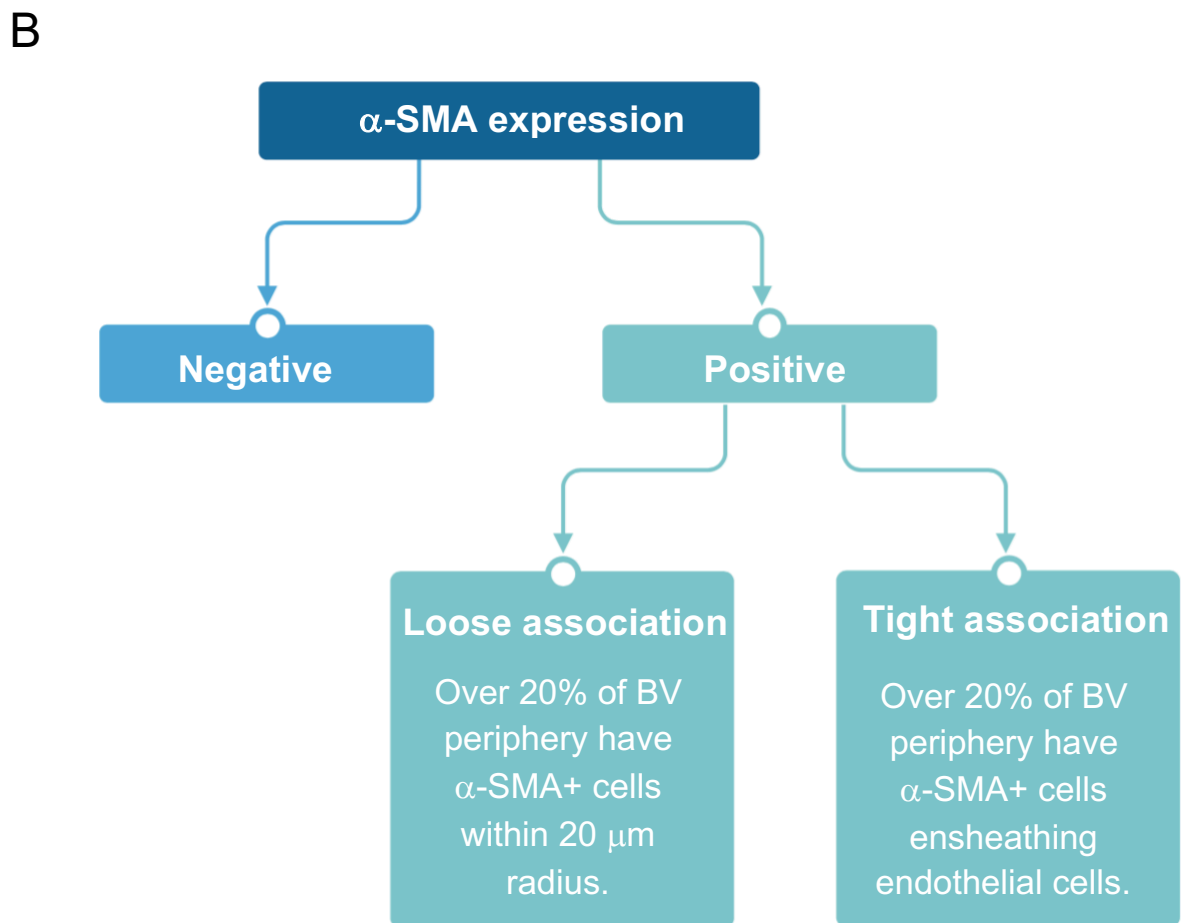
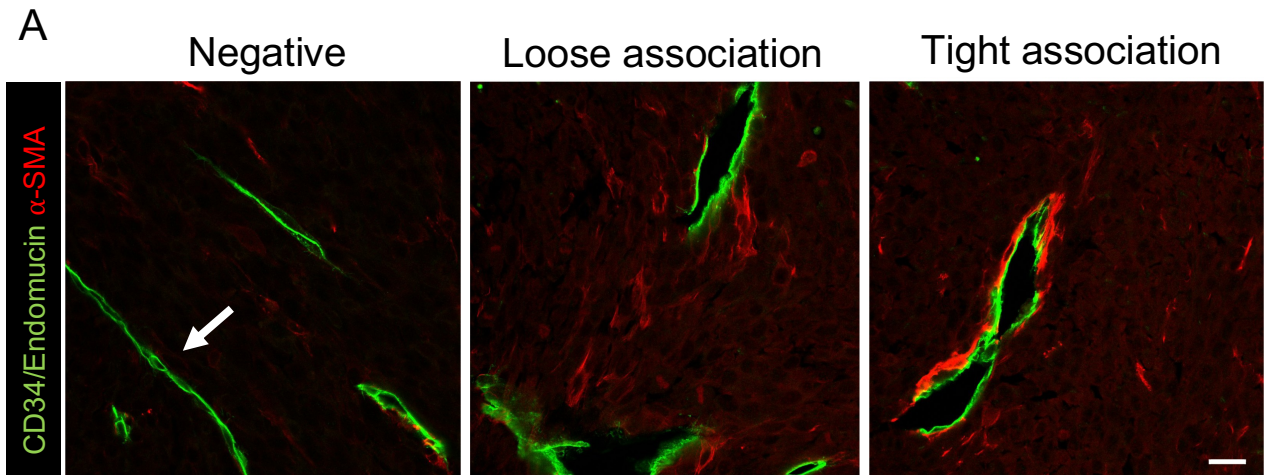
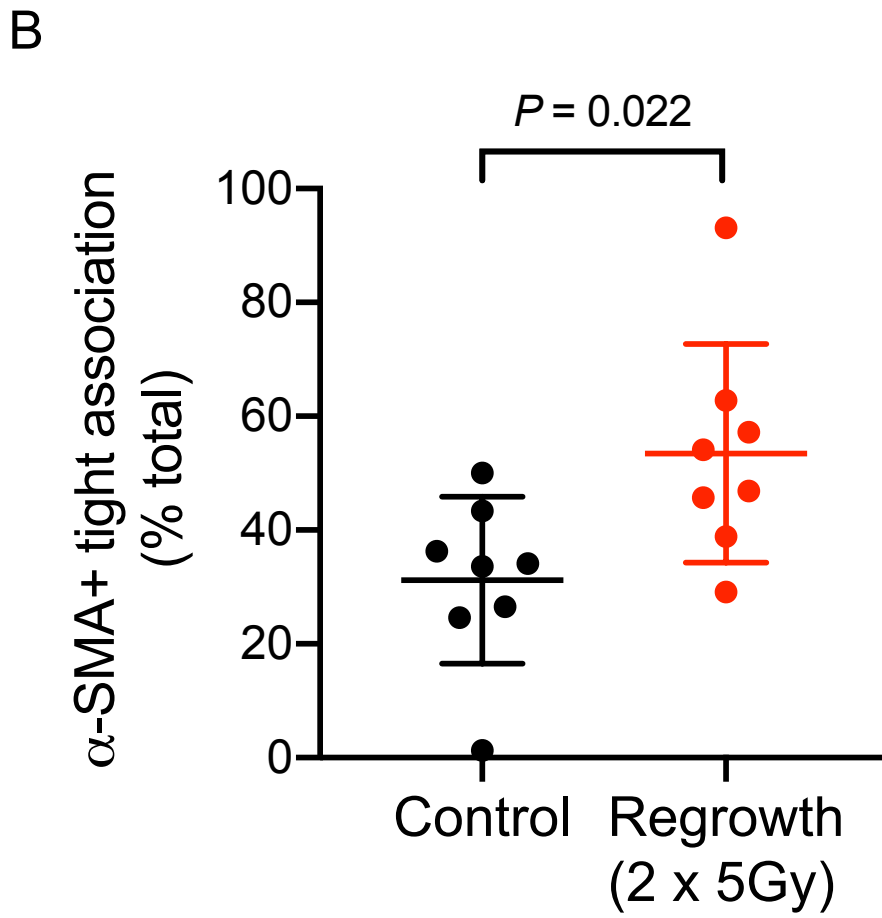
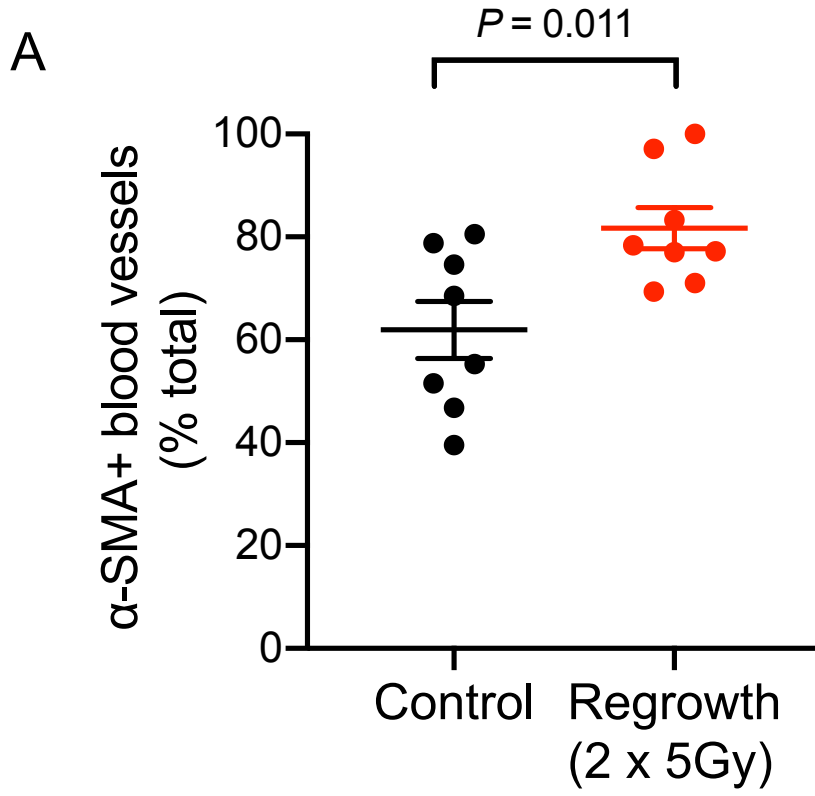


**Figure 4.6 Scoring of blood vessel pericyte association.**

(A) Sections of mouse brains with CT2A tumours were stained for CD34/Endomucin and  $\alpha$ -SMA. Images show examples of pericyte-negative blood vessels, blood vessels with loose pericyte association, and blood vessels with tight pericyte association.

(B) Flowchart shows the scoring system used to quantify pericyte coverage of blood vessels.  $\alpha$ -SMA positive blood vessels: pericytes within 20  $\mu$ m radius of the vessel periphery.  $\alpha$ -SMA negative blood vessels: lack pericytes within the 20  $\mu$ m radius. Tight association: over 20% of the vessel periphery covered by  $\alpha$ -SMA positive pericytes. Loose association: over 20% of the vessel periphery has unattached  $\alpha$ -SMA positive pericytes. Scale bar = 20  $\mu$ m.



C

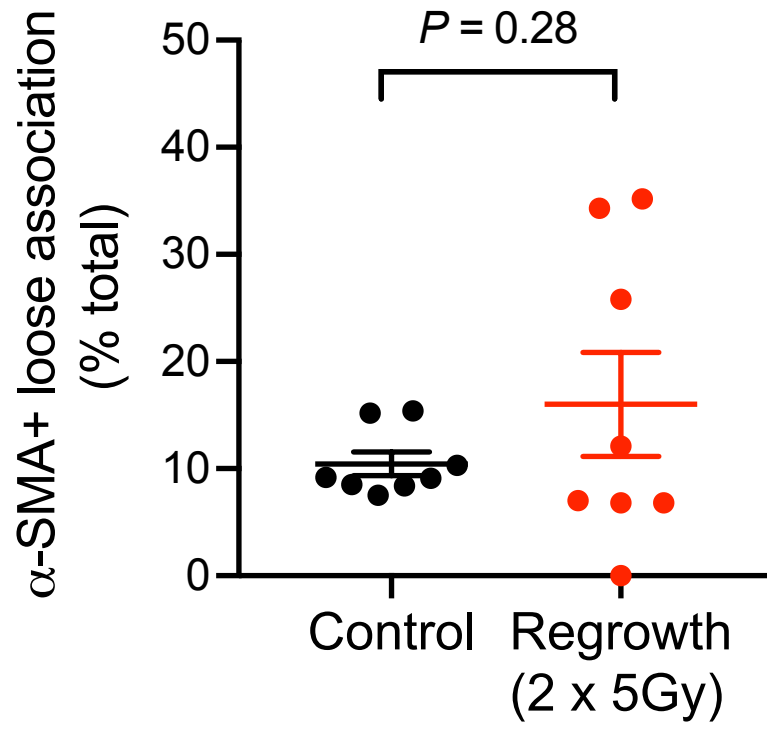


**Figure 4.7 Quantification of  $\alpha$ -SMA+ blood vessels show increase in  $\alpha$ -SMA tight association after radiotherapy.**

Sections of CT2A tumours, control and regrown after irradiation, obtained from areas 100  $\mu$ m apart were stained for CD34/Endomucin,  $\alpha$ -SMA and DAPI. Microscopic fields of CD34/Endomucin positive blood vessels were randomly selected at 60x magnification and images were captured for expression of CD34/Endomucin and  $\alpha$ -SMA. Blood vessels were scored for  $\alpha$ -SMA+ cell association as shown in Figure 4.6.

(A) Dot plot shows significant increase in the percentage of blood vessels associated with  $\alpha$ -SMA+ cells in regrown tumours after radiotherapy compared to untreated controls.

(B) Dot plot shows significant increase in the percentage of blood vessels with tight association of  $\alpha$ -SMA+ cells in regrown tumours after radiotherapy compared to controls.

(C) Dot plot shows no significant difference in the percentage of blood vessels with loose association of  $\alpha$ -SMA+ cells between control tumours and tumours regrown after radiotherapy.

Error bars represent SEM. n = number of tumour sections per group quantified from 4 mice per condition: control = 8, radiotherapy = 8.

## 4.4 Effect of radiotherapy on blood brain barrier (BBB) integrity and blood vessel permeability

In a study published in 2010, Armulik et al. expounded the critical role of pericytes in regulating blood vessel permeability in the CNS. Using intravenous injections of fluorescent-conjugated tracers such as albumin, cadaverin and Evans blue, they demonstrated that brain pericyte deficiency in a *pdgfb*<sup>ret/ret</sup> mouse lacking pericytes by means of genetic deletion of *pdgfrb*, resulted in breakdown of the brain blood-brain barrier (BBB) as manifested by oedema and extravasation of plasma proteins (Armulik et al., 2010). Although the study focused on normal brain, the question of whether pericytes also maintained this role in the blood-tumour barrier (BBB) led to the subsequent experiments in this study. First, we investigated whether there were indications that the BBB was restored in the irradiated regrown CT2A tumours through staining for GLUT1, a marker associated with an intact BBB (Phoenix et al., 2016). The staining experiments were performed by myself and an MSc student in the lab, Laura Heskin and quantification was performed by Laura Heskin. From that analysis, we concluded that there were no changes in BBB integrity in regrown tumours post irradiation as assessed by GLUT1 staining, and that vessel maturation marked by  $\alpha$ -SMA expression was not linked to barrier-genesis in the GBM tumours (Heskin, LK., MRes dissertation) as previously shown in developmental angiogenesis in a zebrafish model (Umans et al., 2018).

I next investigated whether increased association of blood vessels with  $\alpha$ -SMA+ cells influenced blood vessel permeability in regrown tumours post irradiation. For this purpose, I set up experiments of tracer delivery implementing intravascular injection of BSA-AlexaFluor555 based on the published methodology by Armulik and co-workers (Armulik et al., 2010). Albumin-AlexaFluor conjugates (molecular weight 66.5 kDa) have been widely used for the investigation of blood vessel permeability (Armulik et al., 2005; Armulik et al., 2010; Mitra et al., 2012; Watkins et al., 2014). Elevated distribution of albumin in extravascular regions may infer a disrupted BBB and elevated blood vessel permeability (Ahishali and Kaya, 2021).

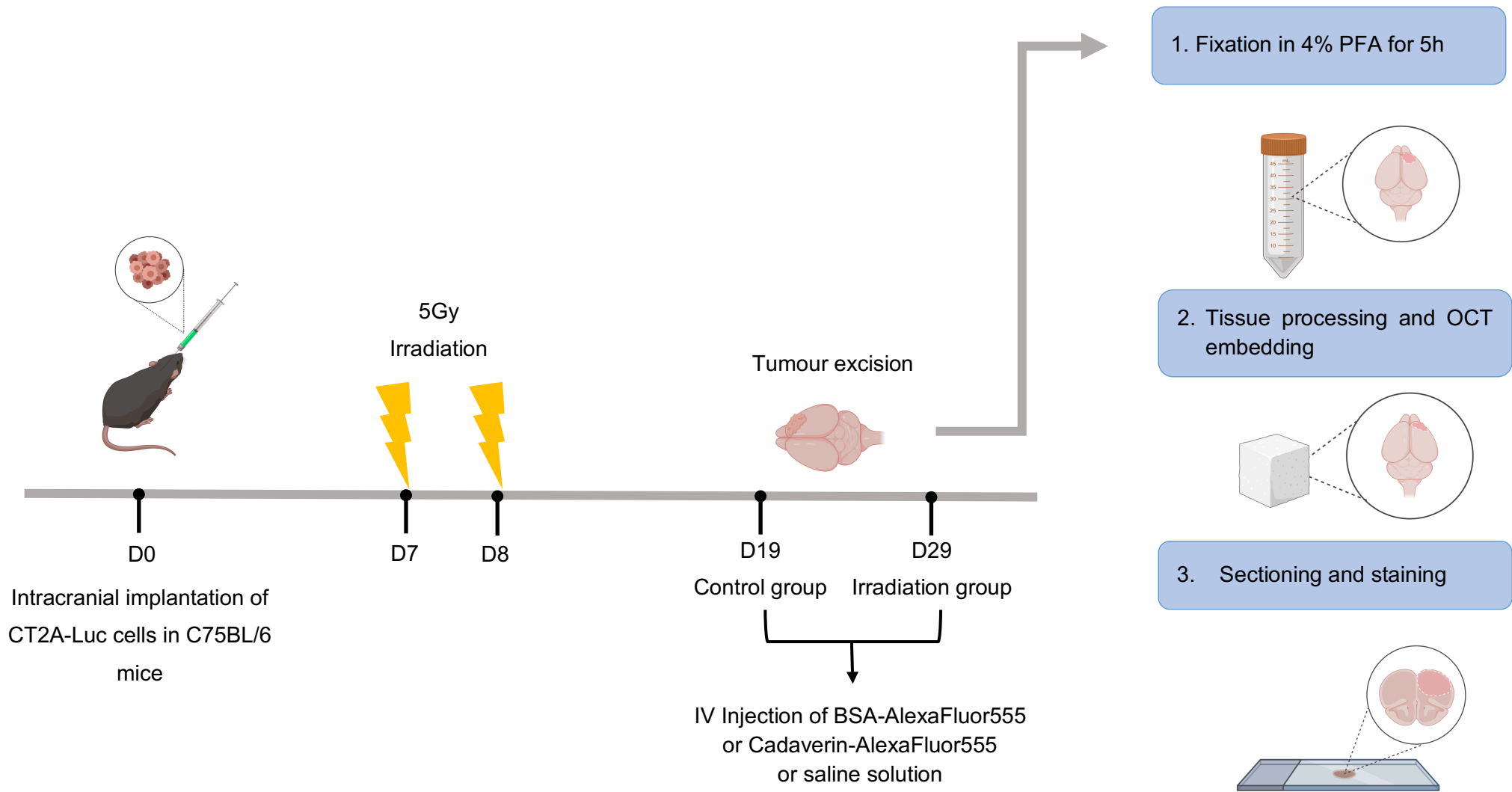


**Figure 4.8 Schedule of CT2A tumour implantation, irradiation, and tracer injection in a pilot experiment.**

CT2A-Luc murine glioma cell line ( $1 \times 10^5$  cells) was injected intracranially into the striatum of C57BL/6 wild type mice. Tumour growth was followed non-invasively by IVIS bioluminescence imaging and on day 6 mice were randomised prior to irradiation. Fractionated irradiation ( $2 \times 5\text{Gy}$ ) was delivered on days 7 and 8 following implantation using SARRP and following regression the irradiated tumours were allowed to regrow. Control mice were sacrificed on day 19 and irradiated mice on day 29 after implantation. Tail vein injections of BSA-AlexaFluor555, Cadaverin-AlexaFluor555 or normal saline solution were performed prior to terminal perfusion. Mouse brains were subsequently excised, embedded in OCT compound and frozen.

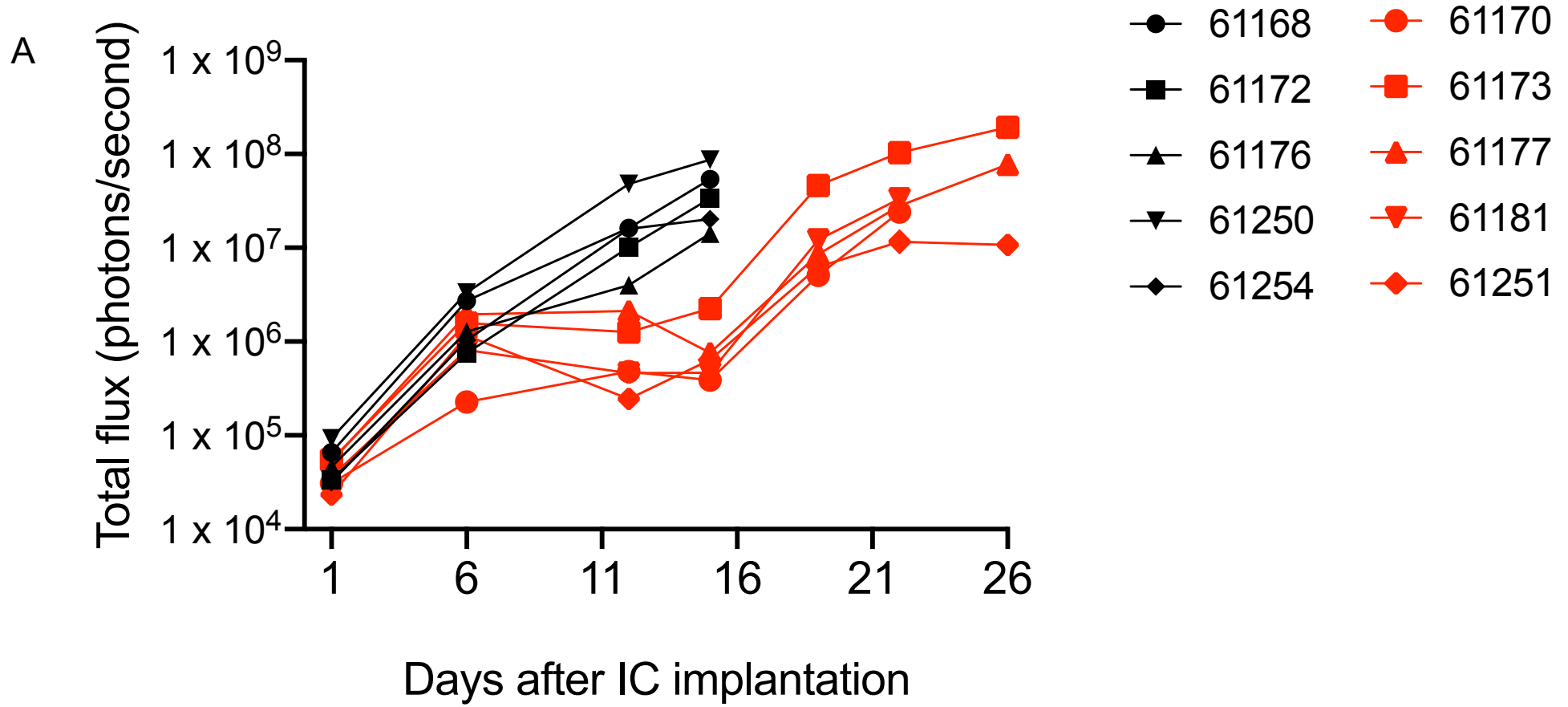
#### **4.5 Pilot experiment for the analysis of blood vessel permeability in response to radiotherapy**

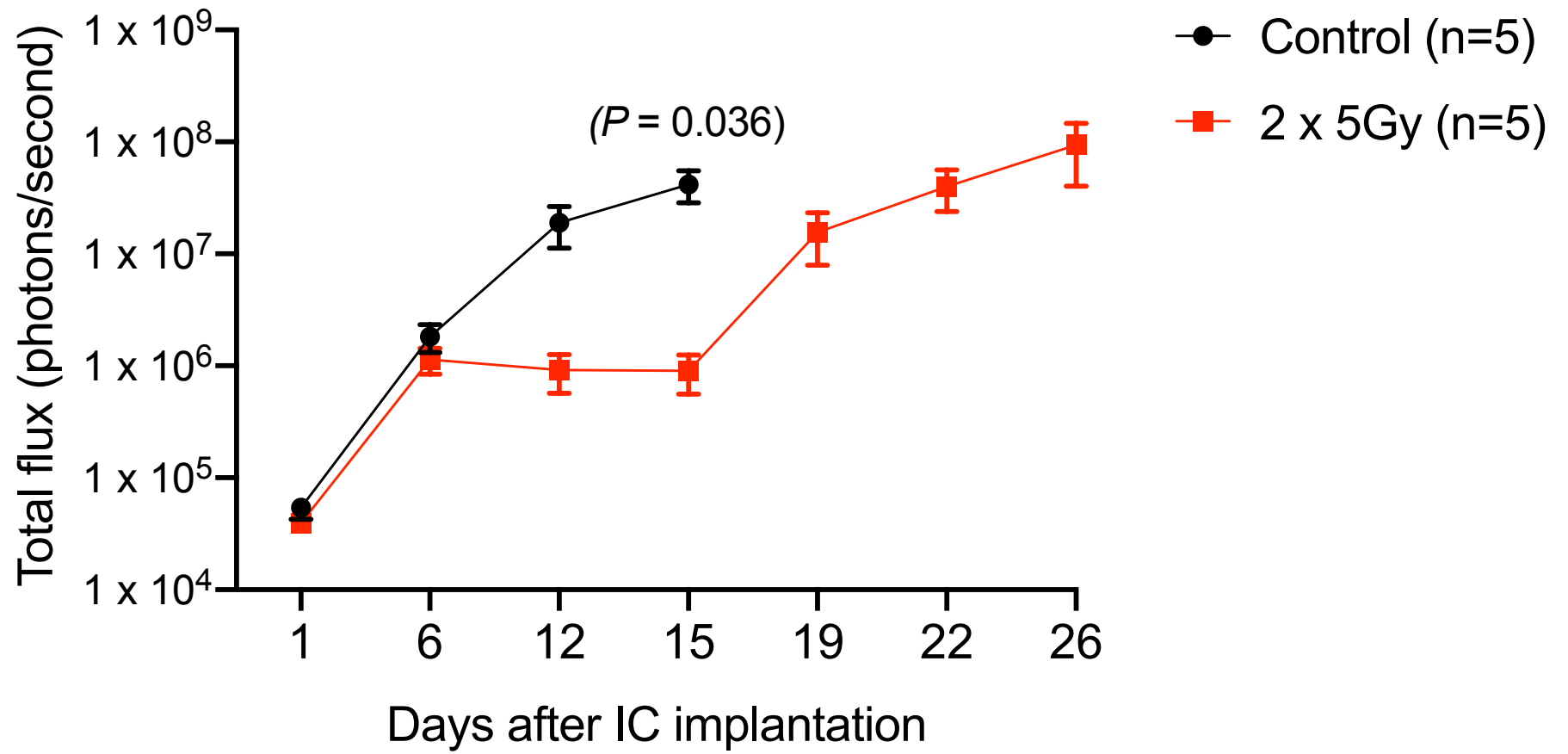
On day 6 following intracranial implantation of CT2A cells mice were randomised for radiation treatment delivered on days 7 and 8 at 5Gy each day, and tumours were excised at day 19 for control group (non-irradiated) and day 29 for irradiated group (Figure 4.8) following intravenous (IV) tail vein injection of fluorescent-conjugated BSA-AlexaFluor555 or Cadaverin-AlexaFluor555 performed 5 hours prior to terminal perfusion (Figure 4.9). All mice were perfused prior to tissue harvest, and brains were fixed for 5 hours and frozen embedded in OCT compound.

Shown in Figure 4.9 for clarity are the growth characteristics of tumours grown in the BSA-AF555 injected mice. The other mice behaved in an equivalent way with regards to tumour growth (data not shown). The IVIS monitoring showed that radiotherapy resulted in a reduced or stunted tumour progression as shown in Figure 4.9 A. At day 15 there was a statistically significant difference in tumour growth between control and irradiated group ( $P = 0.036$ ). In the IVIS images shown in Figure 4.9 B it was visually observable that control mice had a steady increase in tumour growth whereas as expected, radiotherapy treatment resulted in a decrease in tumour growth at day 15, which was followed by tumour regrowth (Figure 4.9 A-B). On day 26 radiotherapy treated tumours reached comparable bioluminescence signal intensity as control non-irradiated mice on day 15. Both groups were excised three days later, at days 18 for the control group and day 29 for the irradiated group.

Post sample processing only two BSA-AF555 injected mice, one control and one irradiated, had detectable tracer in the brain. This may have been due to technical error during IV injection and/ or subsequent sample processing as tumours were erroneously washed in 70% ethanol following fixation, prior to freezing. Therefore, those two samples were used as pilot samples for the establishment of methods and initial quantifications of blood vessel tracer extravasation. Similarly, only one Cadaverin-AF555 injected mouse had detectable tracer in the brain. Cadaverin is a small molecular (molecular weight: 950 Da) fluorescent

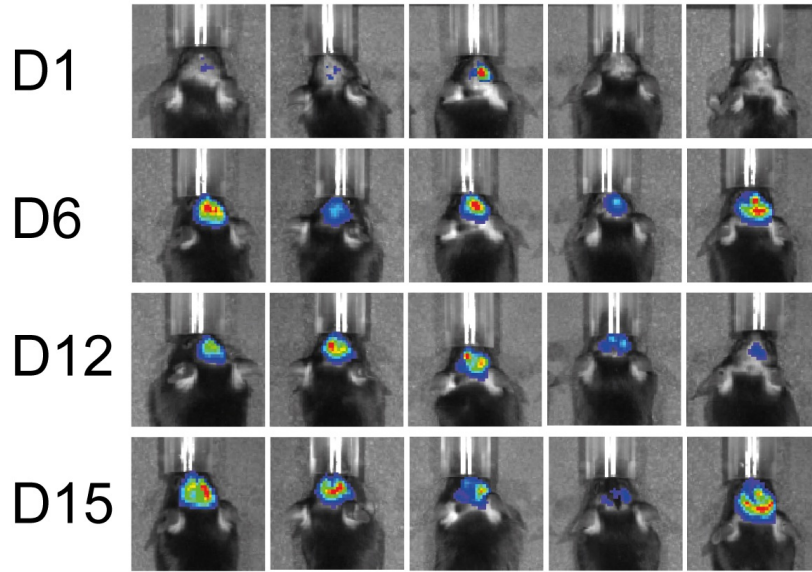
tracer used commonly to assess blood brain barrier integrity *in vivo* (Armulik et al., 2010; Watkins et al., 2014; Zhou et al., 2017). Due to its thick consistency, Cadaverin was more challenging to intravenously inject. BSA extravasation was detectable easily around individual vessels using confocal microscopy whereas Cadaverin extravasation appeared to be speckled and faint. The use of Cadaverin was omitted in subsequent experiments. In summary, this experiment confirmed the effects of irradiation on tumour growth, and regrowth *in vivo* as seen by Dr Tek Egnuni in prior studies. This experiment also provided samples for pilot analyses to quantify BSA-AF555 extravasation in the CT2A tumours.





B

### Control



### 2 x 5Gy

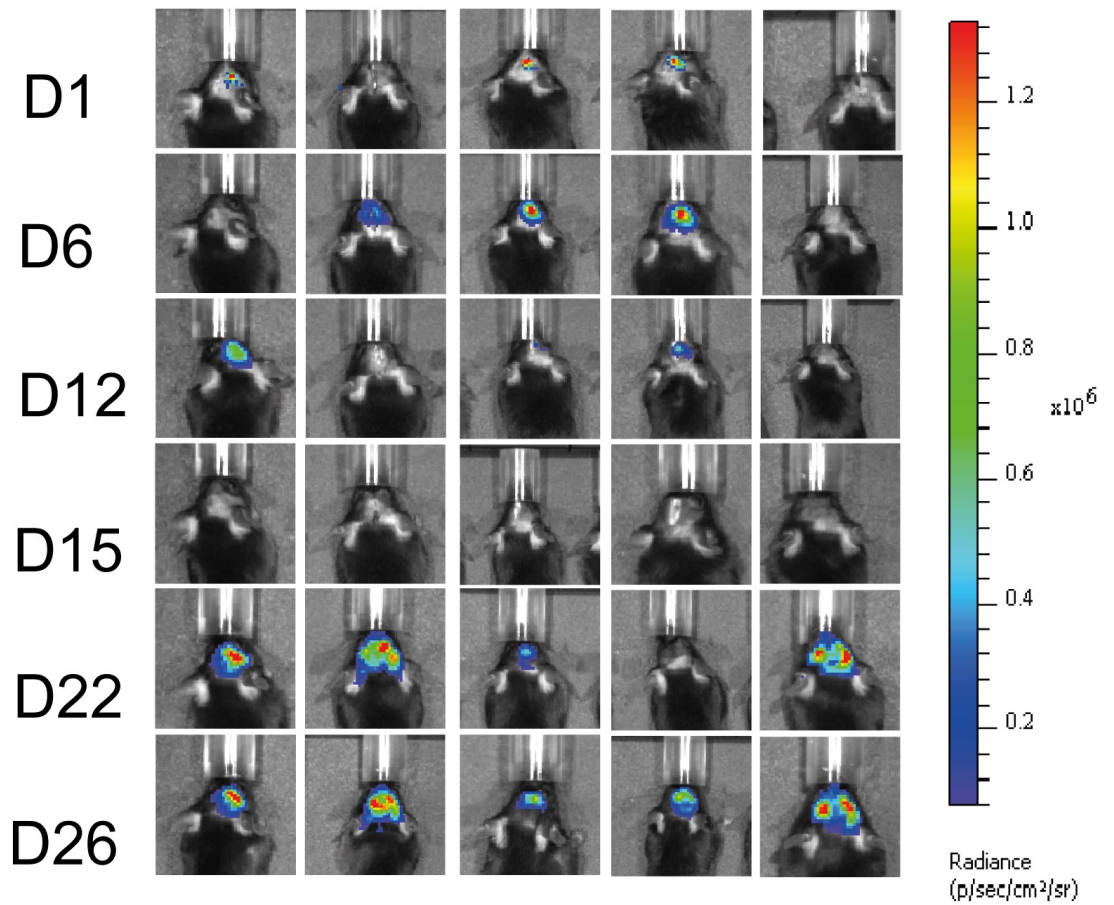


**Figure 4.9 Monitoring of CT2A tumour growth following irradiation in the tracer extravasation pilot experiment.**

CT2A-Luc murine glioma cell line ( $1 \times 10^5$  cells) was injected intracranially into the striatum of C57BL/6 mice. Fractionated irradiation (2 x 5Gy) was delivered on days 7 and 8 following implantation using SARRP. Tumour growth was followed non-invasively by IVIS bioluminescence imaging starting 1 day after tumour implantation.

(A) Graphs present bioluminescence signal intensity as measured in total flux (photons/seconds) following subcutaneous injection of luciferin. Top panel shows individual mouse readings and bottom panel shows average readings  $\pm$ SEM. Note the statistical significance of bioluminescence signal intensity between control and radiation treated group on day 15.

(B) Images taken using IVIS bioluminescence imaging illustrate the progression of tumour growth in mouse brains. Note the reduction in bioluminescence signal on day 15 in the irradiated group.

## 4.6 Establishing a method to analyse BSA-AlexaFluor555 extravasation

In order to assess the effect of radiotherapy on the extravasation of BSA-AlexaFluor555 tracer in regrown tumours, a method for processing and quantification of images needed to be established. Serial sections of CT2A implanted tumour-bearing PFA-fixed mouse brains were cryosectioned at 10  $\mu\text{m}$  thickness coronally from anterior to posterior starting from the olfactory region. Three sections at 100  $\mu\text{m}$  distance apart, were stained for CD34/Endomucin and  $\alpha$ -SMA, and counterstained with DAPI to mark nuclei. Stained sections were imaged using a Nikon A1R confocal microscope, and single channel imaging of CD34/Endomucin was used to select microscopic fields without observing the tracer profiles, in order to limit bias in measurements of extravasation. Following identification of CD34/Endomucin positive blood vessels images were captured of  $\alpha$ -SMA, BSA-AF555 and CD34/Endomucin that were used for quantification (Figure 4.10). Once acquired, images were randomised by a second investigator and analysis was conducted blinded with respect to the identity of the tumours.

Upon initial observation, tracer extravasation was detected in blood vessels, irrespective of their tight pericyte ( $\alpha$ -SMA+) association (Figure 4.11). Furthermore, the tracer could be seen both in blood vessels, and in the tumour parenchyma, as manifested by the extravascular staining (Figure 4.11). As the mice had been perfused, we reasoned that any tracer in blood vessels represents accumulation in the endothelium as shown in Armulik et al., 2010. Blood vessels provide oxygen and nutrients for tumour viability within approximately 100  $\mu\text{m}$  distance (Weinberg, 2014), beyond which radius the tissue becomes hypoxic. Given that albumin extravasates less through the blood vessels, in order to assign extravasation to individual blood vessels, tracer was quantified within 40  $\mu\text{m}$  radius around individual vessels as marked by the white dotted line in Figure 4.11. Tracer trapped within the blood vessel wall, as marked with a yellow dotted line in Figure 4.11, was excluded from the measurement.

For each brain tumour sample, a minimum of ten images from each of the three sections at 100  $\mu\text{m}$  apart was captured at 60x magnification and tracer positive

pixels were quantified using ImageJ software. A macro generated in-house using the ImageJ macro language (IJM), was used to automate quantification as described in Materials and Methods (Chapter 2, Section 2.4.6). Briefly, binary images were generated using minimum and maximum threshold values set on multiple high and low extravasation images from both control and irradiated samples. Next, the BSA-AF555 positive pixels was measured using this macro within a 40um radius around individual blood vessels. As the focus of quantification lies on the tracer in the extravascular area of the blood vessels, accumulation of tracer in the endothelium was deleted from the image using the Image J 'clear' tool and omitted from the quantification. Integrated density (RawIntDen on Image J), which is the sum of all tracer-positive pixels in the region, was measured and taken forward into analysis.

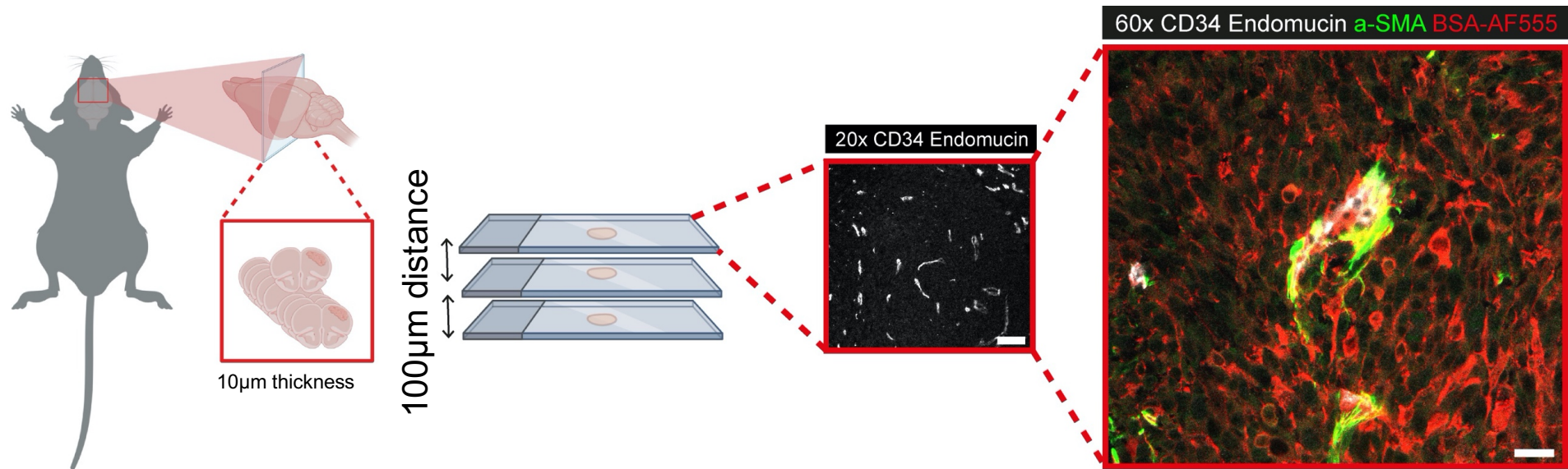


**Figure 4.10 Schematic of processing of CT2A bearing brains for visualisation of BSA-AlexaFluor555 tracer extravasation in histological sections.**

Diagram illustrates the workflow for visualization of BSA-AlexaFluor555 tracer in excised brains. Parallel 10µm thick sections taken 100µm apart were stained using immunofluorescence for CD34/Endomucin and imaged using Nikon A1R confocal microscope. Microscopic fields of CD34/Endomucin positive blood vessels within the tumour area were randomly selected at 20x magnification and images were captured for expression of CD34/Endomucin,  $\alpha$ -SMA and BSA-AF555 at 60x magnification.

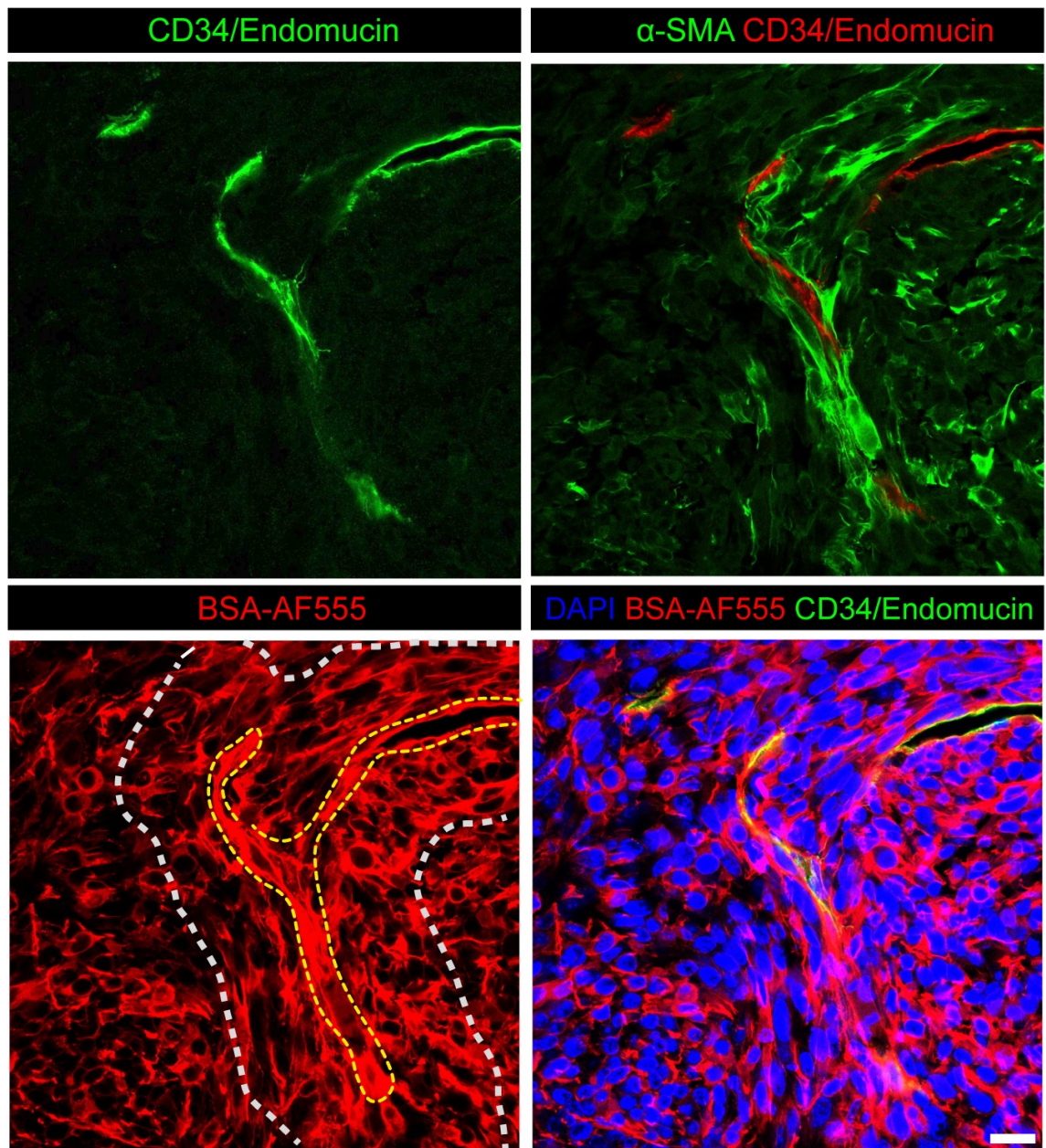


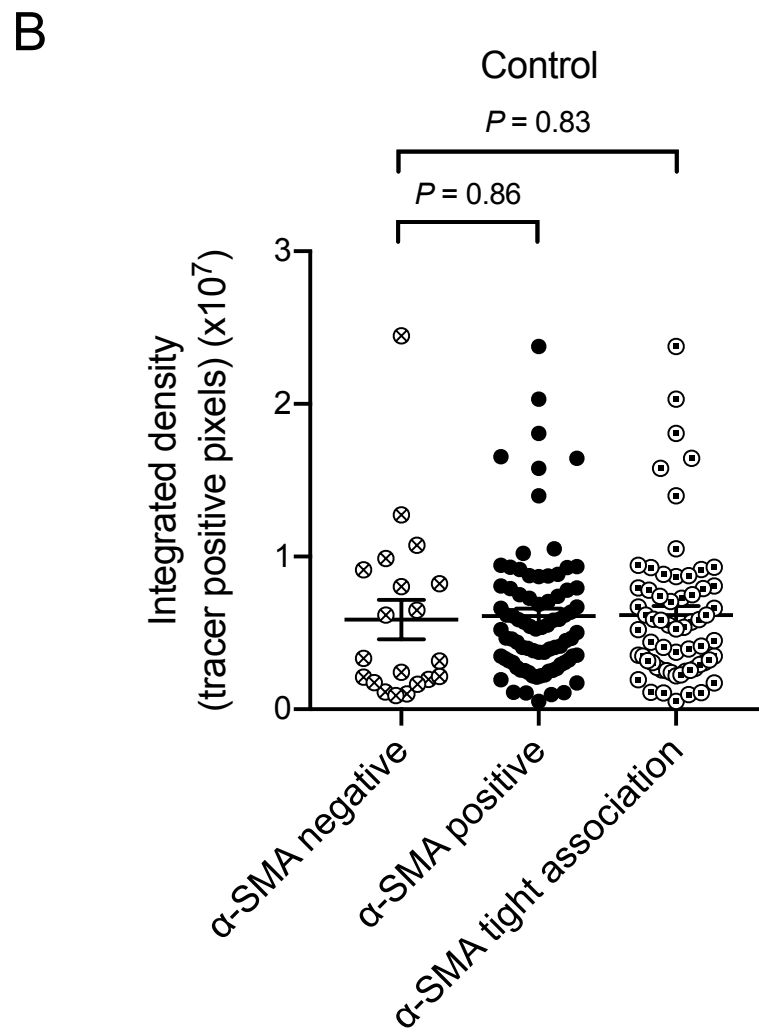
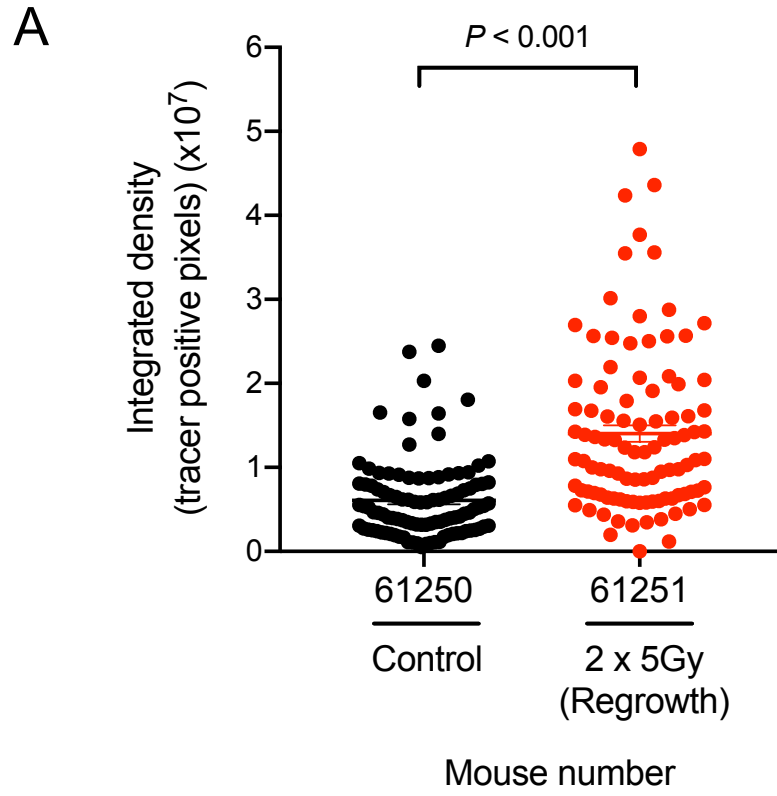
**Figure 4.11 Visualisation of  $\alpha$ -SMA, CD34/Endomucin and BSA-AlexaFluor555 tracer for quantification.**

Images show appearance of BSA-AF555 tracer in CT2A tumours processed as outlined in Figure 4.10. Images were captured using Nikon A1R confocal microscope at 60x magnification. The white dotted line on bottom left panel marks the boundary of quantification for extravascular tracer positivity at 40  $\mu\text{m}$  distance from the blood vessel periphery. Tracer trapped within the blood vessel wall marked by the yellow dotted line was excluded from the analysis. Scale bar = 20  $\mu\text{m}$ .

#### **4.7 Analysis of tracer extravasation in the control and radiotherapy treated regrown tumours in the pilot experiment**

Using the quantification method described in the previous section blood vessels from the control (mouse ID 61250) and the regrown after irradiation tumour (mouse ID 61251) were analysed. Analysis was performed for 103 blood vessels from the control and 98 blood vessels from the radiotherapy treated tumour. The dot plot in Figure 4.12A shows a significant increase ( $P < 0.001$ ) of over 2-fold in the tracer extravasation in the radiotherapy treated regrown tumour compared to control untreated tumour.

When extravasation was analysed with respect to pericyte ( $\alpha$ -SMA+ cell) association, in both the control and the irradiated regrown tumour the association of pericytes with blood vessels did not affect tracer extravasation. Surprisingly, a trend was observed of somewhat increased tracer extravasation from pericyte positive blood vessels and blood vessels with tight association compared to pericyte negative blood vessels in the non-irradiated tumour (Figure 4.12 B), however the difference was not statistically significant ( $P = 0.30$  and  $P = 0.31$  for positivity and tight association respectively). The same trend could be seen in the radiotherapy treated regrown tumour of increased tracer extravasation from pericyte positive blood vessels and blood vessels with tight association compared to pericyte negative blood vessels (Figure 4.12 B) which again was not statistically significant ( $P = 0.30$  and  $P = 0.31$  for positivity and tight association respectively). These results suggest that pericytes could potentially increase tracer extravasation, but they did not account for differences between the irradiated tumour and the untreated control (Figure 4.12 A). Given that these observations were based on only one tumour per condition, it was necessary to increase the number of samples with successful tracer injection for analysis in a subsequent experiment.



C

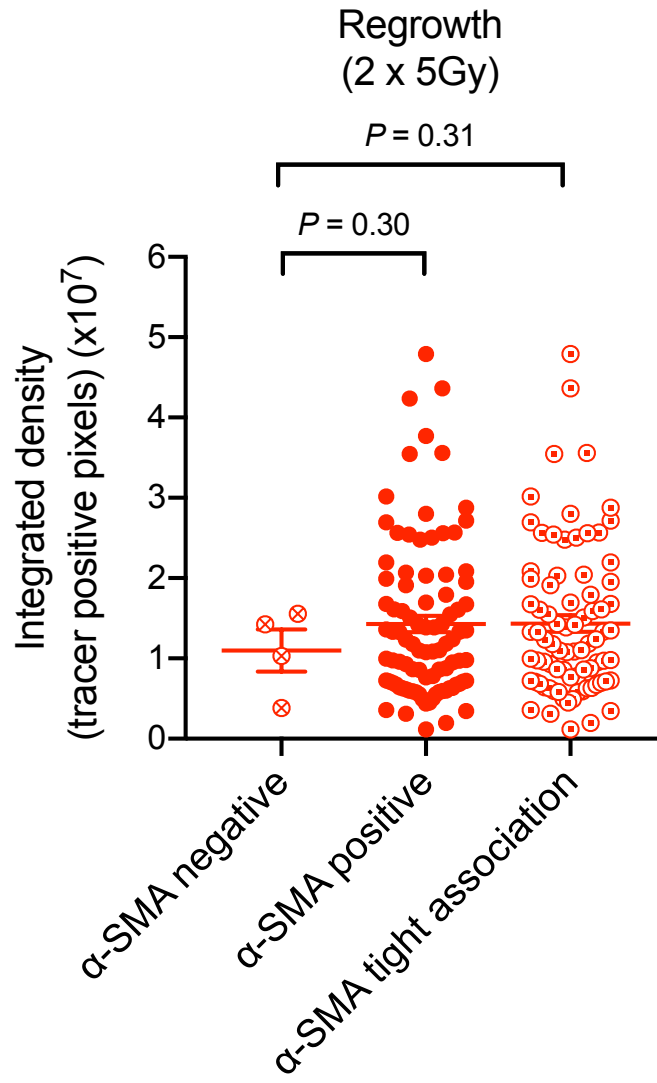


**Figure 4.12 Irradiated regrown tumour in pilot experiment demonstrates higher tracer extravasation.**

Sections of mouse brains bearing CT2A tumours were stained for CD34/Endomucin,  $\alpha$ -SMA and DAPI. 10 images were captured at 60x magnification from three different tumour levels, 100  $\mu$ m apart and analysed for BSA-AlexaFluor555 extravasation and  $\alpha$ -SMA+ cell association using ImageJ.

(A) Dot plot shows an increase in the overall tracer-positive pixels of extravasation in the irradiated mouse compared to control.

(B) Dot plot (black) shows no difference in tracer-positive pixels of extravasation between  $\alpha$ -SMA positive and  $\alpha$ -SMA negative blood vessels in the control mouse.

(C) Dot plot (red) shows no difference in tracer-positive pixels of extravasation between  $\alpha$ -SMA negative and  $\alpha$ -SMA positive tumour blood vessels in the irradiated mouse.

Error bars represent SEM. n = total number of blood vessels quantified from 3 sections from one mouse per condition: control = 103, irradiation = 98.

#### **4.8 Analysis of tracer extravasation in regrown tumours post radiotherapy in a larger tumour cohort**

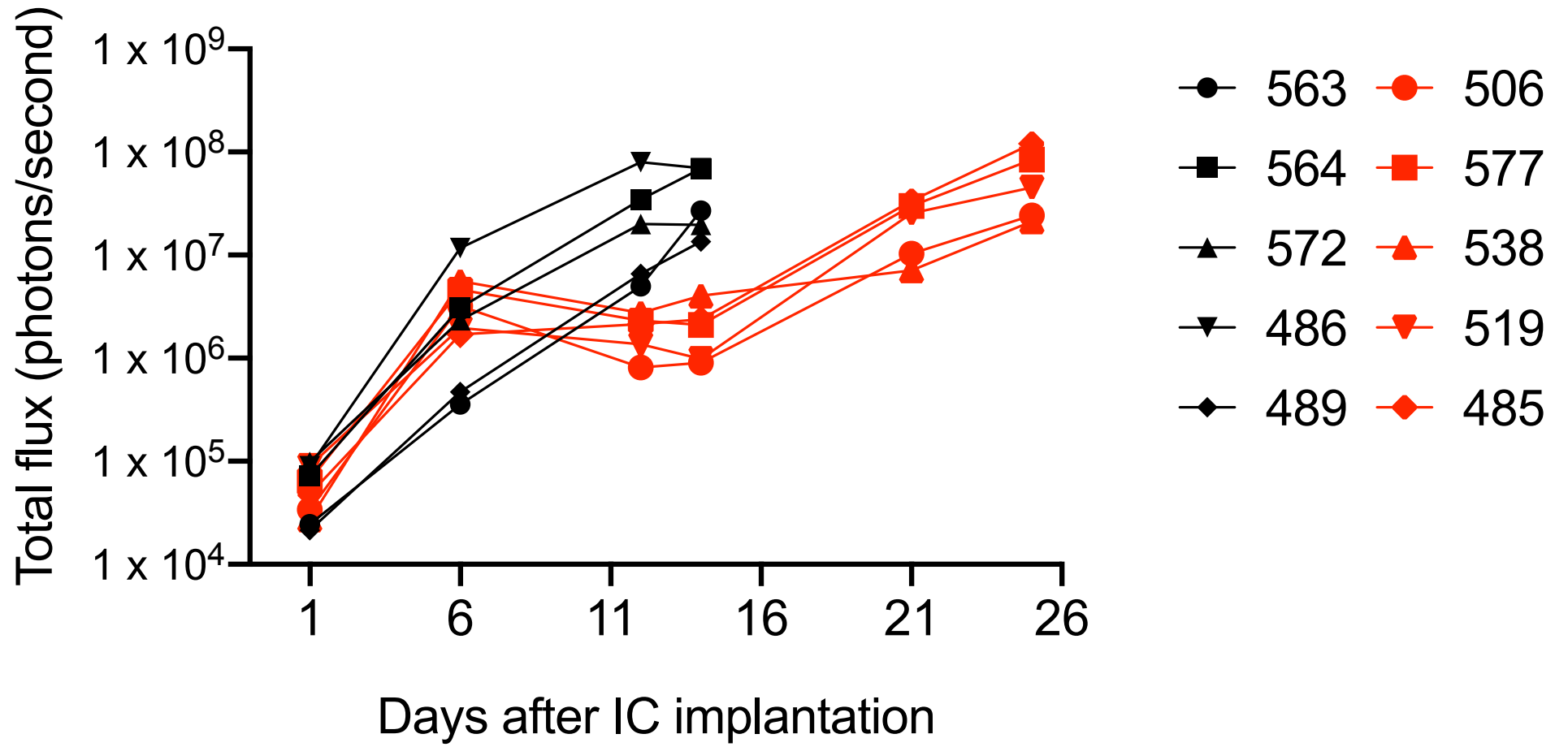
With a method established of staining, visualisation, and quantification of tracer extravasation a new intracranial implantation experiment was performed as previously described (Figure 4.8). As in the earlier pilot experiment mice were intracranially injected with  $1 \times 10^5$  CT2A-Luc cells and tumour growth was monitored by IVIS. Mice were randomised on day 6 and fractionated radiotherapy ( $2 \times 5\text{Gy}$ ) was administered on days 7 and 8. In this experiment the excision time of tumours was on day 18 for control and day 26 for irradiated regrown tumours – when mice began to show neurological symptoms. The average final IVIS reading at the day of excision was  $3.80 \times 10^7$  for control tumours and for irradiated tumours  $4.69 \times 10^7$  with no significant difference between the two groups ( $P = 0.71$ ). The individual growth curves and bioluminescence signal intensity prior to excision are shown in Figure 4.13A and on Table 4.1. As expected, IVIS imaging showed that radiotherapy resulted in a decrease in tumour growth which could be seen from day 12 (Figure 4.13 A). At day 14 when control tumours were excised there was statistically significant difference ( $P = 0.037$ ) in the total flux values of control and radiation groups and irradiated tumours regrew (Figure 4.13 B).

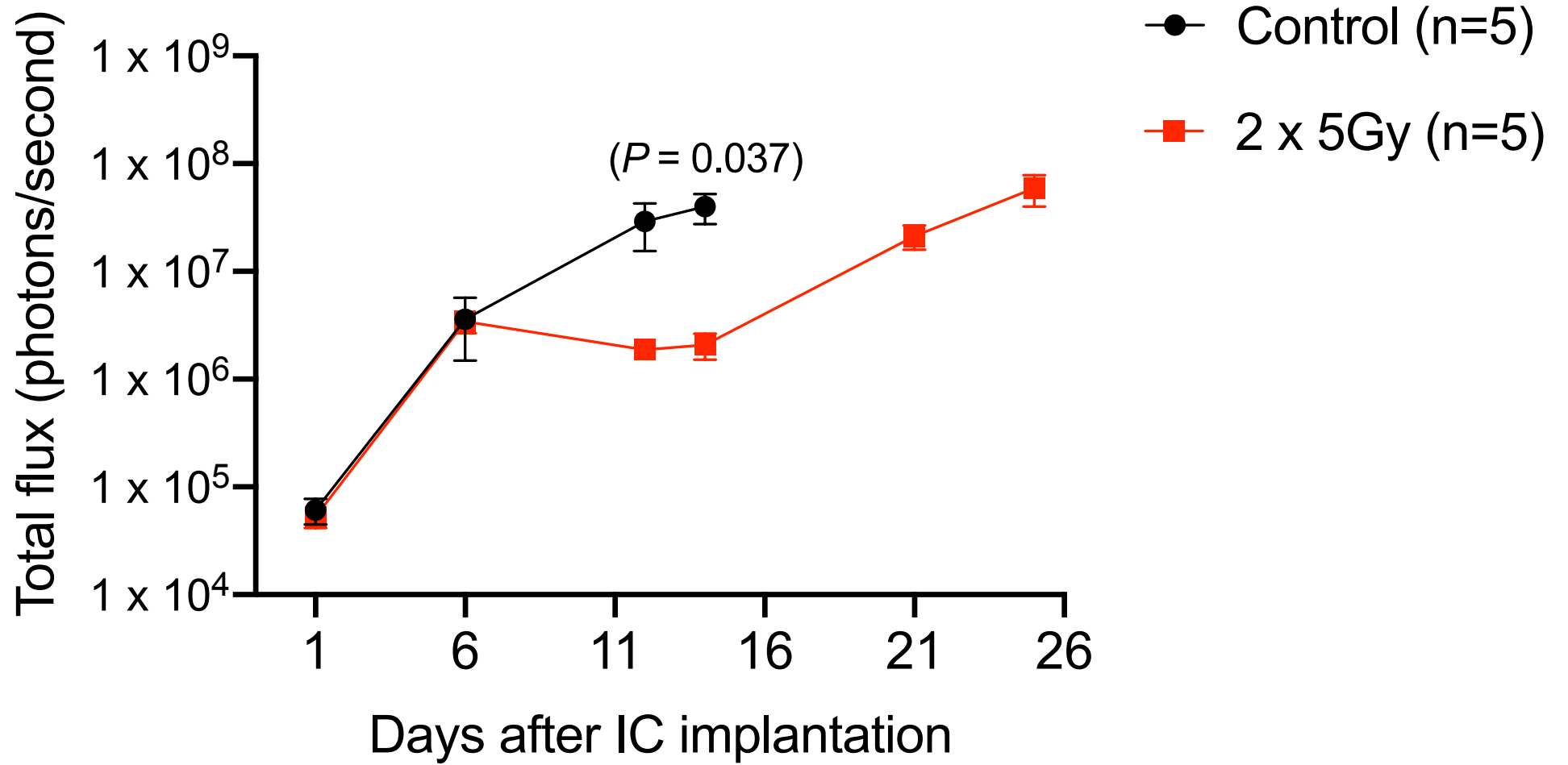
Prior to terminal perfusion mice from each group were injected with BSA-AlexaFluor555 and the tracer was left to circulate for 3 hours (compared to 5 hours in the previous experiment), in order to reduce the overall amount of tracer and clearly identify extravasation around individual blood vessels. Following termination of the experiment the excised tumours were sectioned at  $10 \mu\text{m}$  thickness, three sections at  $100 \mu\text{m}$  apart were stained for CD34/Endomucin and  $\alpha\text{-SMA}$ , counterstained for DAPI and imaged using the Nikon A1R confocal microscope. Randomly selected regions, 10 from each section, were captured at 20x for macroscopic visualisation and at 60x for quantification as described in the previous section.

Livers are highly vascular organs and as all blood passes through the liver for nutrient absorption and filtration of unnecessary substances ((Debbaut et al.,

2014); Kalra and Tuma, 2018), livers were used as valid tracer delivery controls in this study. Hence, the livers of mice were also obtained after terminal perfusion to validate injection success, in order to ensure that a comparable amount of tracer had been injected between mice and any differences seen were not due differences in amount of tracer injected.

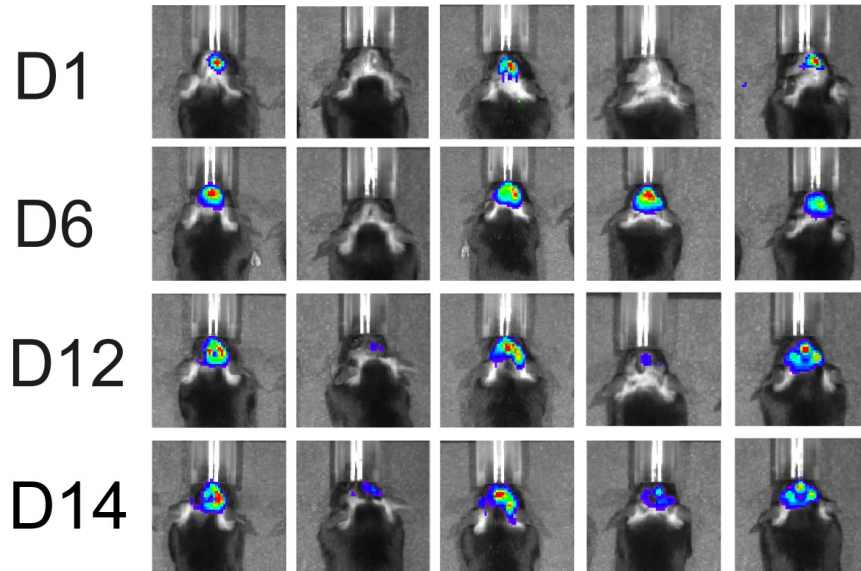
A





B

Control



2 x 5Gy

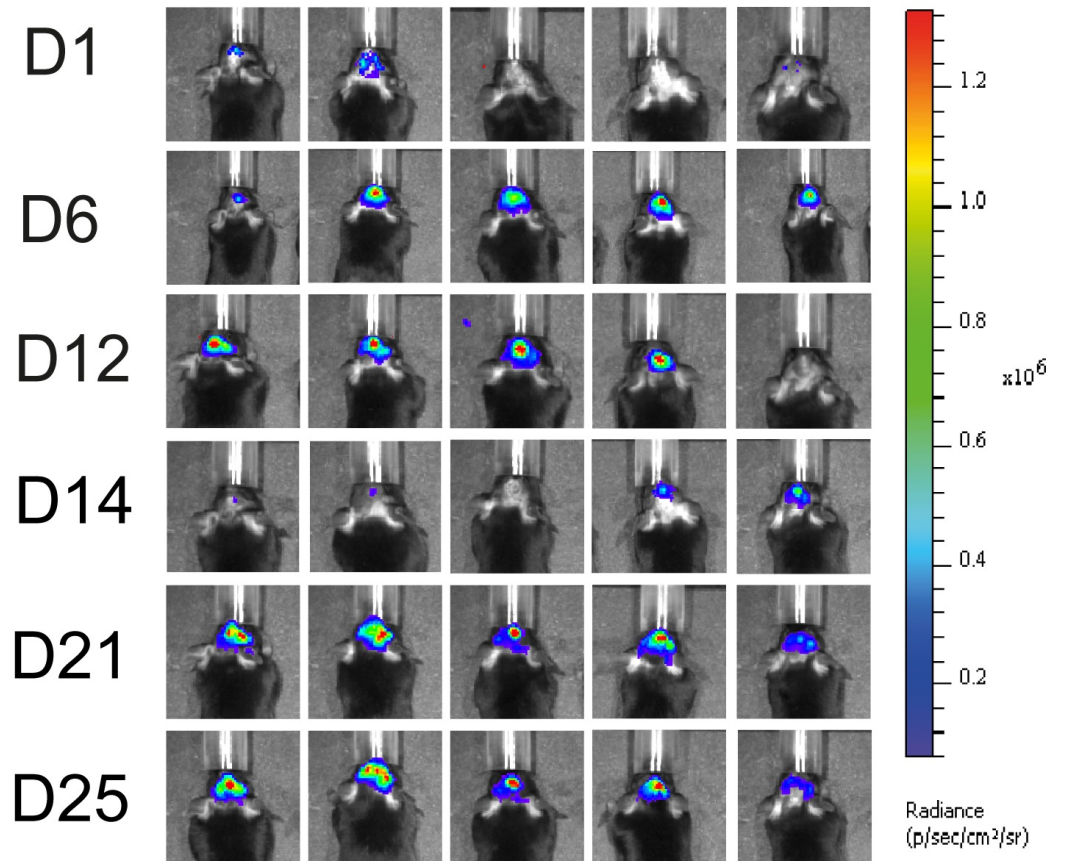


**Figure 4.13 Monitoring of CT2A tumour growth following irradiation in the tracer extravasation repeat experiment.**

CT2A-Luc murine glioma cell line ( $1 \times 10^5$  cells) was injected intracranially into the striatum of C57BL/6 mice. Fractionated irradiation (2 x 5Gy) was delivered on days 7 and 8 following implantation using SARRP. Tumour growth was followed non-invasively using IVIS bioluminescence imaging starting 1 day after tumour implantation. Control mice were sacrificed on day 18 and irradiated mice on day 26 after implantation.

(A) Graphs show the bioluminescence signal intensity of mice (n=5 for control and radiation treated group) following subcutaneous injection of luciferin as measured in total flux (photons/seconds). Top panel shows individual mouse readings and bottom panel shows average readings  $\pm$ SEM. Note the statistical significance of bioluminescence signal intensity between control and radiation treated group on D14.

(B) Images from IVIS scans showing the progression of tumour growth in mouse brains. Note the reduction in bioluminescence signal on day 12 or 14 in the irradiated group which is followed by regrowth.

**Table 4.1 List of CT2A tumour control and irradiated tumour samples analysed in the tracer extravasation experiment.**

<b>Mouse ID</b>	<b>Age (weeks) at intracranial implantation</b>	<b>Sex</b>	<b>Irradiation</b>	<b>Tumour excision day post implantation</b>	<b>Final IVIS signal</b>	<b>Neurological symptoms (Y/N)</b>	<b>Tracer</b>
563	10	F		D18	2.713E+07	Y	BSA-AlexaFluor555
564	10	F		D18	6.944E+07	Y	BSA-AlexaFluor555
489	10	F		D18	1.352E+07	Y	BSA-AlexaFluor555
572	9	F		D18	1.030E+07	Y	BSA-AlexaFluor555
486	10	F		D18	6.985E+07	Y	BSA-AlexaFluor555
519	9	F	X	D26	4.524E+07	Y	BSA-AlexaFluor555
577	19	F	X	D26	2.419E+07	Y	BSA-AlexaFluor555
485	10	F	X	D26	1.196E+08	Y	BSA-AlexaFluor555
506	10	F	X	D26	2.419E+07	Y	BSA-AlexaFluor555
538	10	F	X	D26	2.132E+07	Y	BSA-AlexaFluor555

List of samples in the experiment investigating blood vessel extravasation in control and irradiated tumours including day of excision and IVIS signal. Average final IVIS reading (at the day of excision) for control tumours:  $3.80 \times 10^7$  and irradiated tumours:  $4.69 \times 10^7$ ,  $P = 0.71$ .

Images of sections from control tumours and tumours regrown after irradiation stained for CD34/Endomucin,  $\alpha$ -SMA and DAPI are shown in Figure 4.14, which illustrates the reduced amount of overall tracer extravasation the regrown tumours compared to control in regions with similar number of blood vessels. Figure 4.14 B depicts tracer extravasation patterns in individual blood vessels in control and regrown tumours. On the whole, control blood vessels had a higher amount of tracer extravasation compared to regrown tumours. A consistent pattern regarding effects of pericyte association on extravasation was observed as in the pilot experiment, in that high tracer extravasation was detected despite tight association of  $\alpha$ -SMA+ cells (top control panel, Figure 4.14B). Some blood vessels with tight of  $\alpha$ -SMA+ cell association in irradiated regrown tumours did show low extravasation (top regrowth panel, Figure 14B). It is important to recognise that different regions in the tumour had varied levels of extravasation. Given the level of variability of blood vessel patterns and tracer extravasation, thorough analysis was necessary to determine the differences in extravasation between control and irradiated regrown tumours, and contribution of different blood vessel phenotypes to the patterns of extravasation.

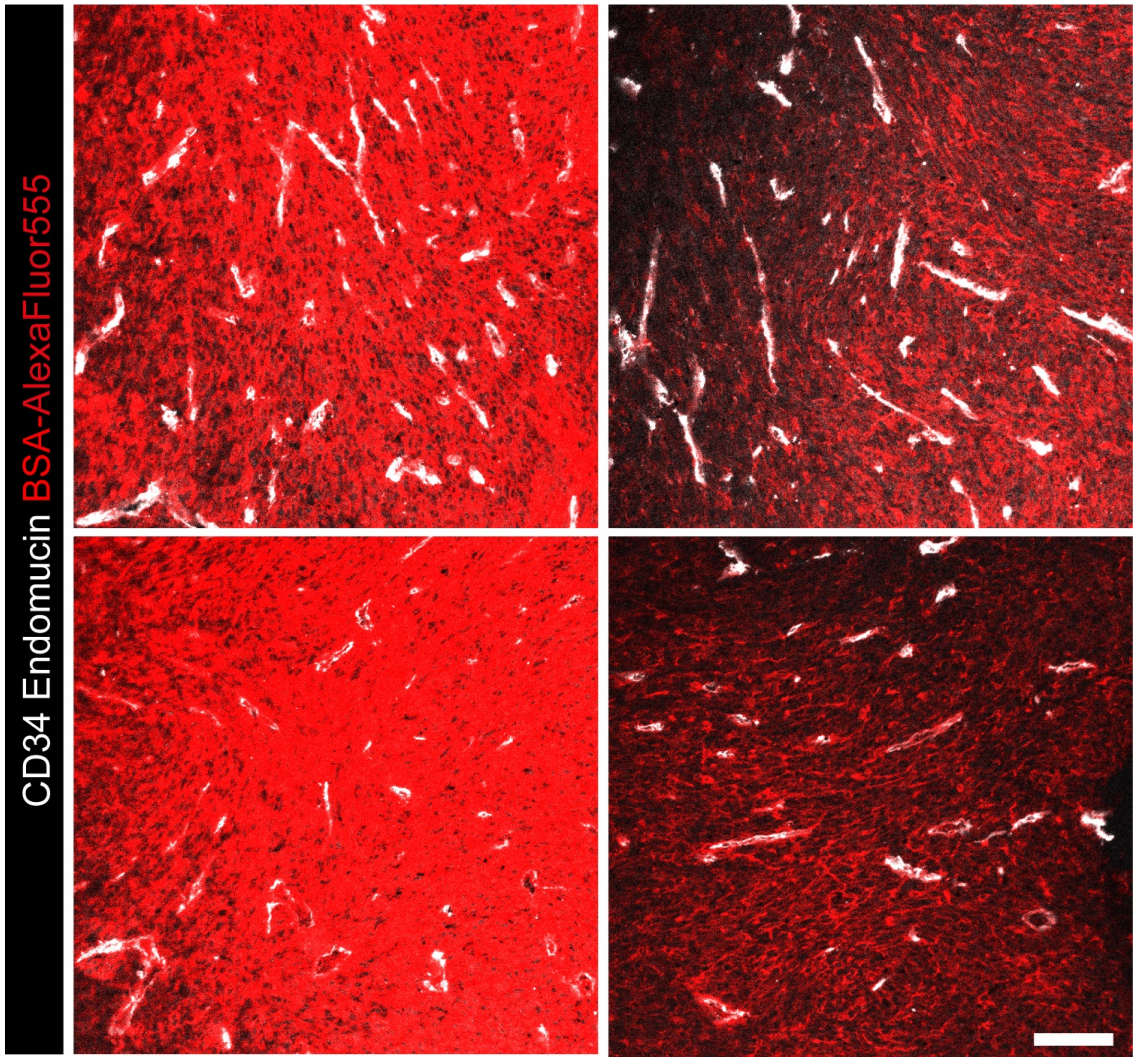
Analysis of multiple tumour regions, and individual blood vessels (control = 222, radiotherapy = 223) imaged at 60x magnification was performed. Figure 4.15 shows the data for tracer-positive pixels of individual blood vessels in each tumour, and the mean extravasation of control and regrown irradiated tumours. The data show variability in the tracer-positive pixels of extravasation amongst different tumours. The highest tracer pixel positivity for control group was 2.06 (a.u.)  $\pm$  1.50 and the lowest was 0.27 (a.u.)  $\pm$  0.57. Whereas in irradiated group, the highest tracer pixel positivity was 1.20 (a.u.)  $\pm$  1.23, and the lowest was 0.09 (a.u.)  $\pm$  0.13 (Figure 4.15 A). When considering the pooled data of blood vessels from each group there was a statistically significant decrease ( $P < 0.001$ ) in the tracer-positive pixels in the irradiated regrown tumours (Figure 4.15 B).

As a control for tracer injection, the mean fluorescence intensity of ten 20x magnified regions of liver sections from the control and regrown irradiated groups sectioned at 10  $\mu\text{m}$  was quantified. The liver of mouse ID 486 in the control group could not be quantified due to experimental collection error. Figure 4.16 provides data on the amount of tracer detected in each individual mouse liver (Figure 4.16 A) and shows the average across each group (Figure 4.16 B), measured in mean fluorescence intensity in the area which is directly proportional to the tracer abundance in the region. Although there was some variability of mean fluorescence intensity between different mice as shown in Figure 4.16A, when looking at the average fluorescence intensity per group, there was no significant difference ( $P = 0.77$ ) in the amount of tracer injected between the control and radiation groups. Livers of the control group had a mean fluorescence intensity of  $119.27 \text{ (a.u.)} \pm 40.99$ , while the mean for irradiated group livers was  $116.75 \text{ (a.u.)} \pm 42.71$ . This confirms that the differences in tracer extravasation seen in the control and the regrown tumours were not due to the variability in the amount of tracer injected.

A

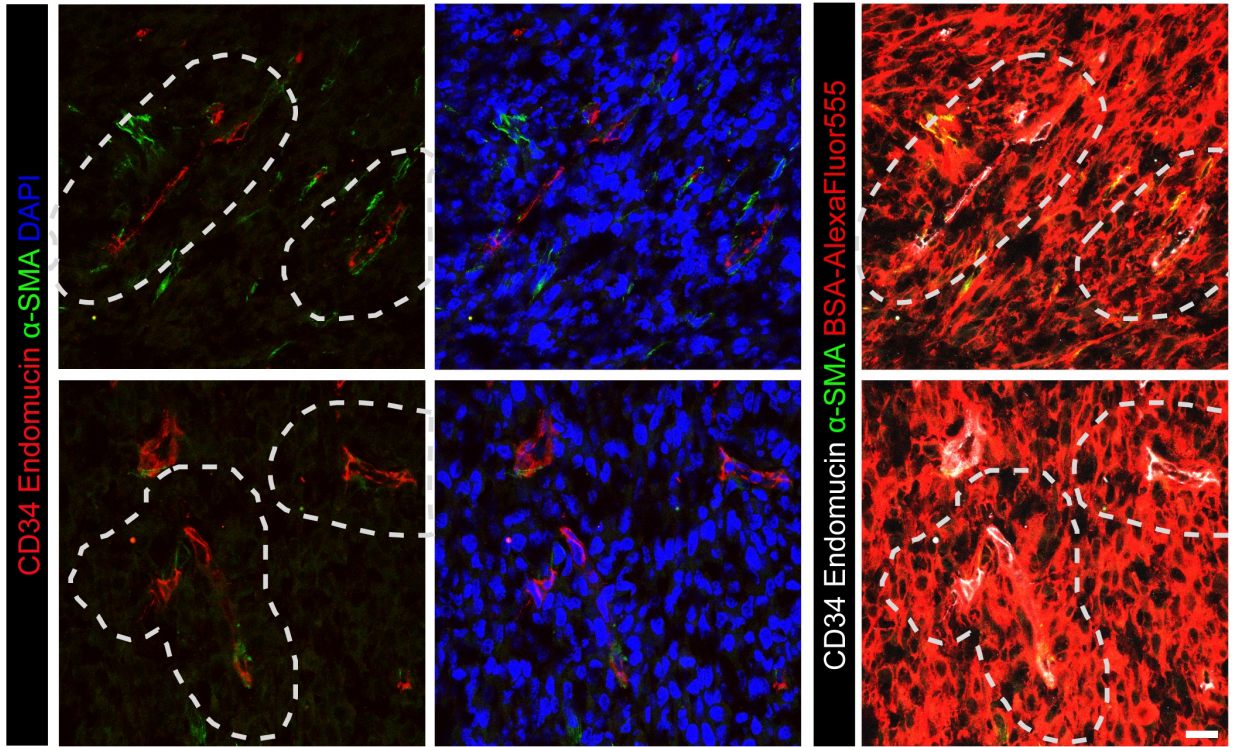
Control

Regrowth  
(2 x 5Gy)



B

Control



Regrowth (2 x 5Gy)

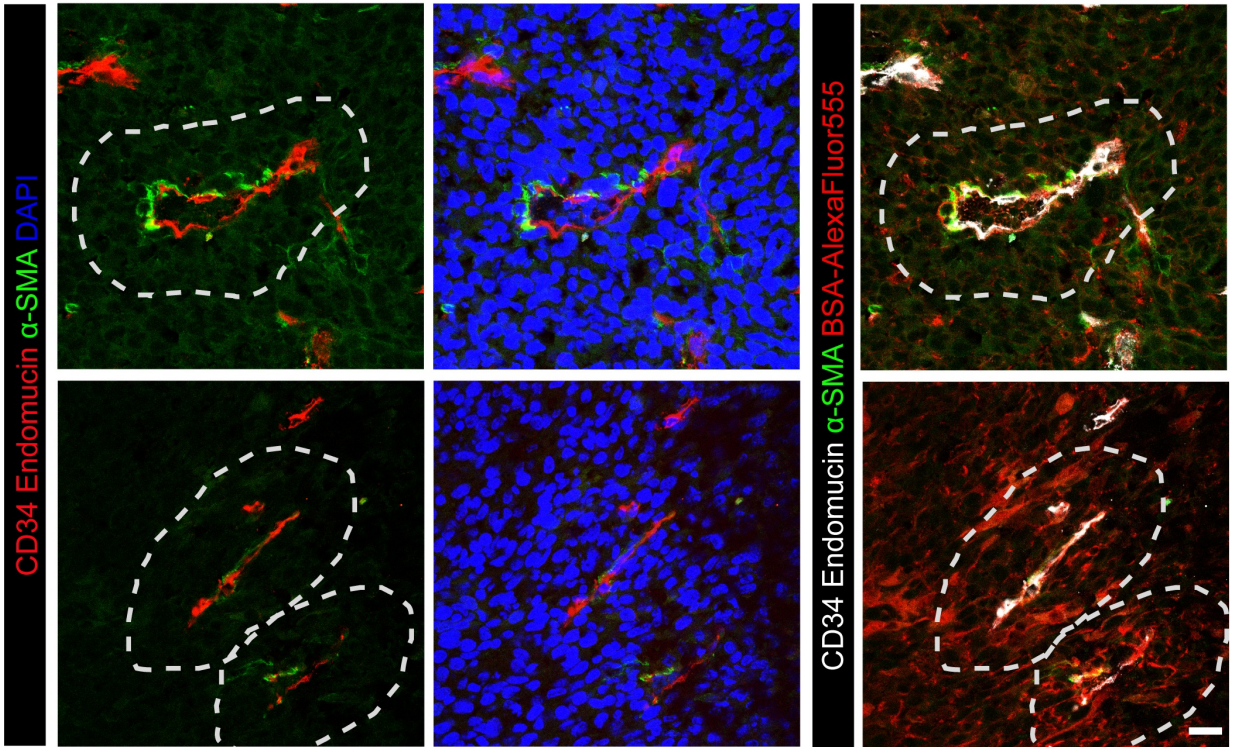


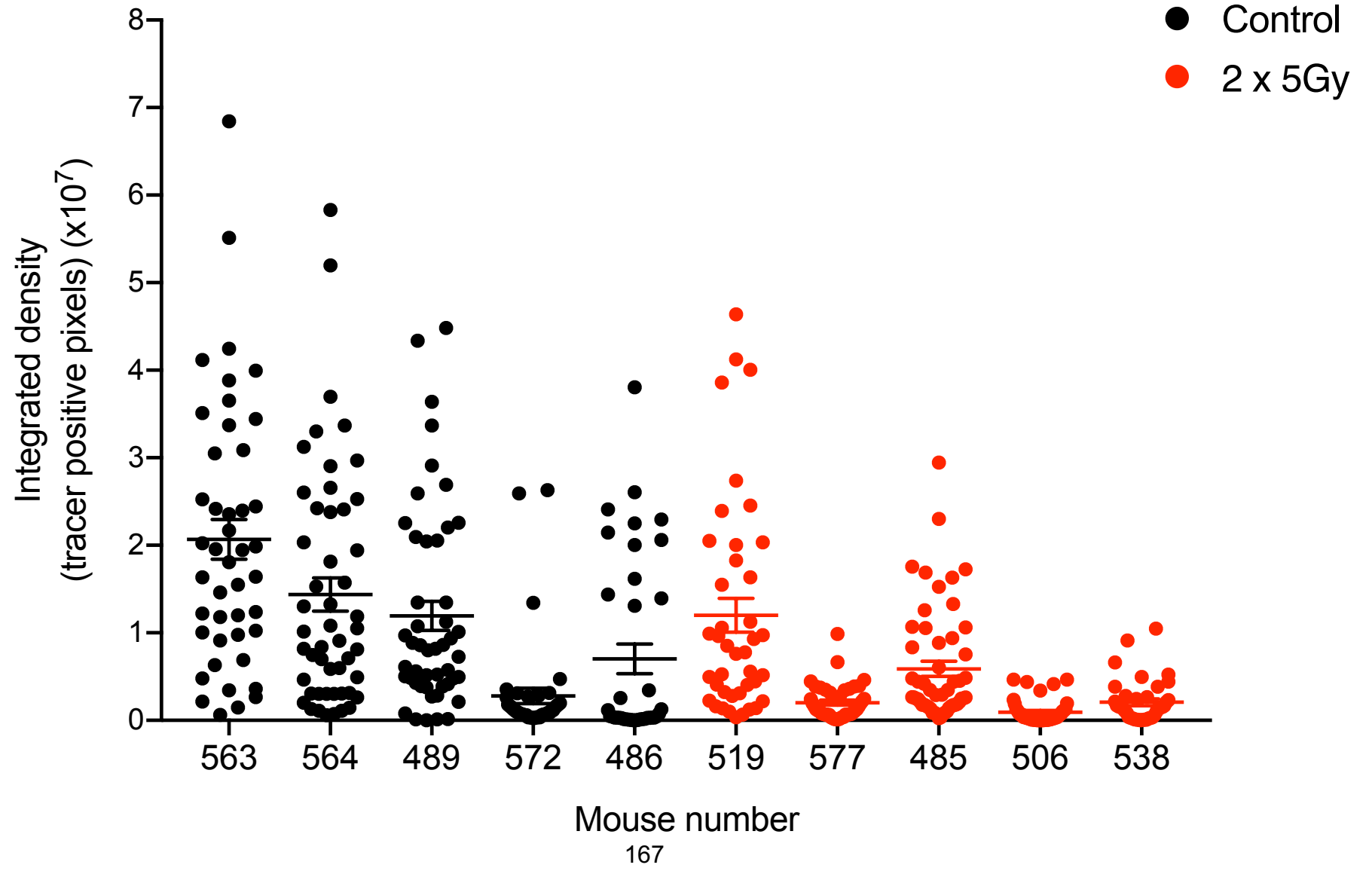
**Figure 4.14 CT2A Tumours regrown after irradiation display reduced tracer extravasation compared to untreated tumours.**

CT2A-Luc murine glioma cell line ( $1 \times 10^5$  cells) was injected intracranially into the striatum of C57BL/6 mice. Fractionated irradiation (2 x 5Gy) was delivered at days 7 and 8 using SARRP and irradiated tumours were allowed to regrow. BSA-AlexaFluor555 was injected intravenously prior to terminal perfusion on days 18 (control) and 26 (radiotherapy). Sections from excised tumours were stained for  $\alpha$ -SMA and CD34/Endomucin for the visualisation of blood vessels. Images were acquired using Nikon A1R confocal microscope and analysed using ImageJ.

(A) Images at 20x magnification show reduced overall extravasation in irradiated tumours ID 506, 577 compared to control tumours ID 563, 564. Scale bar = 100  $\mu$ m.

(B) Images at 60x magnification show reduced tracer extravasation from individual blood vessels in irradiated regrown compared to control tumours. Dotted lines mark a region of 40  $\mu$ m around individual blood vessels for quantification of tracer-positive pixels of extravasation Figure 4.15. Scale bar = 20  $\mu$ m.

A



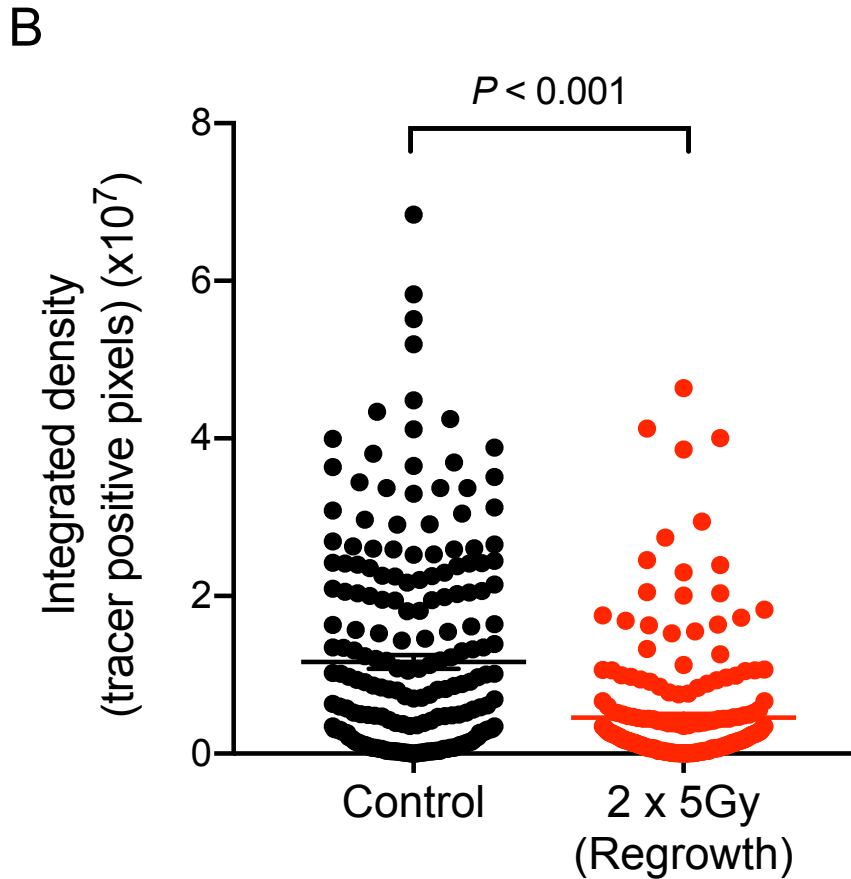


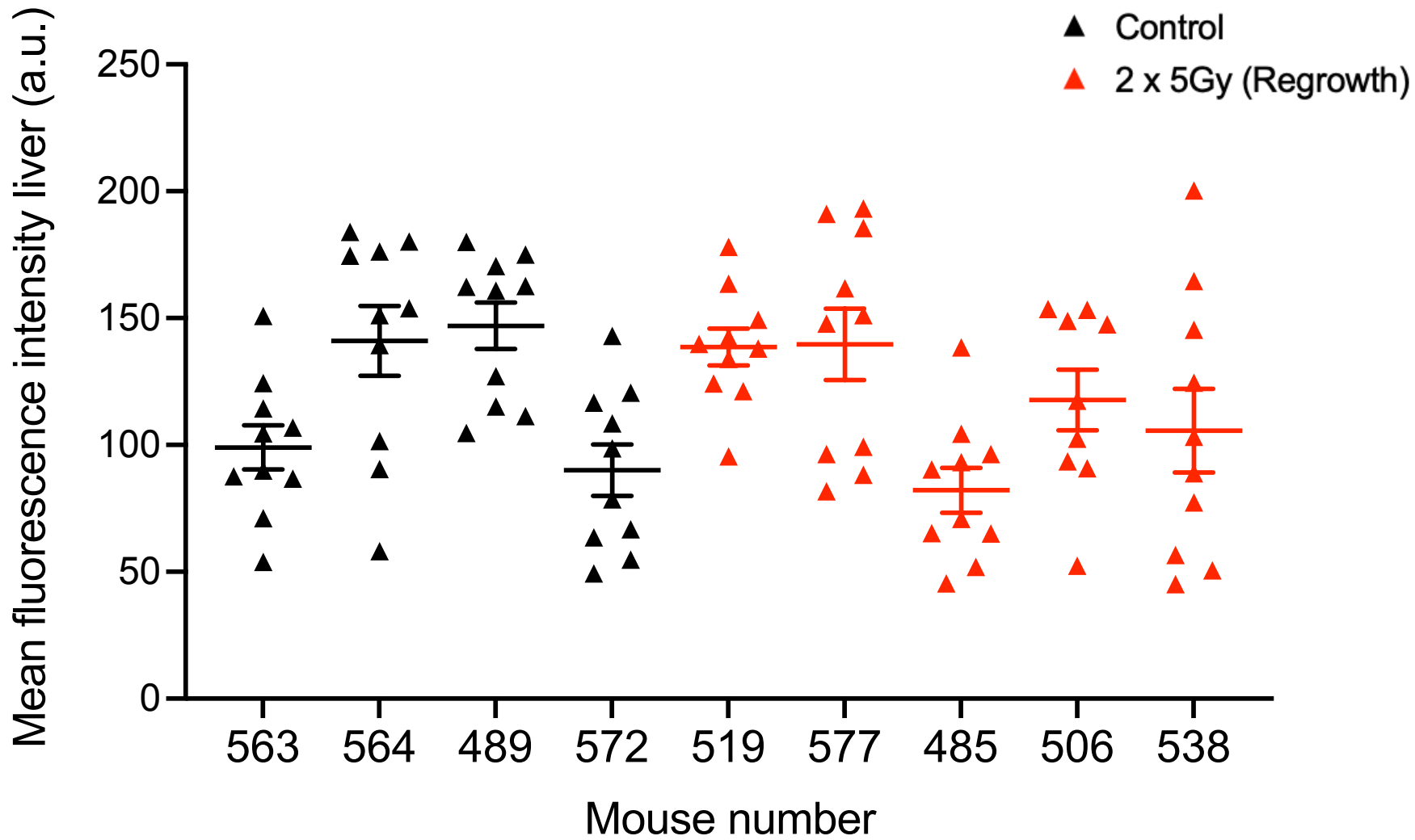
**Figure 4.15 Quantification of tracer-positive pixels of extravasation around blood vessels shows decreased extravasation in irradiated regrown tumours compared to control.**

The tracer-positive pixels of extravasation were measured using ImageJ software in 60x confocal images of control and regrown irradiated tumours as shown in Figure 4.15 B. The fields for quantification were randomly selected from the CD34/Endomucin staining and images were acquired for BSA-AFluor555. Tracer extravasation was quantified within 40  $\mu\text{m}$  of the blood vessel periphery.

(A) Dot plot shows tracer-positive pixels of individual blood vessels for each of the 5 control and 5 regrown tumours.  $n$  = number of blood vessels analysed per individual mouse: control average = 44, radiotherapy average = 45.

(B) Dot plot shows tracer-positive pixels of all blood vessels quantified in control and regrown tumours after irradiation.  $n$  = number of blood vessels analysed from 5 mice per condition: control = 222, radiotherapy = 223.

A



B

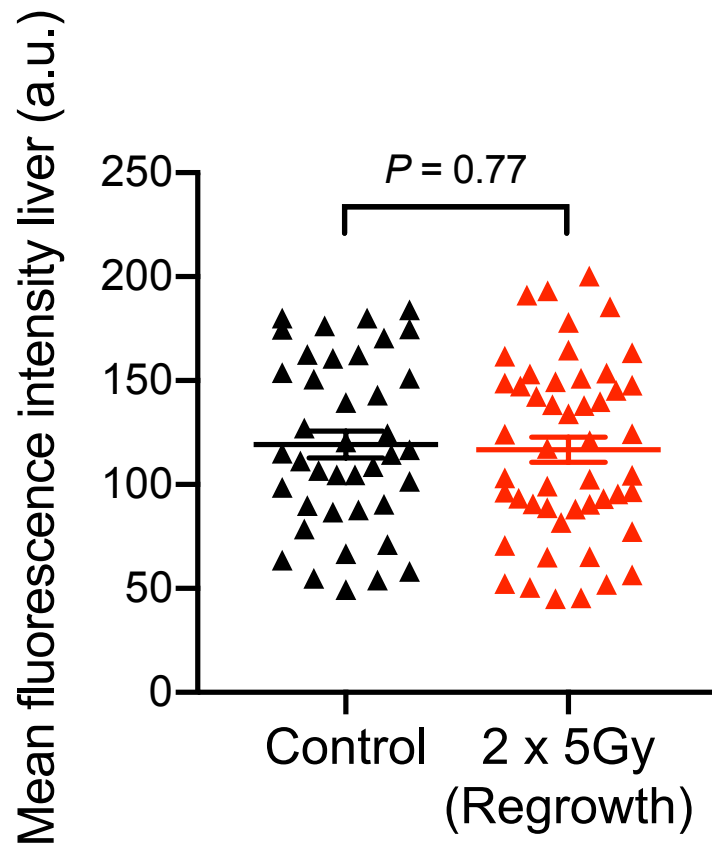


**Figure 4.16 Liver control samples of tracer injected mice display a comparable amount of tracer between control and irradiated group.**

CT2A-Luc tumour bearing C57BL/6 mice were injected intravenously with BSA-AlexaFluor555 prior to terminal perfusion. Fractionated irradiation was performed at days 7 and 8 at 5Gy each using SARRP. Alongside tumour bearing brains the livers were excised and collected at day 18 for control and day 26 for radiotherapy group after intravenous tracer injection and terminal perfusion. Two liver sections 100  $\mu\text{m}$  apart, were quantified for the abundance of tracer within 10 randomly selected areas at 20x magnification that were analysed for mean fluorescence intensity using ImageJ. Note that mouse ID 486 from control group used in further extravasation analysis did not have a liver control due to experimental collection error.

(A) Dot plot shows individual mean fluorescence intensity of tracer in liver sections in individual tracer injected mice. n = number of randomly selected images per liver sample analysed: control and radiotherapy = 10.

(B) Dot plot shows no significant difference between the mean fluorescence intensity of control and radiotherapy group. n = number of randomly selected images analysed from 4 control mice and 5 radiotherapy treated mice: control = 40, radiotherapy = 49.

#### **4.9 Blood vessel association with $\alpha$ -SMA positive cells does not alter tracer extravasation in control tumours or tumours regrown after radiotherapy**

Following the observation of the significant reduction of tracer extravasation in the radiotherapy treated regrown tumours, it was essential to determine which blood vessel phenotypes were affected most and/ or were contributing to the effects seen in the regrown tumours. This investigation was made possible by classifying blood vessels according to traits that had changed in regrown tumours after irradiation:  $\alpha$ -SMA expression, lumen size and vessel length and determining tracer extravasation in relation to those traits.

First, an analysis was performed of the relationship between tracer extravasation and  $\alpha$ -SMA positivity or association with  $\alpha$ -SMA+ cells in 222 blood vessels from control and 223 from regrown tumours. Consistent with the findings in the pilot experiment that  $\alpha$ -SMA cell positivity or association did not affect tracer extravasation in either the control or the irradiated group (Figure 4.12). In the control group (Figure 4.17 A) there was no significant difference in tracer extravasation when  $\alpha$ -SMA negative vessels were compared to blood vessels with  $\alpha$ -SMA positive cells ( $P = 0.59$ ), or blood vessels with  $\alpha$ -SMA+ cells tightly associated ( $P = 0.17$ ). The same observation was made in the radiotherapy treated regrown tumours (Figure 4.17 B) where there was no significant difference in tracer extravasation between blood vessels lacking  $\alpha$ -SMA+ cells and blood vessels with  $\alpha$ -SMA positive cells ( $P = 0.48$ ), or blood vessels tightly associated with  $\alpha$ -SMA+ cells ( $P = 0.07$ ).

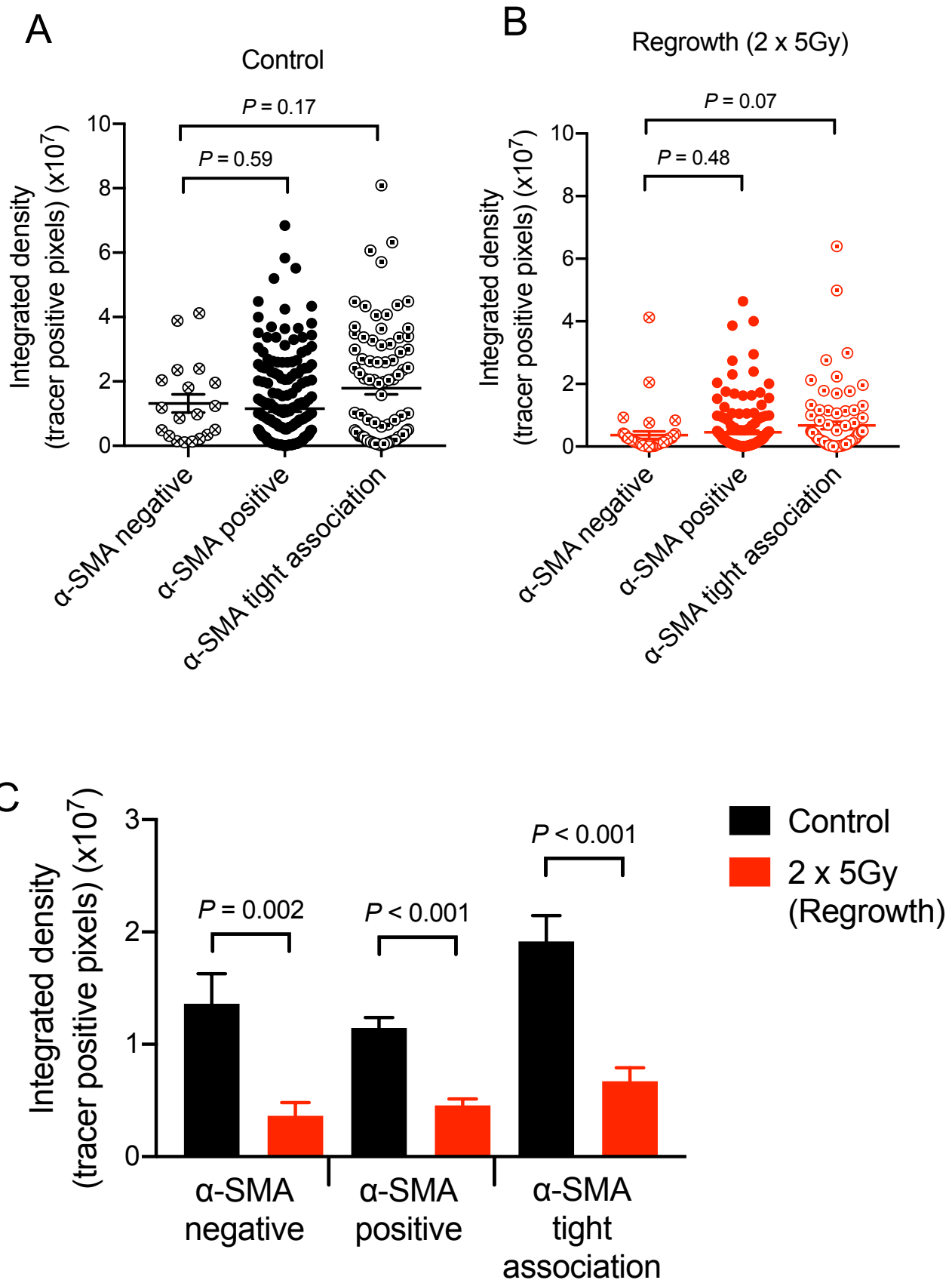


**Figure 4.17  $\alpha$ -SMA+ cell association with tumour blood vessels does not contribute to the differences in tracer extravasation between control and irradiated tumours.**

CT2A-Luc tumour bearing C57BL/6 mice were injected intravenously with BSA-AlexaFluor555 prior to terminal perfusion. Fractionated irradiation was performed at days 7 and 8 at 5Gy each using SARRP. Mouse brains were excised at day 18 for control and day 26 for radiotherapy group. Sections of mouse brains were stained for CD34/Endomucin,  $\alpha$ -SMA and DAPI. CD34/Endomucin positive blood vessels were randomly selected at 60x magnification and images of CD34/Endomucin and  $\alpha$ SMA were captured using a Nikon A1R confocal microscope.  $\alpha$ -SMA scoring, and quantification of tracer positive pixels were performed using ImageJ software.  $\alpha$ -SMA scoring criteria were as described in Figure 4.6 B.

(A) Dot plot (black) shows no significant difference in tracer extravasation between  $\alpha$ -SMA negative and  $\alpha$ -SMA positive blood vessels, or  $\alpha$ -SMA positive blood vessels with tight pericyte association in the control tumours.

(B) Dot plot (red) shows no significant difference in tracer extravasation between  $\alpha$ -SMA negative and  $\alpha$ -SMA positive blood vessels, or  $\alpha$ -SMA positive blood vessels with tight pericyte association in the irradiated tumours.

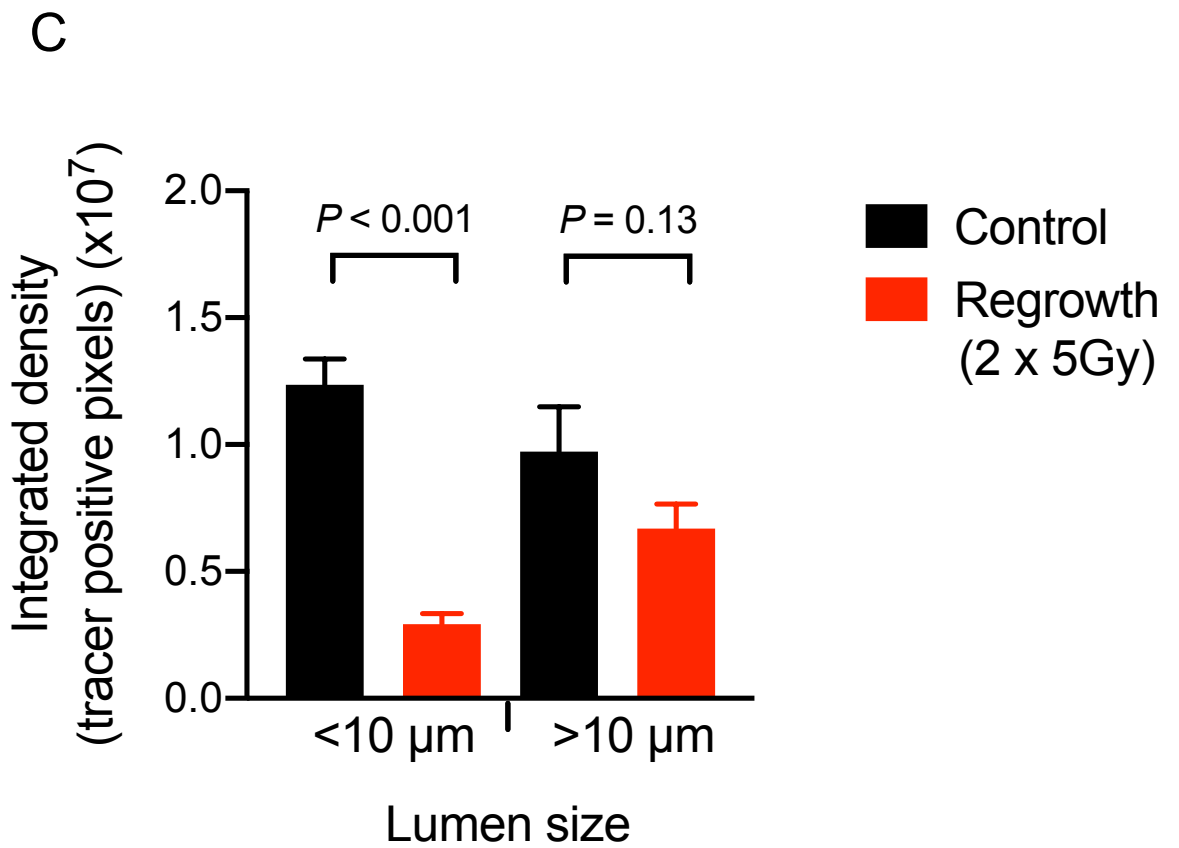
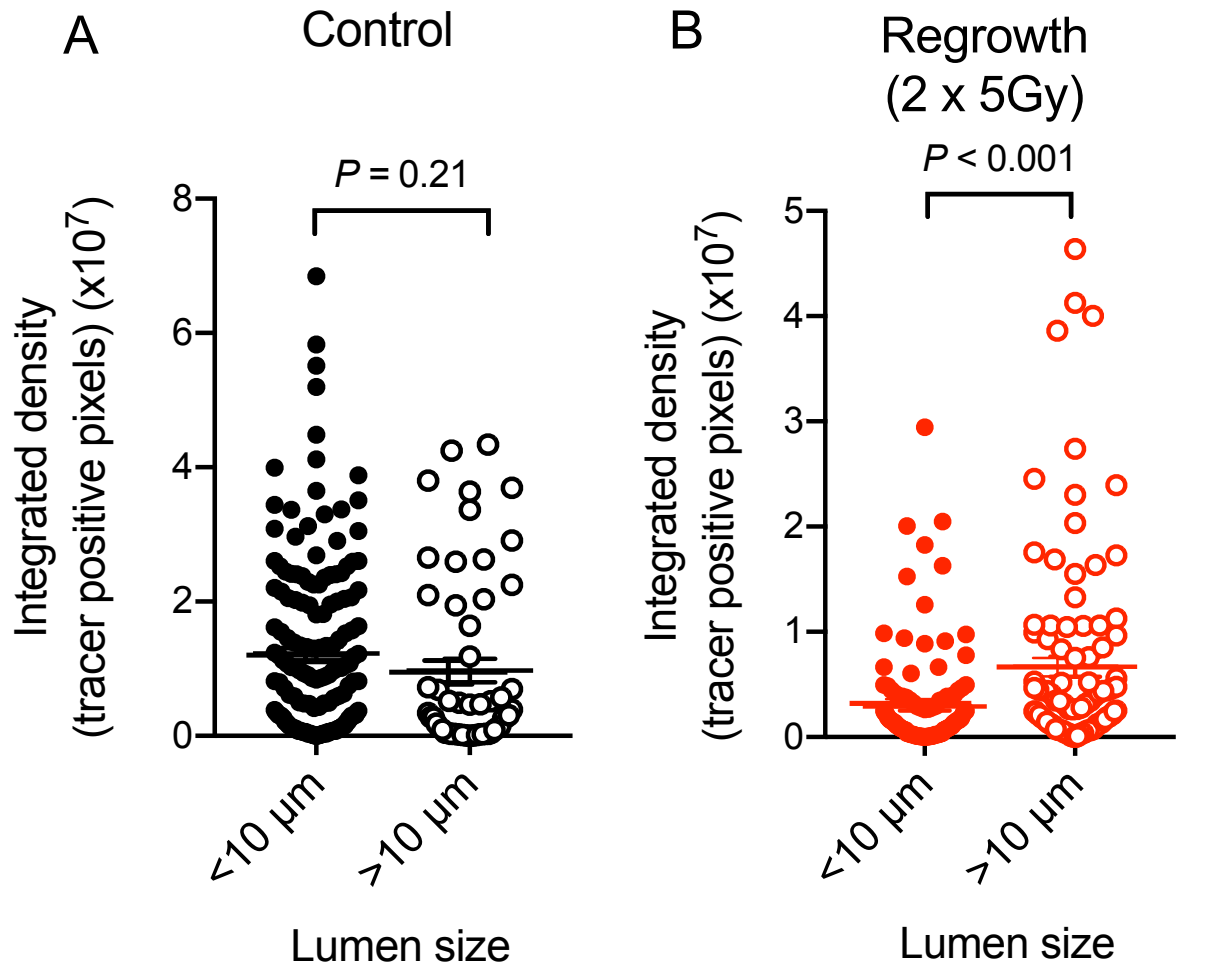
(C) Bar chart shows significant decrease in tracer-positive pixels in irradiated tumours in blood vessels negative for  $\alpha$ -SMA, positive for  $\alpha$ -SMA, and with  $\alpha$ -SMA tight association.

Error bars represent SEM. n = number of blood vessels analysed from 5 mice per condition: control = 222, radiotherapy = 223.

#### **4.10 Decreased tracer extravasation from blood vessels with lumen size $\leq 10\mu\text{m}$ in irradiated regrown tumours**

Another effect observed in the regrown CT2A tumours post radiation as compared to controls was the increase in blood vessel lumen size and percentage of blood vessels with detectable lumens as detailed in the previous chapter (Chapter 3, Figure 3.7). Since the abundance of  $\alpha\text{-SMA}^+$  cells did not seem to play a role in the decrease in tracer extravasation in the regrown tumours, this analysis focused on the parameter of vessel lumen size and its association with their tracer extravasation patterns.

Dot plots as shown in Figure 4.18 A and B highlight the intragroup differences in tracer extravasation between vessels with lumen size, equal or under  $10\mu\text{m}$  and over  $10\mu\text{m}$ . In the control tumours, there was a trend of higher extravasation from lumens with smaller size ( $\leq 10\mu\text{m}$ ) however this difference was not significant between the two lumen sizes. When looking at regrown tumours, there was a significant increase in the tracer-positive pixels in vessels with lumens larger than  $10\mu\text{m}$  as compared to vessels with lumens smaller than or equal to  $10\mu\text{m}$  ( $P < 0.001$ ). When considering intergroup differences, the reduction in tracer extravasation in regrown tumours is more pronounced in vessels with smaller lumens ( $P < 0.001$ ) compared to vessels with lumens over  $10\mu\text{m}$  ( $P = 0.13$ ) as shown in Figure 4.18 C. In order to gain further understanding as to which size of blood vessel lumens best associates to the overall reduction of tracer extravasation, further analysis was conducted as shown in Figure 4.18 D, which showed a positive correlation between vessel lumen size and tracer-positive pixels of extravasation in irradiated regrown tumours that was not observed in controls. Furthermore, a statistically significant difference between control and regrown tumours ( $P = 0.003$ ) could be detected between vessels with lumen size smaller or equal to  $10$  but not in blood vessels of larger lumen size (Figure 4.18 D).



D

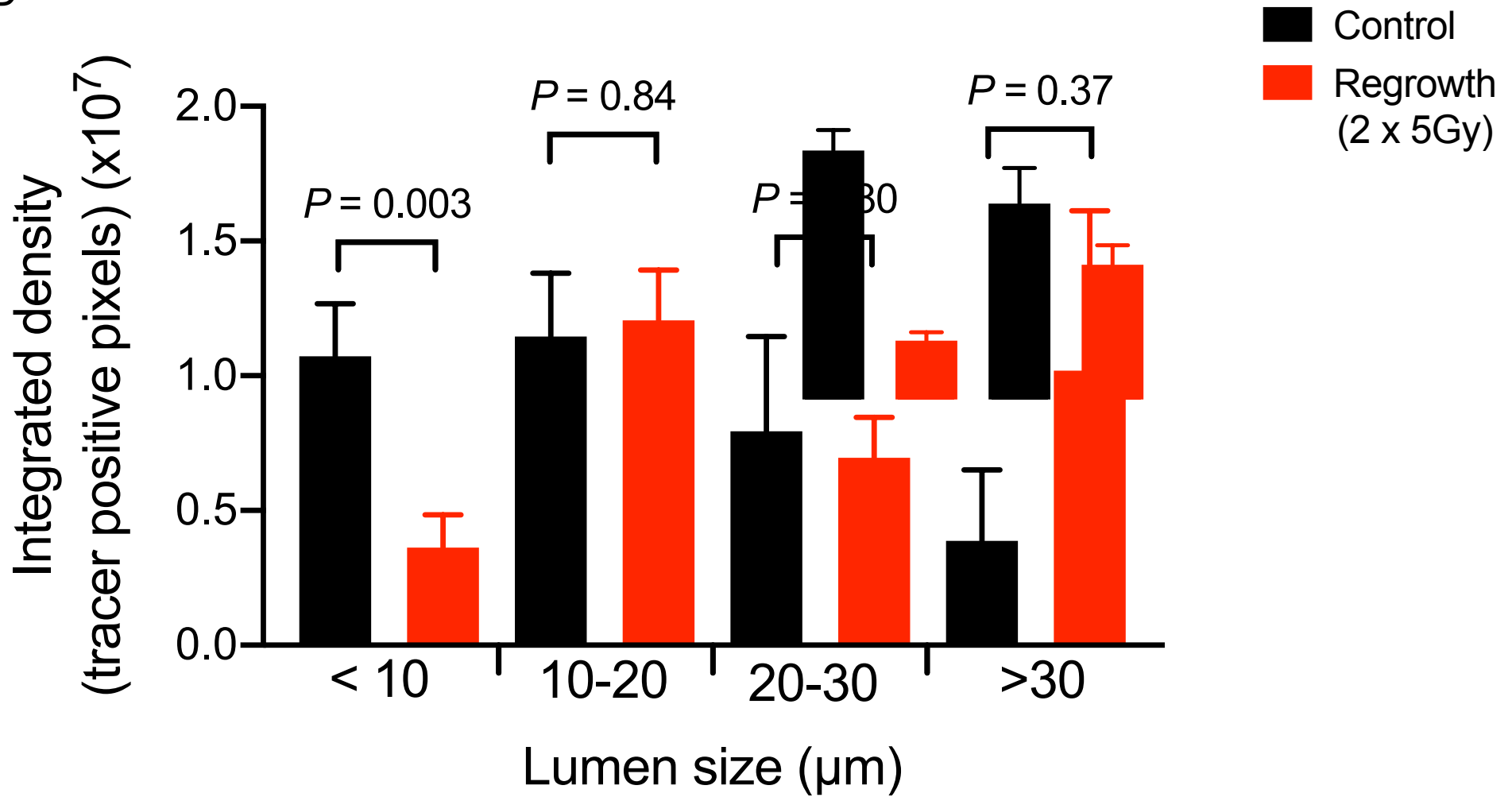


**Figure 4.18 Blood vessels with smaller lumens show the largest reduction in tracer extravasation in CT2A regrown tumours following radiotherapy.**

The tracer-positive pixels of extravasation were measured using ImageJ software in 60x confocal images of control and regrown irradiated tumours as shown in Figure 4.15 B. The fields for quantification were randomly selected from the CD34/Endomucin staining and images were subsequently acquired for BSA-AFluor555. Tracer was quantified within 40  $\mu\text{m}$  of the blood vessel periphery and tracer values were assigned to blood vessels with different lumen size.

(A) Dot plot (black) shows a non-significant difference in tracer-positive pixels of extravasation between vessels with lumens  $< 10 \mu\text{m}$  and  $> 10 \mu\text{m}$  in control tumours.

(B) Dot plot (red) shows a statistically significant difference in tracer-positive pixels of extravasation between vessels with lumens  $< 10 \mu\text{m}$  and  $> 10 \mu\text{m}$  in radiotherapy treated tumours.

(C) Bar chart illustrates a statistically significant difference in tracer-positive pixels of extravasation in vessel with lumens  $< 10 \mu\text{m}$  between control and radiotherapy treated tumours.

(D) Bar chart illustrates a statistically significant difference in tracer-positive pixels of extravasation in vessels with lumen size between 4 - 10  $\mu\text{m}$ .

Error bars represent SEM. n = number of vessels analysed from 5 mice per condition: control = 122, radiotherapy = 123.

#### **4.11 Decreased tracer extravasation from blood vessels with shorter length in irradiated regrown tumours**

Lastly, another phenotype that was observed in the previous chapter and also considered during the quantification of tracer extravasation was an increase in blood vessel length in irradiated regrown tumours compared to controls. When observing intragroup differences within control tumours, there was an inverse correlation between blood vessel size and tracer-positive pixels of extravasation with blood vessels of a length between 5-25  $\mu\text{m}$  having larger tracer positive pixels compared with blood vessels over 25  $\mu\text{m}$  in length ( $P < 0.001$ , Figure 4.19 A). Consistent with the trend seen in the lumen size described in the previous section for irradiated regrown tumours, there is a positive correlation between tracer extravasation with blood vessels of length over 50  $\mu\text{m}$  showing significantly higher extravasation compared to vessels with length under 50  $\mu\text{m}$  ( $P < 0.001$ ) (Figure 4.19 B). When comparing control with irradiated regrown tumours (Figure 4.19 C) it was the smallest calibre tumours (5-25  $\mu\text{m}$ ) that were most affected by irradiation ( $P = 0.001$ ). This implies that the contribution to the reduction in extravasation in regrown tumours and the blood vessels affected, are not only those with small lumen size but also those with smallest vessel length.

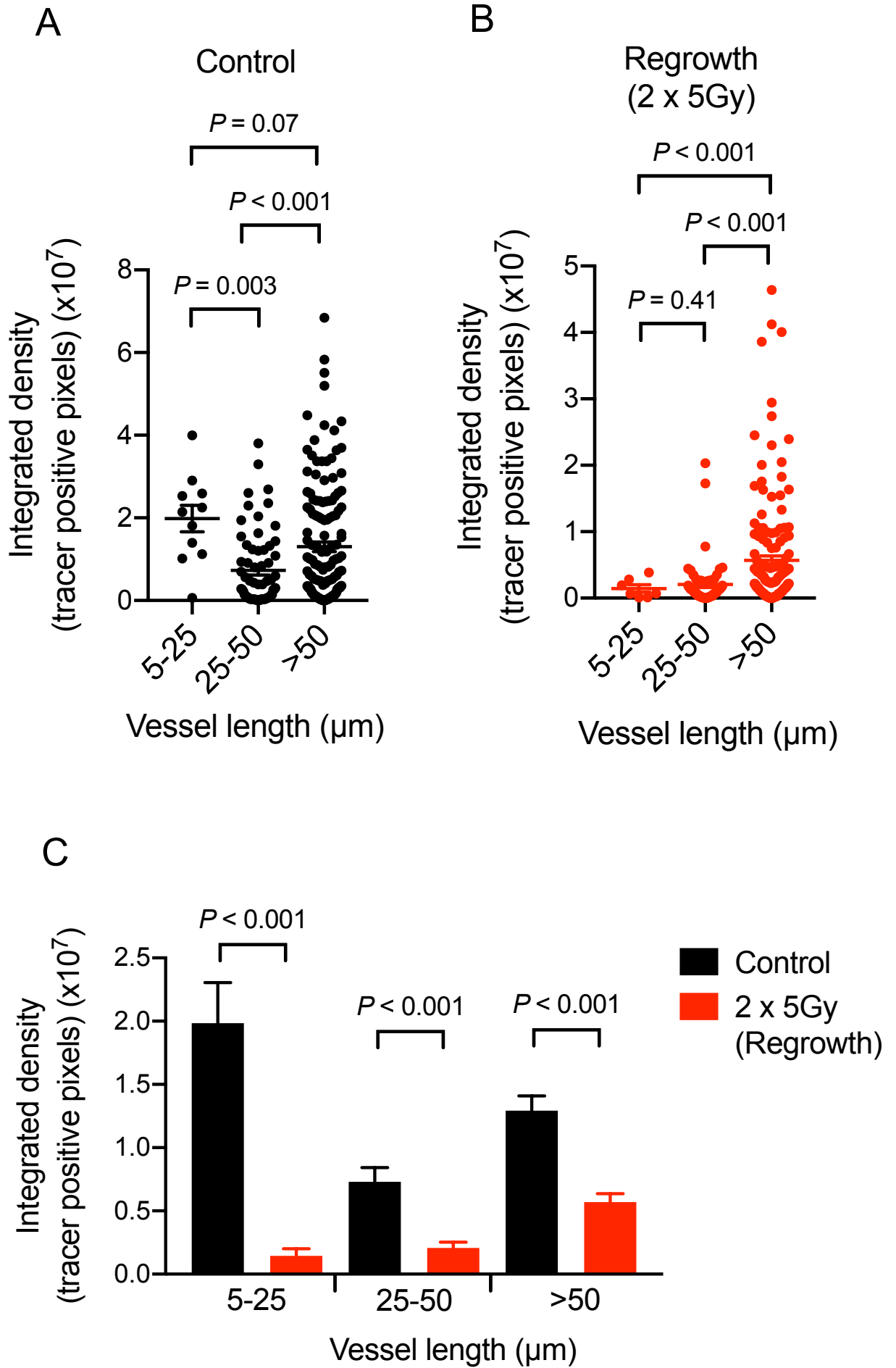


**Figure 4.19 Blood vessels with shorter lengths have the lowest tracer extravasation in irradiated regrown tumours.**

The tracer-positive pixels of extravasation were measured using ImageJ software in 60x confocal images of control and regrown irradiated tumours as shown in Figure 4.15 B. The fields for quantification were randomly selected from the CD34/Endomucin staining and images were acquired for BSA-AFluor555.

(A) Dot plot (black) shows a significantly higher tracer-positive pixels of extravasation of blood vessels with shorter length (5-25  $\mu\text{m}$ ) in control tumours.

(B) Dot plot (red) shows a significantly lower tracer-positive pixels of extravasation of blood vessels with shorter length (5-50  $\mu\text{m}$ ) in irradiated tumours.

(C) Bar chart shows that vessel length between 5 - 25  $\mu\text{m}$  has the largest difference in tracer-positive pixels in control and radiotherapy treated tumours.

Error bars represent SEM. n = number of vessels analysed from 5 mice per condition: control = 122, radiotherapy = 123.

#### **4.12 Increased hypoxia marked by GLUT1 expression in radiotherapy treated regrown tumours**

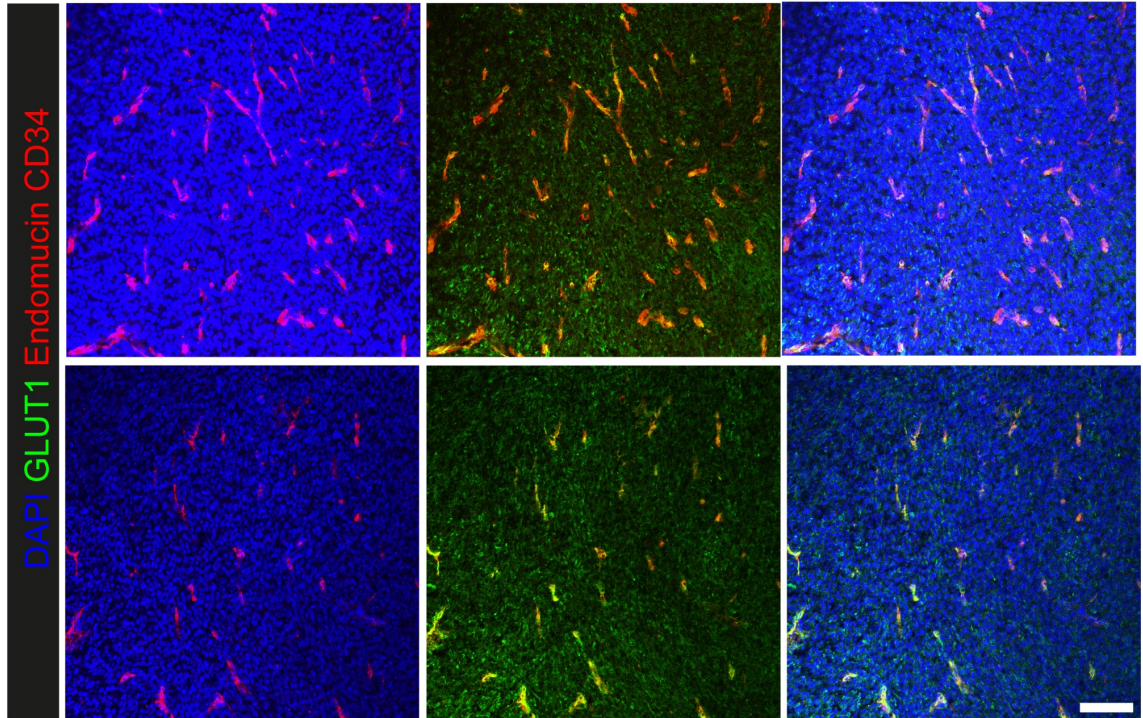
GBM tumours are highly hypoxic due to the defective blood vessel formation. Elevated levels of hypoxia is a major problem for GBM patients as it drives tumour invasion towards healthy brain parenchyma, and functional blood vessels, in order to avoid this complex undesirable environment and maintain its growth (Kaur et al., 2005; Yang et al., 2012). As the reduction in blood vessel permeability may normalise the tumour vasculature alleviating tumour hypoxia or increase hypoxia levels, I set out to investigate how the reduction in blood vessel extravasation impacted on the levels of tumour hypoxia in the irradiated regrown tumours. Glucose transporter-1 (GLUT1) is a uniporter transmembrane protein that allows the facilitated diffusion of glucose which is upregulated at hypoxic conditions due to the increased need for glucose (Airley et al., 2001; Veys et al., 2020). It has been reported previously that its expression in GBM is correlated with hypoxia and HIF1 expression (Mayer et al., 2012) and has been widely used as a hypoxia marker in different cancers (Hoskin et al., 2003; Boström et al., 2016). To investigate whether the recurrent tumours post irradiation in this CT2A implanted GBM model is more hypoxic, GLUT1 antibody was used to mark hypoxia and CD34/Endomucin to mark blood vessels. Two sections 100 µm apart was stained from each tumour. Ten randomly selected images at 20x magnification from each tumour were captured using a Nikon A1R confocal microscope. Following staining quantification to measure GLUT1 expression was based on fluorescence intensity using an ImageJ software. The Image J quantification was performed by Tehniat Ali.

Figure 4.20 A are representative images of GLUT1 stained sections used in the quantification taken at 20x magnification. As shown in Figure 4.20 A, there was a significantly higher GLUT1 expression (green staining) in the irradiated regrown tumours in comparison to the unirradiated control tumours. The fluorescence intensity of these images was subsequently quantified. As shown in Figure 4.20 B and C, there was a significantly higher level of GLUT1 expression in the regrown tumours compared to control ( $P = 0.048$ ). This data suggests that regrown tumours have higher levels of hypoxia compared to control. Therefore, not only that the regrown tumours are less permeable, but there is also

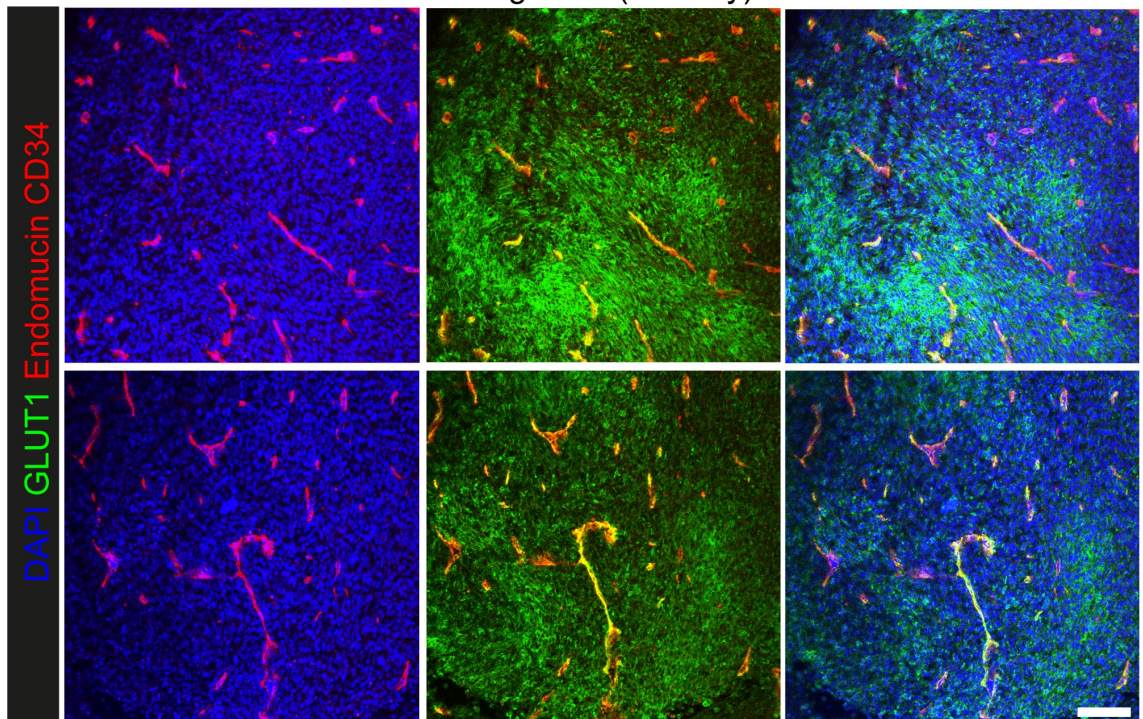
inadequate supply of oxygen in comparison to the demand, in the regrown CT2A implanted tumours.

A

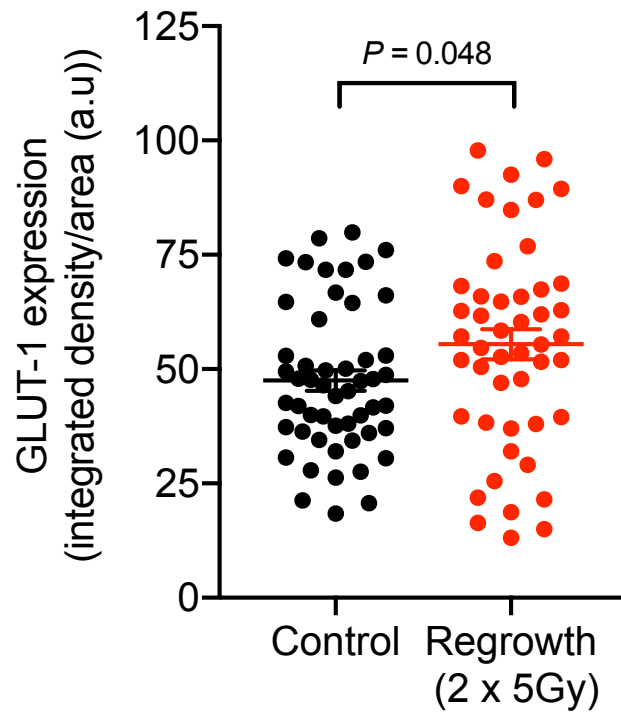
Control



Regrowth (2 x 5Gy)



B



C

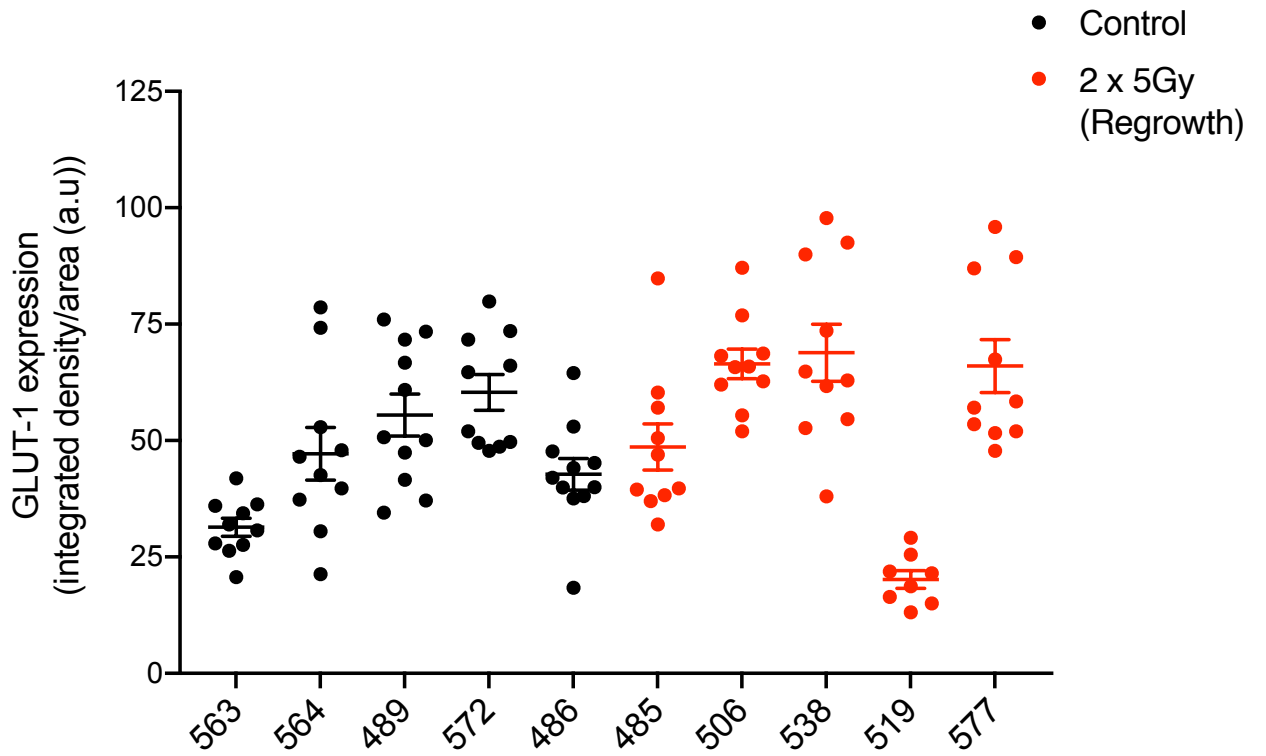


**Figure 4.20 Increased hypoxia in regrown tumours after irradiation marked by GLUT-1 expression.**

CT2A-Luc tumours grown in C57BL/6 mice, control or treated with fractionated irradiation (2 x 5Gy) at days 7 and 8 were excised at day 18 (control) and day 26 (radiotherapy). Sections of mouse brains were stained for CD34/Endomucin, GLUT1 and DAPI. 10 randomly selected CD34/Endomucin positive areas at 20x magnification from 2 sections per condition 100  $\mu$ m apart, were captured for GLUT1 and CD34/Endomucin expression using Nikon A1R confocal microscope, and GLUT1 expression was quantified using ImageJ.

(A) Representative images of CT2A tumour sections of control and regrown CT2A tumours stained with CD34/Endomucin, GLUT1 and DAPI taken at 20x magnification. Scale bar = 100  $\mu$ m.

(B) Dot plot shows a significant increase in GLUT1 levels in irradiated regrown tumours compared with controls.

(C) Dot plot shows GLUT1 expression in individual mice in both control and irradiated regrown tumours.

Error bars represent SEM. n = number of randomly selected images analysed from 5 mice per condition: control = 52, radiotherapy = 48.

### 4.13 Summary

In this chapter, I showed that alongside increase in vascularisation and lumen size, the experimental CT2A implantation GBM model recapitulates the GBM patient samples' blood vessel pericyte expression. Visualisation of pericytes, marked by  $\alpha$ -SMA antibody, present in these tumour samples allowed the characterisation of the three different blood vessel-pericyte association. This includes negative association, pericyte positive tight association and pericyte positive loose association. Initially, pericytes were investigated to understand whether the increase in blood vessel lumen size, was due to the dilation of blood vessels in response to the detachment of pericytes. Through further quantification of these blood vessel-associated pericytes, I have shown that there was an increase in the abundance of pericytes in the radiotherapy treated regrown tumours. This suggests that the increase in lumen size in the regrown tumours was not due to pericyte detachment. Additionally, results from regrown tumours gives evidence of increase in the tight associated pericyte phenotype despite no difference in loose pericyte association between the control and regrown tumours.

Considering the increased abnormal phenotype in the regrown tumours, I then sought to understand the viability and functional integrity of these blood vessels. With the previous result showing evidence of regrown blood vessels having higher number and tighter pericyte association, it was assumed that the regrown blood vessels would be less permeable due to these pericytes. Tracer experiment was subsequently set up to investigate the permeability of these blood vessels through observation of blood vessel tracer extravasation alongside their individual morphology. Using BSA-AlexaFluor555 tracer, I showed that the blood vessels in the radiotherapy treated regrown tumours indeed were less permeable and extravasated less tracer. However, interestingly, when blood vessels were characterized based on their morphology and extravascular tracer positivity, pericytes association did not contribute to the change in tracer extravasation. When these blood vessels were categorised based on size, data showed that the blood vessels with lumens smaller than 10  $\mu$ m contributed to largest reduction of tracer extravasation in the regrown tumours. Lastly, I investigated the hypoxia

status of these tumours by GLUT1 staining. I showed that the radiotherapy treated regrown tumours were more hypoxic compared to the control tumours.

In the future, to fully elucidate the permeability of the blood vessels in the regrown tumours, in addition to the use of an immunohistochemical image quantification of tracer extravasation, a spectrophotometer would ideally be used to quantify overall tracer accumulation. The method used in this study using image quantification was beneficial as it allows the analysis of blood vessel morphology in relation to its tracer extravasation status. Due to the tracer extravasation *in vivo* experiment proving to be highly technical and challenging, the ability to use individual blood vessels in the analysis also allows the reduction of the number of mice used in the study without compromising the data. However, there are limitations that should be considered concerning this method. This includes the problem of the tracer circulating for several hours prior to perfusion, which means that the tracer seen around the vessels might not have directly extravasated to the adjacent vessel but from a distal vessel. In addition to the limitation in the permeability experiment, in the case of the hypoxia experiment, it would be beneficial to add another marker. For example, carbonic anhydrase 9 could be used (CAIX) to further confirm and validate the hypoxia status of these tumours.

In the following chapter, I investigate the role of the GEF *DOCK4*, which has been shown to play a crucial role in blood vessel development including branching, lumenisation using the CT2A implantation GBM model.

## **Chapter 5**

# **Effects of *Dock4* deletion on radiotherapy-induced blood vessel vascular changes**

## 5.1 Introduction

Previous work in the laboratory had shown that the Rac1 exchange factor DOCK4 controls lumen formation in an organotypic angiogenesis model (co-culture of endothelial cells and fibroblasts) and in an intracranial model of breast cancer metastases (Abraham, Scarcia, Bagshaw, McMahon, et al., 2015). Using an EO771 breast cancer cell line intracranially implanted into *Dock4 knockout (ko)* heterozygous mice, as homozygous deletion was embryonic lethal, the authors showed that tumours grown in *Dock4 ko het* mice possessed vessels of smaller mean diameter when compared to tumours grown in wild type (WT) mice. Moreover, when the frequency of lumen size was analysed within a range of lumen diameters, a significant decrease was observed in blood vessel lumens of  $>35\ \mu\text{m}$  in the EO771 tumours (Abraham, Scarcia, Bagshaw, McMahon, et al., 2015). Therefore, given that the analysis of tumours regrown after irradiation showed a significant increase in blood vessels of larger ( $>20\ \mu\text{m}$ ) diameter, in this chapter I set out to investigate whether this increase in response to irradiation was mediated by DOCK4. I hypothesised that *Dock4* deletion may promote normalisation of vascular aberrancy induced by ionising radiation. Due to embryonic lethality in *Dock4*<sup>-/-</sup> homozygous mice, the *Dock4* knockout heterozygous line (referred to as *Dock4het* from this point onwards) was initially employed in experiments designed to assess this hypothesis.

In previous work in the laboratory leading to this thesis when the effects of irradiation on the vasculature of GBM tumours were being assessed, in addition to C75BL/6 WT mice the CT2A cell line was also implanted in *Dock4het* mice and fractionated radiotherapy was delivered to those mice (Chapter 1, Figure 1.9) In this Chapter, I present the quantification of blood vessel parameters (as set out in Chapter 3) in tumours grown in *Dock4het* mice in the absence or presence of radiotherapy. The aim was to assess whether *Dock4* genetic deletion reverses the stimulation of angiogenesis and blood vessel calibre observed in response to irradiation.

Abraham et al. had shown previously that while blood vessel lumen calibre was reduced in *Dock4het* mice compared to controls, perivascular cells were not

affected by global heterozygous *Dock4* deletion, suggesting that downregulation of *Dock4* impacted endothelial cells directly. However, the authors could not exclude the possibility that other cells in the tumour microenvironment may influence angiogenesis in implanted tumours. In order to confirm that the observed effects of *Dock4* deletion were endothelial cell autonomous, a conditional knockout model was generated in the laboratory as described in the section 'Previous work leading to this thesis' (Chapter 1, Section 1.11). Thus, following from the analysis of CT2A tumours in *Dock4*<sup>het</sup> mice, I set up experiments to determine the effect of endothelial *Dock4* deletion on the vascular changes arising from irradiation of CT2A tumours presented in Chapters 3 and 4. The CT2A cell line was implanted in the *Dock4* endothelial conditional knockout mice in order to carry out analysis of blood vessel characteristics including blood vessel length and lumen size in untreated control, and radiotherapy treated regrown tumours. Furthermore, a pilot analysis of blood vessel permeability using BSA-AlexaFluor555 tracer, was conducted in the *Dock4* endothelial conditional knockout mouse model.

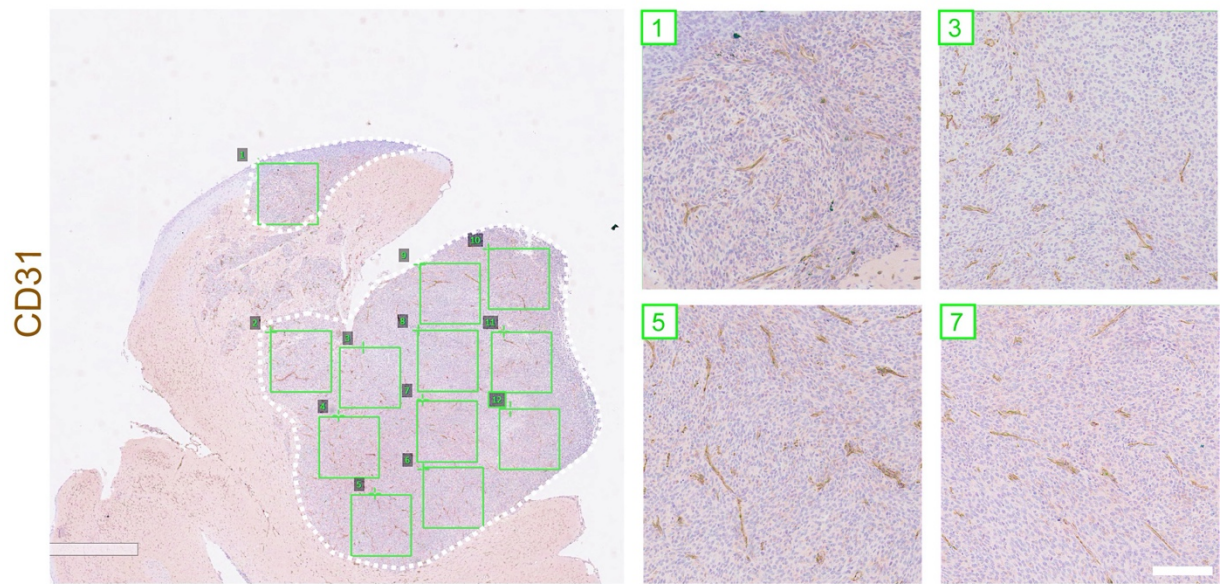
## **5.2 Characterisation of blood vessels in CT2A tumours implanted intracranially in *Dock4* heterozygous knockout mice in response to irradiation**

To elucidate the role of *Dock4* in the modulation of blood vessel growth in the CT2A tumours with and without radiotherapy, an experimental protocol as outlined on 'Prior work leading to this thesis' (Chapter 1, Section 1.11) was performed using *Dock4*het mice.

Figure 5.1 shows representative images of CD31 stained sections of blood vessels grown in WT control (non-irradiated) mice, WT radiotherapy treated mice, *Dock4*het control mice (non-irradiated) and *Dock4*het irradiated mice at 1x magnification and 20x magnification. As described previously in Chapter 3, radiotherapy resulted in the increase in vessel length and lumen size as shown in Figure 3.7-3.8 and Figure 5.1 A and B. When comparing WT control (Figure 5.1 A) and *Dock4*het control (Figure 5.1 B), there did not seem to be a distinguishable difference between the blood vessel morphology. However, when considering the role of *Dock4* heterozygous deletion on blood vessels in radiotherapy treated tumours, it can be observed in Figure 5.1 D that *Dock4*het irradiated tumours have shorter blood vessels and less vessels with distinguishable lumens when compared to WT irradiated tumours (Figure 5.1 C).

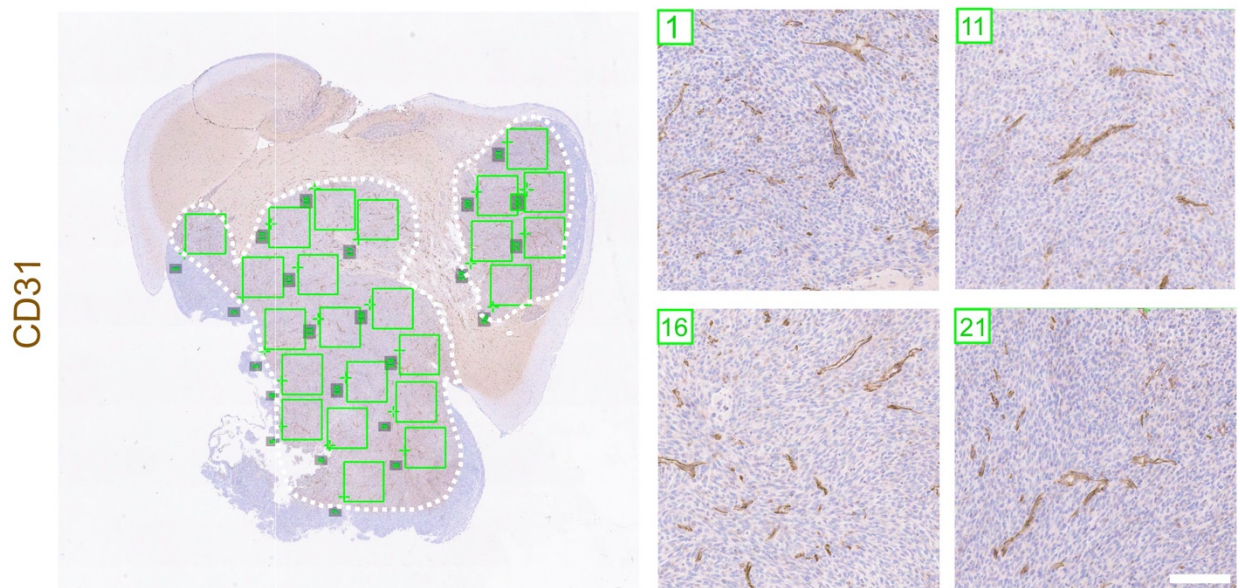
A

WT Control



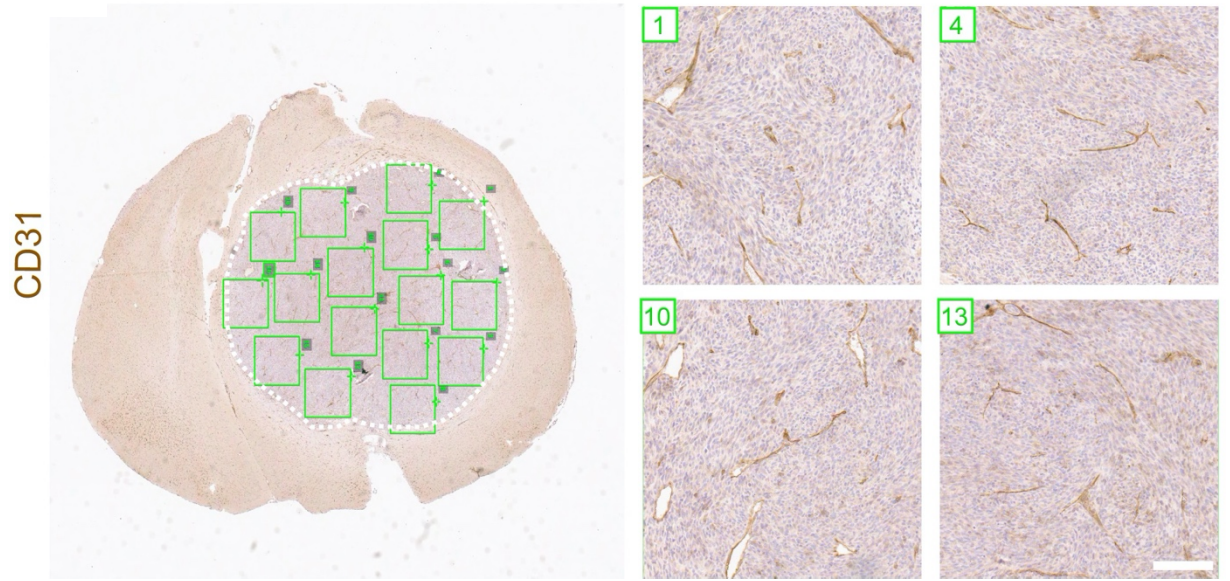
B

*Dock4*het Control



C

WT 2 x 5Gy



D

*Dock4*het 2 x 5Gy

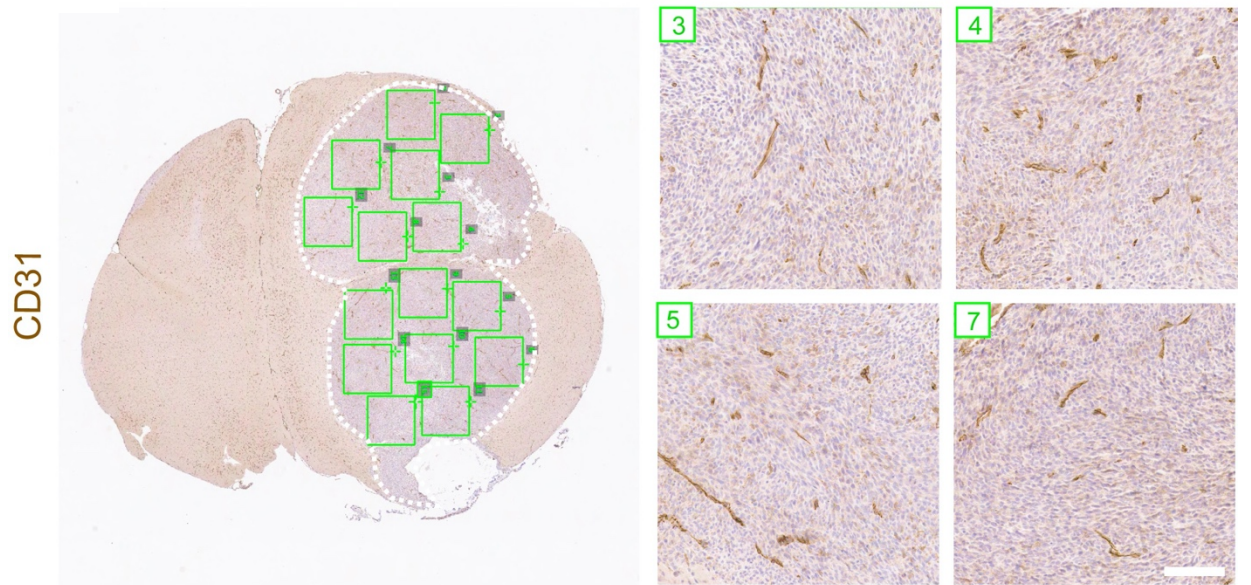


**Figure 5.1 Morphology of blood vessels of CT2A tumours grown intracranially in WT and *Dock4*het mice in control conditions and following irradiation and tumour re-growth.**

Sections of fixed and paraffin embedded CT2A tumours, control and regrown after irradiation in *WT* or *Dock4*het mice, obtained from three different tumour sections 100  $\mu\text{m}$  apart from three mice per condition were stained with an anti-CD31 antibody and haematoxylin by IHC. Slides were scanned using an Aperio AT Virtual Slide scanner and 5 images of 500 x 500  $\mu\text{m}$  (0.25  $\text{mm}^2$ ) were selected using a random number generator at 20x magnification. Images show appearance of blood vessels in non-irradiated control tumours, and irradiated tumours after regrowth in *WT* and *Dock4*het mice. Left-hand panels show 20x objective zoom scanned slides at 1x magnification; right-hand panels show four 0.25  $\text{mm}^2$  images captured at 20x magnification. White dotted lines show the tumour boundary. Scale bar = 100  $\mu\text{m}$ .

### **5.3 *Dock4* heterozygous deletion reverses radiotherapy-induced effects on blood vessel development**

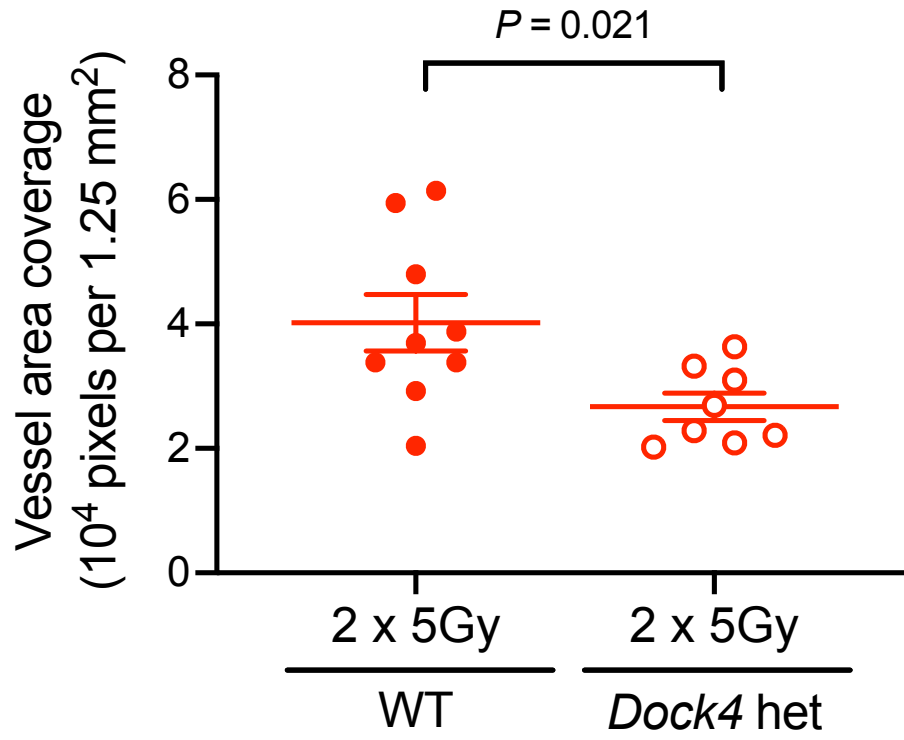
As evidenced in Chapters 3 and 4, radiotherapy promotes vascular abnormalities in the regrown CT2A intracranially injected tumours. As mentioned before, the aim of this section of the study is to understand the potential role of *Dock4* in mediating those changes in blood vessel angiogenesis. Hence, CD31 marked blood vessels in tumours growing in wild type and *Dock4*het tumours shown in Figure 5.1 were quantified using ImageJ for vessel area coverage, lumen size and length as described in Chapter 3 and according to the conventions shown in Table 3.1. The raw data and quantification for WT control and irradiation have been shown in Chapter 3; hence, to avoid repetition, only values for *Dock4*het control and *Dock4*het irradiation are presented. Values shown in fold-increase are shown for the purpose of emphasising any increases in response to irradiation and whether it may be reversed by *Dock4*het deletion. The quantifications showed that tumours grown in *Dock4*het mice treated with radiotherapy had a significantly decreased vessel area coverage ( $P = 0.02$ ) compared to WT mice treated with radiotherapy (Figure 5.2 A). When using fold increase in comparisons, WT irradiated mice showed a 1.35-fold increase in vessel area coverage compared to non-irradiated controls. When WT and *Dock4*het non-irradiated controls were compared, there was no significant difference (Figure 5.2 B). The increase in vessel area in WT mice in response to irradiation was reversed in irradiated *Dock4*het mice (Figure 5.2 C).

Parallel with the differences seen in vessel area coverage, there was a significant decrease in lumen size ( $P = 0.004$ ) in irradiated tumours growing in *Dock4*het mice compared to WT mice (Figure 5.3 A). Accordingly, the 1.52-fold increase in lumen size of WT irradiated tumours compared to non-irradiated control was reversed in the *Dock4*het mice (Figure 5.3 B). There was a no significant difference in lumen size between tumours growing in WT and *Dock4*het non-irradiated controls (Figure 5.3 B) Interestingly, when investigating the percentage of vessels with visible lumens, there was no significant difference ( $P = 0.27$ ) between irradiated tumours growing in WT and *Dock4*het mice (Figure 5.3 C).

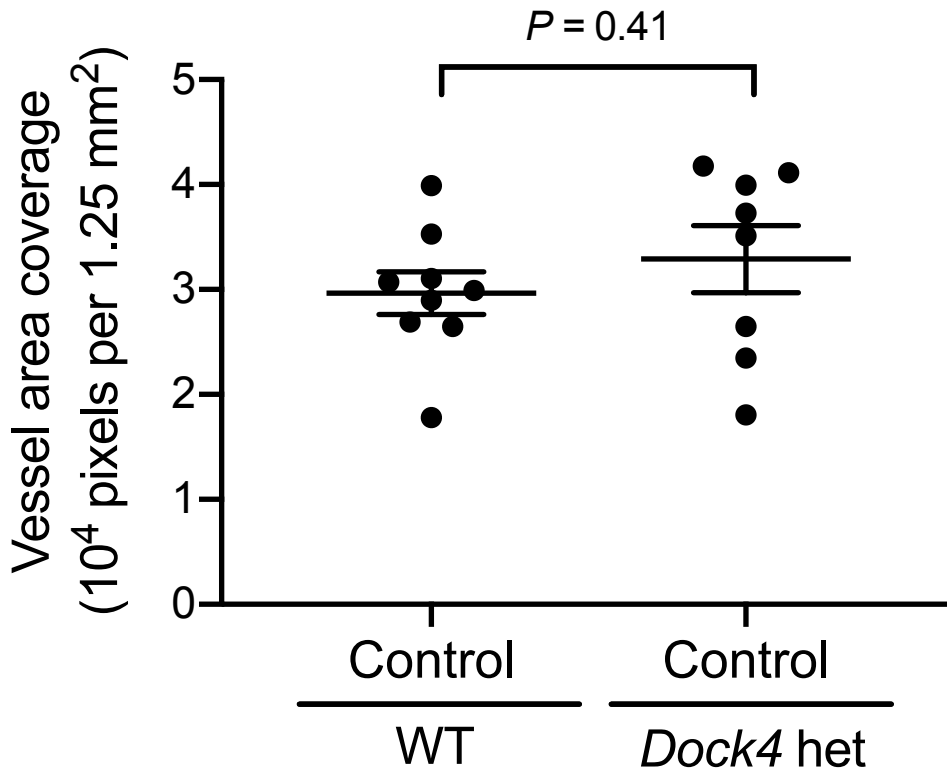
Another readout that was quantified when irradiated CT2A tumours were compared to untreated controls was vessel length showing a consistent pattern with vessel area coverage and lumen size. There was significant decrease ( $P < 0.001$ ) in vessel length between irradiated tumours grown in WT irradiated mice compared to *Dock4*het mice (Figure 5.4 A) and hence reversal of the 1.35-fold increase in vessel length (Figure 5.4 B) However untreated tumours growing in *Dock4*het mice showed no fold change difference in tumour vessel length compared to tumours growing in WT mice (Figure 5.4 B).

Altogether, these results demonstrate that *Dock4* heterozygous deletion in the microenvironment of CT2A tumours results in a reversal of the radiotherapy-induced vessel abnormality, as the increase in blood vessel area coverage, vessel lumen size and length in response to irradiation were reversed when irradiated tumours were grown in *Dock4*het mice. However, this effect was only seen in tumours of mice treated with radiotherapy while *Dock4* heterozygous deletion does not result in any difference in blood vessel development of untreated tumours.

A



B



C

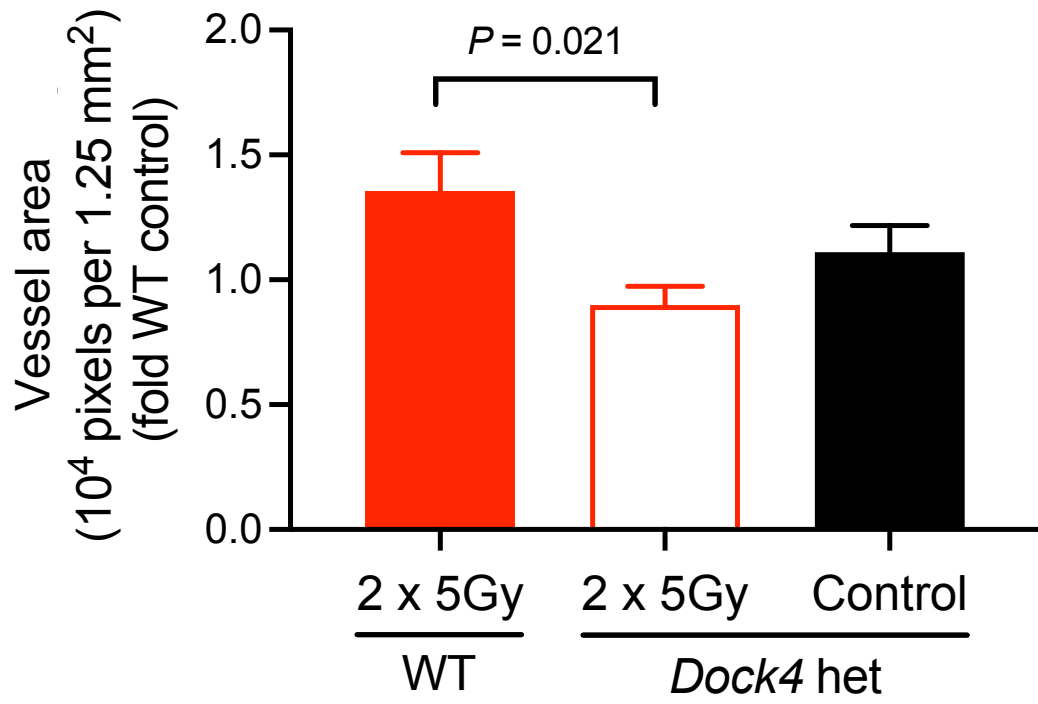


**Figure 5.2 Reduction of overall vessel area of irradiated CT2A tumours grown intracranially in *Dock4het* compared to WT mice.**

Sections of fixed and paraffin embedded CT2A tumours, control and regrown after irradiation, obtained from three different tumour sections 100  $\mu\text{m}$  apart were stained for CD31 expression by IHC, and the overall blood vessel area was quantified from scanned images at 20x magnification using ImageJ software. Values for each section is the sum of blood vessel areas in 5 randomly selected 0.25  $\text{mm}^2$  areas.

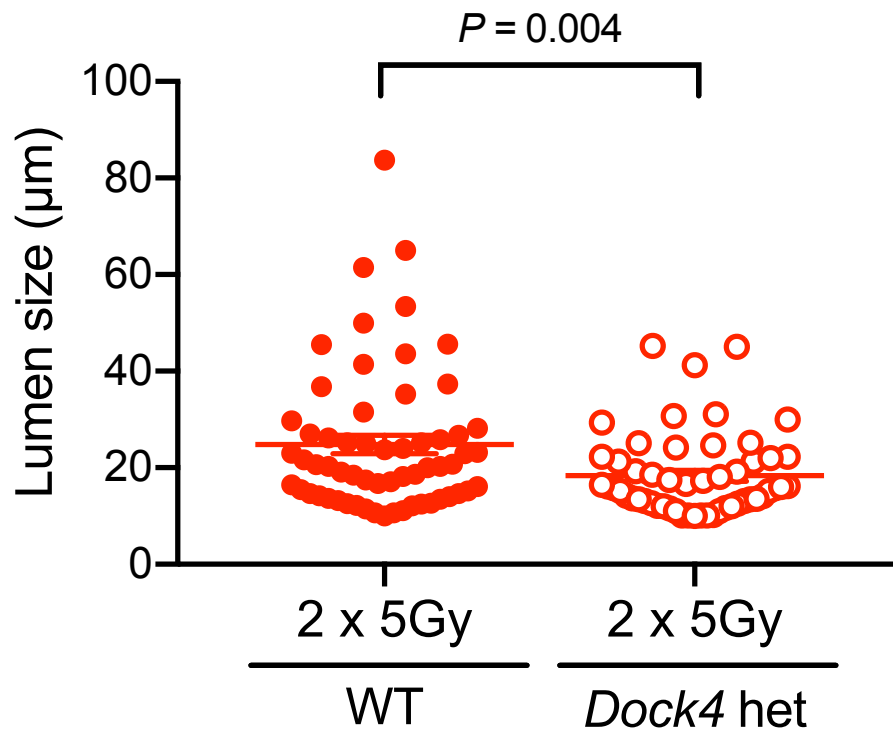
(A) Dot plot shows significant decrease in average blood vessel area in irradiated tumours grown in *Dock4het* mice compared to WT littermate controls.

(B) Dot plot shows no difference in average blood vessel area in non-irradiated control tumours grown in *Dock4het* mice compared to WT littermate controls.

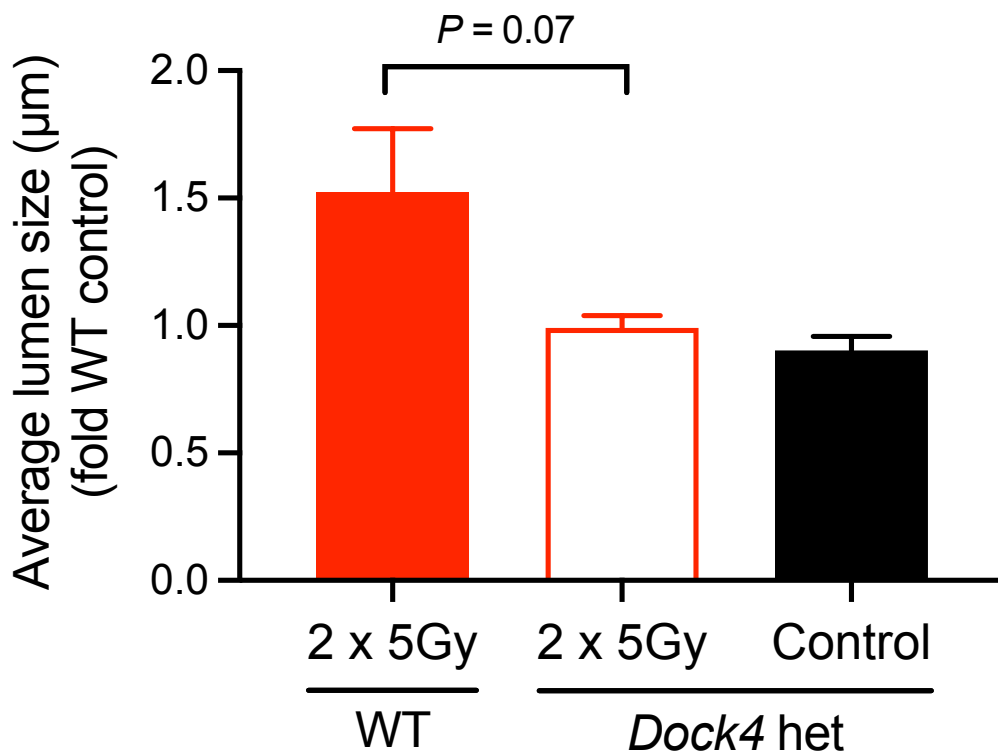
(C) Bar chart shows fold increase (compared to non-irradiated WT control) of blood vessel area following radiotherapy and regrowth is partially reversed in *Dock4het* mice.

Error bars represent SEM. n = number of sections quantified from 3 mice per condition. WT radiotherapy = 9, *Dock4het* radiotherapy = 8, *Dock4het* control = 8, WT control = 9

A



B



C

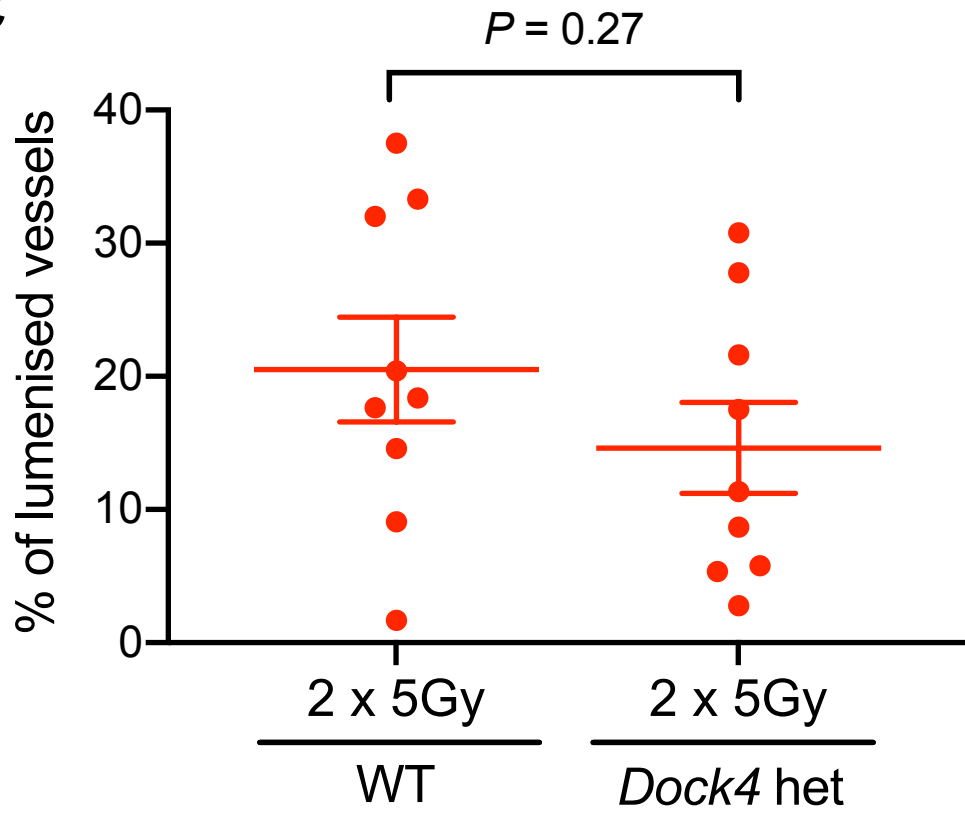


**Figure 5.3 Reduction of blood vessel lumen size of irradiated CT2A tumours grown intracranially in *Dock4het* compared to WT mice.**

Sections of fixed and paraffin embedded CT2A tumours, control and regrown after irradiation, obtained from three different tumour sections 100  $\mu\text{m}$  apart were stained for CD31 expression by IHC, and a best fit circle was used to measure blood vessel lumen size in scanned images at 20x magnification. Blood vessel lumenisation and lumen diameter were quantified using ImageJ. The smallest lumen diameter confidently detected in this magnification was 10  $\mu\text{m}$ .

(A) Dot plot shows significant decrease in lumen size in tumours irradiated and regrown in *Dock4het* compared to WT littermate controls.

(B) Bar chart shows fold increase (compared to non-irradiated WT control) of blood vessel area following radiotherapy and regrowth was reversed in *Dock4het* mice.

(C) Dot plot shows a non-significant decrease in percentage of lumenised blood vessels in irradiated tumours grown in *Dock4het* compared to WT mice.

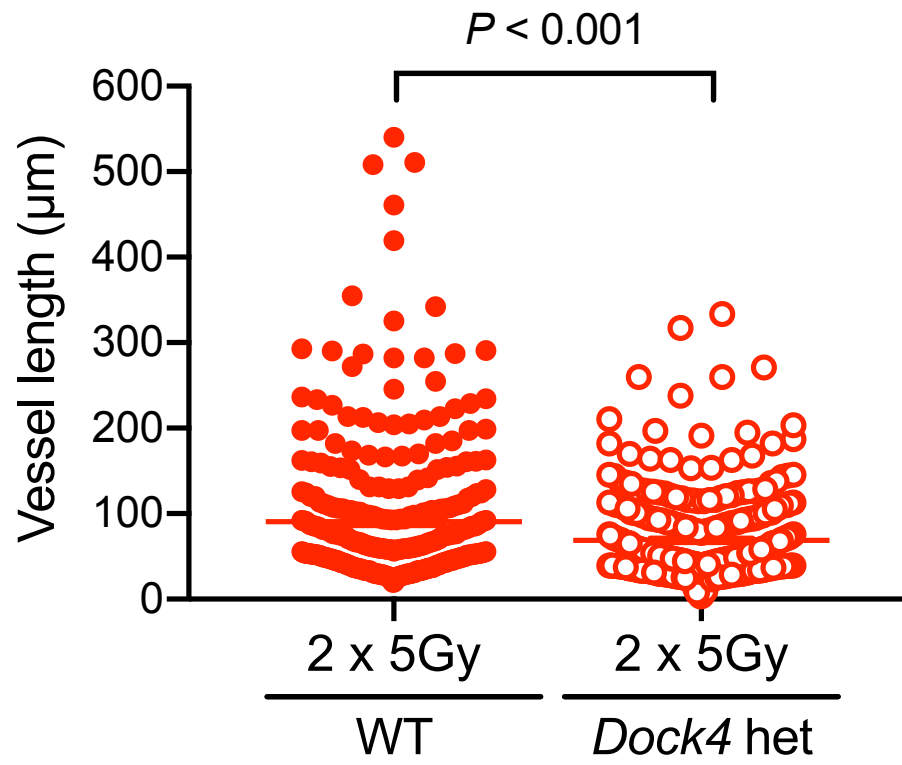
Error bars represent SEM.

A and C: n = number of lumenised blood vessels quantified from 3 mice per condition.

B: n = number of sections quantified from 3 mice per condition. WT radiotherapy = 9, *Dock4het* radiotherapy = 9, *Dock4het* control = 9.

Number of lumenised blood vessels analysed per condition: WT control = 55, WT radiotherapy = 61, *Dock4het* radiotherapy = 54, *Dock4het* control = 63

A



B

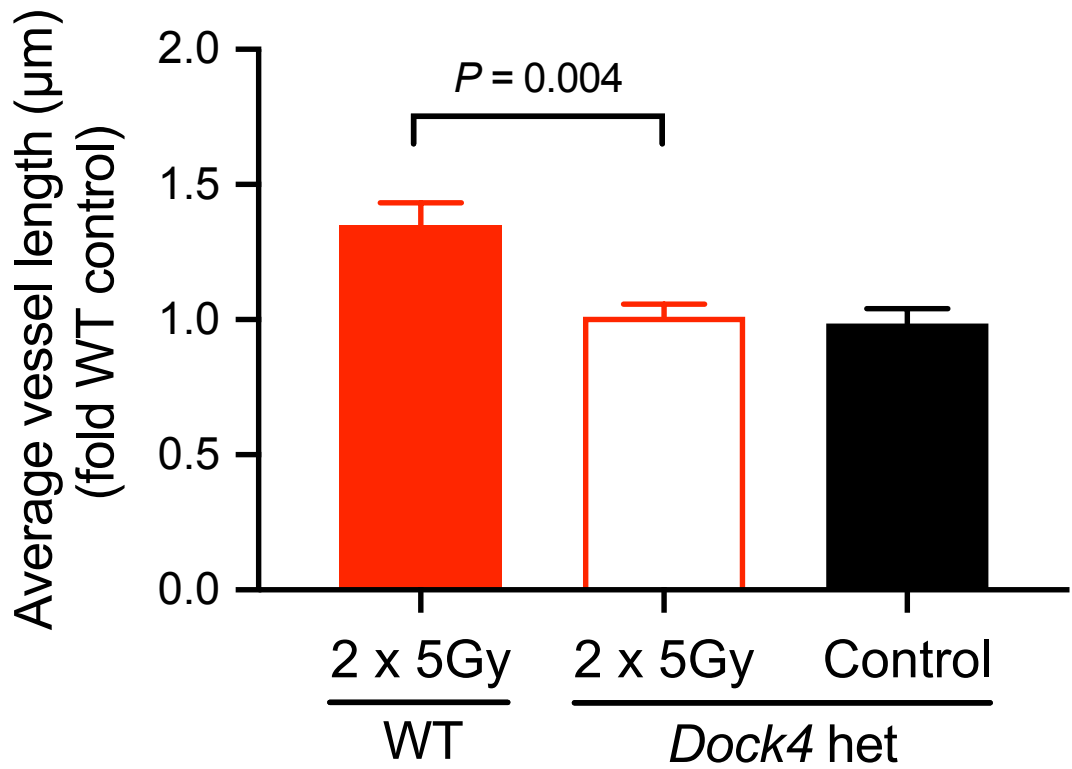


**Figure 5.4 Reduction of blood vessel length of irradiated CT2A tumours grown intracranially in *Dock4het* compared to WT mice.**

Sections of fixed and paraffin embedded CT2A tumours, control and regrown after irradiation obtained from three different tumour levels 100  $\mu\text{m}$  apart were stained for CD31 expression by IHC, and blood vessel length was quantified using ImageJ. Sections were obtained from three different tumour sections at 100  $\mu\text{m}$  apart. All blood vessels with length > 20  $\mu\text{m}$ , were quantified.

(A) Dot plot shows significant decrease in blood vessel length in irradiated tumours grown in *Dock4het* compared to WT mice. n = number of blood vessels quantified from 3 mice per condition.

(B) Bar chart shows fold increase (compared to non-irradiated WT control) of blood vessel length following radiotherapy and regrowth was reversed in *Dock4het* mice.

A and B: Error bars represent SEM. n = number of sections per group quantified from 3 mice per condition. WT control = 9, WT radiotherapy = 9, *Dock4het* radiotherapy = 9, *Dock4het* control = 9

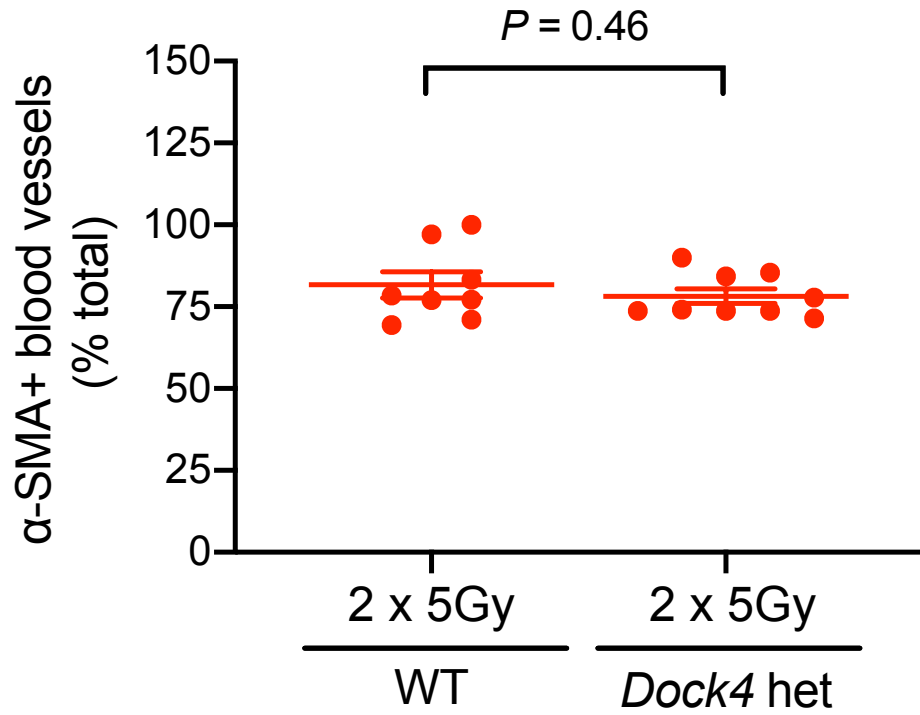
Number of blood vessels quantified for each condition: WT control 574, WT radiotherapy = 346, *Dock4het* radiotherapy = 380, *Dock4het* control = 569.

## 5.4 *Dock4* heterozygous deletion does not reverse the radiation-induced effects of blood vessel– $\alpha$ -SMA+ pericyte association

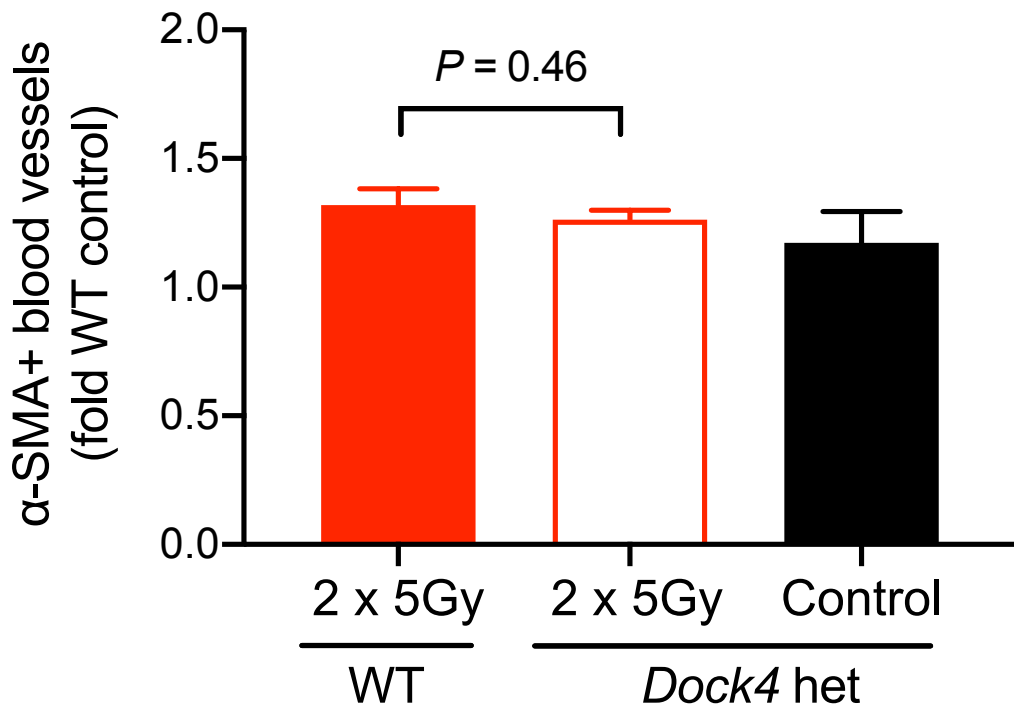
As described in Chapter 4, another radiotherapy-induced effect that was seen in regrown tumours was an increase in the association of blood vessels with  $\alpha$ -SMA positive pericytes. As *Dock4* heterozygous deletion resulted in the reversal of the radiotherapy-induced increase in overall vessel area, length and lumen size, and since lumen size is influenced by pericyte association (Abramsson et al., 2003), I investigated whether *Dock4*het deletion can reverse the increase in pericytes associated with blood vessels. The abundance of vessels associated with  $\alpha$ -SMA positive cells was not significant ( $P = 0.18$ ) between non-irradiated tumours grown in WT (mean = 63.0%) and *Dock4*het mice (mean = 75.2%) (data not shown). Interestingly, there was no difference in the abundance of  $\alpha$ -SMA positive blood vessels when irradiated tumours growing in WT and *Dock4*het mice were compared (Figure 5.5 A). However, the 1.31-fold increase in relation to pericyte positive blood vessels in irradiated tumours compared to untreated controls in WT mice persisted in *Dock4*het irradiated mice (1.26-fold increase) (Figure 5.5 B).

Unexpectedly, in non-irradiated control conditions, when quantification of blood vessel  $\alpha$ -SMA pericyte tight association was performed, there was a significant increase in blood vessels with  $\alpha$ -SMA pericyte tight association in tumours grown in *Dock4*het mice compared to WT control ( $P = 0.029$ ) (Figure 5.5 C). However, when irradiated tumours was observed, aligned with the data on pericyte positivity, *Dock4* heterozygous deletion did not significantly affect  $\alpha$ -SMA pericyte tight association. There was no difference in blood vessels with  $\alpha$ -SMA tight association between irradiated tumours grown in WT and *Dock4*het mice ( $P = 0.21$ ) (Figure 5.5 D). Similarly, when looking at fold-change, *Dock4* heterozygous deletion did not reverse the increase in blood vessels tightly associated with WT irradiated tumours (Figure 5.5 E).

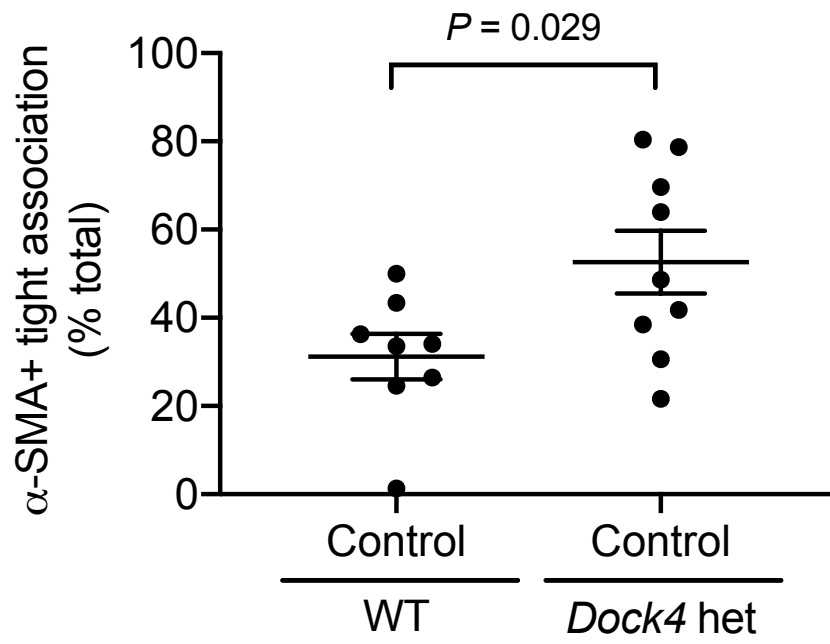
A



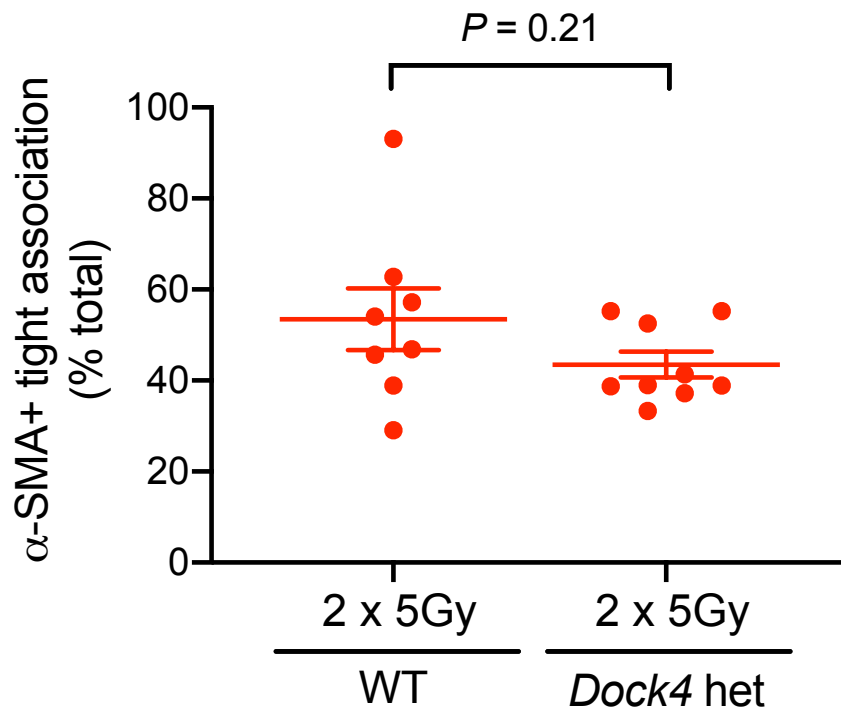
B



C



D



F

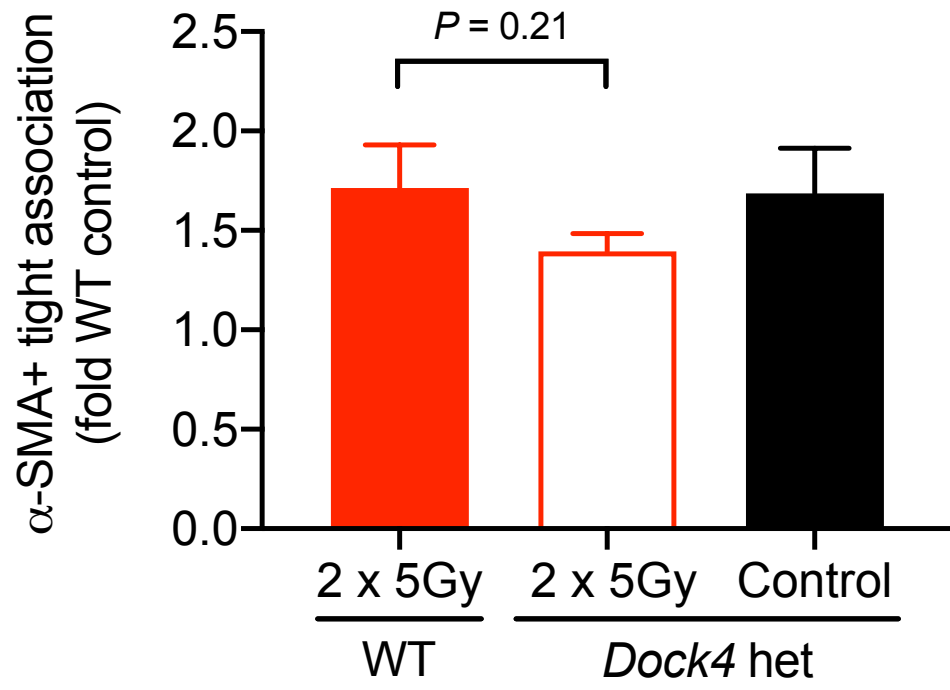


**Figure 5.5 Association of blood vessels with  $\alpha$ -SMA positive cells in response to *Dock4* heterozygous genetic deletion.**

Sections of fixed and paraffin embedded CT2A tumours, control and regrown after irradiation obtained from three different tumour sections 100  $\mu$ m apart were stained for CD34/Endomucin,  $\alpha$ -SMA and DAPI by IF. 10 images at 60x magnification from each tumour section captured using Nikon A1R confocal microscope were analysed using ImageJ according to  $\alpha$ -SMA scoring criteria described in Chapter 4, Figure 4.6 B.

(A) Dot plots show no change in percentage of blood vessels with  $\alpha$ -SMA positive cells in irradiated tumours grown in *Dock4*het mice compared to WT littermate controls.

(B) Bar charts show no change in fold increase (compared to non-irradiated WT control) of blood vessels with  $\alpha$ -SMA positive cells; in tumours grown in *Dock4*het mice.

(C) Dot plots show significant increase in blood vessels with tight  $\alpha$ -SMA association in non-irradiated control tumours grown in *Dock4*het mice compared to WT littermate controls.

(D) Dot plots show non-significant decrease in blood vessels with tight  $\alpha$ -SMA association in irradiated tumours grown in *Dock4*het mice compared to WT littermate controls.

(E) Bar charts show non-significant fold change (compared to non-irradiated WT control) of blood vessels with tight  $\alpha$ -SMA association in tumours grown in *Dock4*het mice.

Error bars represent SEM. n = number of sections quantified from 3 mice per condition. WT radiotherapy = 8, *Dock4*het radiotherapy = 9, *Dock4*het control = 9, WT control = 9.

## 5.5 Intracranial implantation of CT2A glioma cell line in endothelial *Dock4* conditional knockout mice

As the data obtained from the *Dock4* heterozygous knockout model suggests the possibility of normalisation of blood vessels post irradiation with *Dock4* deletion, an experiment was set out using an endothelial specific *Dock4* conditional knockout model to firstly, confirm the effects observed with the global *Dock4* deletion are endothelial cell autonomous and secondly, investigate the effects of deletion of both alleles from endothelial cells. The endothelial *Dock4* conditional knockout mouse line [Cdh5-(PAC)-CreERT2;Dock4 fl/fl] was used for this purpose (Appendix 9) In this model endothelial Dock4 deletion was induced by tamoxifen treatment of mice, which activates the expression of Cre-ERT2 under the control of the endothelial specific Cdh5 (encodes VE-cadherin) promoter. In addition, the line Cdh5(PAC)-CreERT2; Rosa26-Tdtomato; Dock4 fl/fl was used. This line arises from the cross between Cdh5(PAC)-CreERT2; Dock4 fl/fl and Rosa26 Lsl-Tdtomato mouse lines. This allows Cre activity to be monitored by means of expression of Tdtomato (a variant of red fluorescence protein) when Cre recombinase is active.

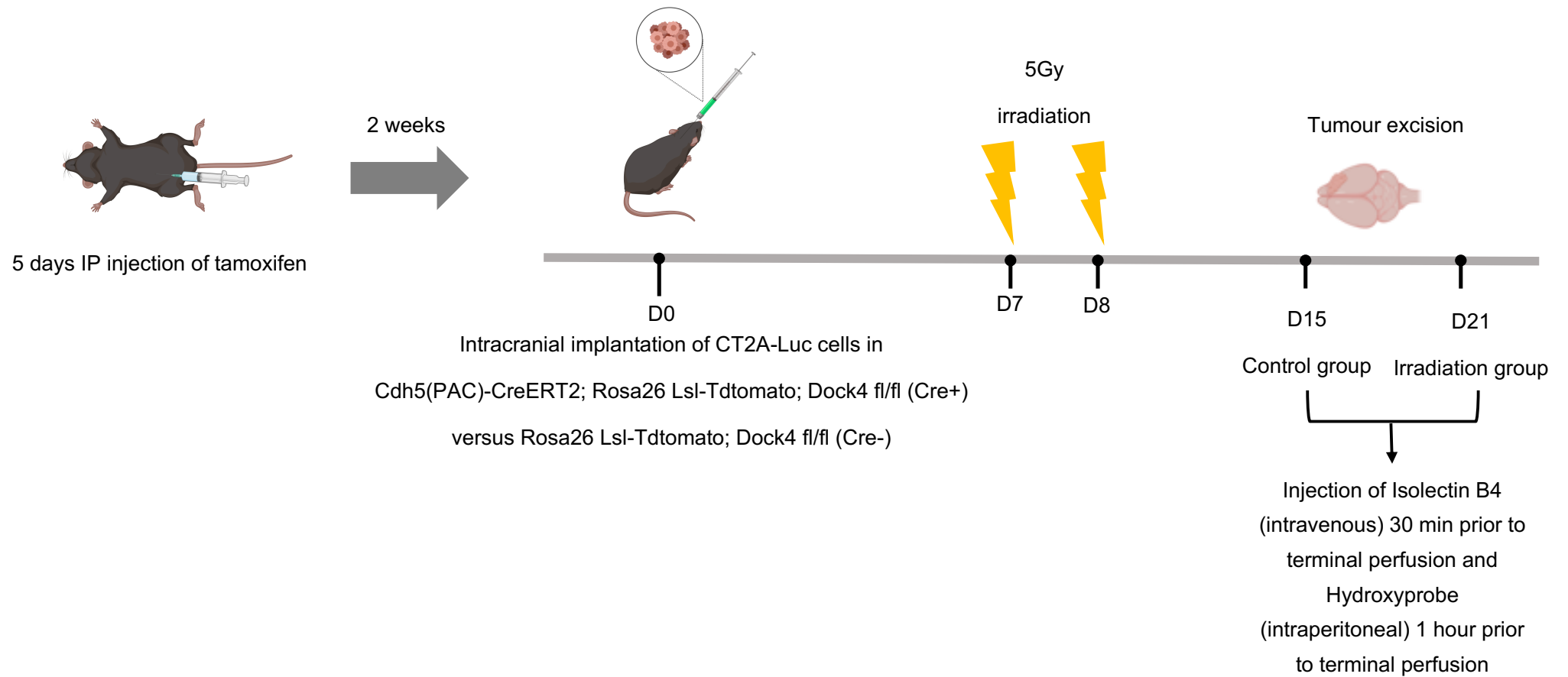
As shown in Figure 5.6, prior to intracranial implantation of the CT2A line the mice were injected with 2mg tamoxifen (Cre+) intraperitoneally for 5 consecutive days to induce the deletion. Control (Cre-) mice were injected with corn oil to leave the *Dock4* gene intact. After 2 weeks  $1 \times 10^5$  CT2A-Luc cells were injected intracranially in Cre+ and Cre- mice and tumour growth was monitored using IVIS bioluminescence imaging. Mice were randomised on day 6 and irradiated on days 7 and day 8 with 5Gy each at day. Mice were taken down at the onset of neurological symptoms at day 15 for the control untreated group and day 18 for the irradiated group. Isolectin B4 was delivered intravenously to two mice from each group for analysis of blood vessel perfusion; and Hypoxyprobe intraperitoneally prior to terminal perfusion for analysis of hypoxia. Following fixation in 4% paraformaldehyde tumours from Isolectin B4 and Hypoxyprobe injected mice were erroneously transferred to 70% ETOH prior freezing in OCT compound which resulted in the formation of ice crystal structures. Those samples were either brittle and could not be sectioned or contained large holes which precluded further analysis. Consequently, only 2 tumours could be

analysed in this experiment per group, except for the irradiated Cre- group which only had 1 tumour suitable for analysis.

Tumour growth was monitored using IVIS bioluminescence imaging. Figure 5.7 A shows the tumour growth curves for the four conditions: Cre+, Cre-, each untreated or irradiated. On day 15 there was a significant difference in tumour growth between untreated and irradiated Cre- mice. However, there was a smaller and non-significant difference between the control and irradiated Cre+ mice, suggesting irradiation was less effective in mice with endothelial Dock4 deletion. Although on day 11 (3 days after irradiation) the decrease in tumour growth appeared more prominent in irradiated Cre+ compared to Cre- mice the difference was not statistically significant (Figure 5.7 B). When observing the last day of imaging at day 19 (two days prior to terminal perfusion), there was also no difference in the bioluminescence signal between Cre- and Cre+ mice (Figure 5.7 C). Given that tamoxifen treatment had induced Cre activity as shown by expression of Tdtomato in blood vessels (Table 5.1 and Figure 5.8) this suggests that endothelial Dock4 deletion does not affect CT2A tumour growth under control or irradiation conditions. The details of samples taken forward for analysis are listed in

Table 5.1. Regrowth of both Cre+ and Cre- tumours post irradiation in this experiment was not as uniform and robust as in the irradiation experiment presented in Chapter 4 (Figure 4.9) despite mice showing neurological symptoms. Confirmation of Cre activity was through detection of TdTomato following deletion of the floxed STOP codon of TdTomato ( Figure 5.8.)

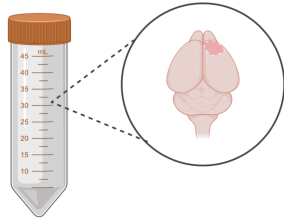
A



B

## Paraffin samples

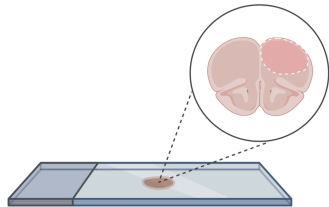
Fixation in 4% PFA for 24h



Tissue processing and paraffin embedding



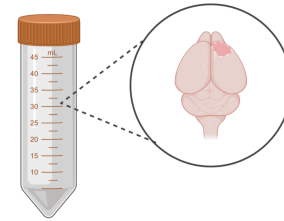
Sectioning and staining



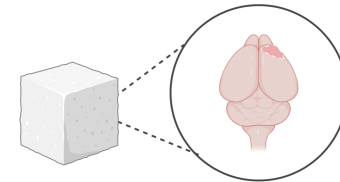
C

## Frozen samples

Fixation in 4% PFA for 5h



Tissue processing and OCT embedding



Sectioning and staining

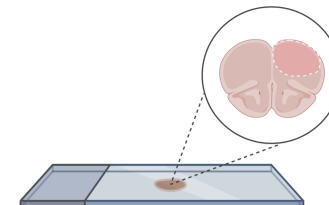


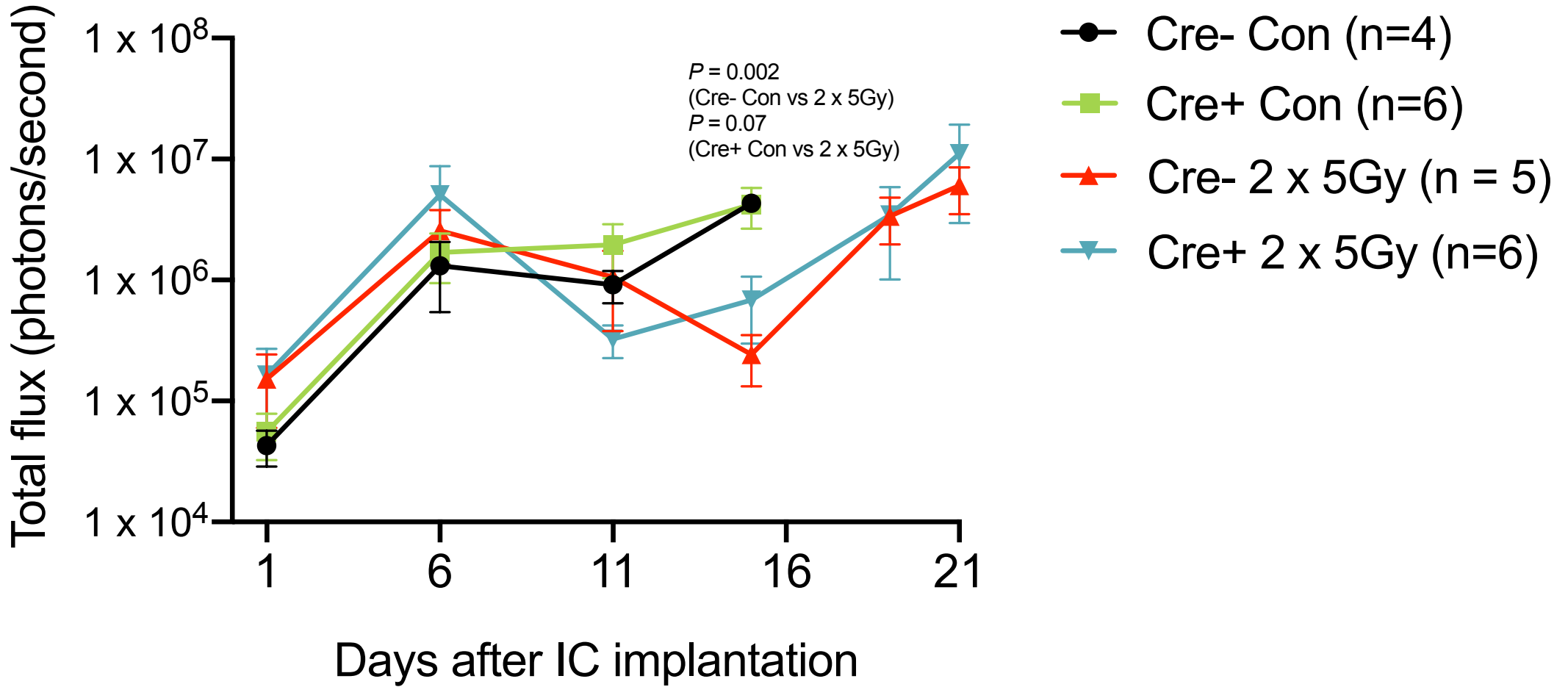
**Figure 5.6 Schedule of CT2A-Luc tumour growth, irradiation, and excision in *Cdh5(PAC)-CreERT2; Dock4 fl/fl* mice (endothelial *Dock4* conditional knockout mice) following tamoxifen induction.**

(A) Intraperitoneal injections of 2 mg tamoxifen per day were performed for 5 consecutive days and mice were monitored for 14 days after the last injection before intracranial implantation of cancer cells. CT2A-Luc murine glioma cell line ( $1 \times 10^5$  cells) was injected intracranially into the striatum of *Cdh5(PAC)-CreERT2; Dock4 fl/fl* (Cre+) and control *Dock4 fl/fl* (Cre-) mice. Tumour growth was followed non-invasively by IVIS bioluminescence imaging from day 1 and mice were randomised for irradiation on day 6. Fractionated irradiation (2 x 5Gy) was delivered on days 7 and 8 following tumour implantation using SARRP. Control (non-irradiated) tumours were excised at day 15, and irradiated tumours were excised at day 21 following terminal perfusion. 2 mice from each group were injected with Isolectin B4 intravenously and Hydroxyprobe intraperitoneally, 30 minutes and 1 hour prior to terminal perfusion, respectively.

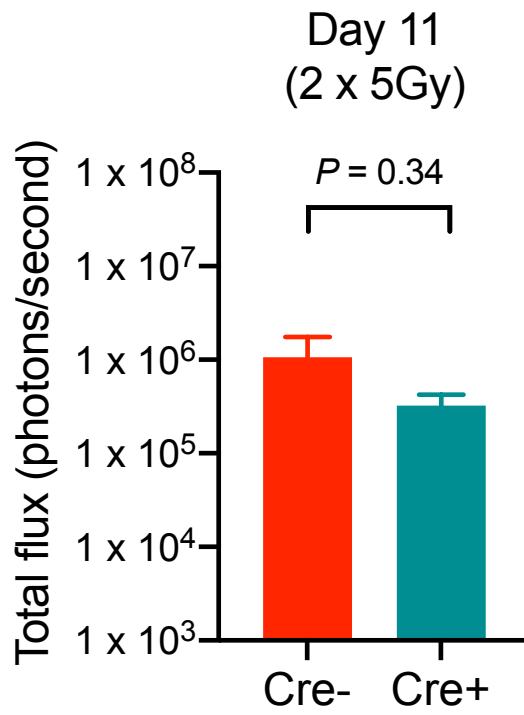
(B) Tumours not injected with Isolectin B4 and Hydroxyprobe were fixed in 4% PFA for 24 hours, transferred to 70% ethanol and paraffin embedded. Samples were sectioned at 5  $\mu$ m.

(C) Tumours injected with Isolectin B4 and Hydroxyprobe were fixed in 4% PFA for 5 hours, transferred to 70% EtOH and frozen in OCT compound using dry ice. Due to formation of ice crystals, tissue samples were damaged and were not used for further analysis.

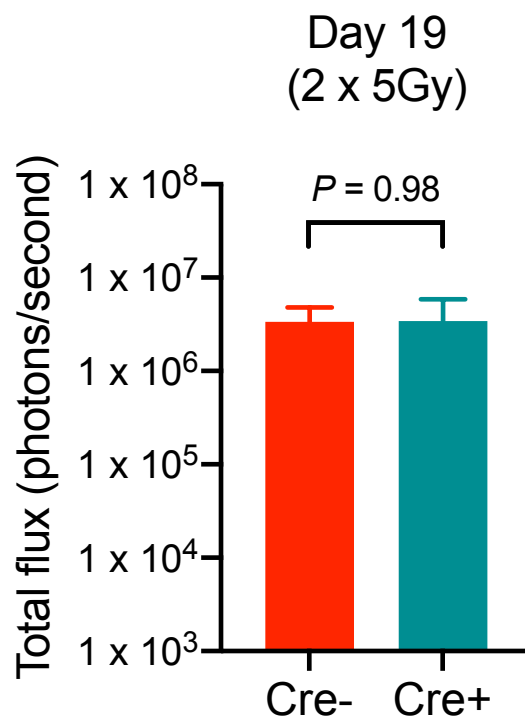
A



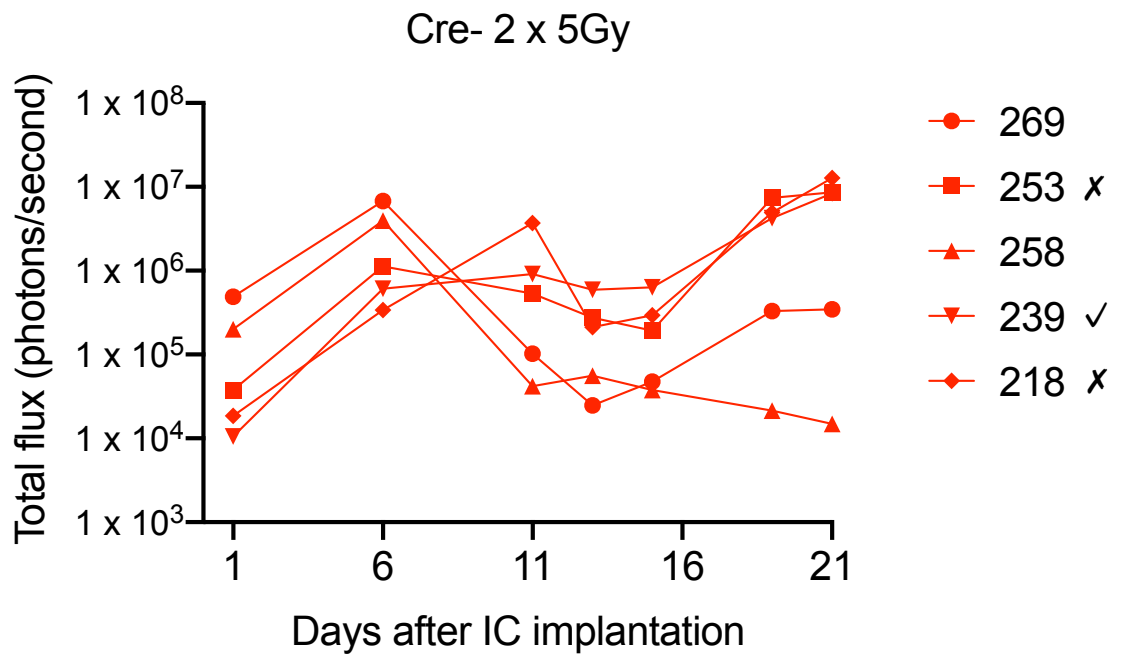
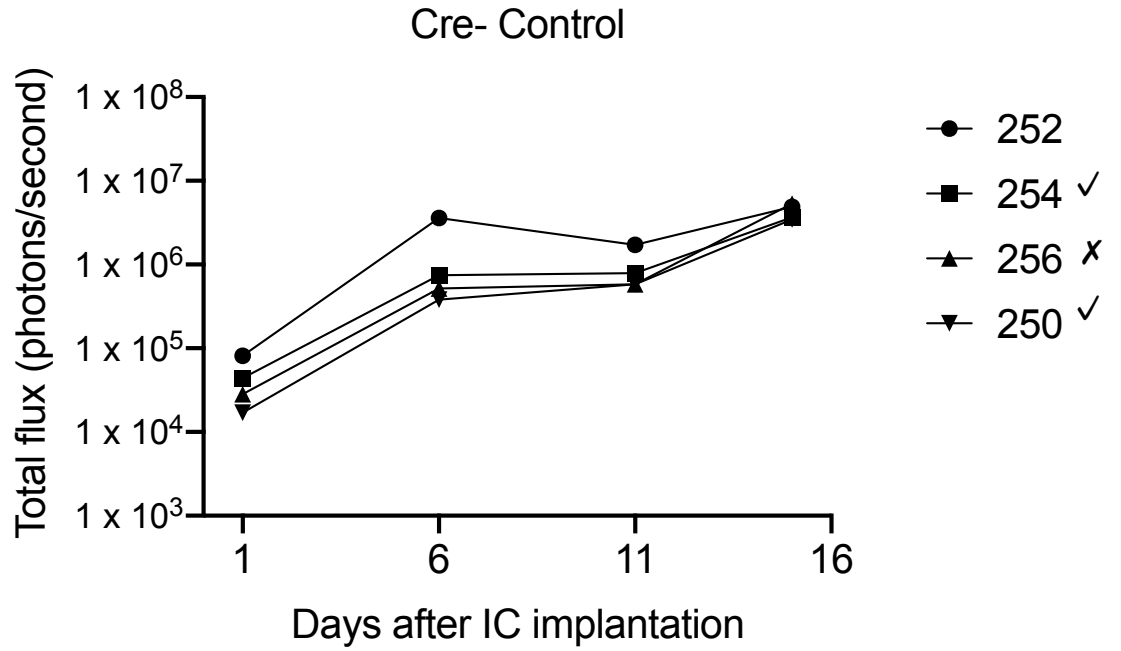
B



C



D



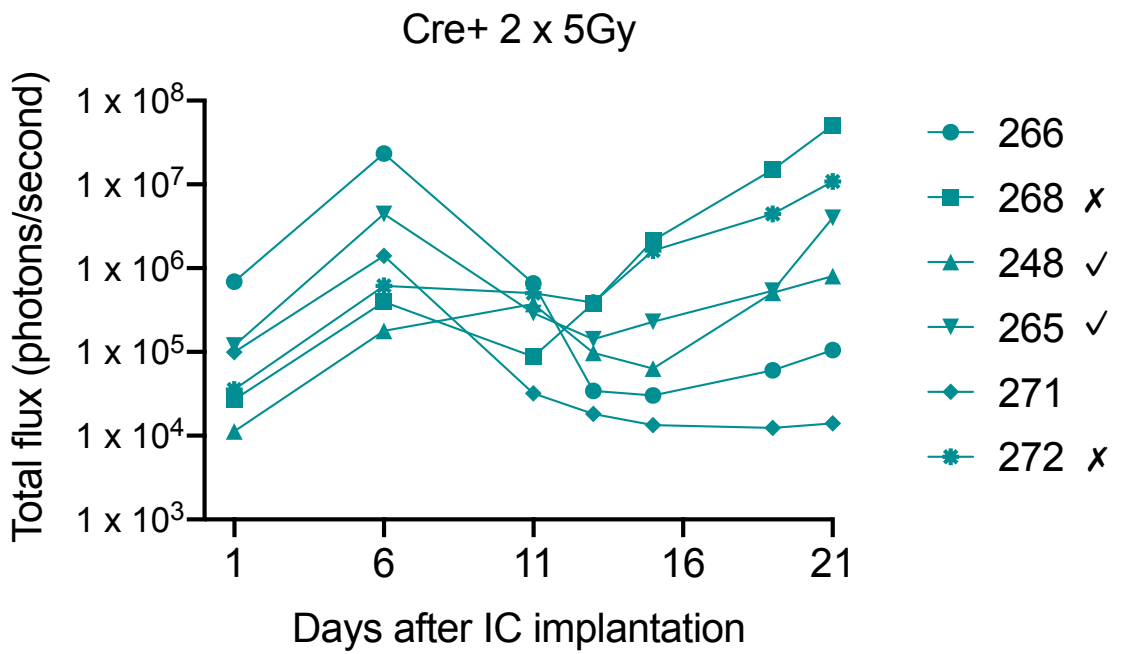
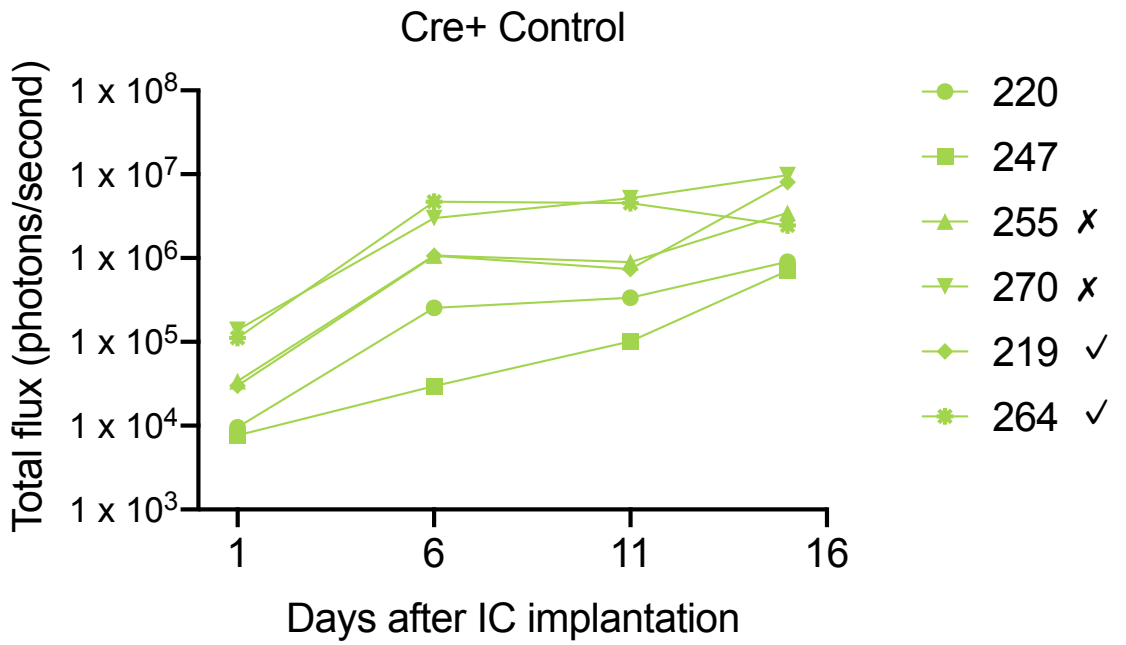


**Figure 5.7 Monitoring of CT2A tumour growth in control and irradiated WT or endothelial *Dock4* conditional knockout mice by bioluminescence imaging.**

CT2A-Luc murine glioma cell line ( $1 \times 10^5$  cells) was injected intracranially into the striatum of WT or *Dock4* conditional knockout mice and *in vivo* experiment was performed as shown in Figure 5.6.

(A) Growth curves of CT2A intracranial tumours in control versus irradiated *Cdh5(PAC)-CreERT2; Dock4 fl/fl (Cre+)* and *Dock4 fl/fl (Cre-)* mice.

(B) Bar graph shows the bioluminescence signal intensity at day 11 for irradiated *Cre+* and *Cre-* mice.

(C) Bar graph shows the bioluminescence signal intensity at day 19 for irradiated *Cre+* and *Cre-* mice.

(D) Growth curves of individual tumours: tick next to mouse number indicates mouse that is taken forward for analysis; cross next to mouse number indicates tumour sample was damaged during processing and could not be analysed. Unmarked mouse numbers indicate tumours were not detected or too small to analyse.

Error bars represent SEM. N = number of mice per condition: *Cre+*, 6; *Cre-*, 5.

**Table 5.1 CT2A tumour samples grown intracranially in endothelial *Dock4* conditional knockout mice.**

<b>Mouse ID</b>	<b>Age at intracranial implantation (weeks)</b>	<b>Sex</b>	<b>Cre</b>	<b>TdTomato</b>	<b>Irradiation</b>	<b>Tumour excision day post injection</b>	<b>Neurological symptoms (Y/N)</b>	<b>RFP staining detected</b>
254	12	F	-			15	N	no
250	12	M	-			15	N	no
264	12	M	+	X		15	N	yes
219	14	M	+	X		15	N	yes
239	13	M	-		X	21	N	no
248	12	F	+	X	X	21	N	yes
265	12	M	+	X	X	21	N	yes

Shown are the genotype of mice, sex, age at injection, treatment, tumour excision day and presence of neurological symptoms at the time of excision. RFP staining was detected in the tumour blood vessels of mice harbouring Td tomato in the Rosa26 locus with a transcription stop codon flanked by loxP sites (Appendix 9) confirming tamoxifen induction of Cre activity in tumour endothelial cells.

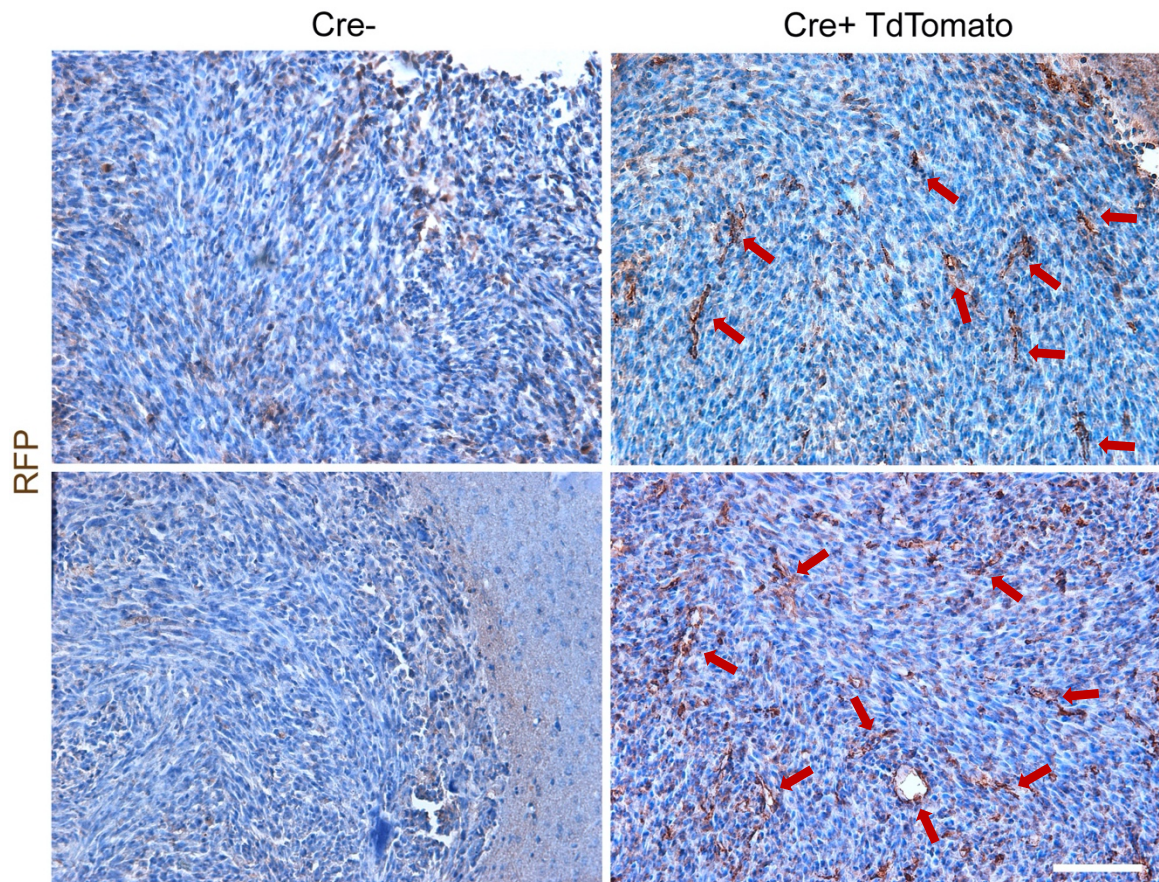


**Figure 5.8 Endothelial Dock4 deletion detected by IHC in CT2A tumours grown intracranially in endothelial *Dock4* conditional knockout mice.**

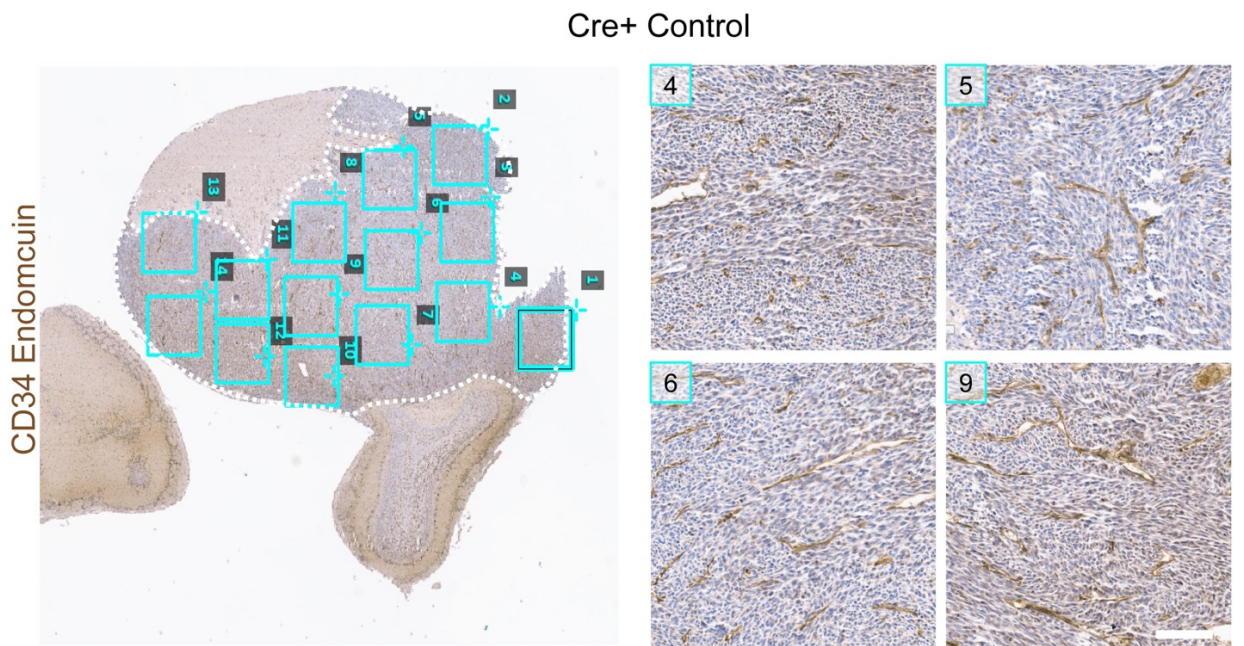
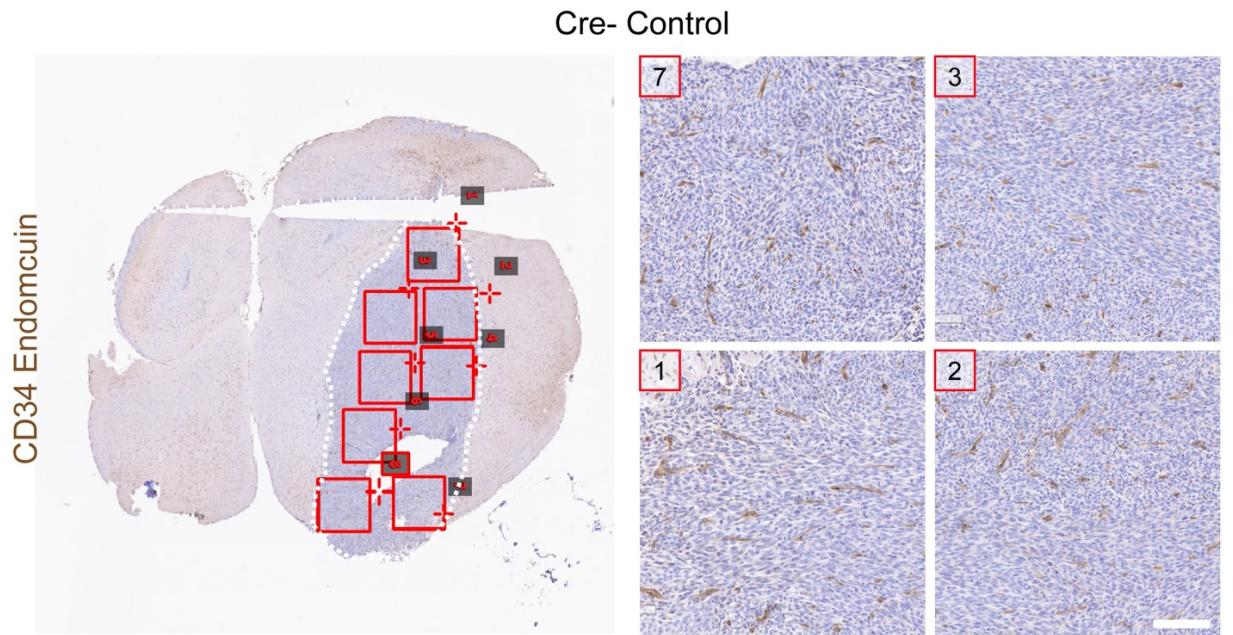
Images show red fluorescent protein (RFP) staining (detects TdTomato) of sections from tumours growing in Cre- and Cre+ *Dock4* conditional knockout mice. Images were acquired using a Nikon Eclipse E1000 microscope at 20x magnification. Red arrows point to RFP-expressing blood vessels in the Cre+ tumours. Scale bar = 100  $\mu$ m.

## 5.6 Characterisation of CT2A tumours injected intracranially in endothelial *Dock4* conditional knockout mice

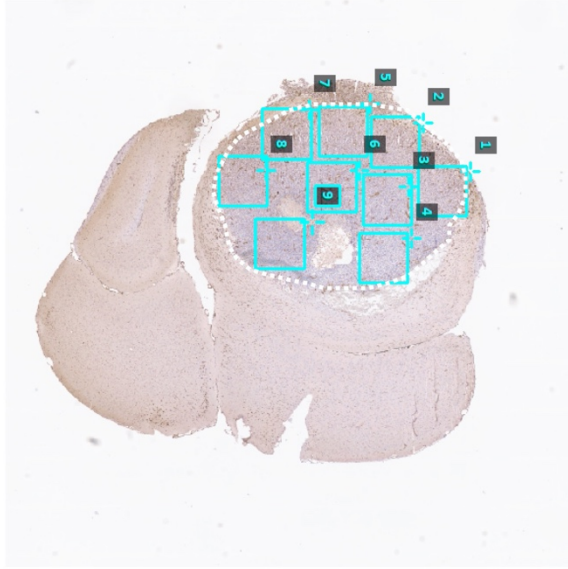
To elucidate the effect of *Dock4* conditional deletion in combination with radiotherapy on CT2A tumour blood vessel development, tumours were stained with CD34/ Endomucin for blood vessel visualisation. CD34/Endomucin antibody was used in this experiment as staining was done simultaneously for pilot (Figure 5.7) and repeat experiment (refer to Section 5.7 in this chapter). Repeat experiment samples were processed frozen and the CD31 antibody did not work effectively on frozen samples. Three sections 100  $\mu\text{m}$  distance apart was obtained from each mouse and was stained by immunohistochemistry. Slides were scanned using Aperio AT Virtual Slide Scanner and 5 images of 500 x 500  $\mu\text{m}$  (0.25  $\text{mm}^2$ ) size at 20x magnification were randomly selected using a random number generator.

Figure 5.9 shows captured images of scanned whole slides at 1x magnification (left panel), and four images for each tumour at 20x magnification (right panel). Visually tumours in Cre<sup>+</sup> control mice demonstrated higher vascularisation when compared to Cre<sup>-</sup> control mice. The blood vessels were longer, lumens were larger and more visible and there was an overall higher number of blood vessels present in the tumour suggesting that endothelial *Dock4* deletion suppresses blood vessel development in control non-irradiated tumours. When looking at the Cre<sup>-</sup> irradiated tumour, there were more lumens compared to non-irradiated control as previously observed, however the lumens were of small calibre and there was a high number of short length blood vessels. As seen in Figure 5.7 D previously, the Cre<sup>-</sup> irradiated tumour (mouse ID 239) did not undergo regression, rather the tumour growth stayed stagnant post irradiation and therefore the effects of radiotherapy may not have fully developed in this tumour. When observing the blood vessels of Cre<sup>+</sup> irradiated mice however, there was not a noticeable difference when compared with Cre<sup>+</sup> control mice. The blood vessel length, lumen size and lumenised vessels of those tumours were then quantified using Image J.

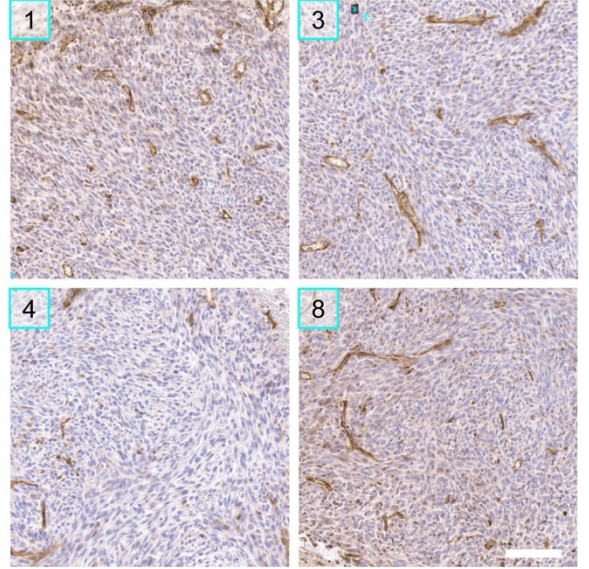
Figure 5.10 shows that in this experiment, there was a trend for increase in length, lumen size and lumenised vessels between tumours grown in non-irradiated Cre- and Cre+ mice (Fig 5.10 A-C) however as the experiment was underpowered (N=2 tumours) the differences did not reach statistical significance. Interestingly, there was statistically significant increase in vessel length between tumours grown in irradiated Cre- and Cre+ mice (Fig 5.10 A) suggesting that blood vessel growth was stimulated in the absence of endothelial *Dock4*, however since there was only one mouse in the irradiated Cre- group the results are not conclusive. Furthermore, while there was a trend of increase in lumen size and percentage lumenisation in Cre- mice post radiotherapy, the differences were not statistically significant, and there were no significant differences between Cre+ irradiated tumours and non-irradiated controls. Since the efficacy of irradiation was questionable and there was only one irradiated Cre- tumour, the only comparable groups in this experiment were the non-irradiated Cre- and Cre+ tumours. However, due to the small number of mice, only a trend of stimulation of blood vessel development in the Cre+ tumours could be observed.



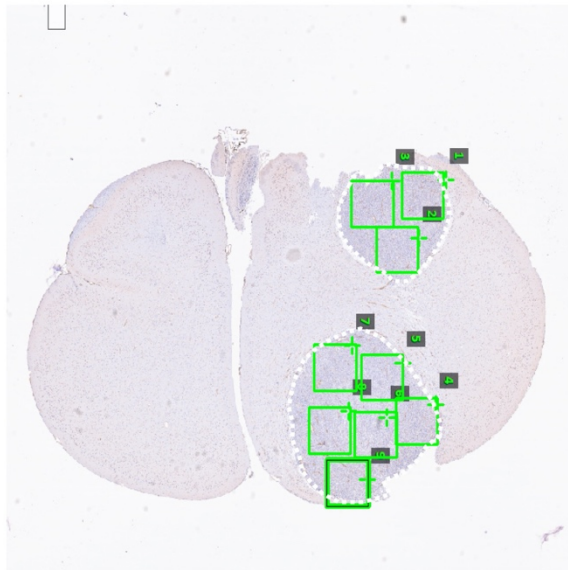
CD34 Endomucin



Cre- 2 x 5Gy



CD34 Endomucin



Cre+ 2 x 5Gy

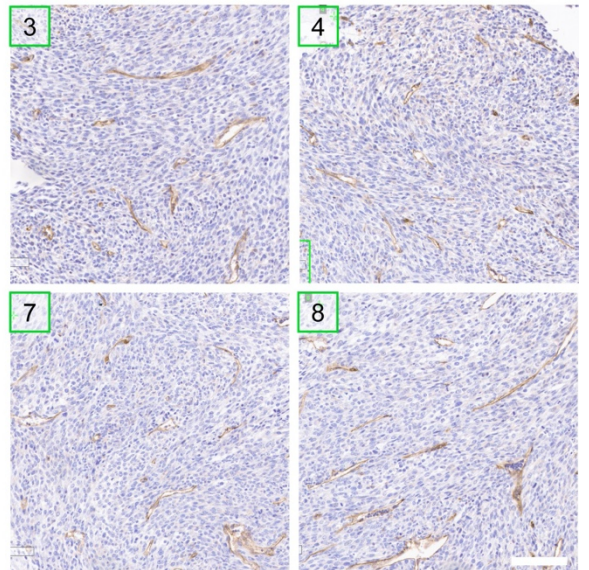
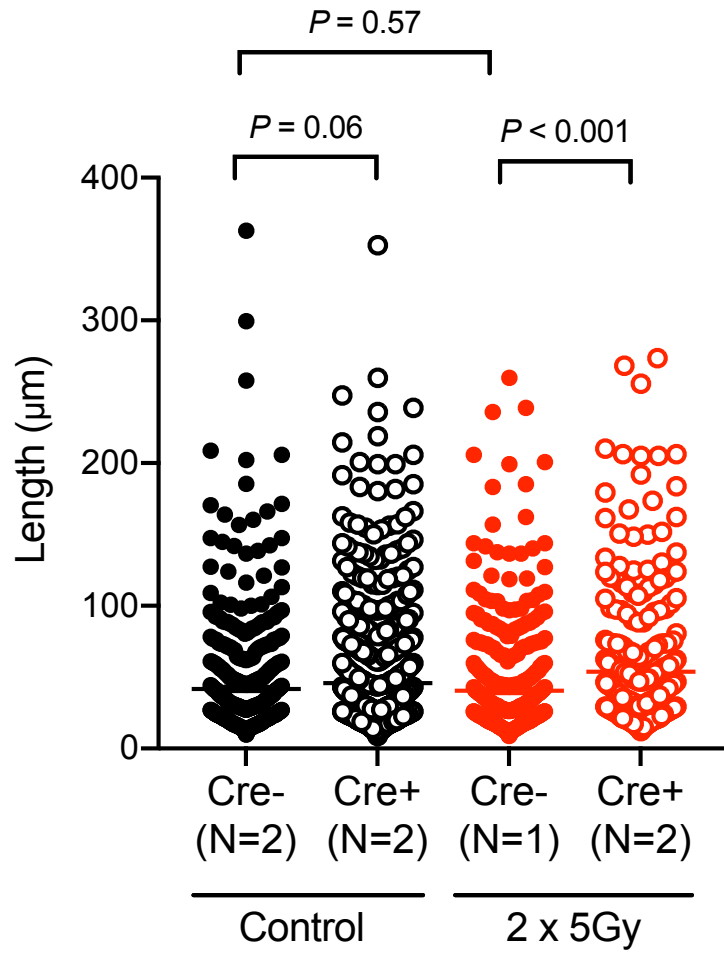


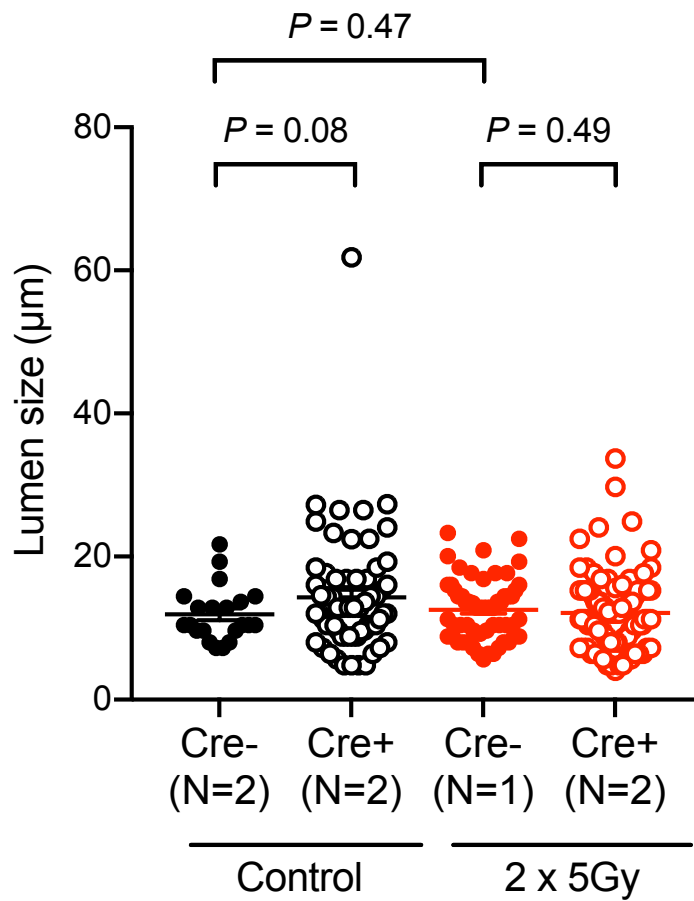
**Figure 5.9 Morphology of blood vessels of CT2A tumours grown intracranially in endothelial *Dock4* conditional knockout mice.**

Sections of fixed and frozen CT2A tumours, control and regrown after irradiation in *Dock4* conditional knockout mice, obtained from three different tumour sections 100  $\mu\text{m}$  apart were stained by IHC for CD34/Endomucin and haematoxylin. Slides were scanned using an Aperio AT Virtual Slide scanner and 5 images of 500 x 500  $\mu\text{m}$  (0.25  $\text{mm}^2$ ) at 20x magnification were selected using a random number generator. Images show appearance of blood vessels in control tumours and tumours regrown after irradiation in WT and endothelial *Dock4* conditional knockout mice. Left-hand panels show images of 20x objective zoom scanned slides at 1x magnification; right-hand panels show four 0.25  $\text{mm}^2$  images captured at 20x magnification from each tumour. White dotted lines indicate the tumour boundary. Scale bar = 100  $\mu\text{m}$ .

A



B



C

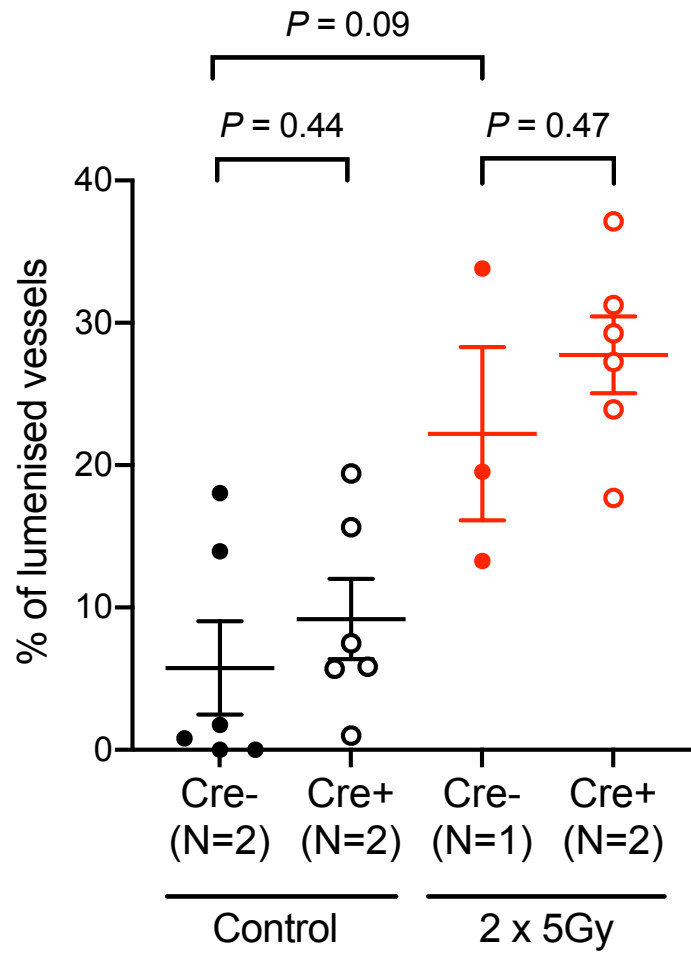


**Figure 5.10 Quantification of blood vessel growth, abundance, and size of blood vessel lumens in control and irradiated CT2A tumours growing intracranially in *Dock4* conditional knockout mice.**

Sections of fixed and frozen CT2A tumours control and regrown after irradiation obtained from three different tumour levels 100  $\mu\text{m}$  apart were stained for CD34/Endomucin and blood vessel length, lumen size and percentage of lumenised vessels were quantified using ImageJ.

(A) Dot plot shows increase in blood vessel length in irradiated tumours grown in Cre<sup>+</sup> compared to Cre<sup>-</sup> mice. n = number of blood vessels quantified: Cre-control = 564, Cre<sup>+</sup> control = 790, Cre<sup>-</sup> radiotherapy = 467, Cre<sup>+</sup> radiotherapy = 315.

(B) Dot plot shows no difference in lumen size in tumours grown in Cre<sup>+</sup> compared to Cre<sup>-</sup> mice. n = number of lumenised blood vessels quantified: Cre-control = 21, Cre<sup>+</sup> control = 63, Cre<sup>-</sup> radiotherapy = 58, Cre<sup>+</sup> radiotherapy = 100.

(C) Dot plot shows no significant difference in the percentage of lumenised vessel in tumours grown in Cre<sup>+</sup> compared to Cre<sup>-</sup> mice. n = number of sections per group quantified: Cre<sup>-</sup> control = 6, Cre<sup>+</sup> control = 6, Cre<sup>-</sup> radiotherapy = 3, Cre<sup>+</sup> radiotherapy = 6.

Error bars represent SEM. Note that the experiment is underpowered because of the small number of mice N = number of mice per condition: Cre<sup>-</sup> control = 2, Cre<sup>+</sup> control = 2, Cre<sup>-</sup> radiotherapy = 1, Cre<sup>+</sup> radiotherapy = 2.

## **5.7 Intracranial implantation of CT2A glioma cell line in endothelial *Dock4* conditional knockout mice in the repeat experiment**

Due to the small number of tumours per group in the earlier experiment employing the *Dock4* conditional knockout model rendering the results inconclusive, a repeat experiment was performed. This experiment was carried out in combination with injection of tracer to observe the effects of endothelial *Dock4* deletion on blood vessel permeability. Prior to the intracranial injections, as in the previous experiment, mice were injected with 2 mg of tamoxifen intraperitoneally for 5 consecutive days and after two weeks,  $1 \times 10^5$  CT2A-Luc cells were injected intracranially (Figure 5.11). Tumour growth was monitored using IVIS bioluminescence imaging and on day 6, mice were randomised prior to irradiation on days 7 and 8 with 5Gy each day. For reasons that are unclear in this experiment some mice developed neurological symptoms more rapidly and were sacrificed earlier than expected, starting from day 11 for control mice, and on days 15 and 21 for irradiated mice. Despite those differences in the schedule of tumour growth and recurrence compared to previous experiments we reasoned that the protocol should be completed, and tumours analysed in order to obtain the maximum amount of information from this *in vivo* experiment.

Prior to terminal perfusion and where the limits of the project license allowed in terms of animal clinical symptoms mice were injected with BSA-AlexaFluor555 at a dosage of 1.2mg/20g. Tracer was left to circulate for 3 hours, and mice were monitored closely. As described previously, given that there was an error with the processing of the frozen samples in the previous (pilot) experiment, in the repeat experiment, some changes were implemented. The erroneous EtOH step of the processing was omitted, and sucrose was used in place which acts as a cryoprotectant by displacing water present in the brain samples and prevent ice crystal formation, resulting in a better tissue morphology. In addition, the use of dry ice was replaced by freezing the tissue in chilled isopentane which prevents tissue expansion and resultant tissue damage.

Tumour growth monitored by IVIS bioluminescence imaging is shown in Figure 5.12. There was rapid growth of the injected tumour cells for all groups from day 1 to day 6 to an average bioluminescence signal of  $6.15 \times 10^6$  photons/seconds for all groups. In this experiment, radiation treatment on days 7 and 8 did not work as intended due to an operational fault of SARRP on day 7. Figure 5.12 B shows individual tumour growth curves with tumours taken forward for analysis marked. For irradiated groups, only mice that responded to radiotherapy were used in the analysis but note that there was no regrowth in the Cre- irradiated group. The remaining tumours were either undetected or did not respond to the SARRP treatment due to the aforementioned technical issues. Interestingly, Cre+ irradiated mice responded better to irradiation compared to Cre- mice. However, tumour in mouse ID 416 regrew in a different area of the brain from where originally injected and therefore was omitted from the analysis. Two Cre- control, 1 Cre- irradiated, 3 Cre+ control mice and 2 Cre+ irradiated mice were analysed (Table 5.2).

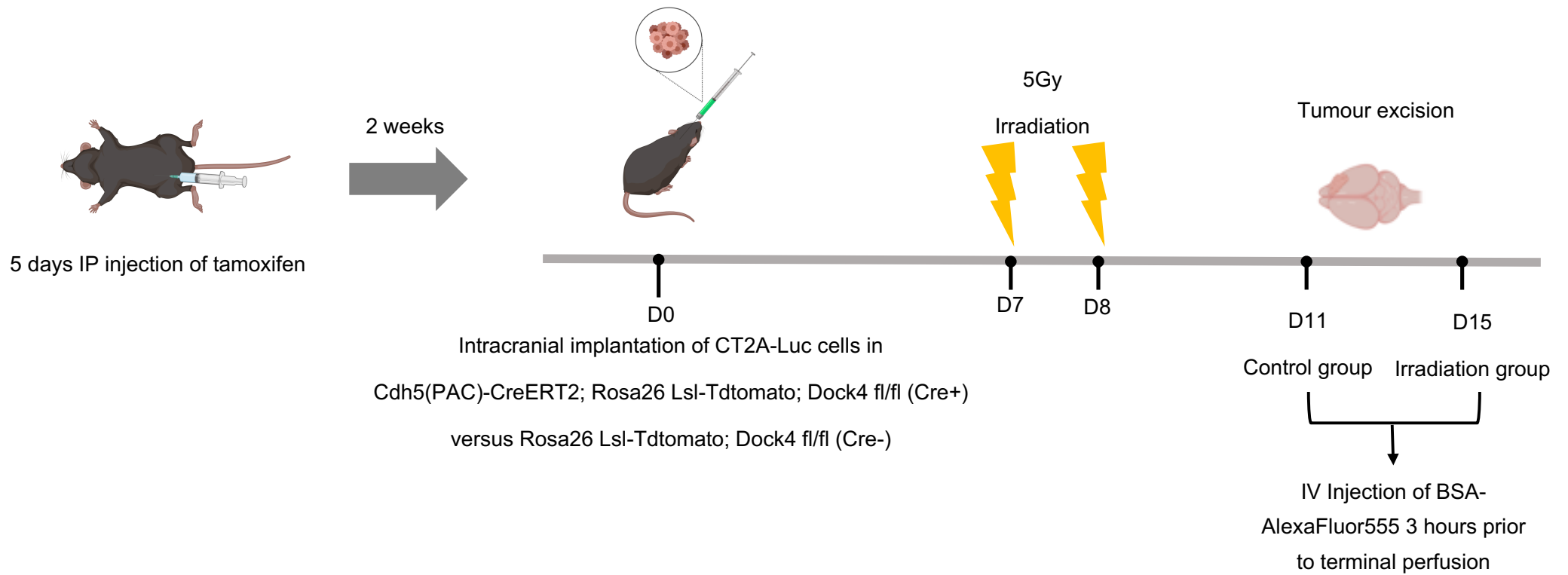
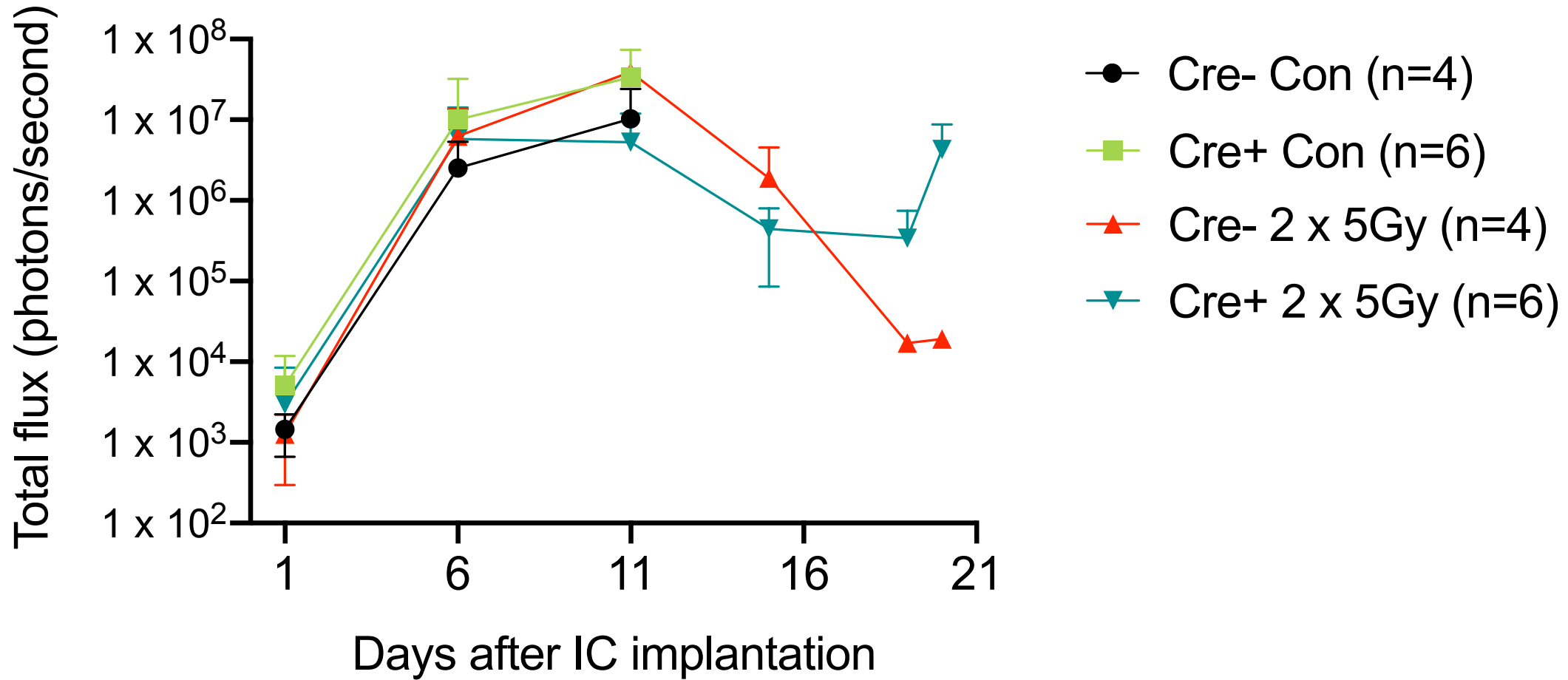


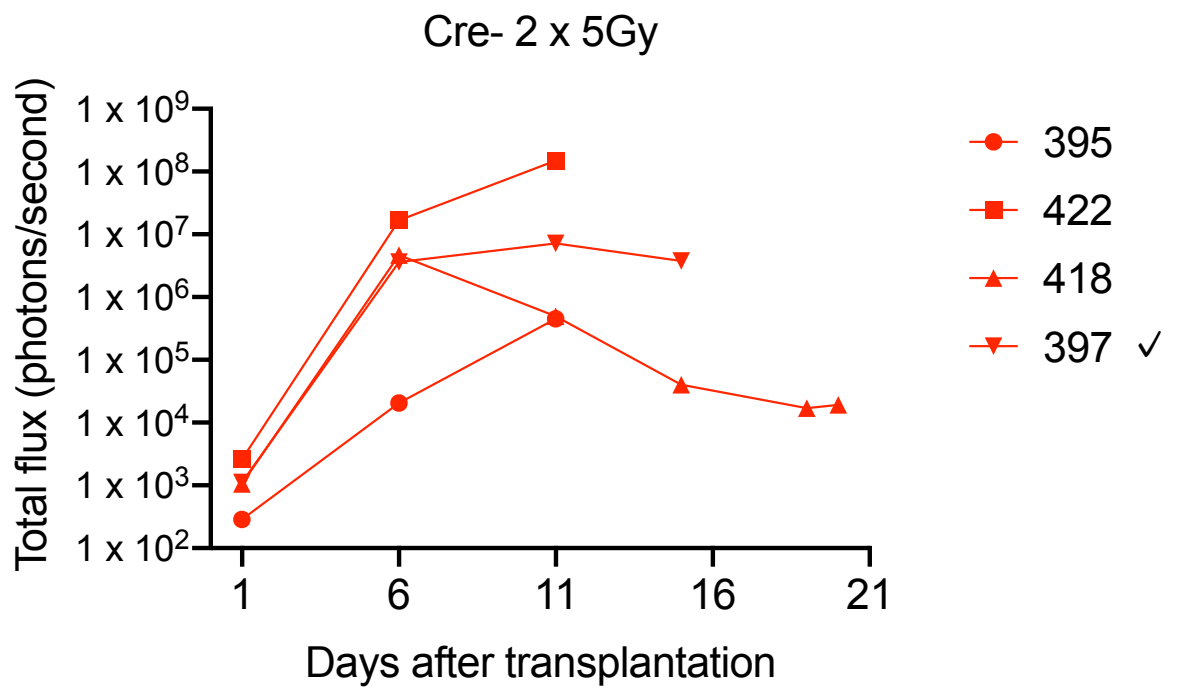
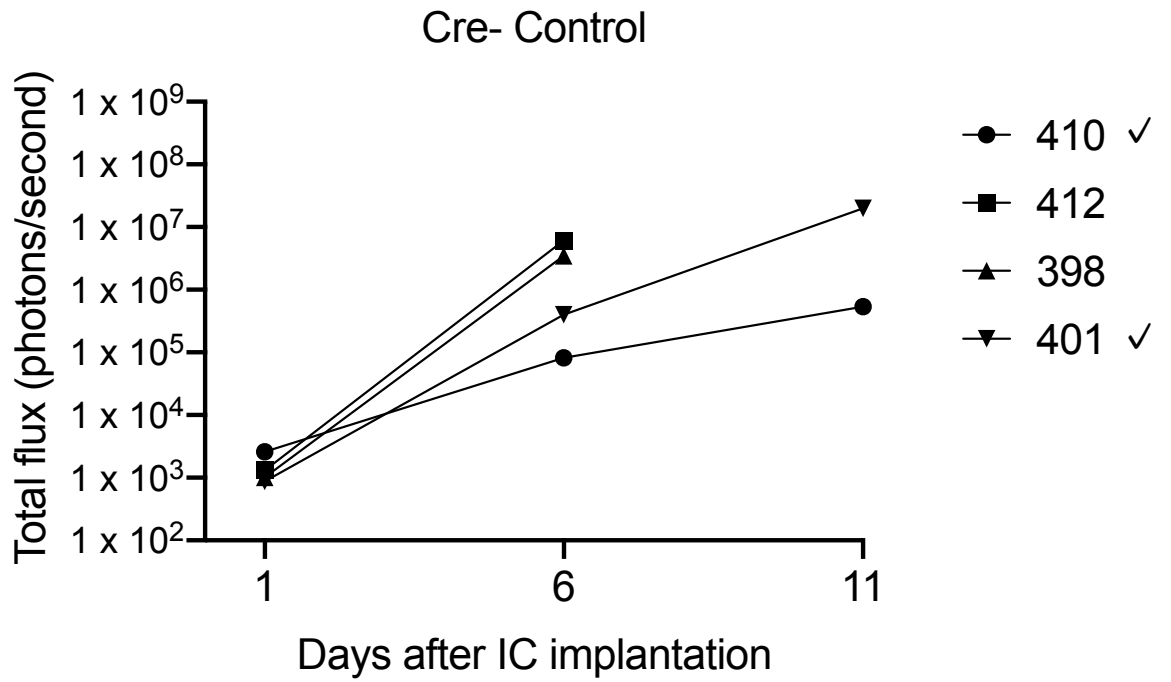
**Figure 5.11 Altered schedule of excision of CT2A tumours in repeat experiment in *Dock4* conditional knockout mice due to early presentation of neurological symptoms.**

CT2A-Luc murine glioma cell line ( $1 \times 10^5$  cells) was injected intracranially into the striatum of Cdh5(PAC)-CreERT2; *Dock4* fl/fl (Cre+) and control *Dock4* fl/fl (Cre-) mice. Tumour growth was followed non-invasively by IVIS bioluminescence imaging and fractionated irradiation ( $2 \times 5$ Gy) was delivered on days 7 and 8 using SARRP. Tumours were excised early due neurological symptoms: control (non-irradiated) tumours were excised between day 11 and 12, and irradiated tumours were excised from day 15. Tracer BSA-AlexaFluor555 was injected intravenously 3 hours prior to terminal perfusion.

A



B



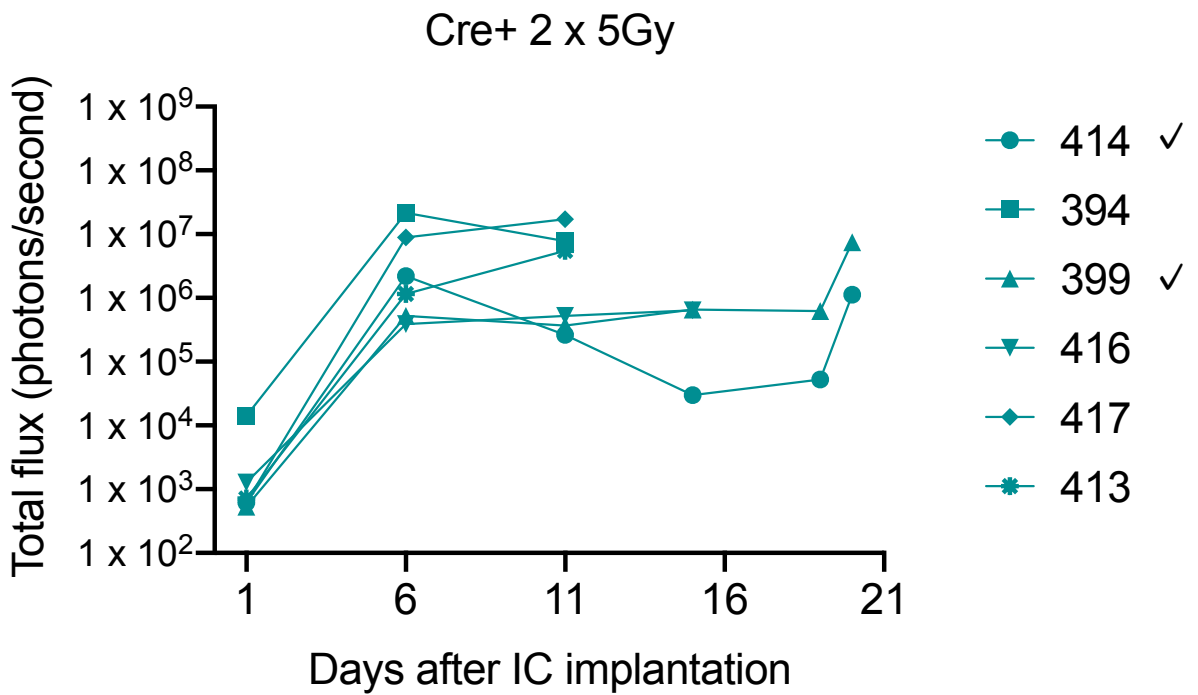
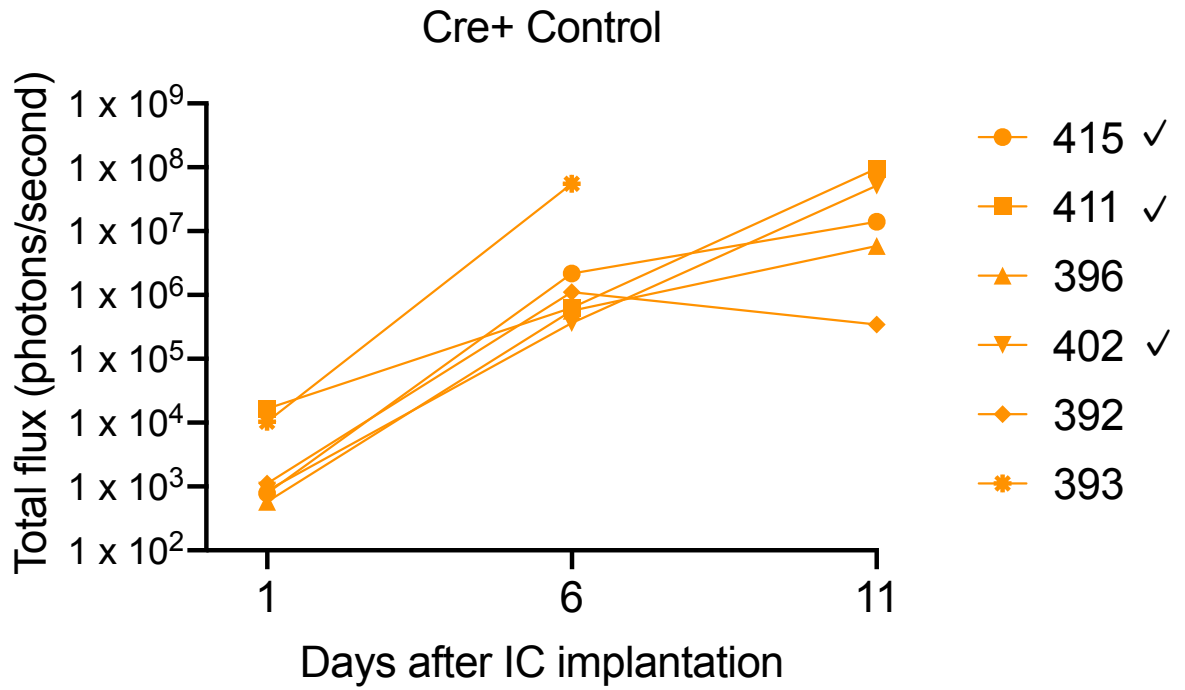


**Figure 5.12 Monitoring of CT2A tumour growth in control and irradiated *Dock4* conditional knockout mice by bioluminescence imaging (repeat experiment).**

(A) Growth curves of CT2A intracranial tumours in control versus irradiated *Cdh5(PAC)-CreERT2; Dock4 fl/fl (Cre+)* and *Dock4 fl/fl (Cre-)* mice.

(B) Growth curves of individual tumours: tick next to mouse number indicate mouse that was taken forward into analysis.

Note in this experiment radiation treatment performed using SARRP did not work as intended due to machine malfunction.

**Table 5.2 CT2A tumour samples grown intracranially in *Dock4* conditional knockout mice (repeat experiment).**

<b>Mouse ID</b>	<b>Age at intracranial implantation (weeks)</b>	<b>Sex</b>	<b>Genotype</b>	<b>TdTomato</b>	<b>Irradiation</b>	<b>Tumour excision day post injection</b>	<b>Tumour excision date</b>	<b>Neurological symptoms (Y/N)</b>	<b>RFP staining detected</b>
410	10	M	Cre-	X		D11	23/11/2020	Y	no
401	10	M	Cre-			D12	24/11/2020	Y	no
411	10	F	Cre+			D11	23/11/2020	Y	yes
402	10	M	Cre+			D12	24/11/2020	Y	yes
415	10	M	Cre+	X		D11	23/11/2020	Y	yes
397	10	M	Cre-		X	D15	27/11/2020	N	no
414	10	M	Cre+	X	X	D21	03/12/2020	Y	yes
399	10	F	Cre+		X	D21	03/12/2020	N	yes

Shown are the genotype of mice, sex, age at injection, treatment, tumour excision dates and presence of neurological symptoms at the time of excision. RFP staining was detected in the tumour blood vessels of mice harbouring Td tomato in the Rosa26 locus with a transcription stop codon flanked by loxP sites (Appendix 9) confirming tamoxifen induction of Cre activity in tumour endothelial cells.

## **5.8 Characterisation of early excised CT2A tumours injected intracranially in endothelial *Dock4* conditional knockout mice.**

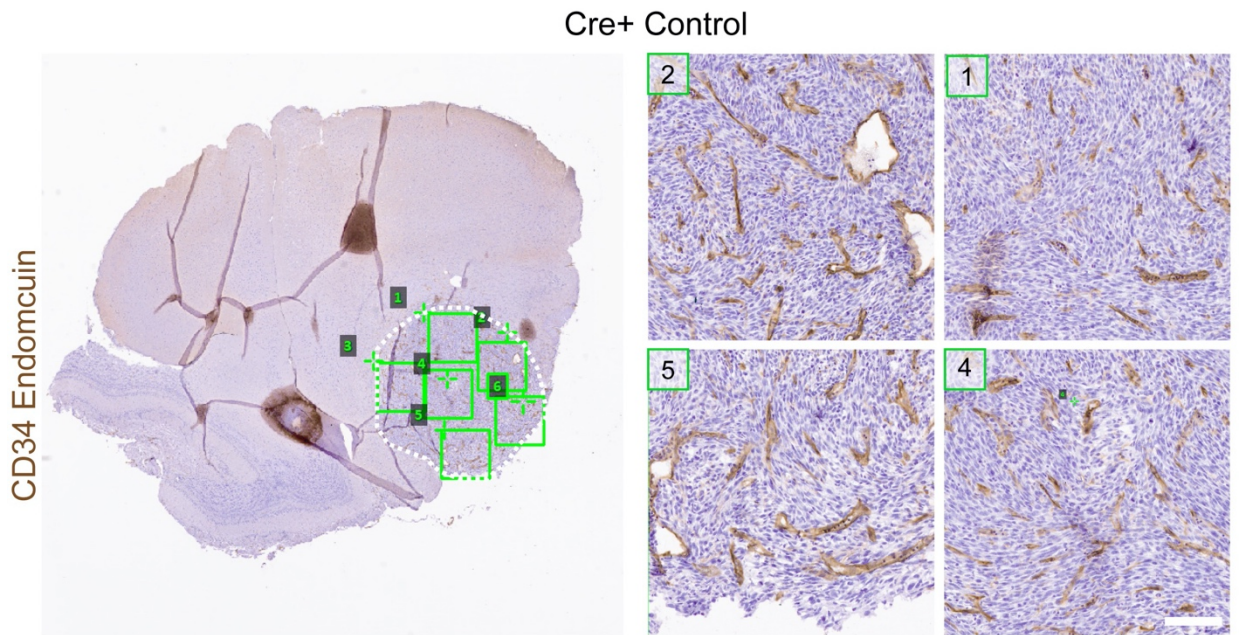
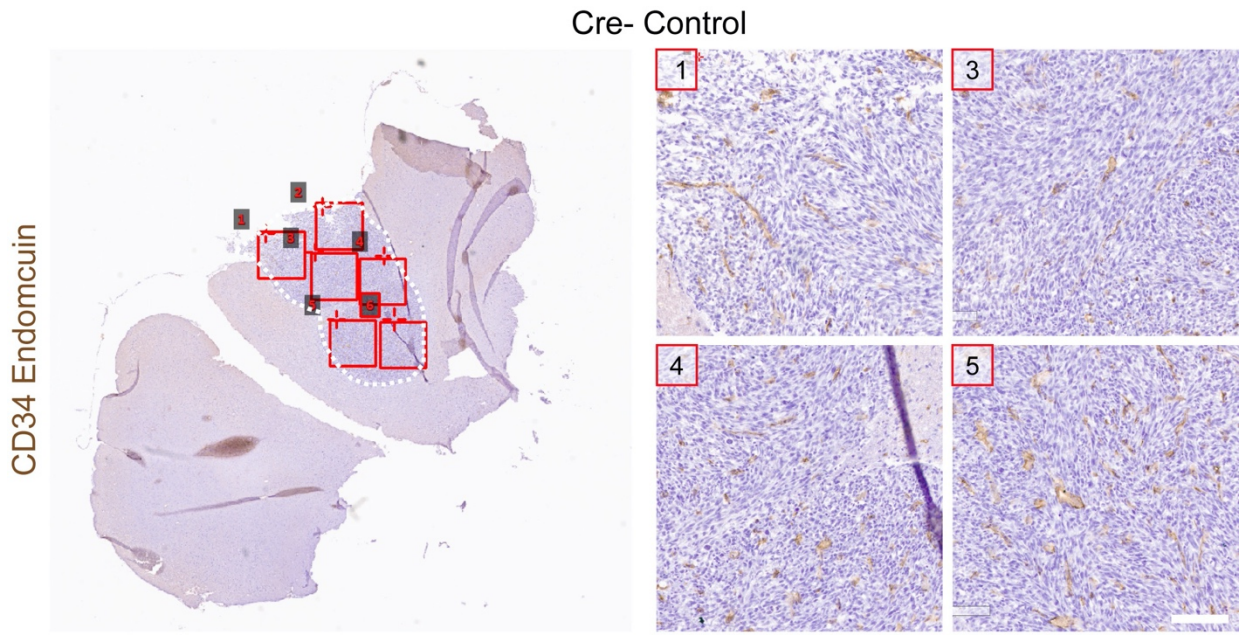
Three sections, 100  $\mu\text{m}$  distance apart, were obtained from each tumour listed in Table 5.2 and stained by IHC for CD34/Endomucin. Slides were scanned using Aperio AT Virtual Slide Scanner and 5 images of 500 x 500  $\mu\text{m}$  (0.25  $\text{mm}^2$ ) size at 20x magnification were randomly selected using a random number generator for vessel analysis. 1x magnification images refer to images scanned using Aperio AT slide scanner, scanned at 20x objective zoom. 20x magnification images refer to images further magnified 20x using ImageScope.

Figure 5.13 shows scanned whole mouse brain at 1x magnification from one tumour from each condition, and right panel shows images taken at 20x magnification using ImageScope from the same tumours. It is evident that the tumour size in this experiment was considerably smaller due to the tumours being excised earlier when compared with the mouse brain tumours from the initial experiment.

When comparing non-irradiated Cre<sup>-</sup> and Cre<sup>+</sup> tumours, Cre<sup>+</sup> tumours had considerably higher levels of vascularisation, blood vessels with larger lumens and longer vessel length. When looking at the Cre<sup>-</sup> irradiated tumour, although vessels with larger lumens were visible, there was no distinguishable difference in morphology compared to Cre<sup>-</sup> non-irradiated control which was expected since this tumour did not respond to irradiation (Figure 5.12) likely due the SARRP malfunction. When looking at the Cre<sup>+</sup> irradiated tumour there was an observable reduction in the number of blood vessel compared to Cre<sup>+</sup> non-irradiated tumour, suggesting that irradiation had worked to some extent.

Using ImageJ, the tumour blood vessels length, lumen size and percentage of lumenised vessels was quantified. As can be seen in Figure 5.14 A, there was a significant increase in tumour length, lumen size and percentage lumenisation in non-irradiated Cre<sup>+</sup> compared to Cre<sup>-</sup> tumours confirming the visual observations

in this experiment, and the trend observed in the previous experiment. Although radiotherapy might have not been administered as intended, Cre<sup>+</sup> irradiated tumour blood vessels showed a decrease in length, lumen size and percentage of lumenised vessels compared to the non-irradiated Cre<sup>+</sup> tumours, suggesting that irradiation had worked to some extent. However, this arm of the experiment was inconclusive because the Cre<sup>-</sup> irradiated tumour had not responded to the SARRP radiation treatment and hence did not show the expected trend of increased lumen size and length. Nonetheless, analysis of these early-excised tumours in this experiment gives evidence of a suppressive function of DOCK4 in GBM vessel development in non-irradiated control conditions.



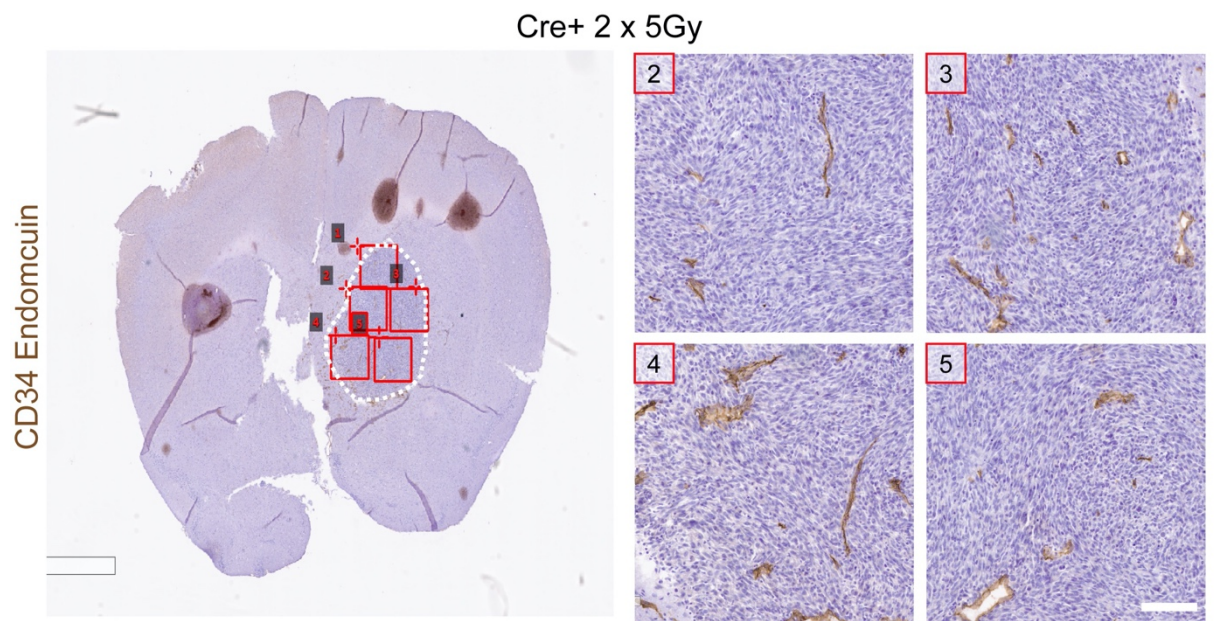
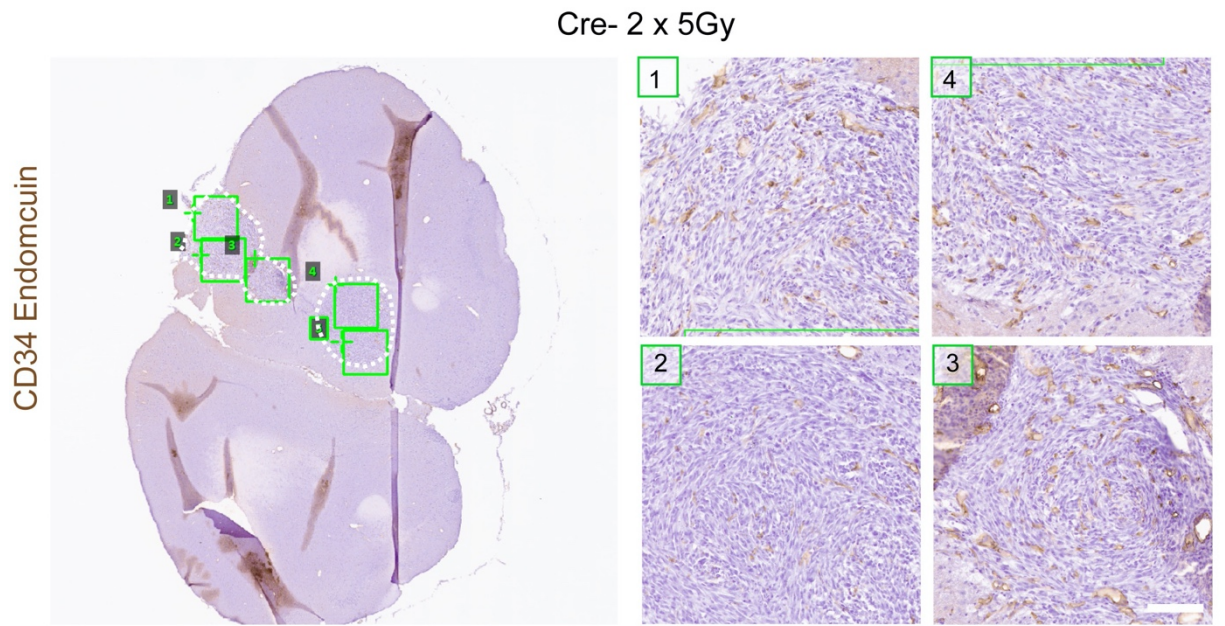
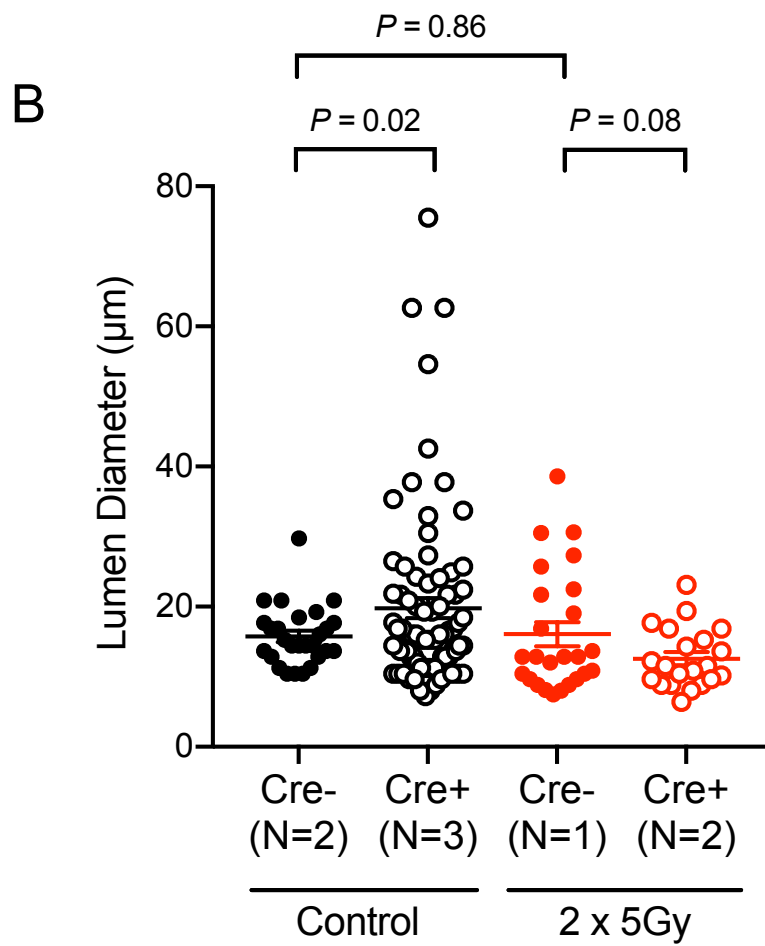
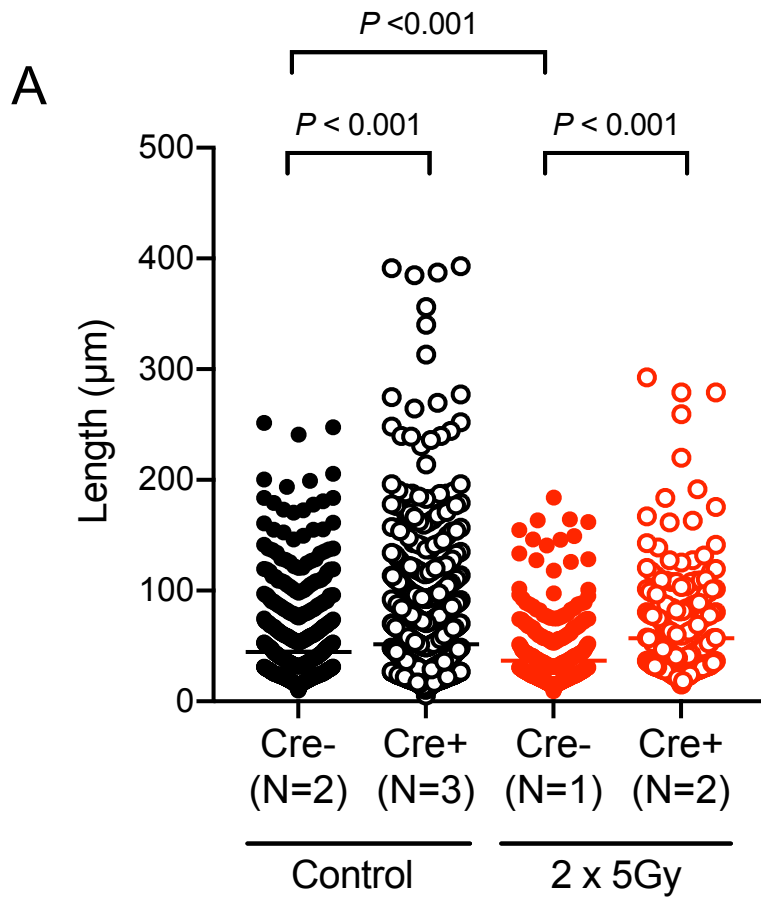


**Figure 5.13 Morphology of blood vessels of CT2A tumours grown intracranially in *Dock4* conditional knockout mice.**

Sections of fixed and frozen CT2A tumours were stained for CD34/Endomucin and haematoxylin by IHC. Slides were scanned using an Aperio AT Virtual Slide scanner and 5 images of 500 x 500  $\mu\text{m}$  ( $0.25 \text{ mm}^2$ ) were randomly selected using a random number generator at 20x magnification. Images show appearance of blood vessels in non-irradiated control tumours, and irradiated tumours in WT and *Dock4*<sup>het</sup> mice. Left-hand panels show 20x objective zoom scanned slides at 1x magnification; right-hand panels show four  $0.25 \text{ mm}^2$  images captured at 20x magnification. White dotted lines show the tumour boundary. Scale bar = 100  $\mu\text{m}$ .



C

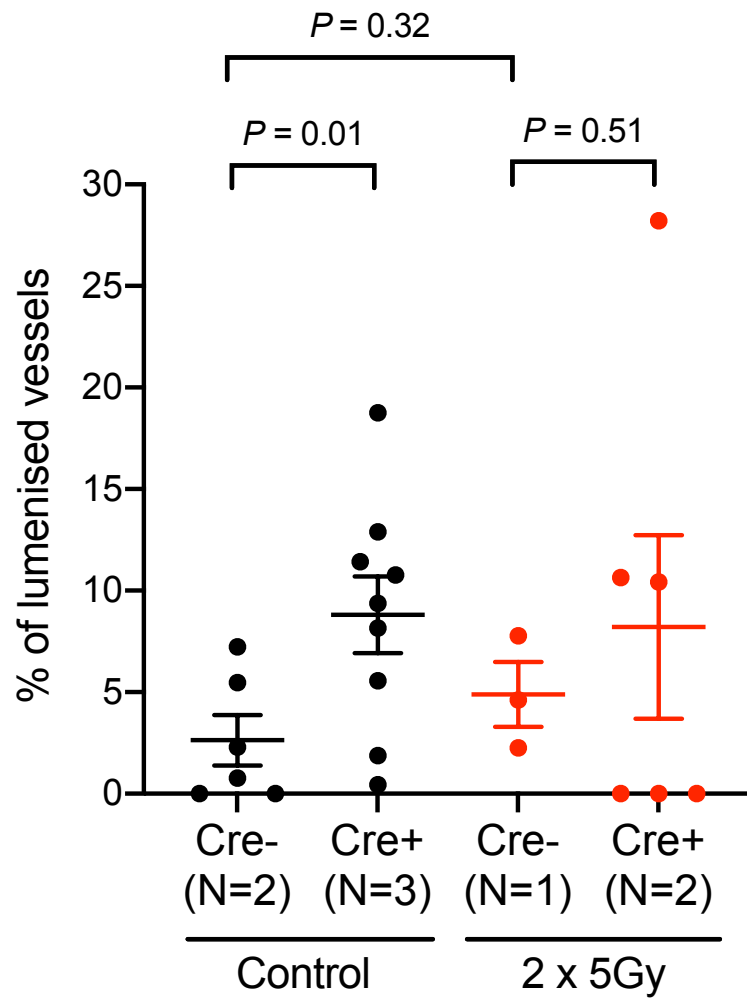


**Figure 5.14 Quantification of blood vessel growth, abundance, and size of blood vessel lumens in early excised CT2A tumours growing intracranially in *Dock4* conditional knockout mice.**

Sections of CT2A tumours were stained with CD34/Endomucin and blood vessel length, lumen size and percentage of lumenised vessels were quantified using ImageJ.

(A) Dot plot shows increase in blood vessel length in tumours grown in Cre+ mice compared to Cre- mice. n = number of blood vessels quantified. Cre- control = 913, Cre+ control = 1221, Cre- radiotherapy = 502, Cre+ radiotherapy = 267.

(B) Dot plot shows significant increase in lumen size in non-irradiated tumours grown in Cre+ compared to Cre- mice. n = number of lumenised blood vessels quantified. Cre- control = 27, Cre+ control = 80, Cre- radiotherapy = 25, Cre+ radiotherapy = 21.

(C) Dot plot shows significant increase in percentage of blood vessels with lumens in non-irradiated tumours grown in Cre+ compared to Cre- mice. n = number of sections quantified. Cre- control = 6, Cre+ control = 6, Cre- radiotherapy = 3, Cre+ radiotherapy = 6.

Error bars represent SEM. N = number of mice per condition: Cre- control = 2, Cre+ control = 3, Cre- radiotherapy = 1, Cre+ radiotherapy = 2

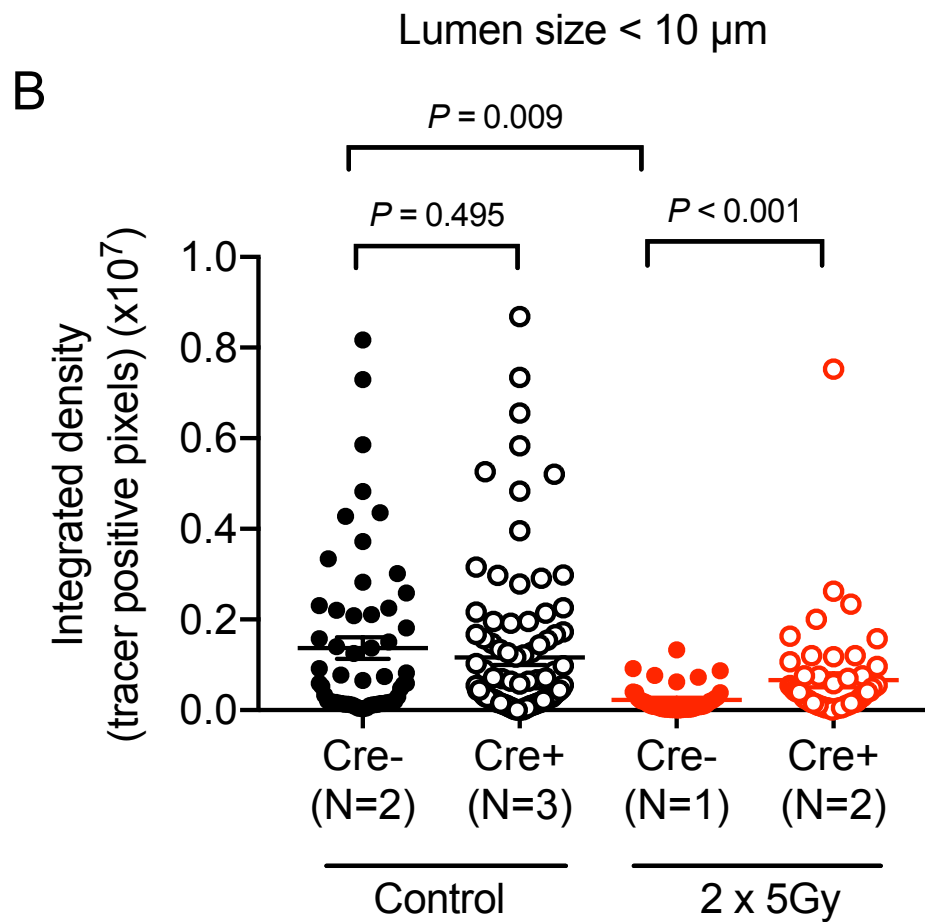
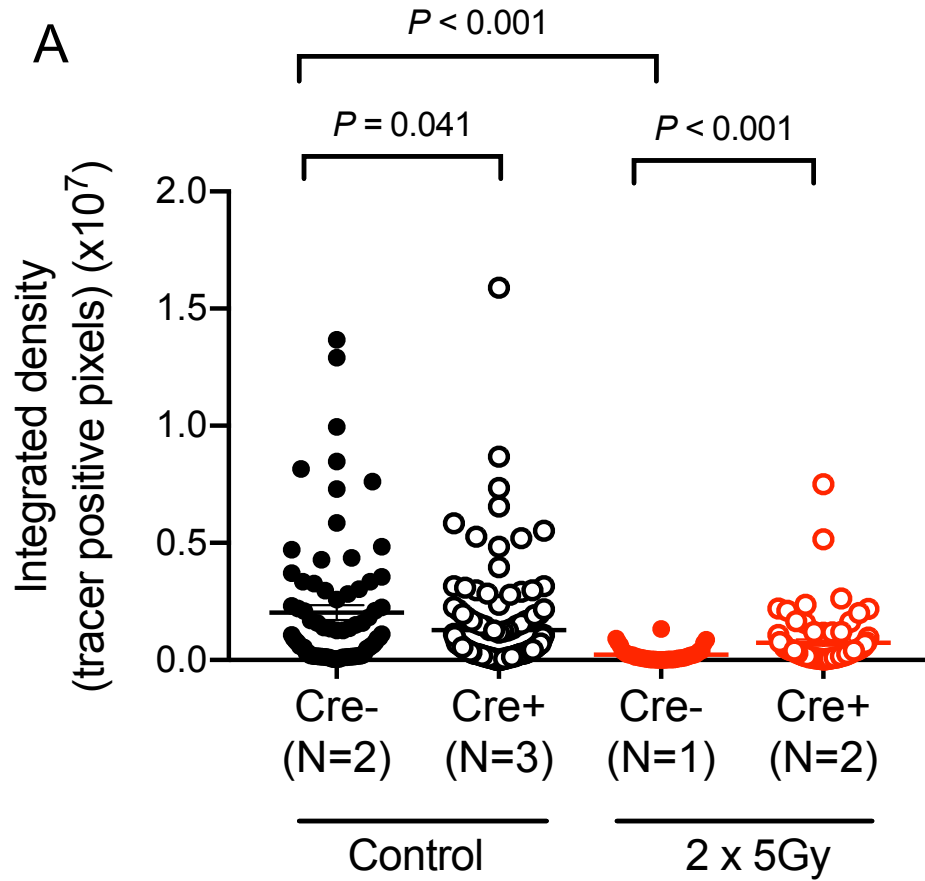
## **5.9 Blood vessel tracer extravasation in early excised intracranial CT2A tumours in endothelial *Dock4* conditional knockout mice**

Alongside blood vessel morphology analysis of the early excised tumours in the conditional *Dock4* experiment, tracer extravasation was assessed as the mice had been injected intravenously with the tracer BSA-AlexaFluor555. Sections of mouse brain tumours stained with CD34/Endomucin were imaged using Nikon A1R confocal microscope and images were captured for quantifications using ImageJ. Using the protocol for analysis of tracer extravasation described in Chapter 4, the analysis was performed to investigate the effects of endothelial *Dock4* deletion on blood vessel permeability.

As shown in Figure 5.15 A, there was a significant decrease in tracer extravasation in tumours grown in the *Dock4* conditional knockout mice compared to WT mice. When classified into different lumen sizes, lumen size larger than 10  $\mu\text{m}$  showed the highest decrease in tracer extravasation between Cre- and Cre+ control tumours. Furthermore, consistent with the data obtained in the previous chapter there was an overall decrease in tracer extravasation post irradiation. However, it was not possible to assess the effect of endothelial *Dock4* deletion under irradiation conditions since there was only one tumour in the Cre-control group (mouse ID = 397). In addition, the tumour had not responded by regression and regrowth but had shown stabilised tumour growth instead.

Control livers were also obtained post terminal perfusion as a control to validate injection success and to compare the amount of tracer injected amongst different mice. Mean fluorescence intensity of ten 20x magnified regions of livers sectioned at 10  $\mu\text{m}$  was quantified as described in Chapter 4. Figure 5.16 shows that when comparing between control and irradiated tumours, there seems to be a higher amount of tracer that was injected into the irradiated tumours. Mice 402, 397, 399 and 414 had an average of three times higher the amount of tracer injected compared to mice 410, 401 and 415, yet tumour blood vessels showed decreased permeability under irradiation conditions supporting further the notion that irradiation decreases blood vessel permeability. Interestingly, although

mouse 397 (Cre- irradiation) had a higher amount of tracer injected, the results still show reduced tracer extravasation in the blood vessels.



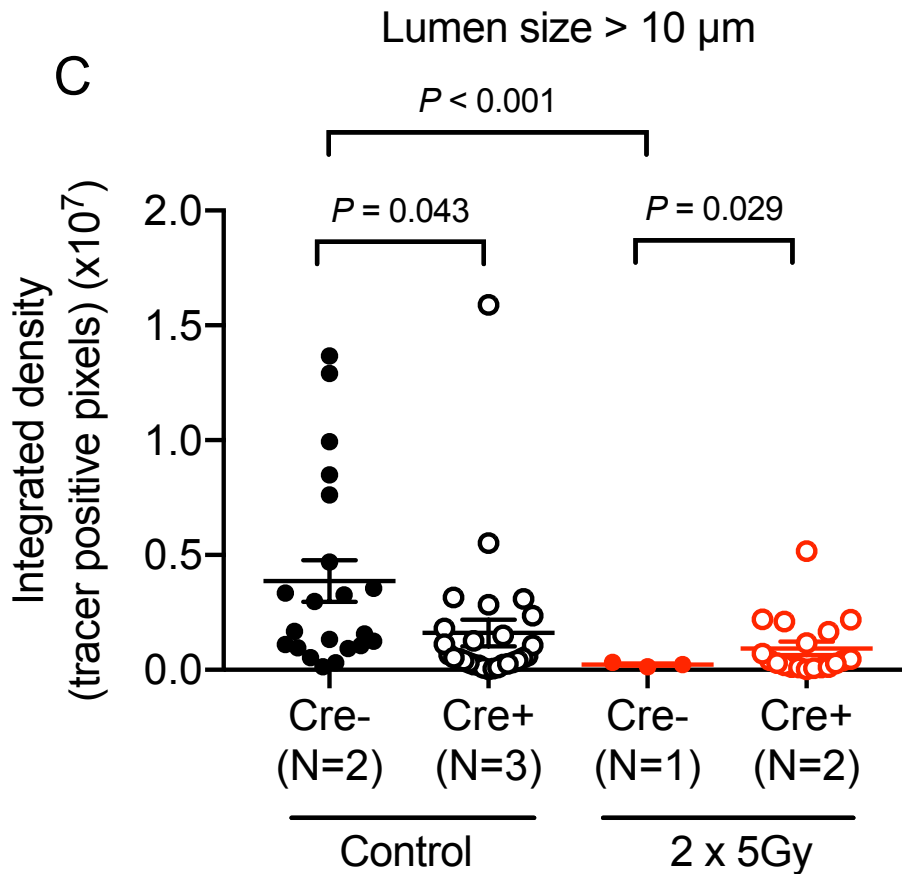


**Figure 5.15 Quantification of tracer extravasation from blood vessels in control and irradiated CT2A tumours growing intracranially in *Dock4* conditional knockout mice.**

CT2A cell line was intracranially injected into *Dock4* conditional mice and tumours were irradiated at 5Gy at day 7 and 8. Prior to terminal perfusion, BSA-AlexaFluor555 was injected to the tail vein of mice. Three tumour sections 100  $\mu\text{m}$  apart, were stained with CD34/Endomucin and imaged using Nikon A1R confocal microscope. Tracer positivity within 40  $\mu\text{m}$  radii around individual blood vessels in 10 regions from each section (total of 30 per mouse) at 60x magnification was quantified using ImageJ.

(A) Dot plot show decrease in the percentage of tracer-positive pixels around blood vessels grown in non-irradiated Cre+ mice compared to Cre- mice. n = number of blood vessels quantified for tracer extravasation. Cre- control = 80, Cre+ control = 124, Cre- radiotherapy = 44, Cre+ radiotherapy = 73.

(B) Dot plot shows lack of significant difference in the percentage of tracer-positive pixels around blood vessels grown in non-irradiated Cre+ mice compared to Cre- mice. n = number of blood vessels with lumen size under 10  $\mu\text{m}$  quantified

for extravasation. Cre- control = 59, Cre+ control = 96, Cre- radiotherapy = 41, Cre+ radiotherapy = 54.

(C) Dot plot shows a decrease in the percentage of tracer-positive pixels around blood vessels with a lumen size over 10  $\mu\text{m}$  in tumours grown in non-irradiated Cre+ mice compared to Cre- mice. n = number of blood vessels with lumen size over 10  $\mu\text{m}$  quantified for extravasation. Cre- control = 21 Cre+ control = 28, Cre- radiotherapy = 3, Cre+ radiotherapy = 19.

Error bars represent SEM. Note that the experiment is underpowered because of the small number of mice. N = number of mice per condition: Cre- control = 2, Cre+ control = 3, Cre- radiotherapy = 1, Cre+ radiotherapy = 2.

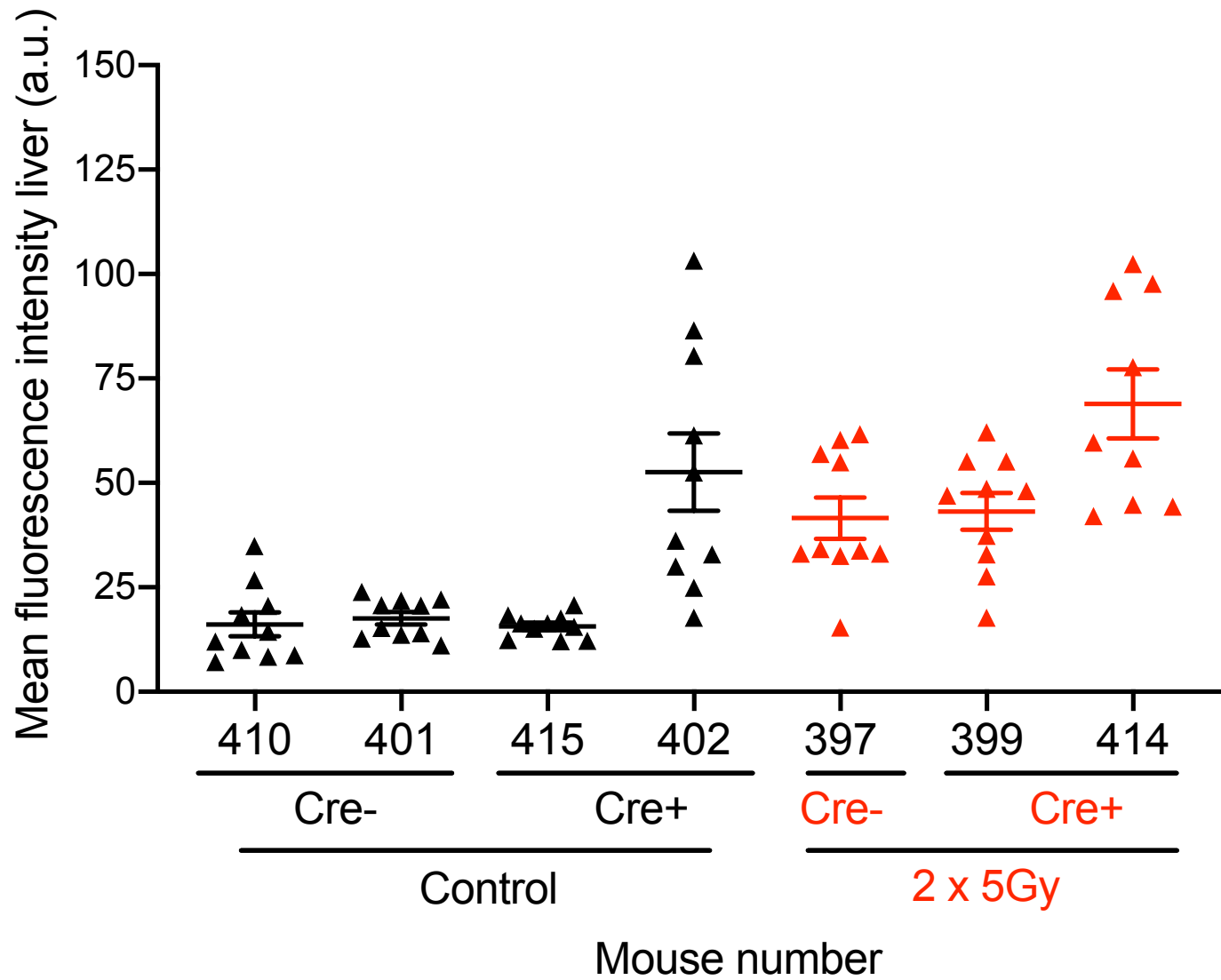


**Figure 5.16 Quantification of tracer abundance in livers of mice injected with BSA-AlexaFluor555.**

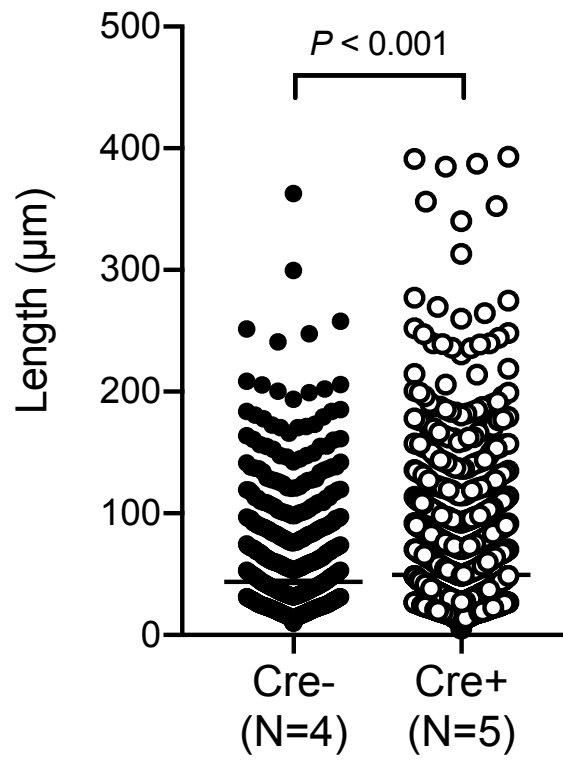
Livers of mice in Figure 5.17 were collected as tracer injection controls. Two 10  $\mu\text{m}$  liver sections were visualized for tracer extravasation from each mouse; 10 randomly selected images per section were captured at 20x magnification and quantified using ImageJ. Value of integrated density divided by area was measured. Note that one liver (mouse ID = 411) was not analysed from control Cre+ group due to processing error. Dot plot shows mean fluorescence intensity of tracer in liver sections. Cre- control mice = 410, 401; Cre+ control mice = 415, 402; Cre- radiotherapy = 397; Cre+ radiotherapy = 399, 414. n = number of liver images analysed for tracer abundance: control = 10; irradiation = 10 (except for mouse ID 414 = 9).

### **5.10 *Dock4* endothelial deletion stimulates blood vessel formation in blood vessels of CT2A tumours injected intracranially**

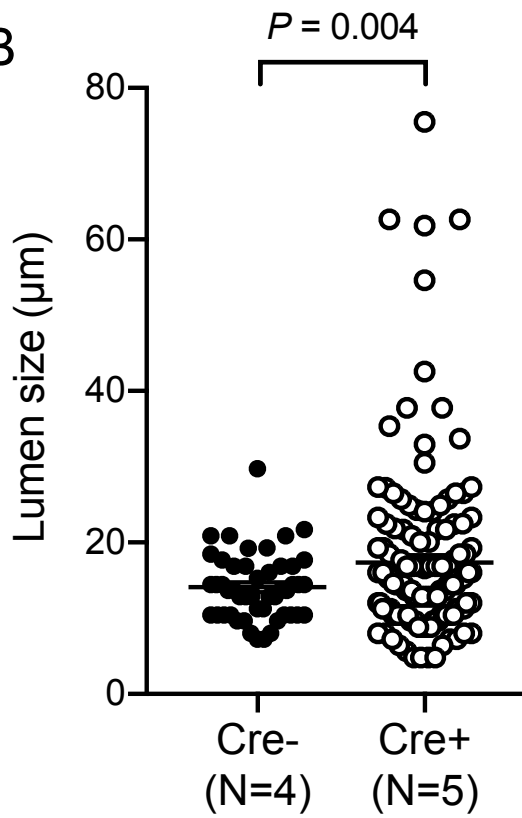
As discussed earlier, the number of irradiated mice suitable for analysis was too small in the first *Dock4* conditional experiment while radiotherapy treatment and tumour response were suboptimal in the second experiment, which was also underpowered due to technical reasons. Therefore, results from the radiotherapy treated mice groups were inconclusive. However, from both experiments there appears to be a consistent effect of *Dock4* conditional deletion in the absence of radiotherapy. Hence, mice were pooled from the two experiments and analysis on length, lumen size and percentage of lumenised vessels were carried out for tumours growing in the 4 C re- and 5 Cre+ non-irradiated mice.

As shown in Figure 5.17 A, interestingly, in the absence of endothelial *Dock4*, there was a significant increase ( $P < 0.001$ ) in tumour blood vessel length from an average of  $43.6 \pm 35.3 \mu\text{m}$  (Cre- mice) to  $49.4 \pm 44.8 \mu\text{m}$  (Cre+ mice). Furthermore, tumours growing in Cre+ mice demonstrated larger lumen size with a mean of  $17.4 \pm 11.4 \mu\text{m}$  compared to Cre- mice with a mean of  $14.1 \pm 4.46 \mu\text{m}$  (Figure 5.17 B). Lastly, the percentage of blood vessels with observable lumens also increased as shown in Figure 5.17 C where the percentage of lumenised vessel had an average increase of 4.7%. These results suggest that *Dock4* endothelial deletion stimulates blood vessel formation in the CT2A model. Although the experiment using global heterozygous *Dock4* knockout mice showed rescue of the increase in vessel size in response to irradiation with *Dock4* deletion, an endothelial cell autonomous effect of *Dock4* in suppressing irradiation driven stimulation of blood vessel development in CT2A tumours could not be discerned due to technical reasons.

A



B



C

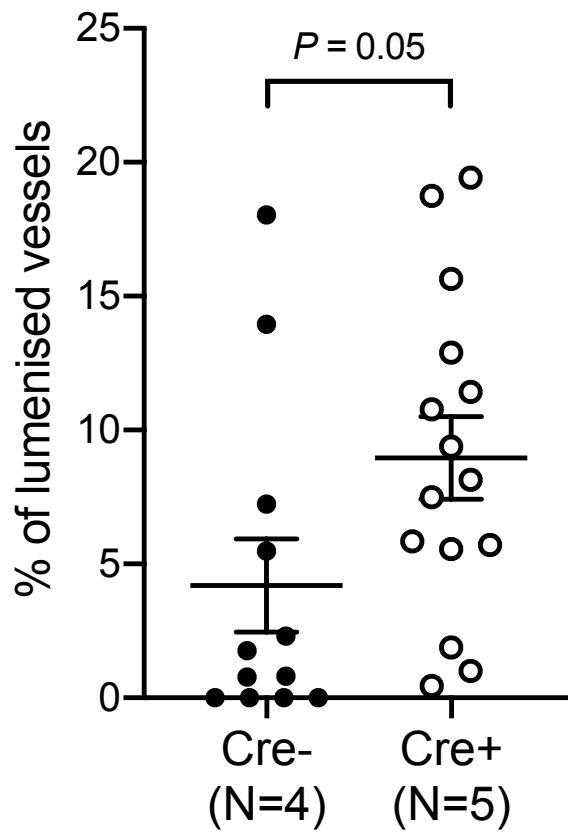


**Figure 5.17 Stimulation of blood vessel growth, abundance, and size of blood vessel lumens in tumours growing intracranially in *Dock4* conditional knockout mice compared to WT controls.**

Sections of CT2A tumours grown in *Dock4* conditional knockout mice were stained for CD34/Endomucin. Blood vessel length, lumen size and percentage of blood vessel with lumen was quantified using ImageJ. Values in graphs are pooled from the two different *Dock4* conditional experiments shown previously for non-irradiated controls.

(A) Dot plot shows significant increase in blood vessel length in tumours grown in control Cre<sup>+</sup> compared to Cre<sup>-</sup> mice. n = number of blood vessels quantified. Cre<sup>-</sup> control = 1477, Cre<sup>+</sup> control = 2011.

(B) Dot plot shows significant increase in blood vessel lumen size in tumours grown in Cre<sup>+</sup> compared to Cre<sup>-</sup> mice. n = number of lumenised blood vessels quantified. Cre<sup>-</sup> control = 48, Cre<sup>+</sup> control = 143.

(C) Dot plot shows increase in percentage of blood vessels with lumens in tumours grown in Cre<sup>+</sup> compared to Cre<sup>-</sup> mice. n = number of sections quantified. Cre<sup>-</sup> control = 12, Cre<sup>+</sup> control = 15.

Error bars represent SEM. N = number of mice per group: Cre<sup>-</sup> = 4, Cre<sup>+</sup> = 5.

## 5.11 Summary

In this chapter, I investigated the role of *Dock4* in CT2A tumour blood vessel pathological development in the context of radiotherapy. Initially, CT2A cancer cells were implanted into the brain of *Dock4* heterozygous knockout mice and blood vessel morphology of tumours grown in *Dock4*het mice with and without irradiation was subsequently analysed. When comparing between tumours grown in WT and *Dock4*het mice under control conditions, there was no difference in area covered by blood vessels, lumen size, percentage of blood vessels with detectable lumens and vessel length. As described previously in Chapter 3, regrown tumours post-irradiation showed an increase in lumen size, percentage of vessels with detectable lumen, blood vessel length and overall surface area covered by blood vessels. Interestingly, this augmentation of abnormal attributes of blood vessel calibre (lumen size and length), but not percentage of lumenised vessels were reversed in tumours implanted in *Dock4*het mice. This suggests that in the CT2A tumours *Dock4* plays a role in vessel regulation only under radiotherapy conditions.

Abraham et al. reported a significant decrease in the abundance of larger calibre lumens ( $> 20 \mu\text{m}$ ) in the global *Dock4* heterozygous knockout mice during embryonic development of the brain vasculature (Abraham, Scarcia, Bagshaw, McMahon, et al., 2015). The authors also reported that analysis of identifiable lumenised vessels in EO771 tumours (breast cancer brain metastasis model) showed that there was a significant decrease of lumen size in tumours grown in *Dock4*het mice compared to WT control (Abraham, Scarcia, Bagshaw, McMahon, et al., 2015). Their study provides an understanding of the role of DOCK4 in lumen morphogenesis both in developmental and pathological angiogenesis. DOCK4-dependent dynamic remodelling via lateral filopodia formation results in lumen formation by endothelial cells. Knockdown of DOCK4 results in loss of lateral cell-cell contact and dysregulation of lumen formation, including in vessels with lumens of smaller calibre.

However, a different observation was made when a conditional knockout model was used in conjunction with the CT2A model. Quantification of tumour blood

vessel morphology showed that under control conditions, tumours grown in *Dock4* conditional knockout mice compared to WT control mice had longer blood vessel length, larger lumen size and higher percentage of vessels with detectable lumens. In the case of irradiated tumours grown in *Dock4* conditional knockout mice, conclusions from the data cannot be made due to the number of mice being highly underpowered due to technical factors.

Interestingly, when looking at the effects of *Dock4* heterozygous deletion on the abundance of blood vessel associated  $\alpha$ -SMA positive cells (pericytes), no difference was observed (Chapter 4). A similar observation with regards to the effects of *Dock4* deletion was made by Abraham et al., as they found that pericyte association with blood vessels was unaffected during brain embryonic development in the *Dock4*het mice. Interestingly, in CT2A tumours growing in *Dock4*het mice, there was an increased abundance of blood vessels tightly associated with pericytes. However, in tumours treated with radiotherapy, *Dock4* deletion did not affect pericyte association.

Altogether, the studies show that *Dock4* deletion can reverse the increase in vessel abnormality including lumen size and length post-irradiation when CT2A tumours are grown in *Dock4* heterozygous deleted mice. In addition, this study shows that when CT2A tumours are grown in *Dock4* conditional endothelial specific knockout mice, there was stimulation of blood vessel growth in control non-irradiated conditions. This insinuates the angio-suppressive activity of conditional homozygous deletion of *Dock4* in the *in vivo* CT2A model of GBM.

# **Chapter 6**

## **Discussion**

## 6.1 Introduction

The concept of interaction between cancer cells and host cells in the tumour microenvironment was first postulated in the context of cancer metastasis by the British surgeon Stephen Paget in 1889 (Paget, 1889). Over a century later, the theory that outlines the influence of the microenvironment on cancer cells has been widely confirmed by both experimental and clinical evidence (Langley and Fidler, 2011). Components of the microenvironment that are crucial for cancer progression have since been elucidated; those include: stromal cells and growth factors they secrete such as angiogenic growth factors; endothelial cells and microvessels supplying the tumour with oxygen and nutrients; cells involved in inflammation such as macrophages; and the extracellular matrix providing a substrate for anchoring during invasion and activation of integrin signalling (Ribatti et al., 2007). Subsequent research in the field of tumour angiogenesis has since highlighted the angiogenic factor VEGF-A as a key player in the formation and growth of the vasculature, leading to the development of anti-angiogenic therapies targeting VEGF or its receptor VEGFR2 (Nagy et al., 2009). However, agents targeting VEGF signalling have not shown the same results in the clinic for all tumours types (Jain et al., 2006). Tumour angiogenesis is a complex orchestra of cellular and molecular interactions occurring amongst many different cell types including endothelial cells, inflammatory cells, stem cells and mural cells (Ribatti et al., 2007), the precise nature of which still remains partially characterised. However, it is known that tumour blood vessels are radically different to normal blood vessels, and they have been long known to be chaotic, structurally abnormal, and functionally defective (Reviewed in Nagy et al., 2009).

Glioblastoma is one of the most vascularised solid tumours and vascular proliferation is directly linked to poor prognosis in GBMs (Hardee and Zagzag, 2012), as described previously in the Introduction Chapter. Recurrence is one of the greatest challenges in GBM treatment, which is invariably followed by therapeutic resistance allowing escaping cells to reignite tumour growth. Despite aggressive therapies including surgical resection, irradiation, and adjuvant chemotherapy, GBM has proven to be some of the most challenging cancers to manage. With anti-angiogenic therapies falling short of expectation, there is a growing appeal in considering alternative ways in which GBM tumours acquire

blood supply in order to target those. Although there have been few studies investigating observing the process of revascularisation and blood vessel abnormality in recurrence tumours (Kioi et al., 2010; Seo et al., 2019), the precise nature of abnormalities, prevalence, and mechanism through which they arise remain uncharacterised. Moreover, while there are numerous studies on the short-term effects of radiotherapy on the vasculature, there is limited understanding on the effects of radiotherapy treatment on the vasculature of regrown tumours in recurrences. This study focused on improving our understanding of the vascular changes occurring in recurrences, both in terms of blood vessel morphology and functionality, specifically in response to radiotherapy of primary tumours, using an experimental *in vivo* model of tumour regression and regrowth post radiotherapy. In addition, the role of DOCK4, a RAC1 activator, was also investigated in GBM using heterozygous global, and conditional endothelial *Dock4* knockout mouse models.

## **6.2 The use of the CT2A tumour model**

The use of *in vivo* intracranial tumour models in studies has offered valuable insights into the pathophysiology of GBM. However, it is widely acknowledged that available models for the study of malignant brain tumours remain imperfect. This is thought to be due to the difficulty in recapitulating the human microenvironment in mouse models of human cancer, while patient derived xenograft models lack an immune component (Akter et al., 2021). With interactions between the blood vessels and cancer cells being the main interest, it was important to employ a model that recapitulated characteristics of the vasculature of human GBM and the invasiveness of cancer cells. Furthermore, the aim to investigate the role of DOCK4 using a knockout model necessitated the use of a syngeneic C57BL/6 mouse GBM model to match the genetic background of the *Dock4* global and conditional knockout models. The limitation of a syngeneic rodent model is the lack of stepwise progression seen in naturally forming human tumours.

This study required the use of a model of GBM recurrence after radiotherapy treatment. Thus, using a CT2A model we followed the published orthotopic GBM

regrown tumour post-irradiation protocol as described previously by Kioi and colleagues, which used an orthotopic U251 model. In this model, prior to irradiation a debulking surgery was not performed, thus while such surgical models are being developed, this model can be used to study the effects of tumour regrowth post irradiation.

Malignant gliomas are characteristically highly infiltrative (Wank et al., 2018) while many syngeneic models grow as a circumscribed tumour (Akter et al., 2021). The CT2A cell line employed in this study is significantly more invasive when compared with the GL621 (Egnuni, PhD thesis). However, when compared to other mouse glioma models such as VM-M3 spontaneous brain tumour model, CT2A has a more distinctive border with less local invasion (Shelton et al., 2010). In a review by Haddad et al. (Haddad et al., 2021), the authors described that although GL261 is widely used as it can be implanted in immunocompetent mice, the underlying genetics are different to human GBM (Szatmári et al., 2006), as GL261 comprises a homogeneous population of cells, and is highly immunogenic compared to human GBM. Like GL261, the line CT2A provides an advantage as a model by its ability to be implanted in immunocompetent mice. Although it has been argued that CT2A tumours show limited invasion into surrounding brain parenchyma (Shelton et al., 2010), in the studies carried out in this thesis I observed considerable peritumoral invasion in both control and regrown tumours (Appendix 4); interestingly, secondary tumour lesions distant from the primary tumour bulk were not observed, however, those are also less prevalent compared to local invasion in patient GBM.

When comparing the blood vessels within the tumour bulk in the CT2A tumours and GBM human tumours, the CT2A model recapitulated a number of different traits observed in the human GBM tumour blood vessels. It was evident that the tumour vasculature of CT2A was structurally abnormal with key differences being significantly larger size and tortuosity (Chapter 3, Figure 3.1). The abnormality of tumour blood vessels has been long known and was elegantly described in a review by R Jain (Jain, 2003). These include abnormal vessel wall structure, uneven diameters, large number of fenestrations in ECs and abundance of pericyte-like cells with abnormal morphology (Jain, 2003). In human tumours,

GBM blood vessels have also been shown to form glomeruloid structures and other abnormal structures such as vascular 'garlands' and 'clusters' indicative of high tortuosity (Rojiani and Dorovini-Zis, 1996; Birner et al., 2003; Chen et al., 2015) that was not observed in CT2A tumours. This may be due to fact that human tumours grow much larger in size prior to surgical resection, and therefore blood vessels become more tortuous as result of increased tumour growth and hypoxia (Mathivet et al., 2017) (Deindl et al., 2001; Boroujerdi et al., 2012). CT2A tumours also appeared to have more sprouting blood vessels potentially representing earlier stages of patient GBM tumour growth. With this study employing the CT2A cell line as a syngeneic tumour model, it would be interesting to investigate the morphology of the vasculature in patient derived tumour models implanted in immunocompromised mice, and genetically engineered mouse models (GEMMs). As GEMMs do not involve the injection of tumour cells directly to the brain and the progression of tumour development appears more similar to human GBM (Haddad et al., 2021), it would be of benefit to find out whether these models develop a more diffused infiltrative growth pattern, and blood vessels with glomeruloid morphology.

### **6.3 The vascularisation of GBM recurrences**

Prior studies have investigated the process of neovascularisation in GBM. It is hypothesised that angiogenesis is the main method of blood vessel formation in primary occurrence; the release of angiogenic factors such as VEGF, EGF and FGF from tumour cells results in blood vessel sprouting that gives rise to the extensive vasculature of GBM tumours (Greenfield et al., 2010). Current antiangiogenic treatments interfere with the VEGF signalling pathway. However, these treatments are only effective in actively growing angiogenic vessels, but not in mature and stable blood vessels (Mukwaya et al., 2021). On the other hand, anti-VEGF therapies have proved ineffective in GBM recurrences, and the mode of revascularisation of tumour recurrences is largely unclear.

Kioi et al., proposed bone marrow-derived endothelial progenitors and the process of vasculogenesis, rather than angiogenesis, as the main mode of revascularisation in recurrence GBM tumours. Their study showed activation of

HIF-1 in regrown intracranial U251 tumours post radiotherapy treatment resulting from elevation of SDF-1 ligand, which activates the CXCR4 pathway, promoting recruitment of BMDCs (Kioi et al., 2010; Greenfield et al., 2010). The authors proposed that BMDCs contribute to the restoration of radiation-targeted vasculature through the process of vasculogenesis. In support, their study showed that inhibition of HIF-1 or of the SDF-1/CXCR4 signalling axis by means of treatment with the small molecule inhibitor AMD3100, cooperated with the VEGF inhibitor DC101 to inhibit tumour regrowth *in vivo*. Their study was the first to propose that vasculogenesis as key mode of revascularisation of recurrence GBM tumours. However, in a commentary published by Kioi et al., it was argued that the dominant mechanism in GBM recurrences is angiogenesis, through the sprouting of surviving endothelial cells after irradiation (Kozin et al., 2011; Kozin et al., 2012). Indeed, to quote the Kozin et al., commentary, “no specific data to support this mechanism (vasculogenesis) exists (in recurrent tumours)” (Kozin et al., 2012) and ‘more work is necessary to elucidate the mechanisms of vascularisation of GBM recurrences’. Kozin et al., further noted that most studies have focused on early vascular effects of irradiation and there is limited understanding of the effects on regrowth post-radiation stages (Kozin et al., 2012).

It is widely accepted that the increased invasiveness of recurrent tumours post-irradiation allows the process of vascular co-option to take place, as resistant and invading cancer cells move towards existing blood vessels in the normal brain parenchyma (Appendix 5) Furthermore, it has been shown that a process of trans-differentiation takes place in primary tumours whereby glioblastoma stem cells transdifferentiate to ECs, which then line the blood vessels. This was documented by laser capture microdissection and identification of cancer cell mutations in ECs (Soda et al., 2011). Interestingly, when patient samples were characterised in this laboratory, no evidence of this process of trans-differentiation was observed in patient recurrences (Egnuni, PhD thesis). To our knowledge, apart from the studies listed here, there no other published studies that describe the detailed characteristics of blood vessels in regrown GBM tumours post irradiation, their functionality, or the mechanism through which they arise.

## **6.4 Blood vessel enlargement in regrown tumours post-irradiation**

The early effects of ionising radiation on the vasculature have been well studied and reported in the literature. Shortly after irradiation, dose-dependent effects ranging from smaller blood vessels size to vessel destruction have been described which particularly affect the microvasculature (Baker and Krochak, 1989; Garcia-Barros et al., 2003; Reviewed in Barker et al., 2015). The higher radiosensitivity of capillaries is thought to be due to their structural composition having only one single layer, the tunica intima, consisting of a single layer of endothelial cells and small amount of connective tissue, which is highly susceptible to radiation (Dimitrievich et al., 1984). In cancers, radiation-induced effects on blood vessels depend on the tumour type and stage, implantation site, and radiation dose and schedule (Park et al., 2012; Karam and Bhatia, 2015).

Park et al., reviewed the short-term radiation-induced changes of the tumour vasculature in a wide range of tumours, in studies published over the past 60 years (Park et al., 2012). Although responses vary, generally, irradiation given at a dose between 10 to 15 Gy per fraction, results in tumour blood flow decreasing soon after irradiation (observed after 24-30 hours), followed by physical vessel abrogation. In an orthotopic human U251 model, a single irradiation dose of 15 Gy decreased blood vessel perfusion to 10% of the original level within 2 weeks of irradiation (Kioi et al., 2010). At the same timepoint, the number of endothelial cells were reduced to 25% of control (Kioi et al., 2010). Consistently, prior work in this laboratory showed that, in the CT2A implantation model, there was significant reduction in blood vessel size three days following tumour irradiation with a dose of 2 x 5Gy (Egnuni, PhD thesis).

Although the early effects of radiation on vascularisation have been studied extensively, there is little understanding of the effects of irradiation on the vasculature in recurrence tumours. In patient samples, prior work by our group had shown increased blood vessel abnormality in recurrences including blood vessel size, tortuosity (glomeruloid morphology), and blood vessel coverage by  $\alpha$ -SMA positive cells (pericytes). In the syngeneic CT2A model in this study, the

abnormal characteristics of the vasculature observed in primary tumours were amplified in the regrown tumours post-irradiation in line with the findings of characterisation of patient recurrences. These abnormalities include increased blood vessel lumen size, vessel length, and overall surface area covered by blood vessels in CT2A tumours. A recent study by Seo et al. is in line with these findings in a different tumour model, patient derived GSC line 83NS grown intracranially in BALB/c mice, showing that tumour regrowth after irradiation results in enlarged vasculature marked by upregulation of CD34 and Von Willebrand factor (VWF) (Seo et al., 2019). The authors suggested that there was enhancement of abnormal vasculogenesis during tumour regrowth post-irradiation (Seo et al., 2019). However, as in the study by Kioi et al., it is unclear whether vasculogenesis is the mode of vascularisation that has taken place. To our knowledge, other than the recent study by Seo et al. of GSC-derived cells of GBM, no other studies have shown the morphological changes of the vasculature post irradiation in GBM tumours.

## **6.5 Elevated hypoxia in regrown tumours post-irradiation**

Published studies suggest that observed blood vessel enlargement may be driven elevated hypoxia and upregulated VEGF signalling. Hovinga et al., showed irradiation may increase VEGF levels secreted by GBM cancer cells in the cell lines U251, U251-NG2 and U87 (Hovinga et al., 2005), while VEGF<sub>121</sub> and VEGF<sub>165</sub> have both been implicated in the regulation of vessel diameter in *in vitro* angiogenesis models (Nakatsu et al., 2003). Furthermore, *in vivo* study of mouse brain and retina vascular development by Ruhrberg and colleagues, demonstrated that the soluble VEGF isoform VEGF<sub>120</sub> generated vessels with large diameters compared to VEGF<sub>188</sub> (Ruhrberg et al., 2002). In this study, VEGF (mouse isoforms 120 and 164 detected by the Quantikine ELISA as specified in manufacturer's specificity information) was significantly elevated in conditioned medium of CT2A cells treated with irradiation at 5 Gy and 10 Gy after 72 hours (Appendix 10).

Studies show that blood vessels enlarge in size in response to hypoxia (Larcher et al., 1998; Carmeliet, 2000; Reviewed in Iruela-Arispe and Davis, 2009) as VEGF is upregulated (Liu et al., 1995; Forsythe et al., 1996; Rankin et al., 2008) in an adaptation response aimed to increase blood flow and oxygenation to counteract hypoxia (Deindl et al., 2001; Boroujerdi et al., 2012). Analysis of hypoxia using GLUT-1 staining in control unirradiated tumours, and tumours regrown post irradiation revealed a significant increase in hypoxia levels in irradiated regrown tumours (Figure 4.20). GLUT-1 expression is regulated by HIF-1 $\alpha$ , which is elevated in hypoxic conditions (Hayashi et al., 2004; Y. Liu et al., 2009) and GLUT-1 has been shown to colocalise with HIF-1 $\alpha$  and mark hypoxic regions in several cancers (Hoskin et al., 2003; Boström et al., 2016). Interestingly, elevated GLUT-1 expression is correlated with shorter GBM patient survival (Flynn et al., 2008).

Low tumour oxygenation has been correlated with poor prognosis in patients, and in cervical cancers, it has been observed that recurring tumours often exhibit higher hypoxia levels compared to primary tumours (Vaupel et al., 2001). Recent published analysis of GBM patient samples treated with standard mode of care by Stadlbauer et al., show that elevated hypoxia may provide as an early sign for tumour recurrence. Those researchers showed that hypoxia continued to intensify post primary tumour treatment and peaked 90 days before recurrence (Stadlbauer et al., 2021). Consistently, analysis of patient samples in our laboratory revealed increased hypoxia in GBM recurrences compared to primary tumours, alongside morphological changes (Egnuni, PhD thesis).

Studies show that hypoxia has critical implications on tumour progression as it promotes tumour aggressiveness. The hypoxic niche in the tumour reprograms resident macrophages into a pro-tumorigenic and immunosuppressive phenotype (Jain, 2014). A hypoxic environment can increase cancer invasion through increased production of pro-migratory proteins such as SDF-1 $\alpha$  and HGF (Semenza, 1999; Finger and Giaccia, 2010). Hypoxia has been implicated in radio-resistance of GBM tumours through maintenance of GSC stemness (Reviewed in Chédeville and Madureira, 2021). Altogether, published studies provide an explanation of why tumours with elevated hypoxia are highly

aggressive, and why hypoxia is associated with poor patient prognosis (Wilson and Hay, 2011). Another hypoxia marker that could be incorporated in our studies is carbonic anhydrase IX (CAIX) as previous studies show that GLUT-1 co-localises with CAIX IX (Hoskin et al., 2003). Additionally, in the future it would be valuable to investigate the migratory ability of CT2A cells under hypoxic conditions using migration assays and identify the drivers of invasion in GBM recurrences.

Altogether, the data obtained in this study together with published data suggest that the observed increase in lumen size and vascularisation in regrown tumours post irradiation may be mediated by the increase in hypoxia levels in the regrown tumours driving higher VEGF levels, and irradiated CT2A cancer cells secreting more VEGF.

## **6.6 Radiotherapy promotes blood vessel association with $\alpha$ -SMA positive cells**

The increase in tight association of blood vessels with  $\alpha$ -SMA positive pericytes in regrown GBM experimental tumours post irradiation uncovered in this study has not been shown previously. This is consistent with the finding in GBM patient samples whereby the GBM patient recurrences showed increased blood vessel association with nestin/ $\alpha$ -SMA positive cells (Egnuni, PhD thesis). The association of pericytes with blood vessels has profound effects on blood vessel stability and functionality (Bergers and Song, 2005). On the other hand, it has been reported that vessel lumen enlargement may result from loss of pericytes (Abramsson et al., 2003). Similar observations of increased pericyte coverage of blood vessels after fractionated radiotherapy, have been reported in mammary carcinoma (Bouchet et al., 2015), colon cancer (Choi et al., 2018), non-small cell lung cancer (Tong et al., 2020) and prostate cancer (Clément-Colmou et al., 2020). However, in contrast to pericyte coverage of blood vessels during development conferring blood vessel stability and maturation, the presence of pericytes in some tumour types has been associated with intravasation of cancer cells into the bloodstream, and increased infiltration of inflammatory cells (Cooke et al., 2012; Park et al., 2016). Hence, the increase in F4/80 positive cells in

regrown tumours post irradiation observed in this study may be associated with the increase in pericyte coverage. Further, studies also show that pericytes can greatly influence GBM patient outcome. Zhou et al., showed that there is an inverse correlation between pericyte coverage and prognosis of GBM patients treated with chemotherapy (Zhou et al., 2017). In the same study, the authors demonstrated that targeting GSC-derived pericytes disrupts the blood-tumour barrier and improves the efficacy chemotherapy and subsequently lengthens survival in mouse models (Zhou et al., 2017). In a recent study Zhang et al., showed that increased pericyte coverage correlates with accelerated tumour recurrence and poor patient prognosis. In addition, the authors observed that GBM pericytes enhance DNA damage repair of tumour cells residing in the GBM perivascular niche, which drive resistance to temozolomide chemotherapy (Zhang et al., 2021).

Early studies show that vascular pericytes are derived from the bone marrow. Using a subcutaneous GL261 murine glioma model, Aghi et al., reported that SDF-1 secretion from tumour cells results in recruitment of bone marrow-derived cells (BMDCs) which differentiate into ECs and pericytes (Aghi et al., 2006). More recent studies demonstrated that blood vessel-associated pericytes in GBMs can arise from GSCs (Cheng et al., 2013). Cheng et al., postulated that elevated SDF-1 signalling may enhance recruitment of GSCs towards ECs, and increase the association of GSC-derived pericytes with tumour blood vessels which results in enhanced protection and resistance to anti-angiogenic therapy (Cheng et al., 2013). Importantly, Cheng et al., showed that selective elimination of GSC-derived pericytes in mice bearing GBM tumours results in the inhibition of tumour growth (Cheng et al., 2013). In those studies, GSCs were transduced to express herpes simplex virus thymidine kinase (HSV-TK) under the control of the desmin promoter, which drives expression in pericytes. HSV-TK specifically metabolises the prodrug ganciclovir (GCV) into a toxic agent. Thus, treatment with GCV eliminated GSCs that differentiated to pericytes in their *in vivo* models and reduced tumour growth (Cheng et al., 2013). GSCs' ability to differentiate into vascular pericytes demonstrates that GSCs can alter the tumour microenvironment to support tumour growth through improving the maturation and stability of the vasculature, and mediate resistance to anti-angiogenic

therapies. Other studies support the notion that SDF-1 and recruitment of pericytes may contribute to resistance to anti-VEGF treatments (Batchelor et al., 2007; Deng et al., 2017). Deng et al., demonstrated that blockage of SDF-1 $\alpha$  by means of administration of Olaptosed pegol (OLA-PEG) could potentiate the anti-tumour efficacy of anti-VEGF treatments (Deng et al., 2017).

Overall, the published literature on the role vascular pericytes in tumour development and progression shows that the role of pericytes is tumour type specific. In some cancers such as breast (Cooke et al., 2012) pericyte coverage suppresses hypoxia and results better patient outcome. In lung cancers, pericyte depletion at early stages of tumour progression enhanced hypoxia but decreased tumour growth (Keskin et al., 2015). In GBM high pericyte coverage is associated with poor therapeutic efficacy to TMZ, may promote resistance to anti-angiogenic therapy and is correlated with poor patient survival (Zhou et al., 2017; Zhang et al., 2021).

In future studies, exploring whether the vascular pericytes in the regrown tumours are of glioma stem cell lineage (Cheng et al., 2013) or bone-marrow derived (De Palma et al., 2005; Aghi et al., 2006) by utilising the  $\alpha$ -SMA-GFP or NG2-GFP transgenic mice would be beneficial to shed light into their origin in recurrences. In addition to their role in vessel integrity, emerging literature has demonstrated the role of vascular pericytes in immune regulation. A study by Valdor et al., has provided evidence of GBM pericytes expressing anti-inflammatory cytokines including IL-10 and TGF- $\beta$  (Valdor et al., 2017). In addition, they showed that glioma pericytes express MHC molecules and could acquire immunosuppressing properties that hinder T cell activation thus promoting tumour growth (Valdor et al., 2017). Consequently, it would be beneficial to find out whether pericyte increase contributes to immune suppression in GBM tumour recurrences.

## **6.7 Blood vessel enlargement but not the increase in $\alpha$ -SMA association is reversed by *Dock4* genetic deletion**

Dedicator of cytokinesis (DOCK) 4 is a GEF for the small GTPase Rac1, which operates downstream of VEGF signalling in ECs (Abraham, Scarcia, Bagshaw, McMahon, et al., 2015). Consistent with the hypothesised role of VEGF in blood vessel enlargement in regrown tumours post irradiation, heterozygous deletion of *Dock4*, a GEF operating downstream of VEGF signalling reversed blood vessel enlargement observed in CT2A regrown tumours post-irradiation (Chapter 5, Figure 5.3).

Normalisation of the vasculature in tumours through regulation of angiogenic factors may result in improved sensitisation of tumour blood vessels to treatments (Jain, 2001; Jain, 2003). VEGF is responsible for vascular development and regulating functions of the vasculature such as permeability during normal and pathological conditions. During development, absence of a single *vegf* allele has been shown to result in improper formation of vascular network, and mice die early in embryogenesis (Carmeliet et al., 1996; Ferrara et al., 1996). Conversely, excess VEGF results in embryonic lethality (Miquerol et al., 2000). These studies show the importance of a balanced level of VEGF in maintaining homeostasis and in development. VEGF signals via different signalling pathways that control angiogenesis (Simons et al., 2016). Furthermore, a study by Lee et al., demonstrated that the effects of VEGF extend beyond its role as a proangiogenic factor as it acts as a survival factors for ECs. Using a transgenic mice model lacking VEGF specifically in the vascular endothelial cells *in vivo* (VEGF<sup>ECKO</sup>), Lee et al., showed that genetic deletion of *vegf* resulted in a progressive endothelial degeneration and apoptosis (Lee et al., 2007). Histologically, VEGF<sup>ECKO</sup> mice had extensive organ failure associated with systemic vascular pathologies and 55% of the mutant mice resulted in sudden death at 25 weeks of age (Lee et al., 2007). However, DOCK4 is not necessary for EC viability (Abraham, Scarcia, Bagshaw, McMahon, et al., 2015) but operates downstream of VEGF signalling to activate Rac1; it mediates the effects of VEGF in regulating filopodia formation *in vitro*; and it controls blood vessel lumen size during brain development and in breast cancer brain tumour metastasis *in vivo* (Abraham, Scarcia, Bagshaw, McMahon, et al., 2015). Hence for these reasons, inhibiting

the downstream pathway of VEGF *via* DOCK4, which is involved in blood vessel morphological modulation, without interfering with EC viability, is a better strategy to interfere with VEGF-driven effects of on lumen size, as compared to inhibiting VEGF. Hence, I investigated whether the absence of DOCK4 could reverse the radiation-induced phenotype observed in the regrown tumours, thus normalising the aberrant enlarged blood vessels. The embryonic lethality of the global homozygous *Dock4* knockout model means that this study had to employ the use of heterozygous *Dock4* (*Dock4*<sup>het</sup>) knockout mice; although recently a viable homozygous *Dock4* global knockout model was generated from a conditional *Dock4* fl-neo/+ line intercrossed with the E11a-Cre germline deleter line (Guo et al., 2021).

The work by Abraham et al., showed that the EO771 (model of breast cancer brain metastases) grown intracranially in the *Dock4*<sup>het</sup> mice, developed vessels with smaller mean diameter compared to tumours grown in wild type mice (Abraham, Scarcia, Bagshaw, McMahon, et al., 2015). Interestingly, a different trend was seen when the CT2A murine glioma cell line was intracranially implanted in the *Dock4*<sup>het</sup> mice. Under control conditions, no difference in vessel length, lumen size, percentage of blood vessels with lumens and area covered by blood vessels could be observed between WT and *Dock4*<sup>het</sup> mice. This could be due to blood vessel mean diameter being smaller in CT2A tumours (approximately 16  $\mu$ m) compared to EO771 tumours which had a considerable proportion of BVs over 35  $\mu$ m (Abraham, Scarcia, Bagshaw, McMahon, et al., 2015), and DOCK4 specifically regulating blood vessel enlargement. Consistently, the radiation-induced augmentation of lumen size and vessel length were reversed in CT2A tumours grown in *Dock4*<sup>het</sup> mice.

When assessing the effect of *Dock4* knockout on  $\alpha$ -SMA pericyte association, the increase in pericyte coverage in response to irradiation was not reversed by heterozygous *Dock4* deletion. This appeared in agreement with the study by Abraham et al., where authors did not find any differences in vessel pericyte coverage (identified by NG2 staining) between the WT and *Dock4*<sup>het</sup> embryos during development (Abraham, Scarcia, Bagshaw, McMahon, et al., 2015). However, in the CT2A tumours in the absence of irradiation, there was a

significant increase in  $\alpha$ -SMA positive cells in tumours grown in *Dock4*het mice compared to WT mice. Thus, although *Dock4* may not play a role in pericyte regulation during normal development, this study suggests a possible role of *Dock4* suppressing blood vessel pericyte association in pathological vessel development in CT2A tumours.

## **6.8 Effects of radiotherapy on blood vessel permeability**

High pericyte coverage is associated with low vascular permeability (Zhou et al., 2017). With the observed increase in pericyte coverage in the regrown tumours, I tested the hypothesis that improved integrity of the tumour vasculature by increased pericyte coverage would reduce blood vessel permeability. The permeability experiments were carried out using bovine serum albumin (BSA) conjugated to AlexaFluor-555. Albumin is the main protein in blood plasma with key role in maintaining osmotic pressure, supply nourishment and nutrients to tissues, and act as transporter for hormones, vitamins, and other essential substances and drugs throughout the body (M.Cameron et al., 2020). In normal physiological conditions albumin does not readily pass through the blood brain barrier (Wanat, 2020), while albumin hyperpermeability is correlated with tissue injury, or pathological vessel development in tumours (Park et al., 2012).

Increase in vascular permeability short-term post-irradiation has been seen shown both in tumour and normal tissues (Reviewed in Park et al., 2012). Among others, Song et al. reported significant increase in extravasation of plasma protein 24 hours post-irradiation, subsequently followed by a marked decrease with time for up to 18 days in Walker 256 strain of rat mammary carcinoma (C. Song et al., 2009). Walker carcinoma 256 treated with radiotherapy at 20 Gy given in a single fraction, 4 daily fractions of 5Gy, or 8 daily fractions of 2.5 Gy resulted in the same outcome of short-term increase in permeability followed by a decrease (C. Song et al., 2009). However, those changes in blood vessel permeability refer to the response of the vasculature in primary tumours. To our knowledge, there are no studies investigating changes in permeability in regrown tumours post irradiation.

When quantification of tracer positive areas around the blood vessel was conducted in control and regrown tumours post irradiation, I observed a decrease in blood vessel permeability consistent with the increase in hypoxia levels in the regrown tumours treated with radiation therapy, compared to control non-irradiated tumours. When blood vessels were further classified based on their morphology, unexpectedly blood vessel pericyte association did not play a role in the reduction in permeability. When classified based on size, while in control tumours smaller blood vessels showed similar extravasation to larger blood vessels, in the irradiated tumours enlarged blood vessels showed higher permeability compared to smaller diameter vessels; supporting the notion that blood vessel enlargement is an adaptation response to increased hypoxia to support blood flow, oxygenation and hence tumour growth.

In developmental angiogenesis, Armulik et al., has shown pericyte is essential in regulating blood vessel permeability (Armulik et al., 2010). By employing a pericyte-deficient mutant mouse model (*Pdgfr<sup>ret/ret</sup>*), they demonstrated that lack of pericytes resulted in breakdown of blood brain barrier and extravasation of plasma proteins (Armulik et al., 2010). Previous studies have shown that pericytes on tumour vessels are distinctively different to that of normal vessels. In RIP-Tag2 mice, Morikawa et al, has shown increased  $\alpha$ -SMA expression in pericytes during tumour progression, while pericytes on normal capillaries typically express desmin and not  $\alpha$ -SMA, (Morikawa et al., 2002). Additionally, pericytes on tumour vessels are abnormal in shape and show abnormal association with endothelial cells (Morikawa et al., 2002). Defective pericyte-endothelial cell interaction results in formation of a disorganised tumour vasculature (Ferland-McCollough et al., 2017). However, the efficiency and functionality of pericytes in tumours as a regulator of the blood brain barrier remains unclear. Since in this study the increase in blood vessel pericyte association did not play a role in the reduction in permeability, this suggests that GBM tumour pericytes do not function effectively in the regulation of the blood brain barrier and blood vessel permeability in GBM.

In future studies it would be critical to elucidate the mechanism of reduced blood vessel permeability in regrown tumours post irradiation. With regards to primary

tumours implanted intracranially, it has been long known that when comparing intracranially implanted tumours with subcutaneously implanted tumours there is a reduction of tumour blood vessels with open endothelial gaps and fenestrated endothelium in the intracranial tumours regardless of the tumour type (Roberts et al., 1998). Out of all the tumours implanted intracranially, only GBM tumours had vessels with open gaps suggesting that GBM specific factors alter the blood brain barrier (Roberts et al., 1998). Consistently, U87 GBM tumours grown intracranially showed 2-fold higher permeability to BSA compared to murine mammary carcinoma grown intracranially (Hobbs et al., 1998). This is aligned with the clinical characteristics of GBM neo-vasculature being highly permeable compared to other tumours. Overall, GBM tumours express elevated levels of angiogenic growth factors such as VEGF which can drive both neovascularisation and blood vessel enlargement of mature blood vessels (Dvorak, 2015). Further, GBM tumours may produce additional, yet unidentified factors that allow them to modify the tight blood vessels in the brain (Risau, 1991; Kubitza et al., 1999), which could be downregulated in regrown tumours post irradiation, leading to the observed reduction in blood vessel permeability.

In future studies it would be essential to identify the molecular factors responsible for the regulation of GBM vascular permeability that may be altered post irradiation. In a study of melanoma tumours, Chen et al., showed that Akt1 – a gene which plays critical roles in many processes including cell survival, metabolism, and angiogenesis – is involved in the regulation of pathological angiogenesis and permeability (Chen et al., 2005). By employing an Akt1 knockout mice (*Akt<sup>-/-</sup>*) they demonstrated that the neovasculature of *Akt* deficient mice is leaky, and immature with less  $\alpha$ -SMA positive cells association (Chen et al., 2005). Additionally, they showed that there was enhanced pathological angiogenesis, characterised by higher vascular density and vascular area (Chen et al., 2005). In a separate *in vitro* study, Li et al., have shown that irradiation induces Akt phosphorylation in a subset of human GBM cell lines, and that it plays a critical role in the sensitivity of these cells to radiotherapy (H.F. Li et al., 2009). Thus, it may be possible that radiation-induced upregulation of Akt may contribute to reduced permeability in the regrown tumours. However, initially, the role of Akt in GBM tumour pathological angiogenesis would need to be evaluated.

In future studies investigating vascular permeability in regrown GBM tumours, it would be beneficial to also perform experiments which investigate whether irradiation affects blood vessel perfusion of regrown tumours by intravascular injection of Isolectin B4. The tracer circulating time of 3 hours employed in this study resulted in perfusion of most blood vessels, while allowing differences between control and recurrent tumours to be identified. Tight junction proteins play a key role in maintaining blood vessel leakiness and analysis of GBM patient tumours have shown downregulation of claudin-1, -3 and -5 (Wolburg et al., 2009; Attwell et al., 2010). Thus, investigating BBB vascular tight junctions by means of staining for zone occludens 1 (ZO-1), Occludin, claudin proteins, combined with visualisation of the basement membrane through transmission electron microscopy (Armulik et al., 2010; Zhou et al., 2017), will aid in identifying the morphological and structural changes seen in the regrown tumours that may impact on permeability. Staining for the plasmalemmal vesicle associated proteins (PLVAP) which have also been used in studies as marker for vascular fenestration and is associated with transcytosis and blood brain barrier breakdown (Xie et al., 2021), could potentially distinguish between angiogenic and co-opted blood vessels in future studies aimed to elucidate the mechanism of reduced blood vessel permeability in the regrown tumours.

The finding that regrown GBM tumours show reduced vessel permeability and increased hypoxia has important implications in the therapeutic options of recurrent tumours. As increased tumour vessel leakiness have been exploited to leverage drug delivery, not only it may provide a disadvantage for the delivery of chemotherapy agents but may also contribute to the reduced efficacy or radiotherapy in recurrent tumours (Gerstner et al., 2020). Reduction of hypoxic regions, which homes slow-proliferating, quiescent GSCs, would improve the efficacy of radiotherapy which eradicates rapidly proliferating cells more readily (Wilson and Hay, 2011; Muz et al., 2015). Furthermore, recent research on selective BBB modulation to improve drug delivery is gaining traction (Reviewed in Luo and Shusta, 2020). In the review, Luo and Shusta et al., iterates that the differential molecular expression profiles of normal brain blood vessels compared to blood vessels in tumours could be used for the selective modulation of the BBB (Luo and Shusta, 2020).

## **6.9 Other changes observed in regrown post radiotherapy CT2A tumours**

Co-option, as described previously, is one of the mechanisms of vascularisation that is frequently overlooked and has plays a considerable influence on disease progression and response to treatments. As the mode of vessel formation affects their structural components, this also influences their radiosensitivity. In various tumours, it has also been demonstrated previously that ionizing radiation increases tumour cell migration and metastatic potential (Su et al., 2012; Shankar et al., 2014; Young and Bennewith, 2017; Li et al., 2020). Although there are no studies yet to demonstrate the correlation between increase in vessel co-option and radiation, it might be possible that radiation-induced migratory capabilities may result in increased vessel co-option. This is an undesirable outcome, as co-opted vessels promote tumour growth and are more resistant to antiangiogenic therapy (Voutouri et al., 2019). Therefore, it would also be interesting to delve into investigating the effects of radiation therapy on mechanisms and prevalence of vessel co-option in the CT2A model (Appendix 5)

In addition to the analysis of blood vessel morphology and functionality, this study was also extended by looking into F4/80 positive macrophages in the regrown tumours. Macrophages have been shown to secrete various pro-angiogenic growth factors including VEGF A, IL-6 and TGF- $\beta$  (Reviewed in Corliss et al., 2016) to name a few. Thus, with the increased vascularisation post radiotherapy, it was postulated that macrophages may contribute to the enlargement of blood vessels as reported previously (Mathivet et al., 2017).

Using quantification of IHC stained sections, I observed that there was a higher expression of F4/80 positive cells in the regrown tumours. This is similar to the observations recorded by Kioi et al. where they observed increased tumour associated macrophage (TAMs) infiltration (marked by F4/80) and CD11b<sup>+</sup> monocytes in the U251 GBM model (Kioi et al., 2010). Studies using other tumour models have also show that radiotherapy treatment can drive macrophage recruitment into the tumour site (Reviewed in Arnold et al., 2018). Increased

chemokine expression, CSF-1 has been shown to play a key role in radiation-induced macrophage recruitment in prostate cancer (Xu et al., 2013). Alternatively, the induction of hypoxia as a result of radiation-induced vessel damage may promote recruitment of macrophages. In a mouse xenograft model of astrocytoma (intracranially implanted ALTS1C1 cells), following a single radiotherapy dose of 8 Gy or 15 Gy, Wang et al., observed that HIF-1-induced expression of stromal-derived factor 1 (SDF-1) promoted the recruitment of CD68 positive TAMs (Wang et al., 2013). Tumour associated microglia and macrophages have been correlated with poor prognosis in patients with high-grade gliomas due to their pro-tumorigenic capabilities (Sørensen et al., 2018). Importantly, a study by Mathivet et al., using intracranially implanted CT2A or GL261 spheroids showed the abundance of F4/80-positive macrophages in close proximity to large calibre blood vessels in late-stage of the tumour growth. The authors showed that promoting macrophage recruitment by means of delivery of recombinant CSF1 drives early blood enlargement and abnormality, whereas macrophage depletion using anti-CSF1 monoclonal antibody treatment, results in restoration of blood vessel calibre and function (Mathivet et al., 2017).

Thus, aligned with the published literature, the CT2A syngeneic mouse glioma model following radiotherapy, showed higher areas of F4/80 positive cells which may contribute to the observed blood vessel enlargement through secretion of angiogenic factors including VEGF. However, in order for this result to be conclusive, in future studies flow cytometry techniques should be utilised to allow quantitative characterisation of TAMs in this experimental GBM model alongside with M1/M2 polarisation. M2 macrophages have been described to be immunosuppressive and favour angiogenesis and tissue repair, whereas M1 macrophages are pro-inflammatory and cytotoxic (Hagemann et al., 2009). Additionally, it would be interesting to further elucidate whether SDF-1 plays a role in radiation-induced recruitment of macrophages in CT2A tumours by staining and quantification for SDF-1 antibody; and whether inhibiting SDF-1 blocks macrophage recruitment in the recurrences.

## 6.10 Effects of endothelial *Dock4* deletion on tumour vessel development

The use of conditional *Dock4* deletion was employed in the studies to confirm that the effects of *Dock4* deletion were endothelial cell autonomous. CT2A cell line was intracranially implanted into the *Dock4* endothelial conditional knockout mice. Unexpectedly, in control conditions, *Dock4* endothelial deletion resulted in longer blood vessel length, larger lumen size and higher percentage of vessels with lumens. This implies that *Dock4* may play a role as a suppressor of vessel formation in the CT2A model. When DOCK4 was first discovered, it was described as a tumour suppressor (Yajnik et al., 2003). Thus, it might be possible that DOCK4 suppresses the growth of endothelial cell development. It is clear that further analysis is required to confirm the role of DOCK4 in suppression of pathological vessel development. Firstly, although induction of Cre activity with tamoxifen was demonstrated by means of Td expression, it would be important to confirm that the blood vessels do not express DOCK4. This was not possible due to time limitation and lab access restrictions during the Covid-19 pandemic. Secondly, assessment of EC proliferation through staining with Ki67 would be valuable to understand further the mechanism of suppression of vessel formation. It is plausible that under non-irradiation conditions blood vessel formation is driven by a variety of factors with DOCK4 acting as suppressor. Work by S. Mohajerani in the laboratory using *in vitro* co-culture angiogenesis assays shows that when angiogenesis is driven by FGF, DOCK4 knockdown stimulates tubule formation (unpublished observations), while in VEGF driven angiogenesis DOCK4 knockdown inhibits angiogenic sprouting (Abraham, Scarcia, Bagshaw, McMahon, et al., 2015). On the other hand, we cannot exclude the possibility that the stimulation of vessel development observed in the *Dock4* conditional homozygous knockout mice was due to a compensatory mechanism in the absence of both *Dock4* alleles in endothelial cells. Further experiments would be required to discover which pathways responsible for vessel formation are activated in the homozygous deletion. An experiment employing a *Dock4* conditional heterozygous mice (fl/+) would shed considerable light to these different possibilities.

In the future, in order to determine the molecular players responsible in the enhanced tumour angiogenesis in the *Dock4* homozygous conditional mice, it would be valuable to employ the angiogenic sponge assay. In this assay, synthetic sponges are injected with the specific angiogenic growth factor of interest. Growth factor impregnated sponges are then implanted into the mice, and sections of excised sponges are then immunostained and blood vessel growth analysed histologically (McCarty et al., 2002; Tavora et al., 2011; Lechertier et al., 2020). As this technique has not been used intracranially, an experiment using subcutaneous CT2A model grown in endothelial *Dock4* knockout mice may be performed, and subcutaneous sponge assay incorporated to dissect the *in vivo* role of *Dock4* in the activity of different angiogenic growth factors.

The effects of endothelial *Dock4* deletion could not be assessed under radiation conditions in neither of the two experiments performed. In the first experiment, lumen size in the two irradiated tumours growing in the endothelial *Dock4* conditional mice was equivalent to the two unirradiated controls, however in the absence of significant upregulation of lumen size in the single irradiated tumour growing in the WT mouse, it is not possible to draw any conclusions; more experiments are needed with tumours implanted in more mice to generate a cohort large enough for analysis. In the second experiment, mice presented neurological symptoms early on that were not due to tumour growth, as the tumours were small in size when excised. Importantly, SARRP had not worked as intended due to machine malfunction resulting in the lack of response in the irradiated tumours.

As early clinical symptoms were observed in both experiments that were not associated with tumour growth, it would be valuable to understand whether *Dock4* deletion itself contributed to the early presentation of clinical symptoms in the tumour bearing mice, and/ or whether tamoxifen injections for Cre activation may have had a contribution to early symptoms. Although considered safe for injection into mice in small doses, there are side effects that may arise from tamoxifen treatment. Post-mortem of a tamoxifen injected mouse that was found dead in the repeat *Dock4* conditional experiment, revealed intestinal bleeding and

inflammation reported previously in the literature in response to tamoxifen injection (Huh et al., 2010; Huh et al., 2012). In the future, it would be beneficial to repeat these experiments to elucidate the effect of *Dock4* endothelial specific deletion on vessel development of CT2A tumours in response to radiotherapy treatments. Those experiments should be performed after allowing more time between tamoxifen treatment, and tumour implantation and irradiation.

### **6.11 Concluding remarks**

Characterisation of orthotopically injected CT2A glioma tumours regrown post radiotherapy in mice showed augmentation of vascular abnormality seen in the control tumours. This includes increase in blood vessels with increased lumen size and length. The findings observed in the *in vivo* model are consistent with those of patient GBM recurrences. The BV enlargement in the regrown tumours treated with radiotherapy is driven by VEGF signalling. This was observed via an *in vivo* experiment targeting DOCK4, which acts downstream of VEGF. CT2A tumours intracranially implanted in *Dock4* heterozygous mice treated with radiotherapy, resulted in a reversal of the augmentation of vessel calibre and abnormality post-irradiation. However, heterozygous deletion of *Dock4* alone had no effect on tumour vessel development under control conditions. In the homozygous *Dock4* conditional endothelial knockout model, there was enhanced blood vessel development in control conditions. However, studies investigating the effect of homozygous *Dock4* deletion in response to radiotherapy must be carried out in the future, as that arm of the *in vivo* studies was not informative due to technical reasons.

Staining of GLUT-1 as a marker for hypoxia revealed that in the regrown tumours, there was an elevated level of hypoxia. It could be observed that while in the control tumours there is relatively low hypoxia levels around small blood vessels, in the radiotherapy treated tumours there is high hypoxia around small blood vessels similar in size with those of control tumours (Chapter 4, Figure 4.22). This is aligned with previous published literature in breast and cervical cancer, showing that recurring tumours often possess higher hypoxic regions compared to primary tumours, although the mechanisms are not fully understood (Vaupel

et al., 2001; Vaupel et al., 2002). Higher hypoxia drives VEGF expression, and subsequent proangiogenic signalling. In GBM tumours, it has been shown that HIF-1 $\alpha$  expression (concomitant with elevated hypoxia) is colocalised with VEGF expression (Zagzag et al., 2006). Furthermore, depletion of macrophage-derived VEGF expression in the tumour has been shown to contribute to restoration of enlarged blood vessel calibre in non-irradiated tumours grown to a large size, while stimulation of macrophage by means of recombinant CSF1 recruitment leads to vessel enlargement early in tumour growth (Mathivet et al., 2017). In this study, we observed an increase in F4/80 expression in regrown tumours treated with radiotherapy compared to unirradiated control, suggesting the possible contribution of macrophages in the regulation of lumen size in the regrown tumours.

Thus, the findings in this study suggest that the radiotherapy-induced effects seen in the regrown tumours including increased lumen size, is mediated by increased hypoxia, increased macrophage recruitment, and VEGF expression – which regulates blood vessel diameter (Nakatsu et al., 2003). In the non-irradiated tumours, small and large vessels are similarly permeable. However, post-irradiation, the larger vessels are more permeable, supporting the notion that vessel enlargement is an adaptation response to hypoxia (Deindl et al., 2001; Boroujerdi et al., 2012). Radiation-induced vascular damage has been shown previously to promote hypoxia (Reviewed in Barker et al., 2015). We propose that in the regrown tumours, there is an elevated number of blood vessels that have been irradiated, damaged, and then co-opted by surviving cancer cells. Those blood vessels were then modified and enlarged as an adaptation response to hypoxia.

Analysis of pericyte association with blood vessels showed that in regrown tumours post-irradiation, there was an increase in pericyte associated with blood vessels. In non-tumour bearing brain, hypoxia-induced increase in vessels with large calibre is correlated with increased numbers of  $\alpha$ -SMA positive blood vessels in C57BL/6 mice (Boroujerdi et al., 2012). Interestingly, although there was a decrease in overall extravasation in the regrown tumours compared to control, this was not dependent on blood vessel-pericyte association. This

suggests that although in developmental angiogenesis pericytes play a key role in maintenance of vessel integrity, pericytes in GBM as in other tumours are less functional.

Future work should focus on deeper analysis and mechanistic studies of the effects of radiation on the vasculature of the regrown tumours. An experiment that unequivocally determines whether the abnormal blood vessels observed in the regrown tumours are remaining, radioresistant vessels that survived radiotherapy which have been co-opted, or whether they are *de novo* vessels, or both would be crucial. Preliminary observation of irradiated brains in the absence of tumour growth supports the notion that irradiation promotes abnormality in the absence of tumour growth (Appendix 7). Understanding the key pathways of revascularisation in the regrown tumours would be beneficial in the context of therapy with the aim of vessel normalisation. The planned next stage of this study is to employ RNA sequencing to identify the key molecular components responsible for the revascularisation post-irradiation. Additionally, while previous research has demonstrated the benefits of targeting GSC-derived pericytes through depleting them (Cheng et al., 2013), it would be valuable to investigate further the origin and role of pericytes in the recurrences. Key question would be whether factors involved in the recruitment of pericytes (for example, angiopoietin-1) are upregulated in the regrown tumours and the mechanism of such potential upregulation. The depletion of pericytes associated with blood vessels, may aid in the reduction of mature radioresistant vessels, and improve the efficacy of radiotherapy.

With regards to the observed decrease in tracer extravasation, key question remains whether those are blood vessels were co-opted post-irradiation. Secondly, the elements that may be responsible for reduction in tracer extravasation such as changes in tight junctions or the basement membrane, or endothelial cell fenestrations will be explored. The use of single-cell RNA sequencing of endothelial cells in the control versus regrown tumours may be implemented (Teuwen et al., 2021). This may provide information on the possible molecular alterations associated with the regrown tumours which render their vasculature less functional.

## 6.12 Model

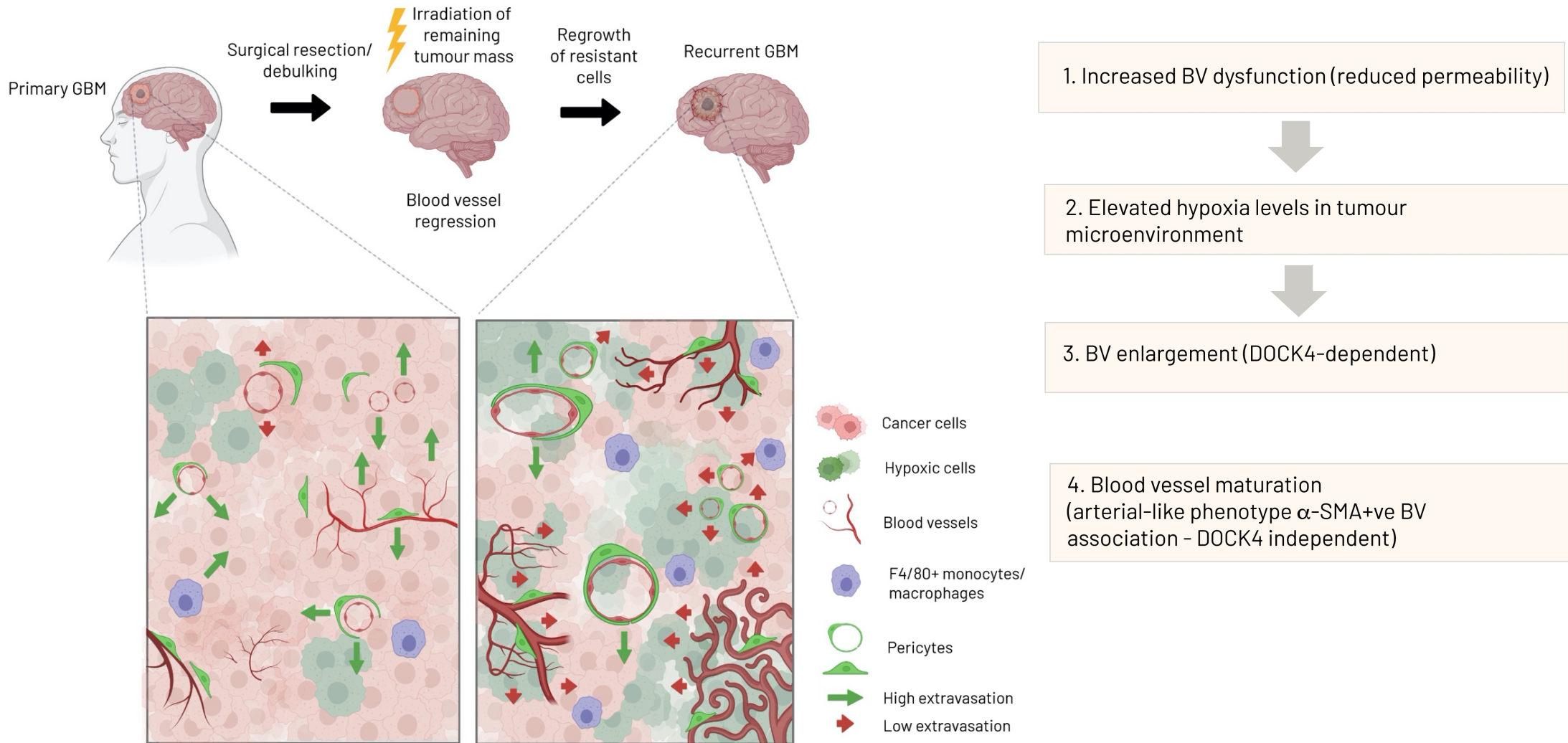


**Figure 6.1 Observed changes in tumour blood vessels of primary and recurrent GBM tumours.**

Illustration shows the proposed model of the changes observed in primary and recurrent GBM tumours post-radiotherapy treatment. The reduction of permeability which suggests increased BV dysfunction post-irradiation, results in elevated hypoxia levels in tumour microenvironment, and in turn results in BV enlargement, which is DOCK4-dependent as modelled in the *in vivo* experimental model. Furthermore, regrown tumours have increased abundance and increased tight association of blood vessels to  $\alpha$ -SMA positive pericytes. Created with BioRender.com.

# Appendices

## Appendix 1

Exp No.	Experiment	Mice strain	Performed by	Licence number	Summary
1.	Investigation on the effects of radiotherapy on vascularisation of CT2A tumours	WT and <i>Dock4</i> het mice	Tek Egnuni	P67C4EBE	Experiment employing WT and <i>Dock4</i> het mice intracranially implanted with CT2A cell line. Treatment group treated with 2 x 5Gy radiotherapy.
2.	Investigation on the effects of <i>Dock4</i> conditional deletion with and without radiotherapy on vascularisation of CT2A tumours	Endothelial <i>Dock4</i> conditional knockout mice	Anastasia, Gary Shaw, Tek Egnuni	PEA0105B1	Pilot experiment employing <i>Dock4</i> endothelial conditional knockout mice intracranially implanted with CT2A cell line. Treatment group treated with 2 x 5Gy radiotherapy.
3.	Investigation on effects of radiotherapy on blood vessel tracer extravasation	WT (C57BL/6)	Anastasia, Gary Shaw, Tek Egnuni	P67C4EBE	Pilot experiment employing WT C57BL6 mice intracranially implanted with CT2A cell line. Treatment group treated with 2 x 5Gy radiotherapy. Mice were intravenously

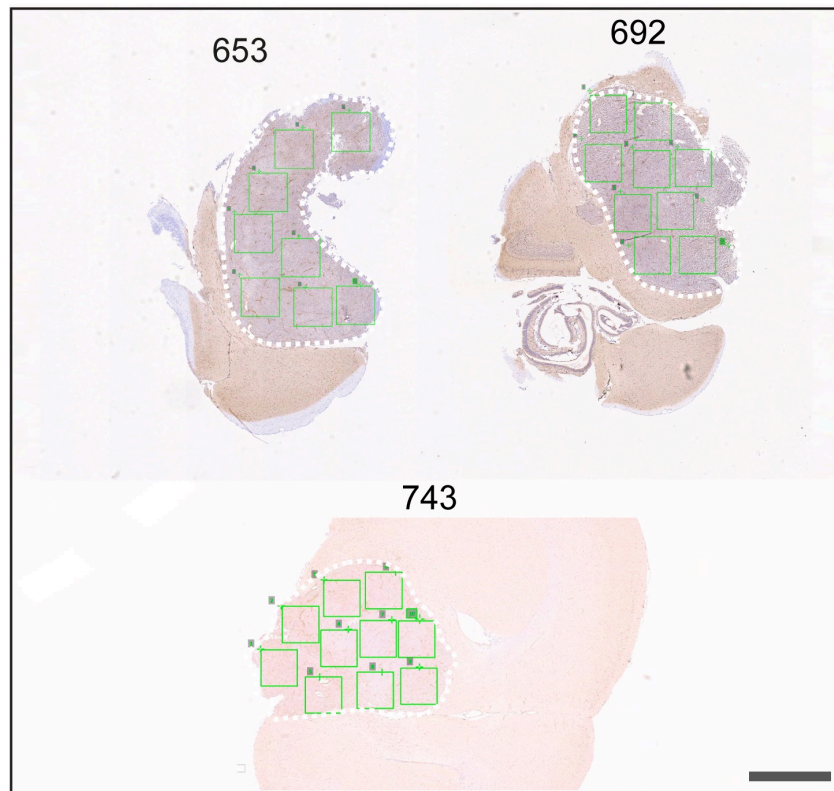
					injected with BSA-AlexaFluor555, Cadaverine-AlexaFluor555 or saline.
4.	Investigation on effects of radiotherapy on normal brain blood vessel tracer extravasation	WT (C57BL/6)	Anastasia Widyadari, Gary Shaw	P85C8BDBF	Experiment employing WT C75BL/6 mice (non-tumour bearing) injected with BSA-AlexaFluor555 or Cadaverine-AlexaFluor555.
5.	Investigation on effects of radiotherapy on blood vessel tracer extravasation (Repeat)	WT (C57BL/6)	Anastasia Widyadari, Gary Shaw, Tek Egnuni	P85C8BDBF	Repeat experiment employing WT C75BL6 mice intracranially implanted with CT2A cell line. Treatment group treated with 2 x 5Gy radiotherapy. Mice were intravenously injected with BSA-AlexaFluor555.
6.	Investigation on the effects of <i>Dock4</i> conditional deletion with and without radiotherapy on vascularisation of CT2A tumours (Repeat)	Endothelial <i>Dock4</i> conditional knockout mice	Anastasia, Gary Shaw	PEA0105B1	Repeat experiment employing 24 x <i>Dock4</i> endothelial conditional knockout mice intracranially implanted with CT2A cell line. Treatment group treated with 2 x 5Gy radiotherapy. SARRP machine malfunction at day 7 of radiotherapy

**Summary of *in vivo* experiments conducted and/or analysed within this study.**

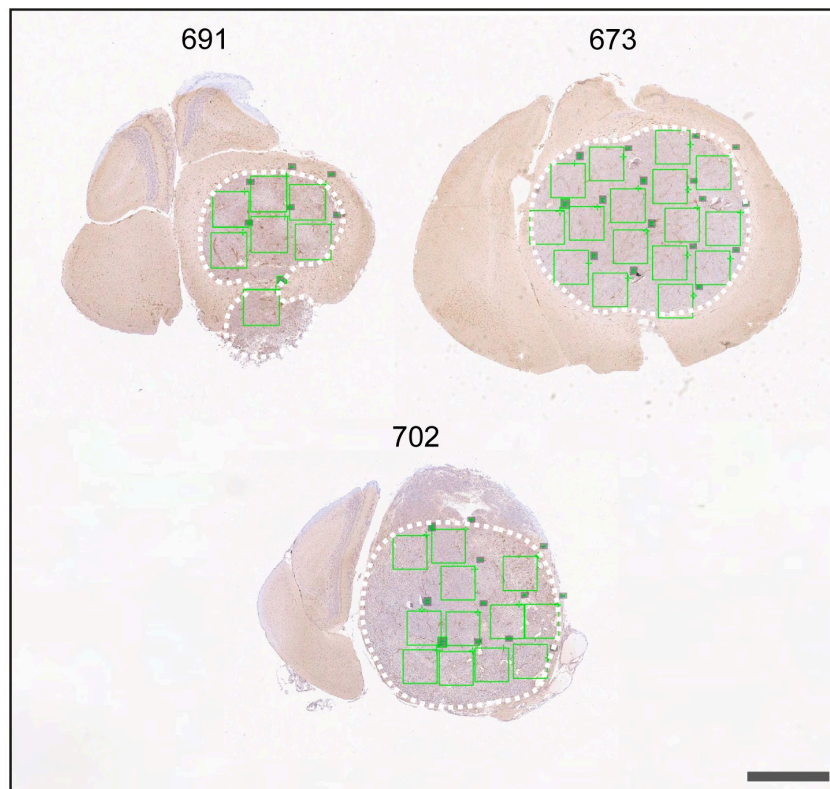
Table shows experiments conducted and/or analysed within this study, mice strain employed in the experiment, name of persons who conducted the experiments, licence, protocol, and summary of each experiment. A total of 6 *in vivo* experiments were analysed in this study, including Experiment 1 which was conducted prior to the start of this study.

Appendix 2

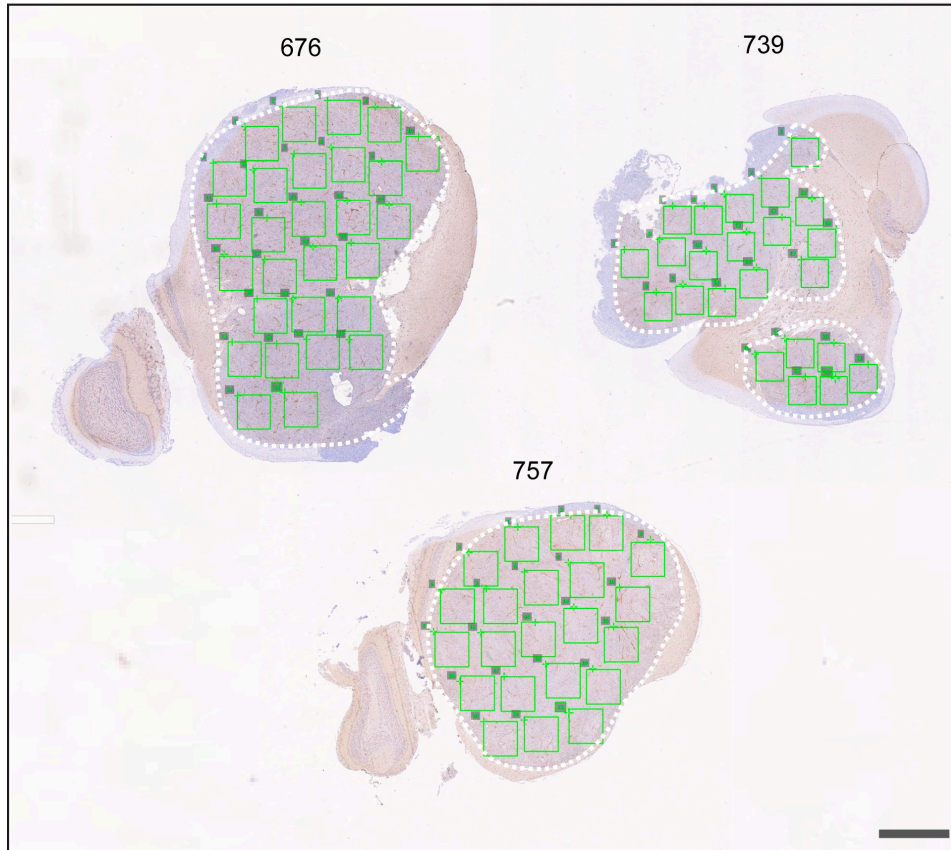
WT Control



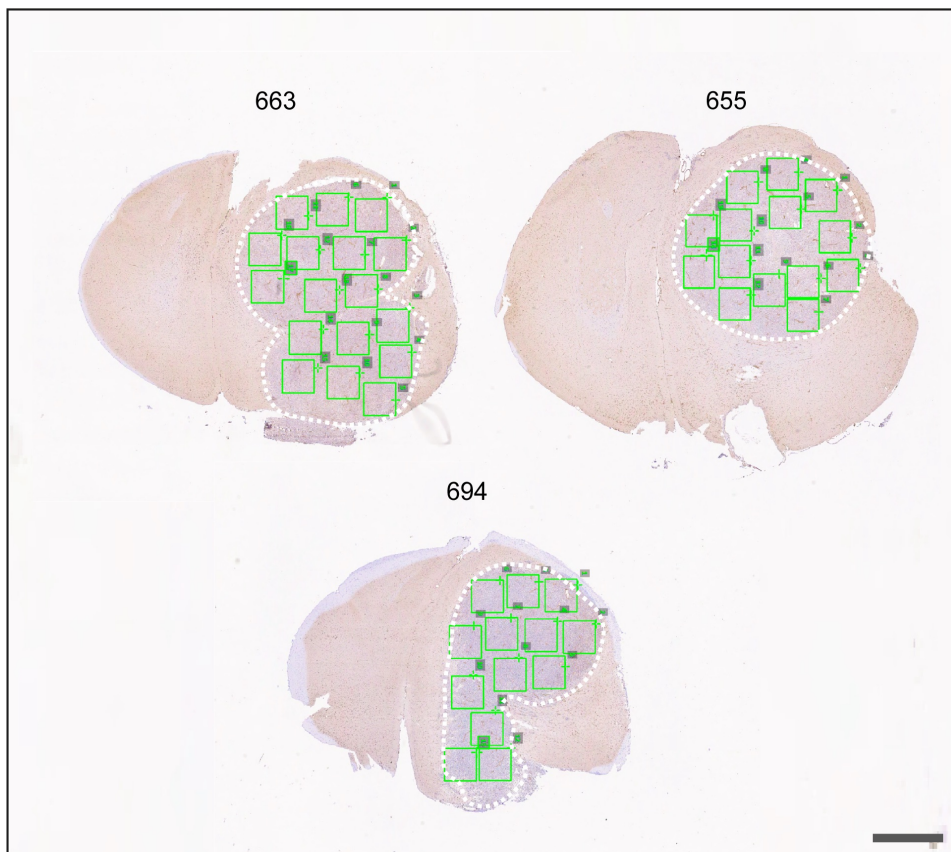
WT 2 x 5Gy (Regrowth)



*Dock4het* Control



*Dock4het* 2 x 5Gy (Regrowth)



**Scanned images of CT2A tumours in WT and *Dock4*het mice, control and regrown post radiotherapy used for quantification.**

Sections of mouse brains bearing CT2A tumour were paraffin embedded, sectioned at 5  $\mu\text{m}$  and stained with CD31 by immunohistochemistry and counterstained using haematoxylin. Stained sections were scanned using Aperio SlideScanner at 20x. Subsequently, images were captured using ImageScope software at 1x magnification. Images show size x size boxes from which images selected for were randomly chosen. Scale bar = 1 mm.

## Appendix 3

### Source code

```
# Program to generate a random number between 0 and 9 (numbers may  
change depending on number of images)  
# Importing the random module  
import random  
print(random.randint(0,9))
```

### Output

```
5
```

### **Python source code and output used in image randomisation for analysis of immunohistochemistry sections.**

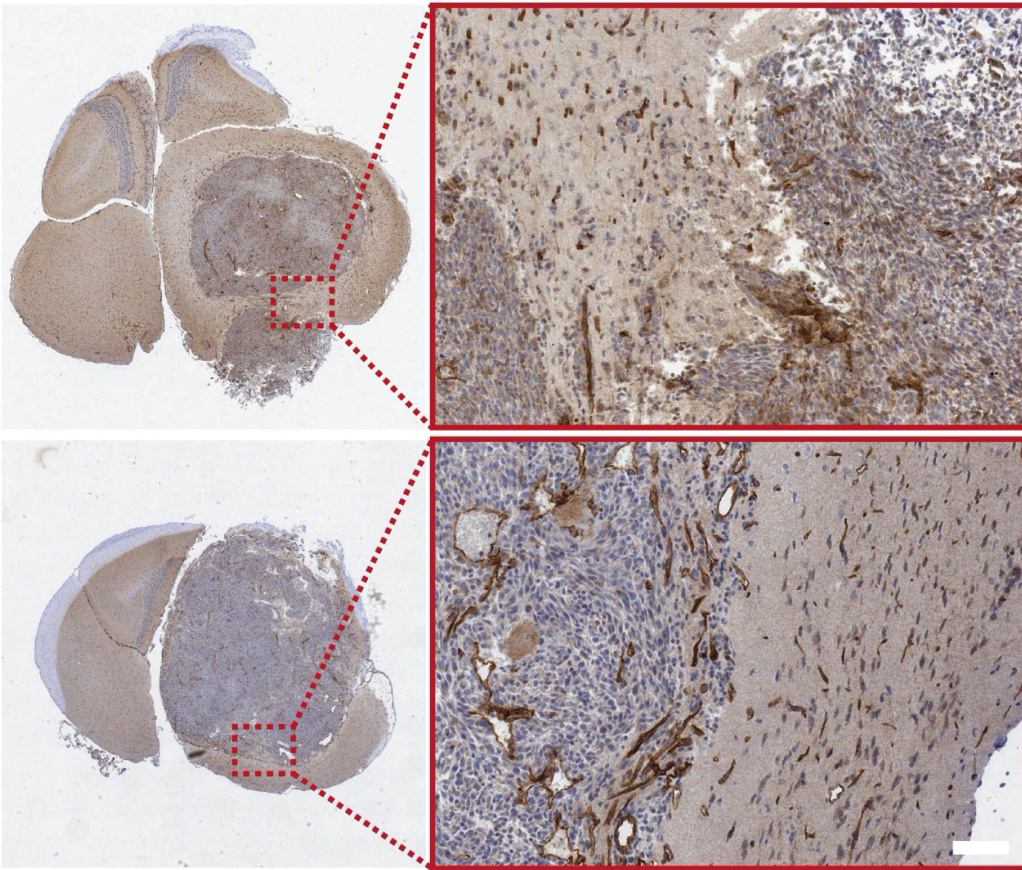
Images of stained tumour samples scanned or captured were chosen for use in the analysis by random via generation of a random number generator using a Python code run on Mac Terminal application.

Appendix 4

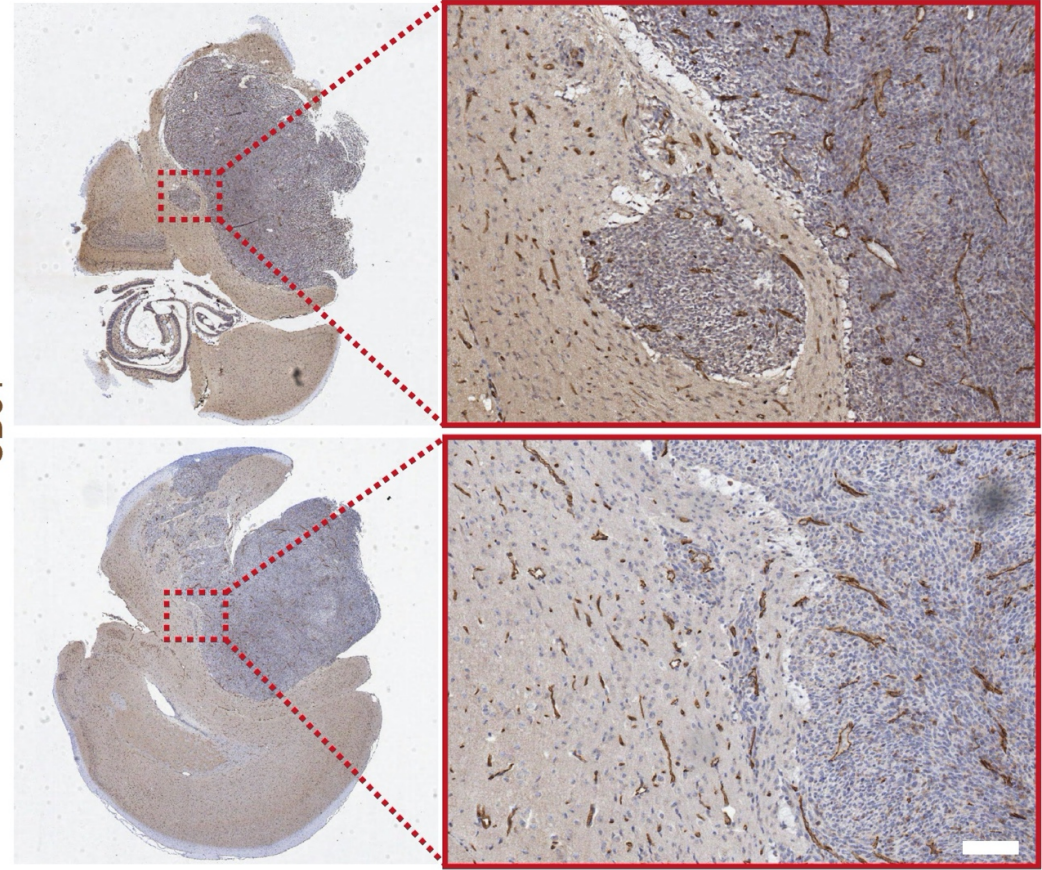
Control

Regrown (2 x 5Gy)

CD31



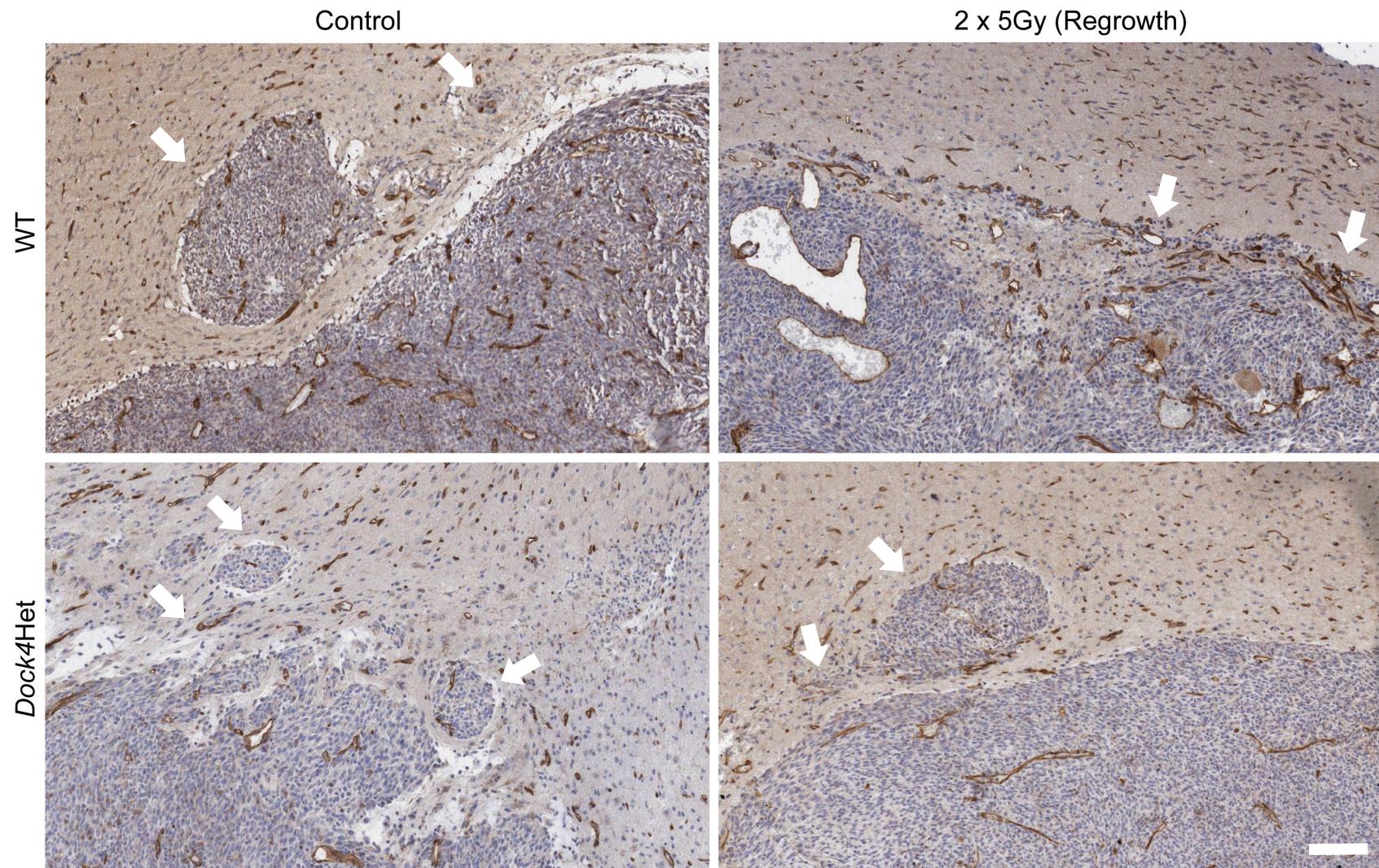
CD31



**Observed peritumoral invasion in control and regrown intracranially implanted CT2A tumours.**

Sections of mouse brains intracranially implanted with CT2A tumours were paraffin embedded, sectioned at 5  $\mu\text{m}$  and stained with CD31 by immunohistochemistry and haematoxylin for visualisation of nuclei. Stained sections were scanned using an Aperio SlideScanner at 20x and captured using ImageScope software. Images show the invasive edge of the peritumoral area of both control and radiotherapy treated regrown CT2A tumours. Scale bar = 100  $\mu\text{m}$ .

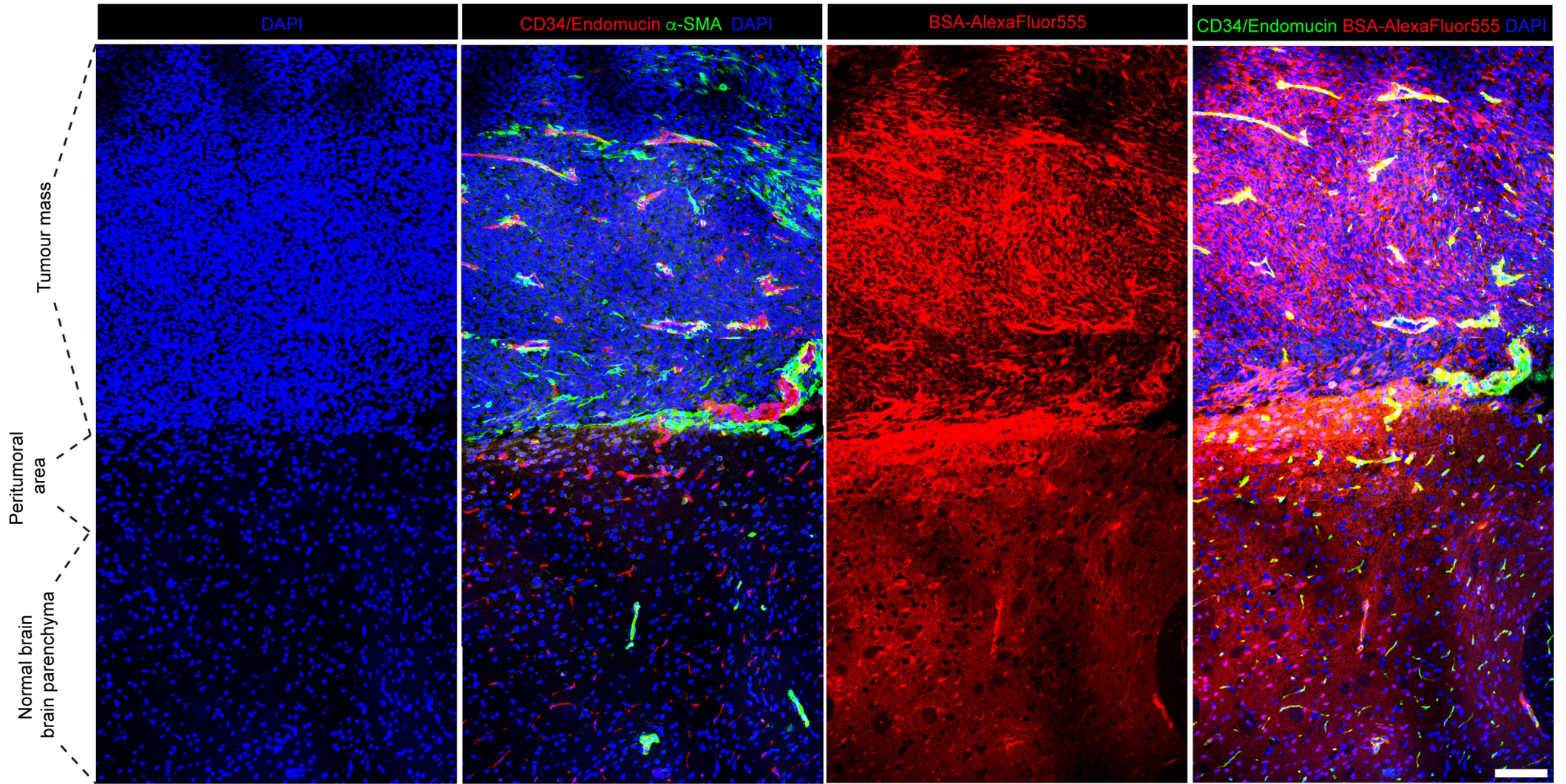
Appendix 5



**Visualisation of blood vessel co-option in CT2A tumours intracranially implanted in WT and *Dock4*Het mice.**

Sections of mouse brains bearing CT2A tumour were paraffin embedded, sectioned at 5  $\mu\text{m}$  and stained with CD31 and counterstained using haematoxylin for visualisation of nuclei by immunohistochemistry. Stained sections were scanned using an Aperio SlideScanner at 20x and captured using ImageScope software. Images show the different patterns of co-option observed in intracranially implanted CT2A tumours. White arrows point to co-opted blood vessels. Scale bar = 100  $\mu\text{m}$ .

# Appendix 6

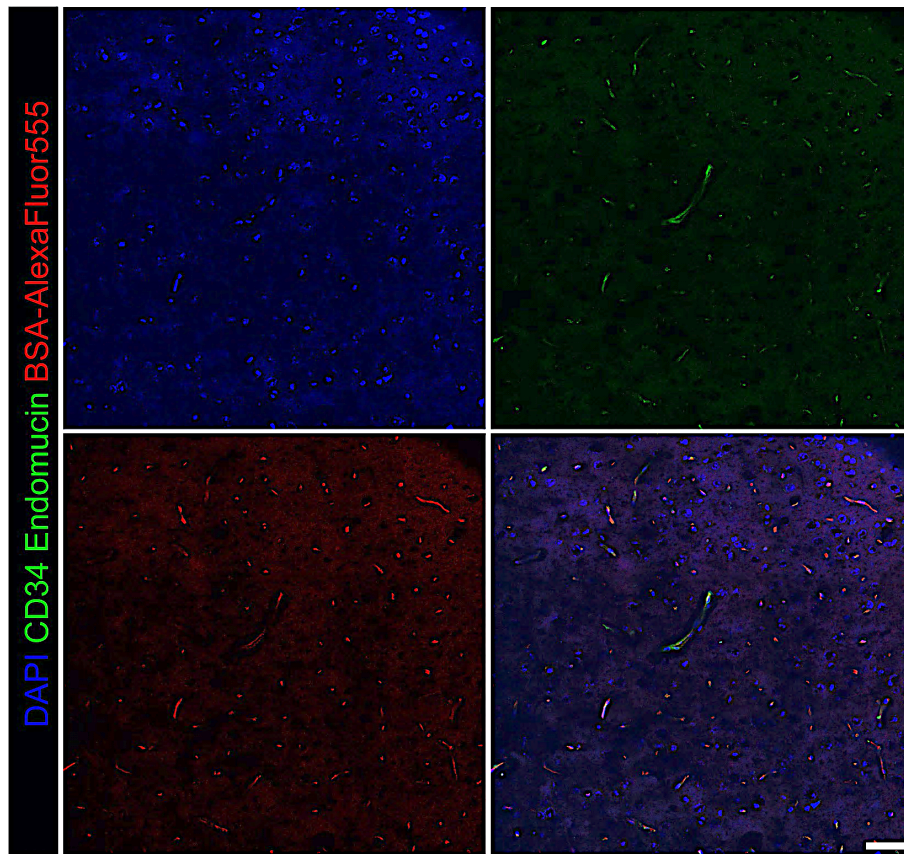


**Pattern of tracer extravasation from tumour mass to non-tumour bearing brain parenchyma in CT2A control non-irradiated tumour.**

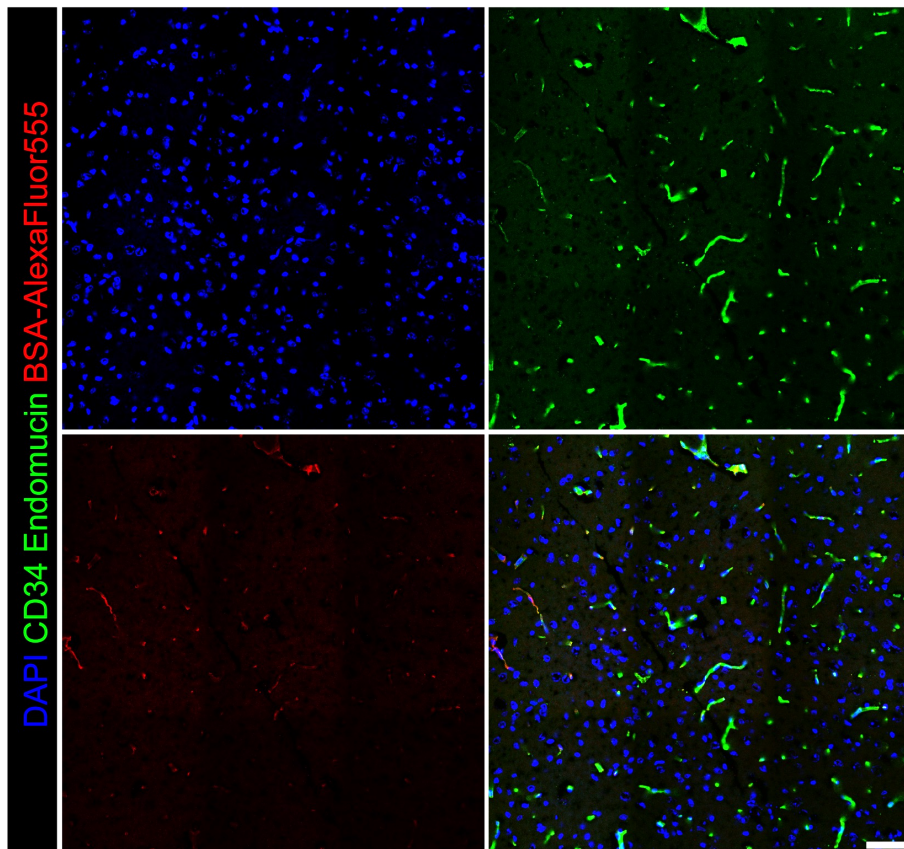
Sections of mouse brains bearing CT2A tumour injected with BSA-AlexaFluor555 were frozen embedded, sectioned at 10  $\mu\text{m}$  and stained with CD34/Endomucin,  $\alpha$ -SMA antibody and DAPI for visualising nuclei. Stained sections were captured using a Nikon A1R confocal microscope at 20x magnification starting from the from tumour mass to the normal brain parenchyma. Peritumoral area lies outside the tumour circumference, with blood vessels appearing morphologically different to the normal brain parenchyma. Note the increased extravasation in the peritumoural area followed by decrease in the normal brain where tracer marks the blood vessels. Scale bar = 100  $\mu\text{m}$ .

## Appendix 7

Control



2 x 5Gy (Regrowth)



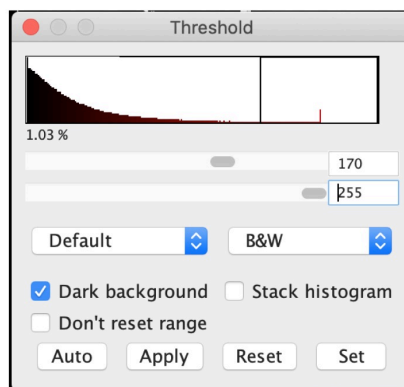
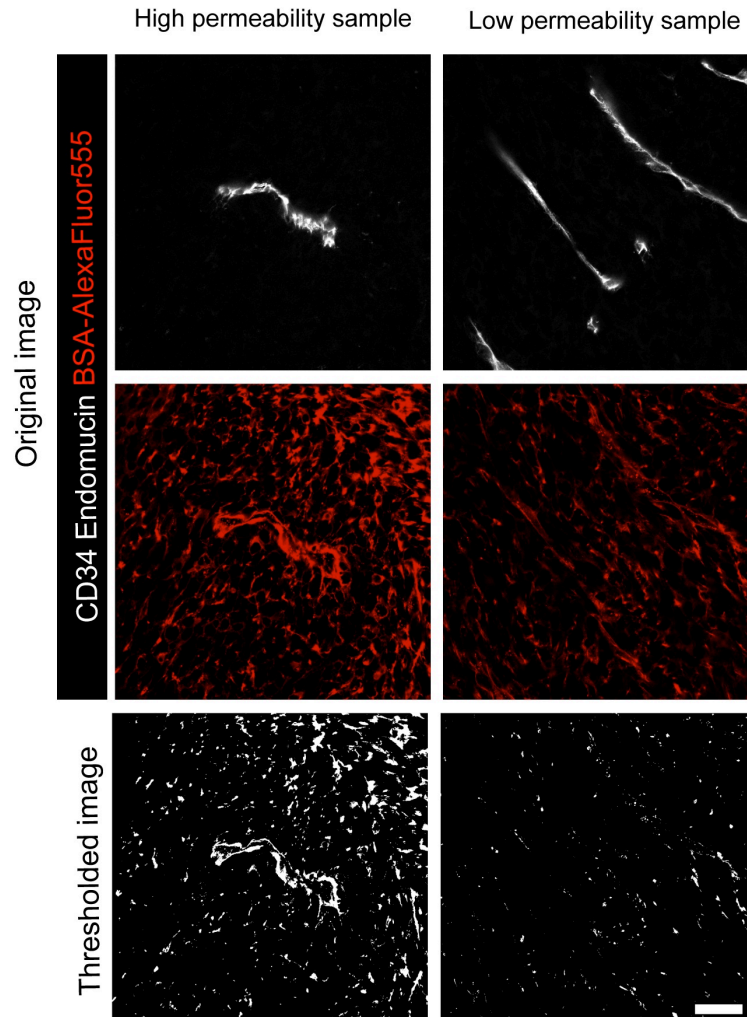
**Vascularisation and tracer extravasation of normal mouse brain 21 days after treatment with 2 x 5Gy radiotherapy.**

Sections of normal (non-tumour bearing) mouse brains injected with BSA-AlexaFluor555 (Appendix 2, Experiment 4) were frozen embedded, sectioned at 10  $\mu\text{m}$  and stained with CD34/Endomucin and DAPI for visualising nuclei. 9 stained sections were captured using a Nikon A1R confocal microscope at 20x magnification and stitched at a 3 x 3 configuration with 5% overlap. Scale bar = 200  $\mu\text{m}$ .

## Appendix 8

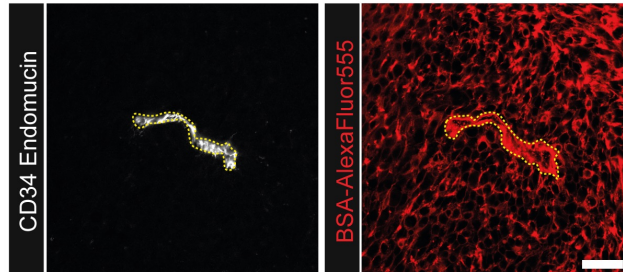
### A

#### 1. Determination of threshold

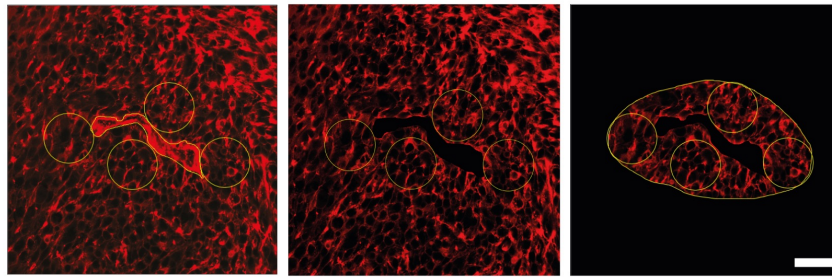


1. Use command *Image > Adjust > Threshold*
2. Manually set threshold using the slider
3. Click Set and Apply

## 2. Determination of ROI

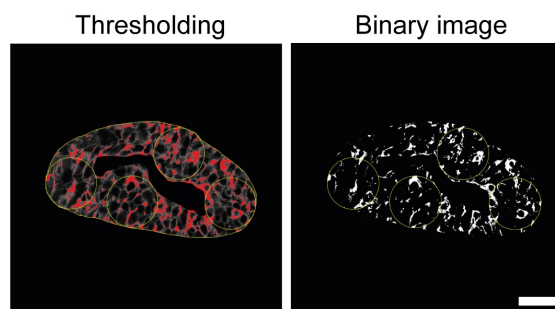


1. Outline the vessel on the tracer channel using the CD34 Endomucin staining as a guide using freehand line tool
2. ROI for tracer extravasation excludes CD34 Endomucin positive area and adjacent pixel positivity including entrapment of tracer in endothelial cell lining



1. Manual placing of 40  $\mu\text{m}$  diameter circles around blood vessel
2. Manual region selection of tracer entrapment
3. Exclusion of tracer entrapment using command *Edit > Clear*
4. Manual region selection of 40  $\mu\text{m}$  diameter around blood vessel
5. Exclusion of area outside ROI using command *Edit > Clear Outside*

## 3. Thresholding and measurement



1. Setting threshold as determined previously
2. Set only to thresholded area and convert to binary
3. Determine pixel positivity with the command *Analyse > Measure*
4. Raw IntDen is the total positive pixels around the blood vessel

## B

```
1 // Macro for making 40um sized circles
2
3 run("Specify...", "width=40 height=40 x=89.53 y=78.05 oval scaled");
4 makeOval(255, 731, 192, 192);
5
6
7
8
9
10
11
12
13
14
15
16
17
18
19
20
21
22
23
24
25
26
27
28
29
30
31
32
33
34
35
36
37
38
39
40
41
42
43
44
45
46
47
48
49
50
51
52
53
54
55
56
57
58
59
60
61
62
63
64
65
66
67
68
69
70
71
72
73
74
75
76
77
78
79
80
81
82
83
84
85
86
87
88
89
90
91
92
93
94
95
96
97
98
99
100
101
102
103
104
105
106
107
108
109
110
111
112
113
114
115
116
117
118
119
120
121
122
123
124
125
126
127
128
129
130
131
132
133
134
135
136
137
138
139
140
141
142
143
144
145
146
147
148
149
150
151
152
153
154
155
156
157
158
159
160
161
162
163
164
165
166
167
168
169
170
171
172
173
174
175
176
177
178
179
180
181
182
183
184
185
186
187
188
189
190
191
192
193
194
195
196
197
198
199
200
201
202
203
204
205
206
207
208
209
210
211
212
213
214
215
216
217
218
219
220
221
222
223
224
225
226
227
228
229
230
231
232
233
234
235
236
237
238
239
240
241
242
243
244
245
246
247
248
249
250
251
252
253
254
255
256
257
258
259
260
261
262
263
264
265
266
267
268
269
270
271
272
273
274
275
276
277
278
279
280
281
282
283
284
285
286
287
288
289
290
291
292
293
294
295
296
297
298
299
300
301
302
303
304
305
306
307
308
309
310
311
312
313
314
315
316
317
318
319
320
321
322
323
324
325
326
327
328
329
330
331
332
333
334
335
336
337
338
339
340
341
342
343
344
345
346
347
348
349
350
351
352
353
354
355
356
357
358
359
360
361
362
363
364
365
366
367
368
369
370
371
372
373
374
375
376
377
378
379
380
381
382
383
384
385
386
387
388
389
390
391
392
393
394
395
396
397
398
399
400
401
402
403
404
405
406
407
408
409
410
411
412
413
414
415
416
417
418
419
420
421
422
423
424
425
426
427
428
429
430
431
432
433
434
435
436
437
438
439
440
441
442
443
444
445
446
447
448
449
450
451
452
453
454
455
456
457
458
459
460
461
462
463
464
465
466
467
468
469
470
471
472
473
474
475
476
477
478
479
480
481
482
483
484
485
486
487
488
489
490
491
492
493
494
495
496
497
498
499
500
501
502
503
504
505
506
507
508
509
510
511
512
513
514
515
516
517
518
519
520
521
522
523
524
525
526
527
528
529
530
531
532
533
534
535
536
537
538
539
540
541
542
543
544
545
546
547
548
549
550
551
552
553
554
555
556
557
558
559
560
561
562
563
564
565
566
567
568
569
570
571
572
573
574
575
576
577
578
579
580
581
582
583
584
585
586
587
588
589
590
591
592
593
594
595
596
597
598
599
600
601
602
603
604
605
606
607
608
609
610
611
612
613
614
615
616
617
618
619
620
621
622
623
624
625
626
627
628
629
630
631
632
633
634
635
636
637
638
639
640
641
642
643
644
645
646
647
648
649
650
651
652
653
654
655
656
657
658
659
660
661
662
663
664
665
666
667
668
669
670
671
672
673
674
675
676
677
678
679
680
681
682
683
684
685
686
687
688
689
690
691
692
693
694
695
696
697
698
699
700
701
702
703
704
705
706
707
708
709
710
711
712
713
714
715
716
717
718
719
720
721
722
723
724
725
726
727
728
729
730
731
732
733
734
735
736
737
738
739
740
741
742
743
744
745
746
747
748
749
750
751
752
753
754
755
756
757
758
759
760
761
762
763
764
765
766
767
768
769
770
771
772
773
774
775
776
777
778
779
780
781
782
783
784
785
786
787
788
789
790
791
792
793
794
795
796
797
798
799
800
801
802
803
804
805
806
807
808
809
810
811
812
813
814
815
816
817
818
819
820
821
822
823
824
825
826
827
828
829
830
831
832
833
834
835
836
837
838
839
840
841
842
843
844
845
846
847
848
849
850
851
852
853
854
855
856
857
858
859
860
861
862
863
864
865
866
867
868
869
870
871
872
873
874
875
876
877
878
879
880
881
882
883
884
885
886
887
888
889
890
891
892
893
894
895
896
897
898
899
900
901
902
903
904
905
906
907
908
909
910
911
912
913
914
915
916
917
918
919
920
921
922
923
924
925
926
927
928
929
930
931
932
933
934
935
936
937
938
939
940
941
942
943
944
945
946
947
948
949
950
951
952
953
954
955
956
957
958
959
960
961
962
963
964
965
966
967
968
969
970
971
972
973
974
975
976
977
978
979
980
981
982
983
984
985
986
987
988
989
990
991
992
993
994
995
996
997
998
999
1000
```

### Graphical representation of the process of blood vessel tracer

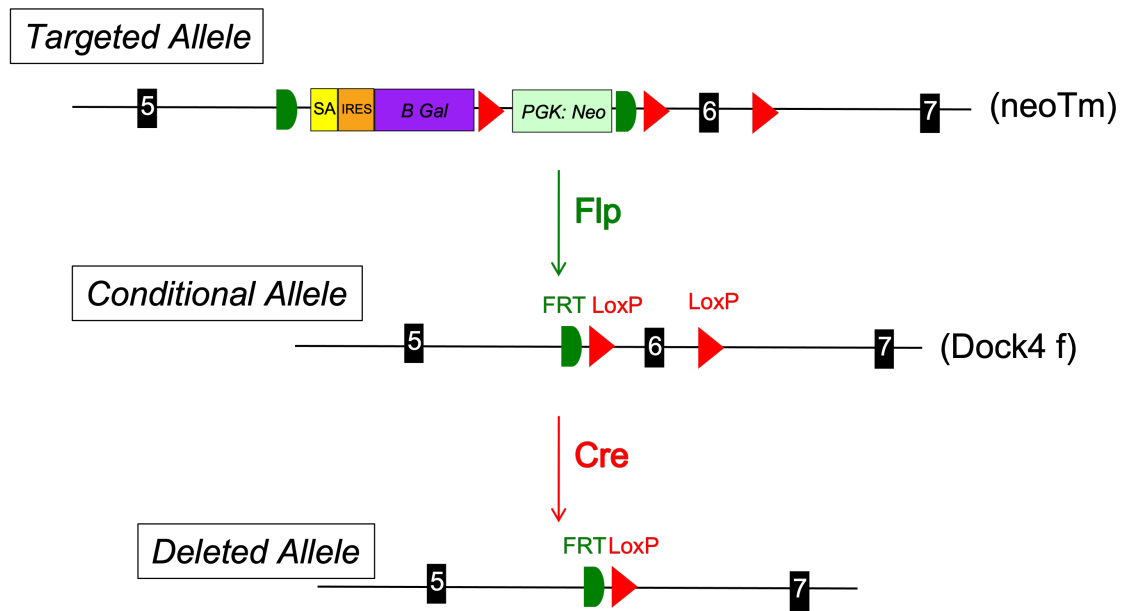
#### quantification and macros generated for automation.

(A) Workflow shows a graphical representation of the process used for blood vessel tracer quantification shown on Chapter 4. The process is described in detail in Chapter 2, Section 2.4.6. Scale bar = 100  $\mu\text{m}$ .

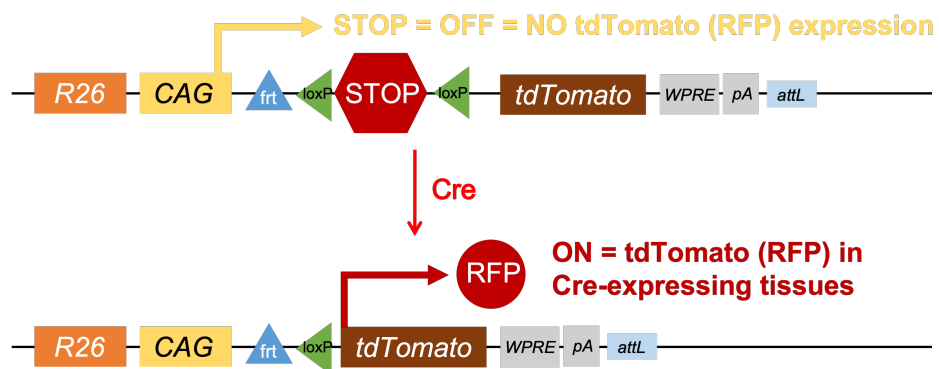
(B) To automate the quantification, a macro was generated using the ImageJ macro language (IJM). Two scripts are shown, top panel shows script for making 40  $\mu\text{m}$  sized circles and bottom panel shows the script for the thresholding process.

## Appendix 9

### Dock4 Conditional Strategy



+ TdTomato strain (<https://www.jax.org/strain/007914>)



Adapted from Madisen, L. 2010. *Nat Neurosci* 13:133.

### + Cdh5(PAC)-CREERT2 strain

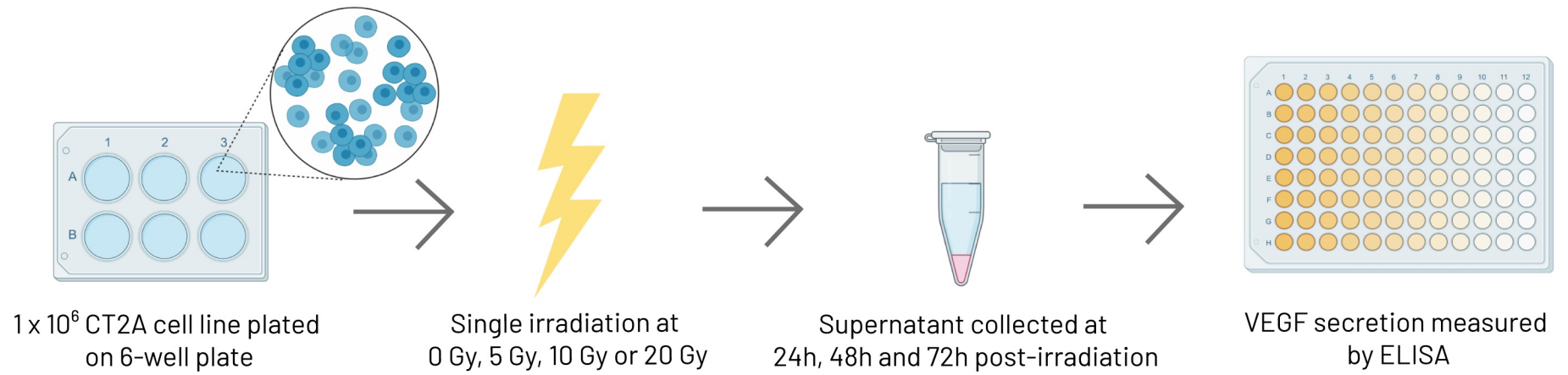
The Cdh5(PAC)-CreERT2 Mouse was developed in the laboratory of Ralf Adams at the London Research Institute. The model was generated by microinjecting a transgene containing a genomic Cdh5(PAC) promoter fragment fused to a CreERT2 cDNA into C57BL/6 zygotes. Founder lines were backcrossed to C57BL/6 for at least five generations. Source: <https://www.taconic.com/mouse-model/cdh5pac-creert2-mouse>.

**Conditional *Dock4* knockout model generated by Ozgene.**

*Dock4* conditional knockout model generated by Ozgene used in this study. *Dock4*<sup>fl/fl</sup> mice were crossed with a VE-cadERT2-CreTdtomato gene carrying mice. For the conditional deletion of *Dock4* and expression of TdTomato, the iVE-Cre;Rosa26Td mice were intraperitoneally injected with tamoxifen for 5 consecutive days prior to experiment. Upon development of neurological symptoms, mice were sacrificed and tumour bearing mouse brains were stained using RFP antibody to confirm Cre deletion (Chapter 5, Figure 5.8).

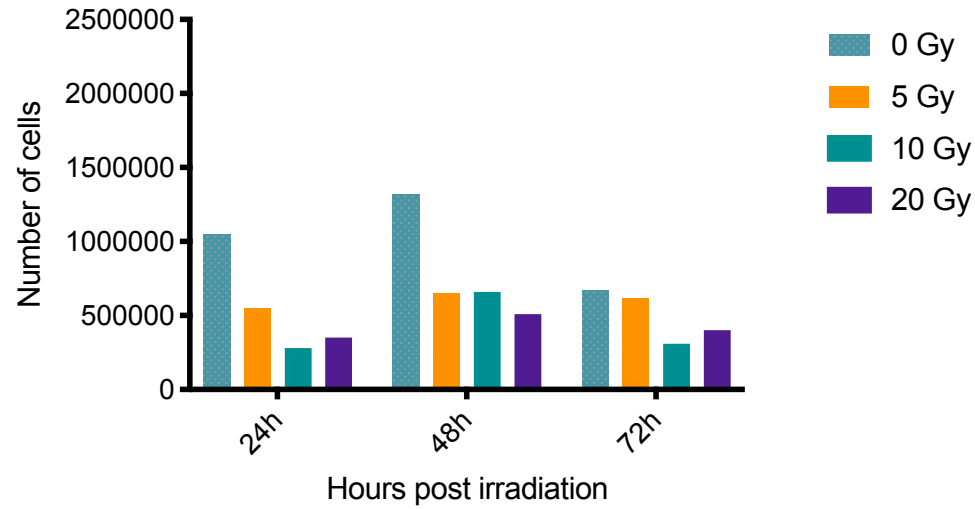
## Appendix 10

A

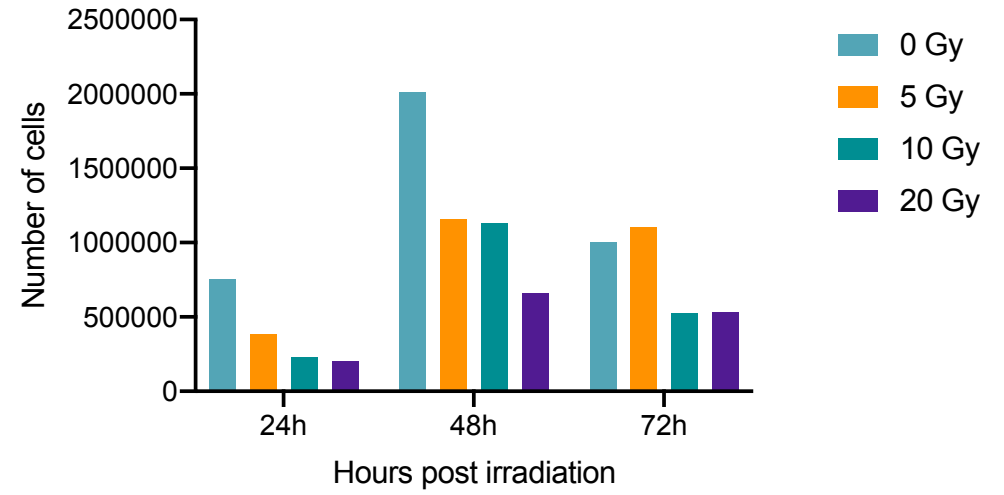


**B**

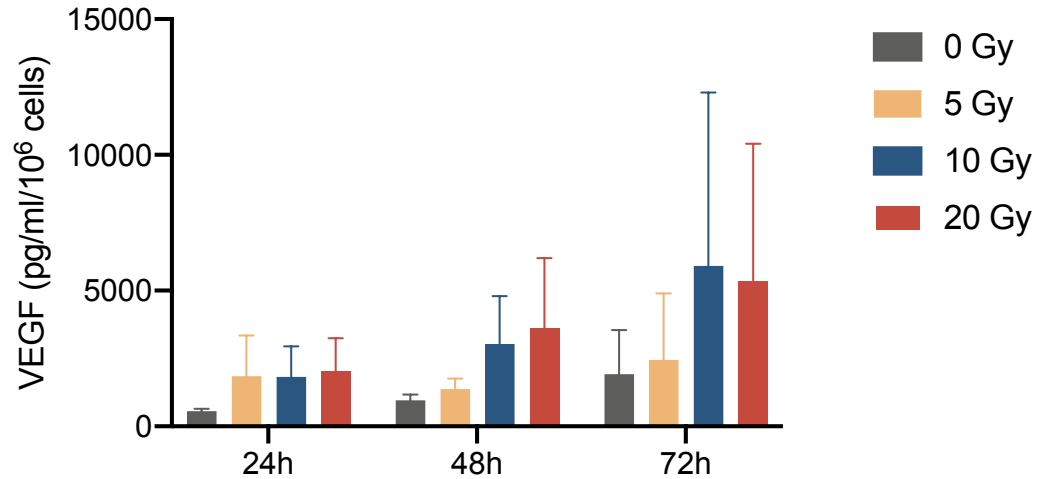
Exp 1



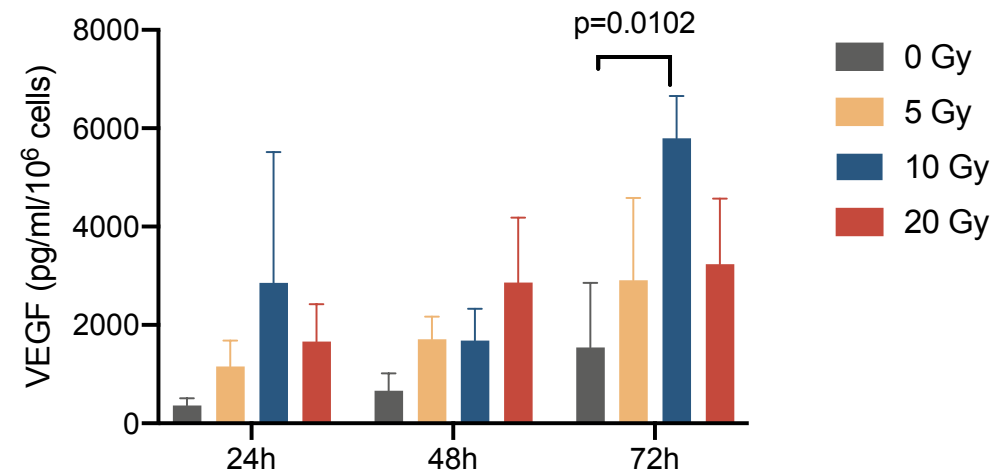
Exp 2

**C**

ELISA 1

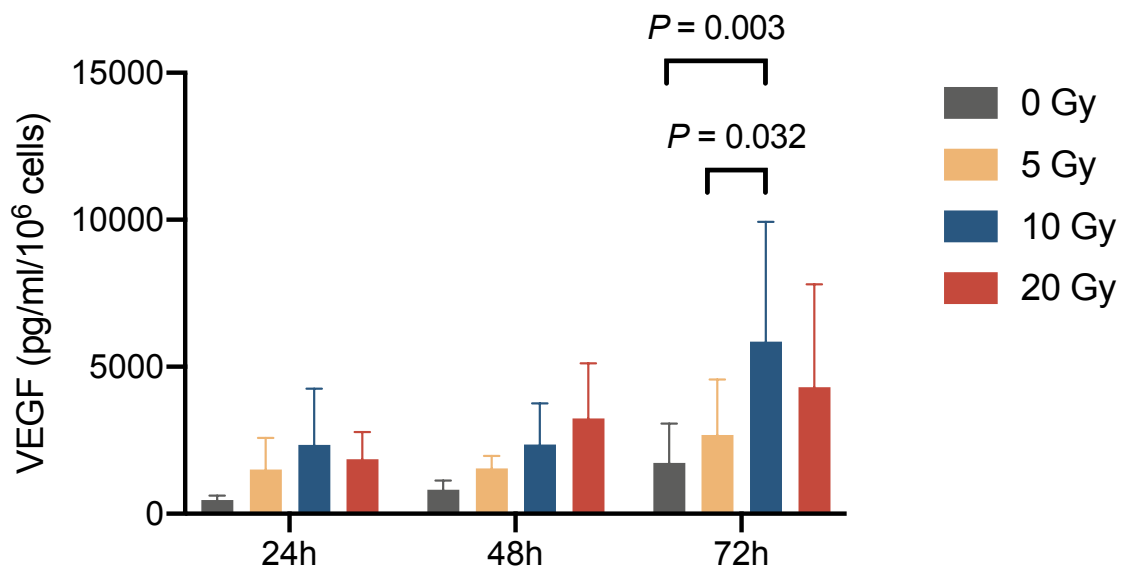


ELISA 2



D

## ELISA 1 and 2



### Increased VEGF secretion in conditioned medium of CT2A cells treated with radiotherapy.

(A) Workflow shows the protocol of ELISA experiment as described in Methods chapter (Section 2.15).  $1 \times 10^6$  cells were cultured in 6-well plates and allowed to attach overnight. Cells were then treated with a single dose of irradiation of 0 Gy, 5 Gy, 10 Gy or 20 Gy. Conditioned medium was collected at 24-, 48- and 72-hours post-irradiation and the number of cells in each well was measured using a haemocytometer and conditioned medium was collected. VEGF levels in the conditioned medium was measured using ELISA. Two experiments were performed and both experiments were done in triplicates.

(B) Graphs show the number of cells in each experiment at 24-, 48- and 72-hours post-irradiation.

(C) Graphs show VEGF protein levels (pg/ml/10<sup>6</sup> cells) in CT2A conditioned medium after 24-, 48- and 72-hours post-irradiation from each of the two experiments. VEGF levels are normalised to cell number.

(D) Graph shows the combined VEGF protein levels (pg/ml/10<sup>6</sup> cells) in CT2A conditioned medium after 24-, 48- and 72-hours post-irradiation from both experiments. VEGF levels are normalised to cell number.

## Appendix 11

### The application of statistical methods: Student's t-test and ANOVA

Student's t-test (also known as t-test) and ANOVA are statistical methods used for the purpose of testing of hypothesis for the comparison of means between separate groups (Mishra et al., 2019). Data tested for hypothesis using these methods should be continuous and normally distributed. The use of correct statistical method is crucial in ensuring key scientific results are reproducible. T-test and ANOVA consists of many statistical tests within themselves.

T-test is a one of the most widely used statistical method used to test whether the mean difference between two groups is statistically significant. There are three types of t-tests, and each should be used depending on the type of data. An independent t-test or also called the unpaired t-test is used to compare the means of two separate unrelated groups. A paired sample t-test is used to compare whether there is a statistically significant change in the mean of a group taken at two different observations (same subjects measured at two time points or observed by two different methods). A one sample t-test, tests whether the mean of a single group is statistically significant against a known mean (a parent population from which the sample is drawn).

ANOVA test or also known as the F Test is a statistical method used to compare the means between three or more groups. A significant *P* value in ANOVA indicates that there is at least one pair which has a statistically significant difference in the mean. To determine which pair is statistically significant, a *post hoc* test of multiple comparisons can be used, where each group is tested against each other. Similar to t-test, ANOVA also contains multiple different tests within itself. When one independent variable is involved in the data, a one-way ANOVA is used, and when there are two independent variables, a two-way ANOVA is used. A one-way ANOVA can be used for independent data sets and a one-way repeated measures ANOVA can be used for dependent data sets (data taken from the same group).

ANOVA and t-test cannot be used interchangeably and, in a case where more than two variables are considered, a *post hoc* multiple comparisons ANOVA should be used rather than individual t-test methods. In using multiple means with multiple t-test, the chances of acquiring a type 1 error in hypothesis testing are high. A Type 1 error is simply, a “false positive” which leads to an incorrect rejection of the null hypothesis (the statistical theory which assumes that no statistical relationship and significant exists between two sets of data) (Banerjee et al., 2009).

In this thesis, although t-test was used to test two groups at a time, in cases where more than two groups were compared in the same experiment, ANOVA would have been a more appropriate statistical test. In cases where the ANOVA test proves to be significant, the ANOVA *post hoc* multiple comparisons method can be utilised to identify differences between pairs. For the improvement of research practices, all data in this study which compares more than two groups should be tested using the appropriate ANOVA test, and data which compares two groups should be tested using the student t-test method. For future publication of the data in this study experiments which compares more than two variables should be tested using the more appropriate ANOVA test.

## References

- Abbott, N.J. 2013. Blood-brain barrier structure and function and the challenges for CNS drug delivery. *Journal of Inherited Metabolic Disease*. **36**(3), pp.437–449.
- Abraham, S., Scarcia, M., Bagshaw, McMahon, K., Grant, G., Harvey, T., Yeo, M., Esteves, F.O.G., Thygesen, H.H., Jones, P.F., Speirs, V., Hanby, A.M., Selby, P.J., Longer, M., Dear, T.N., Pawson, T., Marshall, C.J. and Mavria, G. 2015. A Rac/Cdc42 exchange factor complex promotes formation of lateral filopodia and blood vessel lumen morphogenesis. *Nature Communications*. **6**, pp.1–14.
- Abraham, S., Scarcia, M., Bagshaw, McMahon, K., Grant, G., Harvey, T., Yeo, M., Esteves, F.O.G., Thygesen, H.H., Jones, P.F., Speirs, V., Hanby, A.M., Selby, P.J., Longer, M., Dear, T.N., Pawson, T., Marshall, C.J. and Mavria, G. 2015. A Rac/Cdc42 exchange factor complex promotes formation of lateral filopodia and blood vessel lumen morphogenesis. *Nature Communications*. **6**, pp.1–14.
- Abramsson, A., Lindblom, P. and Betsholtz, C. 2003. Endothelial and nonendothelial sources of PDGF-B regulate pericyte recruitment and influence vascular pattern formation in tumors. *Journal of Clinical Investigation*. **112**(8), pp.1142–1151.
- Aghi, M., Cohen, K.S., Klein, R.J., Scadden, D.T. and Chiocca, E.A. 2006. Tumor stromal-derived factor-1 recruits vascular progenitors to mitotic neovasculature, where microenvironment influences their differentiated phenotypes. *Cancer Research*. **66**(18), pp.9054–9064.
- Agnihotri, S., Burrell, K.E., Wolf, A., Jalali, S., Hawkins, C., Rutka, J.T. and Zadeh, G. 2013. Glioblastoma, a brief review of history, molecular genetics, animal models and novel therapeutic strategies. *Archivum Immunologiae et Therapiae Experimentalis*. **61**(1), pp.25–41.
- Ahishali, B. and Kaya, M. 2021. Evaluation of Blood-Brain Barrier Integrity Using Vascular Permeability Markers: Evans Blue, Sodium Fluorescein, Albumin-Alexa Fluor Conjugates, and Horseradish Peroxidase. *Methods in Molecular Biology*. **2367**, pp.87–103.

- Ahmed, A.U., Auffinger, B. and Lesniak, M.S. 2013. Understanding glioma stem cells: Rationale, clinical relevance and therapeutic strategies. *Expert Review of Neurotherapeutics*. **13**(5).
- Airley, R., Loncaster, J., Bromley, M., Roberts, S., West, C., Davidson, S., Hunter, R., Airley, R., Patterson, A., Stratford, I. and Patterson, A. 2001. Glucose transporter Glut-1 expression correlates with tumor hypoxia and predicts metastasis-free survival in advanced carcinoma of the cervix. *Clinical Cancer Research*. **7**(4).
- Akter, F., Simon, B., de Boer, N.L., Redjal, N., Wakimoto, H. and Shah, K. 2021. Pre-clinical tumor models of primary brain tumors: Challenges and opportunities. *Biochimica et biophysica acta. Reviews on cancer*. **1875**(1), p.188458.
- Al-Khallaf, H. 2017. Isocitrate dehydrogenases in physiology and cancer: Biochemical and molecular insight. *Cell and Bioscience*. **7**(1), pp.1–18.
- Alarcon-Martinez, L., Yilmaz-Ozcan, S., Yemisci, M., Schallek, J., Kilic, K., Can, A., Polo, A. Di and Dalkara, T. 2018. Capillary pericytes express a-smooth muscle actin, which requires prevention of filamentous-actin depolymerization for detection. *eLife*. **7**(34861), pp.1–17.
- Alessandri, G., Chirivi, R.G.S., Fiorentini, S., Dossi, R., Bonardelli, S., Giulini, S.M., Zanetta, G., Landoni, F., Graziotti, P.P., Turano, A., Caruso, A., Zardi, L., Giavazzi, R. and Bani, M.R. 1999. Phenotypic and functional characteristics of tumour-derived microvascular endothelial cells. *Clinical and Experimental Metastasis*. **17**(8).
- Alkelai, A., Lupoli, S., Greenbaum, L., Kohn, Y., Kanyas-Sarner, K., Ben-Asher, E., Lancet, D., Macciardi, F. and Lerer, B. 2012. DOCK4 and CEACAM21 as novel schizophrenia candidate genes in the Jewish population. *The international journal of neuropsychopharmacology*. **15**(4), pp.459–69.
- Alonso, M.M., Gomez-Manzano, C., Bekele, B.N., Yung, W.K.A. and Fueyo, J. 2007. Adenovirus-based strategies overcome temozolomide resistance by silencing the O6-methylguanine-DNA methyltransferase promoter. *Cancer Research*. **67**(24), pp.11499–11504.
- Ammirati, M., Chotai, S., Newton, H., Lamki, T., Wei, L. and Grecula, J. 2014. Hypofractionated intensity modulated radiotherapy with temozolomide in

- newly diagnosed glioblastoma multiforme. *Journal of Clinical Neuroscience*. **21**(4).
- Andor, N., Harness, J. V., Müller, S., Mewes, H.W. and Petritsch, C. 2014. Expands: Expanding ploidy and allele frequency on nested subpopulations. *Bioinformatics*. **30**(1), pp.50–60.
- Antoine, S., Lozano-Sanchez, F., Alice, T., Bertrand, M., Suzanne, T., Karima, M., Marine, G., Yannick, M., Laurent, C., Matthieu, P., Alexandre, C., Loic, F., Marc, S., Khé, H.X., Jérôme, H., Jean-Yves, D., Ducray, F. and Idbaih, A. 2020. Initial surgical resection and long time to occurrence from initial diagnosis are independent prognostic factors in resected recurrent IDH wild-type glioblastoma. *Clinical Neurology and Neurosurgery*. **196**.
- Armulik, A., Abramsson, A. and Betsholtz, C. 2005. Endothelial/pericyte interactions. *Circulation Research*. **97**(6), pp.512–523.
- Armulik, A., Genové, G. and Betsholtz, C. 2011. Pericytes: Developmental, Physiological, and Pathological Perspectives, Problems, and Promises. *Developmental Cell*. **21**(2), pp.193–215.
- Armulik, A., Genové, G., Mäe, M., Nisancioglu, M.H., Wallgard, E., Niaudet, C., He, L., Norlin, J., Lindblom, P., Strittmatter, K., Johansson, B.R. and Betsholtz, C. 2010. Pericytes regulate the blood-brain barrier. *Nature*. **468**(7323), pp.557–561.
- Arnold, K.M., Flynn, N.J., Raben, A., Romak, L., Yu, Y., Dicker, A.P., Mourtada, F. and Sims-Mourtada, J. 2018. The Impact of Radiation on the Tumor Microenvironment: Effect of Dose and Fractionation Schedules. *Cancer Growth and Metastasis*. **11**, p.117906441876163.
- Arrieta, O., Guevara, P., Escobar, E., García-Navarrete, R., Pineda, B. and Sotelo, J. 2005. Blockage of angiotensin II type I receptor decreases the synthesis of growth factors and induces apoptosis in C6 cultured cells and C6 rat glioma. *British Journal of Cancer*. **92**(7).
- Attwell, D., Buchan, A.M., Charpak, S., Lauritzen, M., MacVicar, B.A. and Newman, E.A. 2010. Glial and neuronal control of brain blood flow. *Nature*. **468**(7321).
- Augustin, H.G., Young Koh, G., Thurston, G. and Alitalo, K. 2009. Control of

vascular morphogenesis and homeostasis through the angiopoietin - Tie system. *Nature Reviews Molecular Cell Biology*. **10**(3), pp.165–177.

Azzam, E.I., Jay-Gerin, J.P. and Pain, D. 2012. Ionizing radiation-induced metabolic oxidative stress and prolonged cell injury. *Cancer Letters*. **327**(1–2).

Baker, D.G. and Krochak, R.J. 1989. The response of the microvascular system to radiation: A review. *Cancer Investigation*. **7**(3).

Baker, G.J., Yadav, V.N., Motsch, S., Koschmann, C., Calinescu, A.A., Mineharu, Y., Camelo-Piragua, S.I., Orringer, D., Bannykh, S., Nichols, W.S., deCarvalho, A.C., Mikkelsen, T., Castro, M.G. and Lowenstein, P.R. 2014. Mechanisms of Glioma Formation: Iterative Perivascular Glioma Growth and Invasion Leads to Tumor Progression, VEGF-Independent Vascularization, and Resistance to Antiangiogenic Therapy. *Neoplasia (United States)*. **16**(7).

Balabanov, R., Beaumont, T. and Dore-Duffy, P. 1999. Role of central nervous system microvascular pericytes in activation of antigen-primed splenic T-lymphocytes. *Journal of Neuroscience Research*. **55**(5).

Baldi, I. and Loiseau, H. 2012. Epidemiology of primary brain tumors. *Tumors of the Central Nervous System, Volume 4: Brain Tumors (Part 2)*. **6**(July), pp.3–13.

Banerjee, A., Chitnis, U., Jadhav, S., Bhawalkar, J. and Chaudhury, S. 2009. Hypothesis testing, type I and type II errors. *Industrial Psychiatry Journal*. **18**(2).

Bao, S., Wu, Q., McLendon, R.E., Hao, Y., Shi, Q., Hjelmeland, A.B., Dewhirst, M.W., Bigner, D.D. and Rich, J.N. 2006. Glioma stem cells promote radioresistance by preferential activation of the DNA damage response. *Nature*. **444**(7120).

Bao, S., Wu, Q., Sathornsumetee, S., Hao, Y., Li, Z., Hjelmeland, A.B., Shi, Q., McLendon, R.E., Bigner, D.D. and Rich, J.N. 2006. Stem cell-like glioma cells promote tumor angiogenesis through vascular endothelial growth factor. *Cancer Research*. **66**(16).

Bar, E.E., Lin, A., Mahairaki, V., Matsui, W. and Eberhart, C.G. 2010. Hypoxia increases the expression of stem-cell markers and promotes clonogenicity in glioblastoma neurospheres. *American Journal of Pathology*. **177**(3).

- Barker, H.E., Paget, J.T.E., Khan, A.A. and Harrington, K.J. 2015. The tumour microenvironment after radiotherapy: Mechanisms of resistance and recurrence. *Nature Reviews Cancer*. **15**(7), pp.409–425.
- Barry, D.M., Xu, K., Meadows, S.M., Zheng, Y., Norden, P.R., Davis, G.E. and Cleaver, O. 2015. Cdc42 is required for cytoskeletal support of endothelial cell adhesion during blood vessel formation in mice. *Development (Cambridge)*. **142**(17).
- Baselet, B., Belmans, N., Coninx, E., Lowe, D., Janssen, A., Michaux, A., Tabury, K., Raj, K., Quintens, R., Benotmane, M.A., Baatout, S., Sonveaux, P. and Aerts, A. 2017. Functional gene analysis reveals cell cycle changes and inflammation in endothelial cells irradiated with a single X-ray dose. *Frontiers in Pharmacology*. **8**(APR).
- Baskar, R., Dai, J., Wenlong, N., Yeo, R. and Yeoh, K.W. 2014. Biological response of cancer cells to radiation treatment. *Frontiers in Molecular Biosciences*. **1**(NOV).
- Batchelor, T.T., Sorensen, A.G., di Tomaso, E., Zhang, W.T., Duda, D.G.G., Cohen, K.S., Kozak, K.R., Cahill, D.P., Chen, P.J., Zhu, M., Ancukiewicz, M., Mrugala, M.M., Plotkin, S., Drappatz, J., Louis, D.N., Ivy, P., Scadden, D.T.T., Benner, T., Loeffler, J.S., Wen, P.Y. and Jain, R.K. 2007. AZD2171, a Pan-VEGF Receptor Tyrosine Kinase Inhibitor, Normalizes Tumor Vasculature and Alleviates Edema in Glioblastoma Patients. *Cancer Cell*. **11**(1).
- Baudino, T.A., McKay, C., Pendeville-Samain, H., Nilsson, J.A., Maclean, K.H., White, E.L., Davis, A.C., Ihle, J.N. and Cleveland, J.L. 2002. c-Myc is essential for vasculogenesis and angiogenesis during development and tumor progression. *Genes & development*. **16**(19), pp.2530–43.
- Benjamin, L.E., Hemo, I. and Keshet, E. 1998. A plasticity window for blood vessel remodelling is defined by pericyte coverage of the preformed endothelial network and is regulated by PDGF-B and VEGF. *Development*. **125**(9).
- Bergers, G. and Song, S. 2005. The role of pericytes in blood-vessel formation and maintenance. *Neuro-Oncology*. **7**(4), pp.452–464.
- Bergwerff, M., Verberne, M.E., DeRuiter, M.C., Poelmann, R.E. and

- Gittenberger-de Groot, A.C. 1998. Neural crest cell contribution to the developing circulatory system implications for vascular morphology? *Circulation Research*. **82**(2), pp.221–231.
- Bernier, J., Hall, E.J. and Giaccia, A. 2004. Radiation oncology: A century of achievements. *Nature Reviews Cancer*. **4**(9).
- Bertossi, M., Maiorano, E., Occhiogrosso, M. and Roncali, L. 1997. Ultrastructural and morphometric investigation of human brain capillaries in normal and peritumoral tissues. *Ultrastructural Pathology*. **21**(1).
- Bhat, K.P.L., Balasubramaniyan, V., Vaillant, B., Ezhilarasan, R., Hummelink, K., Hollingsworth, F., Wani, K., Heathcock, L., James, J.D., Goodman, L.D., Conroy, S., Long, L., Lelic, N., Wang, S., Gumin, J., Raj, D., Kodama, Y., Raghunathan, A., Olar, A., Joshi, K., Pelloski, C.E., Heimberger, A., Kim, S.H., Cahill, D.P., Rao, G., DenDunnen, W.F.A., Boddeke, H.W.G.M., Phillips, H.S., Nakano, I., Lang, F.F., Colman, H., Sulman, E.P. and Aldape, K. 2013. Mesenchymal Differentiation Mediated by NF- $\kappa$ B Promotes Radiation Resistance in Glioblastoma. *Cancer Cell*. **24**(3).
- Binda, E., Visioli, A., Giani, F., Lamorte, G., Copetti, M., Pitter, K.L., Huse, J.T., Cajola, L., Zanetti, N., Dimeco, F., Filippis, D., Mangiola, A., Maira, G., Anile, C. and Bonis, P. De 2014. The EphA2 Receptor Drives Self-Renewal and Tumorigenicity in Stem-Like Tumor-Propagating Cells from Human Glioblastomas. *Cancer Cell*. **22**(6), pp.765–780.
- Birner, P., Piribauer, M., Fischer, I., Gatterbauer, B., Marosi, C., Ambros, P.F., Ambros, I.M., Bredel, M., Oberhuber, G., Rössler, K., Budka, H., Harris, A.L. and Hainfellner, J.A. 2003. Vascular patterns in glioblastoma influence clinical outcome and associate with variable expression of angiogenic proteins: Evidence for distinct angiogenic subtypes. *Brain Pathology*. **13**(2).
- Blanco, R. and Gerhardt, H. 2013. VEGF and Notch in tip and stalk cell selection. *Cold Spring Harbor Perspectives in Medicine*. **3**(1), pp.1–19.
- De Bonis, P., Anile, C., Pompucci, A., Fiorentino, A., Balducci, M., Chiesa, S., Lauriola, L., Maira, G. and Mangiola, A. 2013. The influence of surgery on recurrence pattern of glioblastoma. *Clinical Neurology and Neurosurgery*. **115**(1), pp.37–43.
- Boroujerdi, A., Welser-Alves, J. V., Tigges, U. and Milner, R. 2012. Chronic

cerebral hypoxia promotes arteriogenic remodeling events that can be identified by reduced endoglin (CD105) expression and a switch in  $\beta 1$  integrins. *Journal of Cerebral Blood Flow and Metabolism*. **32**(9).

Boström, P.J., Thoms, J., Sykes, J., Ahmed, O., Evans, A., Van Rhijn, B.W.G., Mirtti, T., Stakhovskiy, O., Laato, M., Margel, D., Pintilie, M., Kuk, C., Milosevic, M., Zlotta, A.R. and Bristow, R.G. 2016. Hypoxia marker GLUT-1 (glucose transporter 1) is an independent prognostic factor for survival in bladder cancer patients treated with radical cystectomy. *Bladder Cancer*. **2**(1).

Boucher, Y., Salehi, H., Witwer, B., Harsh, G.R. and Jain, R.K. 1997. Interstitial fluid pressure in intracranial tumours in patients and in rodents. *British Journal of Cancer*. **75**(6).

Bouchet, A., Potez, M., Coquery, N., Rome, C., Lemasson, B., Bräuer-Krisch, E., Rémy, C., Laissue, J., Barbier, E.L., Djonov, V. and Serduc, R. 2017. Permeability of Brain Tumor Vessels Induced by Uniform or Spatially Microfractionated Synchrotron Radiation Therapies. *International Journal of Radiation Oncology Biology Physics*. **98**(5), pp.1174–1182.

Bouchet, A., Serduc, R., Laissue, J.A. and Djonov, V. 2015. Effects of microbeam radiation therapy on normal and tumoral blood vessels. *Physica Medica*. **31**(6), pp.634–641.

Brat, D.J., Bellail, A.C. and Van Meir, E.G. 2005. The role of interleukin-8 and its receptors in gliomagenesis and tumoral angiogenesis. *Neuro-Oncology*. **7**(2).

Brat, D.J., Castellano-Sanchez, A.A., Hunter, S.B., Pecot, M., Cohen, C., Hammond, E.H., Devi, S.N., Kaur, B. and Van Meir, E.G. 2004. Pseudopalisades in Glioblastoma Are Hypoxic, Express Extracellular Matrix Proteases, and Are Formed by an Actively Migrating Cell Population. *Cancer Research*. **64**(3), pp.920–927.

Brighi, C., Reid, L., Genovesi, L.A., Kojic, M., Millar, A., Bruce, Z., White, A.L., Day, B.W., Rose, S., Whittaker, A.K. and Puttick, S. 2020. Comparative study of preclinical mouse models of high-grade glioma for nanomedicine research: the importance of reproducing blood-brain barrier heterogeneity. *Theranostics*. **10**(14), pp.6361–6371.

- Brown, J.M., Recht, L. and Strober, S. 2017. The Promise of Targeting Macrophages in Cancer Therapy. *Clinical Cancer Research*. **23**(13), pp.3241–3250.
- Brugnera, E., Haney, L., Grimsley, C., Lu, M., Walk, S.F., Tosello-Tramont, A.C., Macara, I.G., Madhani, H., Fink, G.R. and Ravichandran, K.S. 2002. Unconventional Rac-GEF activity is mediated through the Dock180-ELMO complex. *Nature Cell Biology*. **4**(8).
- Bryan, B.A. and D'Amore, P.A. 2007. What tangled webs they weave: Rho-GTPase control of angiogenesis. *Cellular and Molecular Life Sciences*. **64**(16).
- Bullitt, E., Zeng, D., Gerig, G., Aylward, S., Joshi, S., Smith, J.K., Lin, W. and Ewend, M.G. 2005. Vessel tortuosity and brain tumor malignancy: A blinded study *In: Academic Radiology*.
- Bulstrode, H., Johnstone, E., Marques-Torres, M.A., Ferguson, K.M., Bressan, R.B., Blin, C., Grant, V., Gogolok, S., Gangoso, E., Gargic, S., Ender, C., Fotaki, V., Sproul, D., Bertone, P. and Pollard, S.M. 2017. Elevated FOXP1 and SOX2 in glioblastoma enforces neural stem cell identity through transcriptional control of cell cycle and epigenetic regulators. *Genes and Development*. **31**(8).
- Burnet, N.G., Jena, R., Burton, K.E., Tudor, G.S.J., Scaife, J.E., Harris, F. and Jefferies, S.J. 2014. Clinical and practical considerations for the use of intensity-modulated radiotherapy and image guidance in neuro-oncology. *Clinical Oncology*. **26**(7).
- Bussink, J., Kaanders, J.H.A.M., Rijken, P.F.J.W., Raleigh, J.A. and Van Der Kogel, A.J. 2000. Changes in blood perfusion and hypoxia after irradiation of a human squamous cell carcinoma xenograft tumor line. *Radiation Research*. **153**(4).
- Bussolati, B., Deambrosio, I., Russo, S., Deregibus, M.C. and Camussi, G. 2003. Altered angiogenesis and survival in human tumor-derived endothelial cells. *The FASEB journal: official publication of the Federation of American Societies for Experimental Biology*. **17**(9).
- Butowski, N., Colman, H., De Groot, J.F., Omuro, A.M., Nayak, L., Wen, P.Y., Cloughesy, T.F., Marimuthu, A., Haidar, S., Perry, A., Huse, J., Phillips, J.,

- West, B.L., Nolop, K.B., Hsu, H.H., Ligon, K.L., Molinaro, A.M. and Prados, M. 2016. Orally administered colony stimulating factor 1 receptor inhibitor PLX3397 in recurrent glioblastoma: An Ivy Foundation Early Phase Clinical Trials Consortium phase II study. *Neuro-Oncology*. **18**(4).
- Van Buul, J.D., Geerts, D. and Huveneers, S. 2014. Rho GAPs and GEFs: Controlling switches in endothelial cell adhesion. *Cell Adhesion and Migration*. **8**(2).
- Cahill, D.P., Levine, K.K., Betensky, R.A., Codd, P.J., Romany, C.A., Reavie, L.B., Batchelor, T.T., Futreal, P.A., Stratton, M.R., Curry, W.T., Lafrate, A.J. and Louis, D.N. 2007. Loss of the mismatch repair protein MSH6 in human glioblastomas is associated with tumor progression during temozolomide treatment. *Clinical Cancer Research*. **13**(7), pp.2038–2045.
- Calabrese, C., Poppleton, H., Kocak, M., Hogg, T.L., Fuller, C., Hamner, B., Oh, E.Y., Gaber, M.W., Finklestein, D., Allen, M., Frank, A., Bayazitov, I.T., Zakharenko, S.S., Gajjar, A., Davidoff, A. and Gilbertson, R.J. 2007. A Perivascular Niche for Brain Tumor Stem Cells. *Cancer Cell*. **11**(1).
- Campos, B., Olsen, L.R., Urup, T. and Poulsen, H.S. 2016. A comprehensive profile of recurrent glioblastoma. *Oncogene*. **35**(45), pp.5819–5825.
- Cancer Research UK 2020. Brain, other CNS and intracranial tumours incidence statistics. [Accessed 24 June 2021]. Available from: <https://www.cancerresearchuk.org/health-professional/cancer-statistics/statistics-by-cancer-type/brain-other-cns-and-intracranial-tumours/incidence#heading-Zero>.
- Carmeliet, P. 2000. Mechanisms of angiogenesis and lymphangiogenesis. *Nature Medicine*. **6**(3), pp.389–395.
- Carmeliet, P., Ferreira, V., Breier, G., Pollefeyt, S., Kieckens, L., Gertsenstein, M., Fahrig, M., Vandenhoek, A., Harpal, K., Eberhardt, C., Declercq, C., Pawling, J., Moons, L., Collen, D., Risaut, W. and Nagy, A. 1996. Abnormal blood vessel development and lethality in embryos lacking a single VEGF allele. *Nature*. **380**(6573).
- Carmeliet, P. and Jain, R.K. 2011. Molecular mechanisms and clinical applications of angiogenesis. *Nature*. **473**(7347), pp.298–307.

- Caspani, E.M., Crossley, P.H., Redondo-Garcia, C. and Martinez, S. 2014. Glioblastoma: A pathogenic crosstalk between tumor cells and pericytes. *PLoS ONE*. **9**(7).
- Charalambous, C., Chen, T.C. and Hofman, F.M. 2006. Characteristics of tumor-associated endothelial cells derived from glioblastoma multiforme. *Neurosurgical focus*. **20**(4), pp.1–5.
- Charalambous, C., Hofman, F.M. and Chen, T.C. 2005. Functional and phenotypic differences between glioblastoma multiforme-derived and normal human brain endothelial cells. *Journal of Neurosurgery*. **102**(4).
- Charalambous, C., Pen, L.B., Su, Y.S., Milan, J., Chen, T.C. and Hofman, F.M. 2005. Interleukin-8 differentially regulates migration of tumor-associated and normal human brain endothelial cells. *Cancer Research*. **65**(22).
- Chauhan, V.P., Martin, J.D., Liu, H., Lacorre, D.A., Jain, S.R., Kozin, S. V., Stylianopoulos, T., Mousa, A.S., Han, X., Adstamongkonkul, P., Popović, Z., Huang, P., Bawendi, M.G., Boucher, Y. and Jain, R.K. 2013. Angiotensin inhibition enhances drug delivery and potentiates chemotherapy by decompressing tumour blood vessels. *Nature Communications*. **4**.
- Chédeville, A.L. and Madureira, P.A. 2021. The role of hypoxia in glioblastoma radiotherapy resistance. *Cancers*. **13**(3), pp.1–16.
- Chen, J., Somanath, P.R., Razorenova, O., Chen, W.S., Hay, N., Bornstein, P. and Byzova, T. V. 2005. Akt1 regulates pathological angiogenesis, vascular maturation and permeability in vivo. *Nature Medicine*. **11**(11), pp.1188–1196.
- Chen, L., Lin, Z.X., Lin, G.S., Zhou, C.F., Chen, Y.P., Wang, X.F. and Zheng, Z.Q. 2015. Classification of microvascular patterns via cluster analysis reveals their prognostic significance in glioblastoma. *Human Pathology*. **46**(1).
- Cheng, L., Huang, Z., Zhou, W., Wu, Q., Donnola, S., Liu, J.K., Fang, X., Sloan, A.E., Mao, Y., Lathia, J.D., Min, W., McLendon, R.E., Rich, J.N. and Bao, S. 2013. Glioblastoma stem cells generate vascular pericytes to support vessel function and tumor growth. *Cell*. **153**(1), pp.139–52.
- Cheng, L., Wu, Q., Guryanova, O.A., Huang, Z., Huang, Q., Rich, J.N. and Bao,

- S. 2011. Elevated invasive potential of glioblastoma stem cells. *Biochemical and Biophysical Research Communications*. **406**(4).
- Chinot, O.L., Wick, W., Mason, W., Henriksson, R., Saran, F., Nishikawa, R., Carpentier, A.F., Hoang-Xuan, K., Kavan, P., Cernea, D., Brandes, A.A., Hilton, M., Abrey, L. and Cloughesy, T. 2014. Bevacizumab plus Radiotherapy–Temozolomide for Newly Diagnosed Glioblastoma. *New England Journal of Medicine*. **370**(8), pp.709–722.
- Choi, S.H., Kim, A.R., Nam, J.K., Kim, J.M., Kim, J.Y., Seo, H.R., Lee, H.J., Cho, J. and Lee, Y.J. 2018. Tumour-vasculature development via endothelial-to-mesenchymal transition after radiotherapy controls CD44v6+ cancer cell and macrophage polarization. *Nature Communications*. **9**(1).
- Christensen, K., Schrøder, H.D. and Kristensen, B.W. 2008. CD133 identifies perivascular niches in grade II-IV astrocytomas. *Journal of Neuro-Oncology*. **90**(2).
- Claes, A., Idema, A.J. and Wesseling, P. 2007. Diffuse glioma growth: A guerilla war. *Acta Neuropathologica*. **114**(5).
- Clayton, N.S. and Ridley, A.J. 2020. Targeting Rho GTPase Signaling Networks in Cancer. *Frontiers in Cell and Developmental Biology*. **8**(April), pp.1–12.
- Clément-Colmou, K., Potiron, V., Pietri, M., Guillonneau, M., Jouglar, E., Chiavassa, S., Delpon, G., Paris, F. and Supiot, S. 2020. Influence of radiotherapy fractionation schedule on the tumor vascular microenvironment in prostate and lung cancer models. *Cancers*. **12**(1), pp.1–11.
- Coleman, M. and Olson, M. 2002. Rho GTPase signalling pathways in the morphological changes associated with apoptosis. *Cell Death and Differentiation*. **9**(493–504).
- Colman, H., Zhang, L., Sulman, E.P., McDonald, J.M., Shooshtari, N.L., Rivera, A., Popoff, S., Nutt, C.L., Louis, D.N., Cairncross, J.G., Gilbert, M.R., Phillips, H.S., Mehta, M.P., Chakravarti, A., Pelloski, C.E., Bhat, K., Feuerstein, B.G., Jenkins, R.B. and Aldape, K. 2010. A multigene predictor of outcome in glioblastoma. *Neuro-Oncology*. **12**(1), pp.49–57.
- Coniglio, S.J., Eugenin, E., Dobrenis, K., Stanley, E.R., West, B.L., Symons, M.H. and Segall, J.E. 2012. Microglial stimulation of glioblastoma invasion

involves epidermal growth factor receptor (EGFR) and colony stimulating factor 1 receptor (CSF-1R) signaling. *Molecular medicine (Cambridge, Mass.)*. **18**(1).

Cooke, V.G., LeBleu, V.S., Keskin, D., Khan, Z., O'Connell, J.T., Teng, Y., Duncan, M.B., Xie, L., Maeda, G., Vong, S., Sugimoto, H., Rocha, R.M., Damascena, A., Brentani, R.R. and Kalluri, R. 2012. Pericyte depletion results in hypoxia-associated epithelial-to-mesenchymal transition and metastasis mediated by met signaling pathway. *Cancer Cell*. **21**(1).

Corliss, B.A., Azimi, M.S., Munson, J.M., Peirce, S.M. and Murfee, W.L. 2016. Macrophages: An Inflammatory Link Between Angiogenesis and Lymphangiogenesis. *Microcirculation*. **23**(2).

Côté, J.F. and Vuori, K. 2002. Identification of an evolutionary conserved superfamily of DOCK180-related proteins with guanine nucleotide exchange activity. *Journal of Cell Science*. **115**(24).

Couturier, C.P., Ayyadhury, S., Le, P.U., Nadaf, J., Monlong, J., Riva, G., Allache, R., Baig, S., Yan, X., Bourgey, M., Lee, C., Wang, Y.C.D., Wee Yong, V., Guiot, M.C., Najafabadi, H., Misic, B., Antel, J., Bourque, G., Ragoussis, J. and Petrecca, K. 2020. Single-cell RNA-seq reveals that glioblastoma recapitulates a normal neurodevelopmental hierarchy. *Nature Communications*. **11**(1).

Cuddapah, V.A., Robel, S., Watkins, S. and Sontheimer, H. 2014. A neurocentric perspective on glioma invasion. *Nature Reviews Neuroscience*. **15**(7).

Cuneo, K.C., Vredenburg, J.J., Sampson, J.H., Reardon, D.A., Desjardins, A., Peters, K.B., Friedman, H.S., Willett, C.G. and Kirkpatrick, J.P. 2012. Safety and efficacy of stereotactic radiosurgery and adjuvant bevacizumab in patients with recurrent malignant gliomas. *International Journal of Radiation Oncology Biology Physics*. **82**(5).

D'Alessio, A., Proietti, G., Sica, G. and Scicchitano, B.M. 2019. Pathological and molecular features of glioblastoma and its peritumoral tissue. *Cancers*. **11**(4).

D'Avella, D., Ciccirello, R., Albiero, F., Mesiti, M., Gagliardi, M.E., Russi, E., D'Aquino, A., Tomasello, F. and D'Aquino, S. 1992. Quantitative study of blood-brain barrier permeability changes after experimental whole-brain

radiation. *Neurosurgery*. **30**(1).

Darmanis, S., Sloan, S.A., Croote, D., Mignardi, M., Chernikova, S., Samghababi, P., Zhang, Y., Neff, N., Kowarsky, M., Caneda, C., Li, G., Chang, S.D., Connolly, I.D., Li, Y., Barres, B.A., Gephart, M.H. and Quake, S.R. 2017. Single-Cell RNA-Seq Analysis of Infiltrating Neoplastic Cells at the Migrating Front of Human Glioblastoma. *Cell Reports*. **21**(5).

Das, S. and Marsden, P.A. 2017. Angiogenesis in Glioblastoma. . **369**(16), pp.1561–1563.

Davies, D.C. 2002. Blood-brain barrier breakdown in septic encephalopathy and brain tumours. *Journal of Anatomy*. **200**(6).

De Bacco, F., D'Ambrosio, A., Casanova, E., Orzan, F., Neggia, R., Albano, R., Verginelli, F., Cominelli, M., Poliani, P.L., Luraghi, P., Reato, G., Pellegatta, S., Finocchiaro, G., Perera, T., Garibaldi, E., Gabriele, P., Comoglio, P.M. and Boccaccio, C. 2016. MET inhibition overcomes radiation resistance of glioblastoma stem-like cells . *EMBO Molecular Medicine*. **8**(5).

Deanfield, J.E., Halcox, J.P. and Rabelink, T.J. 2007. Endothelial function and dysfunction: Testing and clinical relevance. *Circulation*. **115**(10).

Debbaut, C., Segers, P., Cornillie, P., Casteleyn, C., Dierick, M., Laleman, W. and Monbaliu, D. 2014. Analyzing the human liver vascular architecture by combining vascular corrosion casting and micro-CT scanning: A feasibility study. *Journal of Anatomy*. **224**(4).

Debruyne, D.N., Turchi, L., Burel-Vandenbos, F., Fareh, M., Almairac, F., Virolle, V., Figarella-Branger, D., Baeza-Kallee, N., Lagadec, P., Kubiniek, V., Paquis, P., Fontaine, D., Junier, M.-P., Chneiweiss, H. and Virolle, T. 2018. DOCK4 promotes loss of proliferation in glioblastoma progenitor cells through nuclear beta-catenin accumulation and subsequent miR-302-367 cluster expression. *Oncogene*. **37**(2), pp.241–254.

Deindl, E., Buschmann, I., Hoefler, I.E., Podzuweit, T., Boengler, K., Vogel, S., Van Royen, N., Fernandez, B. and Schaper, W. 2001. Role of ischemia and of hypoxia-inducible genes in arteriogenesis after femoral artery occlusion in the rabbit. *Circulation Research*. **89**(9).

Deng, L., Stafford, J.H., Liu, S.C., Chernikova, S.B., Merchant, M., Recht, L. and

- Martin Brown, J. 2017. SDF-1 Blockade Enhances Anti-VEGF Therapy of Glioblastoma and Can Be Monitored by MRI. *Neoplasia (United States)*. **19**(1).
- Dennis, M.K., Field, A.S., Burai, R., Ramesh, C., Whitney, K., Bologna, C.G., Oprea, T.I., Yamaguchi, Y., Hayashi, S., Sklar, L. a, Hathaway, H.J., Arterburn, J.B. and Prossnitz, E.R. 2012. Olig2-regulated lineage-restricted pathway controls replication competence in neural stem cells and malignant glioma. *Neuron*. **53**(4), pp.503–517.
- Deshors, P., Toulas, C., Arnauduc, F., Malric, L., Siegfried, A., Nicaise, Y., Lemarié, A., Larrieu, D., Tosolini, M., Cohen-Jonathan Moyal, E., Courtade-Saidi, M. and Evrard, S.M. 2019. Ionizing radiation induces endothelial transdifferentiation of glioblastoma stem-like cells through the Tie2 signaling pathway. *Cell Death and Disease*. **10**(11).
- Desouky, O., Ding, N. and Zhou, G. 2015. Targeted and non-targeted effects of ionizing radiation. *Journal of Radiation Research and Applied Sciences*. **8**(2).
- Dimitrievich, G.S., Fischer-Dzoga, K. and Griem, M.L. 1984. Radiosensitivity of vascular tissue. I. Differential radiosensitivity of capillaries: A quantitative in vivo study. *Radiation Research*. **99**(3).
- Donnelly, E.F., Geng, L., Wojcicki, W.E., Fleischer, A.C. and Hallahan, D.E. 2001. Quantified power doppler US of tumor blood flow correlates with microscopic quantification of tumor blood vessels. *Radiology*. **219**(1).
- Dvorak, H.F. 2015. Tumors: Wounds that do not heal-redux. *Cancer Immunology Research*. **3**(1).
- E. Benson, C. and Southgate, L. 2021. The DOCK protein family in vascular development and disease. *Angiogenesis*. (0123456789).
- Eckerich, C., Zapf, S., Fillbrandt, R., Loges, S., Westphal, M. and Lamszus, K. 2007. Hypoxia can induce c-Met expression in glioma cells and enhance SF/HGF-induced cell migration. *International Journal of Cancer*. **121**(2).
- Etienne-Manneville, S. and Hall, A. 2002. Rho GTPases in cell biology. *Nature*. **420**(6916).
- Evans, S.M., Judy, K.D., Dunphy, I., Timothy Jenkins, W., Hwang, W.T., Nelson, P.T., Lustig, R.A., Jenkins, K., Magarelli, D.P., Hahn, S.M., Collins, R.A.,

- Grady, S. and Koch, C.J. 2004. Hypoxia is important in the biology and aggression of human glial brain tumors. *Clinical Cancer Research*. **10**(24).
- F.J. II, W., Lämmle, M., Anatelli, F., Lennerz, J. and Perry, A. 2006. Neuropathology for the Neuroradiologist: Palisades and Pseudopalisades. *Pathology Review*. **27**(1), pp.2037–2041.
- Felsberg, J., Thon, N., Eigenbrod, S., Hentschel, B., Sabel, M.C., Westphal, M., Schackert, G., Kreth, F.W., Pietsch, T., Löffler, M., Weller, M., Reifenberger, G. and Tonn, J.C. 2011. Promoter methylation and expression of MGMT and the DNA mismatch repair genes MLH1, MSH2, MSH6 and PMS2 in paired primary and recurrent glioblastomas. *International Journal of Cancer*. **129**(3), pp.659–670.
- Ferland-McCollough, D., Slater, S., Richard, J., Reni, C. and Mangialardi, G. 2017. Pericytes, an overlooked player in vascular pathobiology. *Pharmacology and Therapeutics*. **171**.
- Ferrara, N., Carver-Moore, K., Chen, H., Dowd, M., Lu, L., O'Shea, K.S., Powell-Braxton, L., Hillan, K.J. and Moore, M.W. 1996. Heterozygous embryonic lethality induced by targeted inactivation of the VEGF gene. *Nature*. **380**(6573).
- Finger, E.C. and Giaccia, A.J. 2010. Hypoxia, inflammation, and the tumor microenvironment in metastatic disease. *Cancer and Metastasis Reviews*. **29**(2), pp.285–293.
- Flynn, J.R., Wang, L., Gillespie, D.L., Stoddard, G.J., Reid, J.K., Owens, J., Ellsworth, G.B., Salzman, K.L., Kinney, A.Y. and Jensen, R.L. 2008. Hypoxia-regulated protein expression, patient characteristics, and preoperative imaging as predictors of survival in adults with glioblastoma multiforme. *Cancer*. **113**(5).
- Folberg, R., Hendrix, M.J.C. and J., A.M. 2000. Vasculogenic mimicry and tumor angiogenesis. *American Journal of Pathology*. **156**(2), pp.361–381.
- Folkens, C., Shaked, Y., Man, S., Tang, T., Lee, C.R., Zhu, Z., Hoffman, R.M. and Kerbel, R.S. 2009. Glioma tumor stem-like cells promote tumor angiogenesis and vasculogenesis via vascular endothelial growth factor and stromal-derived factor 1. *Cancer Research*. **69**(18).

- Forsythe, J.A., Jiang, B.H., Iyer, N. V, Agani, F., Leung, S.W., Koos, R.D. and Semenza, G.L. 1996. Activation of vascular endothelial growth factor gene transcription by hypoxia-inducible factor 1. *Molecular and Cellular Biology*. **16**(9).
- Gadea, G. and Blangy, A. 2014. Dock-family exchange factors in cell migration and disease. *European Journal of Cell Biology*. **93**(10–12), pp.466–477.
- Garcia-Barros, M., Paris, F., Cordon-Cardo, C., Lyden, D., Rafii, S., Haimovitz-Friedman, A., Fuks, Z. and Kolesnick, R. 2003. Tumor response to radiotherapy regulated by endothelial cell apoptosis. *Science*. **300**(5622).
- Gerhardt, H. and Betsholtz, C. 2003. Endothelial-pericyte interactions in angiogenesis. *Cell and Tissue Research*. **314**(1), pp.15–23.
- Gerstner, E.R., Emblem, K.E., Chang, K., Vakulenko-Lagun, B., Yen, Y.F., Beers, A.L., Dietrich, J., Plotkin, S.R., Catana, C., Hooker, J.M., Duda, D.G., Rosen, B., Kalpathy-Cramer, J., Jain, R.K. and Batchelor, T. 2020. Bevacizumab reduces permeability and concurrent temozolomide delivery in a subset of patients with recurrent glioblastoma. *Clinical Cancer Research*. **26**(1).
- Gilbert, M.R., Dignam, J.J., Armstrong, T.S., Wefel, J.S., Blumenthal, D.T., Vogelbaum, M.A., Colman, H., Chakravarti, A., Pugh, S., Won, M., Jeraj, R., Brown, P.D., Jaeckle, K.A., Schiff, D., Stieber, V.W., Brachman, D.G., Werner-Wasik, M., Tremont-Lukats, I.W., Sulman, E.P., Aldape, K.D., Curran, W.J. and Mehta, M.P. 2014. A Randomized Trial of Bevacizumab for Newly Diagnosed Glioblastoma. *New England Journal of Medicine*. **370**(8), pp.699–708.
- Goldstein, G.W. 1988. Endothelial Cell-Astrocyte Interactions: A Cellular Model of the Blood-Brain Barrier. *Annals of the New York Academy of Sciences*. **529**(1).
- Van Golen, K.L., Wu, Z.F., Qiao, X.T., Bao, L.W. and Merajver, S.D. 2000. RhoC GTPase overexpression modulates induction of angiogenic factors in breast cells. *Neoplasia*. **2**(5).
- Graeber, M.B., Scheithauer, B.W. and Kreutzberg, G.W. 2002. Microglia in brain tumors. *GLIA*. **40**(2).
- Greenberger, L.M., Horak, I.D., Filpula, D., Sapra, P., Westergaard, M.,

- Frydenlund, H.F., Albæk, C., Schrøder, H. and Ørum, H. 2008. A RNA antagonist of hypoxia-inducible factor-1 $\alpha$ , EZN-2968, inhibits tumor cell growth. *Molecular Cancer Therapeutics*. **7**(11).
- Greenfield, J.P., Cobb, W.S. and Lyden, D. 2010. Resisting arrest: A switch from angiogenesis to vasculogenesis in recurrent malignant gliomas. *Journal of Clinical Investigation*. **120**(3), pp.663–667.
- Griffioen, A.W. 1997. Phenotype of the tumor vasculature; cell adhesion as a target for tumor therapy. *Cancer Journal*. **10**(5).
- Griveau, A., Seano, G., Shelton, S.J., Kupp, R., Jahangiri, A., Obernier, K., Krishnan, S., Lindberg, O.R., Yuen, T.J., Tien, A.C., Sabo, J.K., Wang, N., Chen, I., Kloepper, J., Larrouquere, L., Ghosh, M., Tirosh, I., Huillard, E., Alvarez-Buylla, A., Oldham, M.C., Persson, A.I., Weiss, W.A., Batchelor, T.T., Stemmer-Rachamimov, A., Suvà, M.L., Phillips, J.J., Aghi, M.K., Mehta, S., Jain, R.K. and Rowitch, D.H. 2018. A Glial Signature and Wnt7 Signaling Regulate Glioma-Vascular Interactions and Tumor Microenvironment. *Cancer Cell*. **33**(5), pp.874-889.e7.
- De Groot, J.F., Fuller, G., Kumar, A.J., Piao, Y., Eterovic, K., Ji, Y. and Conrad, C.A. 2010. Tumor invasion after treatment of glioblastoma with bevacizumab: Radiographic and pathologic correlation in humans and mice. *Neuro-Oncology*. **12**(3).
- Guo, D., Peng, Y., Wang, L., Sun, X., Wang, X., Liang, C., Yang, X., Li, S., Xu, J., Ye, W.-C., Jiang, B. and Shi, L. 2021. Autism-like social deficit generated by Dock4 deficiency is rescued by restoration of Rac1 activity and NMDA receptor function. *Molecular Psychiatry*. **26**(5), pp.1505–1519.
- Gupta, K. and Burns, T.C. 2018. Radiation-induced alterations in the recurrent glioblastoma microenvironment: Therapeutic implications. *Frontiers in Oncology*. **8**(NOV), pp.1–11.
- Gutin, P.H., Iwamoto, F.M., Beal, K., Mohile, N.A., Karimi, S., Hou, B.L., Lymberis, S., Yamada, Y., Chang, J. and Abrey, L.E. 2009. Safety and Efficacy of Bevacizumab With Hypofractionated Stereotactic Irradiation for Recurrent Malignant Gliomas. *International Journal of Radiation Oncology Biology Physics*. **75**(1).
- Gzell, C., Back, M., Wheeler, H., Bailey, D. and Foote, M. 2017. Radiotherapy in

- Glioblastoma: the Past, the Present and the Future. *Clinical Oncology*. **29**(1).
- Haddad, A.F., Young, J.S., Amara, D., Berger, M.S., Raleigh, D.R., Aghi, M.K. and Butowski, N.A. 2021. Mouse models of glioblastoma for the evaluation of novel therapeutic strategies. *Neuro-Oncology Advances*. **3**(1).
- Hagemann, T., Biswas, S.K., Lawrence, T., Sica, A. and Lewis, C.E. 2009. Regulation of macrophage function in tumors: The multifaceted role of NF- $\kappa$ B. *Blood*. **113**(14).
- Hambardzumyan, D. and Bergers, G. 2015. Glioblastoma: Defining Tumor Niches. *Trends in Cancer*. **1**(4), pp.252–265.
- Hambardzumyan, D., Gutmann, D.H. and Kettenmann, H. 2015. The role of microglia and macrophages in glioma maintenance and progression. *Nature Neuroscience*. **19**(1).
- Hardee, M.E. and Zagzag, D. 2012. Mechanisms of glioma-associated neovascularization. *American Journal of Pathology*. **181**(4), pp.1126–1141.
- Harrigan, M.R., Ole-Schmidt, N., Black, P.M.L., Laurans, M., Gunel, M., Rutka, J.T. and Parsa, A.T. 2003. Angiogenic factors in the central nervous system. *Neurosurgery*. **53**(3).
- Hayashi, M., Sakata, M., Takeda, T., Yamamoto, T., Okamoto, Y., Sawada, K., Kimura, A., Minekawa, R., Tahara, M., Tasaka, K. and Murata, Y. 2004. Induction of glucose transporter 1 expression through hypoxia-inducible factor 1 $\alpha$  under hypoxic conditions in trophoblast-derived cells. *Journal of Endocrinology*. **183**(1).
- Heckmann, M., Douwes, K., Peter, R. and Degitz, K. 1998. Vascular activation of adhesion molecule mRNA and cell surface expression by ionizing radiation. *Experimental Cell Research*. **238**(1).
- Hegi, M.E., Diserens, A.-C., Gorlia, T., Hamou, M.-F., de Tribolet, N., Weller, M., Kros, J.M., Hainfellner, J.A., Mason, W., Mariani, L., Bromberg, J.E.C., Hau, P., Mirimanoff, R.O., Cairncross, J.G., Janzer, R.C. and Stupp, R. 2005. MGMT Gene Silencing and Benefit from Temozolomide in Glioblastoma. *New England Journal of Medicine*. **352**(10), pp.997–1003.
- Hellström, M., Phng, L.-K., Hofmann, J.J., Wallgard, E., Coultas, L., Lindblom, P., Alva, J., Nilsson, A.-K., Karlsson, L., Gaiano, N., Yoon, K., Rossant, J.,

- Iruela-Arispe, M.L., Kalén, M., Gerhardt, H. and Betsholtz, C. 2007. Dll4 signalling through Notch1 regulates formation of tip cells during angiogenesis. *Nature*. **445**(7129), pp.776–780.
- Helseth, R., Helseth, E., Johannesen, T.B., Langberg, C.W., Lote, K., Rønning, P., Scheie, D., Vik, A. and Meling, T.R. 2010. Overall survival, prognostic factors, and repeated surgery in a consecutive series of 516 patients with glioblastoma multiforme. *Acta Neurologica Scandinavica*. **122**(3).
- Hendrix, M.J.C., Seftor, E.A., Hess, A.R. and Seftor, R.E.B. 2003. Vasculogenic mimicry and tumour-cell plasticity: Lessons from melanoma. *Nature Reviews Cancer*. **3**(6).
- Herbert, S.P. and Stainier, D.Y.R. 2012. Molecular control of endothelial cell behaviour during blood. *Nat Rev Molecular Cell Biology*. **12**(9), pp.551–564.
- Hicks, W.H., Bird, C.E., Traylor, J.I., Shi, D.D., El Ahmadi, T.Y., Richardson, T.E., McBrayer, S.K. and Abdullah, K.G. 2021. Contemporary Mouse Models in Glioma Research. *Cells*. **10**(3), pp.1–18.
- Hiramoto, K., Negishi, M. and Katoh, H. 2006. Dock4 is regulated by RhoG and promotes Rac-dependent cell migration. *Experimental Cell Research*. **312**(20), pp.4205–4216.
- Hobbs, S.K., Monsky, W.L., Yuan, F., Roberts, W.G., Griffith, L., Torchilin, V.P. and Jain, R.K. 1998. Regulation of transport pathways in tumor vessels: Role of tumor type and microenvironment. *Proceedings of the National Academy of Sciences of the United States of America*. **95**(8).
- Holash, J., Maisonpierre, P.C., Compton, D., Boland, P., Alexander, C.R., Zagzag, D., Yancopoulos, G.D. and Wiegand, S.J. 1999. Vessel cooption, regression, and growth in tumors mediated by angiopoietins and VEGF. *Science*.
- Holland, E.C., Celestino, J., Dai, C., Schaefer, L., Sawaya, R.E. and Fuller, G.N. 2000. Combined activation of Ras and Akt in neural progenitors induces glioblastoma formation in mice. *Nature Genetics*. **25**(1).
- Hoskin, P.J., Sibtain, A., Daley, F.M. and Wilson, G.D. 2003. GLUT1 and CAIX as intrinsic markers of hypoxia in bladder cancer: Relationship with vascularity and proliferation as predictors of outcome of ARCON. *British*

*Journal of Cancer*. **89**(7).

- Hovinga, K.E., Stalpers, L.J.A., van Bree, C., Donker, M., Verhoeff, J.J.C., Rodermond, H.M., Bosch, D.A. and van Furth, W.R. 2005. Radiation-enhanced vascular endothelial growth factor (VEGF) secretion in glioblastoma multiforme cell lines - A clue to radioresistance? *Journal of Neuro-Oncology*. **74**(2).
- Hovingaa, K.E., Shimizua, F., Wanga, R., Panagiotakosc, G., Heijdena, M. Van Der and Moaye, H. 2010. Inhibition of Notch Signaling in Glioblastoma Targets Cancer Stem Cells via an Endothelial Cell Intermediate. *Stem Cells*. **28**(6), pp.1019–1029.
- Huang, Z., Cheng, L., Guryanova, O.A., Wu, Q. and Bao, S. 2010. Cancer stem cells in glioblastoma-molecular signaling and therapeutic targeting. *Protein and Cell*. **1**(7).
- Huh, W.J., Khurana, S.S., Geahlen, J.H., Kohli, K., Waller, R.A. and Mills, J.C. 2012. Tamoxifen induces rapid, reversible atrophy, and metaplasia in mouse stomach. *Gastroenterology*. **142**(1).
- Huh, W.J., Mysorekar, I.U. and Mills, J.C. 2010. Inducible activation of Cre recombinase in adult mice causes gastric epithelial atrophy, metaplasia, and regenerative changes in the absence of 'floxed' alleles. *American Journal of Physiology - Gastrointestinal and Liver Physiology*. **299**(2).
- Ignatova, T.N., Kukekov, V.G., Laywell, E.D., Suslov, O.N., Vrionis, F.D. and Steindler, D.A. 2002. Human cortical glial tumors contain neural stem-like cells expressing astroglial and neuronal markers in vitro. *GLIA*. **39**(3).
- Ikeda, H. and Kakeya, H. 2021. Targeting hypoxia-inducible factor 1 (HIF-1) signaling with natural products toward cancer chemotherapy. *Journal of Antibiotics*. **74**(10), pp.687–695.
- Irtenkauf, S.M., Sobiechowski, S., Hasselbach, L.A., Nelson, K.K., Transou, A.D., Carlton, E.T., Mikkelsen, T. and deCarvalho, A.C. 2017. Optimization of Glioblastoma Mouse Orthotopic Xenograft Models for Translational Research. *Comparative medicine*. **67**(4), pp.300–314.
- Iruela-Arispe, M.L. and Davis, G.E. 2009. Cellular and Molecular Mechanisms of Vascular Lumen Formation. *Developmental Cell*. **16**(2), pp.222–231.

- Iwamoto, F.M., Abrey, L.E., Beal, K., Gutin, P.H., Rosenblum, M.K., Reuter, V.E., Deangelis, L.M. and Lassman, A.B. 2009. Patterns of relapse and prognosis after bevacizumab failure in recurrent glioblastoma. *Neurology*. **73**(15).
- Jaffe, A.B. and Hall, A. 2005. Rho GTPases: Biochemistry and biology. *Annual Review of Cell and Developmental Biology*. **21**.
- Jaillet, C., Morelle, W., Slomianny, M.C., Paget, V., Tarlet, G., Buard, V., Selbonne, S., Caffin, F., Rannou, E., Martinez, P., François, A., Foulquier, F., Allain, F., Milliat, F. and Guipaud, O. 2017. Radiation-induced changes in the glycome of endothelial cells with functional consequences. *Scientific Reports*. **7**(1).
- Jain, R.K. 2014. Antiangiogenesis Strategies Revisited: From Starving Tumors to Alleviating Hypoxia. *Cancer Cell*.
- Jain, R.K. 1994. Barriers to drug delivery in solid tumors. *Scientific American*. **271**(1).
- Jain, R.K. 2003. Molecular regulation of vessel maturation. *Nature Medicine*.
- Jain, R.K. 2001. Normalizing tumor vasculature with anti-angiogenic therapy: a new paradigm for combination therapy. *Nature medicine*. **7**(9), pp.987–989.
- Jain, R.K., Duda, D.G., Clark, J.W. and Loeffler, J.S. 2006. Lessons from phase III clinical trials on anti-VEGF therapy for cancer. *Nature Clinical Practice Oncology*. **3**(1).
- Jain, R.K., Tomaso, E., Duda, D.G., Loeffler, J.S., Sorensen, A.G. and Batchelor, T.T. 2007. Angiogenesis in brain tumours. *Nature Reviews Clinical Oncology*. **8**(August), pp.610–622.
- Januel, E., Ursu, R., Alkhafaji, A., Marantidou, A., Doridam, J., Belin, C., Levy-Piedbois, C. and Carpentier, A.F. 2015. Impact of renin-angiotensin system blockade on clinical outcome in glioblastoma. *European Journal of Neurology*. **22**(9).
- Joo, K.M., Kim, J., Jin, J., Kim, M., Seol, H.J., Muradov, J., Yang, H., Choi, Y. La, Park, W.Y., Kong, D.S., Lee, Jung Il, Ko, Y.H., Woo, H.G., Lee, Jeongwu, Kim, S. and Nam, D.H. 2013. Patient-Specific Orthotopic Glioblastoma Xenograft Models Recapitulate the Histopathology and Biology of Human Glioblastomas In Situ. *Cell Reports*. **3**(1).
- Kabacik, S. and Raj, K. 2017. Ionising radiation increases permeability of

endothelium through ADAM10-mediated cleavage of VE-cadherin. *Oncotarget*. **8**(47).

El Kaffas, A., Giles, A. and Czarnota, G.J. 2013. Dose-dependent response of tumor vasculature to radiation therapy in combination with Sunitinib depicted by three-dimensional high-frequency power Doppler ultrasound. *Angiogenesis*. **16**(2).

Kalra, A. and Tuma, F. 2018. *Physiology, Liver*.

Kang, H., Davis-Dusenbery, B.N., Nguyen, P.H., Lal, A., Lieberman, J., Van Aelst, L., Lagna, G. and Hata, A. 2012. Bone morphogenetic protein 4 promotes vascular smooth muscle contractility by activating microRNA-21 (miR-21), which down-regulates expression of family of dedicator of cytokinesis (DOCK) proteins. *The Journal of biological chemistry*. **287**(6), pp.3976–86.

Kang, M.K., Hur, B.I., Ko, M.H., Kim, C.H., Cha, S.H. and Kang, S.K. 2008. Potential identity of multi-potential cancer stem-like subpopulation after radiation of cultured brain glioma. *BMC neuroscience*. **9**.

Karam, S.D. and Bhatia, S. 2015. The radiobiological targets of SBRT: Tumor cells or endothelial cells? *Annals of Translational Medicine*. **3**(19).

Karlsson, R., Pedersen, E.D., Wang, Z. and Brakebusch, C. 2009. Rho GTPase function in tumorigenesis. *Biochimica et Biophysica Acta - Reviews on Cancer*. **1796**(2), pp.91–98.

Katz, A.M., Amankulor, N.M., Pitter, K., Helmy, K., Squatrito, M. and Holland, E.C. 2012. Astrocyte-specific expression patterns associated with the PDGF-induced glioma microenvironment. *PLoS ONE*. **7**(2).

Kaur, B., Khwaja, F.W., Severson, E.A., Matheny, S.L., Brat, D.J. and Van Meir, E.G. 2005. Hypoxia and the hypoxia-inducible-factor pathway in glioma growth and angiogenesis. *Neuro-Oncology*. **7**(2).

Kerstetter-Fogle, A.E., Harris, P.L.R., Brady-Kalnay, S.M. and Sloan, A.E. 2020. Generation of glioblastoma patient-derived intracranial xenografts for preclinical studies. *International Journal of Molecular Sciences*. **21**(14).

Keskin, D., Kim, J., Cooke, V.G., Wu, C.C., Sugimoto, H., Gu, C., De Palma, M., Kalluri, R. and LeBleu, V.S. 2015. Targeting Vascular Pericytes in Hypoxic

- Tumors Increases Lung Metastasis via Angiopoietin-2. *Cell Reports*. **10**(7).
- Keunen, O., Johansson, M., Oudin, A., Sanzey, M., Rahim, S.A.A., Fack, F., Thorsen, F., Taxt, T., Bartos, M., Jirik, R., Miletic, H., Wang, J., Stieber, D., Stuhr, L., Moen, I., Rygh, C.B., Bjerkvig, R. and Niclou, S.P. 2011. Anti-VEGF treatment reduces blood supply and increases tumor cell invasion in glioblastoma. *Proceedings of the National Academy of Sciences of the United States of America*. **108**(9), pp.3749–3754.
- Kil, W.J., Tofilon, P.J. and Camphausen, K. 2012. Post-radiation increase in VEGF enhances glioma cell motility in vitro. *Radiation Oncology*. **7**(1).
- Kim, J., Lee, I.H., Cho, H.J., Park, C.K., Jung, Y.S., Kim, Y., Nam, S.H., Kim, B.S., Johnson, M.D., Kong, D.S., Seol, H.J., Lee, Jung Il, Joo, K.M., Yoon, Y., Park, W.Y., Lee, Jeongwu, Park, P.J. and Nam, D.H. 2015. Spatiotemporal Evolution of the Primary Glioblastoma Genome. *Cancer Cell*. **28**(3), pp.318–328.
- Kim, R.K., Suh, Y., Cui, Y.H., Hwang, E., Lim, E.J., Yoo, K.C., Lee, G.H., Yi, J.M., Kang, S.G. and Lee, S.J. 2013. Fractionated radiation-induced nitric oxide promotes expansion of glioma stem-like cells. *Cancer Science*. **104**(9).
- Kioi, M., Vogel, H., Schultz, G., Hoffman, R.M., Harsh, G.R. and Brown, J.M. 2010. Inhibition of vasculogenesis, but not angiogenesis, prevents the recurrence of glioblastoma after irradiation in mice. *The Journal of Clinical Investigation*. **120**(3), pp.694–705.
- Kjeldsen, E. and Veigaard, C. 2013. DOCK4 deletion at 7q31.1 in a de novo acute myeloid leukemia with a normal karyotype. *Cellular Oncology*. **36**(5), pp.395–403.
- Kobayashi, H., Reijnders, K., English, S., Yordanov, A.T., Milenic, D.E., Sowers, A.L., Citrin, D., Krishna, M.C., Waldmann, T.A., Mitchell, J.B. and Brechbiel, M.W. 2004. Application of a macromolecular contrast agent for detection of alterations of tumor vessel permeability induced by radiation. *Clinical Cancer Research*. **10**(22).
- Kobayashi, M., Harada, K., Negishi, M. and Katoh, H. 2014. Dock4 forms a complex with SH3YL1 and regulates cancer cell migration. *Cellular signalling*. **26**(5), pp.1082–8.

- Komohara, Y., Ohnishi, K., Kuratsu, J. and Takeya, M. 2008. Possible involvement of the M2 anti-inflammatory macrophage phenotype in growth of human gliomas. *Journal of Pathology*. **216**(1).
- Kong, D.S., Lee, J. II, Park, K., Jong, H.K., Lim, D.H. and Nam, D.H. 2008. Efficacy of stereotactic radiosurgery as a salvage treatment for recurrent malignant gliomas. *Cancer*. **112**(9).
- Kostianovsky, A.M., Maier, L.M., Anderson, R.C., Bruce, J.N. and Anderson, D.E. 2008. Astrocytic Regulation of Human Monocytic/Microglial Activation. *The Journal of Immunology*. **181**(8).
- Kouam, P.N., Rezniczek, G.A., Adamietz, I.A. and Bühler, H. 2019. Ionizing radiation increases the endothelial permeability and the transendothelial migration of tumor cells through ADAM10-activation and subsequent degradation of VE-cadherin. *BMC Cancer*. **19**(1).
- Kozin, S. V., Duda, D.G., Munn, L.L. and Jain, R.K. 2011. Is vasculogenesis crucial for the regrowth of irradiated tumours? *Nature Reviews Cancer*. **11**(7), p.532.
- Kozin, S. V., Duda, D.G., Munn, L.L. and Jain, R.K. 2012. Neovascularization after irradiation: What is the source of newly formed vessels in recurring tumors? *Journal of the National Cancer Institute*. **104**(12), pp.899–905.
- Kozma, R., Ahmed, S., Best, A. and Lim, L. 1995. The Ras-related protein Cdc42Hs and bradykinin promote formation of peripheral actin microspikes and filopodia in Swiss 3T3 fibroblasts. *Molecular and Cellular Biology*. **15**(4).
- Krueger, M. and Bechmann, I. 2010. CNS pericytes: Concepts, misconceptions, and a way out. *Glia*. **58**(1), pp.1–10.
- Krusche, B., Ottone, C., Clements, M.P., Johnstone, E.R., Goetsch, K., Lieven, H., Mota, S.G., Singh, P., Khadayate, S., Ashraf, A., Davies, T., Pollard, S.M., De Paola, V., Roncaroli, F., Martinez-Torrecuadrada, J., Bertone, P. and Parrinello, S. 2016. EphrinB2 drives perivascular invasion and proliferation of glioblastoma stem-like cells. *eLife*. **5**, pp.1–32.
- Kubitza, M., Hickey, L. and Roberts, W.G. 1999. Influence of host microvascular environment on tumour vascular endothelium. *International Journal of Experimental Pathology*. **80**(1).

- Kuczynski, E.A., Vermeulen, P.B., Pezzella, F., Kerbel, R.S. and Reynolds, A.R. 2019. Vessel co-option in cancer. *Nature Reviews Clinical Oncology*. **16**(8), pp.469–493.
- Kunkel, P., Ulbricht, U., Bohlen, P., Brockmann, M.A., Fillbrandt, R., Stavrou, D., Westphal, M. and Lamszus, K. 2001. Inhibition of glioma angiogenesis and growth in Vivo by systemic treatment with a monoclonal antibody against vascular endothelial growth factor receptor-2. *Cancer Research*. **61**(18).
- Kuo, K.-T., Guan, B., Feng, Y., Mao, T.-L., Chen, X., Jinawath, N., Wang, Y., Kurman, R.J., Shih, I.-M. and Wang, T.-L. 2009. Analysis of DNA Copy Number Alterations in Ovarian Serous Tumors Identifies New Molecular Genetic Changes in Low-Grade and High-Grade Carcinomas. *Cancer Research*. **69**(9), pp.4036–4042.
- Landry, A.P., Balas, M., Alli, S., Spears, J. and Zador, Z. 2020. Distinct regional ontogeny and activation of tumor associated macrophages in human glioblastoma. *Scientific Reports*. **10**(1), p.19542.
- Langley, R.E., Bump, E.A., Quartuccio, S.G., Medeiros, D. and Braunhut, S.J. 1997. Radiation-induced apoptosis in microvascular endothelial cells. *British Journal of Cancer*. **75**(5).
- Langley, R.R. and Fidler, I.J. 2011. The seed and soil hypothesis revisited-The role of tumor-stroma interactions in metastasis to different organs. *International Journal of Cancer*. **128**(11).
- Larcher, F., Murillas, R., Bolontrade, M., Conti, C.J. and Jorcano, J.L. 1998. VEGF/VPF overexpression in skin of transgenic mice induces angiogenesis, vascular hyperpermeability and accelerated tumor development. *Oncogene*. **17**(3).
- Lechertier, T., Reynolds, L.E., Kim, H., Pedrosa, A.R., Gómez-Escudero, J., Muñoz-Félix, J.M., Batista, S., Dukinfield, M., Demircioglu, F., Wong, P.P., Matchett, K.P., Henderson, N.C., D’Amico, G., Parsons, M., Harwood, C., Meier, P. and Hodivala-Dilke, K.M. 2020. Pericyte FAK negatively regulates Gas6/Axl signalling to suppress tumour angiogenesis and tumour growth. *Nature Communications*. **11**(1), pp.1–14.
- Lee, H.S., Han, J., Bai, H.J. and Kim, K.W. 2009. Brain angiogenesis in developmental and pathological processes: Regulation, molecular and

cellular communication at the neurovascular interface. *FEBS Journal*. **276**(17), pp.4622–4635.

Lee, J., Kotliarova, S., Kotliarov, Y., Li, A., Su, Q., Donin, N.M., Pastorino, S., Purow, B.W., Christopher, N., Zhang, W., Park, J.K. and Fine, H.A. 2006. Tumor stem cells derived from glioblastomas cultured in bFGF and EGF more closely mirror the phenotype and genotype of primary tumors than do serum-cultured cell lines. *Cancer Cell*. **9**(5).

Lee, S., Chen, T.T., Barber, C.L., Jordan, M.C., Murdock, J., Desai, S., Ferrara, N., Nagy, A., Roos, K.P. and Iruela-Arispe, M.L. 2007. Autocrine VEGF Signaling Is Required for Vascular Homeostasis. *Cell*. **130**(4), pp.691–703.

Lewis, C.E., De Palma, M. and Naldini, L. 2007. Tie2-Expressing Monocytes and Tumor Angiogenesis: Regulation by Hypoxia and Angiopoietin-2: Figure 1. *Cancer Research*. **67**(18), pp.8429–8432.

Li, C., Menoret, A., Farragher, C., Ouyang, Z., Bonin, C., Holvoet, P., Vella, A.T. and Zhou, B. 2019. Single-cell transcriptomics-based MacSpectrum reveals macrophage activation signatures in diseases. *JCI Insight*. **4**(10).

Li, H.F., Kim, J.S. and Waldman, T. 2009. Radiation-induced Akt activation modulates radioresistance in human glioblastoma cells. *Radiation Oncology*. **4**, p.43.

Li, J., Wu, D.M., Han, R., Deng, Y.Y.S.H., Liu, T., Zhang, T. and Xu, Y. 2020. Low-dose radiation promotes invasion and migration of a549 cells by activating the cxcl1/ nf-kb signaling pathway. *Oncotargets and Therapy*. **13**.

Li, W. and Graeber, M.B. 2012. The molecular profile of microglia under the influence of glioma. *Neuro-Oncology*. **14**(8).

Li, Z., Bao, S., Wu, Q., Wang, H., Eyler, C., Sathornsumetee, S., Shi, Q., Cao, Y., Lathia, J., McLendon, R.E., Hjelmeland, A.B. and Rich, J.N. 2009. Hypoxia-Inducible Factors Regulate Tumorigenic Capacity of Glioma Stem Cells. *Cancer Cell*. **15**(6).

Liebner, S., Fischmann, A., Rascher, G., Duffner, F., Grote, E.H., Kalbacher, H. and Wolburg, H. 2000. Claudin-1 and claudin-5 expression and tight junction morphology are altered in blood vessels of human glioblastoma multiforme. *Acta Neuropathologica*. **100**(3).

- Liu, G., Yuan, X., Zeng, Z., Tunici, P., Ng, H., Abdulkadir, I.R., Lu, L., Irvin, D., Black, K.L. and Yu, J.S. 2006. Analysis of gene expression and chemoresistance of CD133+ cancer stem cells in glioblastoma. *Molecular Cancer*. **5**.
- Liu, Q., Nguyen, D.H., Dong, Q., Shitaku, P., Chung, K., Liu, O.Y., Tso, J.L., Liu, J.Y., Konkankit, V., Cloughesy, T.F., Mischel, P.S., Lane, T.F., Liao, L.M., Nelson, S.F. and Tso, C.L. 2009. Molecular properties of CD133+ glioblastoma stem cells derived from treatment-refractory recurrent brain tumors. *Journal of Neuro-Oncology*. **94**(1).
- Liu, S.C., Alomran, R., Chernikova, S.B., Lartey, F., Stafford, J., Jang, T., Merchant, M., Zboralski, D., Zöllner, S., Kruschinski, A., Klussmann, S., Recht, L. and Brown, J.M. 2014. Blockade of SDF-1 after irradiation inhibits tumor recurrences of autochthonous brain tumors in rats. *Neuro-Oncology*. **16**(1).
- Liu, Y., Cox, S.R., Morita, T. and Kourembanas, S. 1995. Hypoxia regulates vascular endothelial growth factor gene expression in endothelial cells: Identification of a 5' enhancer. *Circulation Research*. **77**(3).
- Liu, Y., Li, Y. ming, Tian, R. feng, Liu, W. ping, Fei, Z., Long, Q. fa, Wang, X. an and Zhang, X. 2009. The expression and significance of HIF-1 $\alpha$  and GLUT-3 in glioma. *Brain Research*. **1304**.
- Lorger, M., Krueger, J.S., O'Neal, M., Staffin, K. and Felding-Habermann, B. 2009. Activation of tumor cell integrin  $\alpha\beta 3$  controls angiogenesis and metastatic growth in the brain. *Proceedings of the National Academy of Sciences of the United States of America*. **106**(26).
- Louis, D.N., Ohgaki, H., Wiestler, O.D., Cavenee, W.K., Burger, P.C., Jouvett, A., Scheithauer, B.W. and Kleihues, P. 2007. The 2007 WHO classification of tumours of the central nervous system. *Acta Neuropathologica*.
- Louis, D.N., Perry, A., Reifenberger, G., von Deimling, A., Figarella-Branger, D., Cavenee, W.K., Ohgaki, H., Wiestler, O.D., Kleihues, P. and Ellison, D.W. 2016. The 2016 World Health Organization Classification of Tumors of the Central Nervous System: a summary. *Acta Neuropathologica*. **131**(6), pp.803–820.
- Louis, D.N., Perry, A., Wesseling, P., Brat, D.J., Cree, I.A., Figarella-Branger, D.,

- Hawkins, C., Ng, H.K., Pfister, S.M., Reifenberger, G., Soffietti, R., Von Deimling, A. and Ellison, D.W. 2021. The 2021 WHO classification of tumors of the central nervous system: A summary. *Neuro-Oncology*. **23**(8).
- Luo, H. and Shusta, E. V. 2020. Blood–brain barrier modulation to improve glioma drug delivery. *Pharmaceutics*. **12**(11), pp.1–12.
- M.Cameron, J., Bruno, C., Rajan Parachalil, D., J.Baker, M., Bonnier, F., J.Butler, H. and Byrne, H.J. 2020. Chapter 10 - Vibrational spectroscopic analysis and quantification of proteins in human blood plasma and serum *In: Vibrational Spectroscopy in Protein Research* [Online]., pp.269–314. Available from: <https://doi.org/10.1016/B978-0-12-818610-7.00010-4>.
- Mader, S. and Brimberg, L. 2019. Aquaporin-4 Water Channel in the Brain and Its Implication for Health and Disease. *Cells*. **8**(90).
- Maestrini, E., Pagnamenta, A.T., Lamb, J.A., Bacchelli, E., Sykes, N.H., Sousa, I., Toma, C., Barnby, G., Butler, H., Winchester, L., Scerri, T.S., Minopoli, F., Reichert, J., Cai, G., Buxbaum, J.D., Korvatska, O., Schellenberg, G.D., Dawson, G., Bildt, A. de, Minderaa, R.B., Mulder, E.J., Morris, A.P., Bailey, A.J. and Monaco, A.P. 2010. High-density SNP association study and copy number variation analysis of the AUTS1 and AUTS5 loci implicate the IMMP2L–DOCK4 gene region in autism susceptibility. *Molecular Psychiatry*. **15**(9), pp.954–968.
- Mancuso, M.R., Kuhnert, F. and Kuo, C.J. 2008. Developmental Angiogenesis of the Central Nervous System. *Lymphatic Research and Biology*. **6**(3–4), pp.173–180.
- Mandl, E.S., Dirven, C.M.F., Buis, D.R., Postma, T.J. and Vandertop, W.P. 2008. Repeated surgery for glioblastoma multiforme: only in combination with other salvage therapy. *Surgical Neurology*. **69**(5).
- Marucci, G., Fabbri, P. V, Morandi, L., Biase, D. De, Oto, E. Di, Tallini, G., Sturiale, C., Franceschi, E., Frezza, G.P. and Foschini, M.P. 2015. Pathological spectrum in recurrences of glioblastoma multiforme. *Pathologica*. **107**(1), pp.1–8.
- Massagué, J. 2008. TGF $\beta$  in Cancer.pdf. *Cell*. **134**(2), pp.215–230.
- Mathivet, T., Bouleti, C., Van Woensel, M., Stanchi, F., Verschuere, T., Phng, L.,

- Dejaegher, J., Balcer, M., Matsumoto, K., Georgieva, P.B., Belmans, J., Sciot, R., Stockmann, C., Mazzone, M., De Vleeschouwer, S. and Gerhardt, H. 2017. Dynamic stroma reorganization drives blood vessel dysmorphia during glioma growth. *EMBO Molecular Medicine*. **9**(12), pp.1629–1645.
- Mayer, A., Schneider, F., Vaupel, P., Sommer, C. and Schmidberger, H. 2012. Differential expression of HIF-1 in glioblastoma multiforme and anaplastic astrocytoma. *International Journal of Oncology*. **41**(4).
- McCarty, M.F., Baker, C.H., Bucana, C.D. and Fidler, I.J. 2002. Quantitative and qualitative in vivo angiogenesis assay. *International journal of oncology*. **21**(1).
- McDonald, M.W., Shu, H.K.G., Curran, W.J. and Crocker, I.R. 2011. Pattern of failure after limited margin radiotherapy and temozolomide for glioblastoma. *International Journal of Radiation Oncology Biology Physics*. **79**(1).
- Meller, N., Irani-Tehrani, M., Kiosses, W.B., Del Pozo, M.A. and Schwartz, M.A. 2002. Zizimin1, a novel Cdc42 activator, reveals a new GEF domain for Rho proteins. *Nature Cell Biology*. **4**(9).
- Miao, H., Gale, N.W., Guo, H., Qian, J., Petty, A., Kaspar, J., Murphy, A.J., Valenzuela, D.M., Yancopoulos, G., Hambardzumyan, D., Lathia, J.D., Rich, J.N., Lee, J. and Wang, B. 2015. EphA2 promotes infiltrative invasion of glioma stem cells in vivo through cross-talk with Akt and regulates stem cell properties. *Oncogene*. **34**(5), pp.558–567.
- Miebach, S., Grau, S., Hummel, V., Rieckmann, P., Tonn, J.C. and Goldbrunner, R.H. 2006. Isolation and culture of microvascular endothelial cells from gliomas of different WHO grades. *Journal of Neuro-Oncology*. **76**(1).
- Minniti, G., Niyazi, M., Alongi, F., Navarria, P. and Belka, C. 2021. Current status and recent advances in reirradiation of glioblastoma. *Radiation Oncology*. **16**(1), pp.1–14.
- Miquerol, L., Langille, B.L. and Nagy, A. 2000. Embryonic development is disrupted by modest increases in vascular endothelial growth factor gene expression. *Development*. **127**(18).
- Mishra, Prabhaker, Singh, U., Pandey, C., Mishra, Priyadarshni and Pandey, G. 2019. Application of student's t-test, analysis of variance, and covariance.

- Annals of Cardiac Anaesthesia*. **22**(4), p.407.
- Mitra, S., Mironov, O. and Foster, T.H. 2012. Confocal fluorescence imaging enables noninvasive quantitative assessment of host cell populations in vivo following photodynamic therapy. *Theranostics*. **2**(9).
- Mohseni-Meybodi, A., Mozdarani, H. and Mozdarani, S. 2009. DNA damage and repair of leukocytes from Fanconi anaemia patients, carriers and healthy individuals as measured by the alkaline comet assay. *Mutagenesis*. **24**(1).
- Monsky, W.L., Fukumura, D., Gohongi, T., Ancukiewicz, M., Weich, H.A., Torchilin, V.P., Yuan, F. and Jain, R.K. 1999. Augmentation of transvascular transport of macromolecules and nanoparticles in tumors using vascular endothelial growth factor. *Cancer Research*. **59**(16).
- Morantz, R.A., Wood, G.W., Foster, M., Clark, M. and Gollahon, K. 1979. Macrophages in experimental and human brain tumors. Part I. Studies of the macrophage content of experimental rat brain tumors of varying immunogenicity. *Journal of Neurosurgery*. **50**(3).
- Morikawa, S., Baluk, P., Kaidoh, T., Haskell, A., Jain, R.K. and McDonald, D.M. 2002. Abnormalities in pericytes on blood vessels and endothelial sprouts in tumors. *American Journal of Pathology*. **160**(3).
- Mukwaya, A., Jensen, L. and Lagali, N. 2021. Relapse of pathological angiogenesis: functional role of the basement membrane and potential treatment strategies. *Experimental and Molecular Medicine*. **53**(2), pp.189–201.
- Munder, M., Eichmann, K. and Modolell, M. 1998. Alternative metabolic states in murine macrophages reflected by the nitric oxide synthase/arginase balance: competitive regulation by CD4+ T cells correlates with Th1/Th2 phenotype. *Journal of immunology (Baltimore, Md. : 1950)*. **160**(11).
- Murat, A., Migliavacca, E., Gorlia, T., Lambiv, W.L., Shay, T., Hamou, M.F., De Tribolet, N., Regli, L., Wick, W., Kouwenhoven, M.C.M., Hainfellner, J.A., Heppner, F.L., Dietrich, P.Y., Zimmer, Y., Cairncross, J.G., Janzer, R.C., Domany, E., Delorenzi, M., Stupp, R. and Hegi, M.E. 2008. Stem cell-related 'self-renewal' signature and high epidermal growth factor receptor expression associated with resistance to concomitant chemoradiotherapy in glioblastoma. *Journal of Clinical Oncology*. **26**(18).

- Muz, B., de la Puente, P., Azab, F. and Azab, A.K. 2015. The role of hypoxia in cancer progression, angiogenesis, metastasis, and resistance to therapy. *Hypoxia*.
- Nagano, N., Sasaki, H., Aoyagi, M. and Hirakawa, K. 1993. Invasion of experimental rat brain tumor: early morphological changes following microinjection of C6 glioma cells. *Acta Neuropathologica*. **86**(2).
- Nagy, J.A., Chang, S.H., Dvorak, A.M. and Dvorak, H.F. 2009. Why are tumour blood vessels abnormal and why is it important to know? *British Journal of Cancer*. **100**(6).
- Nakada, M., Kita, D., Watanabe, T., Hayashi, Y., Teng, L., Pyko, I. V. and Hamada, J.I. 2011. Aberrant signaling pathways in Glioma. *Cancers*. **3**(3), pp.3242–3278.
- Nakatsu, M.N., Sainson, R.C.A., Pérez-Del-Pulgar, S., Aoto, J.N., Aitkenhead, M., Taylor, K.L., Carpenter, P.M. and Hughes, C.C.W. 2003. VEGF121 and VEGF165 Regulate Blood Vessel Diameter Through Vascular Endothelial Growth Factor Receptor 2 in an in Vitro Angiogenesis Model. *Laboratory Investigation*. **83**(12).
- National Institute of Health 2007. *Phase 2 Study of Panzem Nanocrystal Colloidal Dispersion (NCD) in Combination With Fixed-Dose Temozolomide to Patients With Recurrent Glioblastoma Multiforme (GBM)* [Online]. Available from: <https://clinicaltrials.gov/ct2/show/NCT00481455>.
- Navarro, R., Compte, M., Álvarez-Vallina, L. and Sanz, L. 2016. Immune regulation by pericytes: Modulating innate and adaptive immunity. *Frontiers in Immunology*. **7**(NOV), pp.1–10.
- Navis, A.C., Bourgonje, A., Wesseling, P., Wright, A., Hendriks, W., Verrijp, K., van der Laak, J.A.W.M., Heerschap, A. and Leenders, W.P.J. 2013. Effects of Dual Targeting of Tumor Cells and Stroma in Human Glioblastoma Xenografts with a Tyrosine Kinase Inhibitor against c-MET and VEGFR2. *PLoS ONE*. **8**(3).
- Neri, D. and Bicknell, R. 2005. Tumour vascular targeting. *Nature Reviews Cancer*. **5**(6).
- NICE 2018. *Brain tumours (primary) and brain metastases in adults*.

- Nieder, C., Andratschke, N.H. and Grosu, A.L. 2016. Re-irradiation for recurrent primary brain tumors. *Anticancer Research*. **36**(10).
- Nifterik, K.A. van, Elkhuizen, P.H.M., Andel, R.J. van, Stalpers, L.J.A., Leenstra, S., Lafleur, M.V., Vandertop, W.P., Slotman, B.J., Hulsebos, T.J. and Sminia, P. 2006. Genetic profiling of a distant second glioblastoma multiforme after radiotherapy: recurrence or second primary tumor? *Journal of Neurosurgery*. **105**(5).
- Niyazi, M., Siefert, A., Schwarz, S.B., Ganswindt, U., Kreth, F.W., Tonn, J.C. and Belka, C. 2011. Therapeutic options for recurrent malignant glioma. *Radiotherapy and Oncology*. **98**(1).
- Nobes, C.D. and Hall, A. 1995. Rho, Rac, and Cdc42 GTPases regulate the assembly of multimolecular focal complexes associated with actin stress fibers, lamellipodia, and filopodia. *Cell*. **81**(1).
- Nobusawa, S., Watanabe, T., Kleihues, P. and Ohgaki, H. 2009. IDH1 mutations as molecular signature and predictive factor of secondary glioblastomas. *Clinical Cancer Research*. **15**(19), pp.6002–6007.
- Noorani, I. 2019. Genetically engineered mouse models of gliomas: Technological developments for translational discoveries. *Cancers*. **11**(9).
- O'Brien, C.A., Kreso, A. and Jamieson, C.H.M. 2010. Cancer stem cells and self-renewal. *Clinical cancer research: an official journal of the American Association for Cancer Research*. **16**(12), pp.3113–20.
- O'Brien, E.R., Howarth, C. and Sibson, N.R. 2013. The role of astrocytes in CNS tumors: pre-clinical models and novel imaging approaches. *Frontiers in cellular neuroscience*. **7**, p.40.
- Ohgaki, H. and Kleihues, P. 2013. The definition of primary and secondary glioblastoma. *Clinical Cancer Research*. **19**(4), pp.764–772.
- Olsson, A.K., Dimberg, A., Kreuger, J. and Claesson-Welsh, L. 2006. VEGF receptor signalling - In control of vascular function. *Nature Reviews Molecular Cell Biology*. **7**(5).
- Omuro, A. and DeAngelis, L.M. 2013. Glioblastoma and other malignant gliomas: A clinical review. *JAMA - Journal of the American Medical Association*. **310**(17), pp.1842–1850.

- Orlidge, A. and D'Amore, P.A. 1987. Inhibition of capillary endothelial cell growth by pericytes and smooth muscle cells. *Journal of Cell Biology*. **105**(3).
- Östman, A. and Corvigno, S. 2018. Microvascular Mural Cells in Cancer. *Trends in Cancer*. **4**(12), pp.838–848.
- Pàez-Ribes, M., Allen, E., Hudock, J., Takeda, T., Okuyama, H., Viñals, F., Inoue, M., Bergers, G., Hanahan, D. and Casanovas, O. 2009. Antiangiogenic Therapy Elicits Malignant Progression of Tumors to Increased Local Invasion and Distant Metastasis. *Cancer Cell*. **15**(3).
- Paget, S. 1889. THE DISTRIBUTION OF SECONDARY GROWTHS IN CANCER OF THE BREAST. *The Lancet*. **133**(3421).
- Pagnamenta, A.T., Bacchelli, E., de Jonge, M. V, Mirza, G., Scerri, T.S., Minopoli, F., Chiochetti, A., Ludwig, K.U., Hoffmann, P., Paracchini, S., Lowy, E., Harold, D.H., Chapman, J.A., Klauck, S.M., Poustka, F., Houben, R.H., Staal, W.G., Ophoff, R.A., O'Donovan, M.C., Williams, J., Nöthen, M.M., Schulte-Körne, G., Deloukas, P., Ragoussis, J., Bailey, A.J., Maestrini, E., Monaco, A.P. and International Molecular Genetic Study Of Autism Consortium 2010. Characterization of a family with rare deletions in CNTNAP5 and DOCK4 suggests novel risk loci for autism and dyslexia. *Biological psychiatry*. **68**(4), pp.320–8.
- De Palma, M., Venneri, M.A., Galli, R., Sergi, L.S., Politi, L.S., Sampaolesi, M. and Naldini, L. 2005. Tie2 identifies a hematopoietic lineage of proangiogenic monocytes required for tumor vessel formation and a mesenchymal population of pericyte progenitors. *Cancer Cell*. **8**(3), pp.211–226.
- Papadopoulos, M.C., Saadoun, S., Woodrow, C.J., Davies, D.C., Costa-Martins, P., Moss, R.F., Krishna, S. and Bell, B.A. 2001. Occludin expression in microvessels of neoplastic and non-neoplastic human brain. *Neuropathology and Applied Neurobiology*. **27**(5).
- Park, H.J., Griffin, R.J., Hui, S., Levitt, S.H. and Song, C.W. 2012. Radiation-induced vascular damage in tumors: Implications of vascular damage in ablative hypofractionated radiotherapy (SBRT and SRS). *Radiation Research*. **177**(3), pp.311–327.
- Park, J., Kim, Il-kug, Han, S. and Kim, Injune 2016. Normalization of Tumor

Vessels by Tie2 Activation and Ang2 Inhibition Enhances Drug Delivery and Produces a Favorable Tumor Microenvironment Article Normalization of Tumor Vessels by Tie2 Activation and Ang2 Inhibition Enhances Drug Delivery and Produces . *Cancer Cell*. **30**(6), pp.953–967.

Parsons, D.W., Jones, S., Zhang, X., Lin, J.C.H., Leary, R.J., Angenendt, P., Mankoo, P., Carter, H., Siu, I.M., Gallia, G.L., Olivi, A., McLendon, R., Rasheed, B.A., Keir, S., Nikolskaya, T., Nikolsky, Y., Busam, D.A., Tekleab, H., Diaz, L.A., Hartigan, J., Smith, D.R., Strausberg, R.L., Marie, S.K.N., Shinjo, S.M.O., Yan, H., Riggins, G.J., Bigner, D.D., Karchin, R., Papadopoulos, N., Parmigiani, G., Vogelstein, B., Velculescu, V.E. and Kinzler, K.W. 2008. An integrated genomic analysis of human glioblastoma multiforme. *Science*. **321**(5897), pp.1807–1812.

Pasquale, E.B. 2010. Eph receptors and ephrins in cancer: Bidirectional signalling and beyond. *Nature Reviews Cancer*. **10**(3).

Pekny, M. and Nilsson, M. 2005. Astrocyte activation and reactive gliosis. *Glia*. **50**(4), pp.427–34.

Perry, J.R., Rizek, P., Cashman, R., Morrison, M. and Morrison, T. 2008. Temozolomide rechallenge in recurrent malignant glioma by using a continuous temozolomide schedule: The ‘rescue’ approach. *Cancer*. **113**(8).

Phillips, H.S., Kharbanda, S., Chen, R., Forrest, W.F., Soriano, R.H., Wu, T.D., Misra, A., Nigro, J.M., Colman, H., Soroceanu, L., Williams, P.M., Modrusan, Z., Feuerstein, B.G. and Aldape, K. 2006. Molecular subclasses of high-grade glioma predict prognosis, delineate a pattern of disease progression, and resemble stages in neurogenesis. *Cancer Cell*. **9**(3), pp.157–173.

Phoenix, T.N., Patmore, D.M., Boop, S., Boulos, N., Jacus, M.O., Patel, Y.T., Roussel, M.F., Finkelstein, D., Goumnerova, L., Perreault, S., Wadhwa, E., Cho, Y.J., Stewart, C.F. and Gilbertson, R.J. 2016. Medulloblastoma Genotype Dictates Blood Brain Barrier Phenotype. *Cancer Cell*. **29**(4), pp.508–522.

Potchen, E.J., Kinzie, J., Curtis, C., Siegel, B.A. and Studer, R.K. 1972. Effect of irradiation on tumor microvascular permeability to macromolecules. *Cancer*. **30**(3).

Prager, B.C., Bhargava, S., Mahadev, V., Hubert, C.G. and Rich, J.N. 2020.

- Glioblastoma Stem Cells: Driving Resilience through Chaos. *Trends in Cancer*. **6**(3), pp.223–235.
- Price, S.J. and Gillard, J.H. 2011. Imaging biomarkers of brain tumour margin and tumour invasion. *British Journal of Radiology*. **84**(SPEC. ISSUE 2).
- Pumiglia, K. and Temple, S. 2006. PEDF: Bridging neurovascular interactions in the stem cell niche. *Nature Neuroscience*. **9**(3).
- Pyonteck, S.M., Akkari, L., Schuhmacher, A.J., Bowman, R.L., Sevenich, L., Quail, D.F., Olson, O.C., Quick, M.L., Huse, J.T., Teijeiro, V., Setty, M., Leslie, C.S., Oei, Y., Pedraza, A., Zhang, J., Brennan, C.W., Sutton, J.C., Holland, E.C., Daniel, D. and Joyce, J.A. 2013. CSF-1R inhibition alters macrophage polarization and blocks glioma progression. *Nat Med*. **19**(10), pp.1264–1272.
- Qiang, L., Wu, T., Zhang, H.W., Lu, N., Hu, R., Wang, Y.J., Zhao, L., Chen, F.H., Wang, X.T., You, Q.D. and Guo, Q.L. 2012. HIF-1 $\alpha$  is critical for hypoxia-mediated maintenance of glioblastoma stem cells by activating Notch signaling pathway. *Cell Death and Differentiation*. **19**(2).
- Qin, D.-X., Zheg, R., Tang, J., LI, J.-X. and Hu, Y.-H. 1990. Influence of radiation on the blood-brain barrier and optimum time of chemotherapy. *International Journal of Radiation Oncology Biology Physics*. **19**(June), pp.1507–1510.
- Quail, D.F. and Joyce, J.A. 2013. Microenvironmental regulation of tumor progression and metastasis. *Nature Medicine*. **19**(11), pp.1423–1437.
- Raab, S., Beck, H., Gaumann, A., Yüce, A., Gerber, H.P., Plate, K., Hammes, H.P., Ferrara, N. and Breier, G. 2004. Impaired brain angiogenesis and neuronal apoptosis induced by conditional homozygous inactivation of vascular endothelial growth factor. *Thrombosis and Haemostasis*. **91**(3).
- Racordon, D., Valdivia, A., Mingo, G., Erices, R., Aravena, R., Santoro, F., Bravo, M.L., Ramirez, C., Gonzalez, P., Sandoval, A., González, A., Retamal, C., Kogan, M.J., Kato, S., Cuello, M.A., Osorio, G., Nualart, F., Alvares, P., Gago-Arias, A., Fabri, D., Espinoza, I., Sanchez, B., Corvalán, A.H., Pinto, M.P. and Owen, G.I. 2017. Structural and functional identification of vasculogenic mimicry in vitro. *Scientific Reports*. **7**(1).
- Rak, J., Mitsuhashi, Y., Bayko, L., Filmus, J., Shirasawa, S., Sasazuki, T. and

- Kerbel, R.S. 1995. Mutant ras oncogenes upregulate VEGF/VPF expression: implications for induction and inhibition of tumor angiogenesis. *Cancer research*. **55**(20), pp.4575–80.
- Ramírez-Castillejo, C., Sánchez-Sánchez, F., Andreu-Agulló, C., Ferrón, S.R., Aroca-Aguilar, J.D., Sánchez, P., Mira, H., Escribano, J. and Fariñas, I. 2006. Pigment epithelium-derived factor is a niche signal for neural stem cell renewal. *Nature Neuroscience*. **9**(3).
- Ramsauer, M. and D'Amore, P.A. 2002. Getting Tie(2)d up in angiogenesis. *Journal of Clinical Investigation*. **110**(11).
- Rankin, E.B., Rha, J., Unger, T.L., Wu, C.H., Shutt, H.P., Johnson, R.S., Simon, M.C., Keith, B. and Haase, V.H. 2008. Hypoxia-inducible factor-2 regulates vascular tumorigenesis in mice. *Oncogene*. **27**(40).
- Reddy, K., Damek, D., Gaspar, L.E., Ney, D., Waziri, A., Lillehei, K., Stuhr, K., Kavanagh, B.D. and Chen, C. 2012. Phase II trial of hypofractionated IMRT with temozolomide for patients with newly diagnosed glioblastoma multiforme. *International Journal of Radiation Oncology Biology Physics*. **84**(3).
- Reis, M., Czupalla, C.J., Ziegler, N., Devraj, K., Zinke, J., Seidel, S., Heck, R., Thom, S., Macas, J., Bockamp, E., Fruttiger, M., Taketo, M.M., Dimmeler, S., Plate, K.H. and Liebner, S. 2012. Endothelial Wnt/ $\beta$ -catenin signaling inhibits glioma angiogenesis and normalizes tumor blood vessels by inducing PDGF-B expression. *The Journal of Experimental Medicine*. **209**(9), pp.1611–1627.
- Reiss, Y., Machein, M.R. and Plate, K.H. 2005. The role of angiopoietins during angiogenesis in gliomas. *Brain pathology (Zurich, Switzerland)*. **15**(4), pp.311–7.
- Reiter, L.T., Potocki, L., Chien, S., Gribskov, M. and Bier, E. 2001. A systematic analysis of human disease-associated gene sequences in *Drosophila melanogaster*. *Genome research*. **11**(6), pp.1114–25.
- Ribatti, D., Nico, B., Crivellato, E. and Vacca, A. 2007. Macrophages and tumor angiogenesis. *Leukemia*. **21**(10).
- Ricci-Vitiani, L., Pallini, R., Biffoni, M., Todaro, M., Invernici, G., Cenci, T., Maira,

- G., Parati, E.A., Stassi, G., Larocca, L.M. and De Maria, R. 2010. Tumour vascularization via endothelial differentiation of glioblastoma stem-like cells. *Nature*. **468**(7325), pp.824–828.
- Richmond, A. and Su, Y. 2008. Mouse xenograft models vs GEM models for human cancer therapeutics. *Disease models & mechanisms*. **1**(2–3), pp.78–82.
- Ridley, A.J., Paterson, H.F., Johnston, C.L., Diekmann, D. and Hall, A. 1992. The small GTP-binding protein rac regulates growth factor-induced membrane ruffling. *Cell*. **70**(3).
- Ringel, F., Pape, H., Sabel, M., Krex, D., Bock, H.C., Misch, M., Weyerbrock, A., Westermaier, T., Senft, C., Schucht, P., Meyer, B. and Simon, M. 2016. Clinical benefit from resection of recurrent glioblastomas: Results of a multicenter study including 503 patients with recurrent glioblastomas undergoing surgical resection. *Neuro-Oncology*. **18**(1).
- Risau, W. 1991. Induction of Blood-Brain Barrier Endothelial Cell Differentiation. *Annals of the New York Academy of Sciences*. **633**, pp.405–19.
- Risau, W. 1997. Mechanisms of angiogenesis. *Nature Progress*. **386**, pp.671–674.
- Roberts, T.C., Langer, R. and Wood, M.J.A. 2020. Advances in oligonucleotide drug delivery. *Nature Reviews Drug Discovery*. **19**(10).
- Roberts, W.G., Delaat, J., Nagane, M., Huang, S., Cavenee, W.K. and Palade, G.E. 1998. Host microvasculature influence on tumor vascular morphology and endothelial gene expression. *American Journal of Pathology*. **153**(4).
- Roh-Johnson, M., Bravo-Cordero, J.J., Patsialou, A., Sharma, V.P., Guo, P., Liu, H., Hodgson, L. and Condeelis, J. 2014. Macrophage contact induces RhoA GTPase signaling to trigger tumor cell intravasation. *Oncogene*. **33**(33), pp.4203–4212.
- Rojjani, A.M. and Dorovini-Zis, K. 1996. Glomeruloid vascular structures in glioblastoma multiforme: An immunohistochemical and ultrastructural study. *Journal of Neurosurgery*. **85**(6).
- Rong, Y., Durden, D.L., Van Meir, E.G. and Brat, D.J. 2006. ‘Pseudopalisading’ necrosis in glioblastoma: A familiar morphologic feature that links vascular

- pathology, hypoxia, and angiogenesis. *Journal of Neuropathology and Experimental Neurology*. **65**(6), pp.529–539.
- Rose, S.D. and Aghi, M.K. 2010. Mechanisms of evasion to antiangiogenic therapy in glioblastoma *In: Clinical Neurosurgery*.
- Rossmann, K.L., Der, C.J. and Sondek, J. 2005. GEF means go: turning on RHO GTPases with guanine nucleotide-exchange factors. *Nature Reviews Molecular Cell Biology*. **6**(2), pp.167–180.
- Rubenstein, J.L., Kim, J., Ozawa, T., Zhang, M., Westphal, M., Deen, D.F. and Shuman, M.A. 2000. Anti-VEGF antibody treatment of glioblastoma prolongs survival but results in increased vascular cooption. *Neoplasia*. **2**(4).
- Rubin, P., Gash, D.M., Hansen, J.T., Nelson, D.F. and Williams, J.P. 1994. Disruption of the blood-brain barrier as the primary effect of CNS irradiation. *Radiotherapy and Oncology*. **31**(1).
- Ruhrberg, C., Gerhardt, H., Golding, M., Watson, R., Ioannidou, S., Fujisawa, H., Betsholtz, C. and Shima, D.T. 2002. Spatially restricted patterning cues provided by heparin-binding VEGF-A control blood vessel branching morphogenesis. *Genes and Development*. **16**(20).
- Rycaj, K. and Tang, D.G. 2014. Cancer stem cells and radioresistance. *International Journal of Radiation Biology*. **90**(8).
- Saha, G.B. 2013. *Physics and radiobiology of nuclear medicine*.
- Salmaggi, A., Gelati, M., Pollo, B., Frigerio, S., Eoli, M., Silvani, A., Broggi, G., Ciusani, E., Croci, D., Boiardi, A. and De Rossi, M. 2004. CXCL12 in malignant glial tumors: a possible role in angiogenesis and cross-talk between endothelial and tumoral cells. *Journal of neuro-oncology*. **67**(3), pp.305–17.
- Sandmann, T., Bourgon, R., Garcia, J., Li, C., Cloughesy, T., Chinot, O.L., Wick, W., Nishikawa, R., Mason, W., Henriksson, R., Saran, F., Lai, A., Moore, N., Kharbanda, S., Peale, F., Hegde, P., Abrey, L.E., Phillips, H.S. and Bais, C. 2015. Patients with proneural glioblastoma may derive overall survival benefit from the addition of bevacizumab to first-line radiotherapy and temozolomide: Retrospective analysis of the AVAglio trial. *Journal of Clinical Oncology*. **33**(25), pp.2735–2744.

- Sarkaria, J.N., Carlson, B.L., Schroeder, M.A., Grogan, P., Brown, P.D., Giannini, C., Ballman, K. V., Kitange, C.J., Guha, A., Pandita, A. and James, C.D. 2006. Use of an orthotopic xenograft model for assessing the effect of epidermal growth factor receptor amplification on glioblastoma radiation response. *Clinical Cancer Research*. **12**(7 1).
- Sato, Y. and Rifkin, D.B. 1989. Inhibition of endothelial cell movement by pericytes and smooth muscle cells: Activation of a latent transforming growth factor- $\beta$ 1-like molecule by plasmin during co-culture. *Journal of Cell Biology*. **109**(1).
- Sayan, M., Mustafayev, T.Z., Balmuk, A., Mamidanna, S., Kefelioglu, E.S.S., Gungor, G., Chundury, A., Ohri, N., Karaarslan, E., Ozyar, E. and Atalar, B. 2020. Management of symptomatic radiation necrosis after stereotactic radiosurgery and clinical factors for treatment response. *Radiation Oncology Journal*. **38**(3).
- Scadden, D.T. 2006. The stem-cell niche as an entity of action. *Nature*. **441**(7097).
- Scherer, H.J. 1938. Structural development in gliomas. *American Journal of Cancer*. **34**(3).
- Schiffer, D., Annovazzi, L., Mazzucco, M. and Mellai, M. 2015. The microenvironment in gliomas: Phenotypic expressions. *Cancers*. **7**(4), pp.2352–2359.
- Seano, G. 2018. Targeting the perivascular niche in brain tumors. *Current Opinion in Oncology*. **30**(1), pp.54–60.
- Seidel, S., Garvalov, B.K., Wirta, V., Von Stechow, L., Schänzer, A., Meletis, K., Wolter, M., Sommerlad, D., Henze, A.T., Nistér, M., Reifenberger, G., Lundeberg, J., Frisén, J. and Acker, T. 2010. A hypoxic niche regulates glioblastoma stem cells through hypoxia inducible factor 2 $\alpha$ . *Brain*. **133**(4).
- Semenza, G.L. 1999. Regulation of mammalian O<sub>2</sub> homeostasis by hypoxia-inducible factor 1. *Annual Review of Cell and Developmental Biology*. **15**.
- Seo, Y.S., Ko, I.O., Park, H., Jeong, Y.J., Park, J.A., Kim, K.S., Park, M.J. and Lee, H.J. 2019. Radiation-Induced Changes in Tumor Vessels and Microenvironment Contribute to Therapeutic Resistance in Glioblastoma.

*Frontiers in Oncology*. **9**(November), pp.1–10.

- Shahidi, M., Mozdarani, H. and Bryant, P.E. 2007. Radiation sensitivity of leukocytes from healthy individuals and breast cancer patients as measured by the alkaline and neutral comet assay. *Cancer Letters*. **257**(2).
- Shaifer, C.A., Huang, J. and Lin, P.C. 2010. Glioblastoma cells incorporate into tumor vasculature and contribute to vascular radioresistance. *International journal of cancer*. **127**(9), pp.2063–75.
- Shankar, A., Kumar, S., Iskander, A., Varma, N.R.S., Janic, B., deCarvalho, A., Mikkelsen, T., Frank, J.A., Ali, M.M., Knight, R.A., Brown, S. and Arbab, A.S. 2014. Subcurative radiation significantly increases cell proliferation, invasion, and migration of primary glioblastoma multiforme in vivo. *Chinese Journal of Cancer*. **33**(3).
- Sharma, A., Bendre, A., Mondal, A., Muzumdar, D., Goel, N. and Shiras, A. 2017. Angiogenic gene signature derived from subtype specific cell models segregate proneural and mesenchymal glioblastoma. *Frontiers in Oncology*. **7**(JUL).
- Shelton, L.M., Mukherjee, P., Huysentruyt, L.C., Urits, I., Rosenberg, J.A. and Seyfried, T.N. 2010. A novel pre-clinical in vivo mouse model for malignant brain tumor growth and invasion. *Journal of Neuro-Oncology*. **99**(2), pp.165–176.
- Sheng, J., Chen, W. and Zhu, H.J. 2015. The immune suppressive function of transforming growth factor- $\beta$  (TGF- $\beta$ ) in human diseases. *Growth Factors*. **33**(2).
- Shibao, S., Minami, N., Koike, N., Fukui, N., Yoshida, K., Saya, H. and Sampetean, O. 2018. Metabolic heterogeneity and plasticity of glioma stem cells in a mouse glioblastoma model. *Neuro-Oncology*. **20**(3).
- Shih, A.H. and Holland, E.C. 2006. Platelet-derived growth factor (PDGF) and glial tumorigenesis. *Cancer Letters*. **232**(2).
- Shirai, Y., Chow, C.C.T., Kambe, G., Suwa, T., Kobayashi, M., Takahashi, I., Harada, H. and Nam, J.M. 2021. An overview of the recent development of anticancer agents targeting the hif-1 transcription factor. *Cancers*. **13**(11), pp.1–21.

- Shultz, L.D., Lyons, B.L., Burzenski, L.M., Gott, B., Chen, X., Chaleff, S., Kotb, M., Gillies, S.D., King, M., Mangada, J., Greiner, D.L. and Handgretinger, R. 2005. Human lymphoid and myeloid cell development in NOD/LtSz-scid IL2R gamma null mice engrafted with mobilized human hemopoietic stem cells. *Journal of immunology (Baltimore, Md. : 1950)*. **174**(10), pp.6477–89.
- Simons, M., Gordon, E. and Claesson-Welsh, L. 2016. Mechanisms and regulation of endothelial VEGF receptor signalling. *Nature Reviews Molecular Cell Biology*. **17**(10), pp.611–625.
- Singh, A., Gurav, M., Dhanavade, S., Shetty, O. and Epari, S. 2017. Diffuse glioma – Rare homozygous IDH point mutation, is it an oncogenetic mechanism? *Neuropathology*. **37**(6), pp.582–585.
- Singh, S.K., Hawkins, C., Clarke, I.D., Squire, J.A., Bayani, J., Hide, T., Henkelman, R.M., Cusimano, M.D. and Dirks, P.B. 2004. Identification of human brain tumour initiating cells. *Nature*. **432**(7015).
- Skoda, A.M., Simovic, D., Karin, V., Kardum, V., Vranic, S. and Serman, L. 2018. The role of the hedgehog signaling pathway in cancer: A comprehensive review. *Bosnian Journal of Basic Medical Sciences*. **18**(1).
- Soda, Y., Marumoto, T., Friedmann-Morvinski, D., Soda, M., Liu, F., Michiue, H., Pastorino, S., Yang, M., Hoffman, R.M., Kesari, S. and Verma, I.M. 2011. Transdifferentiation of glioblastoma cells into vascular endothelial cells. *Proceedings of the National Academy of Sciences of the United States of America*. **108**(11), pp.4274–4280.
- Song, C., Park, H.J., Tanaka, N., Kwak, H.J., Park, M.J. and Levitt, S.H. 2009. Implication of Vascular Damage in the Response of Tumors to Ablative High-dose Radiotherapy. *International Journal of Radiation Oncology\*Biophysics\*Physics*. **75**(3).
- Song, S., Ewald, A.J., Stallcup, W., Werb, Z. and Bergers, G. 2009. PDGFR $\beta$ + perivascular progenitor cells in tumours regulate. *Nat Cell Biol*. **7**(9), pp.870–879.
- Songtao, Q., Lei, Y., Si, G., Yanqing, D., Huixia, H., Xuelin, Z., Lanxiao, W. and Fei, Y. 2012. IDH mutations predict longer survival and response to temozolomide in secondary glioblastoma. *Cancer Science*. **103**(2), pp.269–273.

- Sørensen, M.D., Dahlrot, R.H., Boldt, H.B., Hansen, S. and Kristensen, B.W. 2018. Tumour-associated microglia/macrophages predict poor prognosis in high-grade gliomas and correlate with an aggressive tumour subtype. *Neuropathology and Applied Neurobiology*. **44**(2).
- Stadlbauer, A., Kinfe, T.M., Eyüpoglu, I., Zimmermann, M., Kitzwögerer, M., Podar, K., Buchfelder, M., Heinz, G., Oberndorfer, S. and Marhold, F. 2021. Tissue hypoxia and alterations in microvascular architecture predict glioblastoma recurrence in humans. *Clinical Cancer Research*. **27**(6), pp.1641–1649.
- Stankiewicz, T.R. and Linseman, D.A. 2014. Rho family GTPases: Key players in neuronal development, neuronal survival, and neurodegeneration. *Frontiers in Cellular Neuroscience*. **8**(OCT), pp.1–14.
- Stark, A.M., Doukas, A., Hugo, H.H. and Mehdorn, H.M. 2010. The expression of mismatch repair proteins MLH1, MSH2 and MSH6 correlates with the Ki67 proliferation index and survival in patients with recurrent glioblastoma. *Neurological Research*. **32**(8), pp.816–820.
- Stenman, J.M., Rajagopal, J., Carroll, T.J., Ishibashi, M., McMahon, J. and McMahon, A.P. 2008. Canonical Wnt signaling regulates organ-specific assembly and differentiation of CNS vasculature. *Science*. **322**(5905).
- Streubel, B., Chott, A., Huber, D., Exner, M., Jäger, U., Wagner, O. and Schwarzing, I. 2004. Lymphoma-Specific Genetic Aberrations in Microvascular Endothelial Cells in B-Cell Lymphomas. *New England Journal of Medicine*. **351**(3).
- Stupp, R., Hegi, M.E., Mason, W.P., Bent, M.J. Van Den, Taphoorn, M.J.B., Janzer, R.C., Ludwin, S.K. and Allgeier, A. 2009. Effects of radiotherapy with concomitant and adjuvant temozolomide versus radiotherapy alone on survival in glioblastoma in a randomised phase III study: 5-year analysis of the EORTC-NCIC trial. *Lancet Oncology*. **10**(5), pp.459–466.
- Stupp, R., Mason, W.P., Bent, M.J. van den, Weller, M., Fisher, B., Taphoorn, M.J.B., Belanger, K., Brandes, A.A., Marosi, C., Bogdahn, U. and Jürgen Curschmann, M. 2005. Radiotherapy plus Concomitant and Adjuvant Temozolomide for Glioblastoma. *The New England Journal of Medicine*. **352**(10), pp.987–996.

- Stupp, R., Wong, E.T., Kanner, A.A., Steinberg, D., Engelhard, H., Heidecke, V., Kirson, E.D., Taillibert, S., Liebermann, F., Dbalý, V., Ram, Z., Villano, J.L., Rainov, N., Weinberg, U., Schiff, D., Kunschner, L., Raizer, J., Honnorat, J., Sloan, A., Malkin, M., Landolfi, J.C., Payer, F., Mehdorn, M., Weil, R.J., Pannullo, S.C., Westphal, M., Smrcka, M., Chin, L., Kostron, H., Hofer, S., Bruce, J., Cosgrove, R., Paleologous, N., Palti, Y. and Gutin, P.H. 2012. NovoTTF-100A versus physician's choice chemotherapy in recurrent glioblastoma: A randomised phase III trial of a novel treatment modality. *European Journal of Cancer*. **48**(14).
- Su, W.H., Chuang, P.C., Huang, E.Y. and Yang, K.D. 2012. Radiation-induced increase in cell migration and metastatic potential of cervical cancer cells operates via the K-ras pathway. *American Journal of Pathology*. **180**(2).
- Sundaravel, S., Duggan, R., Bhagat, T., Ebenezer, D.L., Liu, H., Yu, Y., Bartenstein, M., Unnikrishnan, M., Karmakar, S., Liu, T.C., Torregroza, I., Quenon, T., Anastasi, J., McGraw, K.L., Pellagatti, A., Boulwood, J., Yajnik, V., Artz, A., Le Beau, M.M., Steidl, U., List, A.F., Evans, T., Verma, A. and Wickrema, A. 2015. Reduced DOCK4 expression leads to erythroid dysplasia in myelodysplastic syndromes. *Proceedings of the National Academy of Sciences of the United States of America*. **112**(46).
- Sundberg, C., Kowanetz, M., Brown, L.F., Detmar, M. and Dvorak, H.F. 2002. Stable expression of angiopoietin-1 and other markers by cultured pericytes: Phenotypic similarities to a subpopulation of cells in maturing vessels during later stages of angiogenesis in vivo. *Laboratory Investigation*. **82**(4).
- Suzuki, M., Nakamatsu, K., Kanamori, S., Okumra, M., Uchiyama, T., Akai, F. and Nishimura, Y. 2003. Feasibility study of the simultaneous integrated boost (SIB) method for malignant gliomas using intensity-modulated radiotherapy (IMRT). *Japanese Journal of Clinical Oncology*. **33**(6).
- Svensmark, J.H. and Brakebusch, C. 2019. Rho GTPases in cancer: friend or foe? *Oncogene*. **38**(50), pp.7447–7456.
- Szatmári, T., Lumniczky, K., Désaknai, S., Trajcevski, S., Hídvégi, E.J., Hamada, H. and Sáfrány, G. 2006. Detailed characterization of the mouse glioma 261 tumor model for experimental glioblastoma therapy. *Cancer Science*. **97**(6).
- Szulzewsky, F., Pelz, A., Feng, X., Synowitz, M., Markovic, D., Langmann, T.,

- Holtman, I.R., Wang, X., Eggen, B.J.L., Boddeke, H.W.G.M., Hambardzumyan, D., Wolf, S.A. and Kettenmann, H. 2015. Glioma-associated microglia/macrophages display an expression profile different from M1 and M2 polarization and highly express Gpnmb and Spp1. *PLoS ONE*. **10**(2).
- Tabatabai, G., Frank, B., Möhle, R., Weller, M. and Wick, W. 2006. Irradiation and hypoxia promote homing of haematopoietic progenitor cells towards gliomas by TGF- $\beta$ -dependent HIF-1 $\alpha$ -mediated induction of CXCL12. *Brain*. **129**(9), pp.2426–2435.
- Takai, Y., Sasaki, T. and Matozaki, T. 2021. Small GTP-Binding Proteins. *Physiological Reviews*. **81**(1), pp.153–208.
- Tamura, K., Aoyagi, M., Ando, N., Ogishimao, T., Wakimoto, H., Yamamoto, M. and Ohno, K. 2013. Expansion of CD133-positive glioma cells in recurrent de novo glioblastomas after radiotherapy and chemotherapy. *Journal of Neurosurgery*. **119**(5).
- Tan, W., Palmby, T.R., Gavard, J., Amornphimoltham, P., Zheng, Y. and Gui, J.S. 2008. An essential role for Rac1 in endothelial cell function and vascular development. *The FASEB Journal*. **22**(6).
- Tang, L., Wei, F., Wu, Y., He, Y., Shi, L., Xiong, F., Gong, Z., Guo, C., Li, Xiayu, Deng, H., Cao, K., Zhou, M., Xiang, B., Li, Xiaoling, Li, Y., Li, G., Xiong, W. and Zeng, Z. 2018. Role of metabolism in cancer cell radioresistance and radiosensitization methods. *Journal of Experimental and Clinical Cancer Research*. **37**(1).
- Tavora, B., Batista, S. and Hodivala-Dilke, K. 2011. Measuring angiogenesis in mice. *Methods in Molecular Biology*. **769**.
- Taylor, A. and Powell, M.E.B. 2004. Intensity-modulated radiotherapy - What is it? *Cancer Imaging*. **4**(2).
- Terabe, M., Matsui, S., Park, J.M., Mamura, M., Noben-Trauth, N., Donaldson, D.D., Chen, W., Wahl, S.M., Ledbetter, S., Pratt, B., Letterio, J.J., Paul, W.E. and Berzofsky, J.A. 2003. Transforming Growth Factor- $\beta$  Production and Myeloid Cells Are an Effector Mechanism through Which CD1d-restricted T Cells Block Cytotoxic T Lymphocyte-mediated Tumor Immunosurveillance: Abrogation Prevents Tumor Recurrence. *Journal of Experimental Medicine*.

**198**(11), pp.1741–1752.

Teuwen, L.A., De Rooij, L.P.M.H., Cuypers, A., Rohlenova, K., Dumas, S.J., García-Caballero, M., Meta, E., Amersfoort, J., Taverna, F., Becker, L.M., Veiga, N., Cantelmo, A.R., Geldhof, V., Conchinha, N. V., Kalucka, J., Treppe, L., Conradi, L.C., Khan, S., Karakach, T.K., Soenen, S., Vinckier, S., Schoonjans, L., Eelen, G., Van Laere, S., Dewerchin, M., Dirix, L., Mazzone, M., Luo, Y., Vermeulen, P. and Carmeliet, P. 2021. Tumor vessel co-option probed by single-cell analysis. *Cell Reports*. **35**(11).

The Cancer Genome Atlas Research 2008. Comprehensive genomic characterization defines human glioblastoma genes and core pathways. *Nature*. **455**(7216), pp.1061–1068.

Tong, F., Xiong, C.J., Wei, C.H., Wang, Y., Liang, Z.W., Lu, H., Pan, H.J., Dong, J.H., Zheng, X.F., Wu, G. and Dong, X.R. 2020. Hypo-fractionation radiotherapy normalizes tumor vasculature in non-small cell lung cancer xenografts through the p-STAT3/HIF-1 alpha signaling pathway. *Therapeutic Advances in Medical Oncology*. **12**, pp.1–12.

Traweek, S.T., Kandalaf, P.L., Mehta, P. and Battifora, H. 1991. The human hematopoietic progenitor cell antigen (CD34) in vascular neoplasia. *American Journal of Clinical Pathology*. **96**(1).

Trnovec, T., Kállay, Z. and Bezek, Š. 1990. Effects of ionizing radiation on the blood brain barrier permeability to pharmacologically active substances. *International Journal of Radiation Oncology, Biology, Physics*. **19**(6).

Tsai, C.Y., Ko, H.J., Huang, C.Y.F., Lin, C.Y., Chiou, S.J., Su, Y.F., Lieu, A.S., Loh, J.K., Kwan, A.L., Chuang, T.H. and Hong, Y.R. 2021. Ionizing radiation induces resistant glioblastoma stem-like cells by promoting autophagy via the wnt/β-catenin pathway. *Life*. **11**(5).

Turcotte, S., Desrosiers, R.R. and Béliveau, R. 2003. HIF-1α mRNA and protein upregulation involves Rho GTPase expression during hypoxia in renal cell carcinoma. *Journal of Cell Science*. **116**(11).

Ueda, S., Fujimoto, S., Hiramoto, K., Negishi, M. and Katoh, H. 2008. Dock4 regulates dendritic development in hippocampal neurons. *Journal of Neuroscience Research*. **86**(14).

- Ueda, S., Negishi, M. and Katoh, H. 2013. Rac GEF dock4 interacts with cortactin to regulate dendritic spine formation. *Molecular Biology of the Cell*. **24**(10).
- Umans, R.A., Henson, H.E., Mu, F., Parupalli, C., Ju, B., Peters, J.L., Lanham, K.A., Plavicki, J.S. and Michael, R. 2018. CNS angiogenesis and barrierogenesis occur simultaneously. *Developmental Biology*. **425**(2), pp.101–108.
- Upadhyay, G., Goessling, W., North, T., Xavier, R., Zon, L. and Yajnik, V. 2008. Molecular association between  $\beta$ -catenin degradation complex and Rac guanine exchange factor DOCK4 is essential for Wnt/ $\beta$ -catenin signaling G. *Oncogene*. **27**(44), pp.5845–5855.
- Valdivia, A., Mingo, G., Aldana, V., Pinto, M.P., Ramirez, M., Retamal, C., Gonzalez, A., Nualart, F., Corvalan, A.H. and Owen, G.I. 2019. Fact or Fiction, It Is Time for a Verdict on Vasculogenic Mimicry? *Frontiers in Oncology*. **9**.
- Valdor, R., García-Bernal, D., Bueno, C., Ródenas, M., Moraleda, J.M., Macian, F. and Martínez, S. 2017. Glioblastoma progression is assisted by induction of immunosuppressive function of pericytes through interaction with tumor cells. *Oncotarget*. **8**(40), pp.68614–68626.
- Vallon, M., Chang, J. and Z, H. 2014. *Developmental and pathological angiogenesis in the central nervous system* [Online]. Available from: <http://www.scopus.com/inward/record.url?eid=2-s2.0-84919783684&partnerID=tZOtx3y1>.
- Vaupel, P., Briest, S. and Höckel, M. 2002. Hypoxia in breast cancer: Pathogenesis, characterization and biological/therapeutic implications. *Wiener Medizinische Wochenschrift*. **152**(13–14).
- Vaupel, P., Thews, O. and Hoeckel, M. 2001. Treatment resistance of solid tumors: Role of hypoxia and anemia. *Medical Oncology*. **18**(4).
- Verhaak, R.G.W., Hoadley, K.A., Purdom, E., Wang, V., Qi, Y., Wilkerson, M.D., Miller, C.R., Ding, L., Golub, T., Mesirov, J.P., Alexe, G., Lawrence, M., O’Kelly, M., Tamayo, P., Weir, B.A., Gabriel, S., Winckler, W., Gupta, S., Jakkula, L., Feiler, H.S., Hodgson, J.G., James, C.D., Sarkaria, J.N., Brennan, C., Kahn, A., Spellman, P.T., Wilson, R.K., Speed, T.P., Gray, J.W., Meyerson, M., Getz, G., Perou, C.M. and Hayes, D.N. 2010. Integrated

Genomic Analysis Identifies Clinically Relevant Subtypes of Glioblastoma Characterized by Abnormalities in PDGFRA, IDH1, EGFR, and NF1. *Cancer Cell*.

- Veys, K., Fan, Z., Ghobrial, M., Bouché, A., García-Caballero, M., Vriens, K., Conchinha, N.V., Seuwen, A., Schlegel, F., Gorski, T., Crabbé, M., Gilardoni, P., Ardicoglu, R., Schaffenrath, J., Casteels, C., De Smet, G., Smolders, I., Van Laere, K., Abel, E.D., Fendt, S.M., Schroeter, A., Kalucka, J., Cantelmo, A.R., Wälchli, T., Keller, A., Carmeliet, P. and De Bock, K. 2020. Role of the GLUT1 Glucose Transporter in Postnatal CNS Angiogenesis and Blood-Brain Barrier Integrity. *Circulation Research*. **127**(4).
- Vlasi, E., Lagadec, C., Vergnes, L., Matsutani, T., Masui, K., Poulou, M., Popescu, R., Della Donna, L., Evers, P., Dekmezian, C., Reue, K., Christofk, H., Mischel, P.S. and Pajonka, F. 2011. Metabolic state of glioma stem cells and nontumorigenic cells. *Proceedings of the National Academy of Sciences of the United States of America*. **108**(38).
- Vleeschouwer, S. De and Bergers, G. 2017. Glioblastoma: To Target the Tumor Cell or the Microenvironment? *In: Glioblastoma*.
- Voutouri, C., Kirkpatrick, N.D., Chung, E., Mpekris, F., Baish, J.W., Munn, L.L., Fukumura, D., Stylianopoulos, T. and Jain, R.K. 2019. Experimental and computational analyses reveal dynamics of tumor vessel cooption and optimal treatment strategies. *Proceedings of the National Academy of Sciences of the United States of America*. **116**(7).
- Voytov, G., Kaufman, S., Hong, T., Pinkerton, A., Simon, R. and Dowsett, R. 2002. Treatment of recurrent malignant gliomas with stereotactic intensity modulated radiation therapy. *American Journal of Clinical Oncology: Cancer Clinical Trials*. **25**(6).
- Wacker, A. and Gerhardt, H. 2011. Endothelial development taking shape. *Current Opinion in Cell Biology*. **23**(6), pp.676–685.
- Walker, M.D., Strike, T.A. and Sheline, G.E. 1979. An analysis of dose-effect relationship in the radiotherapy of malignant gliomas. *International Journal of Radiation Oncology, Biology, Physics*. **5**(10).
- Wanat, K. 2020. Biological barriers, and the influence of protein binding on the passage of drugs across them. *Molecular Biology Reports*. **47**(4).

- Wang, J., Cazzato, E., Ladewig, E., Frattini, V., Rosenbloom, D.I.S., Zairis, S., Abate, F., Liu, Z., Elliott, O., Shin, Y.J., Lee, J.K., Lee, I.H., Park, W.Y., Eoli, M., Blumberg, A.J., Lasorella, A., Nam, D.H., Finocchiaro, G., Iavarone, A. and Rabadan, R. 2016. Clonal evolution of glioblastoma under therapy. *Nature Genetics*. **48**(7), pp.768–776.
- Wang, Q., He, Z., Huang, M., Liu, T., Wang, Y., Xu, H., Duan, H., Ma, P., Zhang, L., Zamvil, S.S., Hidalgo, J., Zhang, Z., O'Rourke, D.M., Dahmane, N., Brem, S., Mou, Y., Gong, Y. and Fan, Y. 2018. Vascular niche IL-6 induces alternative macrophage activation in glioblastoma through HIF-2 $\alpha$ . *Nature Communications*. **9**(1).
- Wang, Q., Hu, B., Hu, X., Kim, H., Squatrito, M., Scarpace, L., DeCarvalho, A.C., Lyu, S., Li, P., Li, Y., Barthel, F., Cho, H.J., Lin, Y.H., Satani, N., Martinez-Ledesma, E., Zheng, S., Chang, E., Sauv e, C.E.G., Olar, A., Lan, Z.D., Finocchiaro, G., Phillips, J.J., Berger, M.S., Gabrusiewicz, K.R., Wang, G., Eskilsson, E., Hu, J., Mikkelsen, T., DePinho, R.A., Muller, F., Heimberger, A.B., Sulman, E.P., Nam, D.H. and Verhaak, R.G.W. 2017. Tumor Evolution of Glioma-Intrinsic Gene Expression Subtypes Associates with Immunological Changes in the Microenvironment. *Cancer Cell*. **32**(1), pp.42-56.e6.
- Wang, S.C., Yu, C.F., Hong, J.H., Tsai, C.S. and Chiang, C.S. 2013. Radiation Therapy-Induced Tumor Invasiveness Is Associated with SDF-1-Regulated Macrophage Mobilization and Vasculogenesis. *PLoS ONE*. **8**(8).
- Wanis, H.A., M oller, H., Ashkan, K. and Davies, E.A. 2021. The incidence of major subtypes of primary brain tumors in adults in England 1995-2017. *Neuro-Oncology*. (April), pp.1–12.
- Wank, M., Schilling, D., Schmid, T.E., Meyer, B., Gempt, J., Barz, M., Schlegel, J., Liesche, F., Kessel, K.A., Wiestler, B., Bette, S., Zimmer, C. and Combs, S.E. 2018. Human glioma migration and infiltration properties as a target for personalized radiation medicine. *Cancers*. **10**(11).
- Watabe-Uchida, M., John, K.A., Janas, J.A., Newey, S.E. and Van Aelst, L. 2006. The Rac Activator DOCK7 Regulates Neuronal Polarity through Local Phosphorylation of Stathmin/Op18. *Neuron*. **51**(6).
- Watkins, S., Robel, S., Kimbrough, I.F., Robert, S.M., Ellis-Davies, G. and

- Sontheimer, H. 2014. Disruption of astrocyte-vascular coupling and the blood-brain barrier by invading glioma cells. *Nature Communications*. **5**.
- Wei, Q., Singh, O., Ekinci, C., Gill, J., Li, M., Mamatjan, Y., Karimi, S., Bunda, S., Mansouri, S., Aldape, K. and Zadeh, G. 2021. TNF $\alpha$  secreted by glioma associated macrophages promotes endothelial activation and resistance against anti-angiogenic therapy. *Acta Neuropathologica Communications*. **9**(1).
- Weinberg, R.A. 2014. *The biology of cancer*.
- Wesseling, P., Schlingemann, R.O., Rietveld, F.J.R., Link, M., Burger, P.C. and Ruiters, D.J. 1995. Early and extensive contribution of pericytes/vascular smooth muscle cells to microvascular proliferation in glioblastoma multiforme: An immuno-light and immuno-electron microscopic study. *Journal of Neuropathology and Experimental Neurology*. **54**(3).
- Westbrook, J.A., Wood, S.L., Cairns, D.A., McMahon, K., Gahlaut, R., Thygesen, H., Shires, M., Roberts, S., Marshall, H., Oliva, M.R., Dunning, M.J., Hanby, A.M., Selby, P.J., Speirs, V., Mavria, G., Coleman, R.E. and Brown, J.E. 2019. Identification and validation of DOCK4 as a potential biomarker for risk of bone metastasis development in patients with early breast cancer. *The Journal of Pathology*. **247**(3), p.381.
- Westphal, M. and Lamszus, K. 2011. The neurobiology of gliomas: From cell biology to the development of therapeutic approaches. *Nature Reviews Neuroscience*. **12**(9).
- Wick, W., Gorlia, T., Bendszus, M., Taphoorn, M., Sahm, F., Harting, I., Brandes, A.A., Taal, W., Domont, J., Idbaih, A., Campone, M., Clement, P.M., Stupp, R., Fabbro, M., Le Rhun, E., Dubois, F., Weller, M., von Deimling, A., Golfopoulos, V., Bromberg, J.C., Platten, M., Klein, M. and van den Bent, M.J. 2017. Lomustine and Bevacizumab in Progressive Glioblastoma. *New England Journal of Medicine*. **377**(20).
- Wilson, W.R. and Hay, M.P. 2011. Targeting hypoxia in cancer therapy. *Nature Reviews Cancer*. **11**(6).
- Winkler, F., Osswald, M. and Wick, W. 2018. Anti-Angiogenics: Their Role in the Treatment of Glioblastoma. *Oncology Research and Treatment*. **41**(4), pp.181–186.

- Wolburg, H., Noell, S., Mack, A., Wolburg-Buchholz, K. and Fallier-Becker, P. 2009. Brain endothelial cells and the glio-vascular complex. *Cell and Tissue Research*. **335**(1).
- Woodroffe, R.W., Zanaty, M., Soni, N., Mott, S.L., Helland, L.C., Pasha, A., Maley, J., Dhungana, N., Jones, K.A., Monga, V. and Greenlee, J.D.W. 2020. Survival after reoperation for recurrent glioblastoma. *Journal of Clinical Neuroscience*. **73**.
- Wright, T.J., Leach, L., Shaw, P.E. and Jones, P. 2002. Dynamics of vascular endothelial-cadherin and  $\beta$ -catenin localization by vascular endothelial growth factor-induced angiogenesis in human umbilical vein cells. *Experimental Cell Research*. **280**(2).
- Wu, C.X., Lin, G.S., Lin, Z.X., Zhang, J.D., Liu, S.Y. and Zhou, C.F. 2015. Peritumoral edema shown by MRI predicts poor clinical outcome in glioblastoma. *World Journal of Surgical Oncology*. **13**(1), pp.1–9.
- Xie, Y., He, L., Lugano, R., Zhang, Yanyu, Cao, H., He, Q., Chao, M., Liu, B., Cao, Q., Wang, J., Jiao, Y., Hu, Y., Han, L., Zhang, Yong, Huang, H., Uhrbom, L., Betsholtz, C., Wang, L., Dimberg, A. and Zhang, L. 2021. Key molecular alterations in endothelial cells in human glioblastoma uncovered through single-cell RNA sequencing. *JCI Insight*. **6**(15).
- Xu, J., Escamilla, J., Mok, S., David, J., Priceman, S., West, B., Bollag, G., McBride, W. and Wu, L. 2013. CSF1R signaling blockade stanches tumor-infiltrating myeloid cells and improves the efficacy of radiotherapy in prostate cancer. *Cancer Research*. **73**(9).
- Yajnik, V., Paulding, C., Sordella, R., McClatchey, A.I., Saito, M., Wahrer, D.C.R., Reynolds, P., Bell, D.W., Lake, R., van den Heuvel, S., Settleman, J. and Haber, D.A. 2003. DOCK4, a GTPase Activator, Is Disrupted during Tumorigenesis. *Cell*. **112**(5), pp.673–684.
- Yan, G.N., Yang, L., Lv, Y.F., Shi, Y., Shen, L.L., Yao, X.H., Guo, Q.N., Zhang, P., Cui, Y.H., Zhang, X., Bian, X.W. and Guo, D.Y. 2014. Endothelial cells promote stem-like phenotype of glioma cells through activating the Hedgehog pathway. *Journal of Pathology*. **234**(1), pp.11–22.
- Yang, L., Lin, C., Wang, L., Guo, H. and Wang, X. 2012. Hypoxia and hypoxia-inducible factors in glioblastoma multiforme progression and therapeutic

- implications. *Experimental Cell Research*. **318**(19).
- Yang, X., Guo, D., Li, K. and Shi, L. 2021. Altered postnatal developmental patterns of ultrasonic vocalizations in Dock4 knockout mice. *Behavioural Brain Research*. **406**(March), p.113232.
- Young, A.G.H. and Bennewith, K.L. 2017. Ionizing Radiation Enhances Breast Tumor Cell Migration in Vitro. *Radiation Research*. **188**(4).
- Yu, J.R., Tai, Y., Jin, Y., Hammell, M.C., Wilkinson, J.E., Roe, J.S., Vakoc, C.R. and Van Aelst, L. 2015. TGF- $\beta$ /smad signaling through DOCK4 facilitates lung adenocarcinoma metastasis. *Genes and Development*. **29**(3), pp.250–261.
- Yuan, F., Salehi, H.A., Boucher, Y., Jain, R.K., Vasthare, U.S. and Tuma, R.F. 1994. Vascular Permeability and Microcirculation of Gliomas and Mammary Carcinomas Transplanted in Rat and Mouse Cranial Windows. *Cancer Research*. **54**(17).
- Yue, W.-Y. and Chen, Z.-P. 2005. Does vasculogenic mimicry exist in astrocytoma? *The journal of histochemistry and cytochemistry: official journal of the Histochemistry Society*. **53**(8), pp.997–1002.
- Zagzag, D., Lukyanov, Y., Lan, L., Ali, M.A., Esencay, M., Mendez, O., Yee, H., Voura, E.B. and Newcomb, E.W. 2006. Hypoxia-inducible factor 1 and VEGF upregulate CXCR4 in glioblastoma: implications for angiogenesis and glioma cell invasion. *Laboratory investigation; a journal of technical methods and pathology*. **86**(12), pp.1221–32.
- Zagzag, D., Zhong, H., Scalzitti, J.M., Laughner, E., Simons, J.W. and Semenza, G.L. 2000. Expression of hypoxia-inducible factor 1 $\alpha$  in brain tumors: association with angiogenesis, invasion, and progression. *Cancer*. **88**(11), pp.2606–2618.
- Zeppernick, F., Ahmadi, R., Campos, B., Dictus, C., Helmke, B.M., Becker, N., Lichter, P., Unterberg, A., Radlwimmer, B. and Herold-Mende, C.C. 2008. Stem cell marker CD133 affects clinical outcome in glioma patients. *Clinical Cancer Research*. **14**(1).
- Zhai, H., Heppner, F.L. and Tsirka, S.E. 2011. Microglia/macrophages promote glioma progression. *GLIA*. **59**(3).

- Zhang, M., Song, T., Yang, L., Chen, R., Wu, L., Yang, Z. and Fang, J. 2008. Nestin and CD133: Valuable stem cell-specific markers for determining clinical outcome of glioma patients. *Journal of Experimental and Clinical Cancer Research*. **27**(1).
- Zhang, P., Xia, Q., Liu, L., Li, S. and Dong, L. 2020. Current Opinion on Molecular Characterization for GBM Classification in Guiding Clinical Diagnosis, Prognosis, and Therapy. *Frontiers in Molecular Biosciences*. **7**(September), pp.1–13.
- Zhang, X., Yang, K., Chen, C., He, Z., Wang, Q., Feng, H., Lv, S., Wang, Y., Mao, M., Liu, Q., Tan, Y., Wang, W., Li, T., Che, L., Qin, Z., Wu, L., Luo, M., Luo, C., Liu, Y., Yin, W., Wang, C., Guo, H., Li, Q., Wang, B., Chen, W., Wang, S. and Shi, Y. 2021. Pericytes augment glioblastoma cell resistance to temozolomide through CCL5-CCR5 paracrine signaling. *Cell Research*. (December 2020), pp.1–16.
- Zhao, C., Gomez, G.A., Zhao, Y., Yang, Y., Cao, D., Lu, J., Yang, H. and Lin, S. 2018. ETV2 mediates endothelial transdifferentiation of glioblastoma. *Signal Transduction and Targeted Therapy*. **3**(1), pp.1–11.
- Zhao, S., Lin, Y., Xu, W., Jiang, W., Zha, Z., Wang, P., Yu, P., Li, Z., Gong, L., Peng, Y., Ding, J., Lei, Q., Guan, K.-L. and Xiong, Y. 2009. Glioma-Derived Mutations in IDH1 Dominantly Inhibit IDH1 Catalytic Activity and Induce HIF-1 $\alpha$  Shimin. *Science*. **324**(5924), pp.261–265.
- Zhou, L., Opalinska, J., Sohal, D., Yu, Y., Mo, Y., Bhagat, T., Abdel-Wahab, O., Fazzari, M., Figueroa, M., Alencar, C., Zhang, J., Kambhampati, S., Parmar, S., Nischal, S., Hueck, C., Suzuki, M., Freidman, E., Pellagatti, A., Boulwood, J., Steidl, U., Sautharajah, Y., Yajnik, V., McMahon, C., Gore, S.D., Plataniias, L.C., Levine, R., Melnick, A., Wickrema, A., Grealley, J.M. and Vermaa, A. 2011. Aberrant epigenetic and genetic marks are seen in myelodysplastic leukocytes and reveal Dock4 as a candidate pathogenic gene on chromosome 7q. *Journal of Biological Chemistry*. **286**(28).
- Zhou, W., Chen, C., Shi, Y., Wu, Q., Gimple, R.C., Fang, X., Huang, Z., Zhai, K., Ke, S.Q., Ping, Y.F., Feng, H., Rich, J.N., Yu, J.S., Bao, S. and Bian, X.W. 2017. Targeting Glioma Stem Cell-Derived Pericytes Disrupts the Blood-Tumor Barrier and Improves Chemotherapeutic Efficacy. *Cell Stem Cell*.

21(5), pp.591-603.e4.

Zhu, H., Acquaviva, J., Ramachandran, P., Boskovitz, A., Woolfenden, S., Pfannl, R., Bronson, R.T., Chen, J.W., Weissleder, R., Housman, D.E. and Charest, A. 2009. Oncogenic EGFR signaling cooperates with loss of tumor suppressor gene functions in gliomagenesis. *Proceedings of the National Academy of Sciences of the United States of America*. **106**(8).

Zhu, T.S., Costello, M.A., Talsma, C.E., Flack, C.G., Crowley, J.G., Hamm, L.L., He, X., Hervey-Jumper, S.L., Heth, J.A., Muraszko, K.M., DiMeco, F., Vescovi, A.L. and Fan, X. 2011. Endothelial cells create a stem cell niche in glioblastoma by providing NOTCH ligands that nurture self-renewal of cancer stem-like cells. *Cancer Research*. **71**(18), pp.6061–6072.